



HAL
open science

Bioinspired catalysis using oligourea helical foldamers

Diane Bécart

► **To cite this version:**

Diane Bécart. Bioinspired catalysis using oligourea helical foldamers. Organic chemistry. Université de Bordeaux; Universidad del País Vasco, 2017. English. NNT : 2017BORD0717 . tel-01968021

HAL Id: tel-01968021

<https://theses.hal.science/tel-01968021>

Submitted on 2 Jan 2019

HAL is a multi-disciplinary open access archive for the deposit and dissemination of scientific research documents, whether they are published or not. The documents may come from teaching and research institutions in France or abroad, or from public or private research centers.

L'archive ouverte pluridisciplinaire **HAL**, est destinée au dépôt et à la diffusion de documents scientifiques de niveau recherche, publiés ou non, émanant des établissements d'enseignement et de recherche français ou étrangers, des laboratoires publics ou privés.

THÈSE EN COTUTELLE PRÉSENTÉE
POUR OBTENIR LE GRADE DE
DOCTEUR DE
L'UNIVERSITÉ DE BORDEAUX
ET DE L'UNIVERSITÉ DU PAYS BASQUE EHU/UPV

ÉCOLE DOCTORALE UBX

ÉCOLE DOCTORALE UPV/EHU

SPÉCIALITÉ Chimie Organique

Par Diane BECART

**BIOINSPIRED CATALYSIS USING OLIGOUREA HELICAL
FOLDAMERS**

Sous la direction de Dr Gilles GUICHARD
et de Professeur Claudio PALOMO

Soutenue le 3 Novembre 2017

Membres du jury :

M. TATON, Daniel
M. CONSTANTIEUX, Thierry
M. SMIETANA, Michael
Mme MIELGO VINCENTE, Antonia
M. SMITH, Martin

Professeur, Université de Bordeaux
Professeur, Université de Marseille
Professeur, Université de Montpellier
Professeur, Univ. del País Vasco (Spain)
Professeur, University of Oxford (Great-Britain)

Président
Rapporteur
Rapporteur
Examinateur
Examinateur

Merci ! Thank you ! Gracias ! Eskerrik asko !

I firstly would like to thank Dr Gilles Guichard who invited me in this big adventure around foldamers and organocatalysis, involving me in a fascinating travel and for all his advices and his special power to give me back motivation when research was hard with me, and the fact he trusted me to present my works in many very nice occasions. I would like to thank very much Professor Claudio Palomo for welcoming me one year in his laboratory in Donostia, with his close regard into my project, all his ideas and all his passion as well as his warm enthusiasm towards the little French girl. I thank IDEX for my fellowship and the funding who allowed among others me to participate to many congresses, CBMN, IECB and UPV for giving me such nice working conditions.

I thank Professor Thierry Constantieux and Professor Michael Smietana for the time they spent on my thesis and for accepting to judge my works. I also thank Professor Martin Smith, Professor Daniel Taton and Professor Antonia Mielgo Vicente who answered present to discuss my project on my PhD defence.

Many persons who almost lived my full PhD as much as me, played a very important role in my three years. Vincent, tu m'as enseigné tous tes trucs, tu m'as appris à être pointilleuse voire même parano pour être complètement sûre et rigoureuse, petit Padawan a bien grandi grâce à toi ! Je me sens incroyablement chanceuse d'avoir eu la chance d'apprendre à tes côtés et de démarrer ce projet avec toi. Un grand merci à Arnaud aussi, qui a établi les bases de ce projet et grâce à qui j'ai pu débiter sereinement ma thèse. Un abrazo enorme a mi Igor de amor, quien fue mi mejor compañero de laboratorio, mi profesor de castellano, el supervisor de mis ensayos, quien me hacía reír cuando los tiempos eran difíciles (LE big mac!), con quien compartía un montón de pintxos y trucos de pokemon, mi amigo...! Pensamientos a mi pichuchi Haizea quien me enseñaba su propio castellano, tu energía, tu entusiasmo, tu franquicia y tu risa me han enseñado a coger la vida con más tranquilidad. A mes amis de chaque instant, qui étaient là pour moi à chaque moment de ma thèse, Léonie et Christophe. Vous êtes bien plus que mes collègues ! Tous nos fous rires, nos coups de gueule, nos pauses chocolat-gâteau, nos SMS, nos réflexions philosophiques (Ooohmmm) ont rendu ces trois ans tellement plus géniaux... A Julen, quien me ha ayudado tanto en mi vuelta de Donosti a Burdeos, para recordarme que la vida es como "¡ Qué alegría, Qué alboroto, Qué perrito (caliente) piloto ! », para darme todos los trucos (del almendruco) de cómo se escriben los menos, las R/S, y para aprovisionarme en sidra, ¡eskerrik asko !

Merci à toute l'équipe Guichard pour ces deux années à m'accompagner et m'encourager au milieu de mes colonnes, à Céline, Christel, Morgane pour leur aide et leurs conseils avisés, à Laura et Johanne mes compatriotes thésardes Guichard 2014-2017, à Steph qui m'a accueillie dans le labo et qui était toujours à fond, à Cate pour sa douceur et sa gentillesse, à Camille, Mégane et Jérémie. Merci à Estelle et Axelle, qui ont été d'une patience et d'une aide incroyable pour toutes mes heures passées au 400, notamment avec mes tubes de dernière minute et transfrontaliers. Merci à Loïc et Frédérique pour toutes les analyses MS et HRMS. Merci à Brice et Stéphane pour les jolies résolutions de structure. Un merci très chaleureux à Mariline qui nous accueille toujours avec le sourire, toujours arrangeante et bienveillante, encore un des soleils de l'IECB... Grazie mille a Valerio, you were my sunshine for the few months we spent together! Hvala to Ivan, we shared so funny moments in the lab and I loved when you taught me Serbian culture and bad words!

Eskerrik asko a todo el laboratorio de Donosti, mi compañera de vitrina Silvia, mi coliflorcita Sandra, Ana, Amaiur, Iñaki B., Iurre, Odei, Olatz, Iñaki U., Joseba, Eider, Lorena, Eider, Mikel, Aitor! Me encantó el año con vosotros, la atmósfera super dinámica llena de energía, todo lo que me habéis enseñado sobre la cultura vasca!! Muchas gracias a mis súper compis del piso bonito, Tere y Erika!!! La llegada en Gros y la Zurriola, los pintxopotes, las noches en frente de emisiones de tele tontas y divertidas, las cenas de croquetas, lo pasaba genial!!! A todos los otros que me han ayudado durante

este año precioso, pero también difícil: Maialen quien me ha enseñado todos los trucos de Donosti y quien me traía sus bolas de amor adorables cuando necesitaba suavidad!

A big big thank you to all my friends from the other lab! Tout d'abord toute la bande des Antoine J., M., R., S., A., B. avec un spécial big up à mes collègues grand Antoine pour ta joie de vivre et ton positivisme et Antoine fine blague pour tes lumières et ta subtilité ! Un gros câlin à ma jolie Camille toute pleine de douceur et de bonne humeur ! A big thank to Albano, Arthur, Joan, Daniela, Pedro, Rich, Maëlle, Drago, all these tea breaks and beers would have been so different without you! A huge thank you to all the PhD students who came each month to our PhD students dinners, I was so glad to see we shared these moments with you in so cool restaurants! Thanks to those who answered present when I started to organise the Friendly Organic Chemistry sessions!!! My thoughts to JJC teams 2015 and 2016! Merci à Carmelo qui m'a fait partager de très beaux moments musicaux pour ma dernière année à Bordeaux.

To my biochemist/biologist/friends from the other side of the corridor: Alba y tu sonrío, mi última traza de Euskal Herria por aquí; Britta, my kindest post-doc with the cutest kitten Grizou, my lovely chamber music, JJC co-organizer, bachata mate, hydrophilic friend, Pessac neighbour Caro, you were always there for me, for each presentation, for each drink we needed to forget about science, and above all for a lot of laugh and many sunflowers.

Un énorme merci à ma famille, mes parents qui m'ont soutenu tout au long de ses trois intenses années (et même depuis toujours !), qui m'ont accompagnée à travers les vignes et les sidrerias, les soucis du quotidien et aussi les petits succès de chaque nouveau résultat positif, mais surtout qui m'ont appris à persévérer et à toujours tirer quelque chose de positif et bénéfique quelle que soit l'expérience ! A mes frérots qui étaient avec moi, et qui m'ont écoutée cent fois parler de mes molécules droites et mes molécules gauches avec mes moules à gâteaux ! A mes grand-parents qui m'ont aussi apporté leur soutien depuis le début de mes études !

Un immense merci à tous ceux qui étaient avec moi et qui m'écoutaient, alors qu'ils venaient de galaxies bien éloignées de la mienne : toute la bande des plus beaux, ma belle Cécile, ma voisine chérie bricoleuse réparatrice de pneus Clémence, mon écolo Caro, mon choucho Victor, mes copines danseuses/chimistes MC et Louisiane. Merci à Alex qui m'a écoutée tellement d'heures et qui m'a faite grandir. Merci à ma majesté Charlène, ma complice depuis la Suisse ! Huge thank you to my handsome Magda, you helped me so much when I arrive in Bordeaux, you were my first person here, the one to who I could tell everything and with who I could dance, cry and laugh, buziaki ma chérie!

A mes meilleures amies, mes coupines de CP: Hélo, Hafssa, Sophie et Mado, vous êtes les meilleures !! Je suis trop heureuse qu'on ait traversé nos trois années toutes ensemble, toutes en parallèle, manips, publis, rédactions, soutenance (ou presque !!). Kiss Love et Bisounours ! A la mas gran de las pequeñas compañeras de piso Patricia! He pasado un año más que genial contigo en nuestra casa preciosa... Ya lo sabes que nunca podré decirte todo lo que quiero en 3 líneas... Un gigantismo gracias por ser como eres, que seamos las que queremos ser <3

Et enfin, un grand merci à tous mes professeurs et tous mes mentors qui m'ont amenée à continuer mes études en chimie et à me lancer dans cette grande aventure qu'est la thèse : Mme Parigot, Mme de la Harpe, Tahar Ayad, Giuseppe Cecere, Andrew Thomas, Guillaume Lessene, Amelia Vom. I would never be here without all of you, thank you!

List of abbreviations

°C	Celsius degree
μ	micro
1,2-DCE	1,2-Dichloroethane
ACN	Acetonitrile
Ala	Alanyl
BB	Building Block
Bn	Benzyl
Boc	<i>tert</i> -butoxycarbonyl
CD	Circular Dichroism
COSY	Correlated Spectroscopy
DCM	Dichloromethane
DIPEA	DiIsoPropylEthylAmine (Hunig's base)
DMF	DiMethylFormamide
DMSO	Dimethyl Sulfoxide
eq.	equivalent
Gly	Glycyl
λ	Wavelength
Leu	Leucyl
MW	Molecular Weight
nm	nanometer
NMR	Nuclear Magnetic Resonance
NOE	Nuclear Overhauser Effect
OSu	O-Succinimidyl
Phe	Phenylalanyl
ppm	parts per million
Pro	Prolyl
PS	PolyStyrene
Res. n	Residue n
RMSD	Root Mean Square Deviation
ROESY	Rotating-frame Nuclear Overhauser effect Spectroscopy
RT	Room Temperature
TFA	Trifluoroacetic Acid
THF	Tetrahydrofuran
TLC	Thin Layer Chromatography
TOCSY	Total Correlation Spectroscopy
Val	Valyl
δ	chemical shift
Δδ	split of chemical shift (ppm)

Nomenclature

Amino-acids will be designated by their full names or their 3-letters codes without difference.

Urea residues will be indicated by the 3-letters codes of the amino acids from which they derive, followed by the letter “u” in superscript. The corresponding residue will be named Ala^u. Thiourea residues will be indicated by the 3-letters codes of the amino acids from which it derives, followed by the letter “s” in superscript. The corresponding residue will be named Ala^s.

Carbons from the principal chain will be indicated by greek letters as presented below:

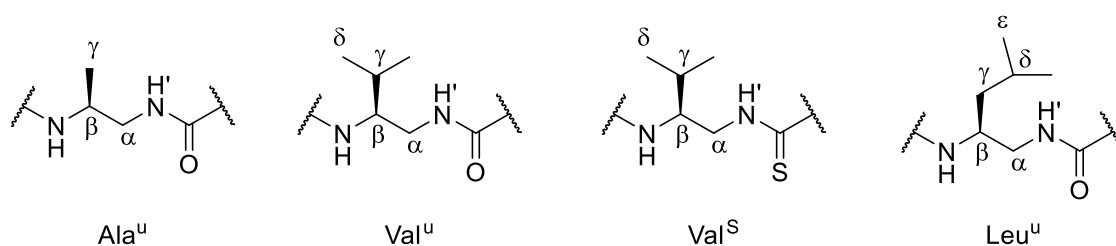


Figure 1: Example of notation of (thio)urea residues

To designate the sequences of synthesized oligoureas, the commonly used nomenclature was used. For instance, a trimer, which is protected with a *tert*-butoxy carbonyl group, synthesized from three residues which derive from valine, alanine and leucine will be noted **Boc-Val^u-Ala^u-Leu^u-NHMe**. The residues will be numbered as below:

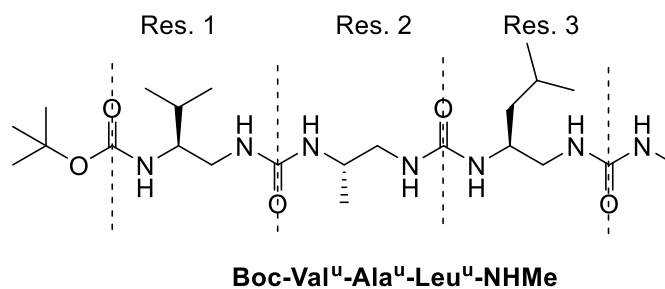


Figure 2: Notation of oligoureas and numbering of residues

Synthesized compounds will be numbered in their apparition order.

TABLE OF CONTENTS

<u>CHAPTER I</u>	2
1.1 TAKING INSPIRATION FROM NATURE TO DEVELOP USEFUL SYNTHETIC TOOLS	6
1.1.1 At the origin of chirality	6
1.1.2 From sophisticated catalysts to simpler bioinspired catalysts	10
1.1.2.1 <i>Natural catalysts for synthetic reactions</i>	10
1.1.2.2 <i>Organometallic small molecules as first simpler synthetic asymmetric catalysts</i>	12
1.1.2.3 <i>Simple designed organic catalysts</i>	16
1.2 FROM (THIO)UREA IN H-BONDS ORGANOCATALYSIS TO FOLDED ORGANOCATALYSTS	23
1.2.1 Importance of urea and thiourea in organocatalysis	23
1.2.2 Multicatalytic systems	24
1.3 MICHAEL ADDITION, A CLASSICAL AND ESSENTIAL WAY TO FORM CARBON-CARBON BOND	28
1.3.1 Asymmetric Michael addition, a common example of organocatalyzed reaction by H-bond	28
1.3.2 Industrial applications of Michael addition	32
1.4 FOLDED SYSTEMS IN ASYMMETRIC CATALYSIS AND ORGANOCATALYSIS	35
1.4.1 Chiral transfer from biomolecules to small molecules	35
1.4.2 Synthetic peptidic catalysts	36
1.4.3 Abiotic bioinspired catalysts	40
1.4.3.1 <i>Mimicking the pocket binding</i>	40
1.4.3.2 <i>Helical abiotic catalysts</i>	41
1.4.3.3 <i>Switchable helical catalysts</i>	44
1.4.3.4 <i>Helical polymer catalysts</i>	46
1.4.4 <i>Foldamers and organocatalysis</i>	48
1.5 OBJECTIVES	51
<u>CHAPTER II</u>	56
2.1 DESIGN OF A FOLDAMER-BASED CATALYTIC SYSTEM	60
2.1.1 Description of oligourea foldamers	60
2.1.2 How to take advantage of oligourea foldamer backbone to design an efficient catalyst?	61
2.1.3 Synthesis of a oligourea catalyst	63
2.1.3.1 <i>Synthesis of building blocks for oligourea synthesis</i>	63
2.1.3.2 <i>Synthesis of oligourea model catalyst 1a</i>	63
2.1.4 Evaluation of the catalytic potential of oligourea 1a	65
2.1.4.1 <i>Fundamental result through the development of a model reaction</i>	65
2.1.4.2 <i>Comparison with Takemoto catalyst</i>	65
2.1.4.3 <i>How to enhance the reactivity and enantioselectivity with the foldamer catalytic system?</i>	66
2.2 COMPARISON BETWEEN UREA VS THIOUREA IN THE MODEL SEQUENCE	68
2.2.1 Structural comparison between urea and thiourea versions of the catalyst	68
2.2.2 Difference of catalytic activity between urea and thiourea catalysts	69
2.3 IMPACT OF THE HELICAL CONFORMATION ON CATALYST EFFICACY	70
2.3.1 Strategy to demonstrate the role of the helicity on catalyst efficiency	70
2.3.2 Structural studies of the catalyst with different chain lengths	71
2.3.3 Catalytic evaluation of the oligoureas with different chain lengths	73
2.3.4 Screw sense inversion: Synthesis of <i>ent-1a</i>	75

2.4 INFLUENCE OF EXTERNAL PARAMETERS ON THE OUTCOME OF THE CATALYZED REACTION	77
2.4.1 Influence of the solvent	77
2.4.2 Impact of the temperature	78
2.5 POTENTIAL BENEFITS OF A SYNERGISTIC CATALYTIC SYSTEM	80
2.5.1 Looking for the minimum catalyst loading	80
2.5.2 Play on the base loading	81
2.5.3 Play on the nature of the base	82
2.5.4 Possibility of match/mismatch effect with chiral bases	83
<u>CHAPTER III</u>	88
3.1 PROBING THE ROLE OF TERMINAL UREAS IN THE CATALYTIC ACTIVITY OF OLIGOUREA FOLDAMERS⁹²	
3.1.1 Strategy and demonstration of the position of the catalytic sites	92
3.1.2 NMR structural study	95
3.1.3 Evaluation of the model reaction with the critical urea positions successively blocked	96
3.2 SUBSTRATES-CATALYST INTERACTIONS OBSERVED BY NMR	99
3.2.1 Preliminaries for NMR study	99
3.2.2 Evaluation of the interaction between the catalyst and nitrostyrene	100
3.2.3 Evaluation of the interaction between the catalyst and deprotonated malonate	102
3.2.4 Competition NMR experiments by successive addition of malonate, nitrostyrene and triethylamine to the catalyst	103
3.2.5 Proposition of mechanism for Michael addition catalysed by 1a	105
3.3 IMPACT OF THE NATURE OF THE FIRST RESIDUE	107
3.3.1 Sequence variations to study the role of the side chain of the first residue	107
3.3.2 Impact of the first residue variation on the catalytic efficiency	108
3.3.3 NMR conformational analysis of sequence modified catalysts and conclusions about possible structural requirements for high catalytic activity	108
3.4 KINETIC STUDIES AND VARIATION OF THE CATALYST ENANTIOMERIC EXCESS	111
3.4.1 Kinetic studies	111
3.4.1.1 Preliminary	111
3.4.1.2 Nitrostyrene order	112
3.4.1.3 Reaction order with respect to malonate, triethylamine and catalyst	113
3.4.2 Study of non-linear effects	115
3.4.2.1 Variation of foldamer catalyst enantiomeric excess	115
3.4.2.2 Impact of the catalyst enantioenrichment on the stereocontrol of the reaction	116
<u>CHAPTER IV</u>	122
4.1 VARIATION OF PRONUCLEOPHILES IN THE MICHAEL ADDITION TO NITROALKENES	126
4.1.1 Evaluation of malonates with ester functions of increasing size	126
4.1.2 Variation around the pronucleophile	127
4.2 VARIATIONS OF ELECTROPHILES IN THE MICHAEL ADDITION OF DIMETHYL MALONATE	129
4.2.1 Variation around aromatic nitroalkenes	129
4.2.2 Aromatic conjugated nitroalkenes	131
4.2.3 Scope aliphatic hindered and linear nitroalkenes	131

4.2.4 Towards a diastereoselective version of the Michael addition	133
4.2.4.1 Addition of deprotonated malonate monoamide 24 on nitrostyrene 1a	133
4.2.4.2 Asymmetric addition of deprotonated ketoester on nitrostyrene 1a	134
4.3 CASCADE MICHAEL ADDITION REACTIONS	135
4.3.1 Cascade Michael addition as a way to access to cyclic ketone with four stereocenters	135
4.3.2 Asymmetric Cascade Michael reaction with oligourea catalyst	136
4.4 JULIÁ-COLONNA EPOXIDATION	138
4.4.1 Comparison between literature catalysts and oligourea foldamers	138
4.3.2 Screening external parameters for asymmetric Juliá-Colonna epoxidation	139
4.3.3 Simple modifications of the hexameric foldamer catalyst for asymmetric Juliá-Colonna epoxidation	141
4.3.4 Synthesis of new substrate with double potential anchoring spots to catalyst	143
4.2 HENRY REACTION	144
<u>CHAPTER V</u>	148
5.1 STRATEGY FOR GRAFTING THE CATALYST ON SOLID PHASE	151
5.2 PRELIMINARY STUDY TO TRANSPOSE THE REACTION FROM A HOMOGENEOUS CATALYTIC SYSTEM TO A HETEROGENEOUS CATALYTIC SYSTEM	153
5.3 OPTIMIZATION OF REACTION PARAMETERS	155
5.3.1 Impact of external parameters on the catalytic activity of 35	155
5.3.2 Impact of the resin loading	156
5.3.3 Fine tuning of experimental conditions with Hunig's base	158
5.4 INTRODUCTION OF A CARBON CHAIN SPACER BETWEEN THE FOLDAMER AND THE RESIN MATRIX	159
5.5 POSSIBILITY TO RECYCLE OF THE CATALYST	162
<u>CHAPITRE VI</u>	166
<u>CHAPTER VII: SUPPORTING INFORMATION</u>	174
7.1 MATERIALS AND GENERAL TECHNIQUES	180
7.2 SYNTHESIS OF BUILDING BLOCKS	182
7.3 SYNTHESIS OF CATALYSTS OF CHAPTER II	184
7.4 SYNTHESIS OF CATALYSTS FROM CHAPTER III	211
7.5 EXPERIMENTAL PART OF CHAPTER IV	231
7.6 EXPERIMENTAL PART OF CHAPTER V	285

CHAPTER I

CHAPTER I: INTRODUCTION

1.1 TAKING INSPIRATION FROM NATURE TO DEVELOP USEFUL SYNTHETIC TOOLS.....	6
1.1.1 At the origin of chirality	6
1.1.2 From sophisticated catalysts to simpler bioinspired catalysts.....	10
1.1.2.1 <i>Natural catalysts for synthetic reactions</i>	10
1.1.2.2 <i>Organometallic small molecules as first simpler synthetic asymmetric catalysts</i>	12
1.1.2.3 <i>Simple designed organic catalysts</i>	16
1.2 FROM (THIO)UREA IN H-BONDS ORGANOCATALYSIS TO FOLDED ORGANOCATALYSTS.....	23
1.2.1 Importance of urea and thiourea in organocatalysis	23
1.2.2 Multicatalytic systems	24
1.3 MICHAEL ADDITION, A CLASSICAL AND ESSENTIAL WAY TO FORM CARBON-CARBON BOND.....	28
1.3.1 Asymmetric Michael addition, a common example of organocatalyzed reaction by H-bond .	28
1.3.2 Industrial applications of Michael addition.....	32
1.4 FOLDED SYSTEMS IN ASYMMETRIC CATALYSIS AND ORGANOCATALYSIS.....	35
1.4.1 Chiral transfer from biomolecules to small molecules	35
1.4.2 Synthetic peptidic catalysts.....	36
1.4.3 Abiotic bioinspired catalysts	40
1.4.3.1 <i>Mimicking the pocket binding</i>	40
1.4.3.2 <i>Helical abiotic catalysts</i>	42
1.4.3.3 <i>Switchable helical catalysts</i>	44
1.4.3.4 <i>Helical polymer catalysts</i>	46
1.4.4 Foldamers and organocatalysis	48
1.5 OBJECTIVES	51

1.1 TAKING INSPIRATION FROM NATURE TO DEVELOP USEFUL SYNTHETIC TOOLS

1.1.1 At the origin of chirality

A left-coiling garden snail has been recently discovered and constituted an important illustration for Angus Davison's research at the University of Nottingham.¹ Whereas all common snails have their shells wound in the right direction (dextral), the extremely rare senestra snail, named Jeremy, is a million exception. Its spirals, but also all its organs are reversed, including its sexual organs, prohibiting any procreation with common dextral snails. The Internet and Twitter community were moved by its situation and tried to find other senestra snails to make a love story possible for Jeremy. Way beyond diverting large audience interest, Angus Davison studied the inherent chirality of snails to improve knowledge about chirality in the human body. It could provide valuable information to help people who were born with organs in wrong orientation. Through funny situations with snails, he demonstrated the importance of chirality for the genome and how far chirality is essential.



Figure I.1: Jeremy the snail, when chirality in snails can help to answer to genetic questions

The macroscopic chirality observable in the snail shell is encoded in its DNA. Through transcription with RNA polymerase and translation with the ribosome, genetic material contained in DNA is translated to proteins constituting living organisms on earth.² Remarkably, all the proteins at the origin of natural living beings are constituted only of (L)-amino acids. This complete stereocontrol on the synthesis of proteins from only (L)-amino acids is due to the selectivity of enzymes translating mRNA into proteins for (L)-amino acids. Nevertheless, the origin of chirality of amino acids is still an enigma for chemists working on the origin of life and the prebiotic formation of polypeptides.³⁻⁴

The main concern for many chemists in all the fields of chemistry is thus to control the chirality of synthetic molecules to access molecules with specific biological or physical properties, which is the biggest challenge of pharmaceutical industry or perfumes industry. For example, the smells of orange and lemon come from two enantiomers of limonene, as well as cumin and mint which are enantiomers of carvone (Figure I.2).

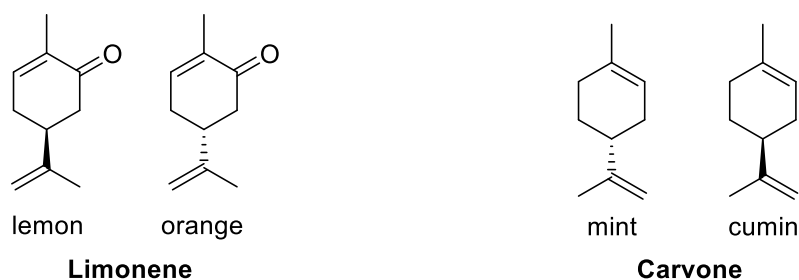


Figure I.2: Different olfactive properties among the enantiomers of Carvone and Limonene

In 1992, the Food and Drug Administration published guidelines in order to produce enantiopure drugs and stimulate the synthesis of enantioenriched compound instead of separation of racemic mixtures. In 2000, the worldwide sales of enantiopure compounds represented 123 billion dollars.⁵ Asymmetric catalysis appeared to be essential because of its numerous advantages: high selectivity, high rate, atom economy, cost efficiency. William Knowles, Ryoji Noyori and Barry Sharpless were awarded the Nobel prize in Chemistry in 2001 for their pioneering work in catalysis. Noyori and Sharpless shared the Wolf prize of Chemistry in 2001 with Henri Kagan, another hero of asymmetric catalysis.

In 2016, the American journal Fortune reported blockbuster pharmaceutical drugs to watch for this year and most of them are chiral compounds (Figure I.3). Intercept Pharmaceuticals and Sumitomo Dainippon Pharm launched obeticholic acid to treat chronic liver diseases. Gilead Sciences and Japan Tobacco developed a treatment against HIV-1 infection with the combination of Emtricitabine and Tenofavir. Merck commercialized Grazoprevir for treating Hepatitis C virus.

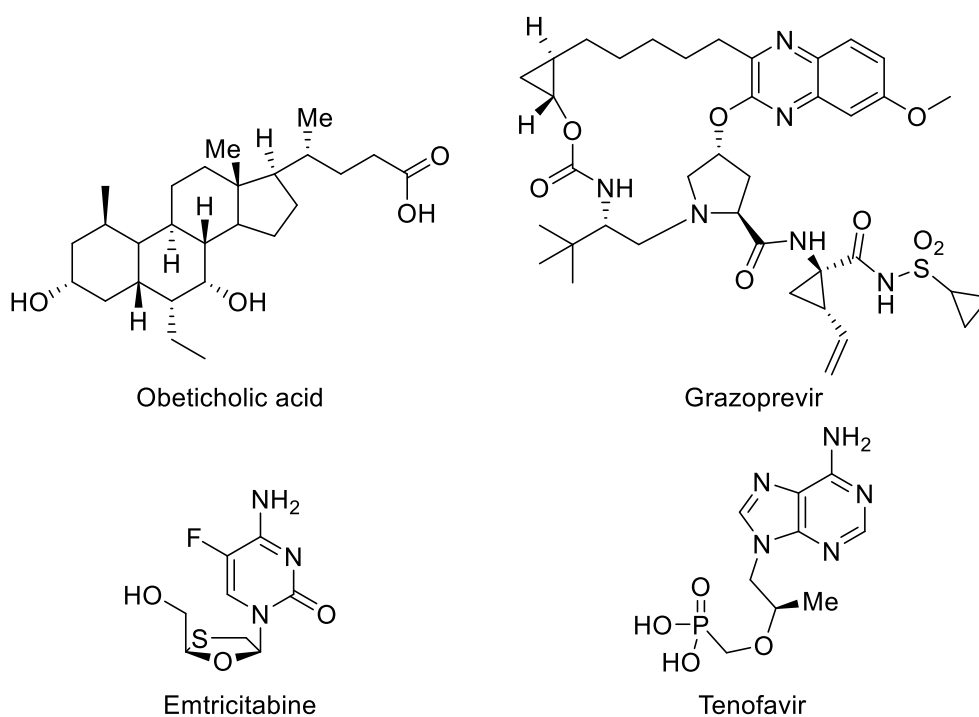


Figure I.3: Potential pharmaceutical blockbusters where chirality is observed

Enantioenrichment is created in nature by enzymes which are themselves inherently chiral. One of the paradigms of biochemistry is the link between protein three-dimensional folding and its catalytic activity. Enzymes increase the rate of chemical reactions by lowering the free energy barrier that separates reactants and products. Serine proteases are a very common and well-studied class of enzymes which cleave peptide bonds by increasing the rate of peptide bond hydrolysis by $\sim 10^{10}$ compared to the uncatalyzed reaction. They are present in almost all living organisms and they are involved in many biological processes such as immune response, digestion or reproduction. Chymotrypsin is a digestion serine protease which cleaves proteins after aromatic or hydrophobic amino acids, such as phenylalanine or tyrosine or tryptophan by accelerating the process (Figure I.4).⁶

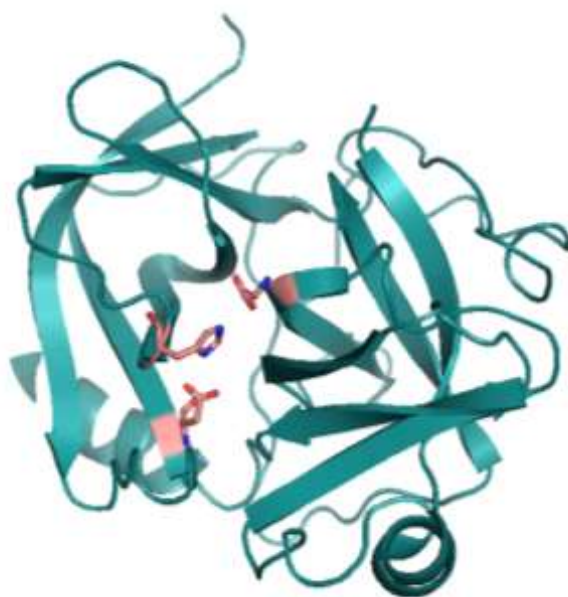
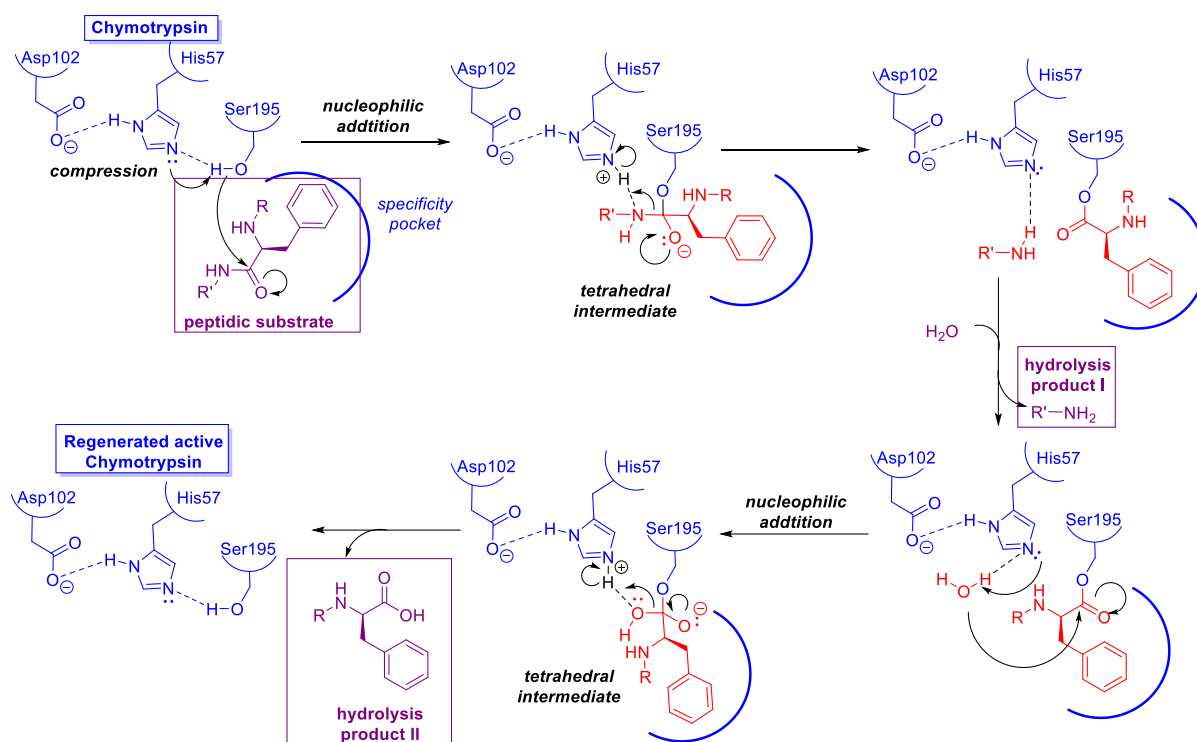


Figure I.4: X-ray structure of Chymotrypsin (PDB: 1CHG)

The mechanism involves a catalytic triad composed of Serine 195, Histidine 57 and Aspartic acid 102 (Scheme I.1) and the transient formation of a catalyst-substrate covalent bond. The serine is first activated by a general acid-base catalysis process involving Asp102 and His57. Nucleophilic addition of the activated Serine results in the formation of a tetrahedral intermediate which is unstable because of the negatively charged oxygen. It rearranges to an O-acyl-enzyme intermediate with concomitant release of the amine part of the substrate peptide. The final step is an attack by water on the ester bond of the O-acyl enzyme. The instability of the second tetrahedral intermediate drives the formation of the carboxylic acid product and the release of the free active enzyme. Preorganization of the triad, electrostatic interactions and the nature of the backbone form a dynamic system which is responsible for the catalytic activity of Chymotrypsin.



Scheme 1.1: Mechanism of peptide bond hydrolysis by Chymotrypsin, serine protease

Chemists have been inspired by enzymes trying to design catalysts that would mimic their modes of action. In addition to appropriate folding of the backbone, which leads to optimal preorganization of catalytic side chains in the three-dimensional space and which enhances the binding between substrates and the enzyme, additional elements such as cofactors (metals, co-substrates) play a critical role in the catalytic activity of a protein. Based on these considerations, several approaches have been envisioned to perform biomimetic catalysis : (i) the engineering and directed evolution of natural enzymes and their use in an artificial environment, (ii) the synthesis of minimalist enzymatic sites with metal cofactors, (iii) the design of small organic molecules with artificial substrate binding pockets.

1.1.2 From sophisticated catalysts to simpler bioinspired catalysts

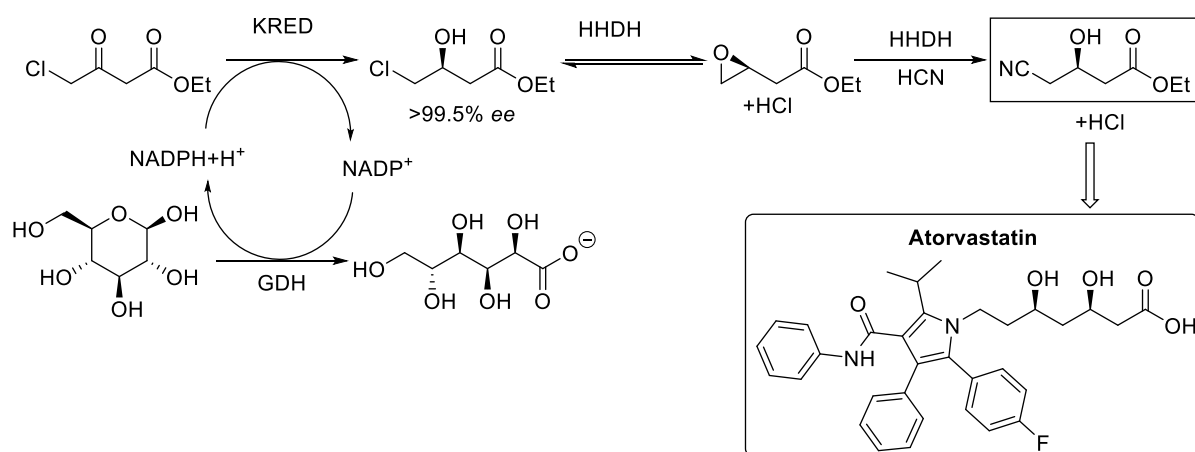
1.1.2.1 Natural catalysts for synthetic reactions

Enzymes are the most efficient stereoselective, regioselective and chemoselective catalysts made by nature. They are compatible with all the principles of green chemistry established by R. Sheldon (Table I.1). A large fraction of enzymes does not need metals, and reactions are often performed under mild conditions, they usually provide high conversion rates and are highly specific, no special equipment is required, and the resulting product is usually obtained with high yield and stereocontrol.

Table I.1: Biocatalysis concurring with the 12 principles of Green Chemistry by R. Sheldon⁷

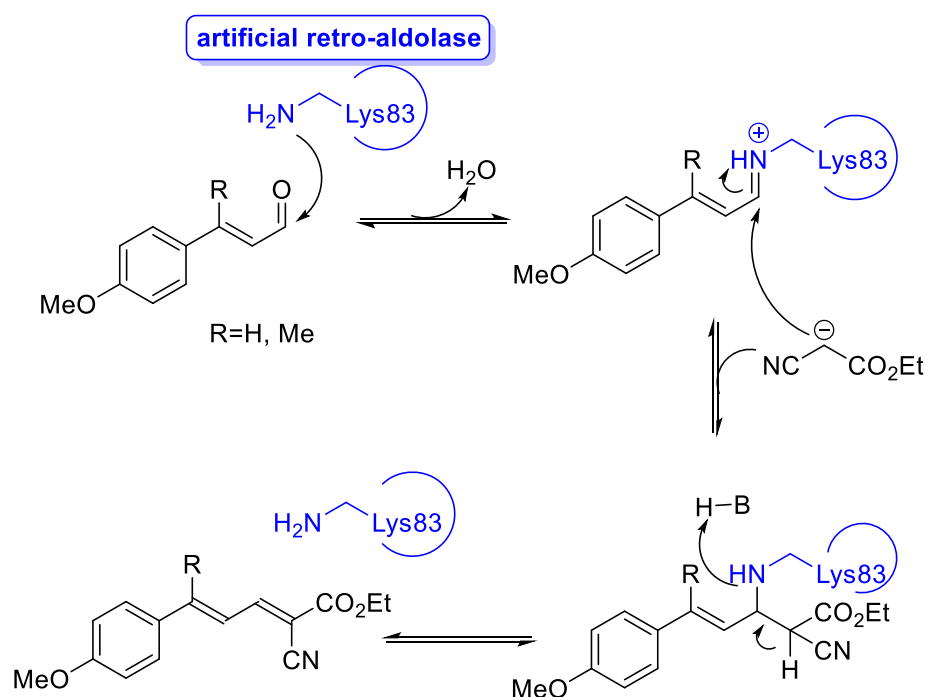
	Green Chemistry Principle	Biocatalysis
1	Waste prevention	Significantly reduced waste
2	Atom economy	More atom and step economic
3	Less hazardous syntheses	Generally low toxicity
4	Design for safer products	Not relevant
5	Safer solvents and auxiliaries	Usually performed in water
6	Energy efficient	Mild conditions
7	Renewable feedstocks	Enzymes are renewable
8	Step economy	No protection / deprotection
9	Catalysis	Enzymes are catalysts
10	Design for Degradation	Enzymes are biodegradable
11	Analytical Methodologies	Applicable to biocatalysis
12	Inherently safer processes	Mild and safe conditions

Protein engineering and computational modelling as well as directed evolution are particularly powerful and useful methods for designing artificial enzymes which can be successful in biocatalysis. The company Codexis[®] developed a process to produce an intermediate of atorvastatin (Lipitor[®], a cholesterol lowering drug), in three steps by the use of an evolved bacterial halohydrin dehalogenase HHDH, and a ketoreductase KRED used with NADP (Nicotinamide Adenine Dinucleotide Phosphate) and glucose as cofactors of oxidation (Scheme I.2). It received the Presidential Green Chemistry Challenge Award in 2006 for developing this process.⁸



Scheme I.2: 3-steps biocatalysed procedure to synthesize building block for Atorvastatin production

Directed evolution of natural enzymes can drive to unprecedented catalytic activities with wide scope as synthetic catalysts, and with high efficiency as natural enzymes. Hilvert *et al.* created an artificial retro-aldolase which is able to cleave the aldol bond of methodol through covalent amine catalysis with lysine⁹, to perform Michael reactions with unsaturated ketones and iminium activation.⁹ A more unprecedented result is the ability of the designed retro-aldolase to perform Knoevenagel condensations with poorly reactive substrates (Scheme I.3) through iminium activation again.¹⁰



Scheme I.3: Knoevenagel Condensation with artificial retro-aldolase designed by Hilvert group¹⁰

Association of natural or artificial enzymes with transition metals allows the combination of the high reactivity and efficiency of enzymes with the broader range of substrates allowed by organometallic catalysis. Artificial metalloenzymes, i.e. the combination of an (un)natural enzyme with an organometallic species, were born from this idea. Hartwig *et al.* created a metalloenzyme by complexing a metal inside an enzymatic pocket. The resulting catalytic activity resides in both the

primary coordination sphere of the metal and the protein folded environment. Hartwig *et al.* replaced iron-protoporphyrin by iridium porphyrin into the P450 enzyme CYP 119 to catalyse insertion of carbenes into C-H bonds with excellent results, 98% *ee* and 35 000 turnovers. The wild type structure of CYP 119 is shown in Figure I.5 with residues targeted to evolve the protein scaffold and increase catalytic activity.¹¹

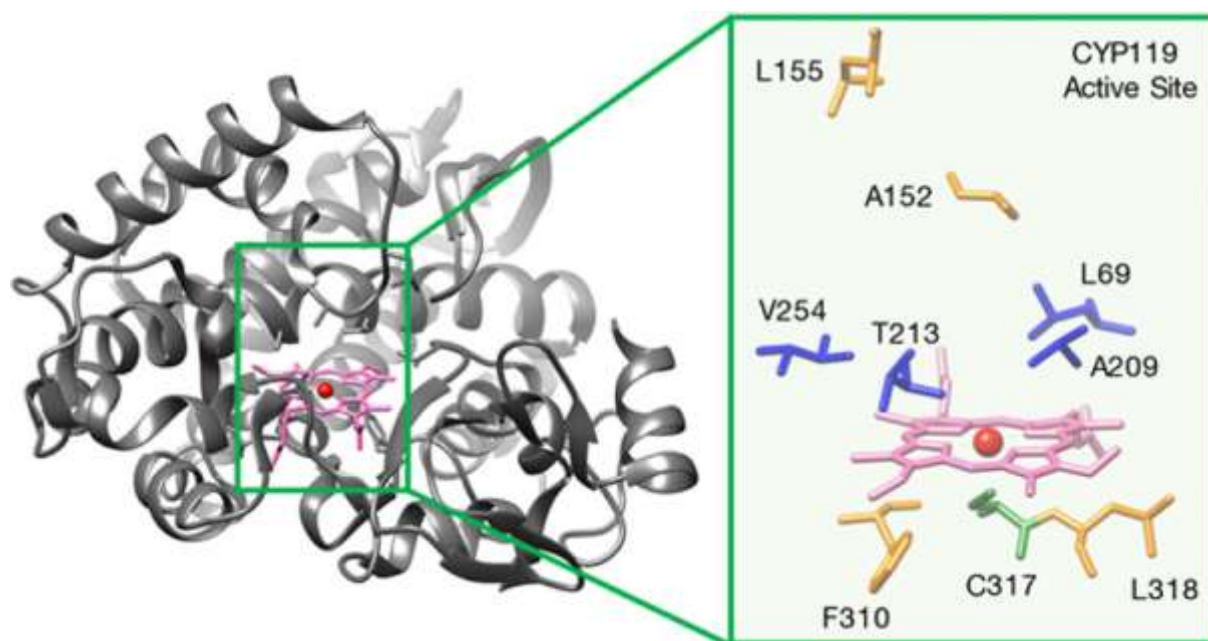


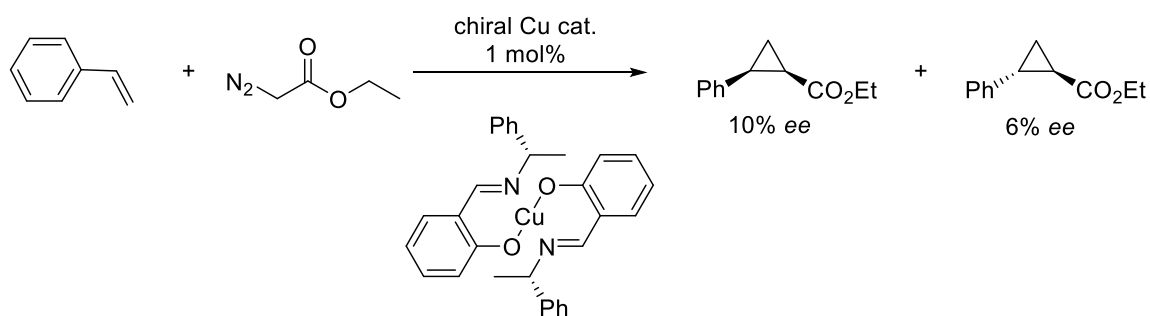
Figure I.5: Highlighted active sites of wild type Fe-CYP119 which have been mutated for increasing catalytic activity of the catalytic system- PDB 11O7¹¹

However, biocatalysis presents a fundamental disadvantage: because of its high specificity, the catalyst has to be adapted for each reaction.⁷ Natural enzymes are less often compatible with commercial processes because of the high substrate specificity. Moreover, directed evolution is not an easy process to perform to access to these new enzymatic abiotic catalysts because of its necessity to work on high-throughput study. The stability of enzymes and the difficulty to immobilize them on solid phase to reuse it may also represent limitations to common use of biocatalysis.¹²

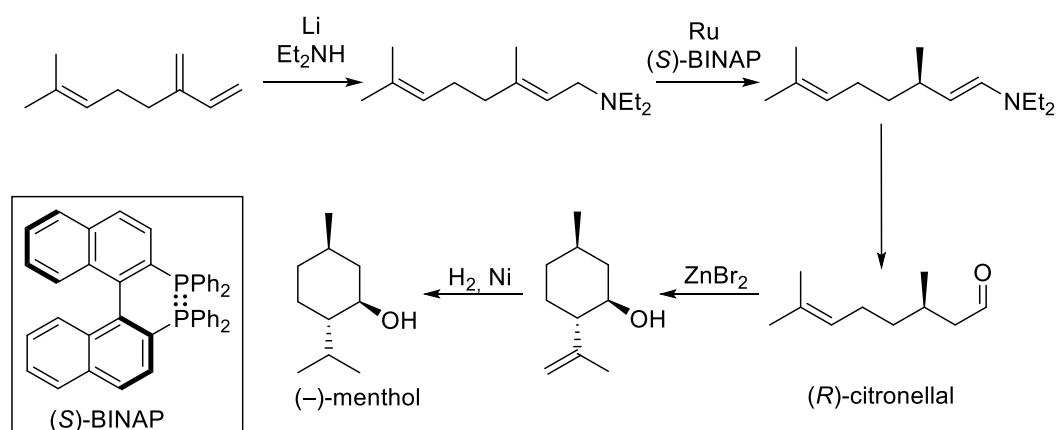
1.1.2.2 Organometallic small molecules as first simpler synthetic asymmetric catalysts

The first commonly used way that chemists found to enantioenrich chemical mixture with a catalytic amount of chiral molecule was the addition of metals. In 1966, Nozaki *et al.* discovered the first induction of chirality with association of chiral Schiff-base complexed with Cu^{II} (Scheme I.4). Noyori developed asymmetric catalysis with elaboration of a new chiral biphosphine ligand BINAP, associated with ruthenium.¹³ It led to asymmetric hydrogenation, at the origin of Takagaso process for

industrial production of (–)-menthol (Scheme I.5), as well as morphine and benzomorphan derivatives, antibiotic levofloxacin, anti 1,3-diols, antidepressant duloxetine, antihistaminic neobenodine.⁵

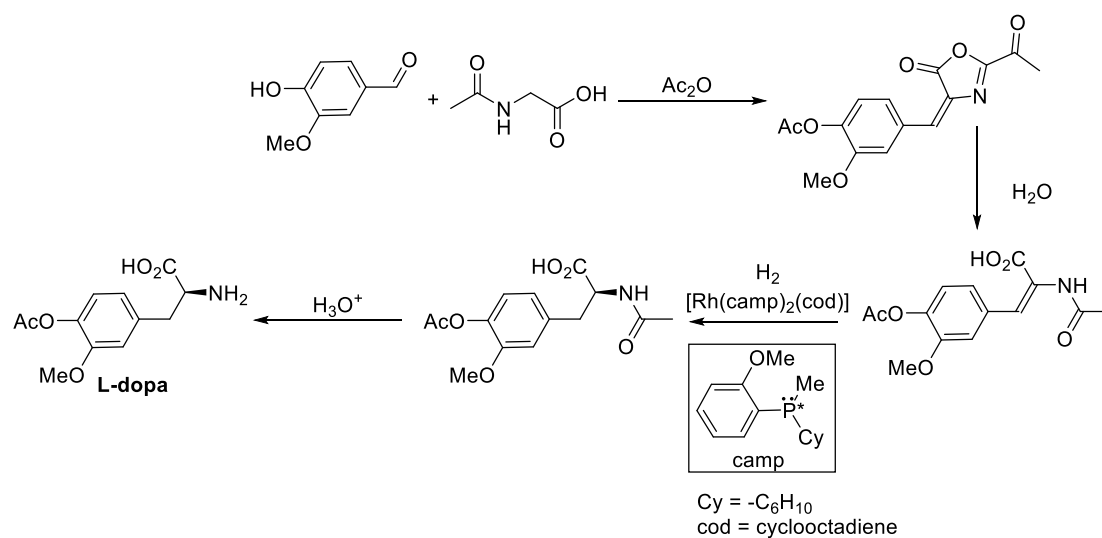


Scheme I.4: Discovery of chirality induction with a chiral organometallic molecule catalyst¹³

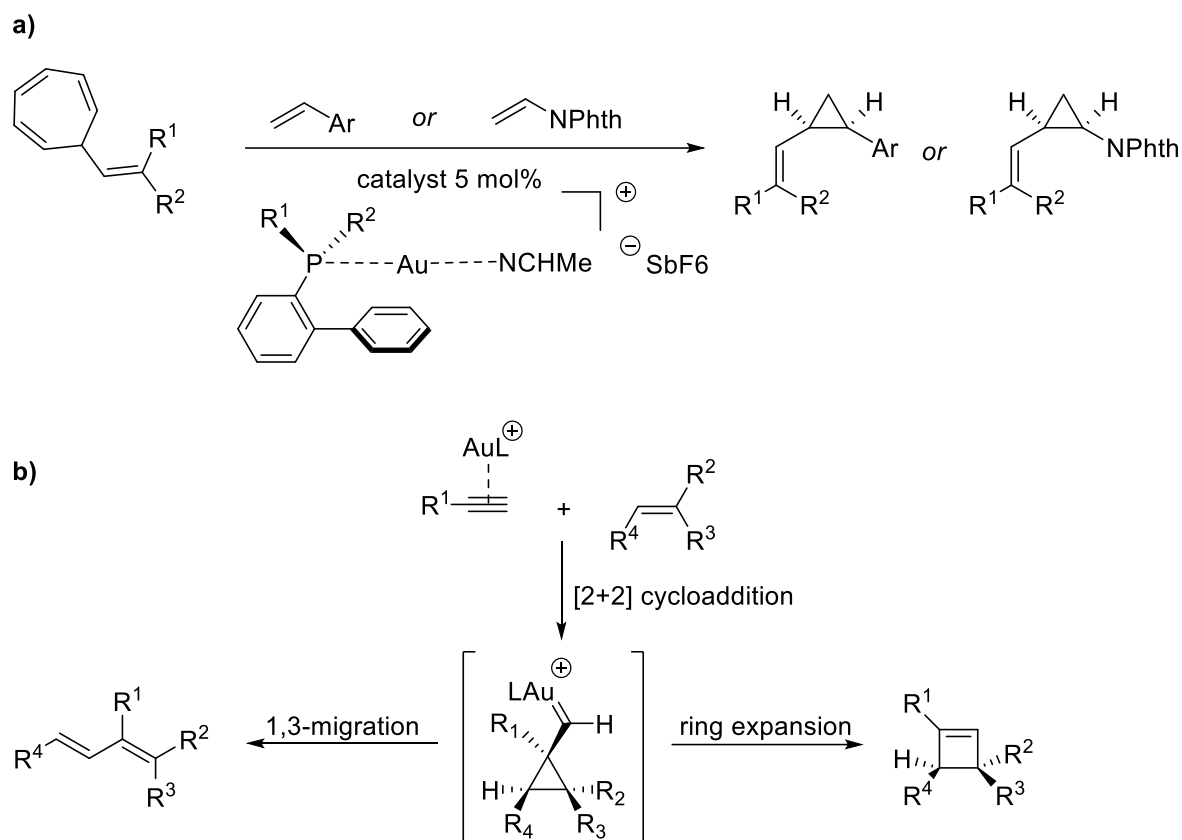


Scheme I.5: Synthesis of (–)-menthol, Takasago process⁵

Knowles and Kagan also worked on asymmetric hydrogenation, with the complexation of chiral ligands with rhodium. This work and the use of the phosphine ligand named camp was applied to a process initially commercialized by Monsanto for the production of L-DOPA a treatment for Parkinsons disease (Scheme I.6). Shortly after the first commercialization, Kagan elaborated the biphosphine ligand (R, R)-DIOP and reached 83% ee in L-DOPA synthesis, then Knowles reported the synthesis of another diphosphine ligand: (R, R)-DIPAMP, pushing to 95% ee (Scheme I.7).¹⁴

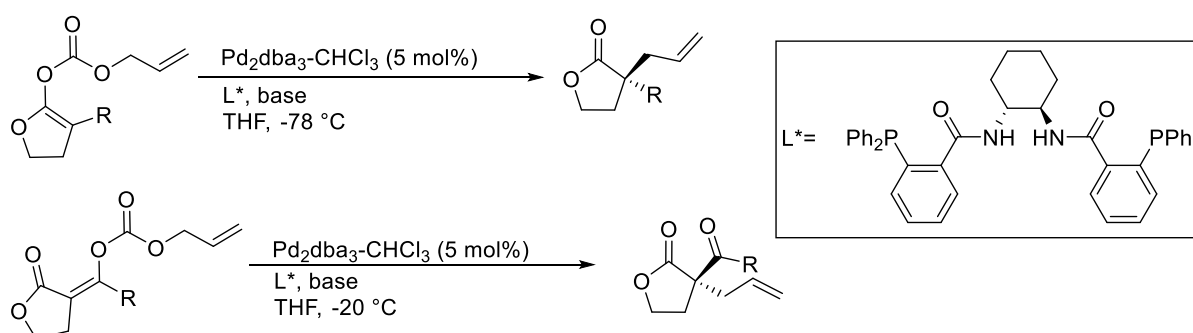


Scheme I.6: Monsanto L-dopa process¹⁴



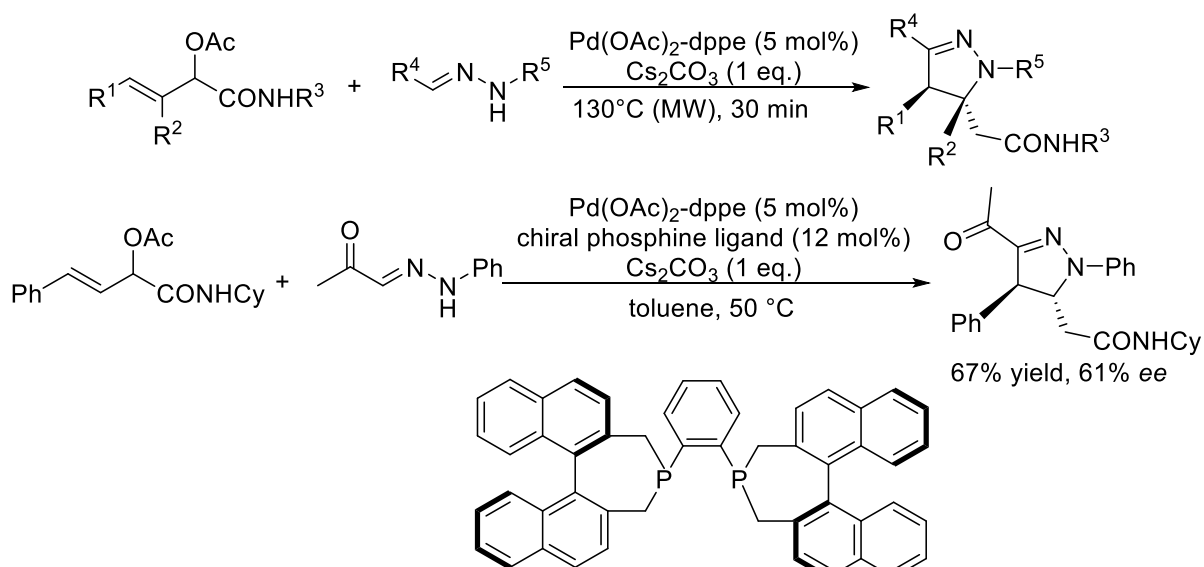
Scheme I.9: Gold catalysis developed by Echavarren group¹⁶⁻¹⁷

Palladium-catalysis has been recently developed to propose through allylic alkylation approach, a mild and efficient way to access to α -quaternary γ -butyrolactones from cyclic enol carbonates, which is a very rich chemical core for medicinal chemistry and access to precursors of natural products (Scheme I.10).¹⁸ The reaction was also very effective with α -acyl-enol carbonates despite their lower reactivity. This new method has been illustrated to synthesise enantioenriched spiroactones with high yield and high enantioselectivity.



Scheme I.10: Palladium-catalyzed asymmetric allylic alkylation¹⁸

The classical palladium-catalysed Tsuji-Trost coupling has been evaluated as a way to access to pyrazolines, very versatile chemical intermediates. Hydrazones have been C-allylated with Passerini adducts to form pyrazolones with tetrasubstituted center. A synergistic use with chiral phosphine ligands with amide led to medium yields and stereocontrols (Scheme I.11).¹⁹

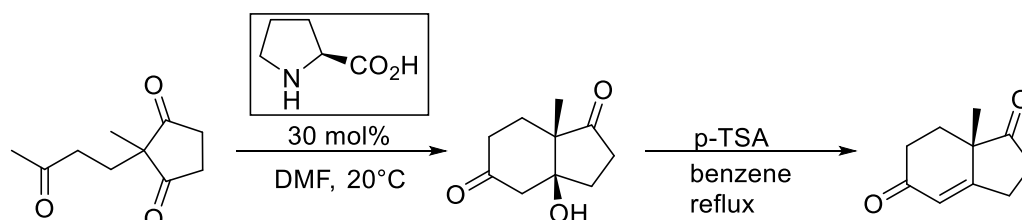


Scheme 1.11: Tsuji-Trost type C-allylation of hydrazones¹⁹

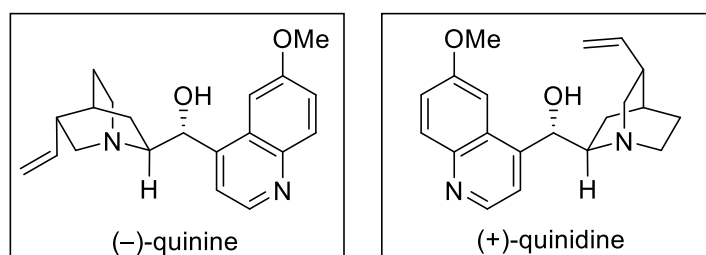
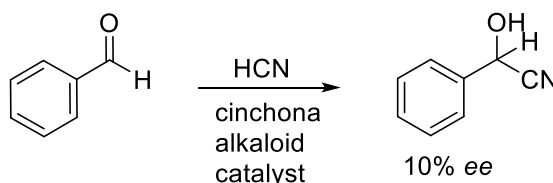
The scope of reactions of metal catalysed-reactions is very large and yields and stereocontrols are often very good. Nevertheless, metals are often toxic, expensive and not environmentally friendly and their use increases the risk of product contamination. Organometallic catalysts are hardly graftable on a solid support, then the purifying steps and recyclability are not so convenient. Since nature is also able to catalyse difficult reactions without metals, chemists have tried to create artificial catalysts without metal. Because many metals in organometallic catalysis are used as Lewis acids, they could in principle be replaced by organic molecules acting in the same way. The challenge is then to design well-defined organic catalysts which can address contemporary problems in asymmetric catalysis such as high reactivity at low catalyst loading, high enantiocontrol in difficult reactions such as the enantioselective synthesis of quaternary stereocenters, as well as site-selectivity and chemoselectivity.

1.1.2.3 Simple designed organic catalysts

Organocatalysts are easier to synthesise, often inexpensive, more stable to air oxidation, and generally more robust than their organometallic counterparts. The very first organocatalyst was discovered accidentally in 1860 by Liebig: acetaldehyde catalysed the hydrolysis of dicyan. It led to Degussa patent for production of oxamide, used to replace urea in fertilizers.²⁰ Before synthesizing new organic catalysts, other chiral natural molecules were used in asymmetric catalysis reactions. Cinchona alkaloids and proline derivatives are at the origin of many classes of asymmetric reactions. Hajos and Parrish from Hoffman-LaRoche and Eder, Sauer and Wiechert from Schering showed the catalytic efficiency of proline for the formation of bicyclic diketone compounds, which allows the access to steroids. (Scheme I.12).²¹ Bredig performed a first enantioenriched synthesis of cyanohydrin with quinine or quinidine, but at the very beginning of the organocatalysis development, he observed a poor enantiomeric excess of 10% *ee* (Scheme I.13).²²



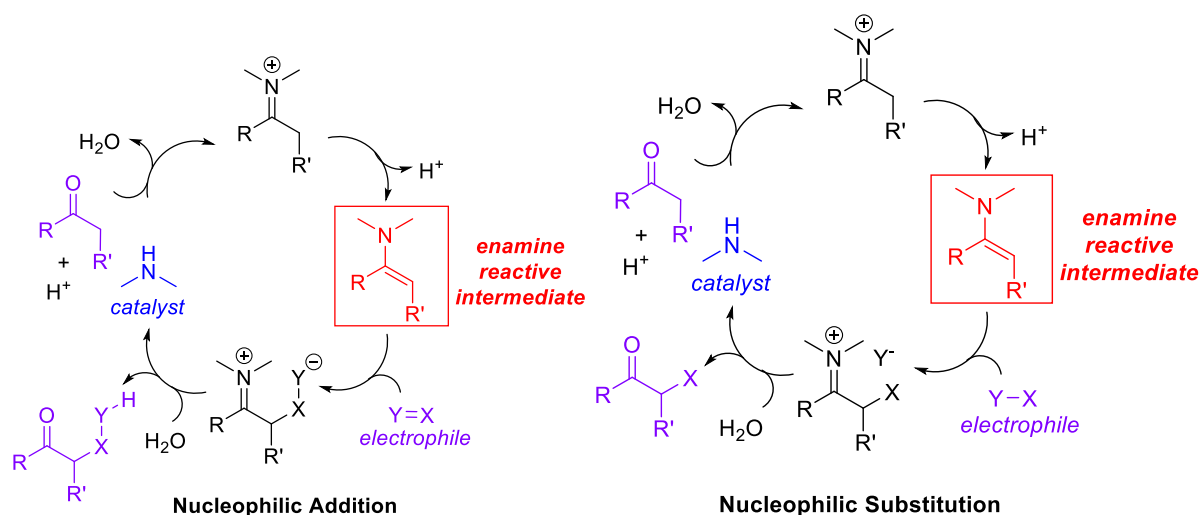
Scheme I.12: Hajos-Parish-Eder-Sauer-Wiechert reaction, with proline catalysis²¹



Scheme I.13: Cyanohydrin synthesis by cinchona catalysis²²

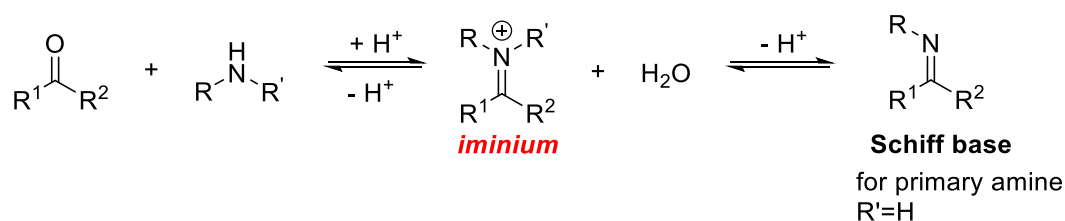
To design efficient fully organic catalysts, chemists have observed in depth the recognition processes at work in nature and the structures at atomic resolution of complexes between enzymes and inhibitors. The spatial and relative rearrangement of key recognition motifs in the catalyst are essential features to improve its capacity to specifically recognize substrates. Several classifications of organocatalysts have been described all along the history of organocatalysis. Dalko & Moisan have classified organocatalysts in four categories according to their main mechanism. The first one encompasses catalytic processes based on the nucleophilic and electrophilic properties of the catalyst whereby the chiral catalyst is not forming covalent bond with the substrate. Next categories include those catalysts which lead to reactive intermediates and are consumed in the reaction and requires regeneration, those which react by phase-transfer process and form host-guest complex, and those which present a molecular cavity and interact with the substrates in a shape and size dependent manner.²³ The most common types of organocatalysis will be described in the next paragraphs.

Enamine catalysis designates electrophilic substitutions α to carbonyl compounds, catalysed by amines which leads to useful and reactive enamine intermediates (Scheme I.14). Stork's work is the basement of enamine catalysis with a stoichiometric approach: addition of secondary amine to a carbonyl compound forms an enamine intermediate on which can react an electrophile to perform a nucleophilic addition or a nucleophilic substitution. The resulting iminium is then hydrolysed to access to the carbonyl products. The catalytic version of both mechanisms has been investigated and is depicted in Scheme I.14.²⁴



Scheme I.14: Mechanism of enamine catalysis process

Iminium catalysis was born with Schiff's work and starts with the addition of an amine on a carbonyl compound, similarly to the first step of the mechanism of enamine catalysis (Scheme I.15). The difference comes from the second substrate which reacts with the iminium intermediate instead of the deprotonated iminium. Following condensations developed by Knoevenagel as first iminium-catalysed reactions. Later, asymmetric version of iminium catalysis has been developed by Yamaguchi (L-Proline catalyst) and MacMillan (imidazolidinone catalysts), Jørgensen (diarylprolineesters) and many others for a large range of reactions including conjugate additions, cycloadditions, epoxidation and hydrogenation of α,β -unsaturated aldehydes.²⁵



Scheme I.15: Formation of Schiff's bases

Jørgensen and Hayashi developed organocatalysts with diarylprolinol silyl ether reagents which were initially used for the asymmetric α -functionalization of aldehydes and then for bond-forming reactions as carbon-halogen or carbon-heteroatom (Figure I.6).^{26, 106} The scope of Jørgensen's catalysts were even more extended with domino conjugated nucleophilic addition-electrophilic amination,²⁷ asymmetric epoxidation,²⁸ and asymmetric hydrophosphinylation leading to valuable phosphine ligands for metal-catalyzed reactions.²⁹⁻³⁰

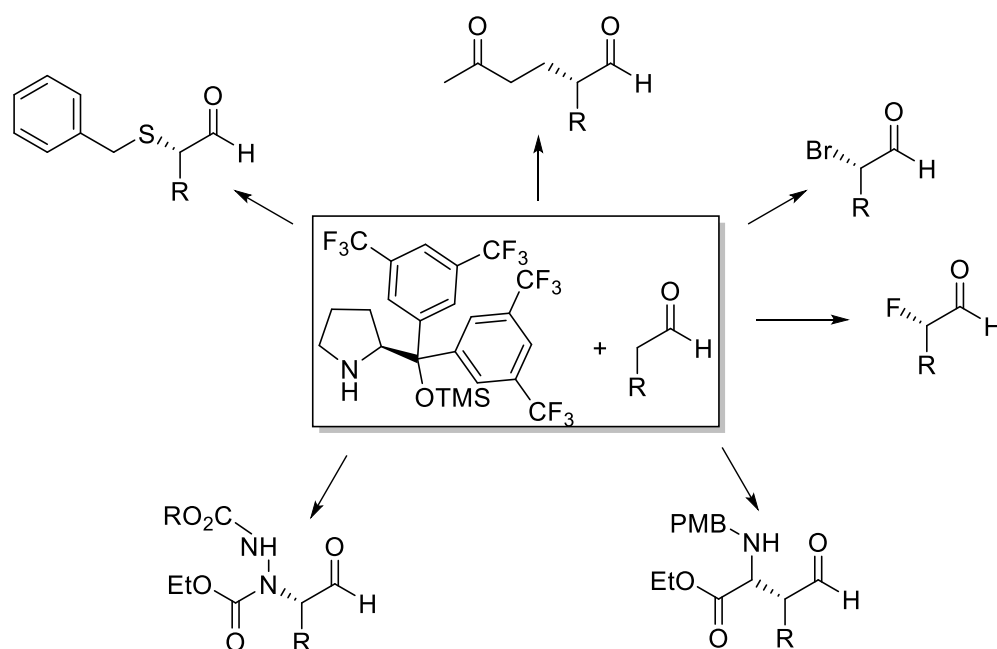


Figure I.6: α -functionalization of aldehydes with Jørgensen catalysts

Macmillan is another pioneer of recent organocatalyzed chemistry. His first advances were performed with Diels-Alder reaction through iminium activation with imidazolidinones.³¹ Asymmetric versions of Friedel-Crafts alkylation,³² α -chlorination,³³ α -fluorination,³⁴ intramolecular Michael addition³⁵ were elaborated with these organocatalysts (Figure I.7). Their high potential was illustrated through synthesis of indoles and synthesis of natural products.³²

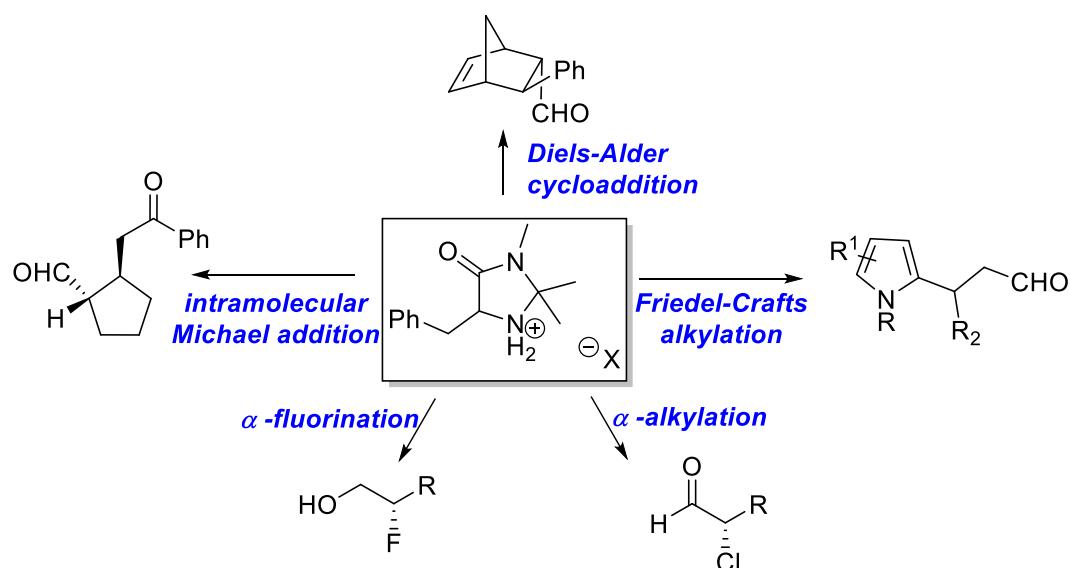
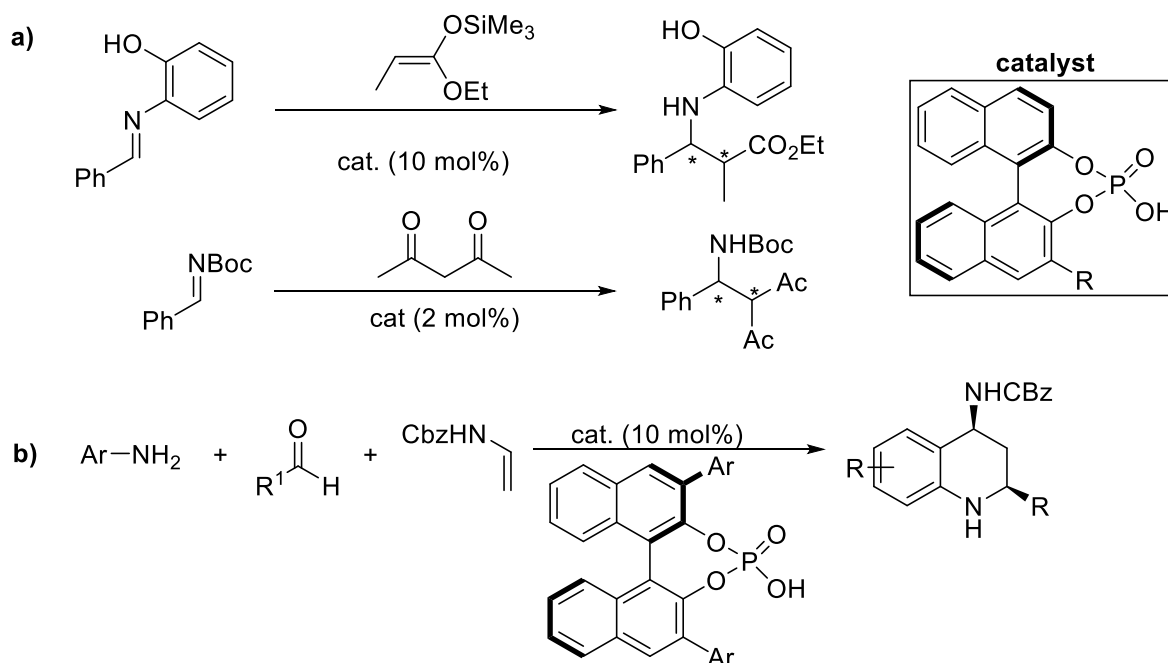


Figure I.7: Asymmetric reactions catalysed by Mac Millan imidazolidinones

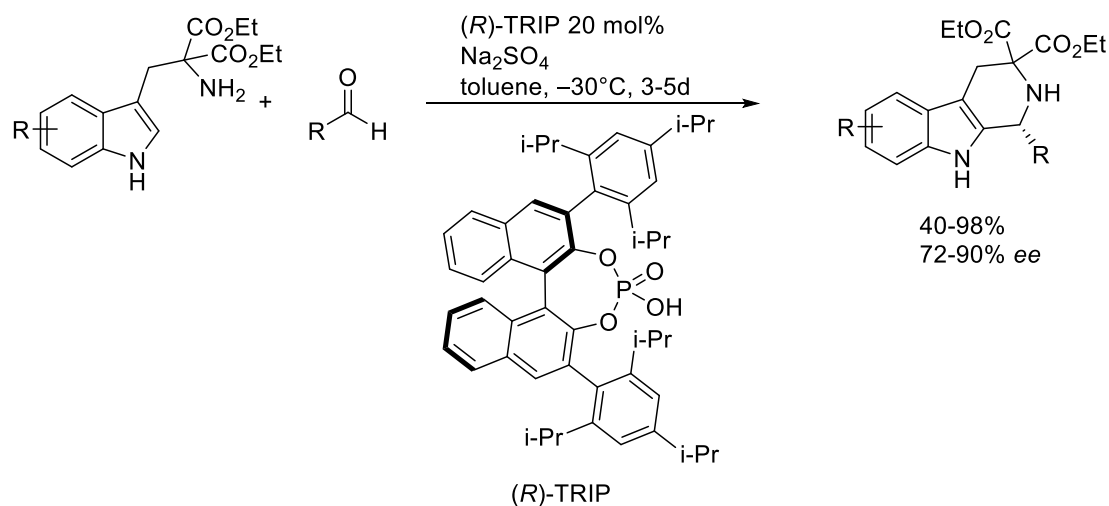
Akiyama and Terada were the first groups to demonstrate their use with relatively low catalyst loading, 2 mol%, with Mannich-type reactions (Scheme I.166a). Masson and Zhu developed a three-component reaction to perform a stereocontrolled Povarov reaction with phosphonic acids as organocatalysts, with relatively high loading (Scheme I.166b).³⁶ The scope of the

demonstrated concept was extended with aromatic and aliphatic aldehydes and anilines. It was illustrated in the total synthesis of Torcetrapib.

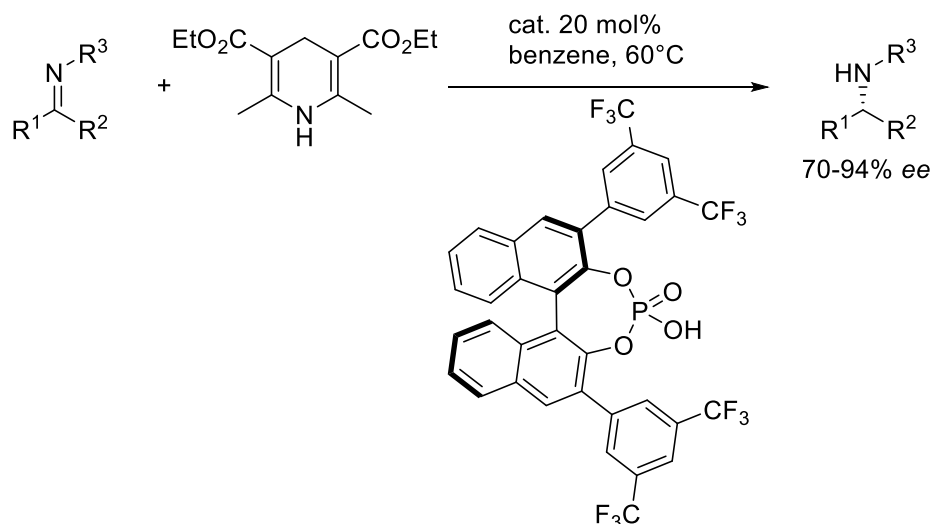


Scheme I.166: a) Phosphoric acid catalysts for Mannich-type reactions³⁷⁻³⁸ b) Three component Povarov reaction with phosphoric acid catalysts³⁶

For more than ten years, chiral phosphoric acids pioneered by Rueping, List and other proved to be a powerful class of organocatalysts. Through their oxide phosphine, there are Lewis base whereas the hydroxyl group is in parallel a Brønsted acid which can target particularly imines for asymmetric additions. List used the chiral phosphoric acid TRIP to catalyse Pictet-Spengler cyclization to form isoquinolines with good yields and very good enantiomeric excesses (Scheme I.17).³⁹ Rueping was the first to demonstrate the use of chiral phosphoric acid to reduce an imine with the use of Hantzsch ester as source of hydrogen (Scheme I.18).⁴⁰ The resulting adducts are protected amines with often a high synthetic utility in synthetic chemistry.

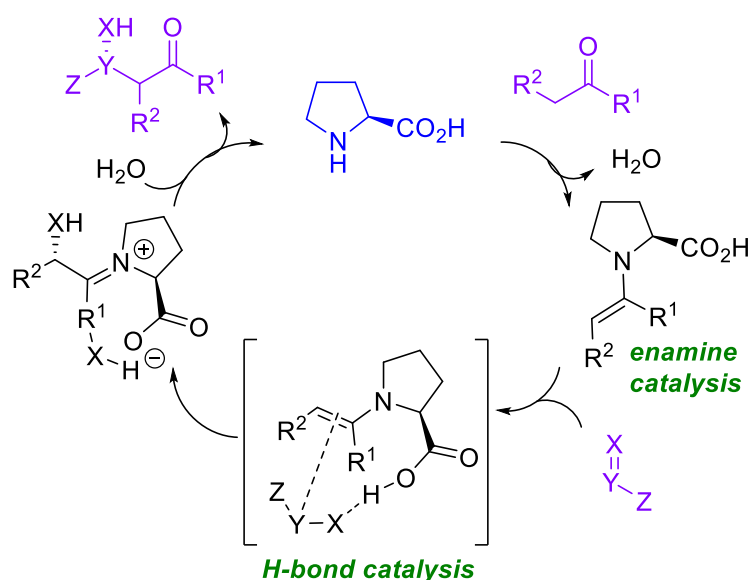


Scheme I.177: Pictet-Spengler cyclization with chiral phosphoric acid catalyst TRIP³⁶



Scheme I.188: Reduction of imine with phosphoric acid catalyst³⁷

Organocatalysts which interact by hydrogen-bonds with the substrates constitute another main activation mode in asymmetric catalysis. They catalyse a large range of carbon-carbon and carbon-heteroatom bond-forming reactions through association of functional and structural frameworks. Crystalline structures with both catalyst and substrates were the milestone of the proof of H-bond catalysis.⁴¹ Etter cocrystallized electron-deficient diaryl ureas with Lewis bases.⁴² Curran and Kuo showed the catalytic potential of urea derivatives.⁴³ Winberg was one of the first to demonstrate the interest of the free -OH groups next to the basic quinuclidine nitrogen in cinchona alkaloid to coordinate with carbonyl groups.⁴⁴ The Hajos-Parrish-Eder-Sauer-Wiechert reaction, previously cited, has been demonstrated to act by enamine catalysis, but the proline also interacts by H-bonding.⁴⁵ The formed H-bond donor is critical to orientate the electrophile relative to the pyrrolidine group and it allows to stabilize the transition state and lower the activation barrier to carbon-carbon bond formation (Scheme I.19).



Scheme I.19: Mechanism of proline-catalysed Hajos-Parrish-Eder-Sauer-Wiechert reaction²⁴

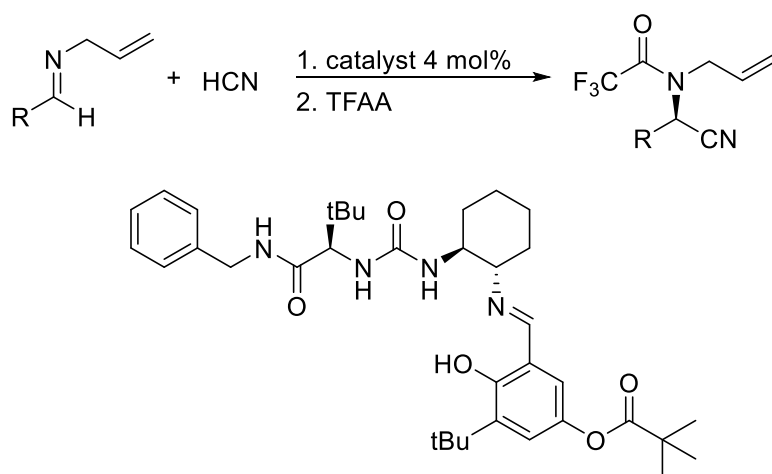
This new mechanistic consideration drove chemists to elaborate new classes of bifunctional catalysts with H-bond donor groups. A wide diversity of structural and functional systems was designed, offering a large range of acidities and which acts by various modes of action. Because of their acidic hydrogens and their lone pairs, ureas and thioureas have been demonstrated as a key motif for organocatalysis based on hydrogen-bond. In the next part, this discovery and its evolution will be reported.

1.2 FROM (THIO)UREA IN H-BONDS ORGANOCATALYSIS TO FOLDED ORGANOCATALYSTS

1.2.1 Importance of urea and thiourea in organocatalysis

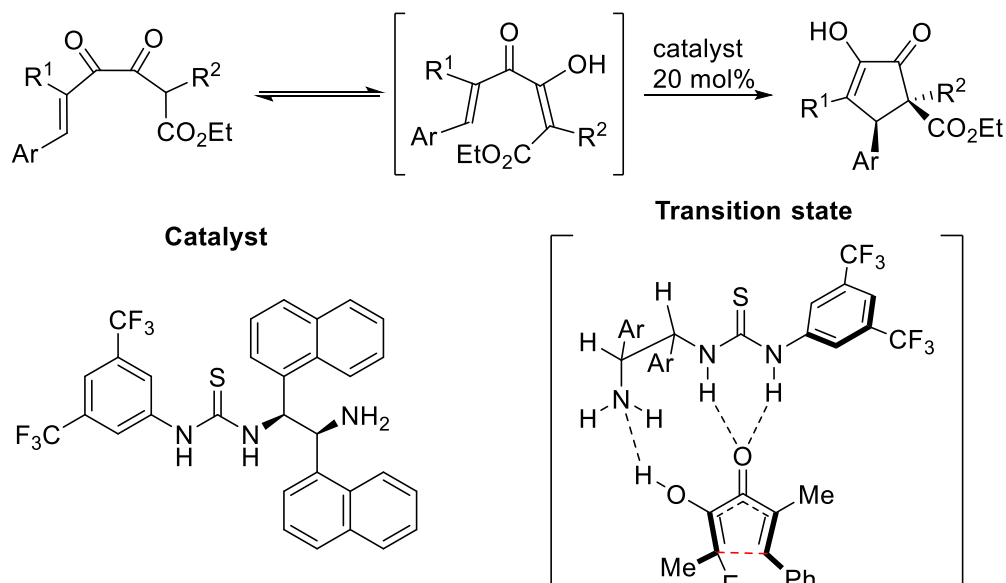
Despite the late development of organocatalysis, the very first example dates from 1829 with acetaldehyde as catalyst as we discussed previously (see 1.1.2.3). In their review, Zhang and Schreiner underline the interest of anion recognition in nature to design thiourea-based catalysts.⁴⁶ Hydrogen bonding is an essential contributor to molecular recognition in enzymatic processes as we showed previously (see 1.1.2.1) and led to the elaboration of “biomimetic chemistry” and “artificial enzymes”. The complexation between carbonyl groups and (thio)urea is associated to the development of partial charged on neutral motifs. They are particularly successful in organocatalysis, particularly because of their similar way of actions than those found in active sites of enzymes. Ureas and thioureas have been shown to well interact well with oxyanions, nitronates, halide anions, carboxylates, cyanides and enolate anions. In 1998, Schreiner demonstrated the advantages of thioureas over ureas among which solubility and better substrates association parameters and he identified one particularly interesting achiral thiourea catalyst, the *N,N'*-bis[3,5-bis(trifluoromethyl) phenyl]thiourea.⁴⁷ As reported Zhang and coworkers, Schreiner’s thiourea is efficient for a wide range of chemical transformation: Diels-Alder reaction, acetalization, Baylis-Hillman reaction, Friedel & Crafts alkylation.⁴⁸

Jacobsen focused his research for several decades on catalysis with thioureas and ureas through hydrogen-bonding catalysis. In 2000, he performed the Strecker reaction with a very powerful catalyst, in urea and thiourea versions, with amino acids derivatives.⁴⁹ The scope was very extended, from aromatic imines to aliphatic and linear imines. The bulkiness of groups in amino acid position and in the 3-position of the salicylimine moiety is the key to create the steric hindrance necessary to the good positioning of substrates and the good stereocontrol of the reaction. (Scheme I.20)



Scheme I.20: Thiourea catalyst for asymmetric Strecker reaction⁴⁹

Thiourea and chirality induction by atropisomers are two major elements which are used in organocatalysis and which can be combined. For Nazarov cyclization developed by Tius, the catalyst was designed with a double bi-aryl pendant inducing helical conformation, associated to a thiourea activated by a 3,5-bis(trifluoromethyl)phenyl group. Tius and Houk performed molecular modelling experiments to explain the mode of interactions between substrates and catalyst. The activating thiourea and amino groups are maintained in a helical conformation by the bulky naphthyl groups (Scheme I.21). The transition-state is a left-handed helix, corresponding to the lowest energetic state. A scope was obtained with good yields and excellent stereocontrol.⁵⁰



Scheme I.21: Organocatalysed Nazarov cyclization⁵⁰

1.2.2 Multicatalytic systems

For controlling the stereoselectivity of an asymmetric reaction, the catalyst could offer two points of anchoring to the system. With a chemical transformation involving two substrates, the catalyst can coordinate one chemical function on each substrate to impose a stereocontrolled approach. It can also be linked on two sites from only one substrate, and by sterical or electrochemical effect, imposing the approach of the second substrate. Moreover, reactions can make contribute more than two substrates: for instance, a base can be necessary to start the reaction. This characteristic has been elegantly used to design bifunctional (thio)urea catalyst whereby the activating urea/thiourea group can be combined in a single molecule with a tertiary amine acting as a base. The design of bifunctional catalysts generally took advantages of rigid backbone as a *trans*-diaminocyclohexane as Takemoto catalyst⁵¹, of cinchona alkaloids derivatives as Soós and Palomo catalysis, of chiral amino acids as Palomo catalyst⁵² (Figure I.8). Another strategy leading to dual catalytic systems is synergistic

activation of the substrates whereby the two catalytic components are not covalently linked but act synergistically (Figure 9, right).

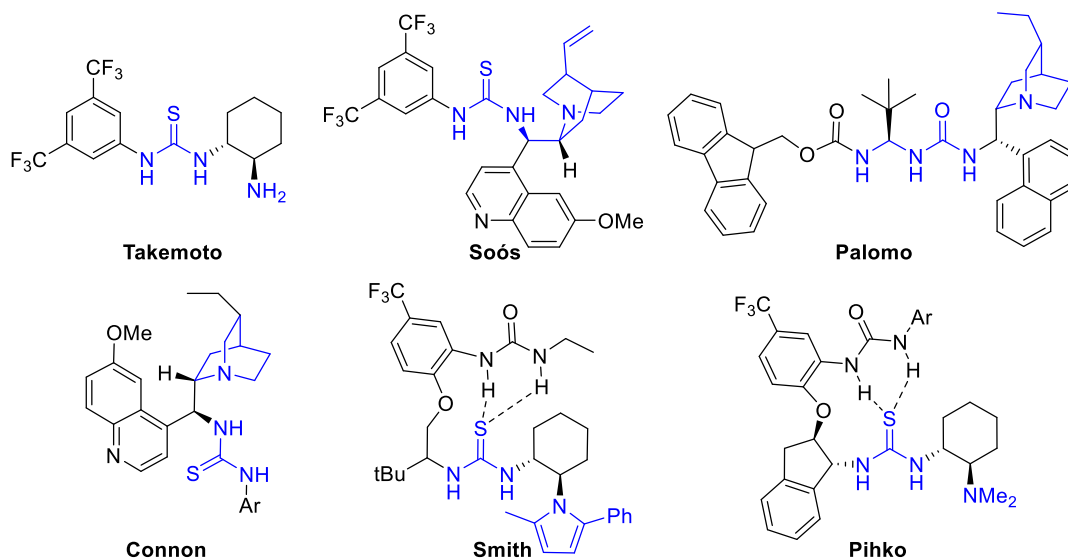


Figure I.8: (Thio)urea bifunctional catalysts with internal tertiary amine

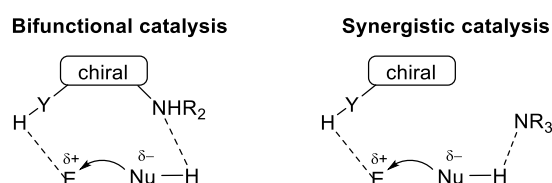
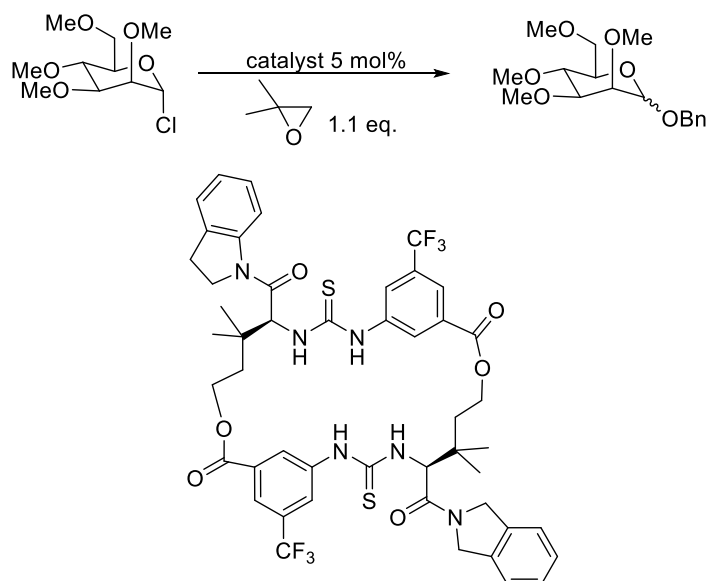


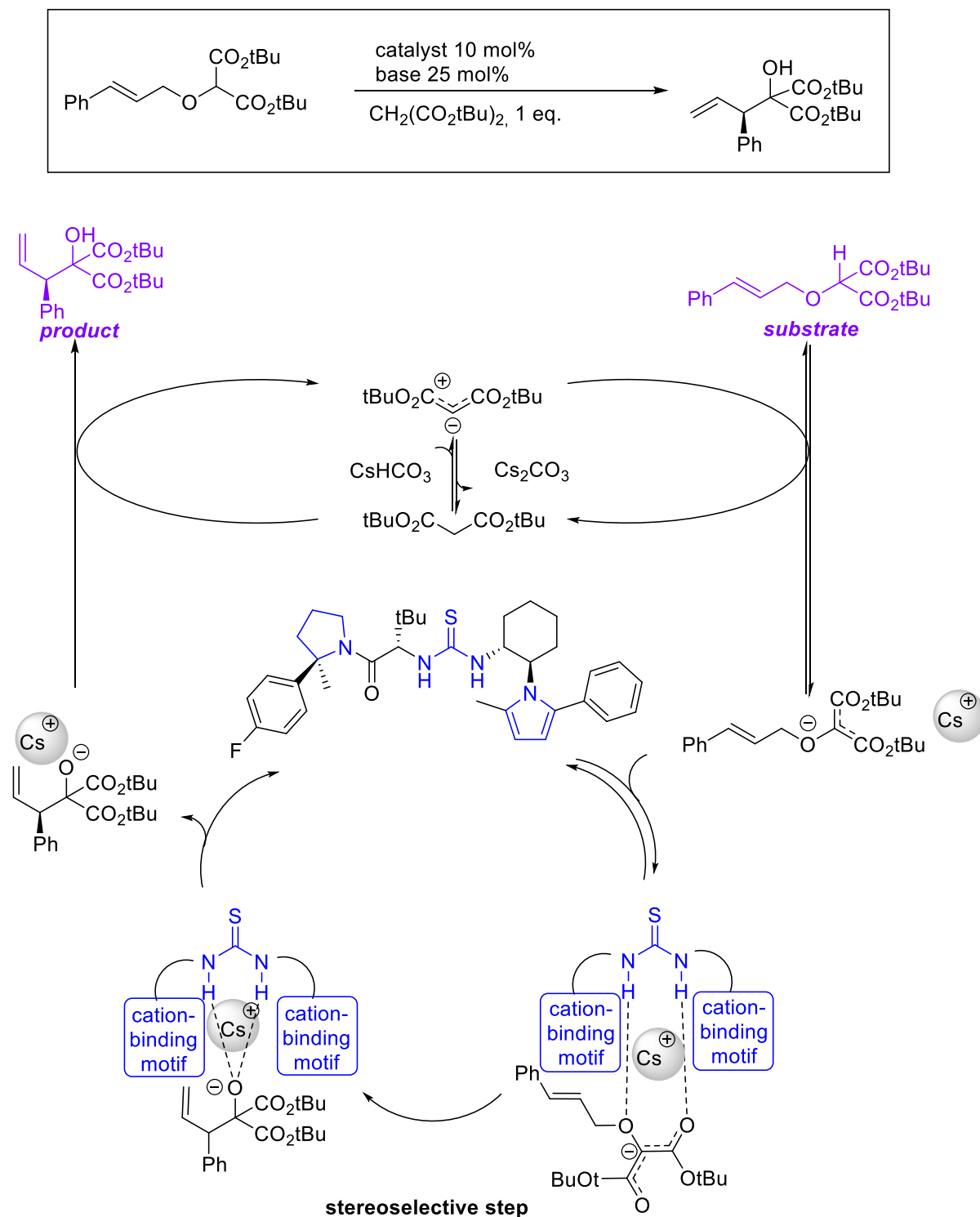
Figure 9: Strategies for dual activation of electrophile and nucleophile

Last year, Jacobsen incorporated two thiourea moieties in a macrocycle, which performed stereospecific glycosylation reactions.⁵³ This system is particularly interesting for the relatively large range of substrates that it tolerates, compared to usual catalysts. Both nucleophile and electrophile had been shown to interact with the catalytic macrocycle and the cooperative effect is responsible of the stereocontrol (Scheme I.22).



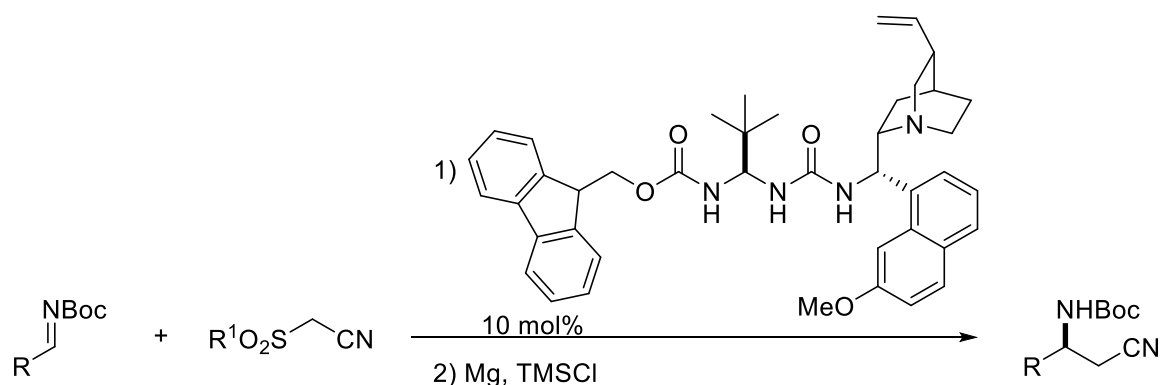
Scheme I.22: Macrocyclic bis-thiourea catalysts for glycosylation⁵³

Jacobsen also developed a thiourea catalyst that mediates [2,3]-Wittig rearrangement through synergistic activation with cation and anion binding. An external base deprotonates the malonate whose counterion is coordinated with the catalyst cation-binding motif and the thiourea allows the simultaneous coordination of two oxygens from the substrates, allowing the stereocontrolled rearrangement into hydroxy malonate (Scheme I.23).

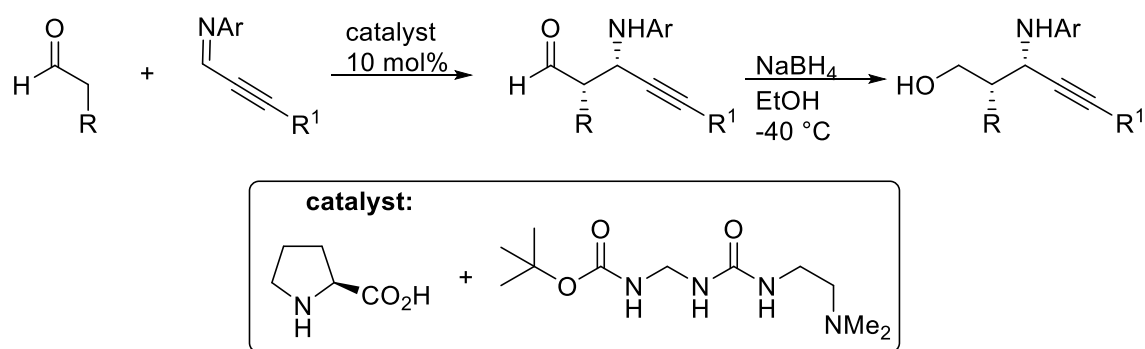


Scheme I.23: Synergistic anion and cation-binding asymmetric catalysis⁵⁴

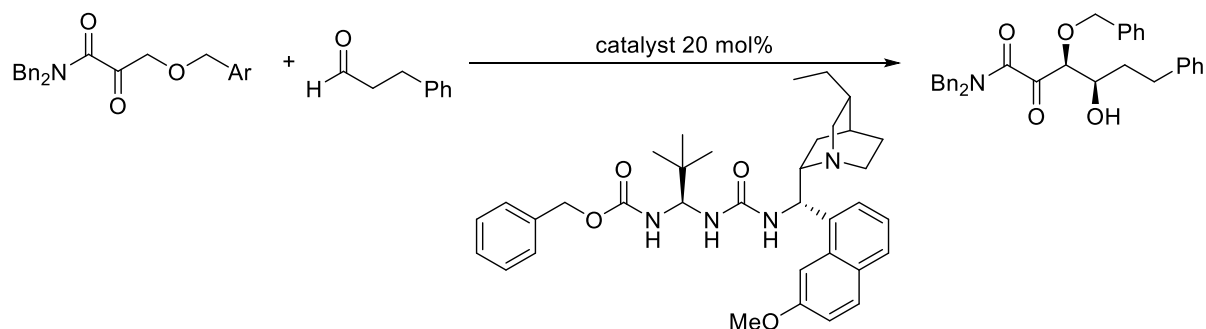
Combination of a Brønsted-base site with a hydrogen bond donor, associated to a cinchona alkaloid derivative illustrated the concept of multiple activation of substrates. Palomo and coworkers developed ureidopeptide-base Brønsted-bases, by simple synthesis from α -amino acids, isocyanates and cinchona alkaloids. This new class of catalysts mediates asymmetric Mannich-type reactions between thiazolones and nitroolefins, and the result was extended between sulfonyl acetonitriles and N-Boc imines (Scheme I.24).⁵⁵ A hydrogen-bonding interaction with four anchoring sites was proposed. Dual activation by Brønsted base catalysts associated to L-proline achieved the Mannich reaction between aldehydes and propargylic imines (Scheme I.25).⁵⁶ This class of catalysts was also successful in the enantioselective direct cross-aldol reaction of α -keto amides with aldehydes and the mode of activation was supported by molecular modelling (Scheme I.26).⁵⁷



Scheme I.24 : Mannich addition of sulfonyl acetonitriles to N-Boc imines with chiral Brønsted bases⁵⁵



Scheme I.25: syn-selective Mannich reaction to access to functionalized propargylic amines⁵⁶

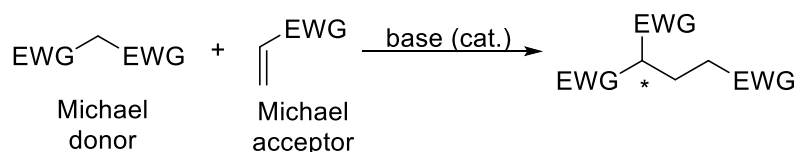


Scheme I.26: Asymmetric aldol reaction of α -keto amides⁵⁷

1.3 MICHAEL ADDITION, A CLASSICAL AND ESSENTIAL WAY TO FORM CARBON-CARBON BOND

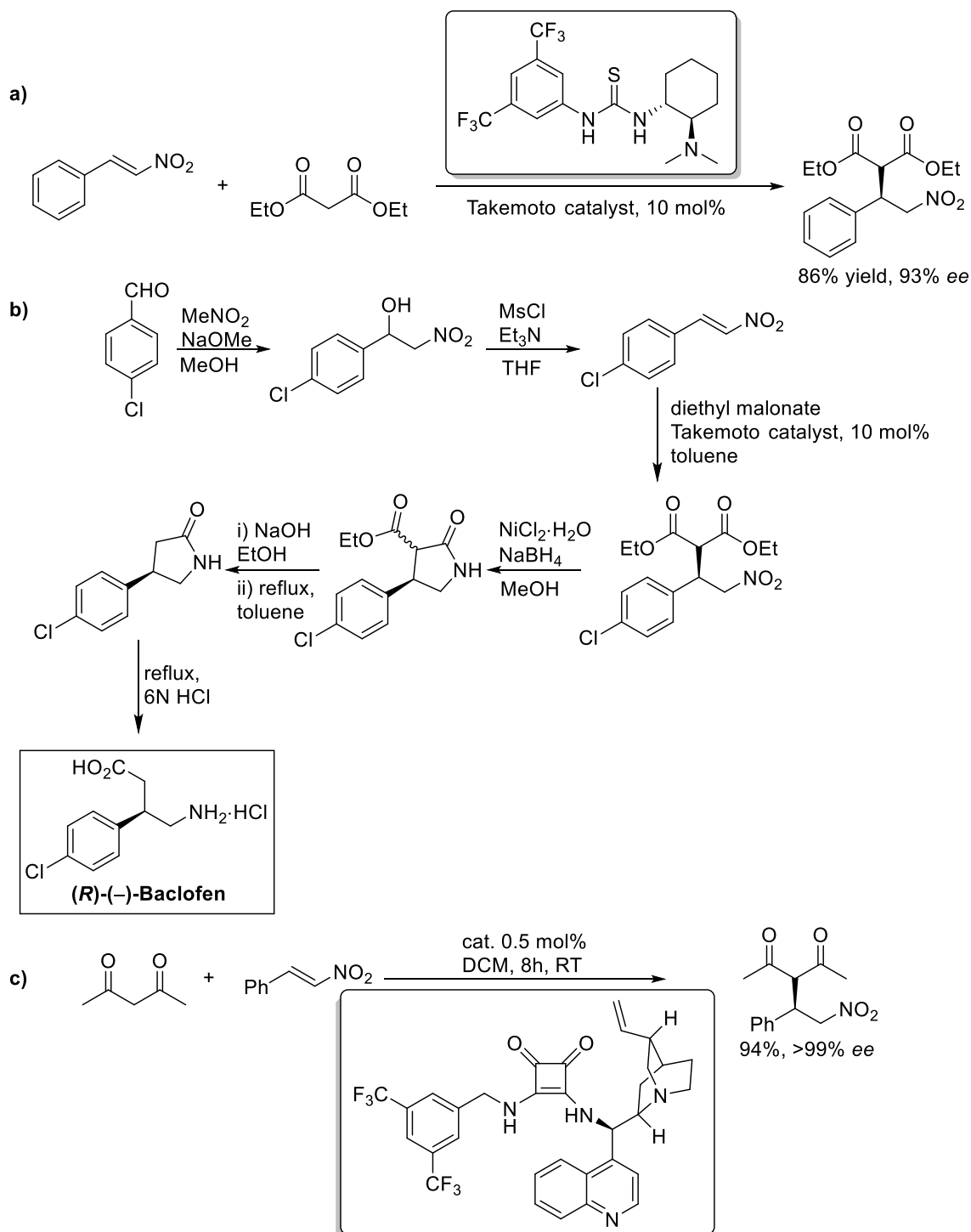
1.3.1 Asymmetric Michael addition, a common example of organocatalyzed reaction by H-bond

The Michael addition is a classical reaction to form carbon-carbon bonds, where a stabilized carbanion is formed through 1,4-addition. Michael acceptors are olefins activated with an electron-withdrawing group, such as α,β -unsaturated carbonyls, nitroalkanes or nitriles. Michael donors are pronucleophiles such as malonates, ketoesters or imidazolones. A catalytic amount of base deprotonates the Michael donor and then performs the addition (Scheme I.27).



Scheme I.27: Michael addition

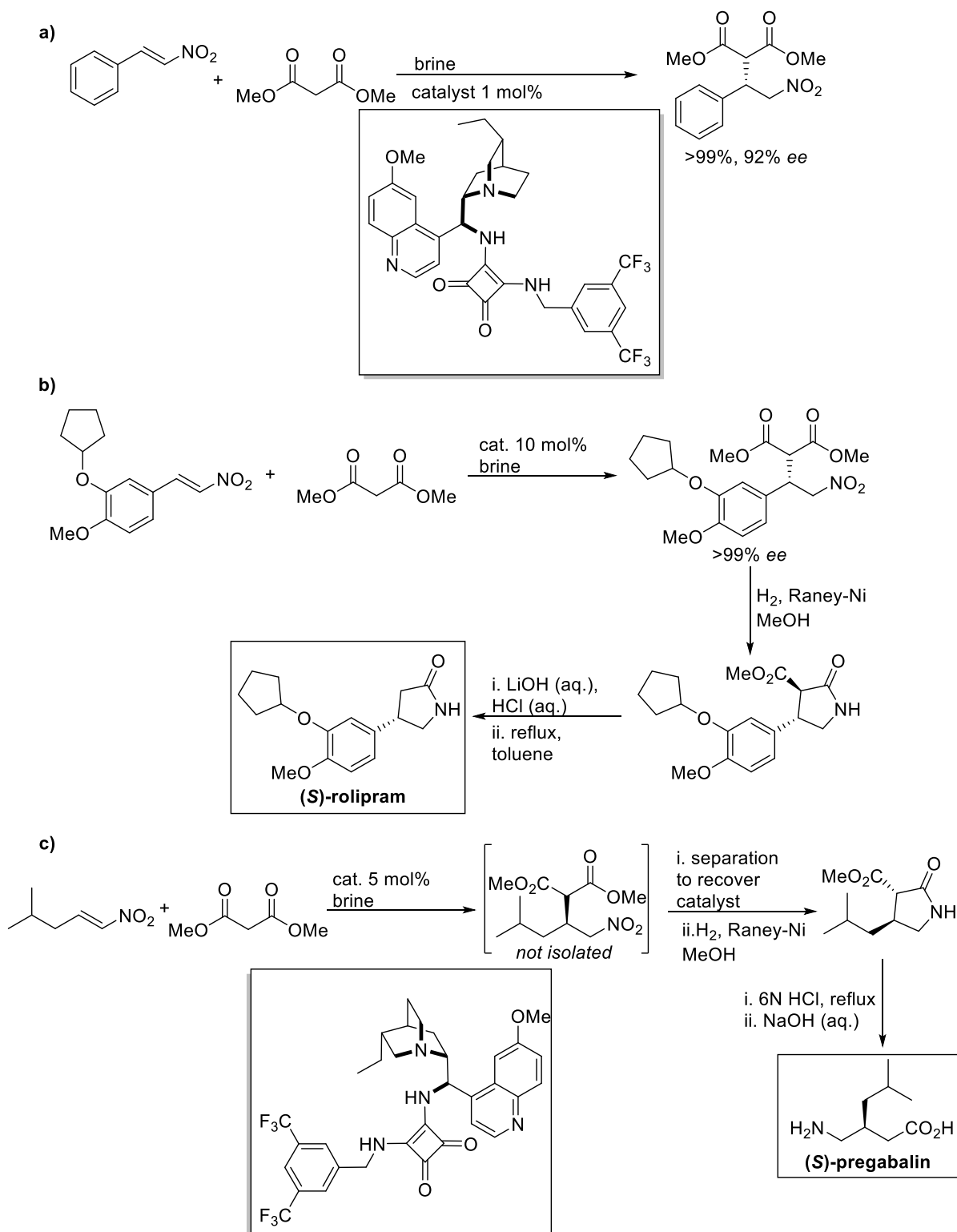
Michael addition can be catalysed through a hydrogen-bonding activation as Xu and coworkers published by the use of hydroxylated quinidine. Bifunctional catalysts containing an internal base associated to urea or thiourea have been a milestone in this research area. Takemoto associated the electron-withdrawing bis-trifluoromethyl phenyl ring, with a thiourea and a tertiary amine to enantioselectively catalyse the addition of malonate to nitrostyrene (Scheme I.28 a).⁵⁸ The substitution on the malonate and the desymmetrization of the malonate by the use of ketoesters were very well tolerated and presented also very good yields and enantioselectivities.⁵¹ On another hand, the scope of aromatic electrophiles was widely extended but the enantioselectivities of aliphatic ones dropped down. Takemoto's group next developed a total synthesis of Baclofen, which is a γ -amino acid derivative acting as an inhibitory neurotransmittant in the CNS and then used as a myorelaxant and more recently as a treatment against alcoholism (Scheme I.28 b). Rawal and coworkers obtained excellent yields and enantioenrichments by the use of a squaramide catalyst they developed (Scheme I.28 c)¹⁰⁷, with very low loading (0.5 mol%). The variety of symmetrical and unsymmetrical 1,3-dicarbonyl pronucleophiles, as well as the variety of electrophiles were well tolerated by this catalyst.



Scheme I.28 : a) Takemoto catalyst for enantioselective Michael addition
 b) Application to Baclofen synthesis⁵⁸ c) Rawal catalyst for enantioselective Michael addition¹⁰⁷

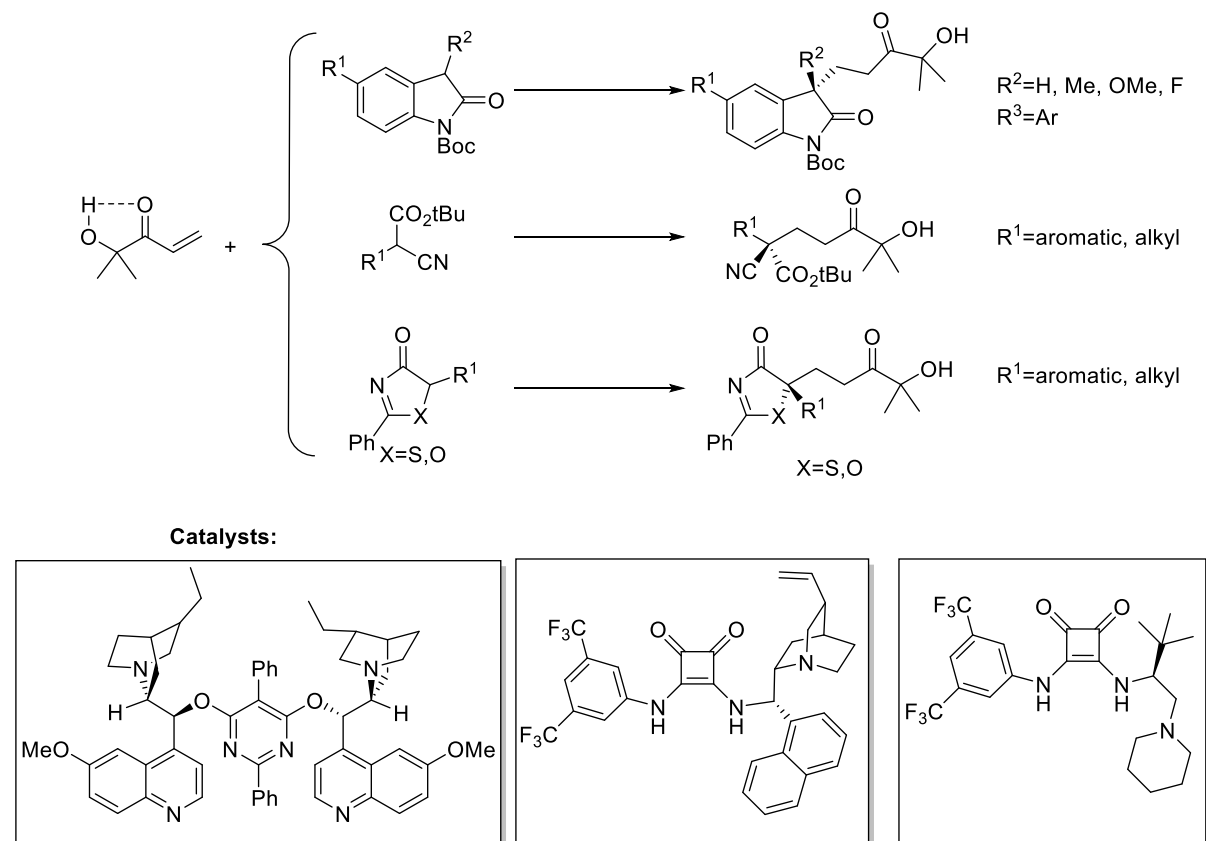
In very recent work, the same reaction with other hydrogen-bonding activating catalyst was performed successfully with the addition of water, which was not expected from all previous studies in literature.⁵⁹ The class of organocatalysts which was used derived from cinchona alkaloids combined with squaramides. A hydrophobic hydration effect linked to the pendant chain on the quinuclidine part allowed to increase rates and obtained very good enantioselectivities even at low catalyst loading. A very broad scope of aromatic and aliphatic nitroalkenes was performed as well as a diastereoselective

example of Michael addition (Scheme I.29). This new method illustrated its interest in the synthesis of pharmaceutical compounds: the antidepressant (*S*)-rolipram and the anticonvulsant blockbuster drug (*S*)-pregabalin (Scheme I.29 b and c).



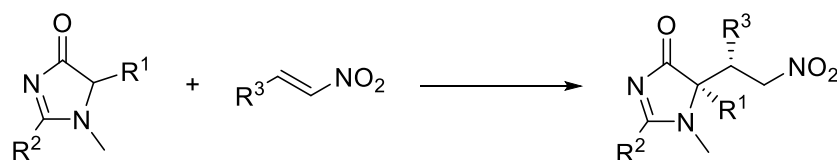
Scheme I.29: a) Biphasic system for asymmetric Michael addition with bifunctional squaramide catalyst. b) Application to the synthesis of (*S*)-rolipram. c) Application to the synthesis of (*S*)-pregabalin.⁵⁹

Palomo *et al.* employed a series of organocatalysts to perform Michael additions with a wide range of electrophile/pronucleophile combinations. Key of the approach is the development of α' -oxy enones as Michael acceptors, containing H-bond acceptor and donor character, with chiral bifunctional Brønsted bases, led to tetrasubstituted carbon stereocenters in high diastereo- and enantioselectivity through the addition of oxindoles, cyanoacetate, 5*H*-thiazolones (Scheme I.30).⁶⁰ The high versatility of the obtained ketol gives access to a wide panel of interesting chemical products.

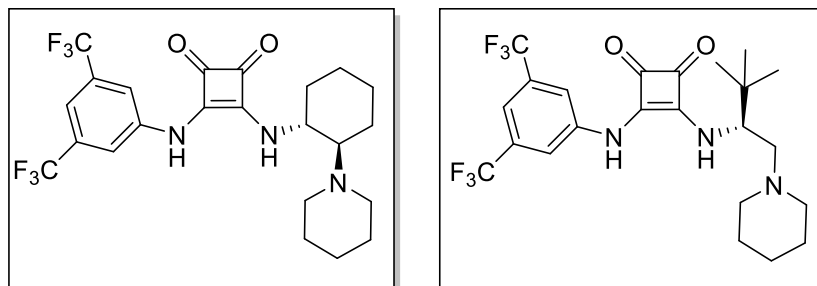


Scheme I.30: α' -hydroxy enones as key enoate equivalent for enantioselective construction of tetrasubstituted stereogenic carbons⁶⁰

Organocatalysts from the same family were also used to synthesize trisubstituted α -amino acid derivatives through an asymmetric Michael addition. 1*H*-Imidazol-4(5*H*)-ones are interestingly used as nucleophilic trisubstituted α -amino acid equivalents (Scheme I.31).⁶¹ The substitution by alkyl, aryl, allyl substituents on the 2-thio-1*H*-imidazol-4(5*H*)-ones is well tolerated. The scope of imidazonoles as pronucleophiles and the scope of nitroolefins are widely extended, giving access to a large range of interesting intermediates for synthesis.



Catalysts:

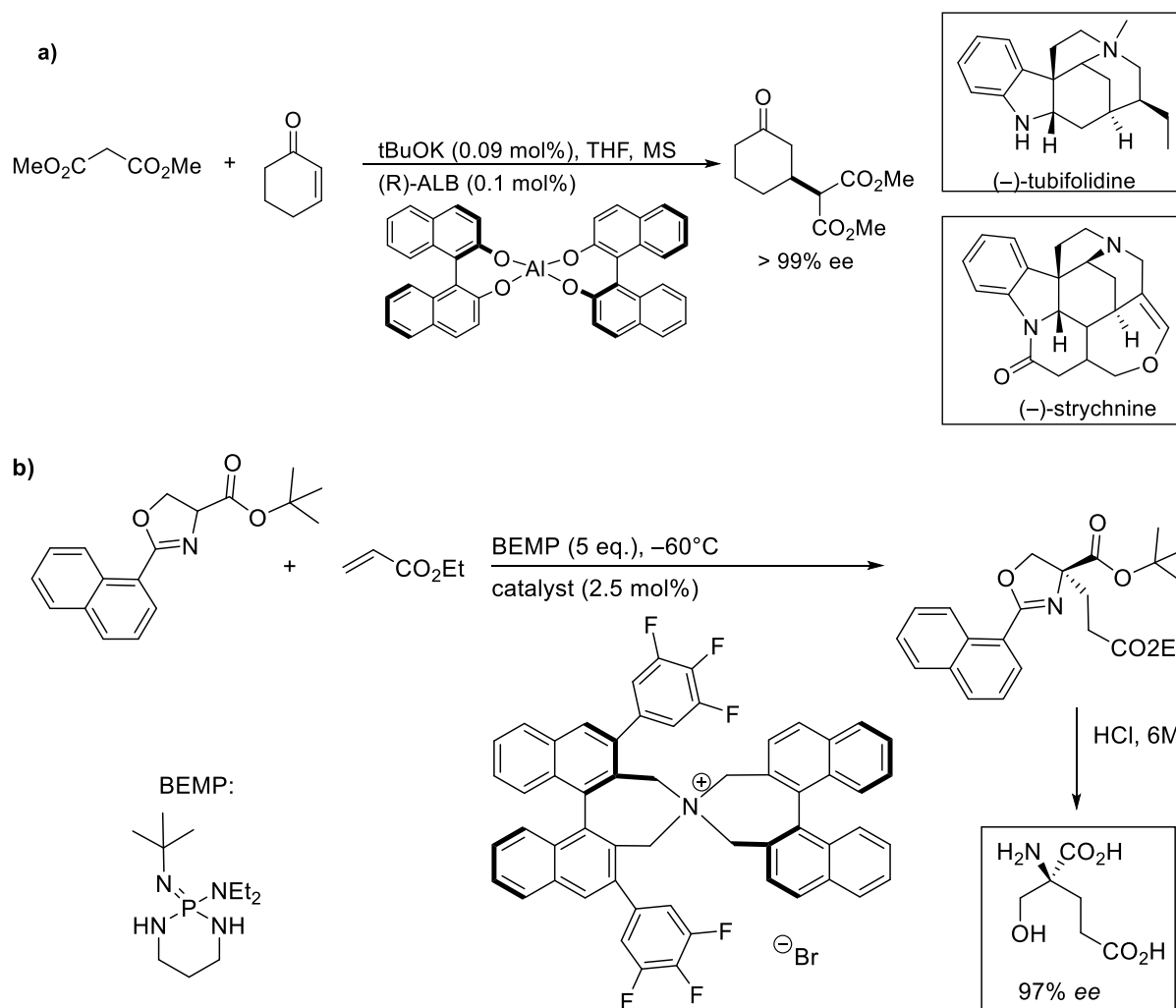


Scheme I.31: Enantioselective addition of imidazolone on nitroolefine to synthesize trisubstituted α -amino acid derivatives⁶¹

Michael addition is one of the most famous and well-studied reaction in organic synthesis. Asymmetric version drives the formation of a tremendous number of biologically active products and natural compounds. Chemical industry developed synthesis processes with this addition. Research performed organometallic and organocatalytic versions of it. The investigation of very versatile catalysts accepting a wide scope of substrates and the improvement of their efficiency are still topic of common concerns for organic chemists.

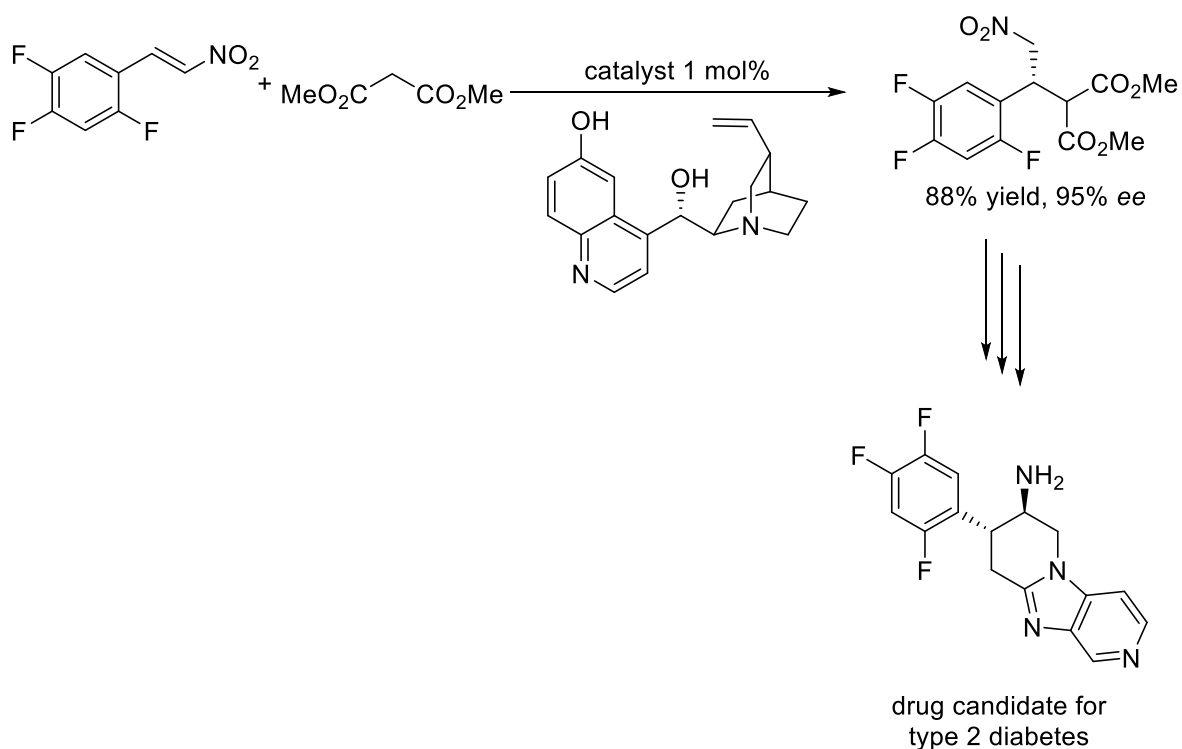
1.3.2 Industrial applications of Michael addition

Michael addition has been used to synthesise natural products and perform the total syntheses of *strychnos* alkaloids. Through metallic catalysis for Michael addition of dimethyl malonate on 2-cyclohexenone on kilogram scale (Scheme I.32 a), Oshima and coworkers obtained (–)-tubifolidine,⁶² and Shimizu and coworkers obtained (–)-strychnine⁶³. Michael addition is also a key step in the synthesis of drugs such as (*S*)- α -(hydroxymethyl)-glutaric acid (Scheme I.32 b) which is an agonist for the metabotropic glutamate receptor 2, and an agonist for the metabotropic glutamate receptor 3, both invested in CNS system.⁶⁴



Scheme I.32: Michael addition to synthesize natural products or bioactive compounds^{62, 64}

Michael addition also found industrial application as published Xu from Merck. He proposed a scalable synthesis of imidazopyridine, which is an inhibitor for the dipeptidyl peptidase IV, involved in the treatment of type 2 diabetes.⁶⁵ The dimethyl malonate is added to nitrostyrene derivative by the use of 1 mol% of cinchona derivative bifunctional catalyst. The deprotonation of the pronucleophile is possible with the quinuclidine moiety of the catalyst. Yield and enantioselectivity are very satisfying (Scheme I.33). A cascade three-component coupling in on pot, followed by organometallic isomerization and couplings leads to the desired drug candidate.



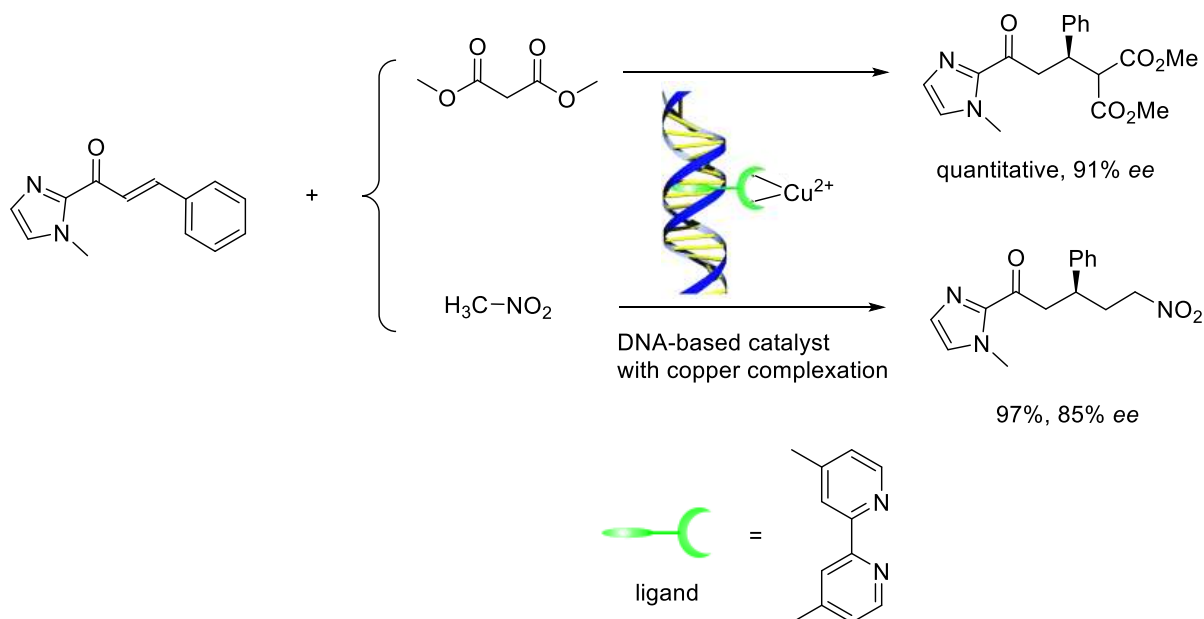
Scheme 1.33: Michael addition as a key step for the synthesis of dipeptidyl peptidase IV inhibitor⁶⁵

Michael addition also takes place in green chemistry as a way to recycle toxic waste. The processing of skin into leather forms chromium collagen as hazardous side products. Thanikaivelan *et al.* designed a nanoparticule core taking profit of this chromium waste with a nanocarbon shell. These new nanoparticles were able to catalyse aza-Michael reaction, speed up the conversion and increase the yield.⁶⁶

1.4 FOLDED SYSTEMS IN ASYMMETRIC CATALYSIS AND ORGANOCATALYSIS

1.4.1 Chiral transfer from biomolecules to small molecules

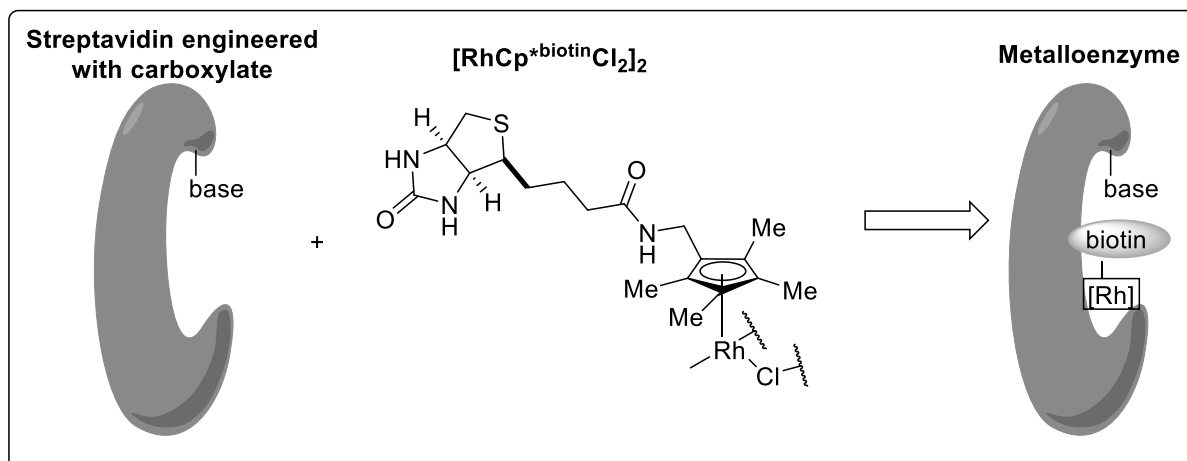
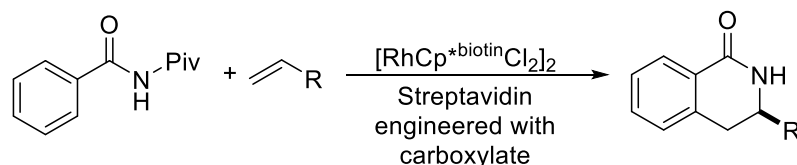
Folding is a key feature selected by nature to achieve complex molecular recognition events and by extension, catalysis. The use of a biopolymer as a chiral inductor for a small molecule catalyst which can be a simple organometallic species is a strategy to develop new efficient chiral catalysts. For instance, the chiral information of a helical system can be transferred to a cofactor and then to the substrates. Roelfes and Feringa took profit of the inherent helicity of the double strand of DNA to associate it with an achiral organocopper catalyst to give a chiral catalyst.⁶⁷ They achieved the catalysis of a Diels-Alder reaction⁶⁸ and also a Michael reaction in water (Scheme I.34).⁶⁹ This elegant transfer of chirality from the DNA double strand to the achiral organometallic catalyst was demonstrated by circular dichroism. Several ligands have been tested, either in association with a DNA-intercalating moiety and a spacer, or with a DNA-binding moiety, to tailor the most adapted to the system. A screening of different bidentate ligands highlighted the close link between ligand nature and stereocontrol.



Scheme I.34: Michael addition with catalyst from double strand DNA complexed with Cu^{2+} ⁶⁷

As we discussed previously, enzymes provide a tailored chiral environment. Combining a protein scaffold and a non-native transition metal permits extension of the scope of possibilities. Ward developed a strategy which combines the folding of natural biological compounds and reactive species to create a potent catalytic system. To synthesize dihydroisoquinolines from pivaloyl-protected benzhydroxamic acids, pentamethylcyclopentadienyl-rhodium complex and streptavidin can be used synergically to catalyse asymmetric C-H activation. As an exogenous base is necessary to enhance the reaction, engineering streptavidin to insert glutamate or aspartate inside its structure will elegantly solve

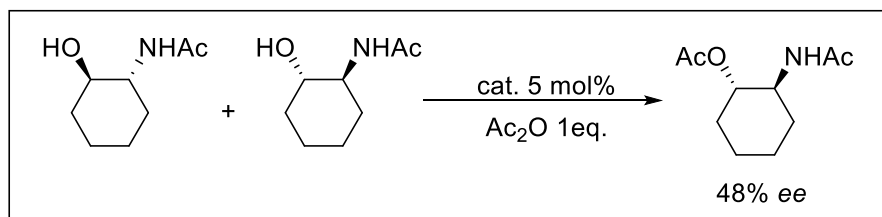
this issue. The organometallic catalyst $[\text{Cp}^*\text{RhCl}_2]_2$ was grafted to biotin to allow the association of the organometallic part of the catalyst with the engineered enzyme (Scheme I.35).⁷⁰



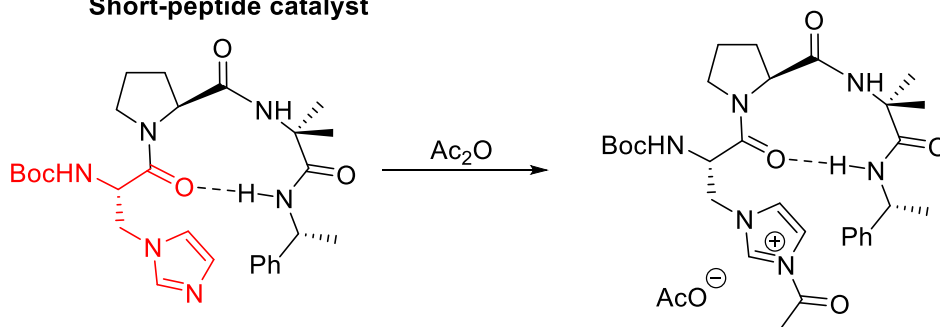
Scheme I.35: Use of the strong natural complex biotin-streptavidin to permit conjugated catalysis between biocatalyst and the organocatalyst⁷⁰

1.4.2 Synthetic peptidic catalysts

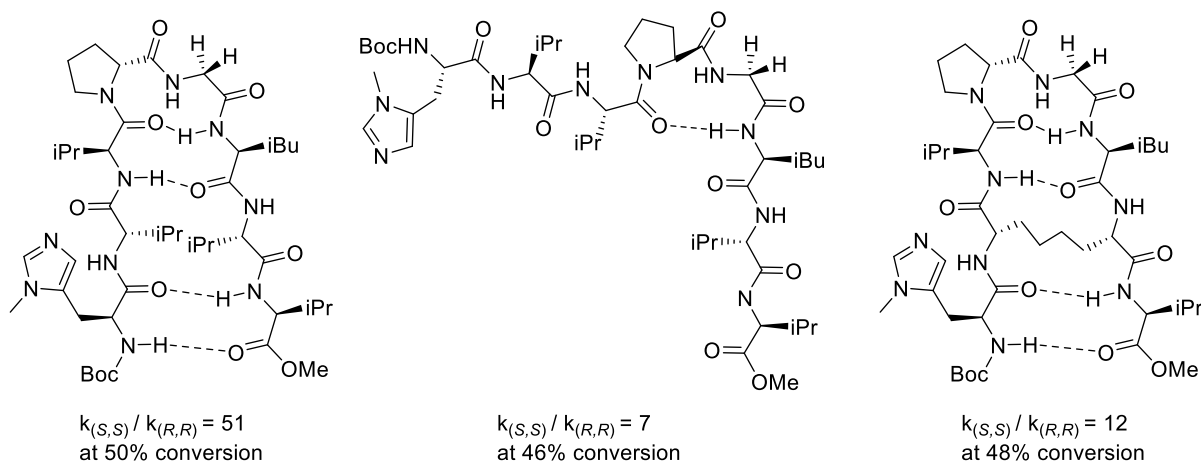
Peptides are small chiral and functional biomolecules which can naturally adopt well-defined conformation in 3D space and thus act as a chiral component to catalyse reactions. Scott J. Miller *et al.* incorporated unnatural amino acids in β -turn short peptides to combine chemical function of the first one and the backbone folding propensity of the second one. 3-(1-imidazolyl)-(*S*)-alanine inserted in β -turn tripeptide catalyses the acylation of secondary alcohols by acetic anhydride and was used for the kinetic resolution of functionalized racemic alcohols (Scheme I.36).⁷¹ Similar octapeptides were synthesized to demonstrate the importance of the turn in the kinetic resolution of alcohols. The role of the secondary structure was proved by NMR and circular dichroism experiments as well as with the synthesis of an open-version of the same peptide catalyst (Scheme I.37). However, an increase of the rigidification of the system by a covalent link had a dramatic effect on selectivity.⁷²



Short-peptide catalyst



Scheme I.36: Kinetic resolution by acylation of alcohols with tetrapeptide catalyst⁷¹

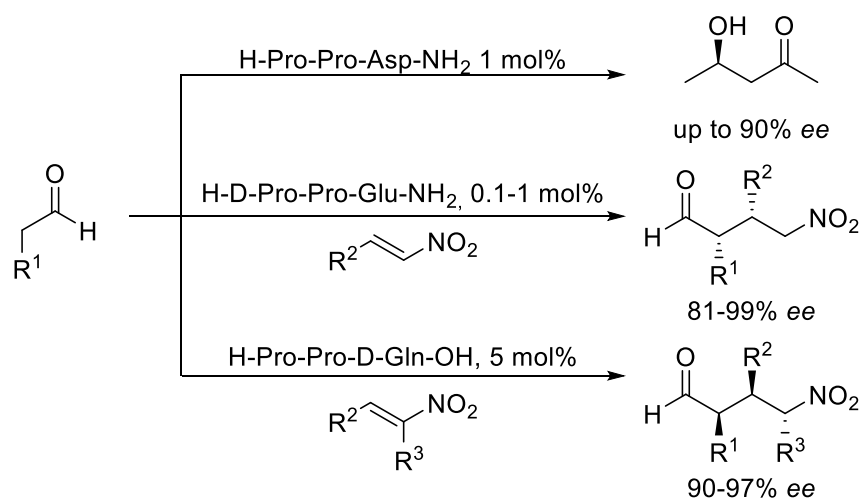


Scheme I.37: Structure-activity relationship of the β -turn octapeptide⁷¹

In their very complete review, B. Lewandowski and H. Wennemers highlighted the strong potential of short peptides in asymmetric catalysis.⁷³ By their high modularity through the synthesis, their catalytic properties can be adapted and improved easily on large scale. They combine features from both enzymes and synthetic catalysts. The authors also discuss the high probability for peptides to have been essential in the development of enzymes.

Miller developed a tetrapeptide able to form atropisomeric tribromo products⁷⁴, but also dynamic kinetic resolution of atropisomers of unsymmetrical tertiary benzamides with two axes of chirality.⁷⁵ Kudo synthesized a solid-supported helical peptide catalyst to access to stereocontrolled nitroaldehydes by Michael addition.⁷⁶ In these examples, catalyst loadings are relatively high, respectively 10 mol% and 20 mol%. Wennemers showed the potential of short peptides able to achieve high chemoselectivity with lower loadings, between 0.1 mol% and 1 mol%, by simple tuning of the catalyst (Scheme I.38).⁷⁷ These tripeptides are particularly active by the well-defined turn on N-terminal

part thanks to the carboxylic acid group.⁷⁸ Moreover, they were grafted on TentaGel resin, which allows to recycle it at least thirty times and to use it in flow chemistry.



Scheme I.38: Chemoselectivity of tripeptide catalysts by the fine tuning of synthesis⁷³

Longer peptides with natural amino acids also played an important role at the beginning of the history of organocatalysis. Juliá mentioned the concept of synthetic enzymes in 1980 with the use of polypeptides to obtain stereoselective epoxydes.⁷⁹ Many studies on the named Juliá-Colona reaction were based on it and the helical poly-leucine catalyst grafted on PEG resin was the most commonly used. Kelly and Roberts demonstrated through X-ray structures and molecular modelling that the helicity of the poly-leucine allows to form an oxy-anion hole with the four terminal N-H, not involved in the H-bond network of the helix, which is at the origin of the stereocontrol of the epoxidation (Figure I.10).⁸⁰ Berkessel *et al.* synthesized oligoleucine versions of different lengths on solid support and demonstrated the direct link between helicity and stereoselectivity.⁸¹ Roberts and coworkers developed helical peptides derivatives with β -amino acids which appear to be efficient for this reaction, but nevertheless not as competitive.⁸²

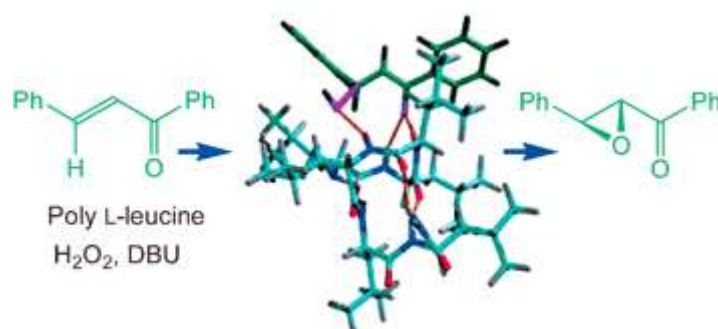
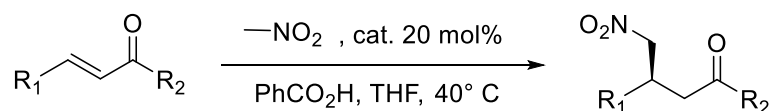


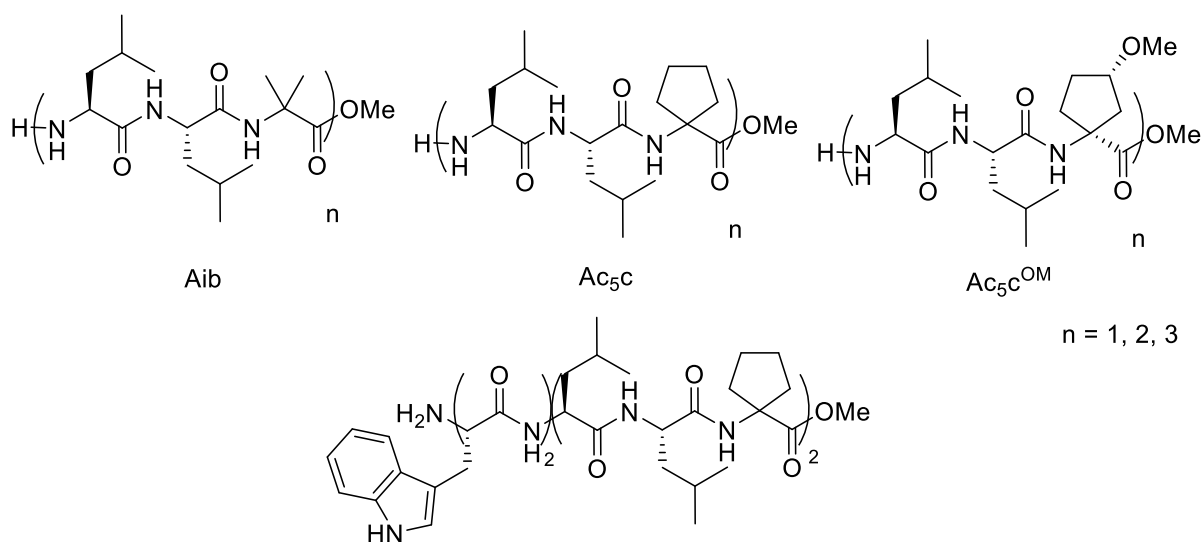
Figure I.10: interaction model for the Julia Colona epoxydation⁸⁰

The possibility to introduce non-natural chemical elements on peptides further expand the possibilities for the design of peptide-based organocatalysts. Ueda and Tanaka demonstrated that an α -helical synthetic depsipeptide with natural and unnatural helicogenic amino acids, (α -aminoisobutyric acid (Aib), 1-aminocyclopentane-1-carboxylic acid (Ac₅c), and para-methoxy substituted Ac₅c ((1*S*,3*S*)-Ac₅c^{OM}) can catalyse Michael addition.⁸³ Similarly, to previous studies, peptides with different

numbers of residues were synthesized to prove the direct link between the helical secondary structure and the selectivity of the system. Tripeptides which are not helical do not catalyse either in terms of conversion or enantioselectivity. However, all the nonapeptides gave notable enantioselectivities and good yields. The peptide with an Aib residue forms a 3_{10} -helix whereas the one with Ac₅c adopts a α -helix. This difference could explain the best results of catalysts with Ac₅c motifs. (Scheme I.39) The best helical peptide they developed was an octapeptide containing a tryptophan on N-terminal site. The sterically demanding indole group probably induced a better stereocontrol. These results were confirmed by X-ray structures (Figure I.11) and NOESY experiments.



Polypeptide abiotic helical catalysts



Scheme I.39: Helical abiotic peptidic catalysts to catalyse Michael addition⁸³

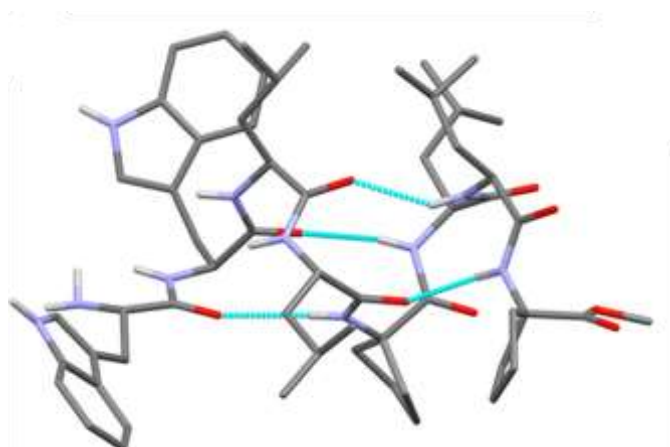
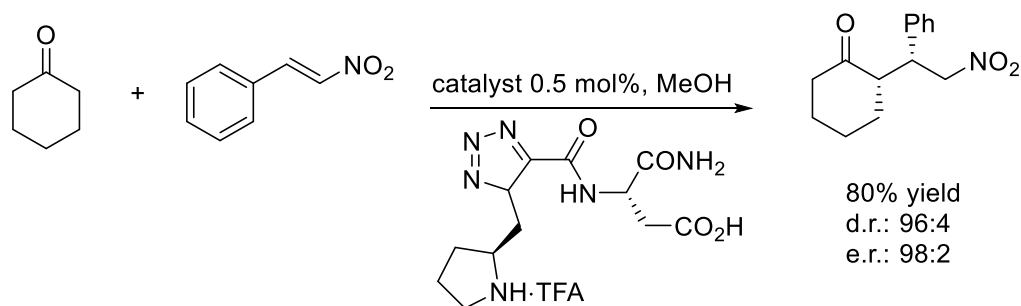


Figure I.11: X-ray structure of helical catalyst $\text{H}_2\text{N-Trp-Trp-(Leu-Leu-Ac}_5\text{c)}_2\text{-OMe}$ ⁸³

Similarly to the concept of the use of turns with amino-acids in organocatalysis, Chandrasekhar and Mainkar developed a dipeptide derivative including a triazole ring which acts as an amide bond

surrogate to access to Michael adduct (Scheme I.40). ROESY experiments supported by DFT calculations demonstrated the turn-like conformation through hydrogen bonds and the mechanism is also similar to proline-like catalysts. There is a synergistic activity with these two elements to reinforce the catalytic efficiency comparing to both taken separately.⁸⁴

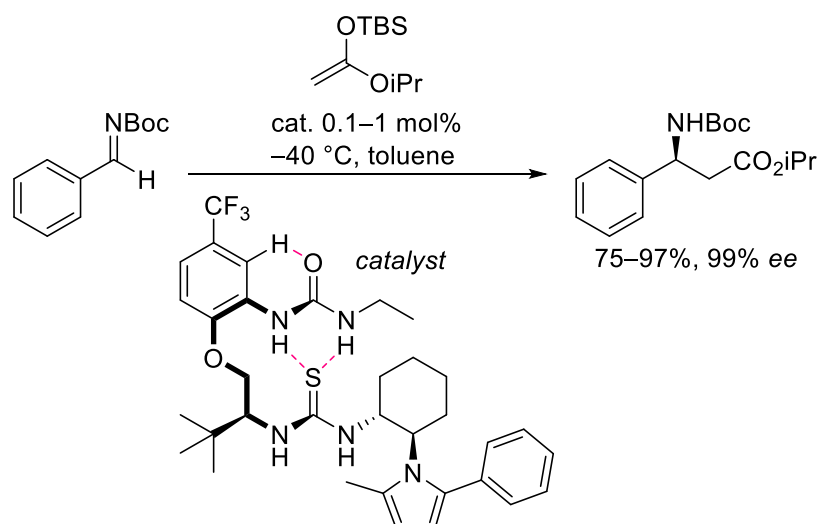


Scheme I.40: Folded dipeptide with triazole ring for Michael addition

1.4.3 Abiotic bioinspired catalysts

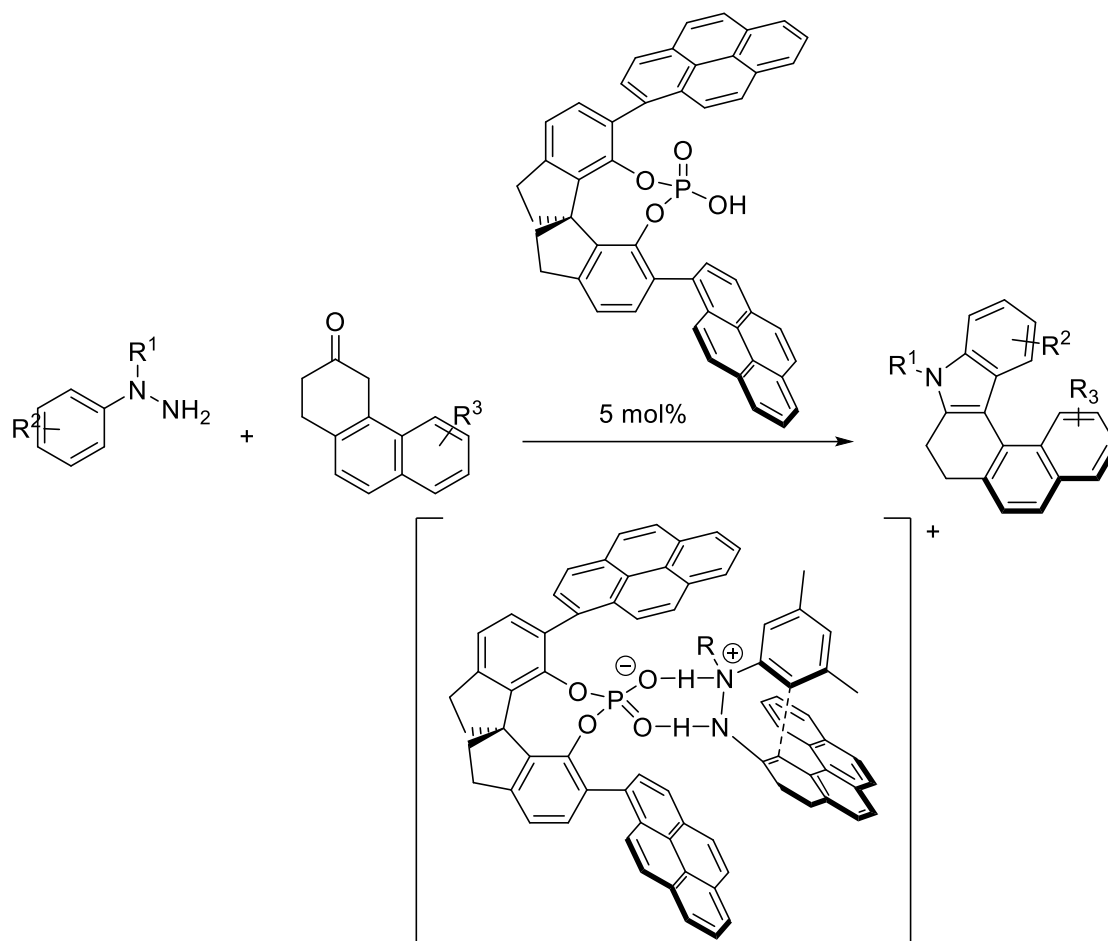
1.4.3.1 Mimicking the pocket binding

Folding helps to reinforce and to provide cooperative interactions, such as in the biological complex streptavidin/biotin. The use of artificially folded backbones leads to a preorganisation of the catalyst, thus it can minimize the entropic cost of transition-state binding catalyst-substrates. In addition, the network of intramolecular non-covalent interactions is reinforced, thus increasing cooperativity in ligand binding and further stabilization of the transition state. This general strategy has been applied to develop new catalysts by Smith and coworkers.⁸⁵ The folding of his bifunctional catalyst was validated by NMR and X-ray. They succeeded to decrease catalyst loading till 0.1 mol% by tailoring the system to perform Mannich reaction (Scheme I.41). Moreover, anion binding experiments confirmed the binding mode between the catalyst and substrate. The synergistic activity of the β -turn folding and the cooperative non-covalent interactions were the key to such a strong catalytic activity.



Scheme I.41: Mannich reaction with folded catalyst designed by the Smith group⁸⁵

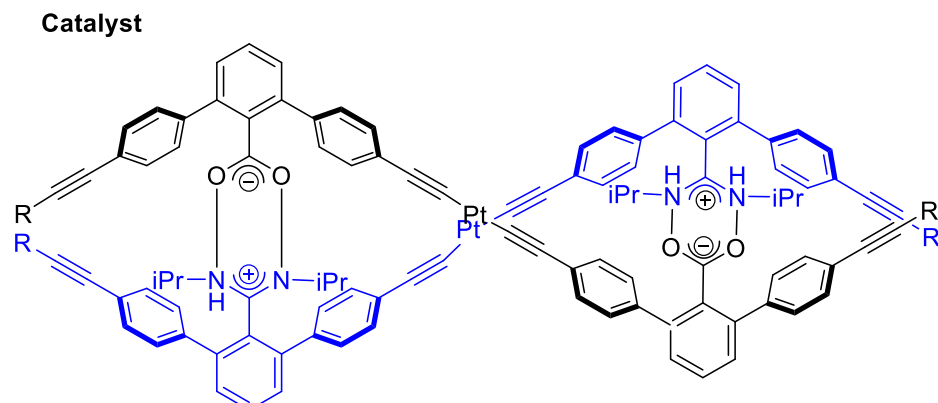
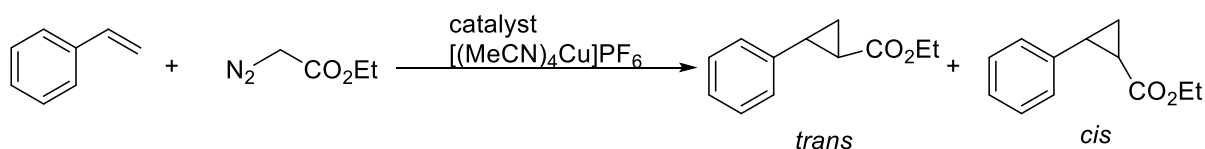
Helicity is a major secondary structural element in nature, which has inspired many chemists to design artificial and well-defined helically folded architectures for molecular recognition and catalysis. In this context phosphoric acid catalysts are very interesting in metallic catalysis and also organocatalysis. List *et al.* demonstrated the use of phosphoric acids to synthesize azahelicenes from Fischer indolization.⁸⁶ The hindered and aromatic substituting groups create a chiral nanometer pocket which induces an excellent stereocontrol (Scheme I.42). Obtained azahelicenes are useful for materials science, catalysis, molecular self-assembly or biological applications. The concept of recognition pocket inspired from enzymatic recognition is observed again in this example.



Scheme I.42: Helicene synthesis by phosphoric acid catalysts⁸⁶

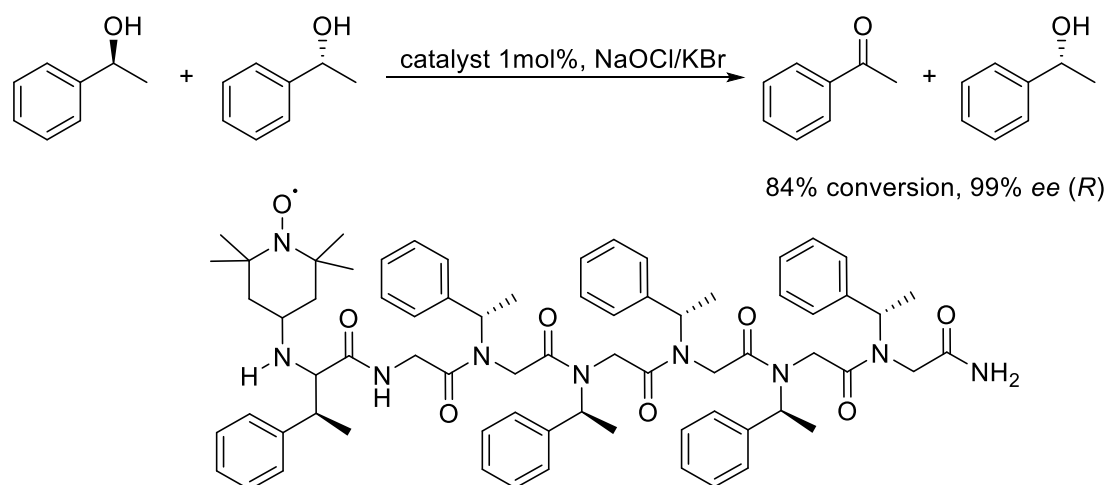
1.4.3.2 Helical abiotic catalysts

Yashima discovered another way to create helicity from double angled molecules with rigid aromatic rings, containing carboxylic acid and amidine, as well as platinum and ligands.⁸⁷ He took advantage of the position of side chains in each strand to form amidinium carboxylate salt bridges to obtain double-helical molecules. He successfully catalysed the asymmetric cyclopropanation of styrene by combining the double helix with copper catalyst (Scheme I.43). The enantiomeric excess of the double helix controlled the ratio of isomers and as previously the screw sense of the helix can be changed with the nature of the solvent.



Scheme I.43: Complementary double helical molecules to catalyze cyclopropanation⁸⁷

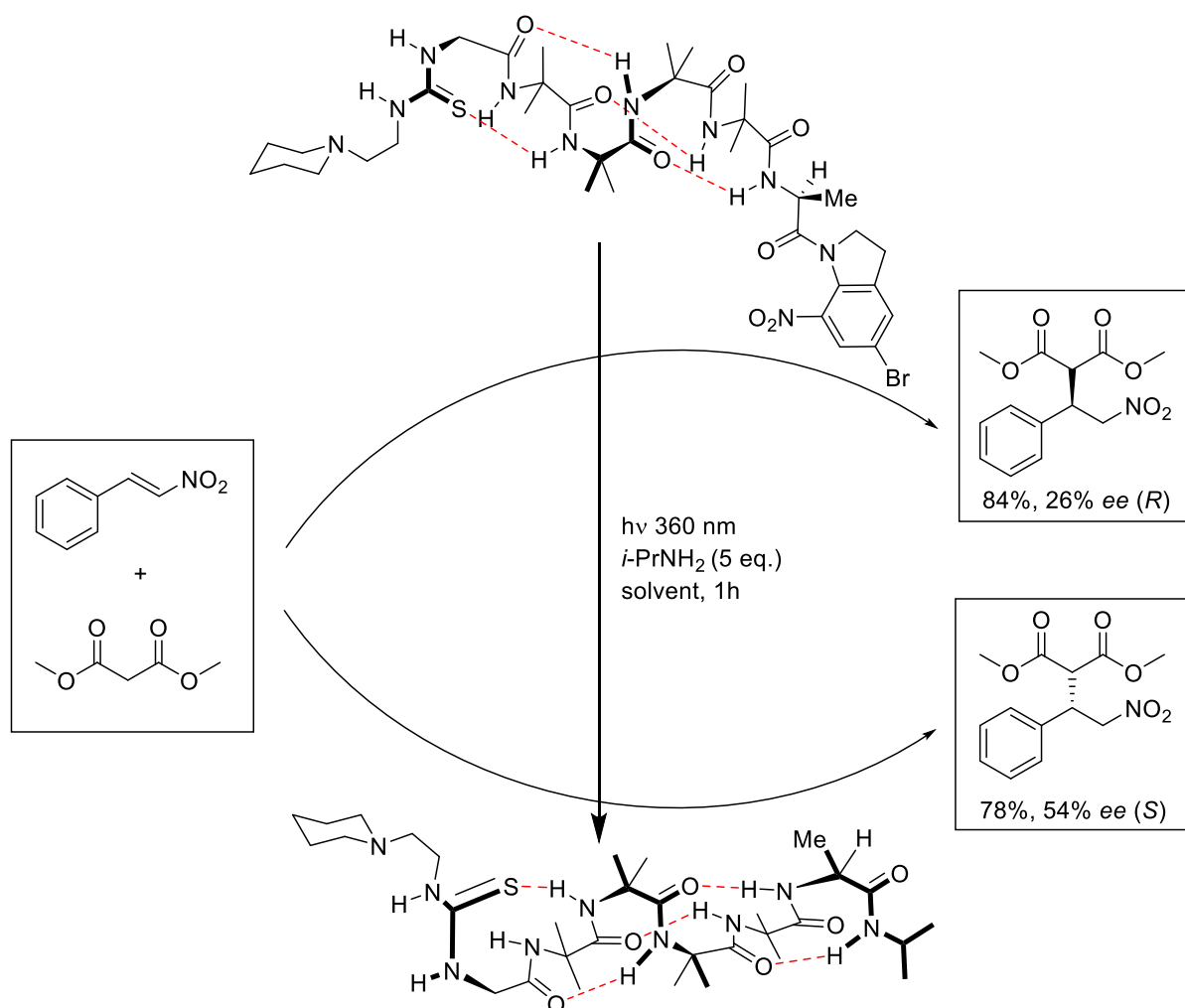
Maayan *et al.* developed her research around peptoids chemistry. Peptoids are oligomers of N-substituted glycine and adopt a well-defined secondary helical structure. The potential of helical artificial system for organocatalysis has not been fully explored yet and Maayan's strategy to deep in this area was to attach a chemical group, known to catalyze chemical transformations.⁸⁸ TEMPO group (2,2,6,6-tetramethylpiperidine-1-oxyl) is known to catalyze oxidations and it was introduced in a peptoid backbone. By the variation of substituents, the variation of the TEMPO position inside the peptoid and the separate use of peptoid compounds and TEMPO simultaneously, a synergistic effect between the helicity of the peptoid has been demonstrated and the catalytic activity of the TEMPO group (Scheme I.44). The position of the oxidative site is also essential to allow the coordination of the substrates to the system.



Scheme I.44: Peptoid catalyst for oxidative kinetic resolution⁸⁸

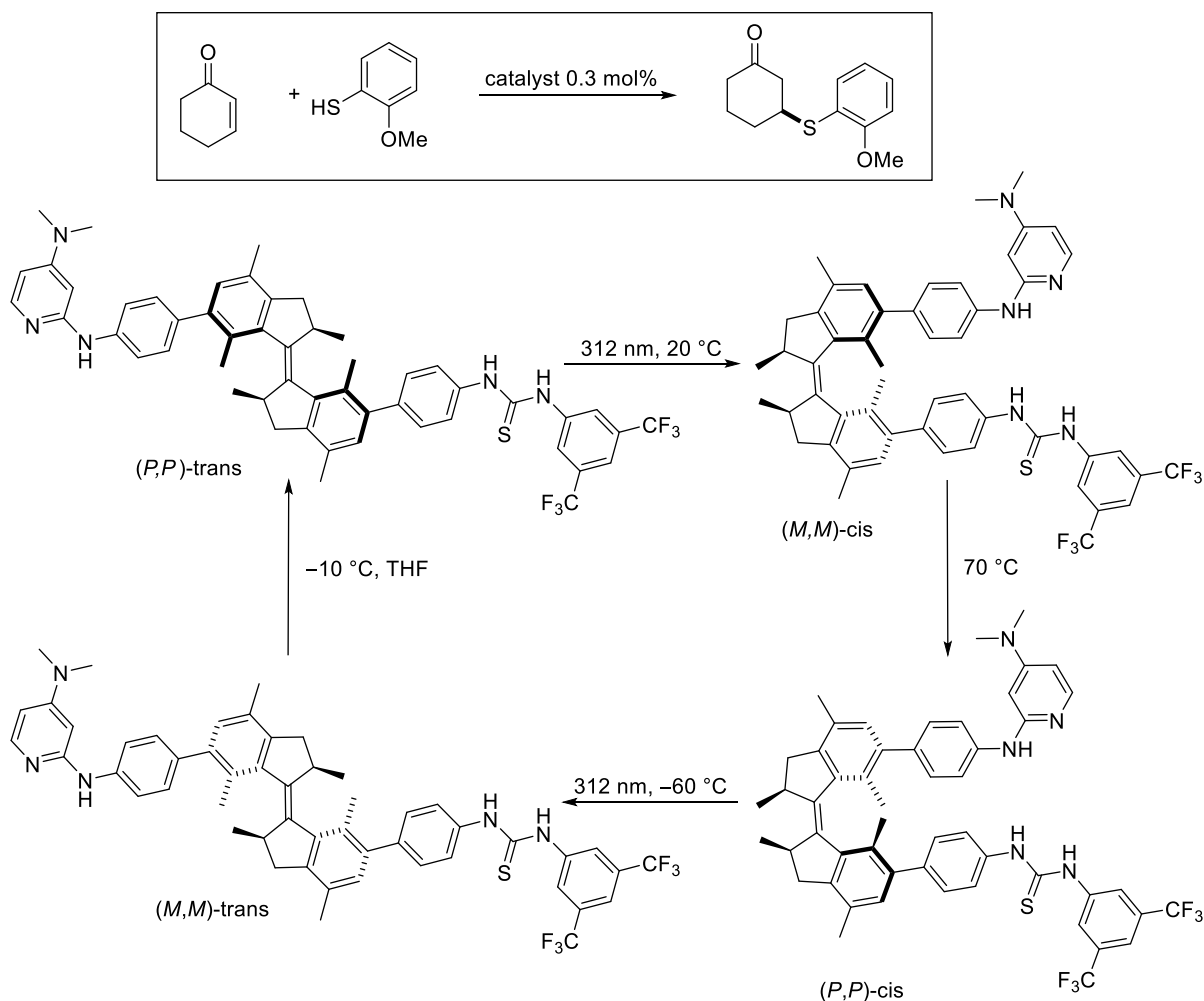
1.4.3.3 Switchable helical catalysts

The folding can also be a dynamic and reversible parameter. Clayden and coworkers designed switchable helices from unnatural achiral quaternary amino acid Aib, from three residues which adopt a 3_{10} -helical conformation. These homo-oligomers coexist with the two screw senses, but a desymmetrization of the balance can be induced in either way by adding a chiral residue at either the N- or C terminal position or even by using chiral groups that bind the helix in a non covalent manner.⁸⁹ Inspired by natural conformationally switchable proteins such as rhodopsin and other G-protein coupled receptors, the Clayden group has designed an Aib-peptide that can be refolded from left-handed helix to right-handed helix following a photochemical cleavage and replacement of the cleaved tertiary amide by a secondary amide. Translation of helix screw sense reversal into a signal was achieved by performing asymmetric catalysis at a remote site of the helical structure where a bifunctional thiourea catalyst with a tertiary amine was introduced.⁹⁰ In this case, the two enantiomers of the Michael addition product can be obtained (Scheme I.45) upon helix screw sense reversal. Of course, this is just a proof of concept and the system was not intended to be developed as a catalyst: the catalyst loading is important (10 mol%) and the stereoselectivity could be improved. Nevertheless, Clayden proposed a mechanism in which 1.22-induction is responsible of the observed chirality of the system, the thiourea engaged in intramolecular H-bonding being able to coordinate the nitro group of the nitrostyrene. This possible mechanism will be discussed in more detail later in this manuscript (see 3.2.4).



Scheme I.45: Photochemically-induced refoldable organocatalyst for Michael addition⁹⁰

In the spirit of the 2016 Chemistry Nobel prizes on molecular machines, Sohtome and Nagasawa illustrated the potential of molecular motors for asymmetric synthesis of thioethers.⁹¹ The motor is constituted of a Brønsted base on one side which is the rotor unit, and a H-bond donor on the other side which is the stator unit. By photoisomerization, the motor can have an open structure or a folded-hairpin structure, along with a *trans* isomer and a *cis* isomer. The enantioenrichment depends on the folding and the configuration of the motor catalyst. It offers a new window of application for molecular motor (Scheme I.46).



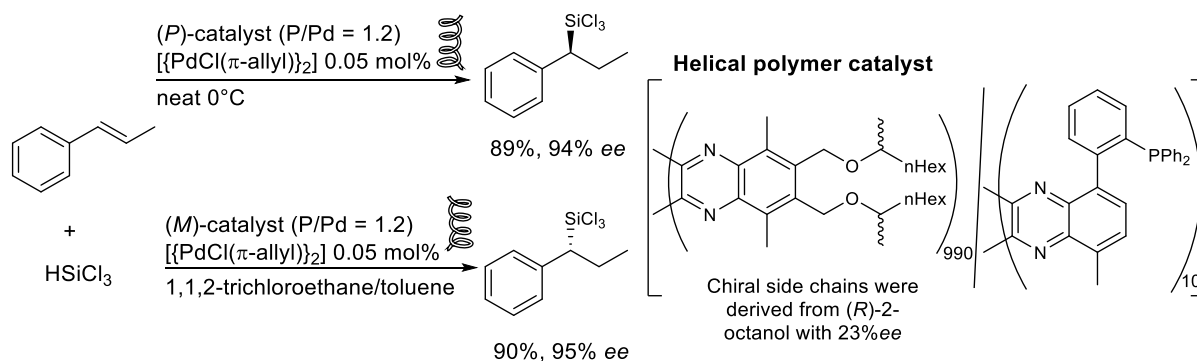
Catalyst	<i>e. r.</i> product (<i>S/R</i>)
(<i>M,M</i>)-cis	75/25
(<i>P,P</i>)-cis	23/77

(*P,P*)-*trans* and (*M,M*)-*trans* were not enantioselective.

Scheme I.46: Molecular motor bifunctional catalyst⁹¹

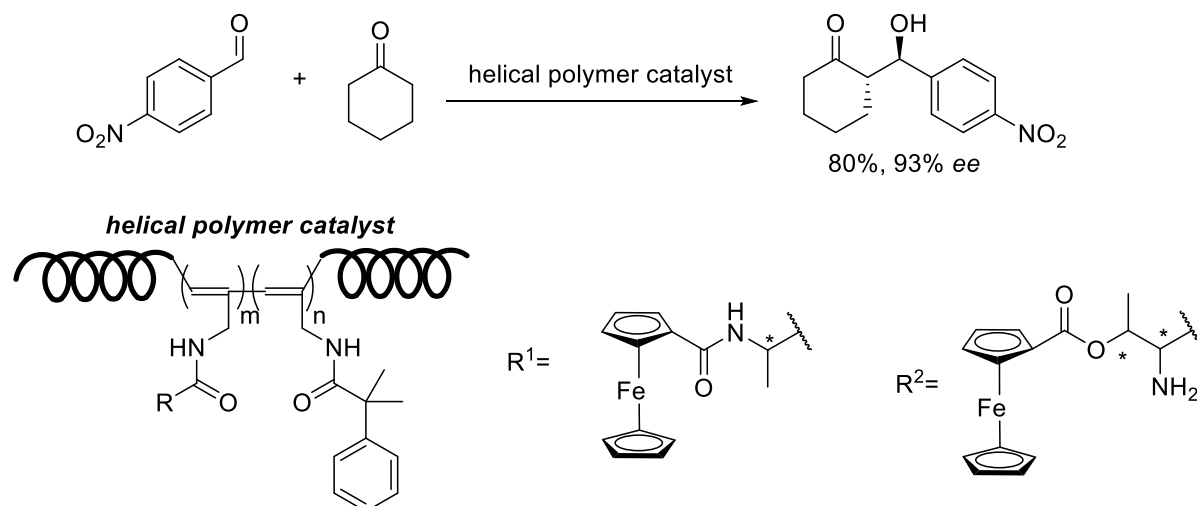
1.4.3.4 Helical polymer catalysts

Suginome *et al.* developed polymers with both achiral and chiral quinoxaline-2,3-diyli units and studied the helicity of the resulting polymers. It is noteworthy that the majority—rule—effects in these systems play a key role leading to remarkable chiral amplification (one single-handed helical structure), even when chiral lateral 2-butoxymethyl side chains are enantioenriched with only 23% *ee*.⁹² The presence of a single helix enables its use in asymmetric catalysis. Interestingly, the system shows a reversibility of helicity depending on the solvent and temperature. Therefore, with one source of chirality, the system can lead to the two enantiomers for asymmetric reaction (Scheme I.47). The amount of metal catalyst is very low (0.05 mol%) and the amount in helical catalyst, measured by the ratio of phosphorous atom in the polymer and the palladium complex, is also very low.



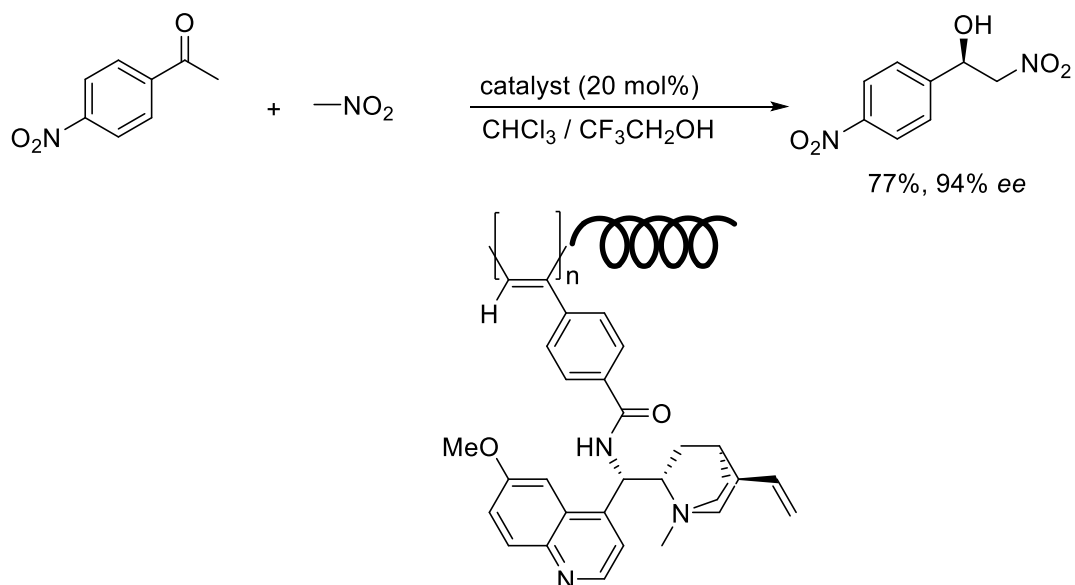
Scheme I.47: A chirality switchable polymer catalyst⁹²

Jianping Deng and coworkers associated a helical polymeric backbone with ferrocenyl amino acids as pendant chains, alanine and threonine.⁹³ The obtained copolymers were used to catalyze aldol reaction between cyclohexanone and *p*-nitrobenzaldehyde and the optimization of the catalyst allowed to reach remarkable results (Scheme I.48). The synergistic activity between the helix and the lipophilic ferrocenyl amino acids was demonstrated by circular dichroism and structure-activity relationship studies.



Scheme I.48: Helical polymer bearing ferrocenyl alanine derivative in pendants⁹³

Yashima also combined helical polymers with cinchona alkaloid pendants to evaluate their potential in organocatalysis (Scheme I.49).⁹⁴ The used polymer was helical poly(phenylacetylene)s, in right-hand version and left-hand version, for asymmetric reaction. By comparison with the equivalent monomer, the helicity of the polymer was demonstrated to be essential to the good catalytic activity. The nature of the link was evaluated: an amide link induced a better stabilization of transition state and was more compatible with the helix structure of the polymer than an ester link. Moreover, it has been demonstrated to be recyclable till five times, with always the excellent activities.



Scheme 1.49: Combination of cinchona alkaloid pendants with helical polymer⁹⁴

1.4.4 Foldamers and organocatalysis

Through all these examples of folded catalysts, several strategies have been used and they can be summed up in the figure below, with catalytic sites highlighted in yellow. Cofactors can be added to a well-structured backbone with transfer of chirality occurring between the folded backbone and the cofactor, as did Ward, Roelfes, Feringa and Suginome. Besides, the folded structure can be used to project requested chemical functions of the lateral side chains in a well-defined manner to catalyse asymmetric reactions, as demonstrated by Miller. On another hand, the folded backbone itself can participate to the catalytic process, as it is the case for Juliá-Colonna epoxidation, and Yashima systems. Finally, these different strategies can also be combined.

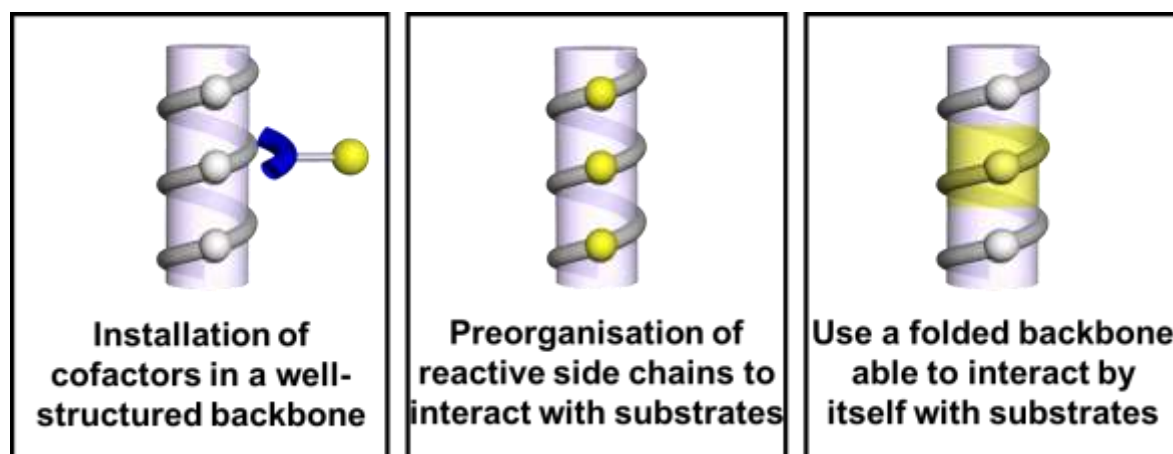


Figure 1.12: Strategies of catalysis with folded systems

With the idea of combining the benefits resulting from folding behaviour and multifunctionality for catalysis, foldamers certainly present a potential, especially those containing urea functions which

can bring effective hydrogen-bonding interactions. Foldamers are “synthetic polymers which adopt a specific conformation in solid state and solution”, as defined for the first time by Gellman in 1998.⁹⁵ A number of helically folded catalysts discussed in the previous section like peptoids, synthetic peptides with unnatural amino acids, double organic strands complexed with metallic ligands can be classified as foldamers. Huc and Guichard illustrated the diversity of backbones, sequences and applications of synthetic foldamers.⁹⁶ In contrast to natural polymers which are able to fold as helices, strands, turns and sheets, abiotic polymers and related oligomers tend more often to fold as helices. β -peptides represent another important class of foldamers which have been reported to adopt well-defined helical conformations. The nature of the building blocks which are used to construct a foldamer can also be mixed to lead to hybrid oligomers with new folding propensities (Figure I.13).

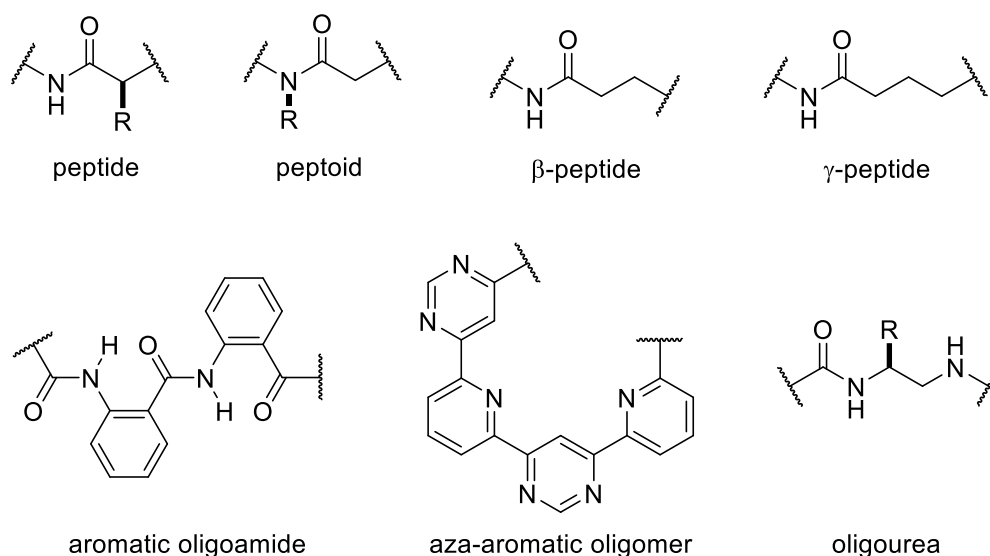


Figure I.13: Homogeneous foldamers constructed from different types of building units either close or remote from natural α -peptides

Abiotic foldamers can be used in biological applications such as DNA delivery for gene transfection,⁹⁷ or the design of antimicrobial drugs⁹⁸ (Figure I.14 a). Zuckermann used the backbone of peptoids to design nanosheet bilayers which could be used for membrane-based separations or templates to grow inorganic materials, or superhelix structure⁹⁹ (Figure I.14 c and d). Quaternary structure formation in aqueous solution (e.g. with oligoureas, Figure I.14b)¹⁰⁰ and recognition of biopolymer surfaces¹⁰¹⁻¹⁰² are also trendy and challenging topics in foldamer chemistry). Furthermore, foldamers are equally useful in molecular recognition of small guests such as sugar derivatives¹⁰³⁻¹⁰⁴ (Figure I.14 e) and anions.¹⁰⁵

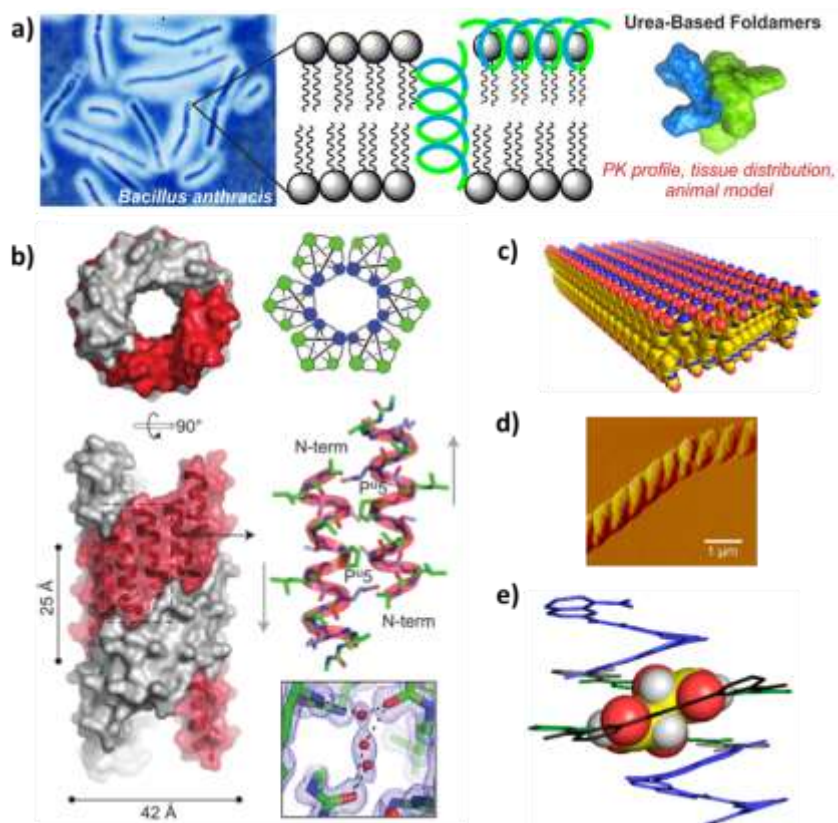


Figure I.14: Variety of applications of foldamers. a) Use of urea-based foldamers as antimicrobial drug against *Bacillus anthracis*. b) Shaping quaternary structures of water-soluble helical foldamers. c) Peptoid nanosheet bilayers. d) Formation of a superhelix from an amphiphilic diblock copolypeptoid imaged by AFM e) X-ray structure of malic acid encapsulated in an aromatic foldamer

1.5 OBJECTIVES

The development of innovative efficient catalysts with a broad scope of substrates and reactions is a current challenge for chemists in academia and industry. The control of chirality and the decrease of catalyst loading are challenging goals responding to ecological problems, the limitation of toxic metals, atom economy principles, and the decrease of waste production. For several decades, organocatalysis emerged as a potential answer to these issues but the lack of efficiency pushes chemists to go further in their investigations.

Through the comparison with the best catalysts present in Nature, combining folding and hydrogen bonding are an interesting pathway to mimic enzymatic route. Precise distribution of chemical functions on a rigid and folded backbone may offer a way to control the selectivity of the reaction. Among synthetic chemical tools, foldamer chemistry and helical backbones in particular appear as a good playground to develop new catalysts, midway between small molecules and biomacromolecules. Moreover, the cooperative effects that could result from optimal preorganisation through helical folding could reinforce the catalytic activity. Because of the importance of urea and thiourea moieties in organocatalysis, oligourea foldamers, developed by the Guichard team, may prove particularly relevant to design new catalysts.

The main objective of this work was thus to explore the potential of oligourea foldamer technology for designing innovative catalysts. The well-defined hydrogen-bonding network, which stabilizes the helix conformation of oligoureas and the preorganization of an anion binding site at the positive pole of the helix, are two important features that could contribute to influence the approach of reactants and the activation of substrates. The use of oligourea foldamers as a new type of hydrogen-bond catalyst was first investigated through the Michael addition of 1,3-dicarbonyl compounds to nitroolefins, for direct comparison with Takemoto bifunctional catalyst.

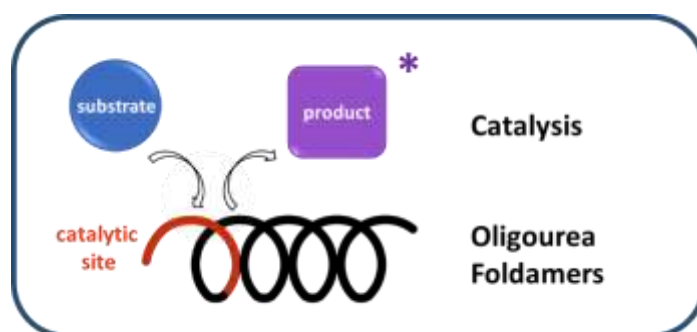


Figure I.15: Strategy to use foldamers for asymmetric reaction

The impact of the inherent constitutive elements of oligoureas have been evaluated in terms of necessity for the catalytic activity. How does the helical folding impact the efficiency of an asymmetric reaction? How do the external parameters influence the catalytic system? Answering all these questions has allowed us to optimize the system in a more effective way and rationalize future designs.

To increase our understanding of the catalytic system and better define the catalytic site, a structure-activity relationship study has been performed using a series of analogues containing selective modifications. NMR experiments have been conducted as another means to observe the interactions between all the species involved in the catalytic process and to gain knowledge of the system from a kinetic point of view.

The extension of the substrate scope in the Michael addition of 1,3-dicarbonyl compounds to nitroolefins also provided useful additional insight into the catalytic process, reinforcing the mechanistic study and helping to propose a general mechanism. First trials have been performed with the designed system on other chemical transformations to evaluate its potential on other reactions. Next, with the goal to further address green chemistry challenges, grafting of the catalyst on solid support was investigated. Preliminary studies have been performed as an attempt to evaluate the feasibility of the transfer of the system from homogeneous to heterogeneous conditions. Because of the introduction of new parameters by working with a biphasic system, systematic optimization of the reaction conditions was necessary to obtain the best results. Finally, the re-consideration of our initial hypotheses could be re-evaluated and the future of the use of oligourea foldamers as organocatalyst could be discussed.

Bibliography

1. Davison, A.; McDowell, G. S.; Holden, J. M.; Johnson, H. F.; Koutsovoulos, G. D.; Liu, M. M.; Hulpiau, P.; Van Roy, F.; Wade, C. M.; Banerjee, R.; Yang, F.; Chiba, S.; Davey, J. W.; Jackson, D. J.; Levin, M.; Blaxter, M. L., *Curr. Biol.* **2016**, *26* (5), 654-60.
2. Crick, F., *Nature* **1970**, *227*, 561-563.
3. Fuss, W., *Chirality* **2009**, *21* (2), 299-304.
4. Caglioti, L.; Micskei, K.; Palyi, G., *Chirality* **2011**, *23* (1), 65-8.
5. Noyori, R., *Angew. Chem. Int. Ed.* **2002**, *41*, 2008-2022.
6. Berg, J. M.; Tymoczko, J. L.; Stryer, L., W.H. Freeman: 2002.
7. Sheldon, R. A.; Arends, I. W. C. E.; Hanefeld, U., Wiley-VCH Verlag GmbH & Co. KGaA: 2007; pp 1-47.
8. Fox, R. J.; Davis, S. C.; Mundorff, E. C.; Newman, L. M.; Gavrilovic, V.; Ma, S. K.; Chung, L. M.; Ching, C.; Tam, S.; Muley, S.; Grate, J.; Gruber, J.; Whitman, J. C.; Sheldon, R. A.; Huisman, G. W., *Nat. Biotechnol.* **2007**, *25* (3), 338-44.
9. Garrabou, X.; Beck, T.; Hilvert, D., *Angew. Chem. Int. Ed.* **2015**, *54* (19), 5609-12.
10. Garrabou, X.; Wicky, B. I.; Hilvert, D., *J Am Chem Soc* **2016**, *138* (22), 6972-4.
11. Dydio, P.; Key, H. M.; Hayashi, H.; Clark, D. S.; Hartwig, J. F., *J. Am. Chem. Soc.* **2017**, *139* (5), 1750-1753.
12. Bornscheuer, U. T.; Huisman, G. W.; Kazlauskas, R. J.; Lutz, S.; Moore, J. C.; Robins, K., *Nature* **2012**, *485* (7397), 185-94.
13. Nozaki, H.; Moriuti, S.; Takaya, H.; Noyori, R., *Tetrahedron Letters* **1966**, *43*, 5239-5244.
14. Knowles, W. S., *Angew. Chem. Int. Ed.* **2002**, *41*, 1998-2007.
15. Sharpless, K. B., *Angew. Chem. Int. Ed.* **2002**, *41*, 2024-2032.
16. Carreras, J.; Kirillova, M. S.; Echavarren, A. M., *Angew. Chem. Int. Ed.* **2016**, *55*, 7121-7125.
17. Herle, B.; Holstein, P. M.; Echavarren, A. M., *ACS Catal.* **2017**, *7* (5), 3668-3675.
18. Nascimento de Oliveira, M.; Fournier, J.; Arseniyadis, S.; Cossy, J., *Org Lett* **2017**, *19* (1), 14-17.
19. El Mamouni, E. H.; Cattoen, M.; Cordier, M.; Cossy, J.; Arseniyadis, S.; Iitki, H.; El Kaim, L., *Chem. Commun.* **2016**, *52* (100), 14490-14493.
20. Liebig, J., *Annalen der Chemie* **1860**, *113* (2).
21. Hajos, Z. G.; Parrish, D. R., *J. Org. Chem.* **1974**, *39* (12), 1615-1621.
22. Bredig, G.; Fiske, P., *Biochem. Z* **1913**, *46*, 7-23.
23. Dalko, P. I.; Moisan, L., *Angew. Chem. Int. Ed.* **2001**, *40*, 3726-3748.
24. Mukherjee, S.; Yang, J. W.; Hoffmann, S.; List, B., *Chem. Rev.* **2007**, *107*, 5471-5569.
25. Erkkila, A.; Majander, I.; Pihko, P. M., *Chem. Rev.* **2007**, *107*, 5416-5470.
26. Franzén, J.; Marigo, M.; Fielenbach, D.; Wabnitz, T. C.; Kjærsgaard, A.; Jørgensen, K. A., *J. Am. Chem. Soc.* **2005**, *127*, 18296-18304.
27. Marigo, M.; Schulte, T.; Franzén, J.; Jørgensen, K. A., *J. Am. Chem. Soc.* **2005**, *127*, 15710-15711.
28. Marigo, M.; Franzén, J.; Poulsen, T. B.; Zhuang, W.; Jørgensen, K. A., *J. Am. Chem. Soc.* **2005**, *127*, 6964-6965.
29. Carlone, A.; Bartoli, G.; Bosco, M.; Sambri, L.; Melchiorre, P., *Angew. Chem. Int. Ed.* **2007**, *46* (24), 4504-6.
30. Ibrahim, I.; Rios, R.; Vesely, J.; Hammar, P.; Eriksson, L.; Himo, F.; Cordova, A., *Angew. Chem. Int. Ed.* **2007**, *46* (24), 4507-10.
31. Ahrendt, K. A.; Borths, C. J.; MacMillan, D. W. C., *J. Am. Chem. Soc.* **2000**, *122*, 4243-4244.
32. Paras, N. A.; MacMillan, D. W. C., *J. Am. Chem. Soc.* **2001**, *123*, 4370-4371.
33. Brochu, M. P.; Brown, S. P.; MacMillan, D. W. C., *J. Am. Chem. Soc.* **2004**, *126*, 4108-4109.
34. Beeson, T. D.; MacMillan, D. W. C., *J. Am. Chem. Soc.* **2005**, *127*, 8826-8828.
35. Hechavarria Fonseca, M. T.; List, B., *Angew. Chem. Int. Ed.* **2004**, *43* (30), 3958-60.
36. Liu, H.; Dagousset, G.; Masson, G.; Retailleau, P.; Zhu, J., *J. Am. Chem. Soc.* **2009**, *131*, 4598-4599.
37. Akiyama, T.; Itoh, J.; Yokota, K.; Fuchibe, K., *Angew. Chem. Int. Ed.* **2004**, *43* (12), 1566-8.
38. Uraguchi, D.; Terada, M., *J. Am. Chem. Soc.* **2004**, *126*, 5356-5357.
39. Seayad, J.; Seayad, A. M.; List, B., *J. Am. Chem. Soc.* **2005**, *128*, 1086-1087.
40. Rueping, M.; Sugiono, E.; Azap, C.; Theissmann, T.; Bolte, M., *Org. Lett.* **2005**, *7* (17), 3781-3783.
41. Doyle, A. G.; Jacobsen, E. N., *Chem. Rev.* **2007**, *107*, 5713-5743.
42. Etter, M. C.; Urbakzyk-Lipkowska, Z.; Zia-Ebrahimi, M.; Panunto, T. W., *J. Am. Chem. Soc.* **1990**, *112*, 8415-8426.
43. Curran, D. P.; Kuo, L. H., *J. Org. Chem.* **1994**, *59*, 3259-3261.
44. Hiemstra, H.; Wynberg, H., *J. Am. Chem. Soc.* **1981**, *103*, 417-430.
45. Hajos, Z. G.; Parrish, D. R., *J. Org. Chem.* **1974**, *39* (12), 1612-1615.
46. Zhang, Z.; Schreiner, P. R., *Chem. Soc. Rev.* **2009**, *38* (4), 1187-98.
47. Schreiner, P. R., *Chem. Soc. Rev.* **2003**, *32* (5), 289.
48. Zhang, Z.; Bao, Z.; King, H., *Org. Biomol. Chem.* **2014**, *12* (20), 3151-62.
49. Sigman, M. S.; Vachal, P.; Jacobsen, E. N., *Angew. Chem. Int. Ed.* **2000**, *39* (7), 1279-1281.
50. Asari, A. H.; Lam, Y. H.; Tius, M. A.; Houk, K. N., *J. Am. Chem. Soc.* **2015**, *137* (40), 13191-9.
51. Okino, T.; Hoashi, Y.; Furukawa, T.; Xu, X.; Takemoto, Y., *J. Am. Chem. Soc.* **2005**, *127*, 119-125.
52. Diosdado, S.; Etxabe, J.; Izquierdo, J.; Landa, A.; Mielgo, A.; Olaizola, I.; Lopez, R.; Palomo, C., *Angew. Chem. Int. Ed.* **2013**, *52*, 11846.
53. Yongho Park, K. C. H., Nadine Kuhl, Eugene E. Kwan, Richard Y. Liu, Eric N. Jacobsen, *Science* **2017**, *355*, 162-166.
54. C. Rose Kennedy, J. A. G., and Eric N. Jacobsen, *ACS Central Science* **2016**, *2*, 416-423.
55. Diosdado, S.; Lopez, R.; Palomo, C., *Chem. Eur. J.* **2014**, *20*, 6526-6531.
56. Lapuerta, I.; Vera, S.; Oiarbide, M.; Palomo, C., *Chemistry* **2016**, *22* (21), 7229-37.
57. Echave, H.; Lopez, R.; Palomo, C., *Angew. Chem. Int. Ed.* **2016**, *55* (10), 3364-8.
58. Okino, T.; Hoashi, Y.; Takemoto, Y., *J. Am. Chem. Soc.* **2003**, *125*, 12672-12673.
59. Bae, H. Y.; Song, C. E., *ACS Catalysis* **2015**, *5* (6), 3613-3619.
60. Badiola, E.; Fiser, B.; Gomez-Bengoa, E.; Mielgo, A.; Olaizola, I.; Urruzuno, I.; Garcia, J. M.; Odriozola, J. M.; Razkin, J.; Oiarbide, M.; Palomo, C., *J. Am. Chem. Soc.* **2014**, *136* (51), 17869-81.
61. Etxabe, J.; Izquierdo, J.; Landa, A.; Oiarbide, M.; Palomo, C., *Angew. Chem. Int. Ed.* **2015**, *54* (23), 6883-6.
62. Shimizu, S.; Otori, K.; Arai, T.; Sasai, H.; Shibasaki, M., *J. Org. Chem.* **1998**, *63*, 7547-7551.
63. Ohshima, T.; Xu, Y.; Takita, R.; Shimizu, S.; Zhong, D.; Shibasaki, M., *J. Am. Chem. Soc.* **2002**, *124*, 14546-14547.
64. Lee, Y.-J.; Lee, J.; Kim, M.-J.; Jeong, B.-S.; Lee, J.-H.; Kim, T.-S.; Lee, J.; Ku, J.-M.; Jew, S.-s.; Park, H.-g., *Org. Lett.* **2005**, *7* (15), 3207-3209.
65. Xu, F.; Corley, E.; Zacuto, M.; Conlon, D. A.; Pipik, B.; Humphrey, G.; Murry, J.; Tschaen, D., *J. Org. Chem.* **2010**, *75* (5), 1343-53.

66. Ashokkumar, M.; Narayanan, N. T.; Gupta, B. K.; Reddy, A. L. M.; Singh, A. P.; Dhawan, S. K.; Chandrasekaran, B.; Rawat, D.; Talapatra, S.; Ajayan, P. M.; Thanikaivelan, P., *ACS Sustainable Chem. Eng.* **2013**, *1* (6), 619-626.
67. Roelfes, G.; Feringa, B. L., *Angew. Chem. Int. Ed.* **2005**, *44* (21), 3230-2.
68. Roelfes, G.; Boersma, A. J.; Feringa, B. L., *Chem. Comm.* **2006**, (6), 635-7.
69. Coquiere, D.; Feringa, B. L.; Roelfes, G., *Angew. Chem. Int. Ed.* **2007**, *46* (48), 9308-11.
70. Hyster, T. K.; Knörr, L.; Ward, T. R.; Rovis, T., *Science* **2012**, *338*, 500-504.
71. S. J. Miller, G. T. C., N. Papaioannou, T. E. Horstmann, E. M. Ruel, *J. Am. Chem. Soc.* **1998**, *120*, 1629-1630.
72. E. R. Jarvo, G. T. C., N. Papaioannou, P. J. Bonitatebus, Jr., S. J. Miller*, *J. Am. Chem. Soc.* **1999**, *121*, 11638-11643.
73. Lewandowski, B.; Wennemers, H., *Curr. Opin. Chem. Biol.* **2014**, *22*, 40-6.
74. Barrett, K. T.; Miller, S. J., *J. Am. Chem. Soc.* **2013**, *135* (8), 2963-6.
75. Barrett, K. T.; Metrano, A. J.; Rablen, P. R.; Miller, S. J., *Nature* **2014**, *509* (7498), 71-5.
76. Akagawa, K.; Kudo, K., *Angew. Chem. Int. Ed.* **2012**, *51* (51), 12786-9.
77. Duschmale, J.; Wennemers, H., *Chemistry* **2012**, *18* (4), 1111-20.
78. Wiesner, M.; Revell, J. D.; Wennemers, H., *Angew. Chem. Int. Ed.* **2008**, *47* (10), 1871-4.
79. Sebastian Julia, J. M., and Juan Carlos Vega, *Angew. Chem. Int. Ed. Engi.* **1980**, *19* (11), 929-931.
80. Kelly, D. R.; Roberts, S. M., *Chem. Commun.* **2004**, (18), 2018-20.
81. Berkessel, A.; Gasch, N.; Glaubitz, K.; Koch, C., *Org. Lett.* **2001**, *3* (24), 3839-3842.
82. Coffey, P. E.; Drauz, K. H.; Roberts, S. M.; Skidmore, J.; Smith, J. A., *Chem. Comm.* **2001**, (22), 2330.
83. Ueda, A.; Umeno, T.; Doi, M.; Akagawa, K.; Kudo, K.; Tanaka, M., *J. Org. Chem.* **2016**, *81* (15), 6343-56.
84. Chandrasekhar, S.; Kumar, C. P.; Kumar, T. P.; Haribabu, K.; Jagadeesh, B.; Lakshmi, J. K.; Mainkar, P. S., *RSC Adv.* **2014**, *4* (57), 30325.
85. Jones, C. R.; Pantos, G. D.; Morrison, A. J.; Smith, M. D., *Angew. Chem. Int. Ed.* **2009**, *48* (40), 7391-4.
86. Kotzner, L.; Webber, M. J.; Martinez, A.; De Fusco, C.; List, B., *Angew. Chem. Int. Ed.* **2014**, *53* (20), 5202-5.
87. Hasegawa, T.; Furusho, Y.; Katagiri, H.; Yashima, E., *Angew. Chem. Int. Ed.* **2007**, *46* (31), 5885-8.
88. Maayan, G.; Ward, M. D.; Kirshenbaum, K., *PNAS* **2009**, *106* (33), 13679-13684.
89. Brown, R. A.; Diemer, V.; Webb, S. J.; Clayden, J., *Nat. Chem.* **2013**, *5* (10), 853-60.
90. Bryden A. F. Le Bailly, L. B., and Jonathan Clayden, *Angew. Chem. Int. Ed.* **2016**, *55*, 2132-2136.
91. Sohtome, Y.; Nagasawa, K., *Chemphyschem* **2011**, *12* (12), 2217-9.
92. Ke, Y. Z.; Nagata, Y.; Yamada, T.; Sugimoto, M., *Angew. Chem. Int. Ed.* **2015**, *54* (32), 9333-7.
93. Deng, J.; Zhao, B.; Deng, J., *Ind. Eng. Chem. Res.* **2016**, *55* (27), 7328-7337.
94. Tang, Z.; Iida, H.; Hu, H.-Y.; Yashima, E., *ACS Macro Lett.* **2012**, *1* (2), 261-265.
95. Gellman, S. H., *Acc. Chem. Res.* **1998**, *31*, 173-180.
96. Guichard, G.; Huc, I., *Chem. Commun.* **2011**, *47* (21), 5933-41.
97. Douat, C.; Aisenbrey, C.; Antunes, S.; Decossas, M.; Lambert, O.; Bechinger, B.; Kichler, A.; Guichard, G., *Angew. Chem. Int. Ed. Engl.* **2015**, *54* (38), 11133-7.
98. Teyssieres, E.; Corre, J. P.; Antunes, S.; Rougeot, C.; Dugave, C.; Jouvion, G.; Claudon, P.; Mikaty, G.; Douat, C.; Goossens, P. L.; Guichard, G., *J. Med. Chem.* **2016**, *59* (18), 8221-32.
99. Sun, J.; Zuckermann, R. N., *ACS Nano* **2013**, *7* (6), 4715-4732.
100. Collie, G. W.; Pulka-Ziach, K.; Lombardo, C. M.; Fremaux, J.; Rosu, F.; Decossas, M.; Mauran, L.; Lambert, O.; Gabelica, V.; Mackereth, C. D.; Guichard, G., *Nat. Chem.* **2015**, *7* (11), 871-8.
101. Jewginski, M.; Granier, T.; Langlois d'Estaintot, B.; Fischer, L.; Mackereth, C. D.; Huc, I., *J. Am. Chem. Soc.* **2017**, *139* (8), 2928-2931.
102. Johnson, L. M.; Gellman, S. H., *Methods Enzymol.* **2013**, *523*, 407-29.
103. Lautrette, G.; Wicher, B.; Kauffmann, B.; Ferrand, Y.; Huc, I., *J. Am. Chem. Soc.* **2016**, *138* (32), 10314-22.
104. Chandramouli, N.; Ferrand, Y.; Lautrette, G.; Kauffmann, B.; Mackereth, C. D.; Laguerre, M.; Dubreuil, D.; Huc, I., *Nat. Chem.* **2015**, *7* (4), 334-341.
105. Diemer, V.; Fischer, L.; Kauffmann, B.; Guichard, G., *Chem. Eur. J.* **2016**, *22* (44), 15684-15692.
106. Jørgensen K. A.; Johannsen M.; Yao S.; Audrain H.; Thorauge J., *Acc. Chem. Res.* **1999**, *32*, 605-613.
107. Malerich J. P.; Hagihara K.; Rawal V. H., *J. Am. Chem. Soc.* **2008**, *130*, 14416-14417.

CHAPTER II

CHAPTER II

2.1 DESIGN OF A FOLDAMER-BASED CATALYTIC SYSTEM.....	60
2.1.1 Description of oligourea foldamers.....	60
2.1.2 How to take advantage of oligourea foldamer backbone to design an efficient catalyst?	61
2.1.3 Synthesis of an oligourea catalyst.....	63
2.1.3.1 Synthesis of building blocks for oligourea synthesis.....	63
2.1.3.2 Synthesis of oligourea model catalyst 1a	63
2.1.4 Evaluation of the catalytic potential of oligourea 1a	65
2.1.4.1 Fundamental result through the development of a model reaction	65
2.1.4.2 Comparison with Takemoto catalyst.....	65
2.1.4.3 How to enhance the reactivity and enantioselectivity with the foldamer catalytic system?.....	66
2.2 COMPARISON BETWEEN UREA VS THIOUREA IN THE MODEL SEQUENCE.....	68
2.2.1 Structural comparison between urea and thiourea versions of the catalyst.....	68
2.2.2 Difference of catalytic activity between urea and thiourea catalysts	69
2.3 IMPACT OF THE HELICAL CONFORMATION ON CATALYST EFFICACY.....	70
2.3.1 Strategy to demonstrate the role of the helicity on catalyst efficiency	70
2.3.2 Structural studies of the catalyst with different chain lengths	71
2.3.3 Catalytic evaluation of the oligoureas with different chain lengths.....	73
2.3.4 Screw sense inversion: Synthesis of <i>ent-1a</i>	75
2.4 INFLUENCE OF EXTERNAL PARAMETERS ON THE OUTCOME OF THE CATALYSED REACTION	77
2.4.1 Influence of the solvent.....	77
2.4.2 Impact of the temperature	78
2.5 POTENTIAL BENEFITS OF A SYNERGISTIC CATALYTIC SYSTEM	80
2.5.1 Looking for the minimum catalyst loading.....	80
2.5.2 Play on the base loading	81
2.5.3 Play on the nature of the base	82
2.5.4 Possibility of match/mismatch effect with chiral bases	83

2.1 DESIGN OF A FOLDAMER-BASED CATALYTIC SYSTEM

2.1.1 Description of oligourea foldamers

Guichard *et al.* have focused their research efforts in the area of oligourea foldamers. Oligourea foldamers are analogues of peptides with γ -amino acid derivatives. They are easily synthesized from amino-acid derivatives through an iterative synthesis.¹ They adopt a 2.5-helical structure from very short sequences: four residues offer five ureas, which is enough for the intramolecular hydrogen-bonding network to confer a helical conformation (Figure II.1).² The backbone is rigidified compared to γ -peptides and the helix stabilization is enhanced. The three-centered H-bonding between C=O (i+3) and urea NH (i) and N'H (i+1) (Figure II.2a), closing 12- and 14-membered pseudoring, is revealed by crystallographic structure and NOESY experiments (Figure II.2b and c).³ Interestingly, the helicity is independent of the nature of lateral side chains. By NMR spectroscopy, the two carbons in the α -position are not equivalent, and the difference between the two chemical shifts defines the diastereotopicity of the residue and is characteristic of the helicity of the foldamer. By circular dichroism experiments, the oligourea 2.5-helix signature corresponds to a maximum band at 203 nm, zero-crossing at 193 nm and a minimum band at 188 nm in trifluoroethanol⁴ (Figure II.2d).

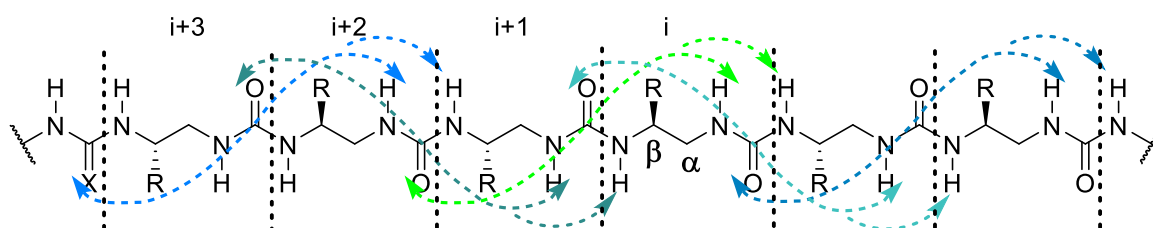


Figure II.1: Oligourea foldamers and hydrogen-bonding framework

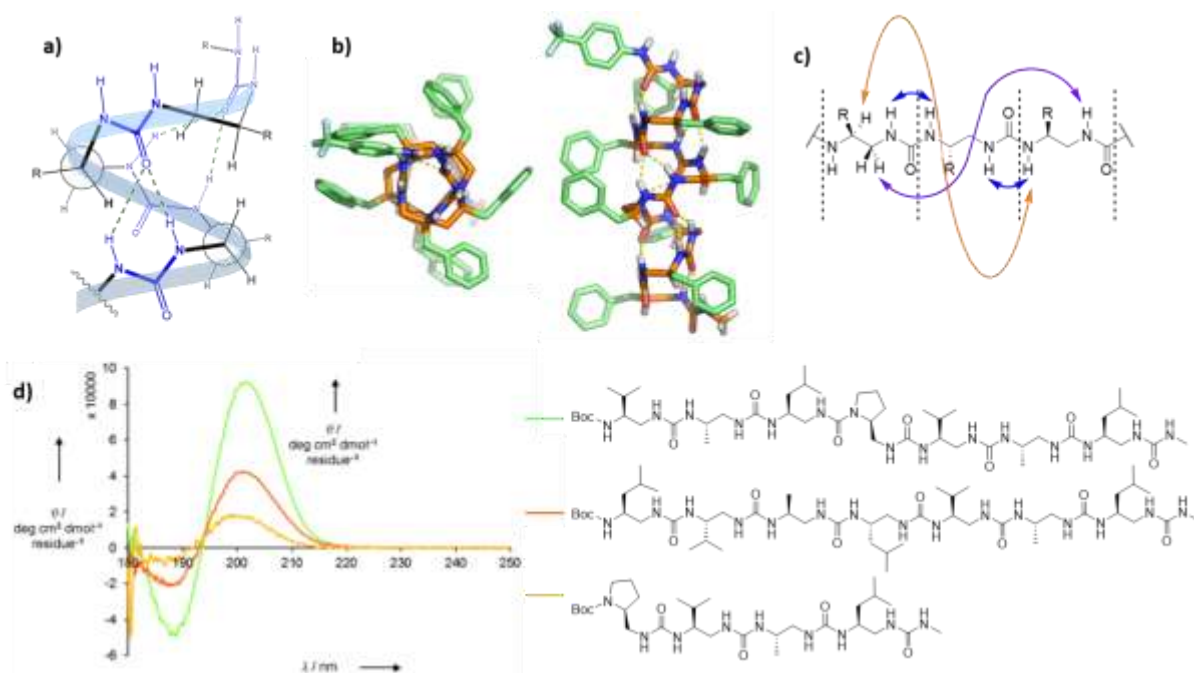


Figure II.2: a) Representation of the three-centered H-bonding. b) X-ray structure of urea oligomers with top view and side view. c) NOE connectivities in oligourea foldamers. d) Circular Dichroism spectra of oligourea foldamers in trifluoroethanol with increase of the length.

Because of their well-structured helical conformation, their ease of synthesis, the possible cooperative effect of the hydrogen-bond network and potential for insertion of a thiourea motif, oligourea foldamers are potentially very interesting organocatalysts. Guichard *et al.* demonstrated the ability of helical oligomers to recognize and complex anions.⁵ The helical conformation is not disturbed by this interaction so we can consider the potential to perform an enantioselective reaction with this system.

2.1.2 How to take advantage of oligourea foldamer backbone to design an efficient catalyst?

N,N'-linked oligoureas are synthetic oligomers derived from natural or unnatural amino acids. The hydrogen bond network described previously (see 2.1.1) confers a helical conformation with 2.5 residues per turn. Four residues and five ureas have been found to be sufficient for the three-centered H-bond pattern between the ureas to develop intramolecularly resulting in helical folding.⁴ The two first ureas at the "N-terminus" of the oligourea sequence are thus free to act as hydrogen-bond donor with external hydrogen-bond acceptor (Figure II.3a). Moreover, the cooperative formation of a directional hydrogen-bond network all along the foldamer confers to it a macrodipole with the two free H-bond donor ureas located close to its positive pole (Figure II.3b). To design a potential catalyst, a 6 residue-sequence with aliphatic (*S*)-configuration side chains isopropyl, methyl and isobutyl, known to present a stable helical conformation in polar and apolar solvent was chosen.⁶ To reinforce the polarity and the

polarizability of the first urea group, a 3,5-bis(trifluoromethyl)phenyl group was attached on the N-terminus part.⁷ The resulting oligomer thus constitutes the first potential catalyst **1a** we intended to evaluate. Inspired by the importance of carbon-carbon formation in industrial and academic chemistry research and the successful developments of bifunctional catalysts acting as hydrogen bond donor described in literature,⁸⁻¹³ we decided to test the catalytic efficiency of **1a** in Michael addition reactions. The bifunctional character of the chiral foldamer scaffold is brought in an innovative way by the two first ureas and without any internal base. To deprotonate the pronucleophile, a catalytic amount of a Brønsted base (e.g. tertiary amine) has to be added. The X-ray structure of oligomer **1a** (CCDC 1534525) proves the helical conformation and the right-handed (*P*)-helicity (Figure II.3c).

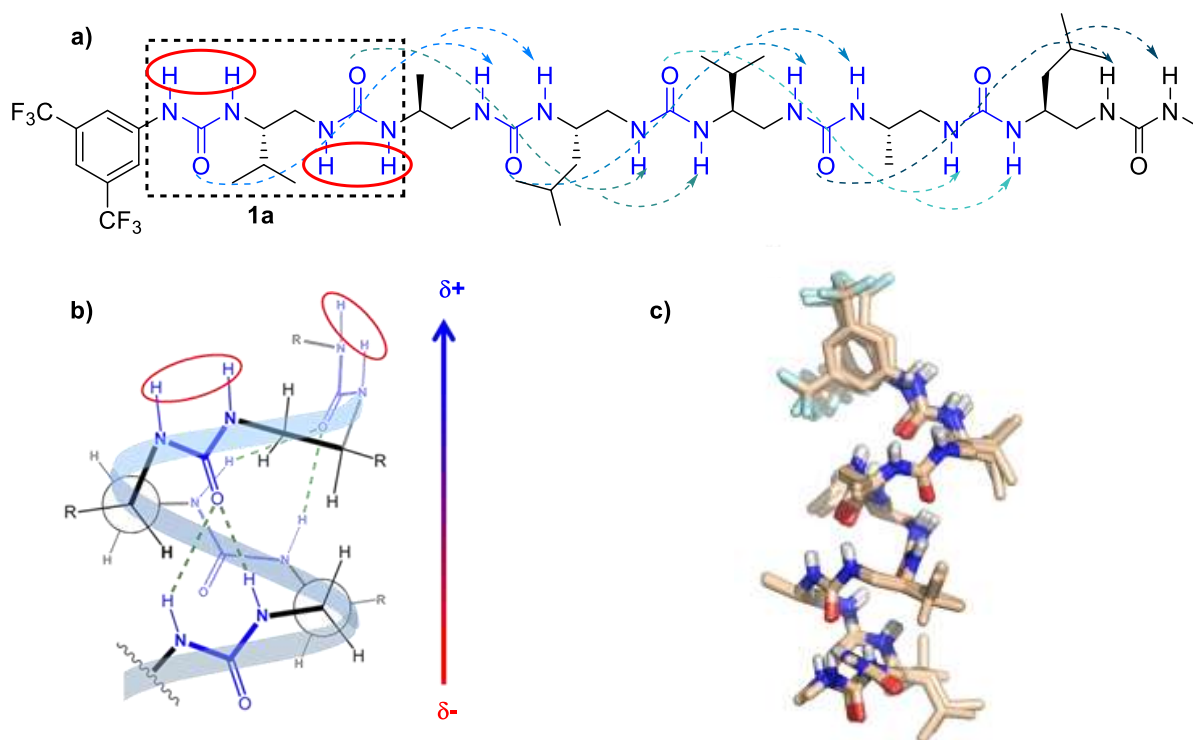
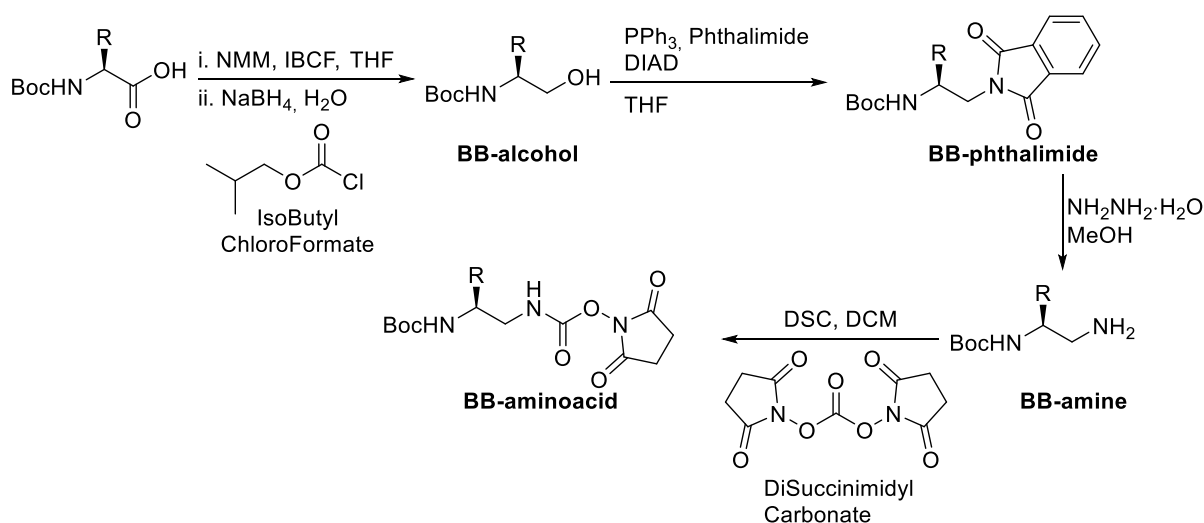


Figure II.3: Design of potential candidate *N,N'*-oligourea foldamer catalyst
 a) Availability of the two ureas at the *N*-terminus part of the oligourea. b) Macrodipole of the oligourea helix. c) X-ray structure of oligomer **1a**.

2.1.3 Synthesis of an oligourea catalyst

2.1.3.1 Synthesis of building blocks for oligourea synthesis

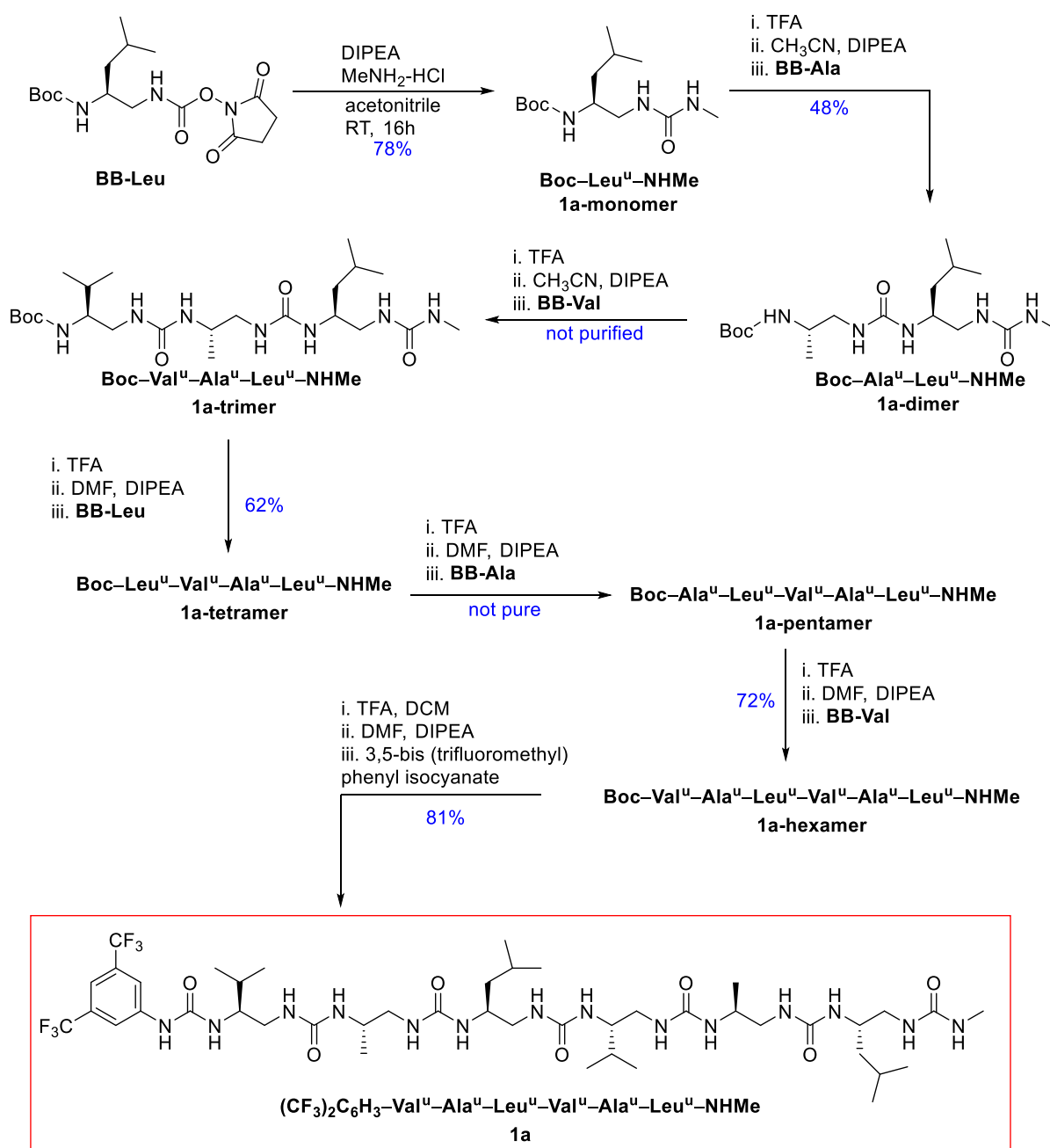
To synthesize oligoureas, amino acids, natural or unnatural, are first transformed to the corresponding 1,2-diamino ethane derivatives which are then activated as succinimidyl carbamates (Scheme II.1)¹⁴. The carboxylic acid is firstly reduced to an alcohol **BB-alcohol** by activation with isobutylchloroformate and treatment of the resulting anhydride with NaBH₄. In a second step, a phthalimide group was installed by a Mitsunobu reaction to form **BB-phthalimide**. The resulting mono-protected 1,2-amine **BB-amine** was obtained by hydrazinolysis. The final step to form the building block **BB-aminoacid** is the activation by coupling with disuccinimidyl carbonate.



Scheme II.1: General procedure of the preparation of building blocks for oligourea synthesis

2.1.3.2 Synthesis of oligourea model catalyst **1a**

The oligomer **1a** was synthesized by an iterative methodology from succinimidyl-activated monomers **BB-aminoacid** by successive deprotection and coupling steps (Scheme II.2). The final capping step with 3,5-bis (trifluoromethyl)phenyl isocyanate activates the catalyst by increasing the acidity of the first urea NHs, thus contributing to further differentiate the H-bond donor capacities of the first two ureas. Because of the high propensity of the intermediates to crystallize, almost the full synthesis was performed with trituration as purification steps and only the final product was purified by flash chromatography. All other oligomer catalysts reported in this work have been synthesized with the same strategy, by adapting the nature of monomers according to the sequence.

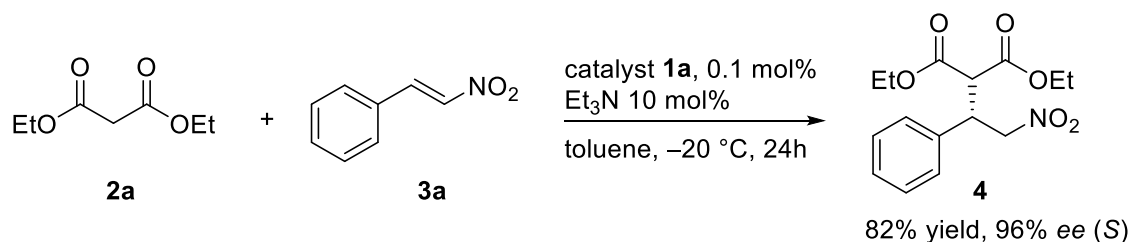


Scheme II.2: General synthesis of oligourea catalyst **1a**

2.1.4 Evaluation of the catalytic potential of oligourea **1a**

2.1.4.1 Fundamental result through the development of a model reaction

The conjugate addition of diethyl malonate esters (e.g. **2**) to nitroalkenes (e.g. **3**) was chosen as a model reaction to test our foldamer catalyst **1a**. It yields to the formation of γ -nitro carbonyl adducts (e.g. **4**), which are versatile intermediates through the rich chemistry of the nitro group¹⁵ and also precursors of pharmaceutical compounds.¹⁶ Because our catalytic system is activated by hydrogen bond interactions, toluene was selected as an aprotic and apolar solvent as a model solvent. Temperature was initially decreased as $-20\text{ }^{\circ}\text{C}$ to limit entropic effect and maximise enantioselectivity. Because oligourea **1a** is only sparingly soluble in toluene, even more at low temperature, it was decided to decrease its concentration from the classical 10 mol% commonly employed with other bifunctional organocatalysts to 0.1 mol%. Because the tertiary amine base is external and its loading can thus be different from the one of the chiral component, the base loading was fixed at 10 mol%. Under these conditions, the adduct **4** was obtained with a very good yield (82%) and with an excellent enantioselectivity (96% *ee*). The catalyst **1a**, synthesized with natural amino acids (L), led to the formation of the adduct (*S*)-**4** (Scheme II.3).

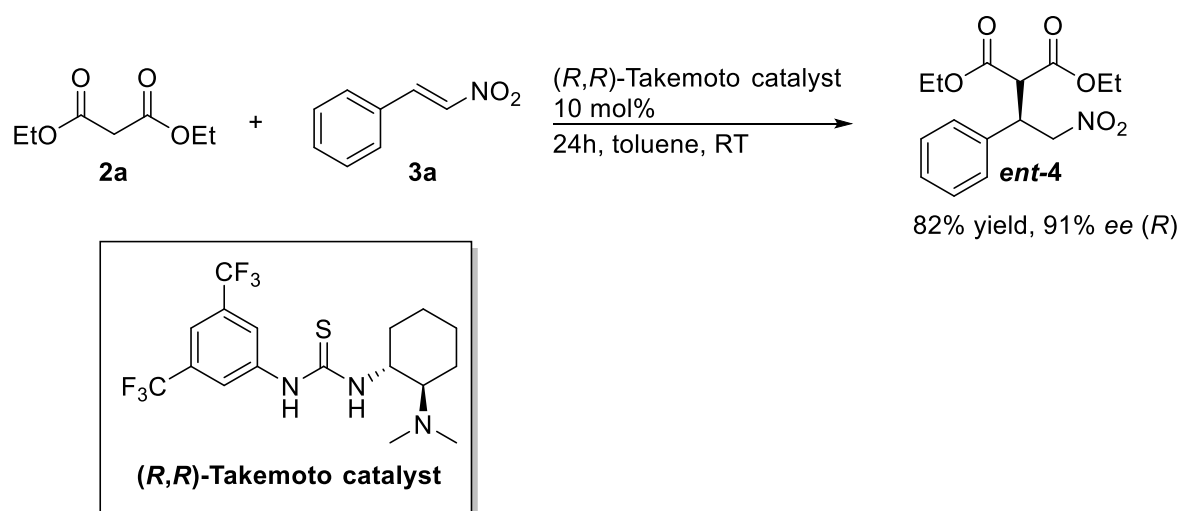


Scheme II.3: Model asymmetric Michael addition to evaluate the catalytic potential of oligomer **1a**

In a subsequent study (see 2.5), the impact of the base loading was evaluated.

2.1.4.2 Comparison with Takemoto catalyst

To compare our results with those from literature (Scheme II.4) and evaluate the potential of our system, we selected (*R,R*)-Takemoto's catalyst and repeated the reaction between **2a** and **3a** under conditions reported by Takemoto in his seminal paper (Table II.1).¹⁷⁻¹⁸



Scheme II.4: Conjugate addition of 2a on 3a with (R,R)-Takemoto catalyst

The results obtained by our group (Entry 1, Table II.1) were similar to those published by the Takemoto group.¹⁷ This catalyst was next evaluated at 0.1 mol% loading (Entry 2, Table II.1): the conversion was almost non-existent and the enantioenrichment decreased. The addition of external triethylamine accelerated the reaction (Entry 3, Table II.1). Nevertheless, it remained slower than the published conditions with 10 mol% of catalyst, which demonstrates the positive cooperative effect on the reaction kinetics of the internal amine and the activating thiourea in the bifunctional Takemoto catalyst. Moreover, the enantioselectivity was highly impacted: the kinetics of the racemic reaction overcomes the enantioenriched one. Overall, these results demonstrate the limited efficacy of Takemoto catalyst at low loading, and that it is not possible to compensate for the low Takemoto catalyst loading by adding an external base.

Table II.1: Evaluation of our catalytic conditions on the addition of 3a on 2a catalysed with Takemoto catalyst

Entry	Loading (mol%)	Base (mol%)	Conversion (%) ^[a]	Yield (%) ^[b]	ee (%) ^[c]
1	10	0	100	86	93
2	0.1	0	7	4	80
3	0.1	10	56	43	29

Reaction conducted on 0.67 mmol scale in 0.67 mL toluene, at RT for 24h. Mol ratio (**2a:3a**, 2:1) [a] Determined by ¹H NMR spectroscopy [b] Isolated compound after chromatographic purification [c] Determined by chiral HPLC analysis. Absolute configuration (*R*) was known and assigned by analogy.

2.1.4.3 How to enhance the reactivity and enantioselectivity with the foldamer catalytic system?

Our first results highlight the high efficiency of the designed oligourea catalyst and the synergistic action with an external Brønsted base (Figure II.4). The background reaction which takes place in the absence of the chiral catalyst leading to a racemic mixture has to be considered in parallel of the catalysed reaction leading to enantioenriched mixture. The control of the kinetic and thermodynamic balance between these two processes is essential to reach good yields and selectivities.

The structure of the catalytic system as well as all external parameters have to be considered. To what extent is the helicity of the oligoureia is involved? Would a thiourea moiety be suitable at the N-terminus and what would be its impact on catalytic activity? How do the nature and the quantity of the external base affect the catalytic process in comparison to the classical internal base found in bifunctional catalysts? How do the external parameters such as temperature and solvent influence the enantiocontrol? All these questions will be studied in the following of this chapter.

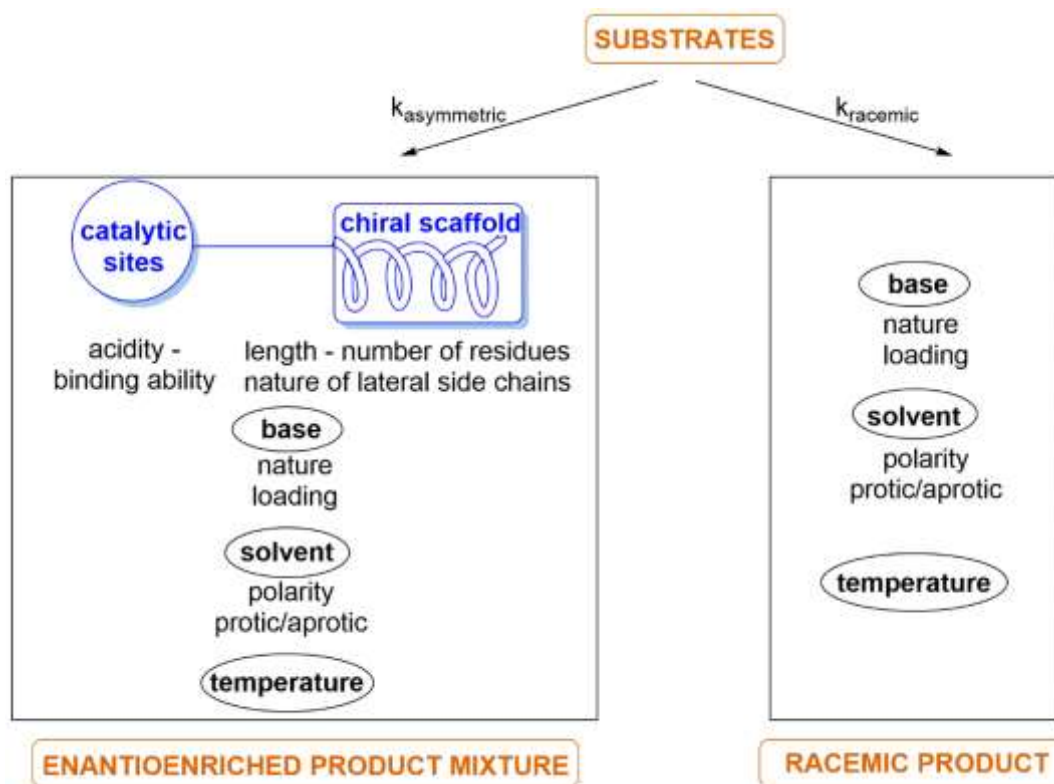


Figure II.4: Competition between background reaction and foldamer catalysed reaction and parameters which can be optimized to enhance the later.

2.2 COMPARISON BETWEEN UREA VS THIOUREA IN THE MODEL SEQUENCE

2.2.1 Structural comparison between urea and thiourea versions of the catalyst

Incorporation of a thiourea moiety at the N-terminal side of the foldamer could increase the acidity of the site which interacts with the substrates and then enhance the catalytic efficiency. The structural consequences of replacing a urea linkage by a thiourea moiety at different positions (but not the first one) in the sequence of an oligourea have been investigated previously by our group.¹⁹ Here TFA treatment of **1a-hexamer**, the free amino group of the oligourea hexamer was treated with 3,5-bis(trifluorophenyl)isothiocyanate to give the catalyst **5a**. Its (*P*)-helicity was proven by X-ray crystallographic analysis (Figure II.5, in white). The head of the helix is the most impacted element because of the variation of the length of the first intramolecular hydrogen bond between the terminal C=X and the NHs of the third urea group (the C=X...N distance increases from an average 2.90 Å in **1a** to 3.42 Å distance in **5a**), which results in a slight rearrangement of the first residue and of the 3,5-bis(trifluoromethyl)phenyl moiety. The chemical synthesis of **5a** is very similar to that of **1a**, except for the purification of the last step which is more difficult because of the formation of side products during formation of thiourea motif.

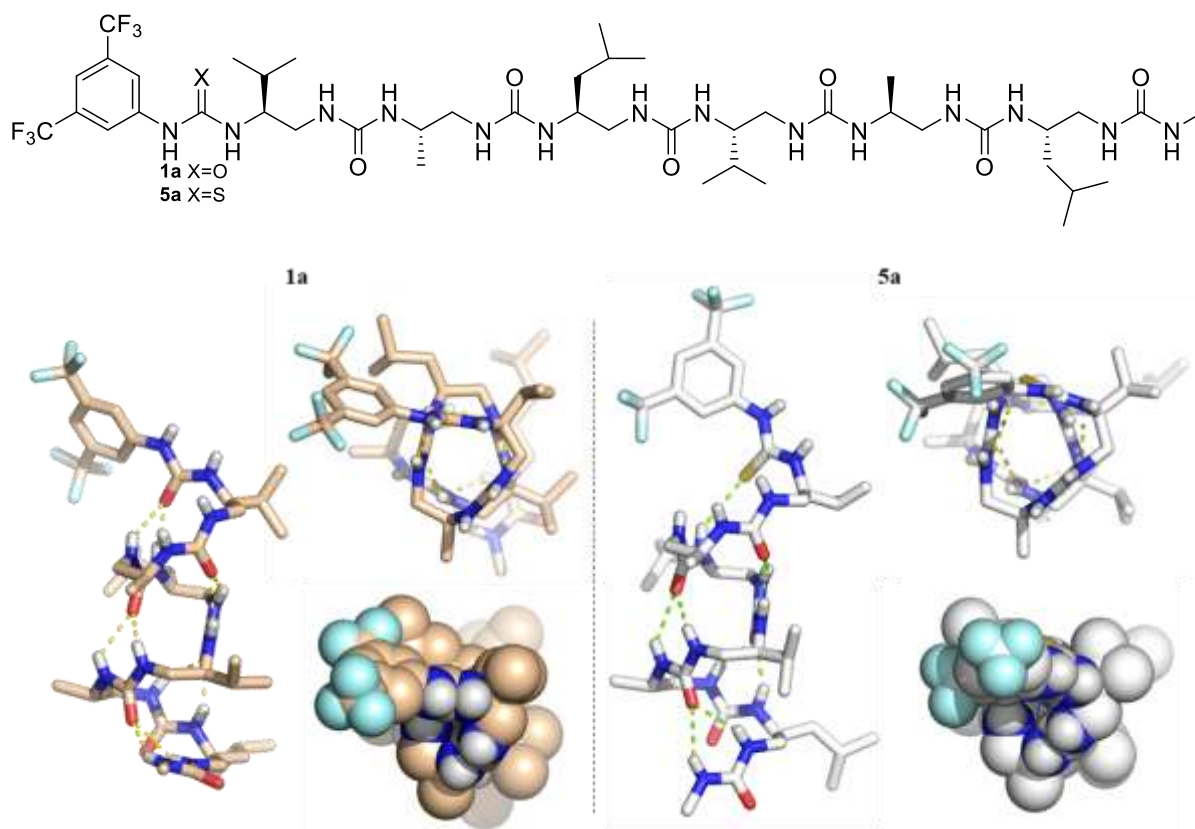


Figure II.5: Structural comparison between urea hexamer foldamer catalyst **1a** and thiourea hexamer foldamer catalyst **5a**

The perturbation of the helix geometry was also observed by NMR. The backbone CH₂^α protons are not equivalent and their differences of chemical shift represent a useful indicator of helix formation. This anisochronicity has been measured for **1a** and **5a** and is reported for every residue in the table below (Table II.2). The helix is locally perturbed at the N-terminus where the thiourea has been inserted, and the extent of the perturbation is more pronounced on residues 1 and 2.

Table II.2: Difference of anisochronicity of backbone CH₂^α protons between urea catalyst **1a** and thiourea catalyst **5a**

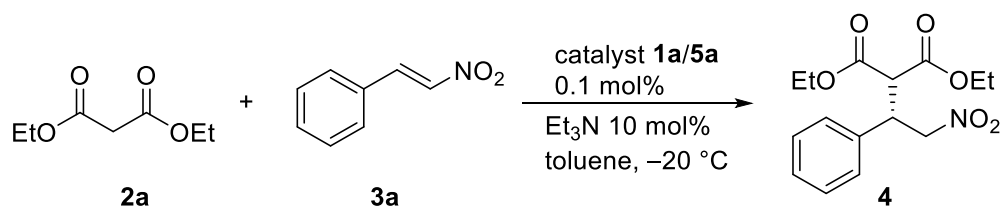
	$\Delta\delta$ (ppm)*					
	res.1	res.2	res.3	res.4	res.5	res.6
1a	1.00	1.28	1.34	1.27	1.20	0.95
5a	0.55	0.97	1.20	1.22	1.19	0.91

*Determined by NMR spectroscopy at 20 °C in CD₃OH.

2.2.2 Difference of catalytic activity between urea and thiourea catalysts

The catalytic potential of **5a** was evaluated with the model Michael addition in comparison with **1a**, at -20 °C, for 24h and 48h. The thiourea catalyst systematically slightly slower in terms of conversion and the observed enantioselectivities are slightly decreased compared to the urea version (Table II.3). The small structural reorganization observed by X-ray and NMR could justify this observation. This result together with the finding that coupling of terminal aromatic isocyanate is cleaner than for the corresponding isothiocyanate, catalyst **1a** was selected for all further studies.

Table II.3: Comparison between urea and thiourea hexamer catalyst, respectively **1a** and **5a**



Catalyst	Reaction time	Conversion (%)	Yield (%)	ee (%)
1a	48	100	80	95
	24	99	63	94
5a	48	99	82	93
	24	94	59	88

Reactions were performed with 0.67 mmol of **3a** and 1.34 mmol of **2a**. Yields correspond to isolated compound after chromatographic purification. The enantiomeric excess (*ee*) was determined by chiral HPLC analysis. Absolute configuration (*R*) was known and assigned by analogy.

2.3 IMPACT OF THE HELICAL CONFORMATION ON CATALYST EFFICACY

2.3.1 Strategy to demonstrate the role of the helicity on catalyst efficiency

Examples of folded catalysts mentioned in the previous chapter (e.g. DNA-based catalysts from Roelfes and Feringa, peptidic β -turns from Scott Miller, peptoid catalysts from Maayan) support a direct relationship between folding propensity and catalytic activity. Berkessel synthesized L-leucine oligomers from 1 to 20 residues and reported that the catalytic potential of each peptide in Juliá-Colonna epoxidation depends on its helix forming ability.²⁰ To test the chain length dependence of oligourea catalysts,²¹ we have prepared two series of oligo(thio)ureas varying in length and bearing either a 3,5-bis(trifluoromethyl) phenylurea or a 3,5-bis(trifluoromethyl) phenylthiourea termination. To evaluate only the impact of the oligourea length, the sequences were carefully designed to preserve the isopropyl lateral side-chain between the two first ureas (Figure II.6). The trimer versions of the catalyst were not evaluated because they were very insoluble and their purifications were not successful. This can be rationalized by the fact that a tri-urea, although it corresponds to the minimum number of ureas necessary to stabilize one helical turn, may also tend to unfold and form large and insoluble intermolecular aggregates.

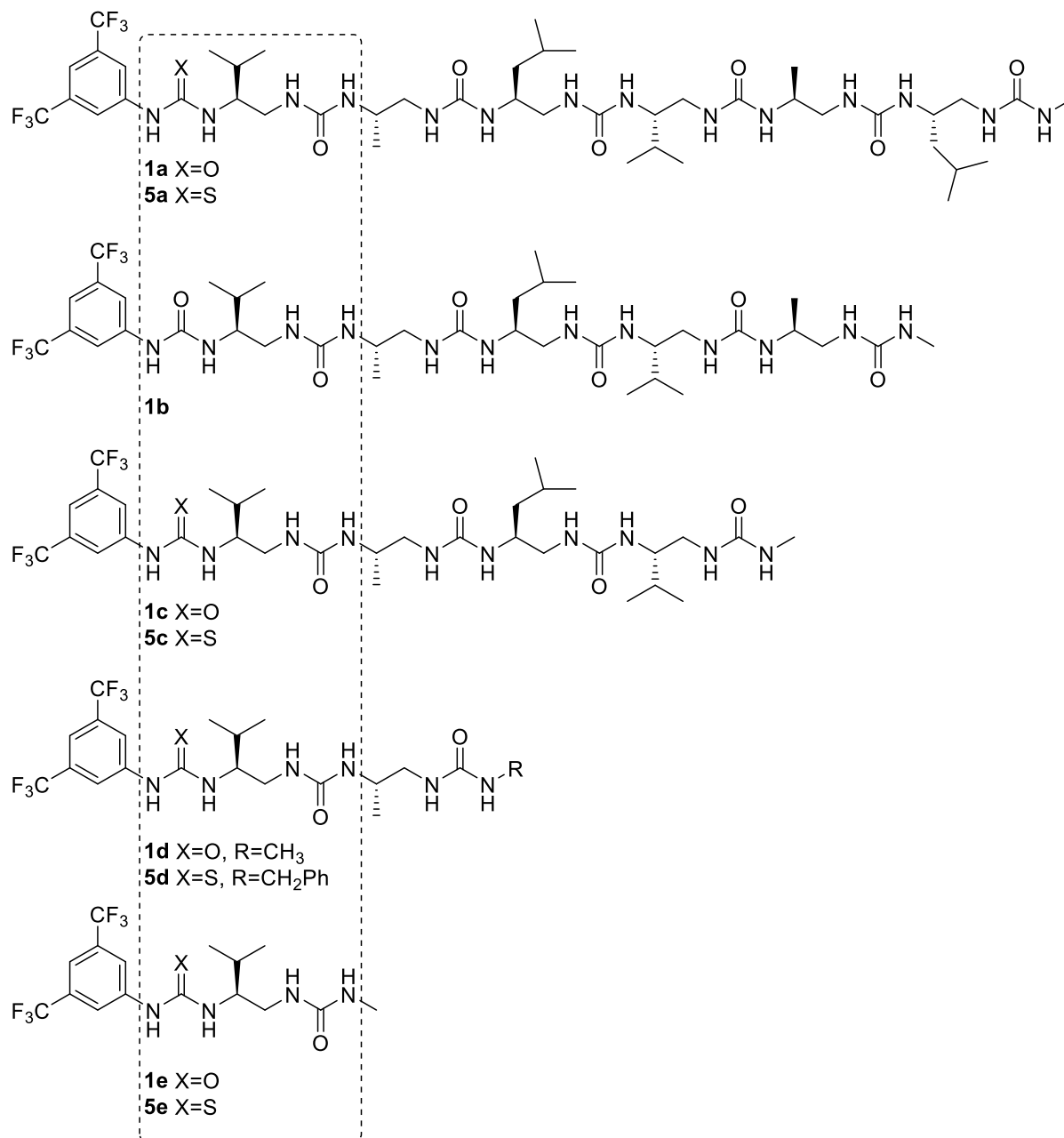


Figure II.6: Structures of catalysts with different chain lengths, in urea version **1a-e** and in thiourea version **5a-e**

2.3.2 Structural studies of the catalyst with different chain lengths

The longer is the oligourea chain length, the longer and stronger is the hydrogen bond network, and the more stable is the helical conformation. The increased helicity of oligoureas as a function of chain length has been studied in depth in earlier studies³⁻⁴ and can be determined by circular dichroism experiments (Figure II.7). The monomer **1e** and dimer **1d** are not helically folded. Helix formation appears for tetramer **1c** and keeps increasing up to hexamer **1a**. Measurement of anisochronicity of

CH_2^α also support helix stabilization with increasing chain length (Table II.4). For each chain length, the difference of anisochronicity between urea and thiourea catalysts is particularly significant on the first two residues and reflects the perturbation of the helicity resulting from thiourea replacement (Table II.5).

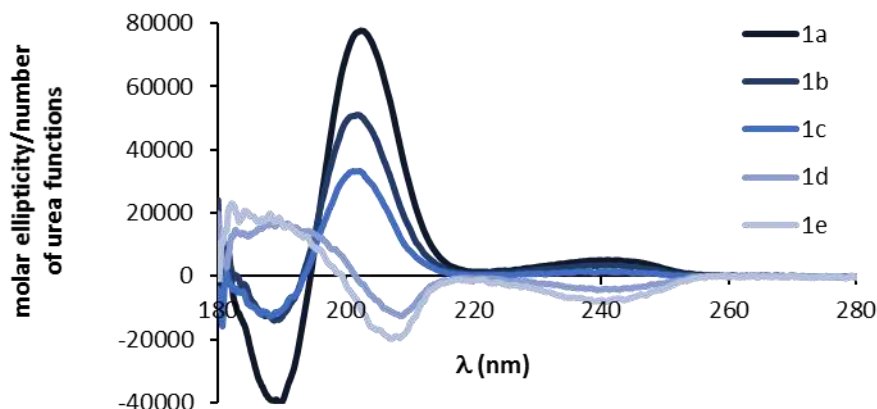


Figure II.7: Electronic circular dichroism (ECD) analysis of oligoureas **1a-1e** in trifluoroethanol. Molar residual ellipticity in $\text{deg.cm}^2.\text{dmol}^{-1}.\text{residue}^{-1}$.

Table II.4 : Anisochronicity of CH_2^α for the various chain lengths of urea catalysts **1a-1e**

Entry	Compounds	Res. 1	Res. 2	Res. 3	Res. 4	Res. 5	Res. 6
1	1e (1 res.)	0.06	/	/	/	/	/
2	1d (2 res.)	0.23	0.28	/	/	/	/
3	1c (4 res.)	0.96	1.19	1.22	0.99	/	/
4	1b (5 res.)	0.92	1.09	1.11	1.02	0.35	/
5	1a (6 res.)	1.00	1.28	1.34	1.27	1.20	0.95

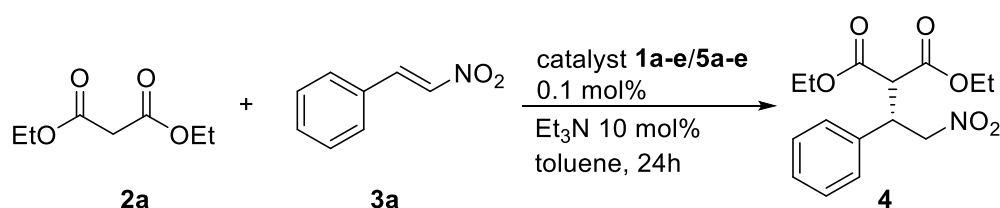
Table II.5: Anisochronicity of CH_2^α for the various chain lengths of thiourea catalysts **5a-5e**

Entry	Compounds	Res. 1	Res. 2	Res. 3	Res. 4	Res. 5	Res. 6
1	5e (1 res.)	0	/	/	/	/	/
2	5d (2 res.)	0.17	0.19	/	/	/	/
3	5c (4 res.)	0.83	0.91	1.02	0.99	/	/
4	5a (6 res.)	0.55	0.97	1.20	1.22	1.19	0.91

2.3.3 Catalytic evaluation of the oligoureas with different chain lengths

The compounds **1a-1e** and **5a-5e** were tested for the conjugate addition of **2a** to **3a**, with 0.1 mol% in oligomer and 10 mol% in Et₃N. Because the relative solubilities of these compounds were not known, reactions were performed at RT (Entries 1-5, Table II.6) and 60 °C (Entries 10-14, Table II.6) for the urea series, to be sure that the observed trend was due to the oligomer structure and not to the insolubility of some these new compounds.

Table II.6: Impact of the oligo(thio)urea chain length on catalysis



Entry	Catalyst	T (°C)	Conversion (%)	Yield (%)	ee (%)
1	1a	RT	98	72	89
2	1b	RT	98	83	87
3	1c	RT	57	47	36
4	1d	RT	57	44	6
5	1e	RT	72	55	5
6	5a	RT	94	74	86
7	5c	RT	87	71	64
8	5d	RT	70	40	14
9	5e	RT	58	28	5
10	1a	60 °C	100	73	75
11	1b	60 °C	100	76	76
12	1c	60 °C	82	58	34
13	1d	60 °C	88	58	5
14	1e	60 °C	93	58	3

Reaction conducted on 0.67 mmol scale in 0.67 mL toluene with 0.1 mol% in catalyst, with Et₃N 10 mol%, for 24h. Ratio mol (**2a**:**3a**, 2:1). Determined by ¹H NMR spectroscopy. Isolated compound after chromatographic purification. Determined by chiral HPLC analysis.

The measured enantiomeric excesses of adduct **4** can be interestingly linked to **1a-e** and **5a-e** structures (Figure II.8). For urea and thiourea versions, enantioenrichment becomes significant at the tetramer level, when the helical conformation starts to form. There is almost no enantio-control in the presence of monomers **1e** and **5e** (Entries 5 and 9, Table II.6) and dimers **1d** and **5d** (Entries 4 and 8, Table II.6) and the highest reactivity and selectivity (respectively 94-98% and 86-89 % *ee*) are obtained for helically folded pentamers and hexamers (**1a** > **1b** > **5a**, Entries 1, 2 and 6, Table II.6). For the folded tetramers **1c** and **5c**, conversions were intermediate and enantioselectivities were significantly

higher for the thiourea than the urea. This can be rationalised by its higher acidity which may compensate for the helical destabilization due to the presence of a thiocarbonyl H-bond acceptor. However, the contribution of the thiourea moiety becomes minor when the helical conformation is well-defined such as in **1a** and **5a**, as both catalysts are almost equipotent (see 2.2).

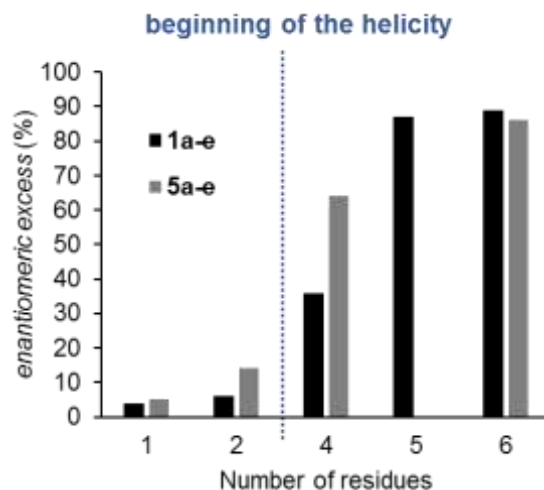


Figure II.8: Enantiomeric excess of the Michael adduct **4** determined by chiral HPLC analysis after purification for reactions conducted in the presence of **1a-e** and **5a-e**. Reactions were performed at RT for 24h, with 0.1 mol% catalyst, 10 mol% Et₃N, on 0.67 mmol scale.

An X-ray crystal structure of pentamer **1b** was obtained. This oligomer is fully helical in the crystal and an overlay with the structure of **1a** (Figure II.9) by fitting the first five pairs of carbonyl C atoms indicates a very close match between the two helices including at the active site (root-mean-square deviation (RMSD) = 0.150 Å). This observation explains the very close catalytic behaviour of both oligoureases **1a** and **1b** although the intensity of their CD profile differs substantially.

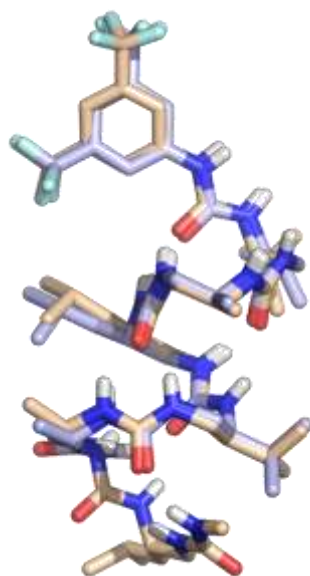


Figure II.9: Structural alignment of the crystal structures of **1a** (carbon atoms in sand) and **1b** (carbon atoms in light blue)

2.3.4 Screw sense inversion: Synthesis of *ent-1a*

The enantiomer of **1a** was synthesised and characterized by circular dichroism (Figure II.10). Whereas **1a** was synthesised from monomers derived from L-amino acids, *ent-1a* was synthesised in the same way, with activation of D-amino acids and the same couplings as previously described. As expected, their circular dichroism spectra were perfectly symmetrical and the enantiomers obtained by the Michael addition of **2** to **3** are opposite according to the helix-sense of the catalyst. The (*P*)-helix **1a** catalyses the formation of the (*R*) enantiomer while the (*M*)-helix of *ent-1a* catalyses the formation of the (*S*)-enantiomer (Figure II.10).

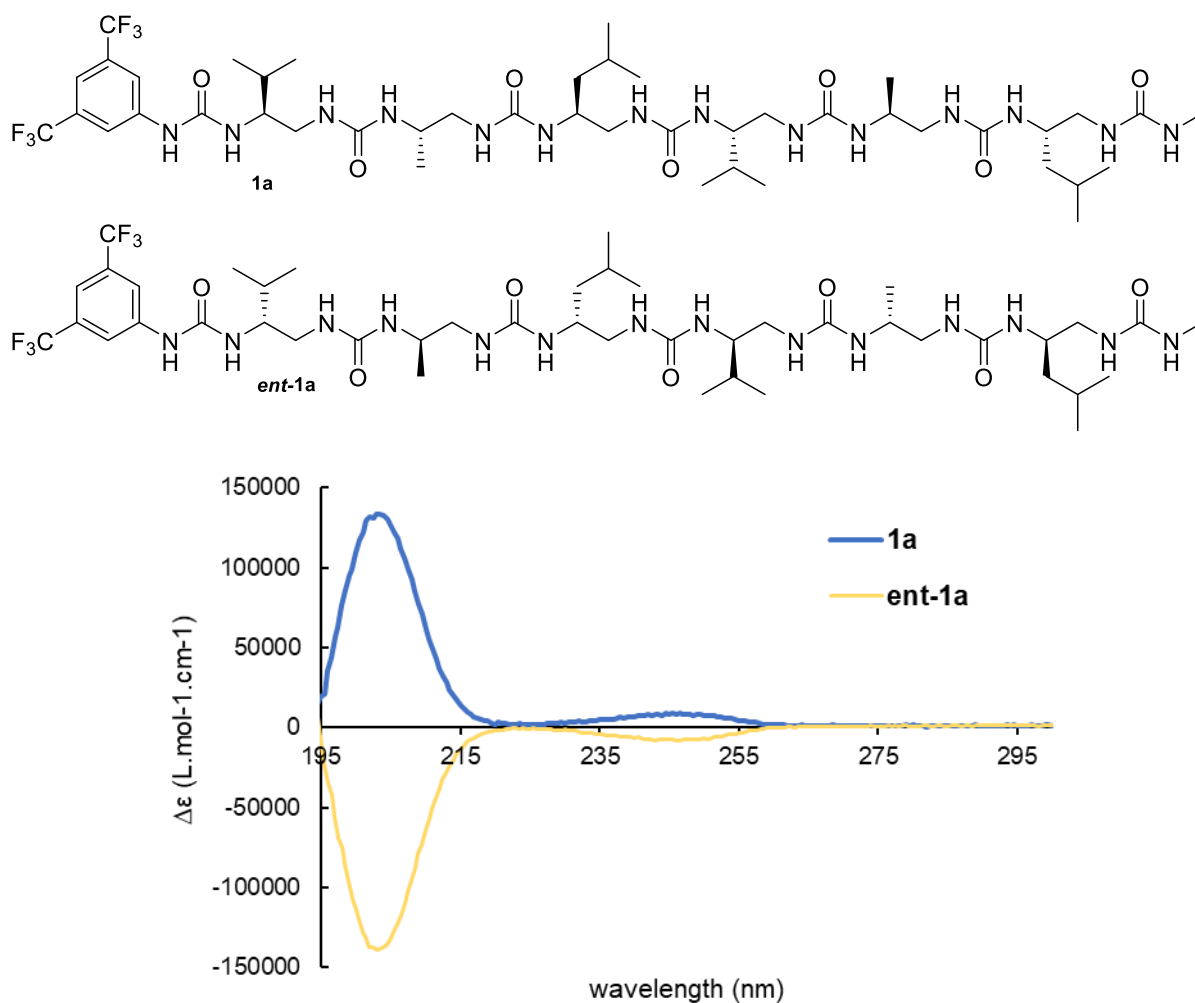
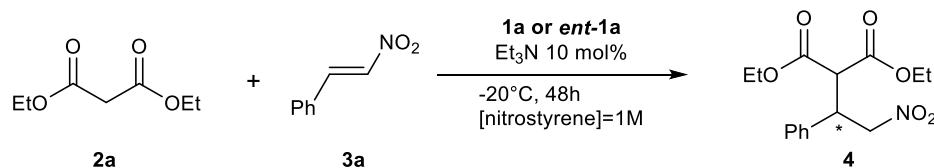


Figure II.10: Reverse helicity for enantiomers **1a** and *ent-1a*

Table II.7: Enantioselective conjugate addition of diethylmalonate to nitrostyrene catalysed by **1a** and its enantiomer **ent-1a**



Entry	Catalyst	Loading (mol %)	Conversion (%)	Yield (%)	ee (%)
1	1a	0.1	100	86	95 (<i>S</i>)
2	ent-1a	0.1	100	84	95 (<i>R</i>)

Conversions were determined by ^1H NMR. Yields were determined after purification on Silica Gel Chromatography. Enantiomeric excesses were determined with Chiral HPLC and absolute configurations were obtained from literature.

Overall, the results obtained in sections 2.2 and 2.3 provide a first rationale for the design of oligoureia-based catalysts: a well-defined helical conformation is required for efficient stereocontrol in the catalytic process at very low loading. Very short sequences such as di-ureas (one monomer unit) and tri-ureas (two monomer units) also catalyse the reaction albeit less effectively in terms of conversion and without stereocontrol. It is likely that much higher loading such as 10 mol% would be needed to reach higher enantiomeric excesses. The efficiency of our catalytic system resides in part in the cooperative interactions between the ureas all along the foldamer, and on the particular geometry of the active site which allow very low loading to be achieved. As expected, the handedness of the catalyst helix is directly linked to the stereochemistry of the formed Michael adduct.

2.4 INFLUENCE OF EXTERNAL PARAMETERS ON THE OUTCOME OF THE CATALYSED REACTION

2.4.1 Influence of the solvent

The solvent allows us to control the balance between the kinetics of the racemic reaction and enantioselective reaction. The goal is to optimise it to have the racemic reaction as a background reaction to enhance only the asymmetric catalysed one and maximise stereocontrol. Protic solvents were irrelevant for our model reaction, because of the necessity of a basic environment to deprotonate the pronucleophile. Solvents with different polarities were first tested without catalyst and then with catalyst in case the racemic reaction was slow: tetrachlorocarbon, benzene, toluene, dichloromethane, 1,2-dichloroethane. (Table II.8) The more polar was the solvent, the faster was the racemic reaction and the lower was the enantiocontrol. Combining this result with the idea to use a convenient solvent for experiments, toluene was chosen to be our model solvent (entries 4-5, Table II.8). The increase in polarity also disturbs the possibility to form robust hydrogen bonds and to coordinate the substrates to the catalyst, which explains the decrease of stereocontrol.

Table II.8: Impact of the solvent polarity on the addition of **2a** on **3a** catalysed by **1a**

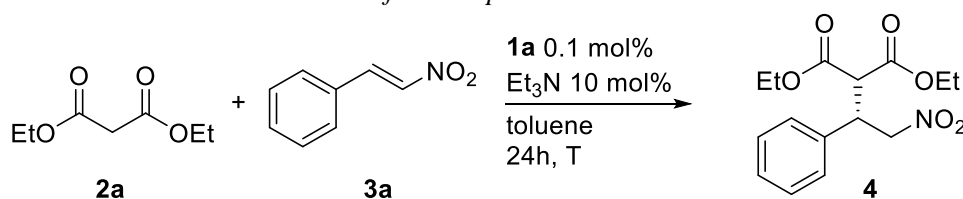
Entry	Solvent	Catalyst	Conversion (%)	ee (%)	Dipole moment (D)
1	CCl ₄	no catalyst	7	-	0
2		5a	95	94	0
3	C ₆ H ₆ *	no catalyst	38	-	0
4	Toluene	no catalyst	6	-	0.43
5		5a	90	91	0.43
6	DCM	no catalyst	26	-	1.55
7		5a	73	71	1.55
8	1,2-DCE	no catalyst	41	-	1.86
9		5a	74	57	1.86

Conversions were determined by ¹H NMR. Yields were determined after purification on Silica Gel Chromatography. Enantiomeric excesses were determined with Chiral HPLC and absolute configuration was obtained from literature. *Reaction with benzene was run at 4 °C.

2.4.2 Impact of the temperature

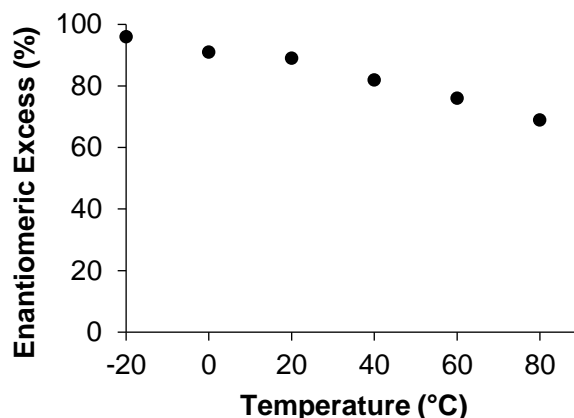
The temperature had been fixed at $-20\text{ }^{\circ}\text{C}$ in our initial conditions to limit entropy and maximise the enantioenrichment. The effect of increasing temperature on the model reaction will be representative of the strength of interaction between the substrates and the catalyst. Besides, the thermal stability of the helicity for oligourea foldamers has been demonstrated in pyridine between $19\text{ }^{\circ}\text{C}$ and $89\text{ }^{\circ}\text{C}$.²² In the model Michael addition, we found that the yield and the enantiomeric excess decreased with increasing temperature. Two elements have to be considered in this study. The first one, as in previous case, is the acceleration of both asymmetric and racemic reactions. The second one is polymerization of nitrostyrene which becomes competitive and impacts the yields of the Michael addition. Nevertheless, the control of selectivity is maintained to a significant extent at elevated temperatures (Table II.9) thus suggesting that the catalyst could be used over a wide range of temperature in case of slow reactions. Moreover, these results confirm that the helical structure of oligoureas and the interaction between the catalyst and the substrates are particularly strong and stable.

Table II.9: Increase of the temperature in the model reaction



Entry	Temperature ($^{\circ}\text{C}$)	Yield (%)	ee (%)
1	-20	82	95
2	0	74	91
3	20	66	89
4	40	70	82
5	60	83	76
6	80	78	69

Conversions were determined by $^1\text{H NMR}$. Yields were determined after purification on Silica Gel Chromatography. Enantiomeric excesses were determined with Chiral HPLC and absolute configuration was obtained from literature.



Scheme II.5: Impact of the temperature on the enantioenrichment

The impact of the temperature was also evaluated with catalyst **5a** over the range -20°C - 20°C . There is a small loss (2-6%) in enantiomeric excess over this temperature range, for both reaction times and both catalysts (Table II.10). The rate of reaction is slightly slower with the thiourea catalyst and this is more visible on reaction with 24h-run (Table II.11). Overall, the yields are very similar but on average, these series of experiments confirm that thiourea catalyst **5a** is less reactive and leads to a slightly lower stereocontrol.

*Table II.10: Comparison of temperature effect between catalysts **1a** and **5a**, after 48h reaction time*

Reaction time: 48h							
Entry	Temperature (°C)	Catalyst 1a			Catalyst 5a		
		Conversion (%)	Yield (%)	ee (%)	Conversion (%)	Yield (%)	ee (%)
1	-20	100	80	95	99	82	93
2	0	100	76	90	99	76	90
3	20	100	75	89	98	71	87

Conversions were determined by ^1H NMR. Yields were determined after purification on Silica Gel Chromatography. Enantiomeric excesses were determined with Chiral HPLC and absolute configuration was obtained from literature.

*Table II.11 : Comparison of temperature effect between catalysts **1a** and **5a**, after 24h reaction time*

Reaction time : 24h							
Entry	Temperature (°C)	Catalyst 1a			Catalyst 5a		
		Conversion (%)	Yield (%)	ee (%)	Conversion (%)	Yield (%)	ee (%)
1	-20	99	63	94	94	59	88
2	0	99	73	92	98	73	91
3	20	98	68	88	94	73	86

Conversions were determined by ^1H NMR. Yields were determined after purification on Silica Gel Chromatography. Enantiomeric excesses were determined with Chiral HPLC.

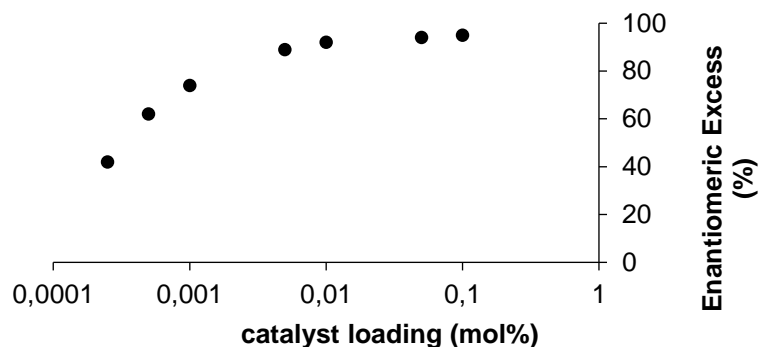


Figure II.11: Impact of the decrease of catalyst loading on the enantioenrichment

2.5.2 Play on the base loading

Here, we evaluated the influence of the base concentration with the aim to identify the minimum amount of base necessary to activate the catalytic system. Triethylamine was selected first for its low cost and because it readily deprotonates malonate. As expected, increasing the amount of Et₃N accelerates the reaction (Table II.13) but surprisingly the enantioselectivity was not affected (at least up to 30 mol% of catalyst, entry 5, Table II.13). Whereas, the catalytic activity was not affected when the amount of Et₃N was divided by two, it was significantly reduced at concentrations ≤ 1 mol% Et₃N. At 1 mol% Et₃N (Entries 1 vs 3, Table II.13), the conversion was moderate but the *ee* remained high (95%).

Table II.13: Impact of triethylamine loading on the model Michael reaction

Entry	Time (h)	Et ₃ N loading (mol%)	Conversion (%)	Yield (%)	<i>ee</i> (%)
1	48	1	56	43	95
2	48	5	100	85	95
3	48	10	100	82	95
4	48	20	100	83	93
5	16	30	100	78	93

Conversions were determined by ¹H NMR. Yields were determined after purification on Silica Gel Chromatography. Enantiomeric excesses were determined with Chiral HPLC and absolute configuration was obtained from literature.

The possibility to change the relative amounts of chiral catalyst and base renders the system more adaptable than other bifunctional catalyst (Figure II.12, Model a). Moreover, in the view of the result obtained with 1 mol% base (Entry 1 Table II.13), it is very unlikely that incorporating the base within the foldamer, either in the backbone or as a side chain, (Figure II.12, Model b) would give satisfactory results, even though a synergistic activity of the base cannot be excluded in such a system.

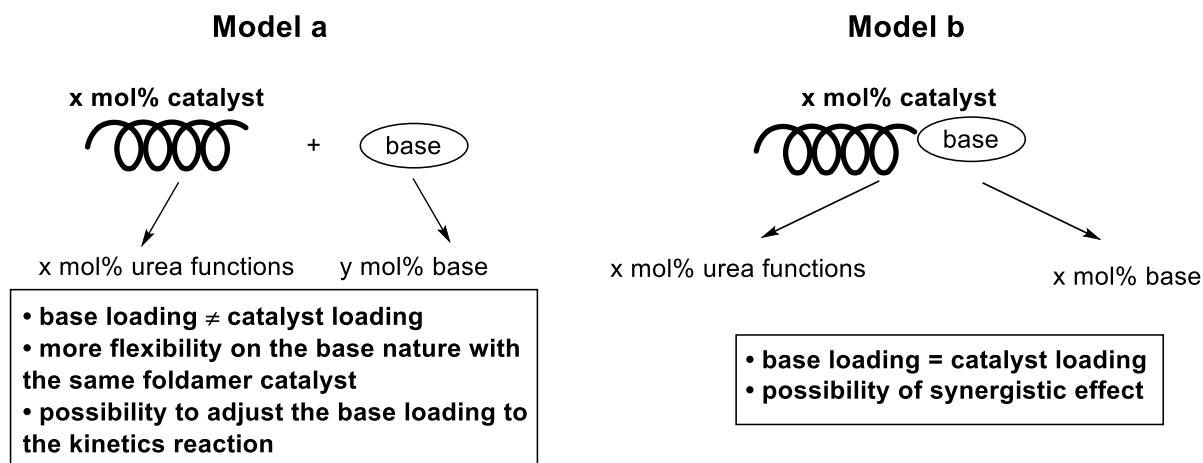
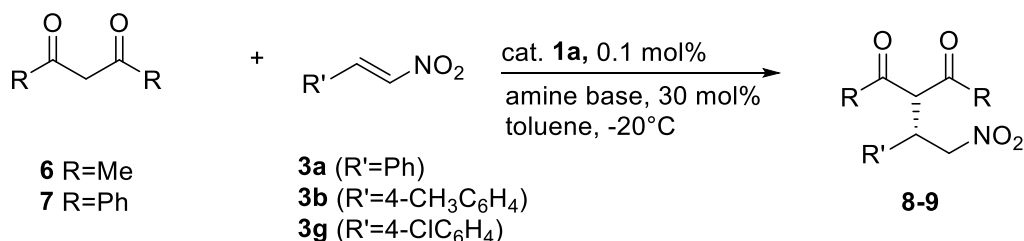


Figure II.12: Characteristics of strategies for base-foldamer association

2.5.3 Play on the nature of the base

While working on more difficult reaction substrates we realized that our catalytic system can be further optimized by tuning the nature of the base. In particular, the addition of acetylacetone **6** to nitrostyrene **3a** with a combination of 0.1 mol% of **1a** and 10 mol% Et₃N led to a modest stereocontrol (63% *ee*, Entry 1, Table II.14). To bring more steric hindrance to the system and possibly improve the stereocontrol, the number of carbons of the alkyl chains of the tertiary amine was increased: i.e. from triethylamine, to *n*-tributylamine, *n*-trihexylamine and *n*-trioctylamine (Entries 1-4, Table II.14). As planned the enantiomeric excess increased when the alkyl chain length increased, but the conversion was slower. On the other hand, using branched tertiary amines such as diisopropylethylamine (Hunig's base) as tertiary external base. The kinetics reaction was as fast as with triethylamine and the enantiocontrol of 92% *ee* was significantly better than with *n*-trioctylamine (83% *ee*). These results were reproducible with the formation of different adducts (Entries 6-14, Table II.14) providing further support for the use of Hunig's base as part of the catalytic system.

Table II.14: Suitability of several 1,3-dicarbonyl compounds as nucleophiles and influence of the nature of the amine base cocatalyst



Entry	Product	Amine base	Time (h)	Yield (%)	ee (%)
1		Et ₃ N	16	92	63
2		<i>n</i> Bu ₃ N	16	90	
3		R': Ph (8a) <i>n</i> Hex ₃ N	120	78	76
4		<i>n</i> Oct ₃ N	120	72	83
5		<i>i</i> Pr ₂ EtN	16	70	92
6		Et ₃ N	16	82	80
7		R': 4-CH ₃ C ₆ H ₄ (8b) <i>n</i> Oct ₃ N	120	98	66
8		<i>i</i> Pr ₂ EtN	16	90	86
9		Et ₃ N	16	87	56
10		R': 4-ClC ₆ H ₄ (8g) <i>n</i> Oct ₃ N	120	80	69
11		<i>i</i> Pr ₂ EtN	16	82	83
12		Et ₃ N	16	64	91
13		9 <i>n</i> Oct ₃ N	72	99	95
14		<i>i</i> Pr ₂ EtN	16	67	>99

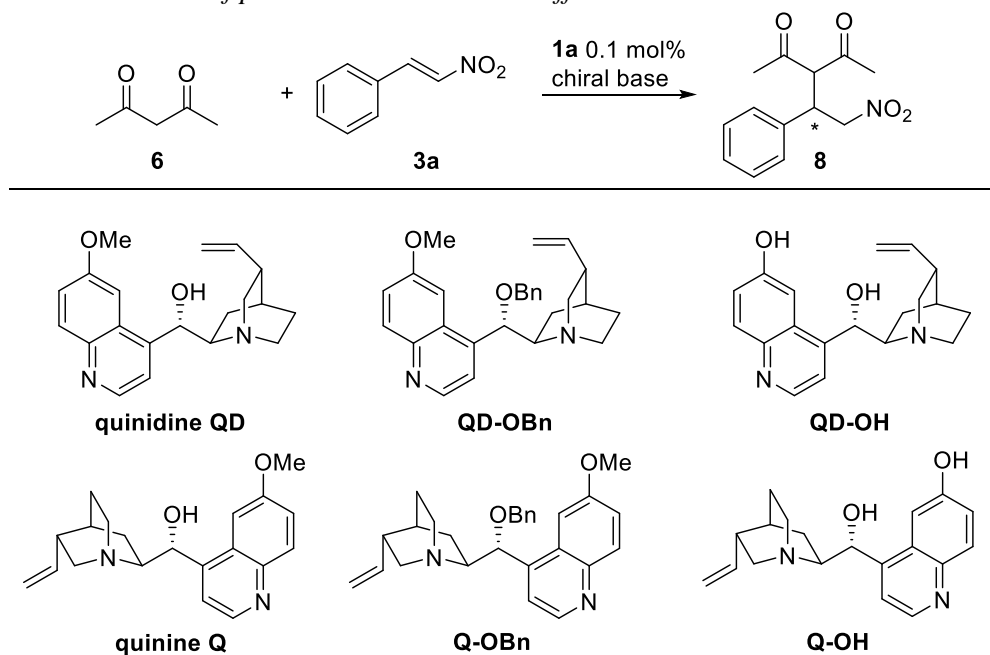
Reactions were performed on 1 mmol scale with 2 equiv. of diketone. Yields correspond to isolated compound after chromatographic purification. The ee was determined by chiral HPLC analysis. Absolute configuration (*R*) or (*S*) was known or assigned by analogy.

2.5.4 Possibility of match/mismatch effect with chiral bases

To go further in these investigations on variations of the nature of the base to fine tune the catalytic system, several combinations between the catalyst and chiral bases were next evaluated (Table II.15). The natural bases quinidine and quinine, commonly used and/or derived to form new organocatalysts^{9, 23-24}, were used firstly without the foldamer catalyst to perform the addition of **6** on **3a**, to evaluate if there was room for improvement (Entries 1–4, Table II.15). The enantioselectivities without catalyst were low, respectively 29% ee (*S*) and –23% ee (*R*), but unfortunately, there was no synergistic effect observed when the reaction was conducted in the presence of the foldamer catalyst. Whereas the association with quinidine gave a small positive effect (Entry 2, Table II.15), the association of quinine and **1a** was found counterproductive (Entry 4, Table II.15). To check whether

the hydroxyl group on the bases could disturb the interaction between the catalyst and the substrates, the bases were *O*-benzylated. The new catalysts QD-OBn and Q-OBn did not give any significant improvement although the mismatch effect observed with the quinine Q in the presence of **1a** was suppressed with QD-OBn. In an opposite way of thinking, the presence of a second hydroxyl group on the base could provide an additional anchoring point for substrate coordination. The corresponding catalysts QD-OH and Q-OH were synthesised. This new class of chiral base was very efficient: with only 1 mol% QD-OH at RT, the enantioselectivity was very good (85% *ee* (*S*), Entry 9 Table II.15). Parameters such as the solvent, the base loading and temperature were also evaluated in parallel, to observe the presence of a match/mismatch effect (Entries 10-13, Table II.15) but it was not successful.

Table II.15 : Evaluation of possible match/mismatch effect with cinchona alkaloids base derivatives



Entry	Cat. loading (mol%)	Base nature	Base loading (mol%)	Solvent	Time	Temperature (°C)	Yield (%)	<i>ee</i> (%)
1	Without	Quinidine	10	DCM	16h	-20	87	29 (<i>S</i>)
2	0.1	QD	10	DCM	we	-20	88	34
3	Without	Quinine Q	10	DCM	16h	-20	82	-23 (<i>R</i>)
4	0.1	Q	10	DCM	we	-20	89	2
5	Without	QD-OBn	10	DCM	40h	-20	85	14
6	0.1	QD-OBn	10	DCM	60h	-20	83	28
7	Without	Q-OBn	10	DCM	40h	-20	88	4
8	0.1	Q-OBn	10	DCM	60h	-20	93	34
9	Without	QD-OH	1	DCM	40h	RT	n.d.	-85
10	Without	Q-OH	1	toluene	-	-20	no conversion	
11	0.1	Q-OH	1	toluene	-	-20	no conversion	
12	Without	Q-OH	0.1	toluene	-	RT	no conversion	

Reactions were performed on 1 mmol scale with 2 equiv. of diketone. Yields correspond to isolated compound after chromatographic purification. The *ee* was determined by chiral HPLC analysis. Absolute configuration (*R*) or (*S*) was determined from literature.

The external base offers a high level of tunability of the catalytic system which can be further adapted to each reagent and reaction of interest. The independence of the base and the catalyst is one of the main reasons why the catalytic system is efficient at low foldamer loading, in addition to the cooperative effect of the intramolecular and polarized arrangement of ureas all along the folded backbone. However, not all bases are compatible with our catalytic system, as demonstrated for the chiral bases. The steric environment imposed by the quinine and quinidine derivatives could preclude a positive cooperation. In any case, mechanistic studies are necessary to further understand how substrates are interacting with each other and with the foldamer.

Bibliography

1. Guichard, G.; Semetey, V.; Didierjean, C.; Aubry, A.; Briand, J.-P.; Rodriguez, M., *J. Org. Chem.* **1999**, *64*, 8702-8705.
2. Pendem, N.; Douat, C.; Claudon, P.; Laguerre, M.; Castano, S.; Desbat, B.; Cavagnat, D.; Ennifar, E.; Kauffmann, B.; Guichard, G., *J. Am. Chem. Soc.* **2013**, *135* (12), 4884-92.
3. Violette, A.; Lancelot, N.; Poschalko, A.; Piotto, M.; Briand, J. P.; Raya, J.; Elbayed, K.; Bianco, A.; Guichard, G., *Chemistry* **2008**, *14* (13), 3874-82.
4. Violette, A.; Averlant-Petit, M. C.; Semetey, V.; Hemmerlin, C.; Casimir, R.; Graff, R.; Marraud, M.; Briand, J.-P.; Rognan, D.; Guichard, G., *J. Am. Chem. Soc.* **2005**, *127*, 2156-2164.
5. Diemer, V.; Fischer, L.; Kauffmann, B.; Guichard, G., *Chem. Eur. J.* **2016**, *22* (44), 15684-15692.
6. Fischer, L.; Claudon, P.; Pendem, N.; Miclet, E.; Didierjean, C.; Ennifar, E.; Guichard, G., *Angew. Chem. Int. Ed. Engl.* **2010**, *49* (6), 1067-70.
7. Zhang, Z.; Bao, Z.; Xing, H., *Org. Biomol. Chem.* **2014**, *12* (20), 3151-62.
8. Bae, H. Y.; Song, C. E., *ACS Catalysis* **2015**, *5* (6), 3613-3619.
9. Kwiatkowski, J.; Lu, Y., *Chem. Commun.* **2014**, *50* (66), 9313-6.
10. Kimmel, K. L.; Weaver, J. D.; Ellman, J. A., *Chem. Sci.* **2012**, *3* (1), 121-125.
11. Etxabe, J.; Izquierdo, J.; Landa, A.; Oiarbide, M.; Palomo, C., *Angew. Chem. Int. Ed.* **2015**, *54* (23), 6883-6.
12. Badiola, E.; Fiser, B.; Gomez-Bengoia, E.; Mielgo, A.; Olaizola, I.; Urruzuno, I.; Garcia, J. M.; Odriozola, J. M.; Razkin, J.; Oiarbide, M.; Palomo, C., *J Am Chem Soc* **2014**, *136* (51), 17869-81.
13. Constantieux, T.; Bugaut, X.; Du, H.; Dudognon, Y.; Sanchez Duque, M.; Goudedranche, S.; Bonne, D.; Rodriguez, J., *Synthesis* **2016**, *48* (20), 3479-3503.
14. Guichard, G.; Semetey, V.; Didierjean, C.; Aubry, A.; Briand, J.-P.; Rodriguez, M., *J. Org. Chem.* **1999**, *64*, 8702-8705.
15. Cobb, A.; Aitken, L.; Arezki, N.; Dell'Isola, A., *Synthesis* **2013**, *45* (19), 2627-2648.
16. Sukhorukov, A. Y.; Sukhanova, A. A.; Zlotin, S. G., *Tetrahedron* **2016**, *72* (41), 6191-6281.
17. Okino, T.; Hoashi, Y.; Takemoto, Y., *J. Am. Chem. Soc.* **2003**, *125*, 12672-12673.
18. Okino, T.; Hoashi, Y.; Furukawa, T.; Xu, X.; Takemoto, Y., *J. Am. Chem. Soc.* **2005**, *127*, 119-125.
19. Nelli, Y. R.; Antunes, S.; Salaün, A.; Thinon, E.; Massip, S.; Kauffmann, B.; Douat, C.; Guichard, G., *Chem. Eur. J.* **2014**, *21*, 2870-2880.
20. Berkessel A., Gasch N., Glaubitz K., Koch C., *Org. Lett.* **2001**, *3* (24), 3839-3842.
21. Stone, M. T.; Heemstra, J. M.; Moore, J. S., *Acc. Chem. Res.* **2006**, *39*, 11-20.
22. Hemmerlin, C.; Marraud, M.; Rognan, D.; Graff, R.; Semetey, V.; Briand, J.-P.; Guichard, G., *Helvetica Chimica Acta* **2002**, *85*, 3692-3711.
23. Bartoli, G.; Bosco, M.; Carlone, A.; Cavalli, A.; Locatelli, M.; Mazzanti, A.; Ricci, P.; Sambri, L.; Melchiorre, P., *Angew. Chem. Int. Ed.* **2006**, *45* (30), 4966-70.
24. Iriarte, I.; Olaizola, O.; Vera, S.; Gamboa, I.; Oiarbide, M.; Palomo, C., *Angew. Chem. Int. Ed.* **2017**, *56* (30), 8860-8864.

CHAPTER III

CHAPTER III

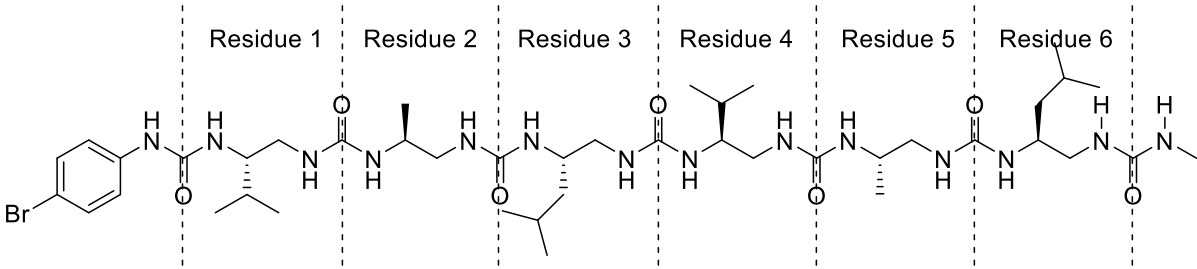
3.1 PROBING THE ROLE OF TERMINAL UREAS IN THE CATALYTIC ACTIVITY OF OLIGOUREA FOLDAMERS	92
3.1.1 Strategy and demonstration of the position of the catalytic sites	92
3.1.2 NMR structural study.....	95
3.1.3 Evaluation of the model reaction with the critical urea positions successively blocked	96
3.2 SUBSTRATES-CATALYST INTERACTIONS OBSERVED BY NMR.....	99
3.2.1 Preliminaries for NMR study.....	99
3.2.2 Evaluation of the interaction between the catalyst and nitrostyrene	100
3.2.3 Evaluation of the interaction between the catalyst and deprotonated malonate	102
3.2.4 Competition NMR experiments by successive addition of malonate, nitrostyrene and triethylamine to the catalyst.....	103
3.2.5 Proposition of mechanism for Michael addition catalysed by 1a	105
3.3 IMPACT OF THE NATURE OF THE FIRST RESIDUE	107
3.3.1 Sequence variations to study the role of the side chain of the first residue	107
3.3.2 Impact of the first residue variation on the catalytic efficiency.....	108
3.3.3 NMR conformational analysis of sequence modified catalysts and conclusions about possible structural requirements for high catalytic activity	108
3.4 KINETIC STUDIES AND VARIATION OF THE CATALYST ENANTIOMERIC EXCESS.....	111
3.4.1 Kinetic studies.....	111
3.4.1.1 Preliminary	111
3.4.1.2 Nitrostyrene order.....	112
3.4.1.3 Reaction order with respect to malonate, triethylamine and catalyst.....	113
3.4.2 Study of non-linear effects.....	115
3.4.2.1 Variation of foldamer catalyst enantiomeric excess	115
3.4.2.2 Impact of the catalyst enantioenrichment on the stereocontrol of the reaction.....	116

3.1 PROBING THE ROLE OF TERMINAL UREAS IN THE CATALYTIC ACTIVITY OF OLIGOUREA FOLDAMERS

3.1.1 Strategy and demonstration of the position of the catalytic sites

The rationale for the design of oligourea-based catalysts was the accessibility of the two first ureas at one end of the helical structure. Only the C=O groups of these ureas are directly involved in the intramolecular hydrogen bond network, so the corresponding four NHs are potentially free to interact with substrates that contain suitable H-bond acceptor groups. Because these NHs are located at the positive pole of the helix macrodipole, binding to anions or transient negatively charged species should be enhanced. Guichard *et al.* investigated anion recognition by oligourea helices in detail and demonstrated that anion binding by oligourea foldamers does not affect the helix folding propensity of the compound (Table III.1).¹ Co-crystallisation of one molecule of DMSO with two oligourea foldamers showed the importance of these two first ureas in the binding process and suggest a possible binding mode for anions (Figure III.1).

Table III.1: Anisochronicity of oligourea backbone CH₂^a protons after addition of increasing amounts of tetrabutylammonium chloride



Entry	Equiv. Anion	$\Delta\delta$ (ppm)*					
		Res. 1	Res. 2	Res. 3	Res. 4	Res. 5	Res. 6
1	0	1.12	1.35	1.25	1.31	1.26	1.04
2	0.7	1.12	1.33	1.23	1.26	1.21	0.92
3	2.0	1.08	1.33	1.24	1.32	1.24	0.99
4	5.5	ND	1.33	1.22	1.30	1.22	ND

*Determined by NMR spectroscopy at 20 °C in a mixture of [d₆]-DMSO/CD₃CN (5/95 v/v).

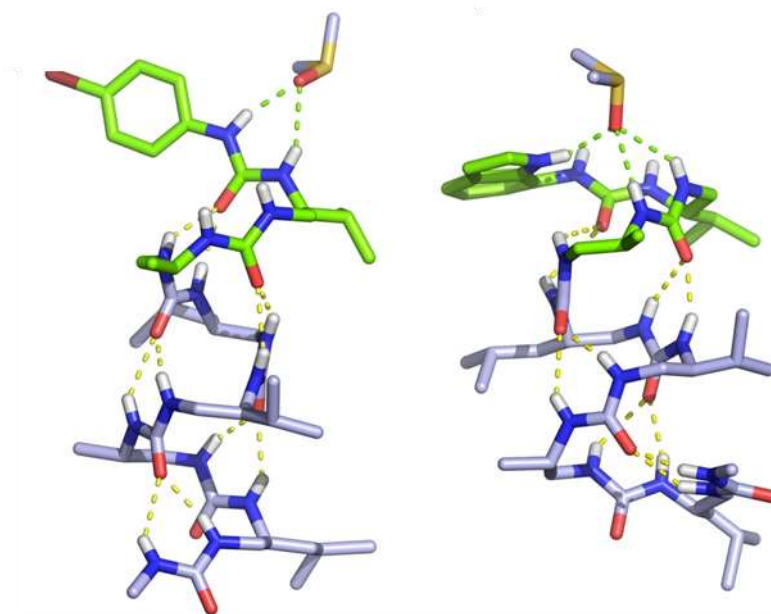


Figure III.1: Co-crystallization of one molecule of DMSO with two oligourea foldamers differing in their helix termination

To demonstrate the role of these terminal ureas on the catalytic process, monosubstituted analogues of catalyst **1a** were synthesised with the goal to block each of the two urea sites independently (Figure III.2). Oligomer **10** contains a pyrrolidine ring blocking the first urea, whereas catalyst **11** has a pyrrolidine ring blocking the second urea, and **12** is an analogue of **11** with a thiourea anchored at the first residue instead of a urea (Figure III.3). The insertion of a pyrrolidine moiety inside the foldamer backbone between CH^β and vicinal NH (a proline type residue Pro^u) was shown previously to be compatible with the 2.5-helical structure of oligoureas.² In particular, the constrained dihedral ‘Phi’ angle value in the pyrrolidine containing residues is very similar to the ‘Phi’ angles of acyclic residues in the canonical 2.5-helical structure. Furthermore, in the particular case of **10**, **11** and **12** the position of the pyrrolidine ring at the end of the sequence does not impair the intramolecular hydrogen bond network. The synthesis of **10**, **11** and **12** were performed as previously described for **1a/5a**, except that **Boc-Pro^u-OSu** was coupled at the last and penultimate positions in place of Val^u and Ala^u , respectively. The X-ray structure of Boc-protected precursor of **11** (**11-hexamer**) demonstrates the formation of a canonical 2.5-helical structure with the pyrrolidine moiety pointing towards the solvent and blocking the access to the second catalytic site as expected (Figure III.4 in orange). An overlay with the structure of the corresponding precursor of **1a**, show a very good match between the two structures as revealed by the small RMSD 0.7.

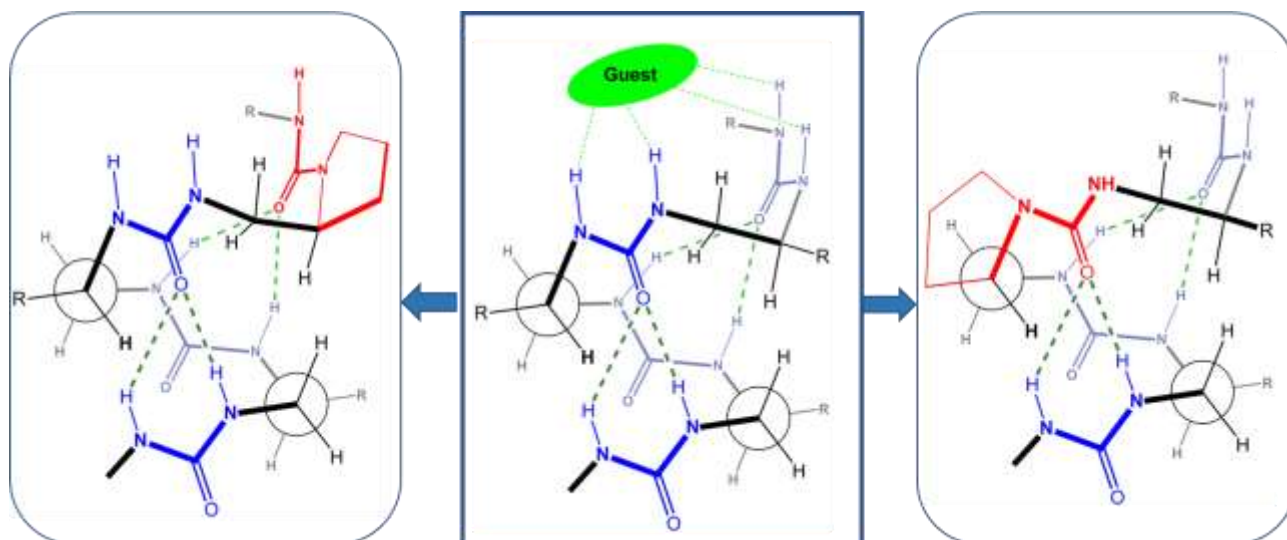


Figure III.2: Pro^H based strategy to block urea NHs demonstrate the role of the two first urea in the catalytic process

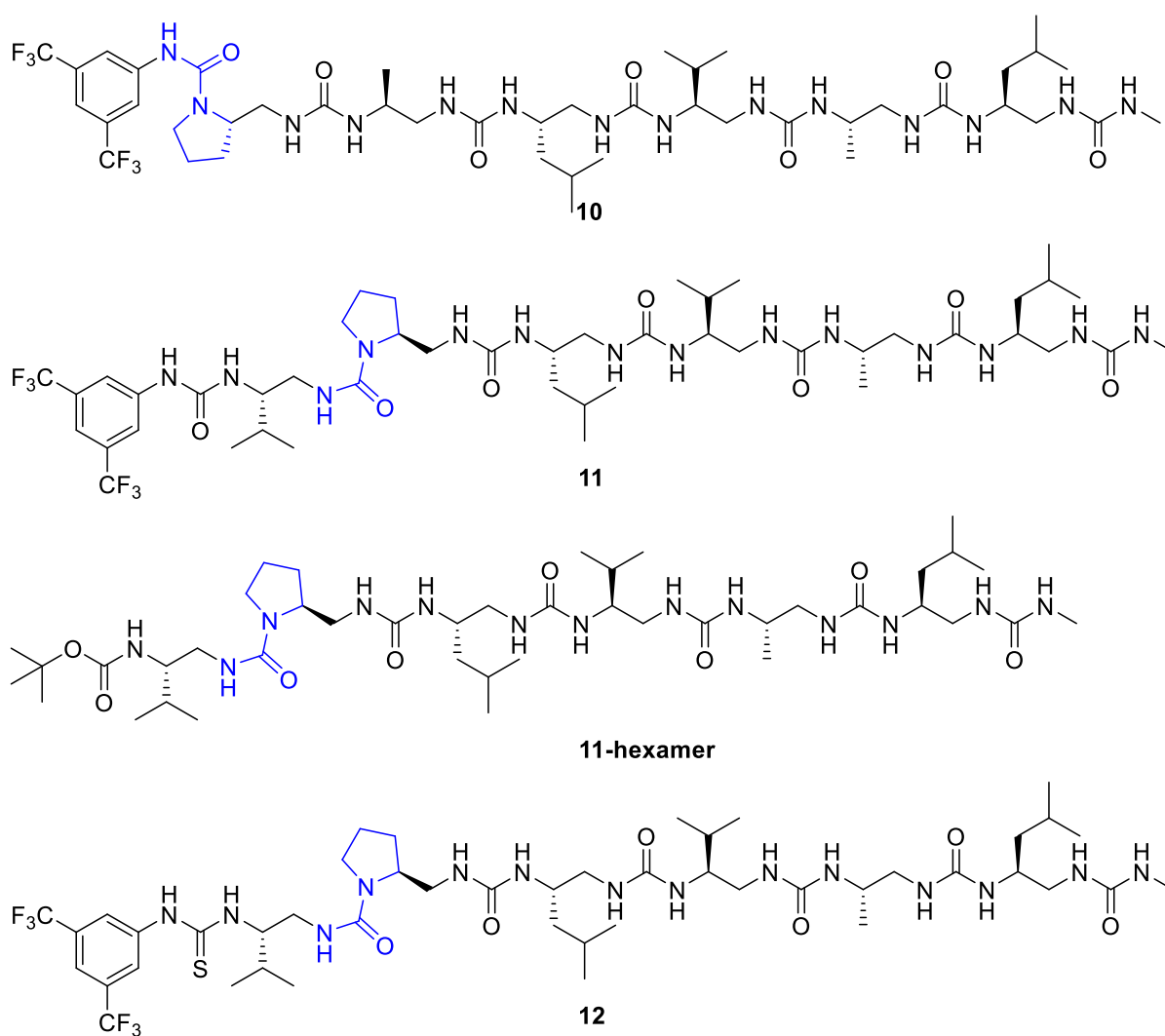


Figure III.3: Synthesized catalysts **10**, **11** and **12** with a pyrrolidine-ring included in the model sequence

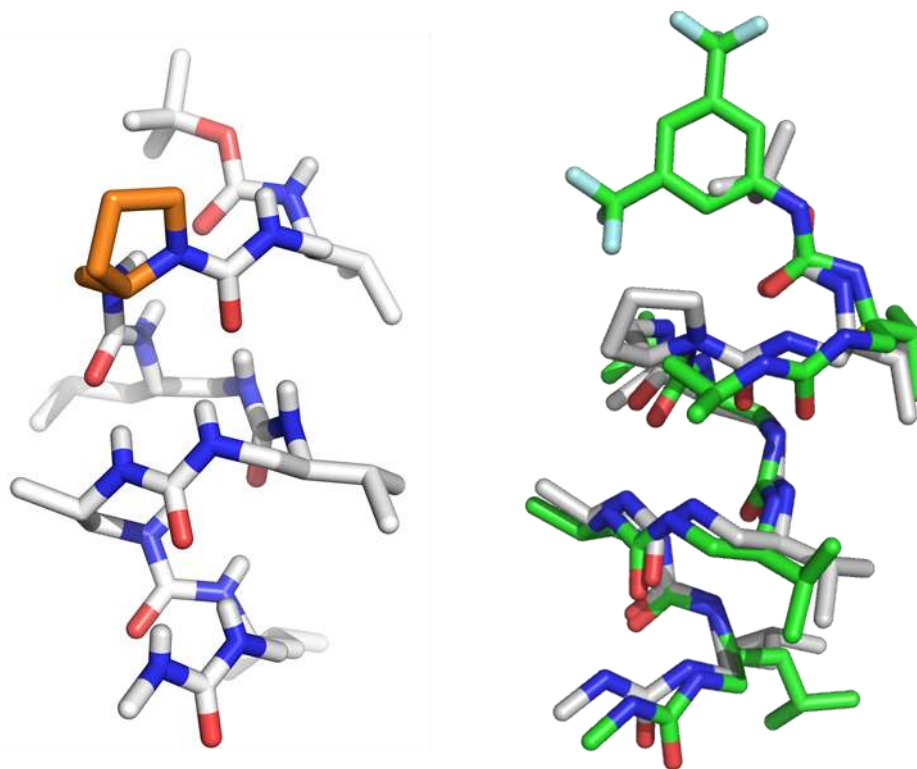


Figure III.4: X-ray structure of **11-hexamer**, *Boc*-protected precursor of **11**

3.1.2 NMR structural study

NMR experiments were used to evaluate the impact of the pyrrolidine and/or thiourea moieties insertion (compounds **10-12**) on the conformation in solution of the reference structure **1a**, and its thiourea analogue **5a**. The anisochronicity of backbone diastereotopic protons all along the sequence was measured for all oligomers and reported on the graph below (Figure III.5). These values suggest that the insertion of pyrrolidine locally disturbs the helicity around the inserted position, but a good proportion of helicity is conserved. From the third residue to the sixth, in urea and thiourea versions, the anisochronicity values are very similar suggesting a close helical conformation. So the impact of these modifications on the catalytic efficiency will essentially reflect local effects including restricted access to catalytic sites but not global variations of the secondary structure.

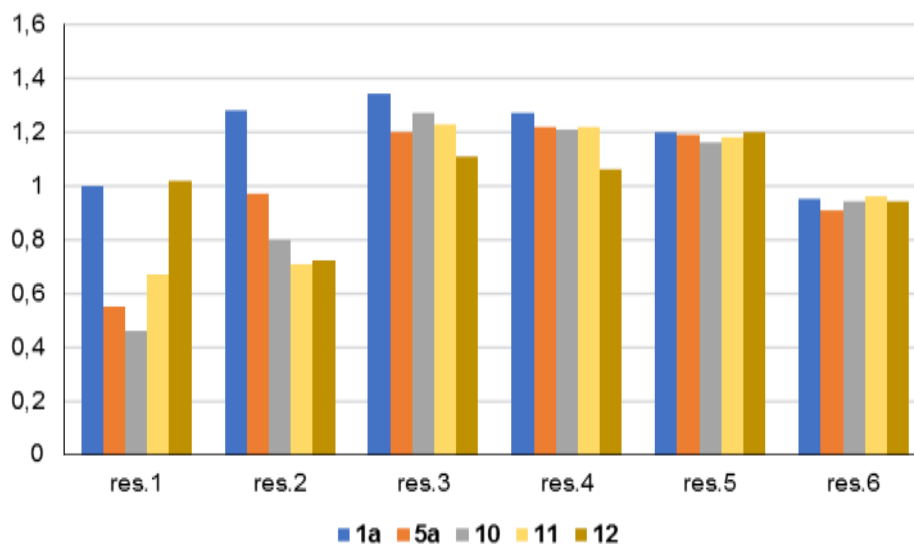
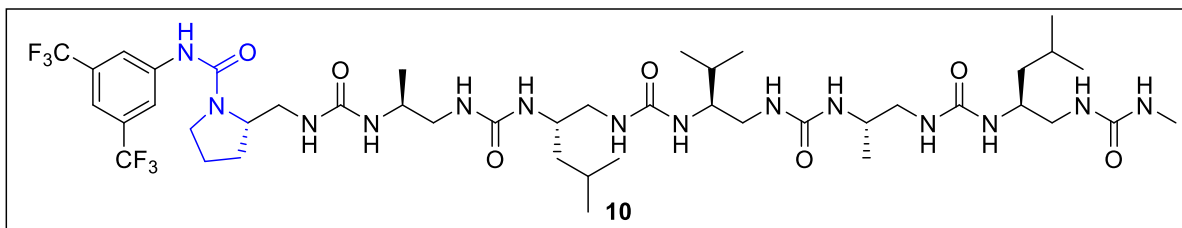
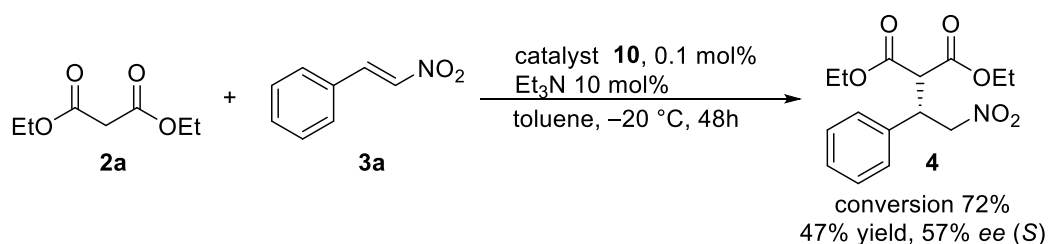


Figure III.5: Anisochronicity of CH₂^α protons extracted from NMR spectra of pyrrolidine-containing oligoureas **10** and **11**, pyrrolidine-containing oligo(thio)urea **12** and comparison to values in **1a** and **5a**

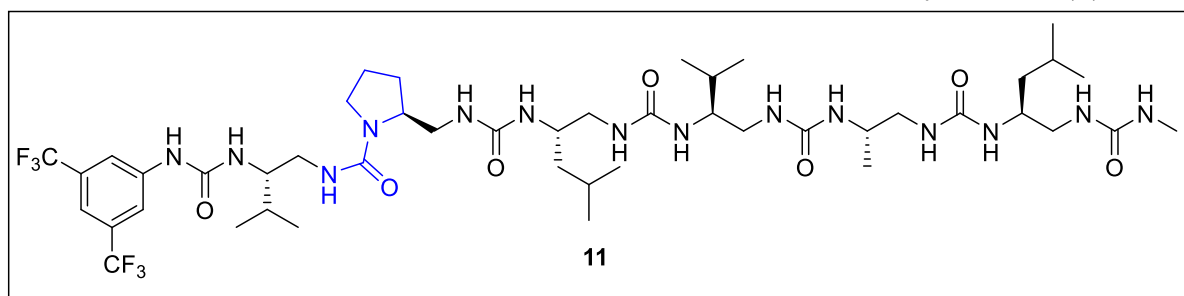
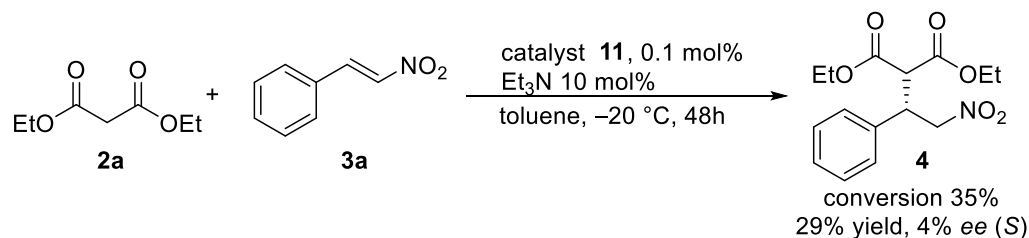
3.1.3 Evaluation of the model reaction with the critical urea positions successively blocked

The evaluation of the catalytic efficiency of oligomer **10** was established by running the Michael addition of **2a** to **3a**, with 10 mol% of Et₃N, for 48h in toluene at -20 °C. In contrast to the process catalysed by **1a**, the conversion using **10** under the same conditions did not go to completion, suggesting slower kinetics (Scheme III.1). The yield was consequently lower (47% instead of 82%). Moreover, the important loss of enantiomeric excess (from 96% *ee* to 57% *ee*) perfectly reflects the key roles of the NHs of the first urea.



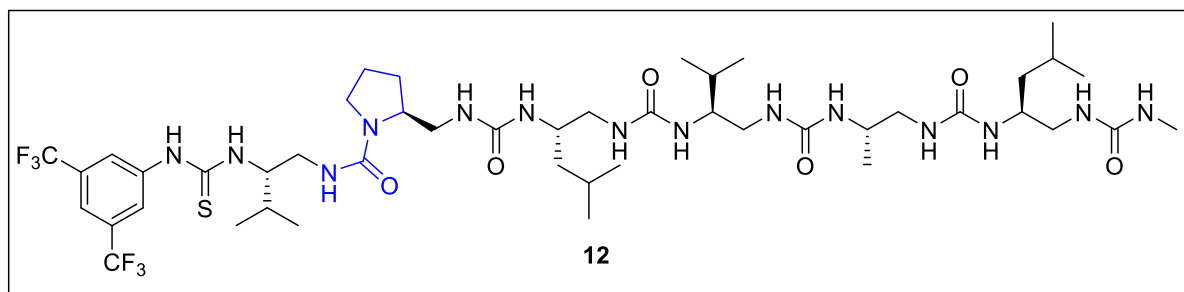
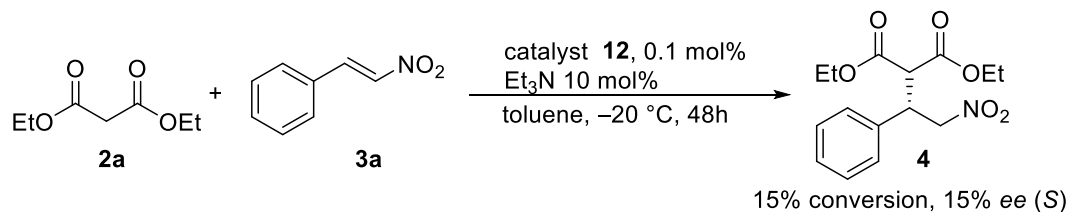
Scheme III.1: Catalytic activity of **10**

The catalyst **11** was also evaluated under same conditions and the resulting reaction conversion was even slower than with catalyst **10**, giving low yield after 48h (29%, Scheme III.2). The enantioenrichment is almost inexistent for the Michael adduct. The dramatic fall in enantiomeric excess from 95% *ee* to 4% *ee* strongly supports a major role of the NHs of the second urea to the catalytic process.



Scheme III.2: Catalytic activity of 11

The catalyst **12** was significantly less reactive than its urea analogue (15% conversion instead of 29% conversion) but it was slightly more stereospecific than its urea analogue, 15% *ee* instead of 4% *ee*, (Scheme III.3). The thiourea changes the electronic environment and increases the acidity of the first residue, and also the local geometry of the catalytic site, which could explain the slightly better enantioenrichment.



Scheme III.3: Catalytic activity of 12

Overall, this study confirms that the catalytic site of the reaction is most-likely formed of the two first ureas which both play a key role in the catalytic process. Although blocking either site is detrimental to the reaction rate and enantiocontrol, careful examination suggests that the two ureas are not acting equally. Although essential to obtain high conversion and *ee*'s, the NH of the first (thio)urea is not as critical as the NH of the second urea which seems absolutely critical. Additional insight could be gained by selectively blocking the aromatic urea nitrogen the NH' of the first residue (Figure III.6). It is synthetically more challenging to build catalyst with only these positions blocked selectively. Alternatively, one could think about blocking both NHs of a given urea by constructing an imidazolidinone ring to further study these effects.

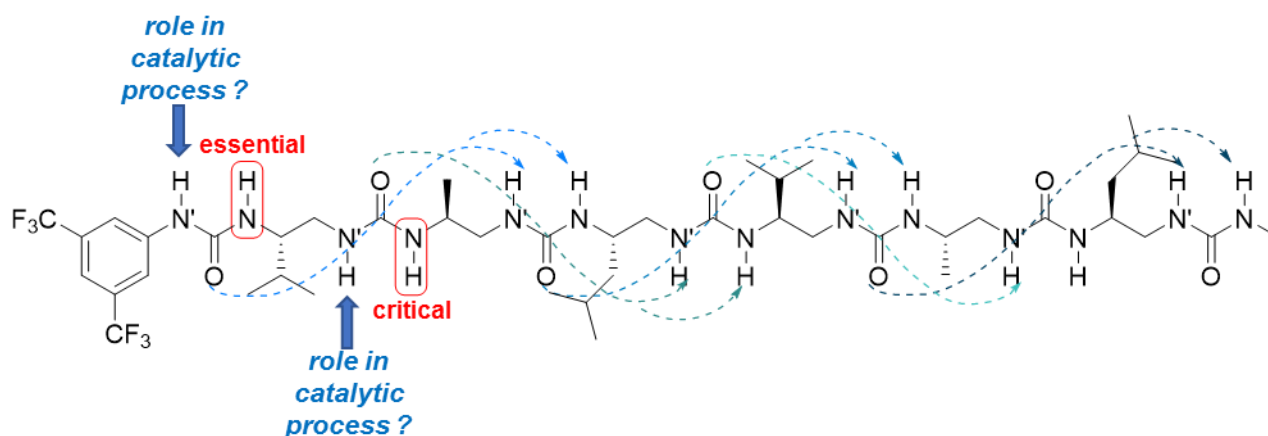
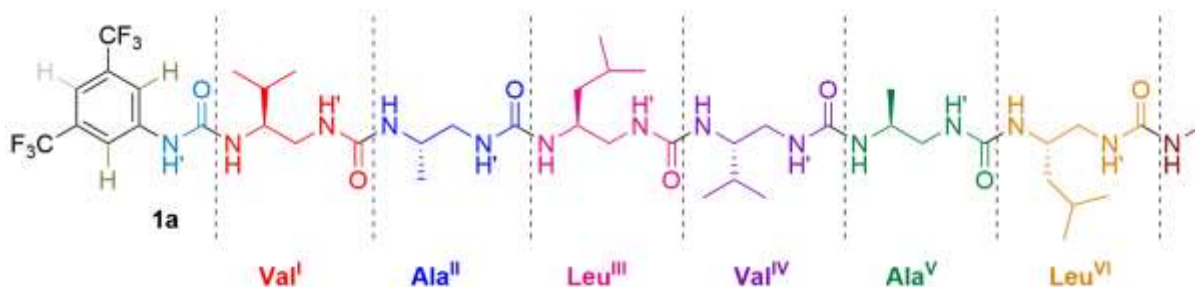


Figure III.6: Conclusion from the study with selective pyrrolidine replacement on **1a**

3.2 SUBSTRATES-CATALYST INTERACTIONS OBSERVED BY NMR

3.2.1 Preliminaries for NMR study

This section describes my efforts to understand the interaction between the substrates of the reaction and the foldamer catalysts using NMR spectroscopy. The NMR analysis of helical oligoureia foldamers in a well-chosen deuterated solvent can provide well dispersed urea NH and NH' signals suitable for titration studies. Because we know that the catalyst interacts with the substrates of the reaction through hydrogen bonds and ureas, an NMR titration experiment of the catalyst with increasing amount of substrates could potentially provide useful information. As already reported for other catalytic system in the literature, this method can help to clarify the way substrates interact with the catalyst.³⁻⁶ One difficulty is to find the right solvent in which the catalyst **1a** is soluble, where the NH region is well-resolved and in which the interaction between the solvent and catalytic sites is negligible. To check whether these conditions can be filled, **1a** was fully characterized by NMR in a mixture acetonitrile- $[d_3]$ /DMSO- $[d_6]$ (88/12 v/v) and all the NH and NH' signals were unequivocally assigned (Figure III.7 and Figure III.8). DMSO was needed to solubilise the oligoureia in acetonitrile, its volume was minimised to avoid the perturbation of the interaction between substrates and catalyst. Several titration experiments have been considered: (i) addition of nitrostyrene to the NMR tube containing the catalyst to monitor the affinity between the nitrostyrene and the catalyst (ii) addition of solution of malonate and triethylamine (molar ratio 1:1) (iii) successive addition of all the reactants to mimic the model reaction.



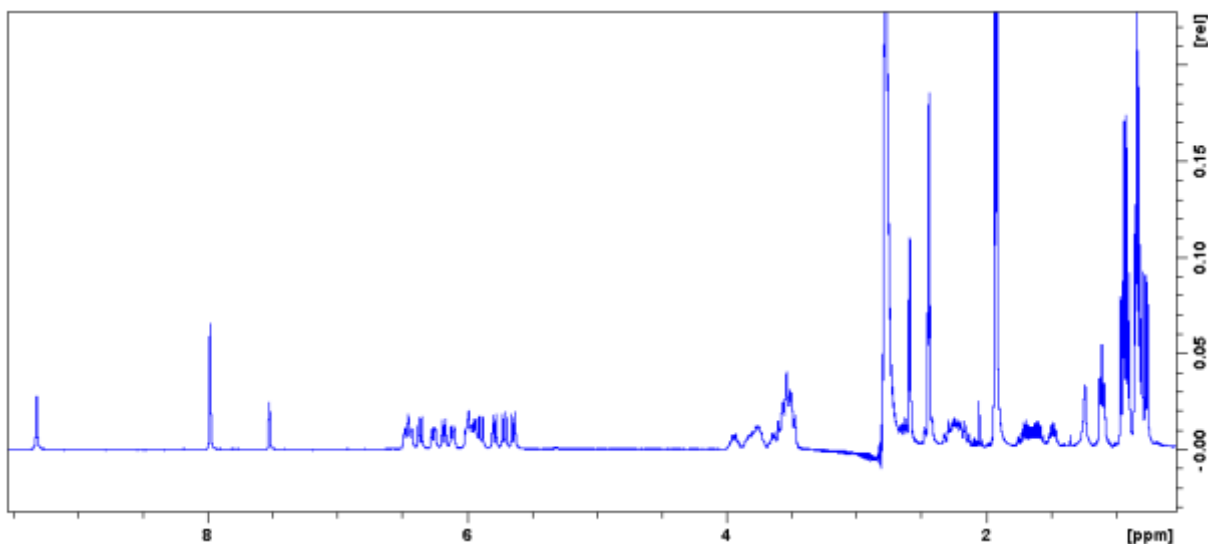


Figure III.7: ^1H NMR spectra of **1a** in acetonitrile- $[\text{d}_3]$ /DMSO- $[\text{d}_6]$ (88/12 v/v)

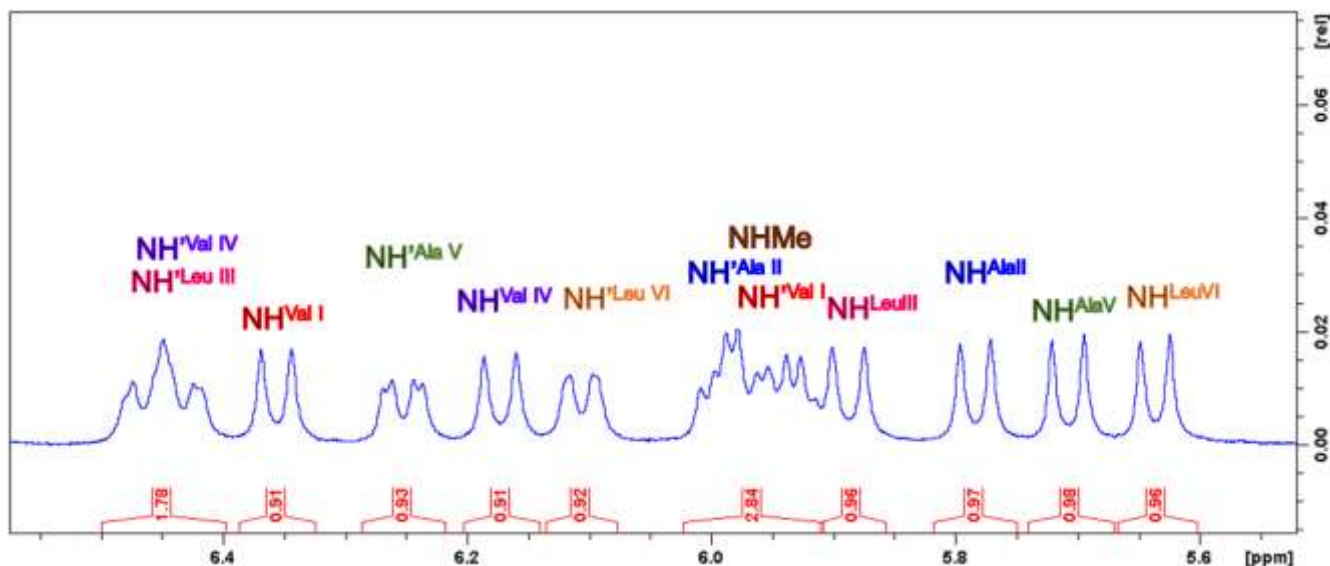


Figure III.8: full attribution of NH and NH' region in NMR spectra of **1a** (corresponding to structure in Figure III.7)

3.2.2 Evaluation of the interaction between the catalyst and nitrostyrene

Starting from the same stock solution which was used to perform the reference NMR spectra of **1a** (Figure III.7), a new tube of **1a** was prepared and titrated with nitrostyrene (up to 108 equiv). No visible change was observed in the spectra of **1a** even when more than 100 added nitrostyrene equivalents were added (Figure III.9). This suggests that there is no strong interaction between nitrostyrene and the catalyst observable by NMR under these solvent conditions. If we assume that this result can be translated to toluene which is the solvent of the catalysed Michael addition reaction, it might question some of the early proposed mechanisms for the Michael addition catalysed by bifunctional catalysts (Figure III.10).⁷

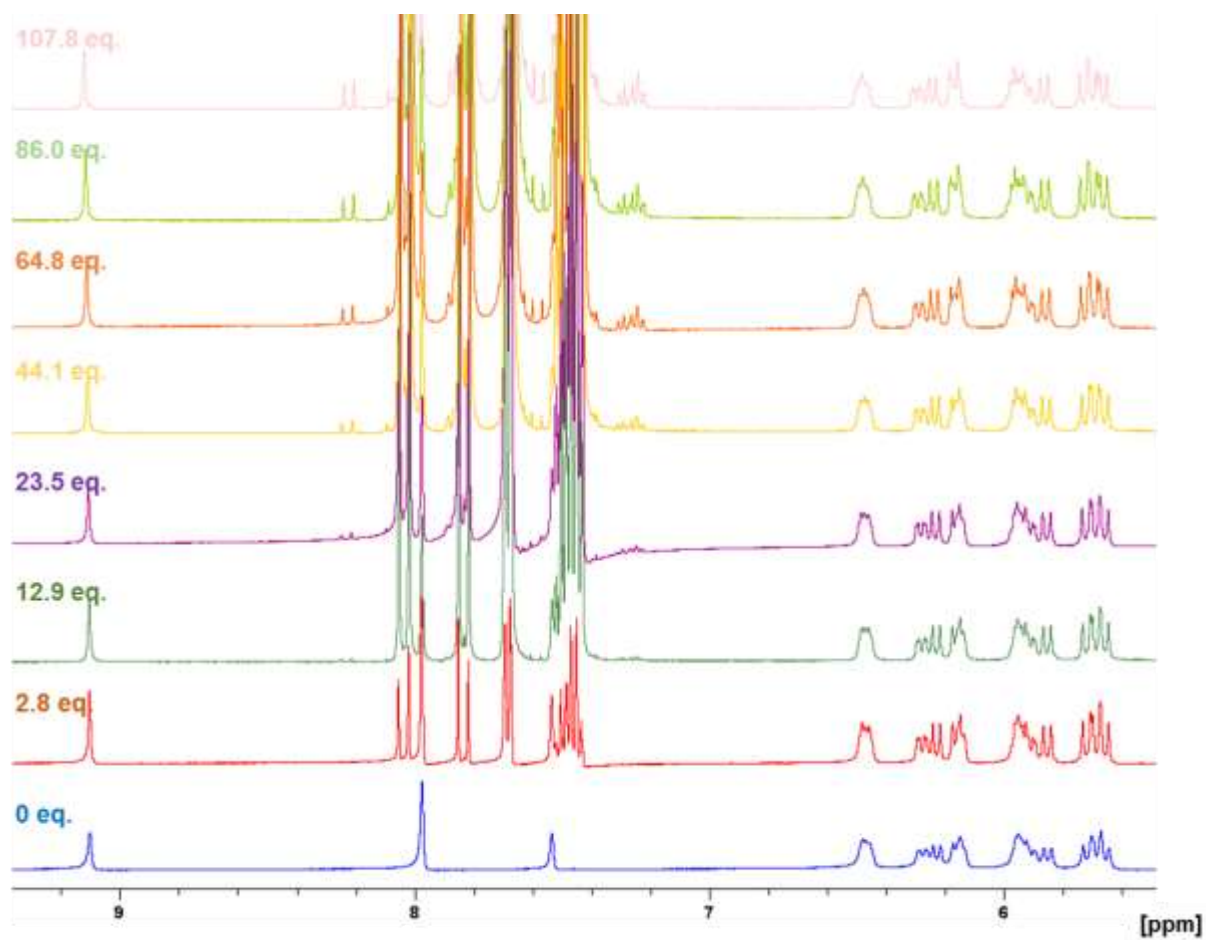


Figure III.9: Titration with nitrostyrene

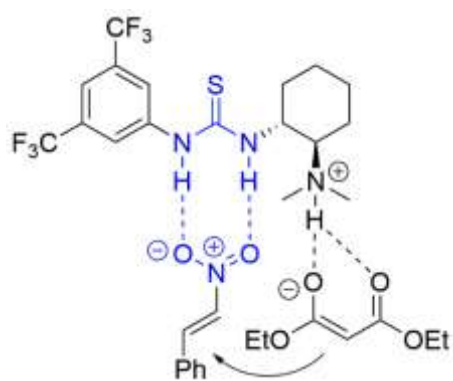


Figure III.10: One proposal of mechanism for Michael addition activated by Takemoto catalyst⁸

3.2.3 Evaluation of the interaction between the catalyst and deprotonated malonate

With the same methodology, an equimolar stock solution of malonate:Et₃N 1:1 was progressively added to an NMR tube containing catalyst **1a**. Two signals were found to progressively shift: the most significant chemical shift difference corresponds to the (most acidic) proton NH' between the aromatic ring and the first catalytic site, the second one, still very clear, corresponds to the proton NH of the first residue Val^I (Figure III.11). The difference of chemical shift was measured and reported in a graph for the two protons (Figure III.12). Although the interaction may seem quite weak one must keep in mind the presence of DMSO which is necessary to solubilize the oligomer but which also compete for binding to ureas.

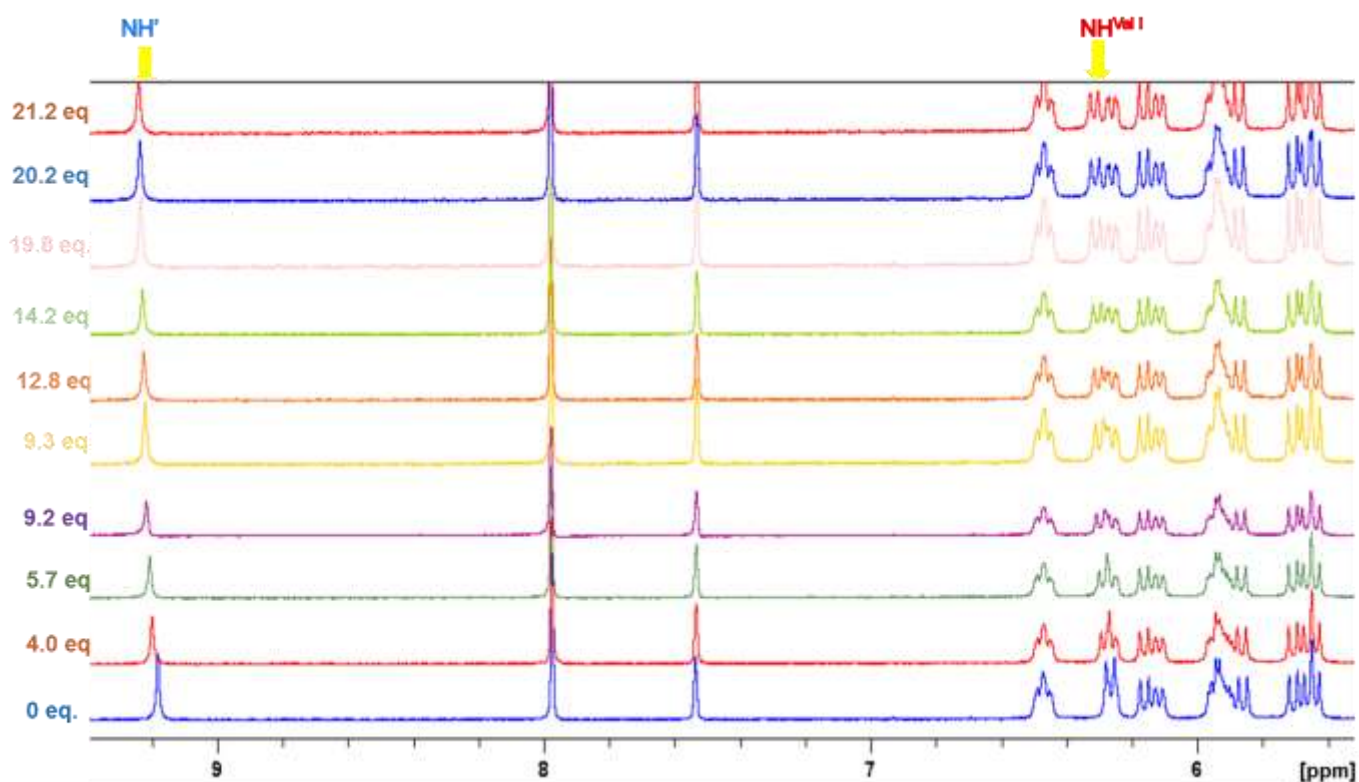


Figure III.11: Titration with deprotonated malonate

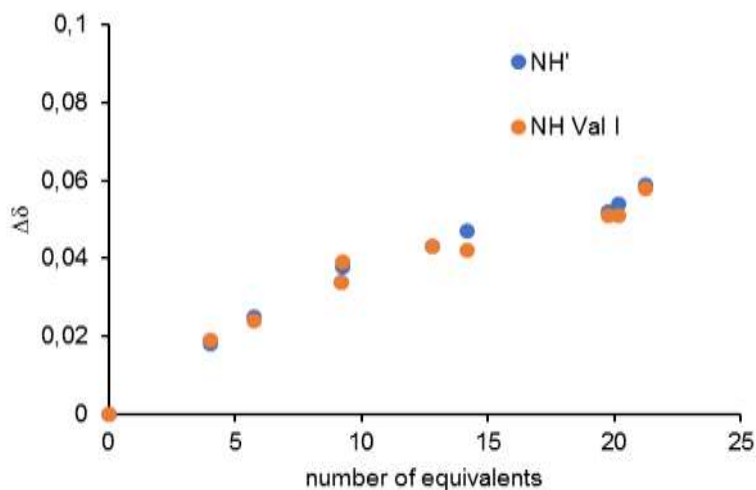


Figure III.12: Chemical shift of NH' and NH(Val^I) from **1a** with the addition of deprotonated malonate

This observation is more in line with another model which was proposed by Pápai where the malonate is activated by the thiourea H-bond donor of the Takemoto catalyst (Figure III.13). According to this model, the nitro group of nitrostyrene interacts with the protonated base, similarly to Pápai proposal. To strengthen this hypothesis and be able to propose a mechanism, we thought to perform a successive addition of the different reactants to an NMR tube containing the catalyst **1a**.

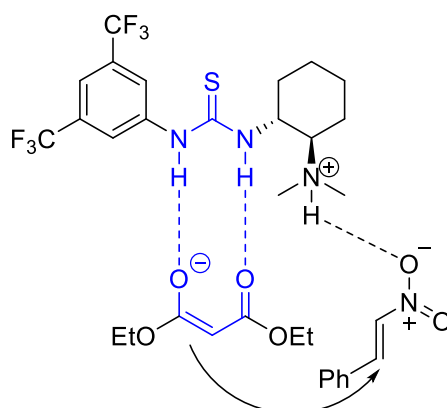


Figure III.13: Pápai model for Michael addition activated by Takemoto catalyst⁹

3.2.4 Competition NMR experiments by successive addition of malonate, nitrostyrene and triethylamine to the catalyst

In the literature, there are many examples of the use of NMR to gain information about the location of catalytic sites.⁵⁻⁶ One strategy is to add separately and then successively the different substrates to the catalyst and observe which proton signal is shifted. Moreover, the order of substrates addition can have an influence and can reveal a competitive coordination of the substrates on the same catalytic site. With this goal, two experiments were run. The first one consisted of the successive

addition of malonate, triethylamine and nitrostyrene, in this order (*Figure III.14*). The addition of malonate induced a very light downfield shift: only the NH' (indicated in light blue) in α -position of the aromatic group presented a shift of 0.0155 ppm. The addition of triethylamine induced a more significant downfield-shift of the NH' (indicated in light blue) in α -position of the aromatic group (0.0776 ppm from the reference spectra). The final addition of nitrostyrene impacted again the NMR spectra with a downfield shift: 0.1308 ppm for NH' signal from the reference catalyst spectra (indicated in light blue) and 0.0552 ppm for NH^{Val I} (indicated in red).

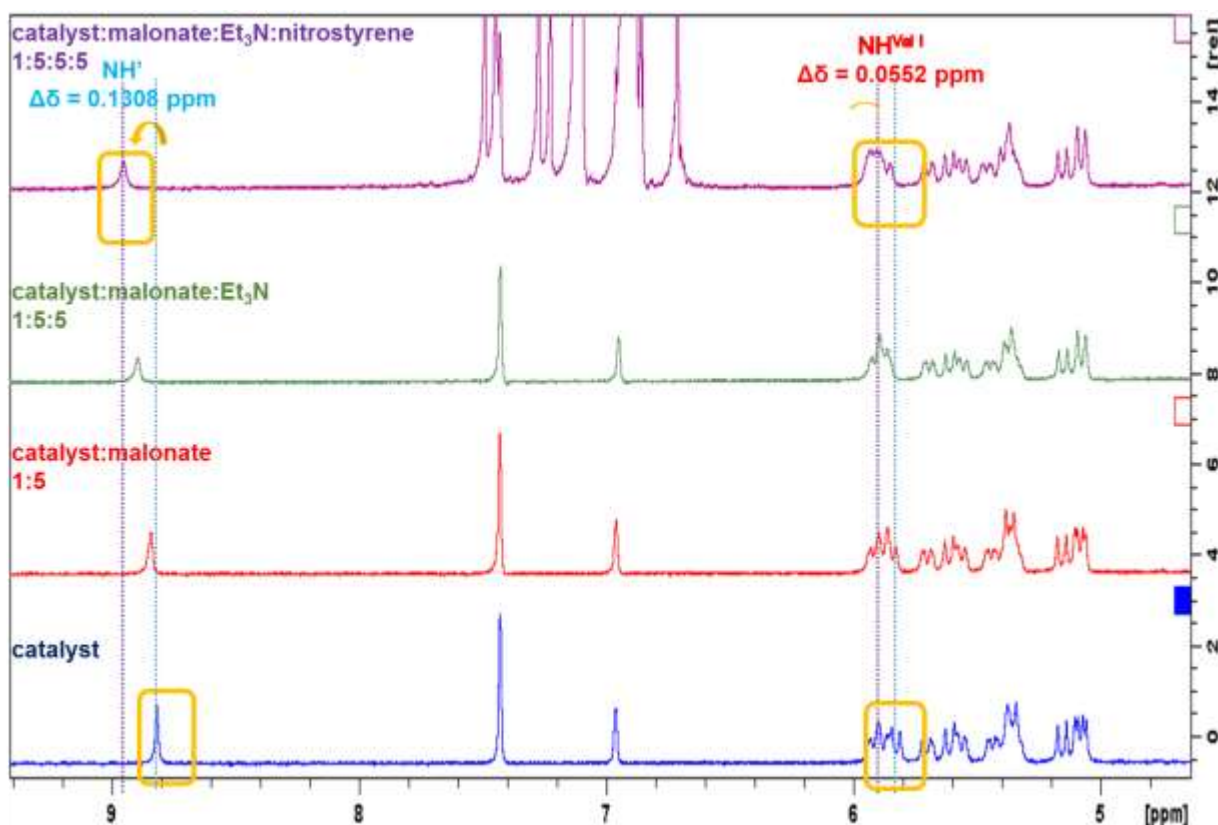


Figure III.14: ¹H-NMR analysis of interactions between catalyst and malonate, triethylamine, nitrostyrene
*Experiments conducted on 300 MHz spectrometer, in DMSO-*d*₆:CD₃CN (12% v:v), at 298K*

The same experiment was run with a different order of addition of the substrates: triethylamine, nitrostyrene, malonate. The triethylamine addition to the catalyst solution did not induce a shift. A downfield-shift appeared upon the nitrostyrene addition (0.0764 ppm for the NH' signal indicated in light blue), and the final malonate addition clearly impacted the NMR spectra by shifting the terminal NHs downfield: 0.1290 ppm for NH' signal (indicated in light blue) and 0.1147 ppm for NH^{Val I} signal (indicated in red) (*Figure III.15*). The difference in the final shifts in the three previous experiments can be explained by the small variation of volume of malonate which has been introduced in each tube.

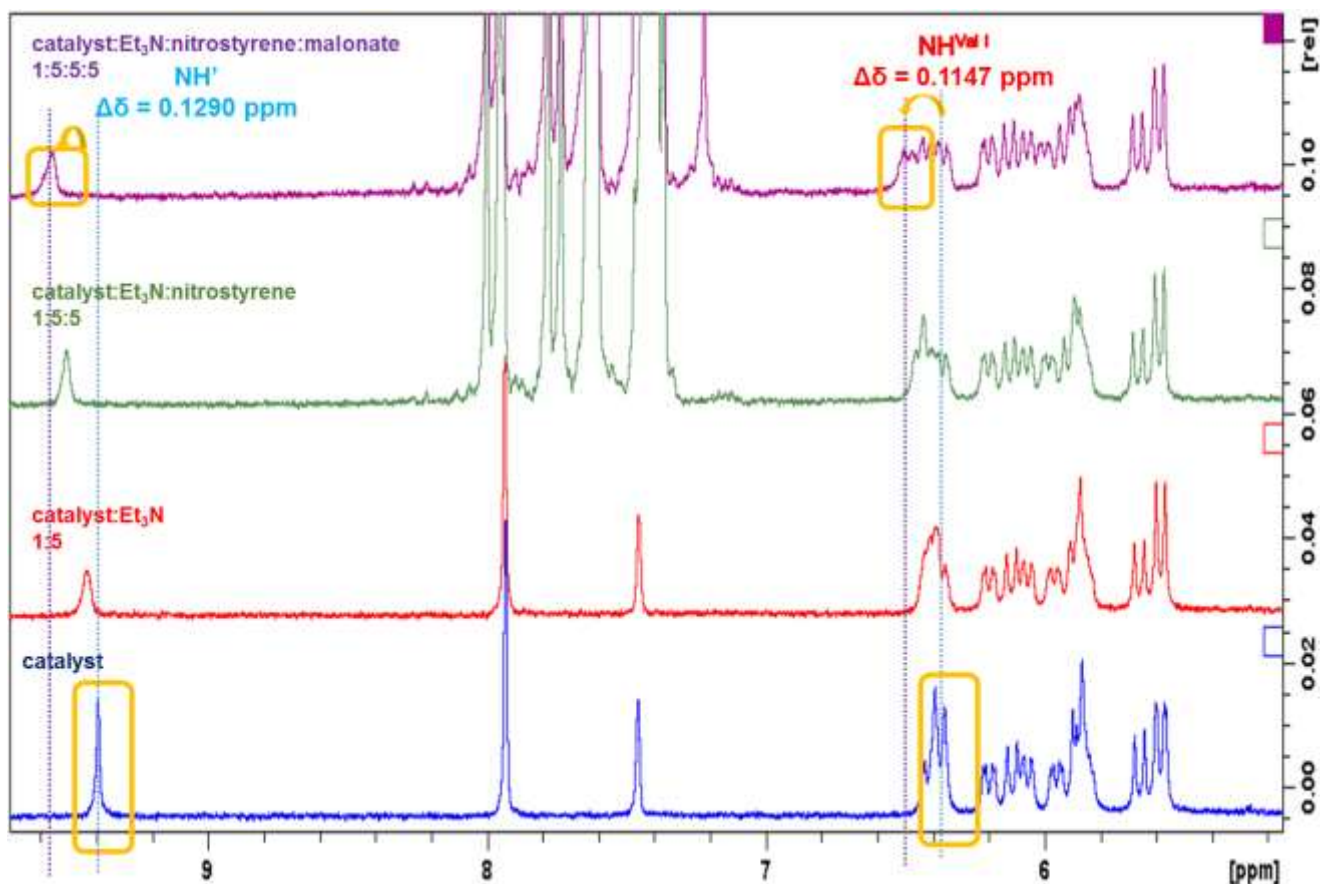


Figure III.15: ¹H-NMR analysis of the interaction between catalyst triethylamine, nitrostyrene and malonate - Experiments conducted on 300 MHz spectrometer, in DMSO-*d*₆:CD₃CN (12% v:v), at 298K

3.2.5 Proposition of mechanism for Michael addition catalysed by 1a

All these experiments allow us to give several conclusions which of course are dependent on the solvent conditions we used: (i) nitrostyrene is not interacting directly with the catalyst (ii) the deprotonated malonate is interacting with the catalyst, more than the cognate malonate (iii) triethylamine critically controls the interaction process because nitrostyrene and malonate do not lead significant modification of the spectrum in its absence (iv) triethylamine alone does not have an impact as strong as the three nitrostyrene-malonate-catalyst on NH chemical shifts. Altogether, these trends may suggest a possible binding model that can be used to explain the mechanism of the catalytic process (Figure III.16). The deprotonated malonate interacts with the two first ureas of the oligomer catalyst at the positive pole of the helix macrodipole, with the protonated triethylamine as a counterion. The nitro group of nitrostyrene may then interact with the protonated base, and this way is indirectly linked to the catalyst by the formation of a supramolecular tetrameric-complex. With the current data, we cannot explain the selectivity of the substrates approach, but we can only propose something which is coherent

with what is observed in the experiments. The downfield shift observed in all these experiments translates a contribution of electrons of the deprotonated malonate to the two first ureas of the catalyst. According to this model, the steric hindrance of the base should have a strong impact as already seen previously and this may explain why the cinchona derivatives were not suitable bases for our system. This model could be reinforced by theoretical calculations that could be performed in the future.

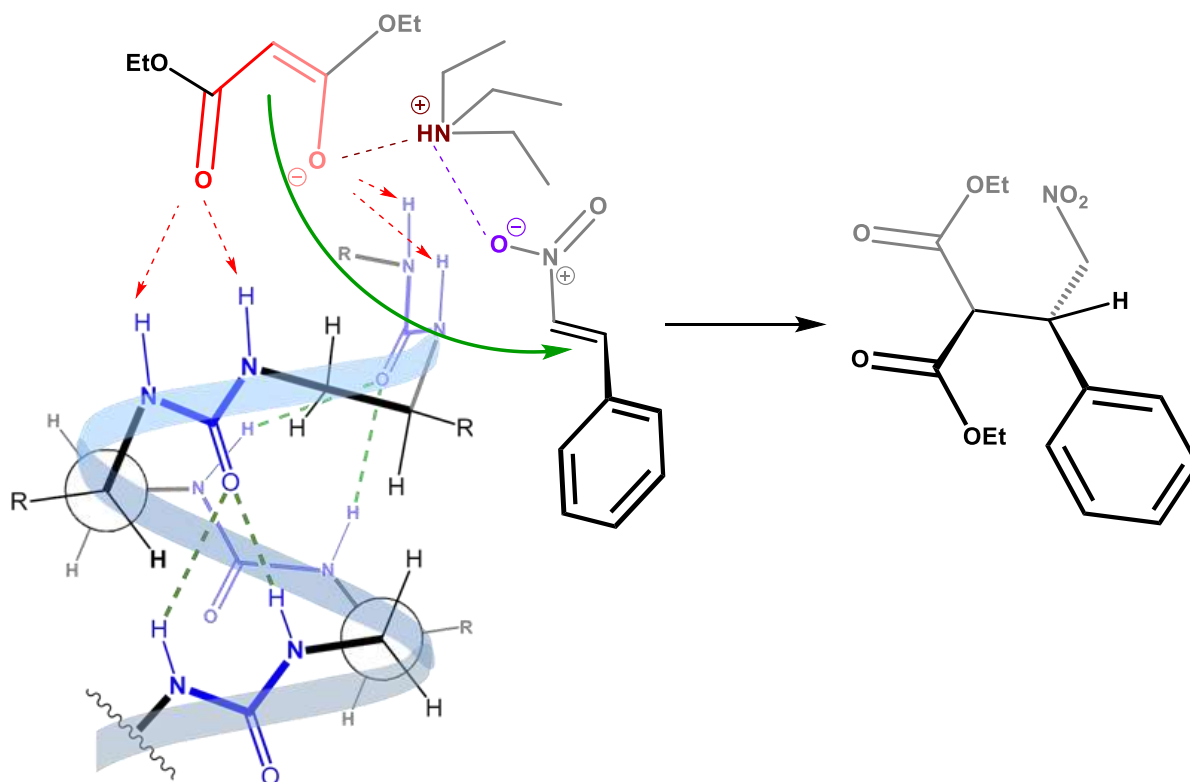
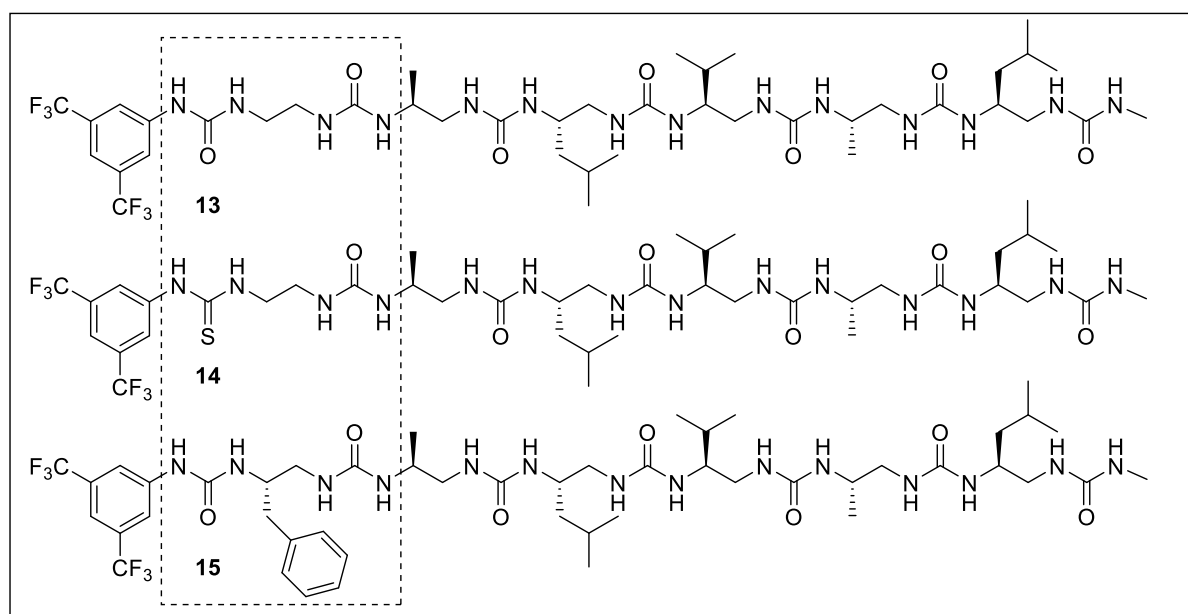
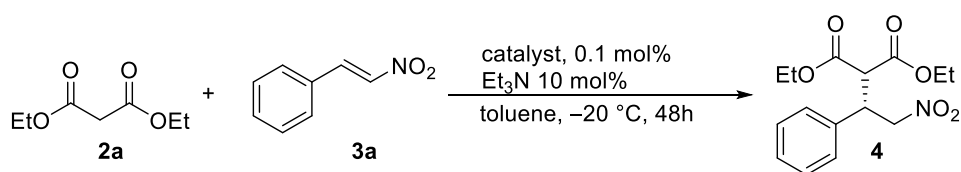


Figure III.16: A possible model of the catalytic process with oligourea foldamers involving the formation of a supramolecular tetrameric complex between the catalyst, the base and the two substrates of the reaction.

3.3 IMPACT OF THE NATURE OF THE FIRST RESIDUE

3.3.1 Sequence variations to study the role of the side chain of the first residue

The catalytic activity results from the two first ureas and the folded backbone which brings both chiral information and synergistic activation through cooperative H-bonding between ureas all along the foldamer and helix polarity. However, the origin of the high stereocontrol observed previously is not fully clarified and it remains to be seen whether the chirality brought by the backbone is enough to control the enantiomeric excess of the adduct or if the nature of the side chain (steric hindrance, functionality) of the first residue (Val^u in **1a**) also play a key role. Catalysts without lateral side chains at the first residue were synthesized by replacing Val^u monomer by a Gly^u derivative, in both urea (catalyst **13**) and thiourea (catalyst **14**) version. Gly^u side residue has been shown previously to be compatible with helix geometry but to have a destabilization effect when inserted in the middle of a short oligourea sequence.¹⁰ Moreover, to evaluate the influence of the chiral side chain in this strategic position, the Val^u residue was replaced by the corresponding Phe^u residue with a Bn side chain to give catalyst **15** (Scheme III.4).



Scheme III.4: Variation of the lateral side chain of the residue between the two catalytic sites

3.3.2 Impact of the first residue variation on the catalytic efficiency

The three new catalysts **13**, **14** and **15** were tested in the addition of **2a** to **3a** using Et₃N 10 mol%, and 0.1 mol% catalyst loading, in toluene at -20 °C for 48h (Table III.1 Table III.2). The removal of the chirality source of information within the catalytic site from structure **1a** (catalyst **13**) slows down the conversion (92% conversion) and affected the enantiomeric excess to a limited extent (decrease from 95% *ee* to 83% *ee*) suggesting that global helicity more than steric hindrance of the side chain of the first residue is important for enantiocontrol. Conversely, in the thiourea version (catalyst **14**), the absence of a chiral side chain has a more dramatic effect on both kinetics and stereocontrol: conversion in 48h dropped from 92% yield to 45% yield and enantiomeric excess fell from 83% *ee* to 35% *ee*. Changing the nature of the chiral unfunctionalized residue (catalyst **15**) between the two catalytic sites does not have an important impact: conversion was almost complete in 48h (94%) and stereocontrol was very good (88% *ee*).

Table III.2: Evaluation of the catalytic efficiency after sequence modification and side modification on the first residue

Entry	Catalyst	Conversion (%)	Yield (%)	<i>ee</i> (%)
1	13	92	75	83
2	14	45	40	35
3	15	94	75	88

Reactions were performed with 0.5 mmol of **3a** and 1.0 mmol of **2a**. Yields correspond to isolated compound after chromatographic purification. The enantiomeric excess (*ee*) was determined by chiral HPLC analysis. Absolute configuration was determined from literature.

3.3.3 NMR conformational analysis of sequence modified catalysts and conclusions about possible structural requirements for high catalytic activity

Structural studies have then been performed to evaluate whether this loss of activity between **1a**, **13** and **14** can be attributed to the absence of chirality at the first position, or to the local perturbation of the helix. The anisochronicity of CH₂^α of each residue along the backbone was measured by ¹H-NMR and the values are presented on the graph below (Figure III.17).

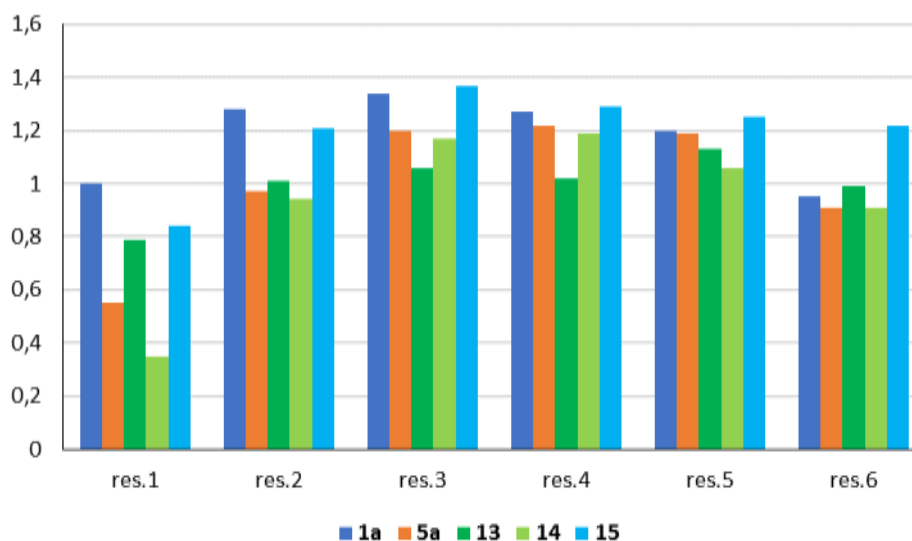


Figure III.17: Anisochronicity of CH_2^α along the backbone of oligoureas with of a glycine-like motif at first position (**13**), a glycine-like motif in first position and a terminal thiourea moiety (**14**), a phenylalanine-like motive in first residue (**15**) and comparison with that of **1a** and **5a**

The chirality of the first residue has an impact on the catalytic efficiency, but the persistence of a well-defined helical structure at the catalytic site is a clearly requirement for the efficiency of the catalytic process. The nature of the lateral side chains between the two first catalytic ureas does not have a major impact on stereocontrol provided that the helicity is maintained. However, the close combination of two modifications (thiourea and Gly^u residue) that locally impact the helical structure of the oligomer (**14**) and thus the catalytic site (Figure III.17), is detrimental for the outcome of the reaction.

Of course, steric hindrance imposed by the side chain and helicity are intimately linked and it is difficult to interrogate both aspects separately when introducing sequence variation close to the catalytic site. However, chain length variations above a minimum known to provide a well-defined helical structure could be used next to evaluate more specifically the impact of helix rigidification and also address the possible role of the helix macrodipole. A longer catalyst with nine residues for instance presents a longer hydrogen-bond network, reduced fraying and increased rigidity at both ends of the helix (Figure III.18). Alternatively, sequences of equal length but incorporating residues with a high helix propensity could be tested. For example, it has been shown that for oligoureas (unpublished results from the Guichard group) like for β^3 -peptides,¹¹ involving branched residues (e.g. β^3 -Val) are stronger stabilizer of helical structures. Hence, oligourea sequences made of the repetition of one type of building block such as $(\text{Val}^u)_n$ are expected to adopt a more rigid helical structure which could be compared to that of **1a** in catalysis (Figure III.18). Moreover, the use of only one type of building block would be very interesting from a synthetic and economic points of view.

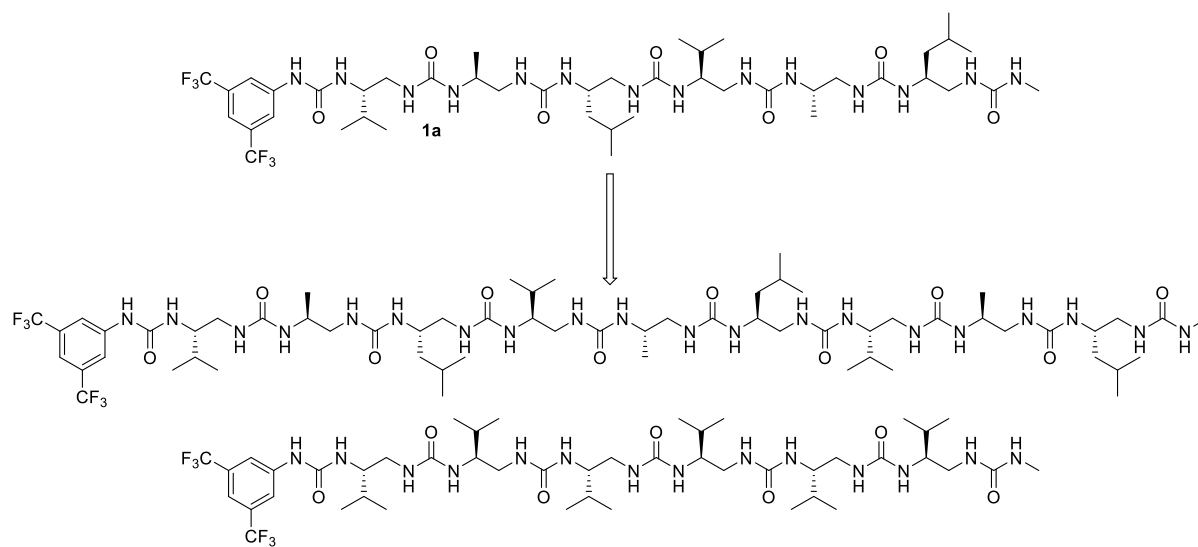


Figure III.18: Two potential catalysts which could bring more mechanistic information on the catalytic system

3.4 KINETIC STUDIES AND VARIATION OF THE CATALYST ENANTIOMERIC EXCESS

3.4.1 Kinetic studies

3.4.1.1 Preliminary

Kinetic analysis is another approach to deepen the mechanistic understanding of the catalytic process. The determination of the order of the reaction for each reactant will give us access to the number of each molecule which is involved in the catalytic process. To answer this question, we used NMR spectroscopy with temperature control (25 °C) in toluene- $[d_8]$. Trimethylphenylsilane was added as an internal reference in order to integrate properly signals of each component and generate quantitative data. A preliminary study (Figure III.19) with the same reagent ratio as in the model reaction: nitrostyrene **3a** : diethyl malonate **2a** : Et_3N : catalyst **1a** 1:2:0.1:0.001. allowed to monitor the almost complete consumption of nitrostyrene, the decrease of almost 50% of the malonate concentration, and the appearance of adduct **4** which reaches a step concentration after 16h (960 min).

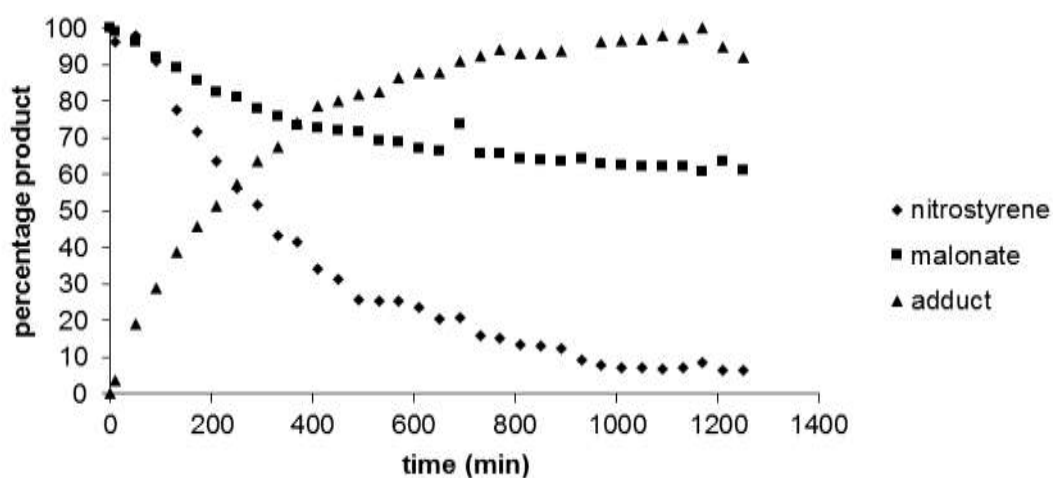


Figure III.19: Kinetic profile of the reaction between malonate **2a** and nitrostyrene **3a** in the presence of oligourea **1a** and triethylamine in toluene at 20 °C. 400MHz ^1H NMR spectra were recorded every 40 minutes. Conditions $[\mathbf{3a}] = 1 \text{ M}$, $[\mathbf{2a}] = 2 \text{ M}$, $[\mathbf{1a}] = 0.001 \text{ M}$, $[\text{Et}_3\text{N}] = 0.1 \text{ M}$.

3.4.1.2 Nitrostyrene order

To determine the order in each reagent, there are many methods described in the literature: method of initial rates,¹² method of flooding,⁸ integral method^{4, 13}. To determine the order in nitrostyrene, we used the method of flooding. The reaction was performed with an excess of malonate (ratio **2a:3a** 10:1), then its influence can be considered as negligible and it will be part of the kinetics constant (Figure III.20). If the reaction kinetics is apparent to a pseudo-order 1, plotting the logarithm of ratio between nitrostyrene initial concentration and nitrostyrene concentration at time t, will give a straight line. If the reaction kinetic reaction is apparent to a pseudo-order 2, plotting the difference of inversed concentrations will result in a straight line. In this manner, it was found that in our case the reaction exhibits a first-order with respect to nitrostyrene (Figure III.21).

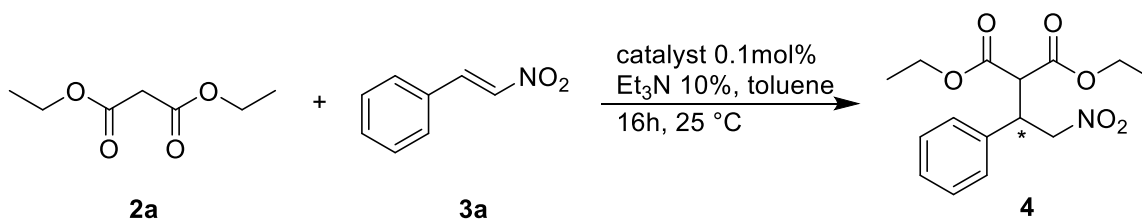
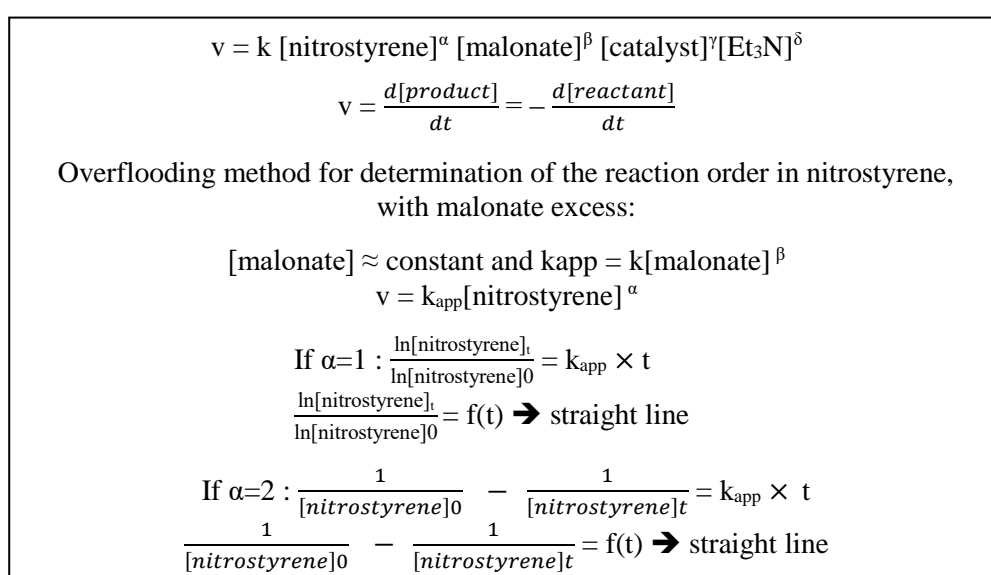


Figure III.20: Overflooding method to determine the nitrostyrene order

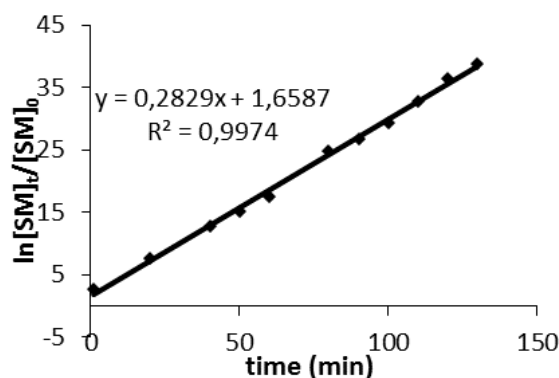


Figure III.21: Determination of the reaction order with respect to nitrostyrene **3a** using the method of flooding

3.4.1.3 Reaction order with respect to malonate, triethylamine and catalyst

The overflowing method is not always an adapted method because the excess of one reagent can completely modify the physical properties of the reaction mixture, for instance an excess of nitrostyrene makes the mixture too dense and viscous to allow reliable data to be obtained. The method of initial rates is useful to cope with this difficulty but also to evaluate orders in components which acted in a catalytic way (Figure III.22). We used this method to determine the orders in malonate, base and foldamer catalyst. To determine the reaction order in one component, several experiments are run with different initial concentrations of this components, all the other parameters being fixed. The initial rate is estimated graphically by the tangent to the curve. For a first-order reaction, the plotting of the initial rate in function of the different concentrations of the evaluated component gives a straight line. For a second order reaction, the plotting of the initial rate in function of the squares of the different concentrations of the evaluated component gives a straight line. Another way to demonstrate it is to plot the logarithm of initial rates in function of the logarithm of the evaluated component concentration. The slope will correspond to the order in the evaluated component.

$$v = k [\text{nitrostyrene}]^\alpha [\text{malonate}]^\beta [\text{catalyst}]^\gamma [\text{Et}_3\text{N}]^\delta$$

$$v = \frac{d[\text{product}]}{dt} = - \frac{d[\text{reactant}]}{dt}$$

$$\text{At } t = 0^+ \quad v_0 = \frac{d[\text{product}]}{dt}_{(\text{at } t=0^+)} = k [\mathbf{3a}]_0^\alpha [\mathbf{2a}]_0^\beta [\text{catalyst}]^\gamma [\text{Et}_3\text{N}]^\delta$$

For triethylamine order determination:

$$[\mathbf{3a}]_0 = \text{constant}$$

$$[\mathbf{2a}]_0^\beta = \text{constant}$$

$$[\text{catalyst}]^\gamma = \text{constant}$$

$$\frac{d[\text{product}]}{dt}_{(\text{at } t=0^+)} = k_{\text{app}} [\text{Et}_3\text{N}]_0^\alpha$$

Figure III.22: Initial rate method, illustrated with the determination of the order in trimethylamine

The orders for malonate and triethylamine were demonstrated to be order 1 (see Figure III.23 and Figure III.24, respectively). For the catalyst, a breaking slope was observed from 0.2 mol% (Figure III.25). From these orders, we can deduce the molecularities of the catalytic process. One molecule of malonate is deprotonated by one molecule of triethylamine to be added with one molecule of nitrostyrene. The interaction with the molecules of catalyst depends on the catalyst loading **1a**.

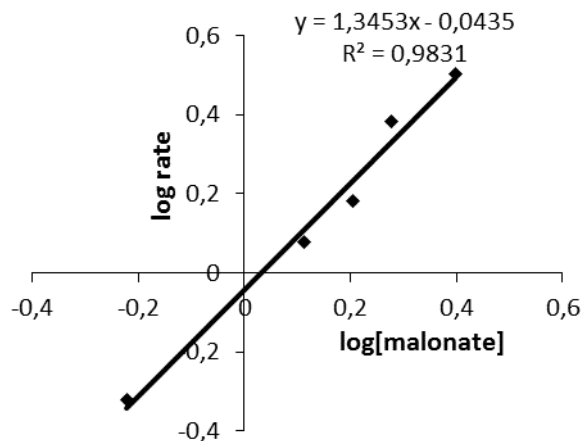


Figure III.23: The catalysed reaction is first-order in malonate **2a**

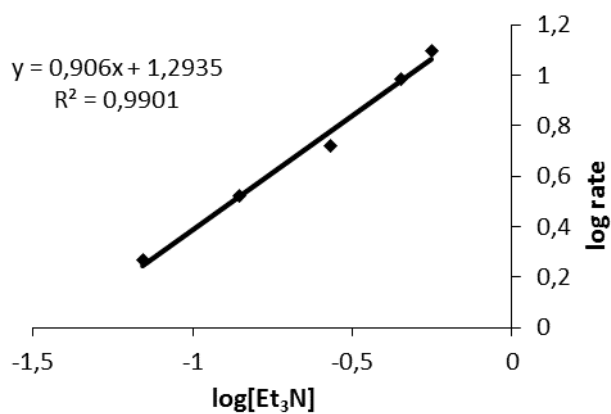


Figure III.24: The catalysed reaction is first-order in triethylamine

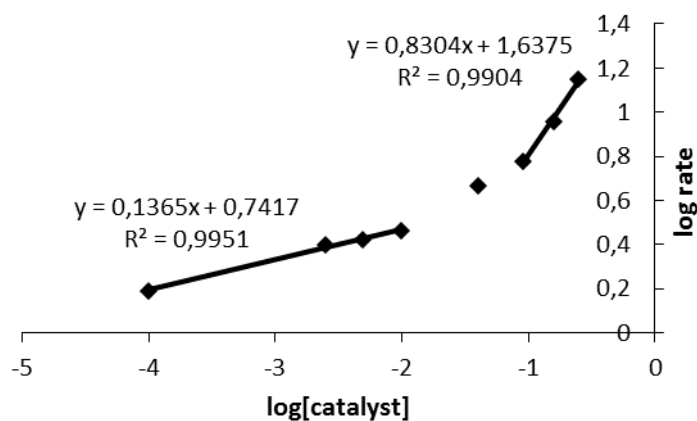


Figure III.25: Observation of two behaviours when determining the reaction order in catalyst

3.4.2 Study of non-linear effects

The association of the two catalyst enantiomers can be precious to gain additional information about the mechanism of the reaction. If only one catalyst molecule interacts with the substrates, then the relationship between the adduct enantiomeric excess and the catalyst enantiomeric excess will be linear. In contrast, if more than one molecule of catalyst interacts with the substrates, a curve will be observed in the graphical representation (Figure III.26). These non-linear effects and associated mathematical models have been developed by Kagan.¹⁴ The existence of a non-linear effect reflects an aggregation effect between the catalysts.

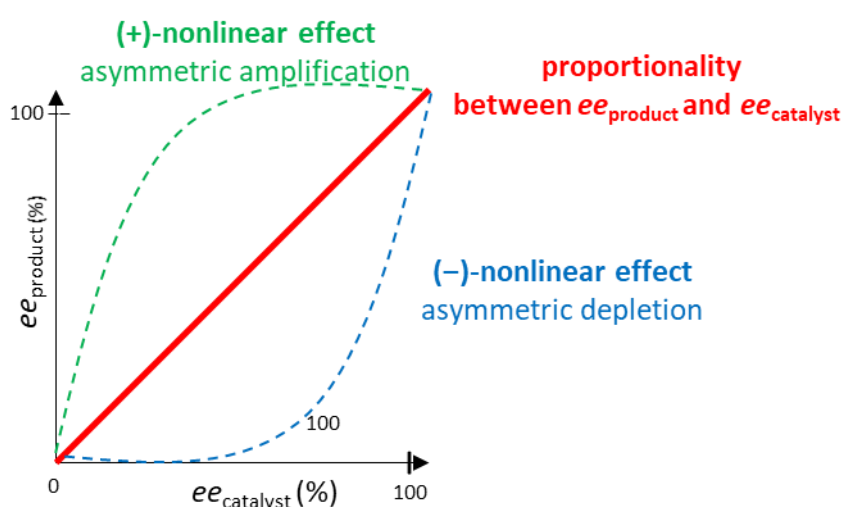


Figure III.26: Representation of non-linear effect

3.4.2.1 Variation of foldamer catalyst enantiomeric excess

The two enantiomers **1a** and *ent-1a* have been mixed in a different ratio to form solutions wherein catalyst **1a** has different enantiomeric excesses: 0% *ee*, 20% *ee*, 40% *ee*, 60% *ee*, 80% *ee*, 100% *ee* (with **1a**), 100% *ee* (with *ent-1a*). Enantiomeric excesses of catalyst solutions which are not enantiopure correspond to mixtures with **1a** as major enantiomer: 20% *ee* corresponds to 60% **1a** and 40% *ent-1a*. The variation of enantiomeric excess was checked by measurement of the relative helicities by circular dichroism in methanol (Figure III.27). The UV band absorption of the aromatic ring was used to normalise all the spectra. The resulting graph was coherent with the mixtures.

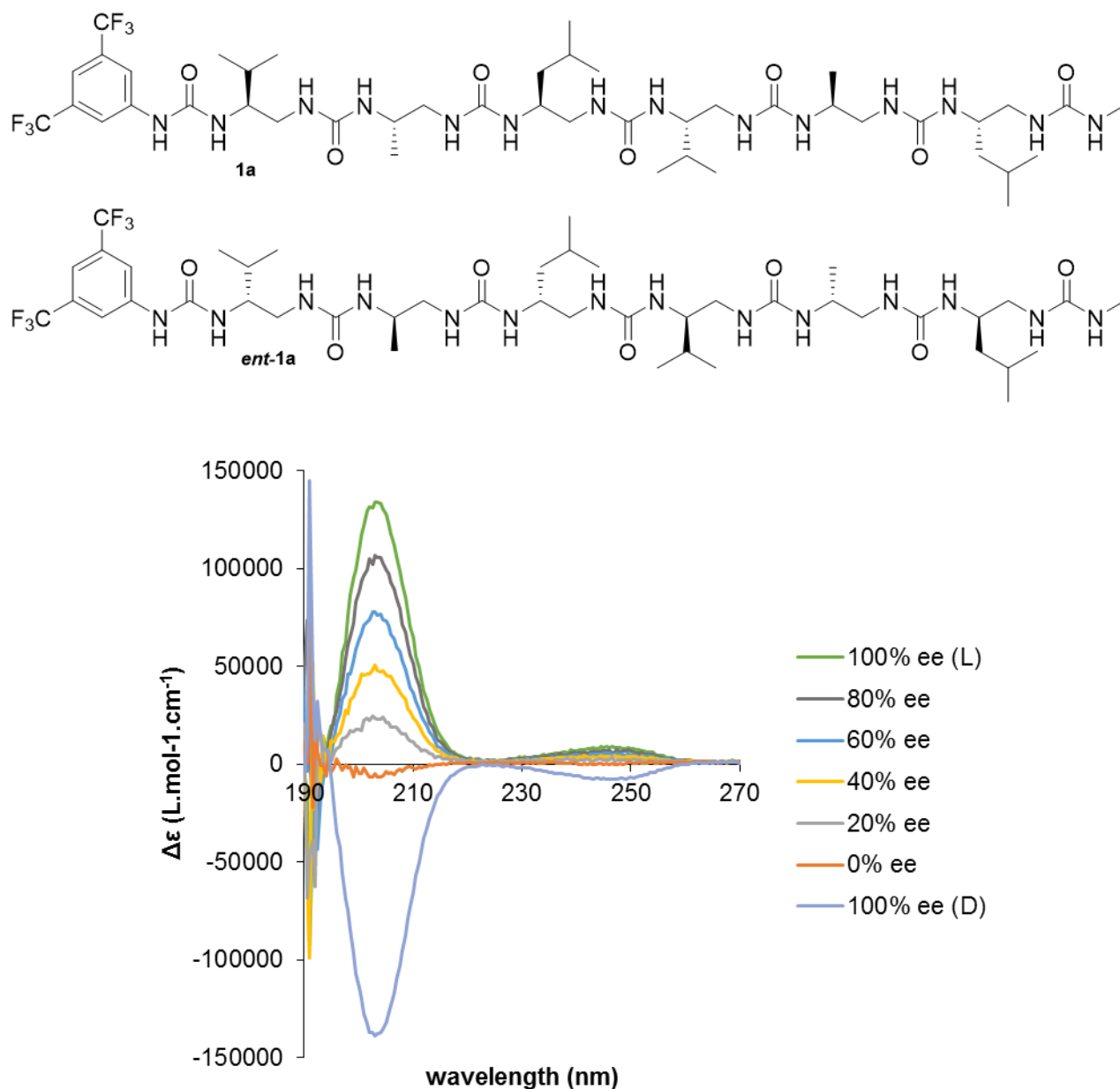


Figure III.27: Preparation of solutions with different enantiomeric ratio from **1a** and **ent-1a**

3.4.2.2 Impact of the catalyst enantioenrichment on the stereocontrol of the reaction

The previously prepared solutions of foldamer catalysts at different enantiomeric ratio were used as stock solution to perform the model reaction with 10 mol% Et₃N, in toluene at -20 °C for 48h. Different catalyst loadings from these solutions were tried, because if the phenomenon of aggregation exists, it can appear at a specific critical concentration: experiments were thus run at 0.1 mol%, 0.02 mol%, and 0.001 mol% of catalyst. Results are given in the table below (Table III.3). For the graphic representation, the enantiomeric excess of the adduct obtained with pure **1a** was normalised to 100%

(Figure III.28). At 0.001 mol% in catalyst loading, the relation is perfectly linear. From 0.02 mol% in catalyst loading, the curve starts to move away from the straight line. With 0.1 mol% which is our reference catalyst loading, the asymmetric depletion is substantial although not massive.

Table III.3: Impact of catalyst ee on adduct **4a** ee

Catalyst loading (mol%)	Entry	Catalyst ee (%)	$[\Delta\theta]$ (deg.cm ² .dmol ⁻¹)	Conversion (%)	Yield (%)	Adduct ee (%)
0.001	1	100	438749	43	30	55
	2	80	334381	45	34	43
	3	60	238733	48	37	31
	4	40	149242	46	34	19
	5	20	59554	49	37	8
	6	0	-33523	47	37	-3
0.02	7	100	438749	97	84	91
	8	80	334381	97	85	59
	9	60	238733	98	82	38
	10	40	149242	98	83	23
	11	20	59554	98	83	9
	12	0	-33523	98	82	-5
0.1	13	100	438749	100	84	95
	14	80	334381	100	83	52
	15	60	238733	100	74	33
	16	40	149242	100	83	19
	17	20	59554	100	85	8
	18	0	-33523	100	88	-3

Reactions were performed with 0.5 mmol of **3a** and 1.0 mmol of **2a**. Yields correspond to isolated compound after chromatographic purification. The enantiomeric excess (ee) was determined by chiral HPLC analysis. Absolute configuration was determined from literature. Molar ellipticity was determined by circular dichroism.

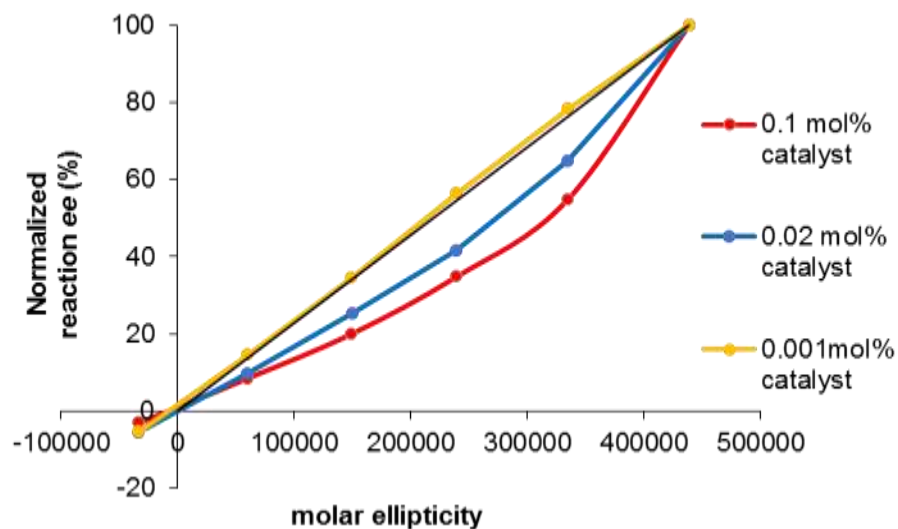


Figure III.28: Graphical representation of the non-linear effect observed in the catalytic process at increasing concentration of the catalyst.

Results of kinetic studies and measurements of non-linear effects both tend to support a trend for aggregation of catalyst molecules above a certain loading. It would be of interest to know more precisely about how the molecules are interacting, whether the catalyst molecules have an arrangement head-to-head or head-to-tail. Molecular modelling, ideally co-crystallization between the catalyst and one or more of the substrates together, could provide useful answers. Modifying the substrates of the model reaction and try to explore other reactions is also a possibility to improve our understanding of the catalytic mechanism.

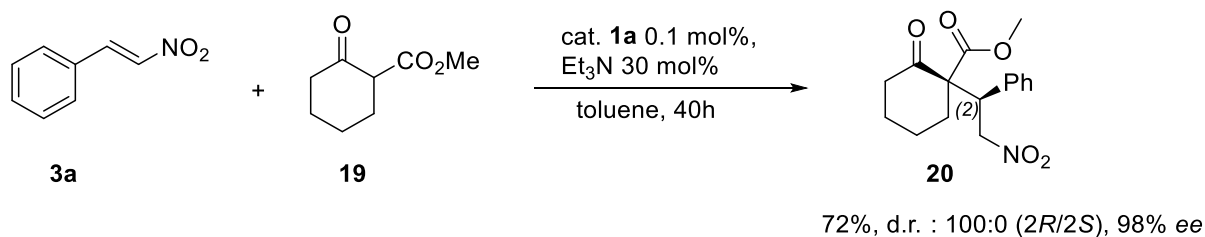
Bibliography

1. Diemer, V.; Fischer, L.; Kauffmann, B.; Guichard, G., *Chem. Eur. J.* **2016**, *22* (44), 15684-15692.
2. Fremaux, J.; Kauffmann, B.; Guichard, G., *J. Org. Chem.* **2014**, *79* (12), 5494-502.
3. Azuma, T.; Kobayashi, Y.; Sakata, K.; Sasamori, T.; Tokitoh, N.; Takemoto, Y., *J. Org. Chem.* **2014**, *79* (4), 1805-17.
4. Quintard, A.; Cheshmedzhieva, D.; Sanchez Duque Mdel, M.; Gaudel-Siri, A.; Naubron, J. V.; Genisson, Y.; Plaquevent, J. C.; Bugaut, X.; Rodriguez, J.; Constantieux, T., *Chemistry* **2015**, *21* (2), 778-90.
5. Etxabe, J.; Izquierdo, J.; Landa, A.; Oiarbide, M.; Palomo, C., *Angew. Chem. Int. Ed.* **2015**, *54* (23), 6883-6.
6. Zhu, J. L.; Zhang, Y.; Liu, C.; Zheng, A. M.; Wang, W., *J. Org. Chem.* **2012**, *77* (21), 9813-25.
7. Okino, T.; Hoashi, Y.; Takemoto, Y., *J. Am. Chem. Soc.* **2003**, *125*, 12672-12673.
8. Okino, T.; Hoashi, Y.; Furukawa, T.; Xu, X.; Takemoto, Y., *J. Am. Chem. Soc.* **2005**, *127*, 119-125.
9. Hamza, A.; Schubert, G.; Soos, T.; Papai, I., *J. Am. Chem. Soc.* **2006**, *128* 13151-13160.
10. Pendem, N.; Douat, C.; Claudon, P.; Laguerre, M.; Castano, S.; Desbat, B.; Cavagnat, D.; Ennifar, E.; Kauffmann, B.; Guichard, G., *J. Am. Chem. Soc.* **2013**, *135* (12), 4884-92.
11. Raguse, T. L.; Lai, J. R.; Gellman, S. H., *Helvetica Chimica Acta* **2002**, *85*, 4154-4164.
12. Zuend, S. J.; Jacobsen, E. N., *J. Am. Chem. Soc.* **2007**, *129*, 15872-15883.
13. Wiesner, M.; Upert, G.; Angelici, G.; Wennemers, H., *J. Am. Chem. Soc.* **2010**, *132*, 6-7.
14. Guillaneux, D.; Zhao, S.-H.; Samuel, O.; Rainford, D.; Kagan, H. B., *J. Am. Chem. Soc.* **1994**, *116*, 9430-9439.

CHAPTER IV

CHAPTER IV

4.1 VARIATION OF PRONUCLEOPHILES IN THE MICHAEL ADDITION TO NITROALKENES	126
4.1.1 Evaluation of malonates with ester functions of increasing size	126
4.1.2 Variation around the pronucleophile.....	127
4.2 VARIATIONS OF ELECTROPHILES IN THE MICHAEL ADDITION OF DIMETHYL MALONATE.....	129
4.2.1 Variation around aromatic nitroalkenes	129
4.2.2 Aromatic conjugated nitroalkenes	131
4.2.3 Scope aliphatic hindered and linear nitroalkenes.....	131
4.2.4 Towards a diastereoselective version of the Michael addition	133
4.2.4.1 Addition of deprotonated malonate monoamide 24 on nitrostyrene 1a	133
4.2.4.2 Asymmetric addition of dissymmetric ketoester on nitrostyrene 1a	134
4.3 CASCADE MICHAEL ADDITION REACTIONS.....	135
4.3.1 Cascade Michael addition as a way to access to cyclic ketone with four stereocenters	135
4.3.2 Asymmetric Cascade Michael reaction with oligourea catalyst	136
4.4 JULIÁ-COLONNA EPOXIDATION	138
4.4.1 Comparison between literature catalysts and oligourea foldamers	138
4.4.2 Screening external parameters for asymmetric Juliá-Colonna epoxidation.....	139
4.4.3 Simple modifications of the hexameric foldamer catalyst for asymmetric Juliá-Colonna epoxidation.....	141
4.4.4 Synthesis of new substrate with double potential anchoring spots to catalyst.....	143
4.2 HENRY REACTION.....	144



*Scheme IV.1: Formation of quaternary centre with the diastereoselective addition of cyclic ketoester **19** to nitrostyrene **3a***

Malononitrile (pKa = 11.1 in DMSO from Bordwell pKa Table) was tested with the catalyst but despite a good conversion and a good yield, no stereocontrol was observed. Probably, the nitrile function is not suitable for a good coordination with the catalyst. Moreover, the possibility of variation on the base nature offers the possibility to use very strong base to deprotonate harsh substrates. In this idea, the sulfones bis(phenylsulfonyl)methane (pKa = 12.2 in DMSO from Bordwell pKa Table), benzodithiol tetraoxide and 2-substituted benzodithiol tetraoxide were tested as pronucleophiles (Figure IV.1), in association with DBU as base (1,8-diazabicyclo[5.4.0]undec-7-ene, pKa = 13.8²). Unfortunately, like in the reaction of **3a** with **17**, whatever the temperature and solvents conditions employed, polymerization of nitrostyrene was faster than deprotonation and addition of the corresponding sulfones.

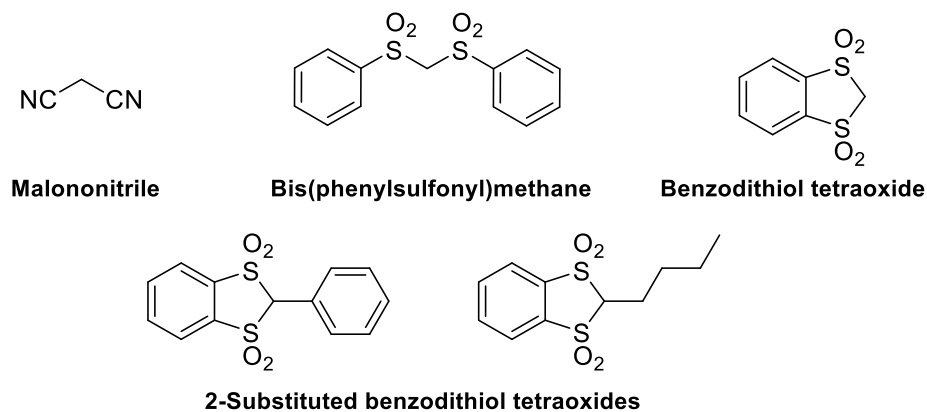


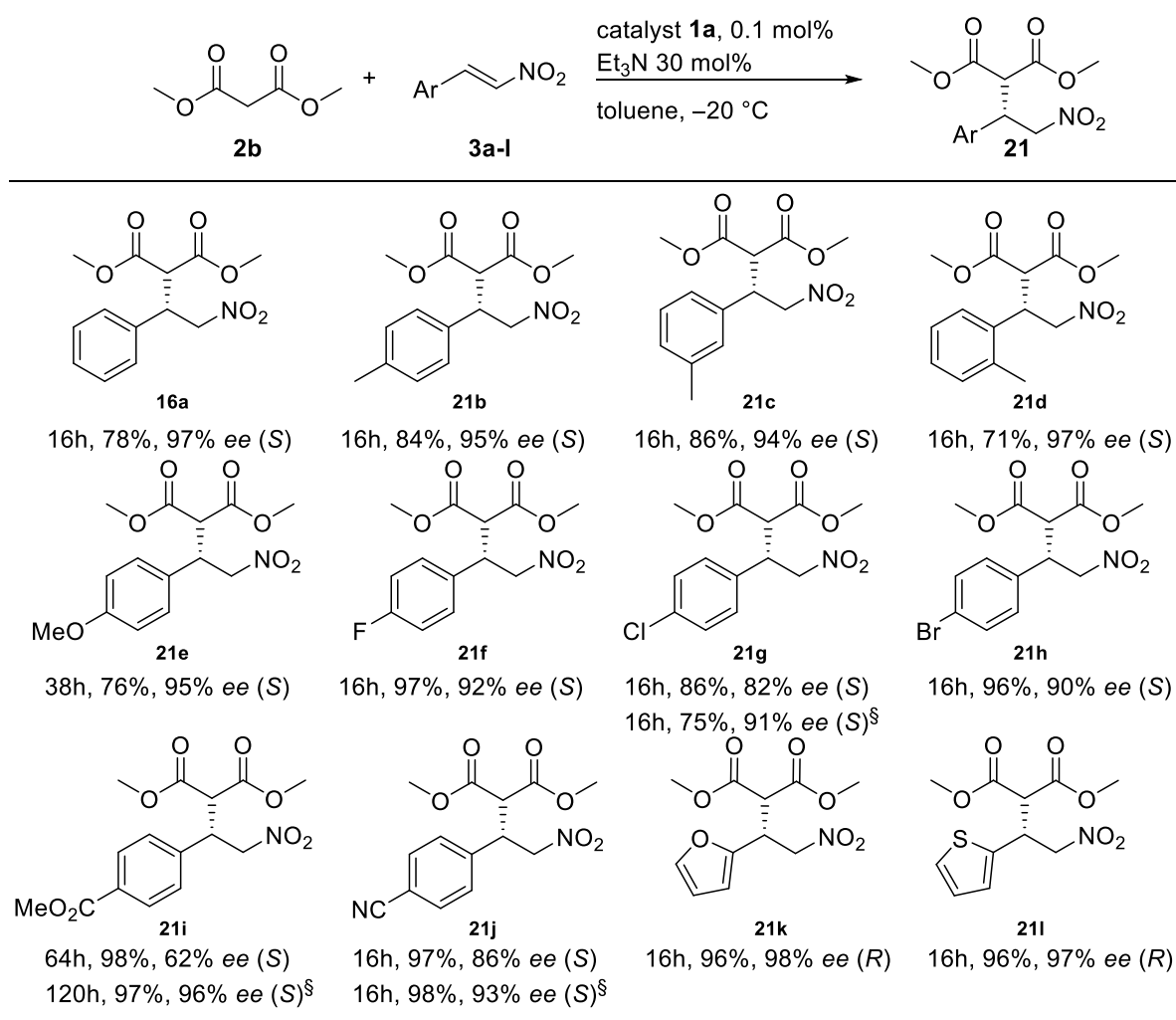
Figure IV.1: Pronucleophiles selected to further evaluate the potential of our catalytic system

4.2 VARIATIONS OF ELECTROPHILES IN THE MICHAEL ADDITION OF DIMETHYL MALONATE

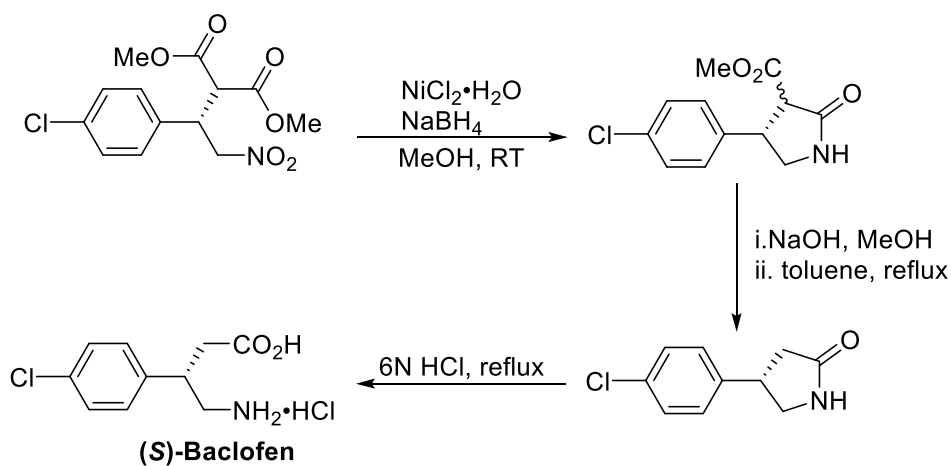
4.2.1 Variation around aromatic nitroalkenes

As stated previously (see 4.1.1), the dimethyl malonate **2b** was chosen as pronucleophile to maximise enantiomeric ratios when performing the scope of electrophiles. Methyl substituted nitrostyrene in position *ortho*-, *meta*-, and *para*- were very well tolerated with excellent yields and enantioselectivities (**21b-21d**, Table IV.3). Substituents with different electroactivities were tested in *para*-position. We already showed that an inductive donating group such as methyl was accepted by the system. Methoxy group, with mesomeric donor and inductive attractor, slowed down the kinetics but gives good results (**21e**, Table IV.3). Halogens were very well tolerated in both reactivities and selectivities (**21f-21h**, Table IV.3). Substrate **21g** is a Baclofen precursor (Scheme IV.2), a product with pharmaceutical interest commercialized under the name of Lioresal by Novartis, and used as myorelaxant. Ester and nitrile substituents, both mesomeric acceptors and inductive attractors, presented modest stereocontrol with triethylamine, but it was improved by the use of diisopropylethylamine (**21i-21j**, Table IV.3). Heteroaromatic also led to excellent results (**21k-21l**, Table IV.3). All the simple modifications on the aromatic group of the nitroalkenes are tolerated by the system: positions of substituents on the aromatic ring, electronic activity of the substituents, insertion of a heteroatom inside the aromatic group. A next challenge around the aromatic electrophiles can be the conjugated ones, such as derivatives of cinnamaldehyde.

Table IV.3: Scope with aromatic nitroalkenes



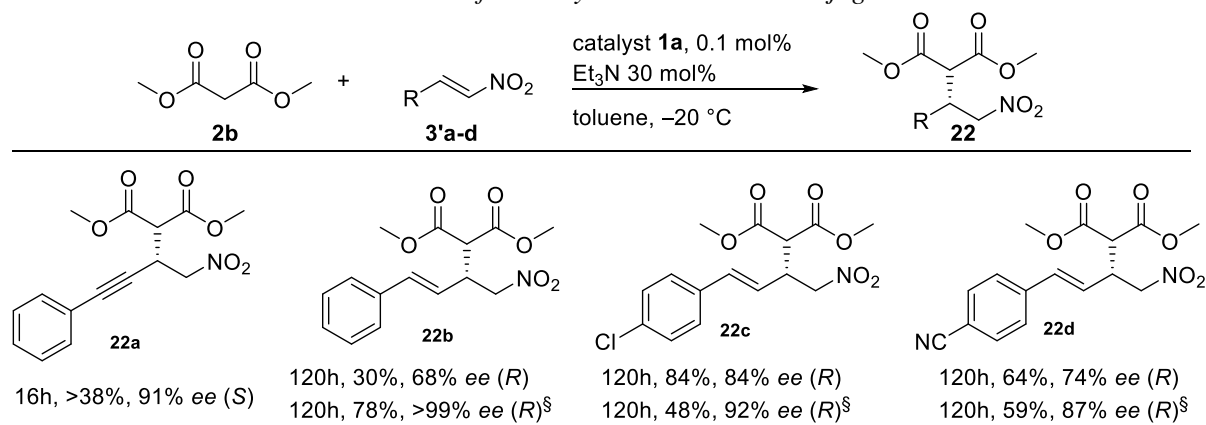
[§] with DIPEA 30 mol%. Yields were determined after purification on Silica Gel Chromatography. Enantioselectivities were determined by analytical Chiral HPLC. Relative configuration (*R*) or (*S*) was determined by comparison with literature.

Scheme IV.2: Synthesis of (*S*)-Baclofen from Michael adduct **21g**¹

4.2.2 Aromatic conjugated nitroalkenes

Conjugated aromatic nitroalkenes present a competitive double bond or triple bond for the addition of the pronucleophile. The yields with these new substrates were lower but the enantioselectivities were still very satisfying (**22a-22d**, Table IV.4). Reactions were led to complete conversion, the decrease in yield was due to the formation of subproducts. Moreover, the use of Hunig's base allowed, once again, to access to products with excellent enantioselectivities (**22b-22d**, Table IV.4). These results enforce the demonstration of the high variety of nitroalkenes which are accepted by our catalytic system.

Table IV.4: Michael addition of dimethyl malonate **2b** to conjugated nitroalkenes **3'a-d**



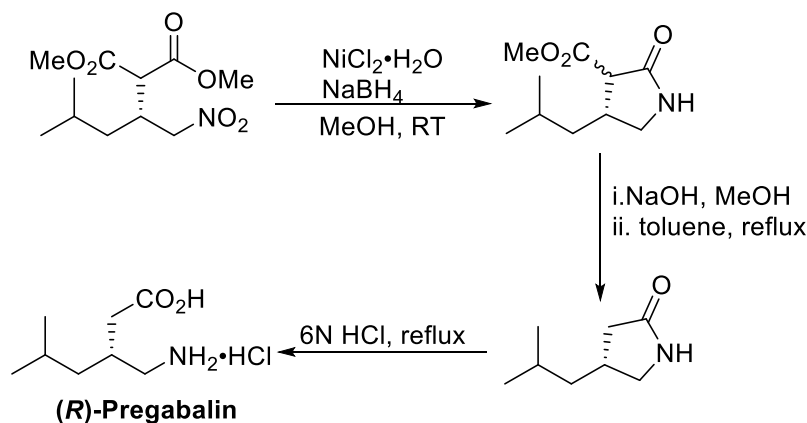
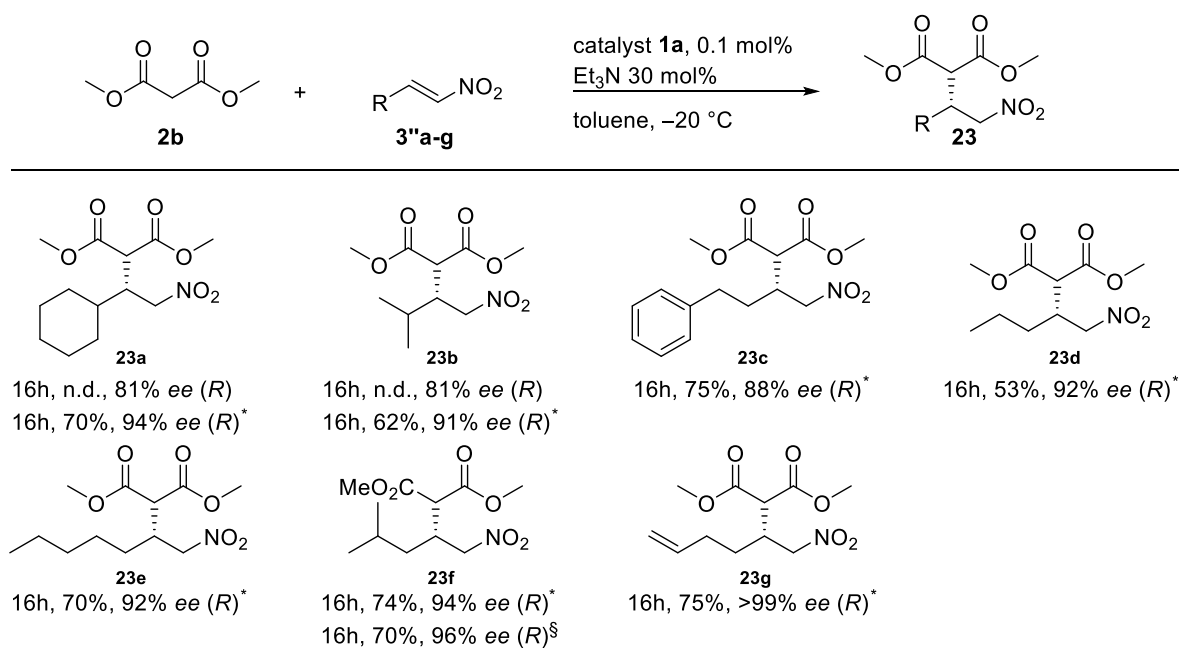
[§] with DIPEA 30 mol%. Yields were determined after purification on Silica Gel Chromatography. Enantioselectivities were determined by analytical Chiral HPLC. Relative configuration (R) or (S) was determined by comparison with literature.

4.2.3 Scope aliphatic hindered and linear nitroalkenes

Regarding the very large possibilities of our catalytic system with the aromatic nitroalkenes, the discussion was then orientated to aliphatic nitroalkenes which are generally less reactive.^{1, 3} The analogue of nitrostyrene with a cyclohexyl group, leading to substrate **23a**, presented good results in our standard conditions (0.1 mol% in catalyst **1a**, Et₃N 30 mol%, toluene, -20 °C) and enantiocontrol reached 94% ee with 0.3 mol% in catalyst **1a**, Et₃N 30 mol%, toluene, -30 °C (**23a**, Table IV.5). This result suggests that there is no critical π -stacking interaction between aromatic nitroalkene electrophiles and the electron-withdrawing aromatic group of the catalyst. An acyclic analogue of nitrovinylcyclohexane also presented similar results, which shows the tolerance of more flexible aliphatic nitroalkenes by our system (**23b**, Table IV.5). Less hindered aliphatic nitroalkenes were tested as electrophiles under these new conditions, with 0.3 mol% catalyst **1a** at -20 °C in toluene with Et₃N 30 mol%. Results were very satisfying with good yields and excellent enantiomeric excesses (**23c-23g**, Table IV.5). Interestingly, adduct **23f** is a Pregabalin precursor (Scheme IV.3), commercialized by

Pfizer under the name of Lyrica, to treat epilepsy. Synthesis of **23f** was also performed very successfully with only 0.1 mol% catalyst **1a**, by replacing Et₃N by DIPEA as base.

Table IV.5: Scope with aliphatic nitroalkenes **3''a-g**



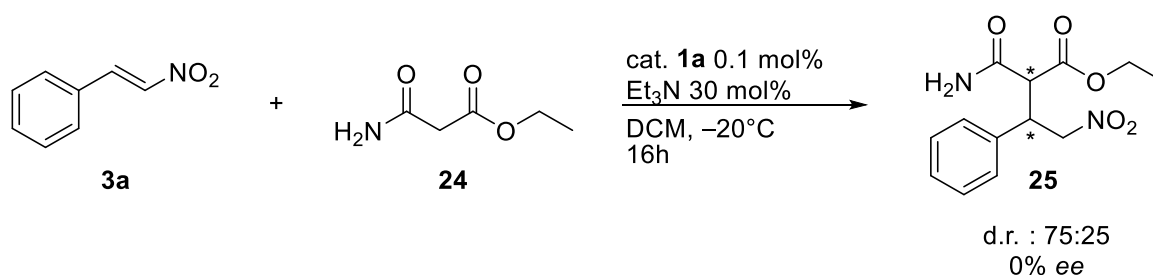
Scheme IV.3: Synthesis of (R)-Pregabalin from Michael adduct **23f**[†]

The very wide range of possibilities around the nitroalkene is coherent with the mode of action we proposed previously (See 3.2.4). Aromatic, substituted, conjugated, aliphatic hindered and linear nitroalkenes are very well tolerated by the designed catalytic system. The external base was shown one more time to be an advantage as it can be adapted to the substrates to maximize the enantiocontrol at low catalyst loading.

4.2.4 Towards a diastereoselective version of the Michael addition

4.2.4.1 Addition of deprotonated malonate monoamide **24** on nitrostyrene **1a**

Following the excellent results in the enantioselective addition of 1,3-diketones on nitroalkenes, pronucleophiles which are able to drive to two pairs of diastereomers have been tested. Ethyl malonate monoamide **24** contains two C=O bonds with the same 1,3-relationship as symmetric dimethyl malonate. The desymmetrisation due to the amide group is interesting since it would be possible to observe if the oligourea catalyst is able to differentiate the amide function from the ester function, and then foster the formation of one pair of diastereoisomer relative to the other.



*Scheme IV.4: Addition of pronucleophile **24** on nitrostyrene **3a**, catalysed by oligourea catalyst **1a***

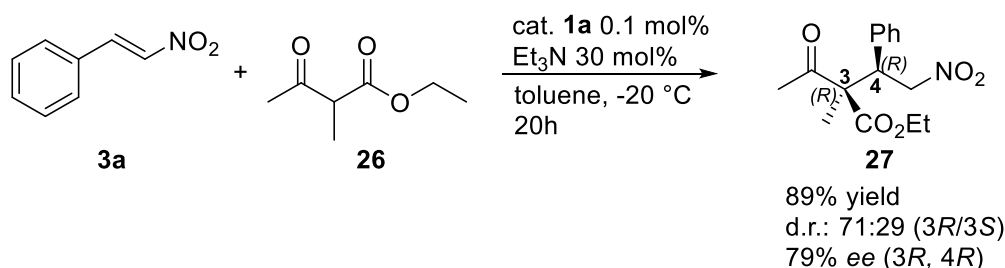
Because of the very low solubility of ethyl malonate monoamide **24**, the racemic and asymmetric reactions were both performed in DCM. The racemic reaction led to complete conversion overnight and the formation of two pairs of diastereomers with a ratio 75:25. Surprisingly, the same reaction with catalyst **1a** had no impact on the diastereomeric ratio, d.r. : 75:25 with 0.1 mol% of catalyst **1a** and 30 mol% of Et₃N, but did not conduct to any enantiomeric ratio either (Scheme IV.4). The free amide in substrate **24** can form competitive hydrogen bonds between substrates, avoiding the coordination of the nucleophile with the oligourea **1a**, resulting to the absence of enantiocontrol. To pursue this direction of investigation, bi-alkylated amide should be synthesized to avoid the malonate monoamide to be a potential hydrogen bond donor (Figure IV.2).

Figure IV.2: Potential malonate monoamide to test for diastereomeric Michael addition



4.2.4.2 Asymmetric addition of dissymmetric ketoester on nitrostyrene **1a**

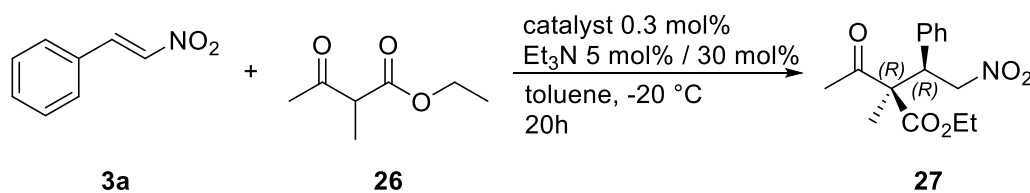
Dissymmetric ketoester ethyl 2-methyl acetoacetate **26** was also tested in the asymmetric Michael addition on nitrostyrene **3a** (Scheme IV.5). With catalyst **1a** 0.1 mol%, the conversion was complete after 20h, leading to a very good yield (89%) after purification on Silica Gel chromatography, with relatively good stereocontrol, 71:29 dr and 79% *ee*.



Scheme IV.5: Asymmetric addition of pronucleophile **26** on nitrostyrene **3a** catalysed by oligourea **1a**

The loading in catalyst **1a** was increased to 0.3 mol% in order to try to improve the diastereocontrol. Moreover, two base loadings were tested, 30 mol% and 5 mol%, with the goal to decrease the background reaction. Conversion was followed by ^1H NMR and each aliquot was used to measure enantiomeric excess in function of the reaction time (Table IV.6). In both cases, the enantiomeric excess and diastereomeric ratio were very satisfying at the early stage of the reaction, and decreased when the conversion increased. The increase of catalyst loading did not improve significantly the final selectivity of the reaction, such as the decrease of base loading. However, these results seems to be very promising for further optimization.

Table IV.6: Asymmetric addition of pronucleophile **26** on nitrostyrene **3a** catalysed by oligourea 0.3 mol% of **1a**, with ^1H NMR kinetics following

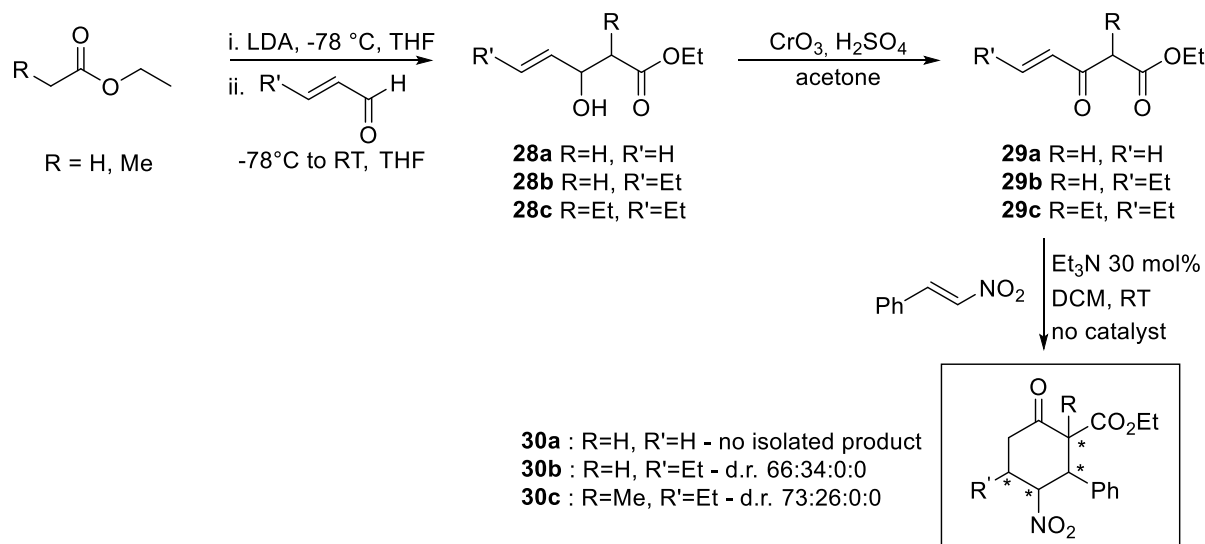


time	30 mol% Et ₃ N			5 mol% Et ₃ N		
	conversion (%)	d.r.	<i>ee</i> (%)	conversion (%)	d.r.	<i>ee</i> (%)
75 min	54	89:11	95	24	94:6	97
140 min	87	79:21	84	63	87:13	96
300 min	100	76:24	81	77	84:16	94
2.5 days	-	-	-	100	73:27	82

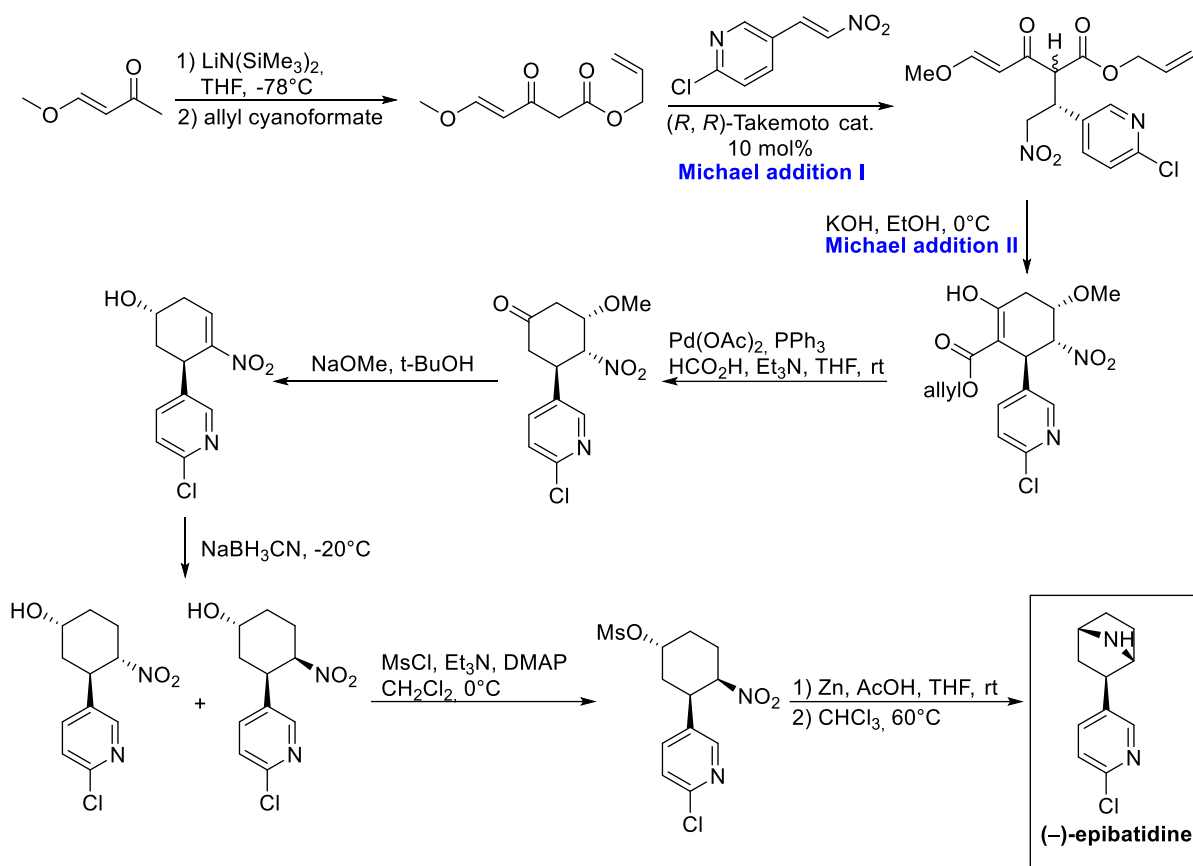
4.3 CASCADE MICHAEL ADDITION REACTIONS

4.3.1 Cascade Michael addition as a way to access to cyclic ketone with four stereocenters

One interesting extension of the model catalysed Michael addition of 1,3-dicarbonyl compounds to nitroalkenes is a tandem Michael addition to form cyclic ketoesters with high added value.⁵ This reaction is interesting to be tested with our catalyst to evaluate the potential to form quaternary centres. The resulting cyclic adduct **30** is a useful intermediate to versatile classes of compounds. It is a way to access to epibatidine⁵ (Scheme IV.7), which is extracted from the skin of the Ecuadorian frog *Epibatidores tricolor* and which interacts with receptors involved in pain feeling. However its use as a drug was not developed because even very low doses were lethal⁶. The strategy to access to this class of intermediates is to use a γ,δ -unsaturated β -ketoester **29** (Nazarov reagents) which can be added to nitrostyrene after deprotonation. The resulting adduct can cyclize by the presence of the double bond to lead to the 6-membered ring (Scheme IV.6).



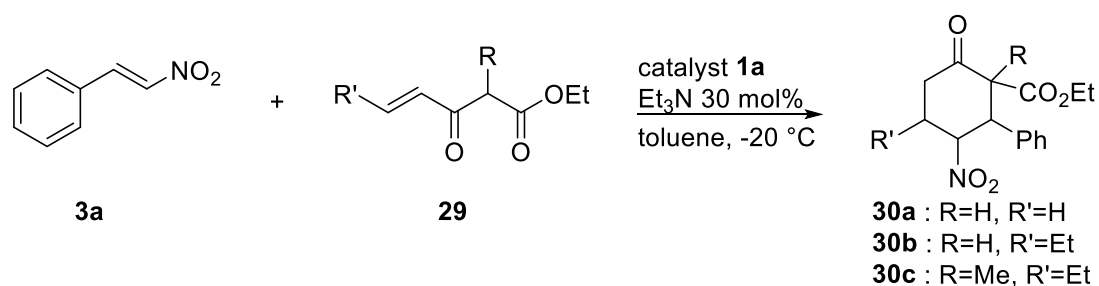
Scheme IV.6: Synthesis of Nazarov reagents and their use in Tandem Michael addition to lead cyclic derivatives **30** without catalyst



Scheme IV.7: Synthesis of (-)-epibatidine with Tandem Michael addition with Takemoto catalyst⁵

4.3.2 Asymmetric Cascade Michael reaction with oligourea catalyst

To form the starting γ,δ -unsaturated β -ketoester derivatives **29**, we used a procedure described in the literature.⁷ Deprotonation of the commercially available ester, followed by addition on an unsaturated aldehyde led to the γ,δ -unsaturated β -hydroxyester **28** (**28a** yield = 64% , **28b** yield = 28%, **28c** yield = 37%). The alcohol function was oxidized with Jones reagent, since Pyridinium Chlorochromate was not strong enough, and the desired compounds **29** were obtained in very poor yields. (**29a** yield = 14%, **29b** yield = 28%, **29c** yield = 24%), (Scheme IV.6). In these cases, a second by-product was formed which was not identified. The only base which was tried for the tandem Michael addition was triethylamine. The addition reaction of ethyl acetate to acrolein led to the adduct **29a** which was not able to further produce the cyclic desired ketone **30a** because of its instability (Entry 1, Table IV.7), as reported by Takemoto group.⁵ An ethyl substituent was installed at the vinylic position ($R' = \text{Et}$) leading to **29b**. This Nazarov reagent reacted with **3a** and led to the expected **30b** with 70:30 dr and excellent 96% ee for the major diastereomer (Entry 2, Table IV.7). Using **29c**, however, the yield was quite low in comparison to the previous example, the diastereoselectivity was slightly improved and the enantiomeric excess was decreased (Entry 3, Table IV.7).

Table IV.7: Asymmetric Tandem Michael addition with oligourea catalyst **1a**

Entry	Adduct	Catalyst Loading	R	R'	Yield (%)	d.r.	<i>ee</i> _{major} (%)
1	30a	0.1	H	H	–	–	–
2	30b	0.05	H	Et	85	70:30:0:0	96%
3	30c	0.1	Et	Et	35	78:22:0:0	78%

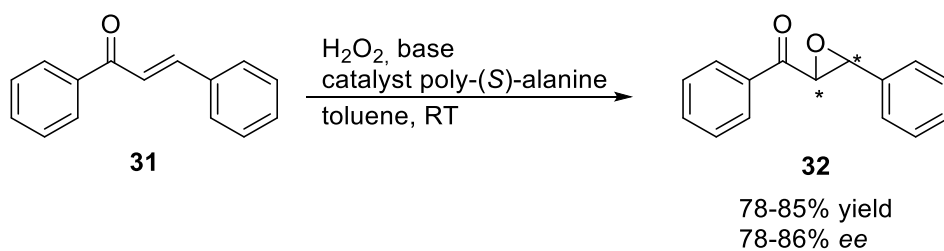
Yields were determined after Silica Gel Chromatography. Diastereomeric ratio and enantiomeric excesses were determined after analysis on Chiral HPLC.

Although more improvement is needed, this preliminary example shows that our catalytic system could be applied to tandem Michael reactions. More studies should be done to determine precisely the nature of the configuration of the stereogenic centres. Finally, this example also shows that the methyl substitution between the two C=O bonds of the 1,3-dicarbonyl derivative, results in a decrease of both reactivity and stereocontrol (compare results with substrates **30b** and **30c**). Besides other reactions with analogues of **29** with different substituents (different alkyl chain lengths) can be tried to go further in the mechanistic investigations.

4.4 JULIÁ-COLONNA EPOXIDATION

4.4.1 Comparison between literature catalysts and oligourea foldamers

Juliá-Colonna epoxidation is well studied case of an asymmetric reaction catalysed with helically folded polypeptides (i.e. poly-alanine or poly-leucine).⁸⁻¹⁰ Chalcone is epoxidized by a source of oxidation (hydrogen peroxide) associated to a strong base (DBU or NaOH), (Scheme IV.8).



Scheme IV.8 : Juliá-Colonna epoxidation of chalcone⁹

The mechanism of action proposed by Kelly *et al.* is very similar to the one with our oligourea catalytic system. The four terminal N-H at the N-terminal part of the polypeptide are not directly involved in the hydrogen-bond network. They have then the possibility to form an oxy-anion hole, which is stabilized by the macrodipole of the peptide, just as our oligourea catalyst. The main difference resides in the geometry of the helices formed by the polypeptide and the polyurea. The polypeptide forms a (*P*)-3.6₁₃- α -helix, with 3.6 residues per turn and 13-membered rings whereas the oligourea forms a (*P*)-2.5₁₄-helix with 2.5 residues per turn and both 12- and 14-membered H-bond rings (Figure IV.3).

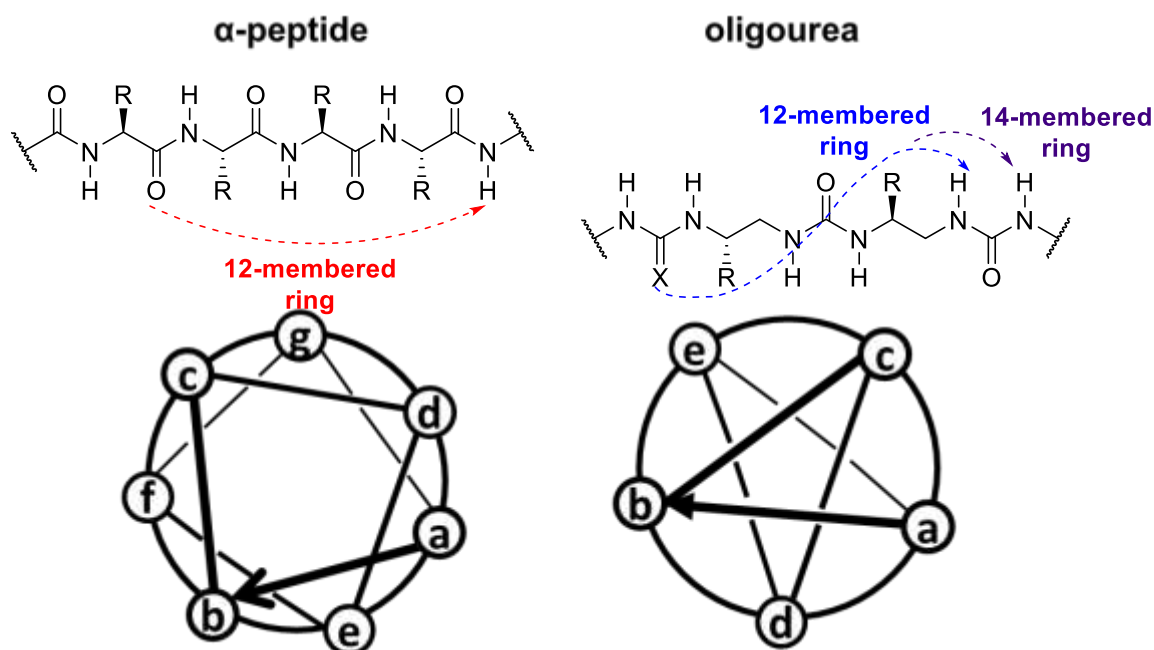


Figure IV.3: Structural comparison between α -peptide and oligourea

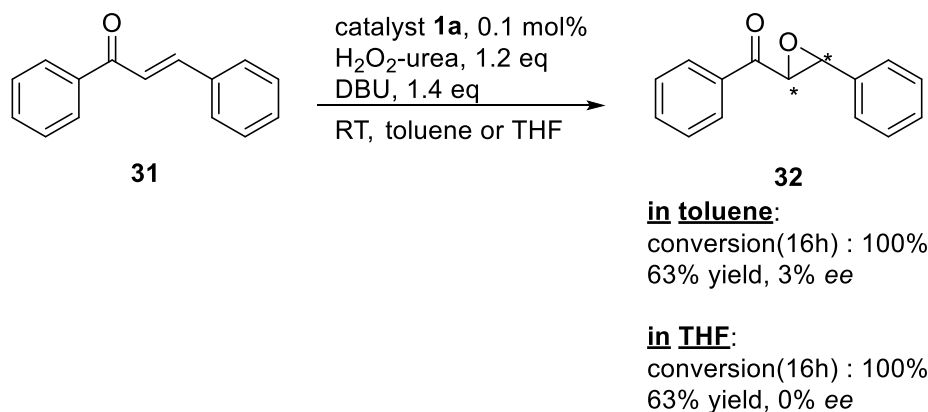
In the literature, several procedures based on the use of poly-amino acids to catalyse Juliá-Colonna epoxidation, different solvent conditions and different sources of hydroperoxide with different bases have been proposed. The first example used poly-leucine, which was fully insoluble in organic solvents and in water, which allows an easy recovery of the catalyst. The oxidant was aqueous peroxide hydrogen, coupled with sodium hydroxide as base. This triphasic system (insoluble catalyst, aqueous oxidant and base, organic solvent and substrates) gave good enantioselectivities but slow conversions.⁹ ¹¹ Then a biphasic version of the Juliá-Colonna epoxidation has been developed (insoluble catalyst, organic base, substrates, solvent, oxidant) through the use of urea-hydrogen peroxide, which is perfectly soluble in organic solvents as THF or DCM. The conversions are faster (less than one hour instead of several days for cyclohexyl derivative) and the substrate scope is wider.⁸

Two decades after the first works on Juliá-Colonna epoxidation, Roberts *et al.* demonstrated that β -peptides, which are also insoluble in both organic and aqueous solvents, are powerful catalysts for this reaction.¹² The new class of catalysts was tested in both triphasic (insoluble β -peptide, aqueous hydrogen peroxide, aqueous sodium hydroxide, toluene) and biphasic (insoluble β -peptide, urea hydrogen peroxide, DBU, toluene) conditions. He also developed triblock polyethylene glycol-poly amino acid catalysts which were soluble in THF, allowing monophasic system and leading to good yields and excellent stereocontrols.¹³

In this context, we thought to evaluate whether our oligourea catalytic system could also be relevant to perform asymmetric Juliá-Colonna epoxidation.

4.3.2 Screening external parameters for asymmetric Juliá-Colonna epoxidation

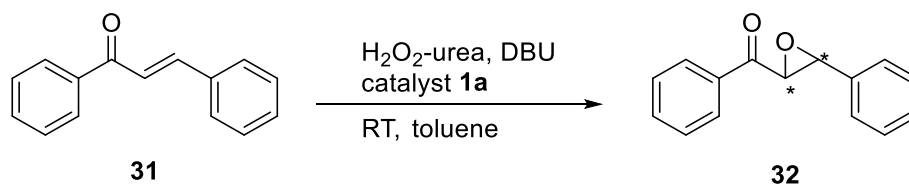
To evaluate the potential of our catalytic model with the Juliá-Colonna epoxidation, the classical conditions used in the literature were chosen to perform a reference reaction: with 1.2 equivalent of oxidant H₂O₂-urea, 1.4 equivalent of DBU, at room temperature. Toluene and THF, which are the most common reaction solvents, were both tried. The catalyst loading was firstly fixed at 0.1 mol% to observe the potential of our catalyst at very low loading in this new reaction. In both cases, the conversion was complete after 16h, the yields were both at 63%, the enantiomeric excesses were 3% for the reaction in toluene and 0% for the reaction in THF (Scheme IV.9).



*Scheme IV.9: Reference reaction with catalyst **1a** for Juliá-Colonna epoxidation*

The catalyst loading was increased to observe if the relationship between catalyst loading and selectivity is linear or if a step tends to appear (Entries 1-2, Table IV.8). The clear improvement of kinetics and enantiomeric excess proves that the interaction catalyst/substrates exists, but because the evolution is not linear with the increase of catalyst loading, structural modifications on the oligourea catalyst should be performed to fit with Juliá-Colonna epoxidation system. The concentration in initial reagents changes the kinetics and then the stereocontrol, so three additional initial concentrations in chalcone were tested (Entries 3-5, Table IV.8). The most concentrated is the initial concentration in chalcone, the faster is the kinetics and the lower is the stereocontrol. A catalytic amount of base was also tried (Entries 6-8, Table IV.8) but the conversion was either barely observable after 4 days or no visible at all. Moreover, because the source of hydrogen peroxide used was the complexed form with urea which could possibly compete with our oligourea, we tested the effect of removing urea (by treatment of the H_2O_2 -urea solution with DBU and filtration to remove the urea) but the results were not improved (Entry 9, Table IV.8). Both reagents were tested as limiting reagent (Entries 10-11, Table IV.8), and working with an excess of hydrogen peroxide allows a faster conversion but without apparent effect on the selectivity. Temperature was the last external parameter which was tested (Entries 12-13, Table IV.8) but decreasing the temperature did not improve selectivity and has a strong impact on the reaction rate. These conclusions led us to re-consider the nature and the design of the catalyst to perform Juliá-Colonna epoxidation.

Table IV.8: Influence of external parameters on asymmetric Juliá-Colonna epoxidation with catalyst **1a**



Entry	Evaluated parameter	Catalyst loading	Base loading	H ₂ O ₂ loading	[chalcone] (M)	Time, Conversion ^a	Yield (%)	ee (%)
1	Catalyst loading	1 mol%	1.4 eq	1.2 eq	1	16h: 100%	89 ^b	19
2		5 mol%		1.2 eq	1	16h: 100%	quant ^b	29
3	Chalcone concentration	0.5 mol%		1.2 eq	2	2h : 65%	31 ^{b, c}	1
4				1.2 eq	0.5	2h : 42%	62 ^d	9
5				1.2 eq	0.25	2h : 28%	28 ^d	11
6			30 mol%			6d : 18%	ND	-
7	Base loading	0.1 mol%	10 mol%	1.2 eq	0.5	4d: 0%	ND	-
8			1 mol%			4d: 0%	ND	-
9	Filtration of competitive urea	0.1 mol%	1.2 eq	1.2 eq	1	5d: 18%	12 ^e	3
10	H ₂ O ₂ in excess	0.5 mol%	2 eq	2 eq	0.8	16h: 100%	79 ^b	3
11	Chalcone in excess	0.5 mol%	1 eq	1 eq	2	4d: 43%	ND	5
12	Temperature	0.5 mol%	1.4 eq, -4°C	1.2 eq.	1	5d: 100%	quant ^b	4
13			1.4 eq, -20°C			5d : 10%	-	-

Reactions were performed on 0.5 mmol scale at room temperature. Enantiomeric excesses were determined on analytic chiral HPLC.

^a The conversion was measured by ¹H NMR at the given time to inform about the kinetics of the reaction.

^b Yield was determined after complete conversion of the reaction and purification of the crude on Silica Gel Chromatography.

^c The very low yield is due to the high polymerization of the chalcone, because of the high concentration of the reaction mixture.

^d Yield was determined when the conversion was stable but not complete, after 3 days of reaction, after purification on Silica Gel Chromatography.

^e Yield was determined when the conversion was stable but not complete, after 5 days of reaction, after purification on Silica Gel Chromatography

^f ND= not determined.

4.3.3 Simple modifications of the hexameric foldamer catalyst for asymmetric Juliá-Colonna epoxidation

Taking inspiration from catalysts reported in the literature, two other catalysts were synthesised and tested in different conditions (Figure IV.4). Because all the reported polyamino acids catalysts have a free amine at the terminus, a similar free amine hexamer catalyst **33** was synthesized from the Boc-protected hexamer **1a-hexamer**. However, there was almost no stereocontrol (Entry 3, Table IV.9) in this case. An analogue of **1a** was grafted on solid support leading to catalyst **35** (polystyrene resin, 0.33 mmol/g). Its synthesis will be described in next chapter. A pyrrolidine ring has been added to the C-

terminus part to allow direct condensation of the oligourea on the resin, as has been published by our group¹⁴. Its use in toluene did not improve the stereocontrol (Entry 5 Table IV.9) and its reactivity was slower than in its soluble version. These three catalysts were then used in biphasic/triphasic conditions with a mixture toluene/water and sodium hydroxide as a base (Entries 2, 4, 6, Table IV.9). Under these conditions, the reaction was very slow and there was almost no any stereocontrol.

Figure IV.4: New catalysts around hexameric oligourea backbone tested for Juliá-Colonna epoxidation

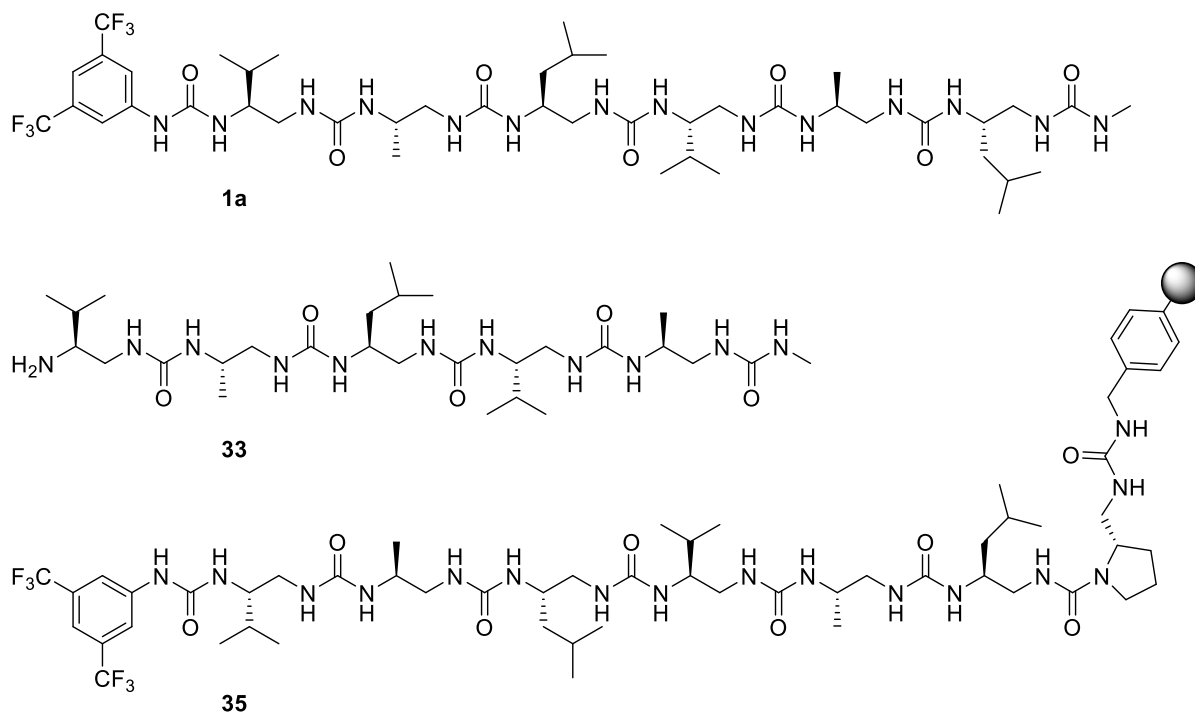


Table IV.9: Comparison between oligourea catalysts inspired from potent polyamino acids catalysts for Juliá-Colonna epoxidation

Entry	Catalyst	Solvent	Base	[chalcone] (M)	Time, Conversion ^a	Yield (%)	ee (%) ^b
1	1a , 1 mol%	Toluene	DBU, 1.4 eq.	1	16h: 100%	62	9
2	1a , 0.5 mol%	Toluene+H ₂ O	NaOH, 1.4 eq	0.5	3d: 6%	ND ^c	2
3	33 , 0.5 mol%	Toluene	DBU, 1.4 eq	1	17h; 64%	ND ^c	5
4	33 , 0.5mol%	Toluene+H ₂ O	NaOH, 1.4 eq	0.5	3d: 26%	ND ^c	0
5	35 , 1 mol%	Toluene	DBU, 1.4 eq	1	3d: 46%	ND ^c	3
6	35 , 1 mol%	Toluene+H ₂ O	NaOH, 1.4 eq.	0.5	3d: 0%	not treated	

Reactions were performed on 0.5 mmol scale at room temperature.

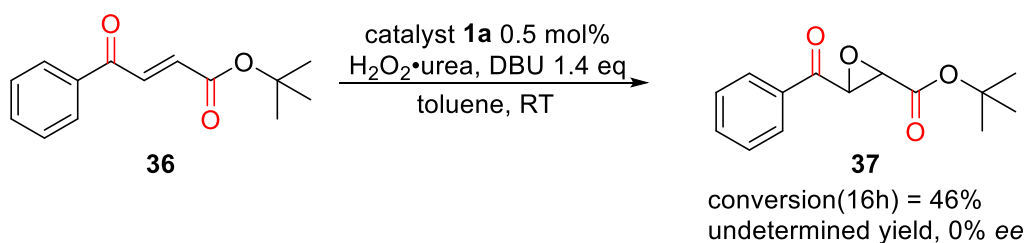
^a The conversion was measured by ¹H NMR at the given time to inform about the kinetics of the reaction.

^b Enantiomeric excesses were determined on analytic chiral HPLC.

^c ND = not determined

4.3.4 Synthesis of new substrate with double potential anchoring spots to catalyst

In the previous chapter, we proposed a mechanism for the foldamer catalysed version of the Michael addition of 1,3-dicarbonyl compounds to nitroalkenes, whereby one substrate of the reaction (i.e. the nucleophile) is tightly bound to the catalyst by interacting simultaneously the two first ureas. According to this model, optimal substrate binding would then be achieved with substrates bearing two appropriately spaced hydrogen bond acceptor groups. We were thus wondering whether chalcones bearing a second anchoring point to the catalyst could be better substrates for the foldamer catalysed Juliá-Colonna epoxidation. We have thus considered one additional substrate, a γ -*tert*-butyl carbamate chalcone **36** which was synthesized in order to be tested with catalyst **1a** for the epoxidation reaction (Scheme IV.10).



*Scheme IV.10: Juliá-Colonna epoxidation with substrate **36** containing two carbonyl oxygens*

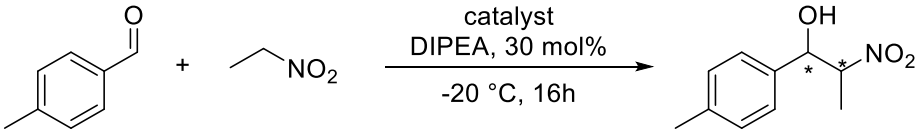
Employing catalyst **1a** under the described conditions did not lead to any stereocontrol for the selected substrate. Having two oxygen atoms on the substrate potentially able to interact with the catalyst was clearly not sufficient here to bring stereocontrol. However, this substrate does not have the same arrangement of H-bond acceptor groups than in 1,3-dicarbonyl compounds and it is difficult to definitely conclude that enantiocontrol in the Juliá-Colonna epoxidation catalysed by an oligourea catalyst could not be achieved for certain classes of substrates.

Despite the unsuccessful results of our catalytic system for Juliá-Colonna epoxidation, it brings more information about the mechanism of action of the catalyst. Other oligourea catalysts could also be designed to offer other possibilities of interaction with substrates such as chalcones and/or with the hydroperoxide anion, by the insertion of functionalized lateral chains for instance or by introducing urea surrogates at specific positions

4.2 HENRY REACTION

Another possibility to expand the potential applications of our designed catalytic foldamer is the Henry reaction (also called the Nitro Aldol Reaction). The Henry reaction is a typical carbon-carbon bond forming reaction which enable access to versatile intermediates with hydroxyl and nitro groups, and allows investigation of diastereomeric control. Here, we evaluated the addition of nitroethane **39** ($pK_a > 15$) to *p*-tolualdehyde **38** with catalyst **1a** and its thiourea version **5a**. The rationale for using **1a** as a catalyst was the possibility to activate and stabilize both the deprotonated nitroalkane and carbonyl derivative through H-bonding. DIPEA is a convenient base for this system which is able to both deprotonate nitroethane and avoid polymerization of *para*-tolualdehyde. THF, DMF and toluene were tested as solvents (Entries 1-3, Table 10) and toluene was the only one in which a certain stereocontrol was observed. Not surprisingly, the solvent was found to have a strong impact on the diastereomeric ratio, the more polar solvents being less effective: DMF gave neither diastereomeric nor enantiomeric control, THF gave a diastereomeric ratio of 70:30 but the enantiocontrol was non-existent. The catalyst loading was increased by a factor of 10 but the enantiomeric excess was only improved from 12% to 26% and the diastereomeric control surprisingly decreased (Entry 4, Table 10). Thiourea catalyst **5a** was tested; the enantiomeric control was similar to urea version but the diastereomeric ratio was diminished, which shows that the control of stereoselectivity is very subtle in this particular case.

Table 10: Evaluation of hexameric oligourea foldamer as catalyst for the asymmetric Henry reaction



Entry	Catalyst, loading	Solvent	d.r.	ee (%)
1	1a , 0.1 mol%	DMF	45:55	0
2	1a , 0.1 mol%	THF	70 : 30	0
3	1a , 0.1 mol%	toluene	85:15	12
4	1a , 1 mol%	toluene	53:47	26
5	5a , 0.1 mol%	toluene	44:56	15

The results obtained so far are not spectacular but provide a hint that some stereocontrol is possible by using 0.1 mol% of **1a** as a catalyst. Other bases could be scanned and the design of the catalyst could be tuned to match with these substrates and perform the Henry reaction. To improve these preliminary results, one could think of reinforcing the interaction between the deprotonated nitroalkane and the catalyst by incorporating guanidinium groups in the main chain (either close or remote from the

urea-based catalytic site) of the catalyst as previously reported for small-molecular weight catalysts.¹⁵⁻
¹⁶ These family of modified oligoureas have recently been prepared in the laboratory (unpublished work from Karolina Pulka-Ziach and Stéphanie Antunes). As reported in the previous section, the lack of two stable anchors on the substrate can also be a reason of the lack of stereocontrol. Substrates such as α -ketoesters¹⁷ and α -ketophosphonates¹⁸ could be evaluated to test this hypothesis. Finally, one could also think of exploring a broader range of electrophiles such as imines in the aza-henry reaction.¹⁹ Previous studies with Takemoto catalysts have shown that the nature of the electrophile may be critical from the standpoint of selectivity; substrates such as imines and N-alkoxycarbonyl imines (e.g. N-Boc imines) in particular could be tested for comparison. Tandem Michael/Henry reaction by combining H-bond catalysis and amino catalysis on the same catalyst (e.g. by introducing a primary or a secondary amine in our catalyst)²⁰⁻²¹ could also be a strategy to introduce more functionalized substrates and allowing a better recognition with the catalyst.

Bibliography

1. Okino, T.; Hoashi, Y.; Furukawa, T.; Xu, X.; Takemoto, Y., *J. Am. Chem. Soc.* **2005**, *127*, 119-125.
2. Kaupmees, K.; Trummal, A.; Leito, I., *Croatica Chemica Acta* **2014**, *87* (4), 385-395.
3. McCooney, S. H.; Connon, S. J., *Angew. Chem. Int. Ed.* **2005**, *44* (39), 6367-70.
4. Bae, H. Y.; Song, C. E., *ACS Catalysis* **2015**, *5* (6), 3613-3619.
5. Hoashi, Y.; Yabuta, T.; Yuan, P.; Miyabe, H.; Takemoto, Y., *Tetrahedron* **2006**, *62* (2-3), 365-374.
6. Jensen, K. L.; Weise, C. F.; Dickmeiss, G.; Morana, F.; Davis, R. L.; Jørgensen, K. A., *Chemistry* **2012**, *18* (38), 11913-8.
7. Zibuck, R.; Streiber, J. M., *J. Org. Chem.* **1989**, *54*, 4717-4719.
8. Adger B. M., Barkley J. V., Bergeron S., Cappi M. W., Flowerdew B. E., Jackson M. P., McCague R., Nugent T. C., Roberts S. M. Roberts, *J. Chem. Soc. Perkin Trans. I* **1997**, 3501-3507.
9. Juliá S., Guixer J., Masana J., Rocas J., Colonna S., Annuziata R., Molinari H., *J. Chem. Soc. Perkin Trans. I* **1982**, 1317-1324.
10. Kelly, D. R.; Roberts, S. M., *Chem. Commun.* **2004**, (18), 2018-20.
11. Juliá S., Masana J., Vega J.C., *Angew. Chem. Int. Ed. Engl.* **1980**, *19* (11), 929-931.
12. Coffey, P. E.; Drauz, K.-H.; Roberts, S. M.; Skidmore, J.; Smith, J. A., *Chem. Comm.* **2001**, (22), 2330.
13. Flood R. W., Geller T. P., Petty S. A., Roberts S. M., Skidmore J., Volk M., *Org. Lett.* **2001**, *3* (5), 683-686.
14. Fremaux J., Fischer L., Arbogast T., Kauffmann B., Guichard G., *Angew. Chem. Int. Ed. Engl.* **2011**, *50* (48), 11382-5.
15. Sohtome, Y.; Hashimoto, Y.; Nagasawa, K., *Adv. Synth. Cat.* **2005**, *347* (11-13), 1643-1648.
16. Sohtome, Y.; Takemura, N.; Takada, K.; Takagi, R.; Iguchi, T.; Nagasawa, K., *Chem. Asian J.* **2007**, *2* (9), 1150-60.
17. Takada, K.; Takemura, N.; Cho, K.; Sohtome, Y.; Nagasawa, K., *Tet. Lett.* **2008**, *49* (10), 1623-1626.
18. Mandal, T.; Samanta, S.; Zhao, C.-G., *Org. Lett.* **2007**, *9* (5), 943-945.
19. Xu, X.; Furukawa, T.; Okino, T.; Miyabe, H.; Takemoto, Y., *Chemistry* **2006**, *12* (2), 466-76.
20. Wang, Y. F.; Zhang, W.; Luo, S. P.; Li, B. L.; Xia, A. B.; Zhong, A. G.; Xu, D. Q., *Chem. Asian J.* **2009**, *4* (12), 1834-8.
21. Uehara, H.; Imashiro, R.; Hernandez-Torres, G.; Barbas, C. F., 3rd, *PNAS* **2010**, *107* (48), 20672-7.

CHAPTER V

CHAPTER V

5.1 STRATEGY FOR GRAFTING THE CATALYST ON SOLID PHASE.....	151
5.2 PRELIMINARY STUDY TO TRANSPOSE THE REACTION FROM A HOMOGENEOUS CATALYTIC SYSTEM TO A HETEROGENEOUS CATALYTIC SYSTEM.....	153
5.3 OPTIMIZATION OF REACTION PARAMETERS.....	155
5.3.1 Impact of external parameters on the catalytic activity of 35	155
5.3.2 Impact of the resin loading.....	156
5.3.3 Fine tuning of experimental conditions with Hunig's base	158
5.4 INTRODUCTION OF A CARBON CHAIN SPACER BETWEEN THE FOLDAMER AND THE RESIN MATRIX.....	159
5.5 POSSIBILITY TO RECYCLE OF THE CATALYST	162

5.1 STRATEGY FOR GRAFTING THE CATALYST ON SOLID PHASE

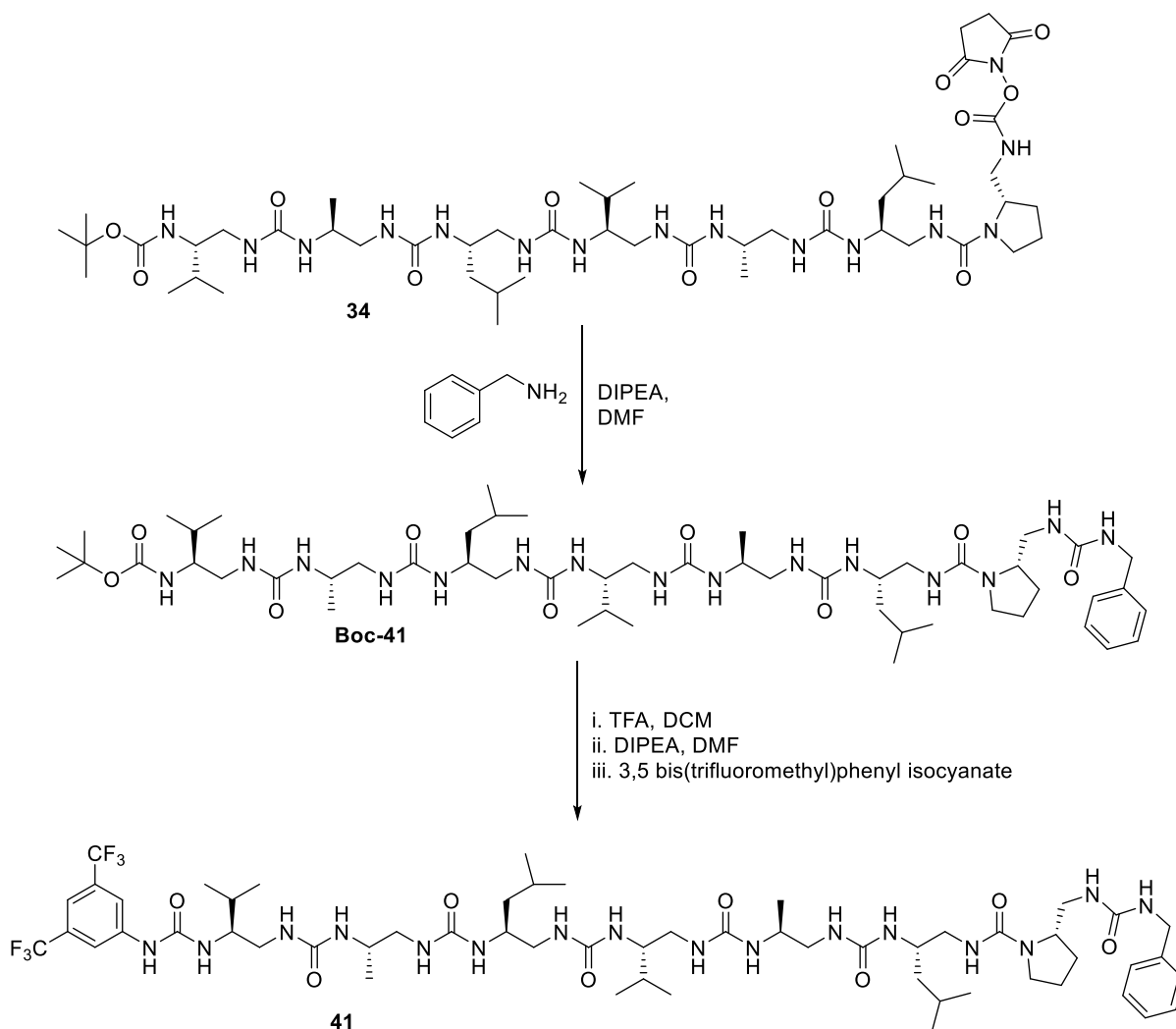
Several strategies are possible to synthesize solid-supported catalysts. The full synthesis of the foldamer could be performed stepwise on the resin beads (a modular approach but at the expense of the catalyst purity), or the foldamer can be synthesized in solution and grafted on the solid support in one final step. Alternatively, both ways can be combined by grafting an advanced precursor on the solid support and then finalizing the synthesis of the catalyst (limited to one or two steps). The strategy we considered was to use a Boc-protected oligourea hexamer, with a pyrrolidine moiety as the first residue from the C-terminal part, synthesized in solution, activated by a succinimidyl group and to graft it on solid support. Only two steps on solid support would then be required to access the solid-supported catalyst: the removal of the Boc protecting group and the final coupling with the 3,5-bis(trifluoromethyl)phenyl isocyanate for example. The main advantage of this strategy is its modularity: the termination (urea, thiourea, ...) can be readily varied from the same oligourea precursor on solid support. (Scheme V.1)

Guichard *et al.* demonstrated that grafting an oligourea foldamer (via its C-terminal end) on solid support does not preclude helix formation.¹ This is a critical result to validate the whole approach developed in this chapter. Because, the penultimate step is the removal of the Boc-protecting group by TFA prior to isocyanate coupling, it is critical to choose a solid-support with a linker which tolerates acidic conditions, to avoid undesired release of the grafted foldamer. Moreover, the matrix has to be suitable with our catalysis conditions, which means that it should (*i*) not contain chemical groups that could compete for hydrogen-bonding and (*ii*) have good swelling properties in toluene. The aminomethyl polystyrene resin which meets these criteria was thus used to synthesize the first solid-supported catalyst **35** (Scheme V.1).

The next step was to investigate the catalytic properties of this new heterogeneous catalyst. As a continuation of our work in solution, we selected the Michael addition of 1,3-dicarbonyl compounds to nitroalkenes as a model reaction to start with. We decided to fully re-evaluate the experimental procedure for using this solid-supported catalytic system (as compared to the one developed with **1a**) with a new screen of parameters such as temperature, base loading, base nature, the reactants concentrations. Moreover, introducing a solid-support provides more parameters to play on such as the nature of the matrix, the resin loading, the linker (chemical properties, chain length). Thereby, having a solid-supported catalyst in hand will allow us to study the possibility to recycle the catalyst.

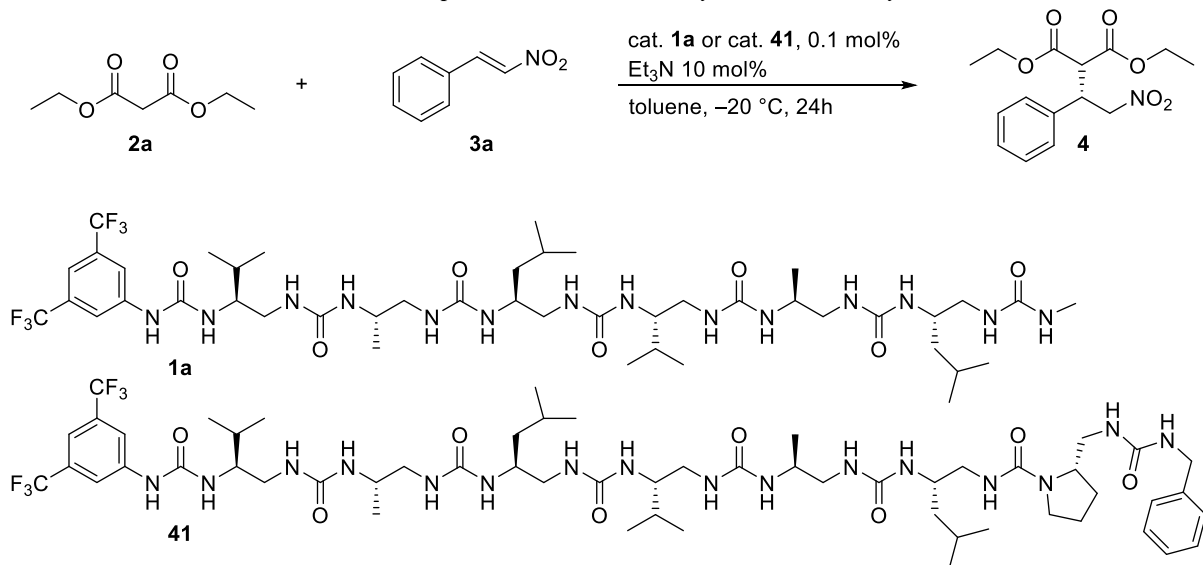
5.2 PRELIMINARY STUDY TO TRANSPOSE THE REACTION FROM A HOMOGENEOUS CATALYTIC SYSTEM TO A HETEROGENEOUS CATALYTIC SYSTEM

To enable head-to-head comparison of catalyst **35** with a homogeneous catalyst counterpart, we synthesized compound **41**, close analogue of catalyst **1a**, with a pyrrolidine residue at the C terminus. In addition, the C-terminus part was capped with a benzyl group to mimic the aminomethyl polystyrene resin.



Scheme V.2: Synthesis of oligourea catalyst **41**

This new catalyst **41** was evaluated in the model Michael addition of malonate to nitroalkenes and gave almost the same results than the reference catalyst **1a** (Table V.1). This preliminary study confirms that C-terminal modifications of the catalyst have little influence on the catalytic activity and that heterogeneous catalysis with **35** can be directly compared with homogeneous phase catalysis with **1a**.

Table V.1: Comparison between catalyst **1a** and catalyst **41**

Entry	Catalyst	Temperature	Conversion (%)	Yield (%)	ee (%)
1	1a	RT	100	75	89
2	41	RT	100	84	86
3	1a	-20°C	100	80	95
4	41	-20°C	100	81	96

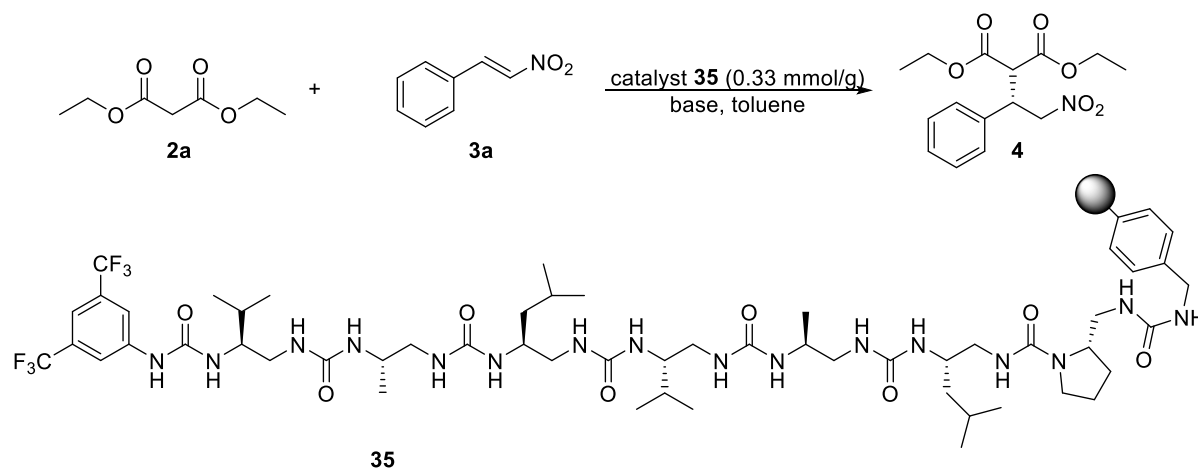
Yield was determined after purification on Silica Gel Chromatography. Enantiomeric excess was determined by analysis on Chiral HPLC. Relative configuration was determined by comparison with literature.

5.3 OPTIMIZATION OF REACTION PARAMETERS

5.3.1 Impact of external parameters on the catalytic activity of **35**

The Michael addition of diethyl malonate **2a** to nitrostyrene **3a** was performed with the new solid-supported catalyst **35**. Different parameters were evaluated and the reaction compared to the homogeneous catalytic system. The reaction mixture was always stirred by mechanic stirring. Two catalyst loadings were tried (0.6 mol% and 0.06 mol%), with a 2-fold higher concentration in nitrostyrene, $[\text{nitrostyrene}]_0 = 2 \text{ M}$ instead of $[\text{nitrostyrene}]_0 = 1 \text{ M}$ in homogeneous solution. In this preliminary experiment, the enantiocontrol was surprisingly low and the yield was very bad at 0.06 mol% catalyst with significant nitrostyrene polymerization (Entries 1-2, Table V.2). The grafted catalyst on aminomethyl polystyrene resin, with 0.33 mmol/g loading, was thus much less efficient than the reference catalyst **1a** under these conditions. The initial nitrostyrene concentration was then evaluated (Entries 2-4, Table V.2). The less concentrated in nitrostyrene the reaction mixture is, the slower is the racemic background reaction and the better is the enantiocontrol. However, with $[\text{nitrostyrene}]_0 = 0.5 \text{ M}$, the conversion is not complete after four days. In general, when low conversions were observed, yields were not determined and the *ee*'s were obtained from the partially converted reaction mixture.

The nature and the loading of the base were then varied (Entries 3, 5-9, Table V.2). With 5 mol% Et_3N , the conversion was not complete in five days and decreasing the triethylamine loading did not improve the enantiocontrol. The heterogeneous system was tested with DIPEA as base (entries 6-8 Table V.2) and the enantiocontrol was improved but the reaction rate was decreased. However, further increase of the amount of DIPEA (up to one equivalent, Entry 8, Table V.2), the reaction was faster but the enantiocontrol decreased slightly. DBU (pKa 24 in MeCN in Bordwell pKa Table) was also tested as a base, but with only 10 mol% loading in reason of its strong basicity (Entry 9, Table V.2). The conversion was still not complete in four days, and the stereocontrol was very low.

Table V.2: Screening external parameters during heterogeneous catalysis with **35**

Entry	Catalyst loading	base, loading	[nitrostyrene] ₀ (M)	Time, conversion ^a	Yield (%) ^b	ee (%) ^c
1	0.6 mol%	Et ₃ N, 10 mol%	2	Conv (16h) = 100%	71	48
2	0.06 mol%	Et ₃ N, 10 mol%	2	Conv(24h) = 100%	18	11
3	0.6 mol%	Et ₃ N, 10 mol%	1	Conv (48h) = 100%	ND ^d	59
4	0.6 mol%	Et ₃ N, 10 mol%	0.5	Conv (4d) = 60%	ND ^d	69
5	0.6 mol%	Et ₃ N, 5 mol%	1	Conv (5d) = 86%	ND ^d	59
6	0.6 mol%	DIPEA, 5 to 15 mol%	1	Conv (16h) = 13%	ND ^d	69
7	0.6 mol%	DIPEA, 30 mol%	0.5	Conv (6d) = 58%	ND ^d	79
8	0.6 mol%	DIPEA, 1 eq	0.5	Conv(4d) = 59%	45	72
9	0.6 mol%	DBU, 10 mol%	0.5	Conv(4d) = 72%	ND ^d	24

^aConversions were determined by ¹H NMR.

^bYields were determined after purification on Silica Gel Chromatography.

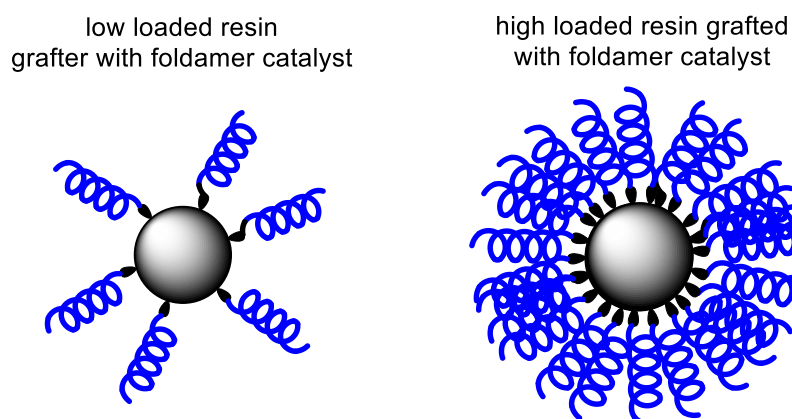
^c Enantiomeric excesses were determined by analysis on Chiral HPLC from reaction mixture if the conversion was not complete, from isolated desired adduct if the conversion was complete.

^dND: not determined

5.3.2 Impact of the resin loading

The loading of the resin is a central parameter which did not exist in homogeneous conditions. A low loaded resin would allow bigger repartition of the grafted catalytic foldamers and a better availability for the substrates in solution (Scheme V.3). Two catalysts grafted on aminomethyl polystyrene resins that differ by their initial loading, (0.55 mmol/g and 0.37 mmol/g) were evaluated. After the oligourea grafting and the final activation, the resin substitution was 0.33 mmol/g and 0.23 mmol/g respectively. The resin loading with the grafted oligourea was determined by the weighing of the grafted weight on the resin, by weighing the dried resin beads at the balance. Because of the low reactivity, the reactions were stopped before complete conversions and the enantiomeric excesses were determined from the partially converted reaction mixtures. It will not be the same result than the final

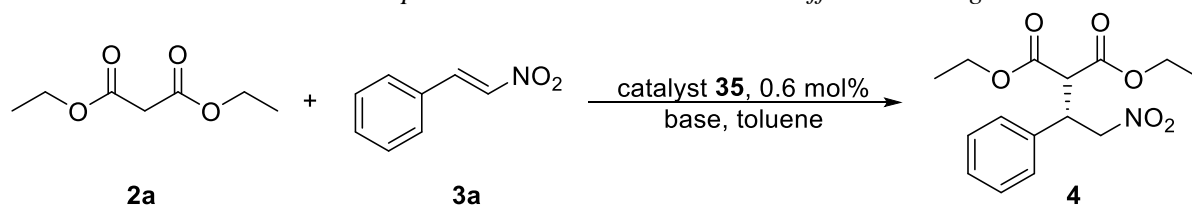
enantiomeric ratio which would have been obtained with complete conversion, but it gives a tendency which is representative for concluding on the impact of each evaluated parameter.



Scheme V.3: Comparison between a low loaded resin and a high loaded resin (in black), and its impact on the grafting of oligourea catalysts (in blue)

At room temperature, with triethylamine, $[\text{nitrostyrene}]_0 = 0.5 \text{ M}$, 0.6 mol% catalyst, the stereocontrol and the reactivity are similar overall (Entry 1 and Entry 3, Table V.1/ Table V.3). The impact of the temperature and the base nature were then evaluated with the less loaded resin. The decrease of temperature slowed down the reaction but did not significantly affect the stereoselectivity (Entry 4, Table V.3). The use of Hunig's base instead of triethylamine significantly increased the stereocontrol but as in the previous study, it slowed down the reactivity (Entry 5, Table V.3).

Table V.3: Comparison between resins with two different loadings



Entry	Resin loading	Temperature	Base loading	$[\text{nitrostyrene}]_0$ (M)	conversion, time ^a	ee (%) ^b
1	0.33 mmol/g	RT	Et ₃ N, 10 mol%	0.5	conv(4d) = 60%	69
2		RT	DIPEA, 30 mol%	1	conv(6d) = 58%	79
3	0.23 mmol/g	RT	Et ₃ N, 30 mol%	0.5	conv(42h) = 41%	64
4		-20°C	Et ₃ N, 30 mol%	0.5	conv(42h) = 25%	69
5		-20°C	DIPEA, 30 mol%	1	conv(60h) = 47%	84

^a Conversion was determined by ¹H NMR.

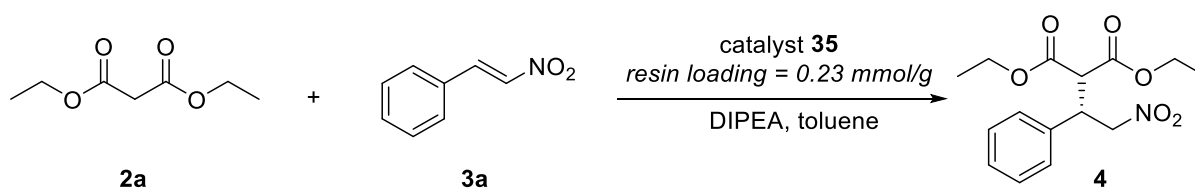
^b Enantiomeric excesses were determined by analysis on Chiral HPLC on aliquots from reaction mixture at the indicated time of conversion measurement.

The difference of effectiveness between the resins at 0.33 mmol/ and 0.23 mmol/g was not visible by our studies. To conclude on the effect of the resin loading on the catalyst efficiency, another resin with a higher difference in substitution should be tried. Moreover, the porosity of the beads which could influence both kinetics and stereocontrol of the system could also be tested by comparing standard polystyrene beads with more rigid macroporous beads.

5.3.3 Fine tuning of experimental conditions with Hunig's base

The low loaded resin (0.23 mmol/g) was used in combination with DIPEA to further optimise the reaction conditions. When the catalyst loading was doubled, the kinetics was faster and stereocontrol was kept high (Entry 2, Table V.4). The reaction was performed without solvent to go further in the perspective of developing a greener catalyst: the beads were just swollen in the minimum of toluene which was necessary, then nitrostyrene **3a**, diethylmalonate **2b** and DIPEA were added at the desired temperature. In this case, the amount of DIPEA was decreased to 10 mol% to slow down background reactions. The conversion was complete in 24h, the yield was decreased because of the nitrostyrene polymerization, and stereocontrol was still high. The impact of the reactor diameter was also evaluated. The larger is the diameter, the most spread will be the catalyst beads, the better will be the contact surface between the catalyst and the reagents, the faster should be the kinetics and the better should be the enantiocontrol. However, the conversion was very slow and the enantiocontrol was not impacted (Entry 4, Table V.4). To improve the system and try to reach the same results which were demonstrated in homogeneous catalysis, structural elements of the foldamer grafted on the resin beads have been considered.

Table V.4: Optimization of heterogeneous catalysis with low loaded catalysis and Hunig's base



Entry	Temp	Catalyst loading	Base	[nitrostyrene] ₀ (M)	reactor diameter (m)	Conversion, time ^a	Yield (%) ^b	ee (%) ^c
1	-20°C	0.6 mol%	DIPEA, 30 mol%	1	9	conv(60h) = 47%	undet.	84
2	-20°C	1.2 mol%	DIPEA, 30 mol%	1	9	conv(80h) = 100%	72	86
3	-20°C	0.6 mol%	DIPEA, 10 mol%	Neat	9	conv (24h) = 100%	49	74
4	RT	0.6 mol%	DIPEA, 30 mol%	0.5	14	conv(192h)=100%	52	78

Reactions were run on 0.5 mmol scale. Conversions were determined by ¹H NMR. Yields were determined after purification on Flash Chromatography.

^a Conversion was determined by ¹H NMR.

^b Yield was determined after purification on Silica Gel Chromatography.

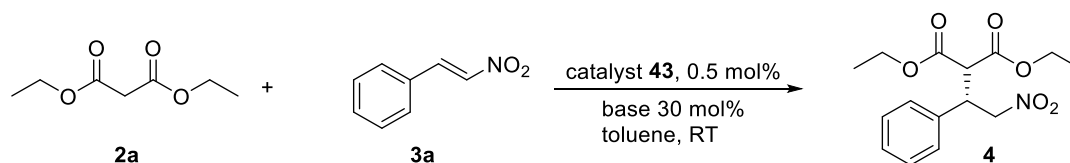
^c Enantiomeric excesses were determined by analysis on Chiral HPLC on aliquots from reaction mixture at the indicated time of conversion measurement.

5.4 INTRODUCTION OF A CARBON CHAIN SPACER BETWEEN THE FOLDAMER AND THE RESIN MATRIX

The grafting of the catalytic foldamer on the resin brings a certain hindrance in the C-terminal part as well as a possible rigidification of the system. To check whether these elements have an impact on the catalytic efficiency, a new solid-supported catalyst **43** was synthesised by the introducing an additional spacer of eight carbons (8-(Boc-amino)caprylic acid), on the same low loading resin (0.37 mmol/g for the ungrafted aminomethyl polystyrene). Briefly, the N-Boc-amino-caprylic acid derivative was coupled to the resin by standard peptide coupling with HBTU and after TFA deprotection, the catalyst was attached as previously described (Scheme V.4). The resulting catalyst **43** presented a grafted resin loading of 0.25 mmol/g.

Catalysts **35** and **43**, without 8 carbons-linker and with 8 carbons-linker, were evaluated in the same conditions. The kinetics, the yields and the enantiocontrol were very similar. There is then no significant impact of the additional spacer arm between the resin and the catalytic oligourea (Entries 1-2, Table V.5). The previous studies were confirmed by a new study of the influence of the reactor diameter, the nature of the base, and initial nitrostyrene concentration (Table V.5). The increase of the reactor diameter slowed down the kinetics and did not impact the stereocontrol (Entry 3, Table V.5). The replacement of triethylamine by Hunig's base slowed down the reaction but improved the enantiomeric excess (Entry 4, Table V.5). The decrease of initial nitrostyrene reaction slows down the kinetics and in this case, it had no significant impact on enantiomeric ratio (Entry 5, Table V.5).

Table V.5: Impact of different parameters with solid-supported catalyst **43**

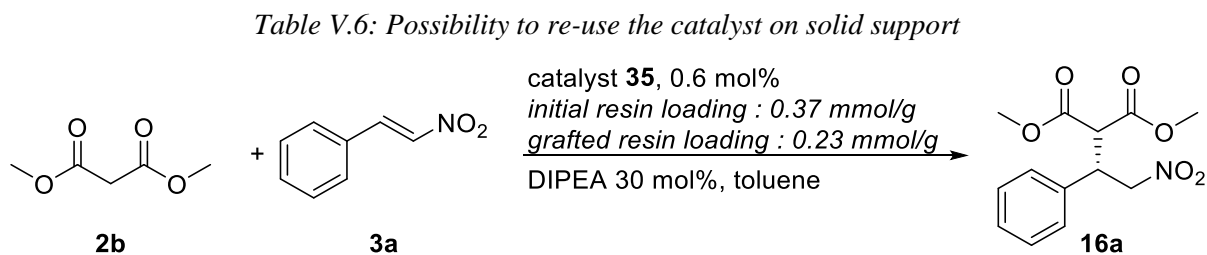


Entry	Catalyst	Reactor diameter (cm)	base	[nitrostyrene] ₀ (M)	Conversion	Yield (%)	ee (%)
1	35	0.9	Et ₃ N	1	conv (19h) = 70%	79	64
2	43	0.9	Et ₃ N	1	conv (19h) = 79%	82	64
3	43	1.4	Et ₃ N	1	conv (19h) = 58%	55	61
4	43	0.9	DIPEA	1	conv (19h) = 54%	79	80
5	43	0.9	Et ₃ N	0.5	conv (23h) = 54%	49	64

Reactions were run on 0.5 mmol scale. Conversions were determined by ¹H NMR. Yields were determined after Flash Chromatography after complete conversion. Enantiomeric excesses were determined on purified desired adducts by analysis on Chiral HPLC.

5.5 POSSIBILITY TO RECYCLE OF THE CATALYST

To evaluate the possibility to recycle the catalyst, the addition of dimethyl malonate to nitrostyrene was carried out using catalyst **35** with low loading (with 0.23 mmol/g grafted resin loading), and DIPEA 30 mol%, at two different temperatures (Room Temperature and 4 °C), in dry toluene. The reactions were run to complete conversion, which corresponds to three days for the batch experiment at RT, and to five days for the batch experiment at 4 °C. Catalytic beads were recovered by filtration after each experiment, rinsed with dichloromethane, dried under high vacuum and swollen in dry toluene before being reused in a new experiment. In both cases, the enantioselectivity remained largely unaffected from one run to another (Table V.6). The higher stability of both yields and enantiomeric excess observed in the series of experiments run at -4°C (Entries 6-8 Table V.6) can be explained by the fact the temperature of the reaction mixture is controlled whereas the first series (Entry 1-5 Table V.6) is dependent on variations of the room temperature.



Entry	Temperature	Run	Yield (%)	ee (%)
1	RT	I	40	88
2		II	68	81
3		III	54	90
4		IV	58	83
5		V	53	80
6	4 °C	I	57	88
7		II	63	85
8		III	54	86

Reactions were run on 0.5 mmol scale with 0.6 mol% catalyst. The yields were determined after purification on Flash Chromatography after complete conversion. The enantiomeric excess was determined by analysis on Chiral HPLC.

The grafting of the catalytic oligourea on solid support allowed us to demonstrate clearly the possibility to re-use the catalyst without loss of the catalytic efficiency between the different runs. There is still room to improve the inherent catalytic efficiency of this heterogeneous foldamer-based catalytic system for example by further investigation on the nature and the porosity of the matrix. Such a catalytic system could possibly be further optimized by adapting it to flow chemistry process.

Bibliography

1. Violette, A.; Lancelot, N.; Poschalko, A.; Piotto, M.; Briand, J. P.; Raya, J.; Elbayed, K.; Bianco, A.; Guichard, G., *Chemistry* **2008**, *14* (13), 3874-82.

CHAPTER VI

CHAPTER VI: CONCLUSION AND PERSPECTIVES

Oligourea foldamers have turned out to be powerful helical backbones with the ability to catalyse Michael addition reactions at very low loading with good yields and excellent enantiocontrol. The possibility to decrease the catalyst loading to 0.1 mol% and even 0.01 mol%, which is 100 to 1000-fold lower than classical organocatalysts for the same reaction, is directly correlated to the helical conformation of the oligourea, and to the synergy which results from the strength of the hydrogen bond network. The second singularity of this system is the combination of the organocatalyst with an external base. It offers a higher flexibility on both catalyst and base loadings, as well as on the nature of the external base. Mechanistic studies demonstrated the location of catalytic sites and NMR experiments gave information which allowed the proposal of a model of interaction between the substrates, the base and the catalyst. Co-crystallisation experiments between substrates and catalysts, coupled to theoretical studies would certainly allow to this model to be examined further.

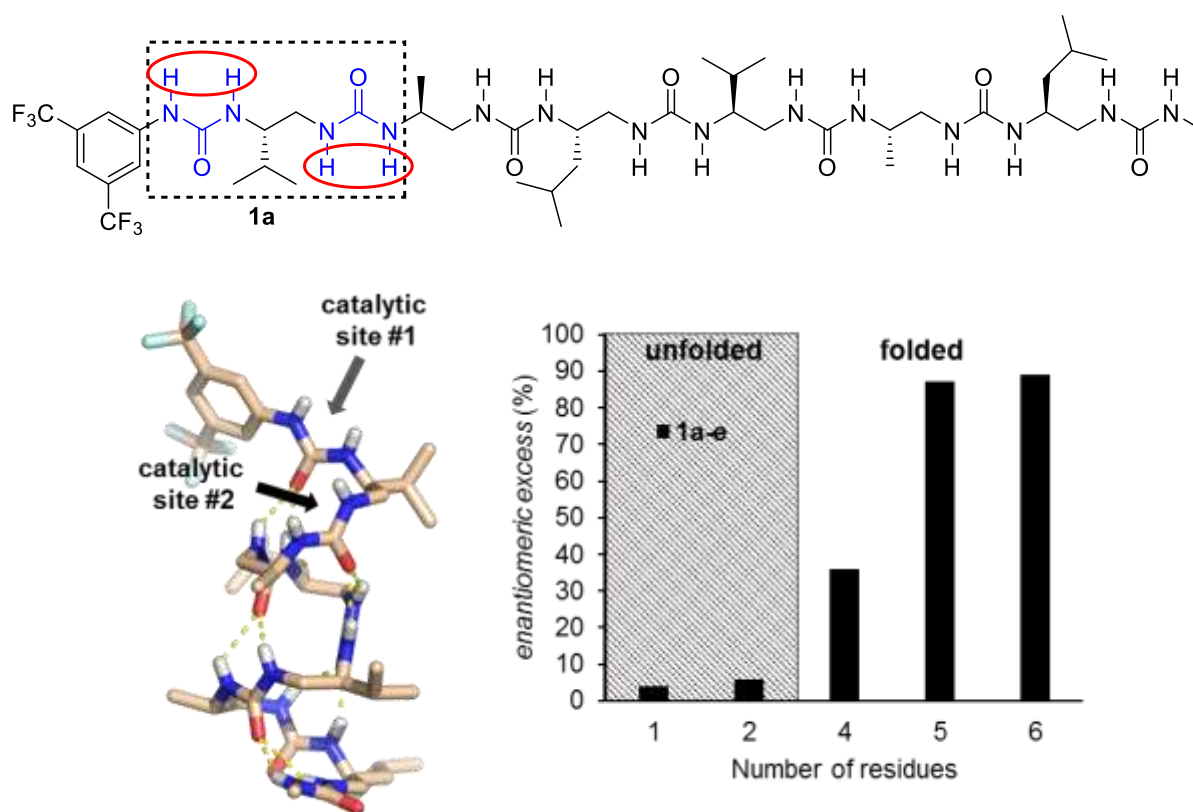


Figure VI.1: Principles governing oligourea-foldamer based organocatalysis

The scope of the Michael addition between 1,3-dicarbonyl pronucleophiles with nitroalkene electrophiles has been extensively studied, with satisfying results, in terms of yields and stereocontrols. The relatively large scope in terms of electrophiles reinforce the proposition of interaction model, whereby the electrophile in the Michael addition is not interacting directly with the catalyst but rather in a coordination complex involving all the compounds. The developed catalytic system has been

applied to the synthesis of cyclohexyl nitro-ketoester with a high number of stereocenters, which can serve as a precursor in the synthesis of natural products, through a double Michael addition. Preliminary results towards the development of reactions with diastereoselective control gave encouraging results but efforts in this direction need to be pursued. A better understanding of the mechanism of action may also help to reach good results for the Michael addition with a diastereocontrol.

Juliá-Colonna epoxidation and Henry addition have been tested with the designed oligourea catalyst in a second part, to investigate its possibilities to be used for other reactions. Despite the lack of stereocontrol, these studies were very complementary with the mechanistic study because they involve other substrates and binding modes to the catalyst. Particularly, the catalyst presented weak stereocontrol for Henry reaction, which showed there is still room for improving the understanding of the catalytic system and for having successful results for the diastereoselective formation of nitroalcohols, which are versatile intermediates.

To explore the possibility to reach a greener system, the catalyst has been grafted on polystyrene beads, allowing an easy recovery of the catalyst. The system was still performant in biphasic conditions. The catalyst beads have been demonstrated to be effective during at least five cycles without no loss of yield and enantiocontrol in the Michael addition reaction. Nevertheless, the catalyst grafted on solid support is not as active as the one in homogeneous phase. There is still place for investigation to optimize the system. Other types of polymers may be screened as a support matrix. The porosity and the resin substitution should be investigated in more detail. A possible solution to improve the solid-supported version of this system is to perform neat reaction, avoiding the use of toxic solvents. Another possibility is to use the catalyst in flow chemistry, which would allow the transfer of the system to industrial process. With the same perspectives, one could envisage the synthesis of a catalyst made of only one residue type (one side chain) which would reduce the price of the catalyst synthesis. Adapting the optimized lateral side chain and the optimized oligourea length would then allow the synthesis of a very competitive and effective catalyst for industrial syntheses.

Because of the key role of the acidity of the two first urea on N-terminus part, the terminal urea at the positive pole of the foldamer macrodipole can be modified to vary the electronic properties of the catalytic sites. As urea and thiourea have been compared, squaramide group and sulfonyl group are very interesting scaffolds to incorporate at the extremity of a oligourea backbone. Their effects on foldamer helicity have first to be studied, then their effects on catalysed reactions can be tested. N-sulfinyl-urea is another electron-withdrawing activating group which will modulate acidity of the catalytic sites and which will modify also the steric hindrance (Figure VI.2).

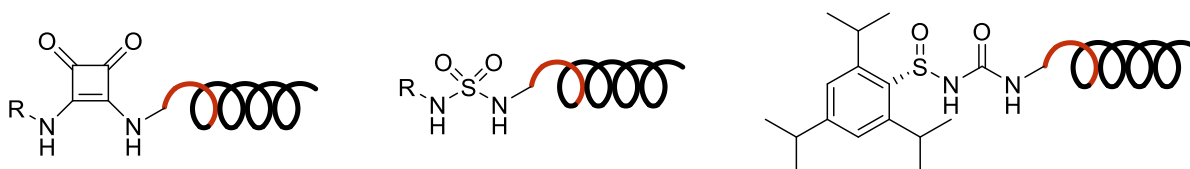


Figure VI.2: Urea isosteres to modify acidity of catalytic sites of the oligourea foldamer

At this point, a wider range of oligourea-based foldamer catalysts could be synthesized in order to screen an even greater variety of chemical reactions. A first option could be the modification of the lateral side chains, in terms of both position and nature. Chemical functions can be added into the lateral side chains towards the purpose to make them interact with the substrates. Derivatives from natural amino acids such as serine, glutamine, cysteine or tyrosine could be used in the oligourea catalyst to complement the aliphatic valine, alanine and leucine derived building blocks. This approach would then combine two elements that would mediate catalysis: on one hand, the folded backbone and on the other hand the chemical functions of the lateral side chains (Figure VI.3 left). The two methylenes bridging the two first urea catalytic sites constitute a strategic position to bring additional functionality and/or more hindrance to the system. The association of the organic foldamer catalyst with metals through coordination is also another option for combining two catalytic elements and widen the possible application fields of oligourea-based foldamer (Figure VI.3 right).

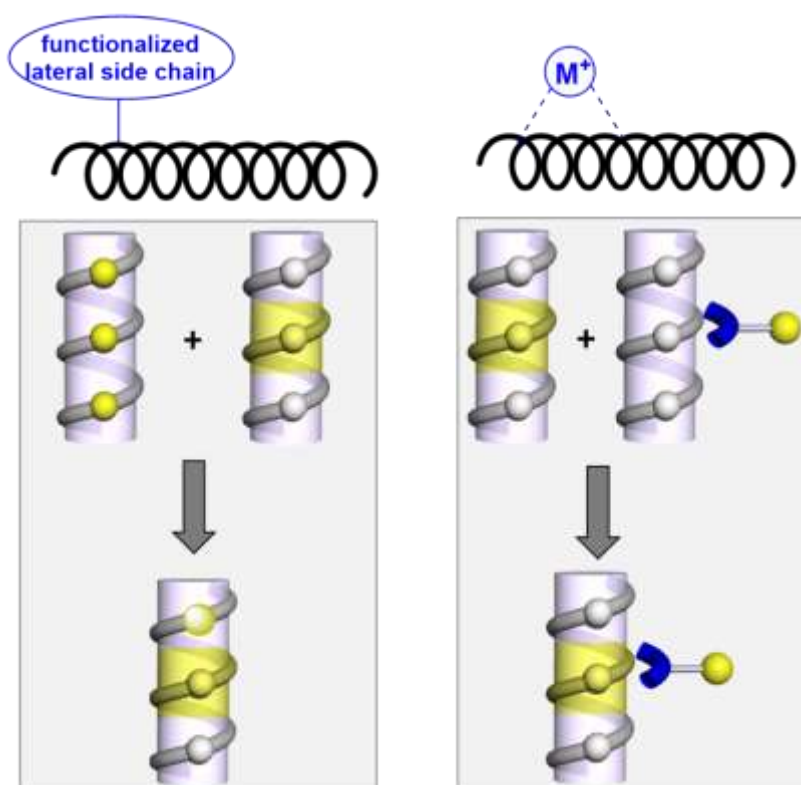


Figure VI.3: Modification of the foldamer catalyst by insertion of functionalized lateral side chain(s) (left) or insertion of metallic cofactors (right)

Structural changes can be realised on the foldamer backbone to bring other properties to the catalyst, and perform other reactions with other kind of activation. For instance, incorporation of a terminal pyrrolidine derivative in the oligourea backbone would allow catalysis through hydrogen bond activation to be combined with enamine or iminium activation (Figure VI.4 left). Oligourea helices have been demonstrated to be compatible with peptides helices, thus bringing the possibility to generate oligourea/peptide chimeras which could be used to further modulate the catalytic activities and would be even cheaper to produce than homo-oligoureas (Figure VI.4 right).

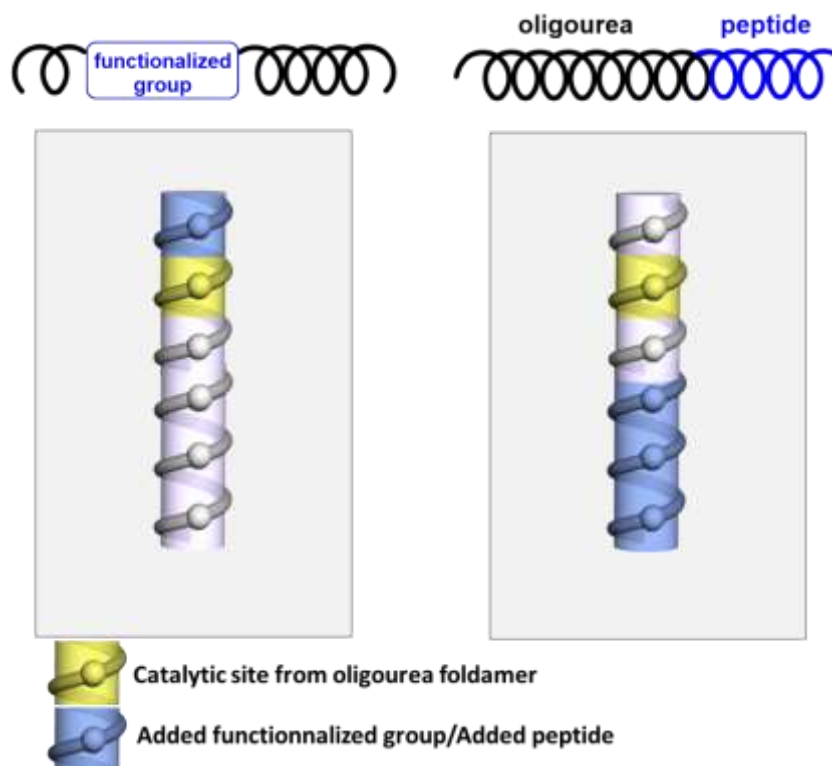


Figure VI.4 : Structural modification of the foldamer catalyst by insertion of a functional segment or residue inside the oligourea backbone (left) or by mixing oligourea and peptide helical backbones

Oligourea have been demonstrated to be able to fold into other architectures (such as β -turns) and to self-assemble in aqueous solution into nanostructures with cavities and pores, which in turn could also be of interest organocatalyzed reaction. For the future, each approach to bring diversity to the oligourea backbone or to its sequence to modify its propensity to self-assemble is of potential interest for the future of catalysis with urea-based foldamers. As with enzymatic catalysis, the perfect control of the coordination sphere between substrates and catalyst enhance the catalytic properties of the designed system. But like enzymes, a high control of the geometric and electrostatic environment of the catalytic sites in the foldamer is also inherently associated with an increase of the specificity of the system. The main perspective of bioinspired catalysis with oligourea foldamers resides in exploiting the modularity and sequence diversity of the system to access to a higher variety of mode of action and more catalysed reactions to enrich the toolbox for synthetic chemists.

CHAPTER VII

CHAPTER VII : SUPPORTING INFORMATION

7.1 MATERIALS AND GENERAL TECHNIQUES	180
7.1.1 Solvents and reagents.....	180
7.1.2 General methods	180
7.1.3 Chromatography	180
7.1.4 Mass spectra.....	180
7.1.5 NMR spectra	180
7.1.6 Determination of enantiomeric excesses.....	181
7.1.7 Optical rotations.....	181
7.1.8 X-Ray diffraction analysis	181
7.2 SYNTHESIS OF BUILDING BLOCKS.....	182
7.2.1 Valine-derivative Building Block	182
7.2.2 Alanine-derivative Building Block	182
7.2.3 Leucine-derivative Building Block.....	182
7.2.4 Proline-derivative Building Block.....	183
7.2.5 Glycine-derivative Building Block.....	183
7.2.6 Phenylalanine-derivative Building Block.....	183
7.3 SYNTHESIS OF CATALYSTS OF CHAPTER II	184
7.3.1 Synthesis of (CF ₃) ₂ PhNHCO-Val ^u -Ala ^u -Leu ^u -Val ^u -Ala ^u -Leu ^u -NHMe (1a)	184
7.3.2 Synthesis of (CF ₃) ₂ PhNHCO-Val ^u -Ala ^u -Leu ^u -Val ^u -Ala ^u -NHMe (1b)	187
7.3.2.1 Boc-Ala ^u -NHMe	188
7.3.2.2 Boc-Val ^u -Ala ^u -NHMe	188
7.3.2.3 Boc-Leu ^u -Val ^u -Ala ^u -NHMe.....	188
7.3.2.4 Boc-Ala ^u -Leu ^u -Val ^u -Ala ^u -NHMe	189
7.3.2.5 Boc-Val ^u -Ala ^u -Leu ^u -Val ^u -Ala ^u -NHMe	189
7.3.2.6 (CF ₃) ₂ PhNHCO-Val ^u -Ala ^u -Leu ^u -Val ^u -Ala ^u -NHMe (1b)	190
7.3.3 Synthesis of (CF ₃) ₂ PhNHCO-Val ^u -Ala ^u -Leu ^u -Val ^u -NHMe (1c).....	193
7.3.3.1 Boc-Val ^u -NHMe	194
7.3.3.2 Boc-Leu ^u -Val ^u -NHMe.....	194
7.3.3.3 Boc-Ala ^u -Leu ^u -Val ^u -NHMe.....	195
7.3.3.4 Boc-Val ^u -Ala ^u -Leu ^u -Val ^u -NHMe	195
7.3.3.5 (CF ₃) ₂ PhNHCO-Val ^u -Ala ^u -Leu ^u -Val ^u -NHMe (1c)	196
7.3.4 Synthesis of (CF ₃) ₂ PhNHCO-Val ^u -Ala ^u -NHMe (1d)	198
7.3.5 Synthesis of (CF ₃) ₂ PhNHCO-Val ^u -NHMe (1e)	200
7.3.6 Synthesis of (CF ₃) ₂ PhNHCS-Val ^u -Ala ^u -Leu ^u -Val ^u -Ala ^u -Leu ^u -NH ^u -Me (5a)	202
7.3.7 Synthesis of (CF ₃) ₂ PhNHCS-Val ^u -Ala ^u -Leu ^u -Val ^u -NHMe (5c)	204

7.3.8 Synthesis of (CF ₃) ₂ PhNHCS-Val ^u -Ala ^u -NHBn (5d).....	206
7.3.9 Synthesis of (CF ₃) ₂ PhNHCS-Val ^u -NHMe (5e).....	209
7.4 SYNTHESIS OF CATALYSTS FROM CHAPTER III	211
7.4.1 Synthesis of 3,5-(CF ₃) ₂ PhNHCO-Pro ^u -Ala ^u -Leu ^u -Val ^u -Ala ^u -Leu ^u -NHMe (10).....	211
7.4.1.1 Boc-Pro ^u -Ala ^u -Leu ^u -Val ^u -Ala ^u -Leu ^u -NHMe	211
7.4.1.2 3,5-(CF ₃) ₂ PhNHCO-Pro ^u -Ala ^u -Leu ^u -Val ^u -Ala ^u -Leu ^u -NHMe (10).....	212
7.4.2 Synthesis of 3,5-(CF ₃) ₂ PhNHCO-Val ^u -Pro ^u -Leu ^u -Val ^u -Ala ^u -Leu ^u -NHMe (11).....	215
7.4.2.1 Boc-Pro ^u -Leu ^u -Val ^u -Ala ^u -Leu ^u -NHMe	216
7.4.2.2 Boc-Val ^u -Pro ^u -Leu ^u -Val ^u -Ala ^u -Leu ^u -NHMe	216
7.4.2.3 3,5-(CF ₃) ₂ PhNHCO-Val ^u -Pro ^u -Leu ^u -Val ^u -Ala ^u -Leu ^u -NHMe (11).....	217
7.4.3 Synthesis of (CF ₃) ₂ PhNHCS-Val ^u -Pro ^u -Leu ^u -Val ^u -Ala ^u -Leu ^u -NHMe (12).....	219
7.4.4 Synthesis of 3,5-(CF ₃) ₂ PhNHCO-Gly ^u -Ala ^u -Leu ^u -Val ^u -Ala ^u -Leu ^u -NHMe (13).....	222
7.4.4.1 BocGly ^u -Ala ^u -Leu ^u -Val ^u -Ala ^u -Leu ^u -NHMe.....	222
7.4.4.2 3,5-(CF ₃) ₂ PhNHCO-Gly ^u -Ala ^u -Leu ^u -Val ^u -Ala ^u -Leu ^u -NHMe.....	223
7.4.5 Synthesis of 3,5-(CF ₃) ₂ PhNHCS-Gly ^u -Ala ^u -Leu ^u -Val ^u -Ala ^u -Leu ^u -NHMe (14).....	225
7.4.6 Synthesis of 3,5-(CF ₃) ₂ PhNHCO-Phe ^u -Ala ^u -Leu ^u -Val ^u -Ala ^u -Leu ^u -NHMe (15).....	227
7.4.7.1 Boc-Phe ^u -Ala ^u -Leu ^u -Val ^u -Ala ^u -Leu ^u -NHMe	227
7.4.7.2 3,5-(CF ₃) ₂ PhNHCO-Phe ^u -Ala ^u -Leu ^u -Val ^u -Ala ^u -Leu ^u -NHMe (15).....	228
7.5 EXPERIMENTAL PART OF CHAPTER IV.....	231
7.5.1 General procedure for synthesis of nitroalkenes	231
7.5.1.1 General procedure to synthesize aromatic nitroalkenes.....	231
7.5.1.2 General procedure to synthesize aliphatic nitroalkenes.....	231
7.5.1.3 General procedure to synthesize aromatic conjugated nitroalkenes	231
7.5.1.4 Characterization of synthesized nitroalkenes	233
7.5.2 General procedure for the asymmetric conjugate addition of 1,3-dicarbonyl compounds to nitroalkenes	235
7.5.2.1 Asymmetric reaction	235
7.5.2.2 Racemic reaction.....	235
7.5.3 Characterisation of adducts 4 , 18c-e , 16a with variation of malonate hindrance	236
7.5.4 Characterisation of adducts 21b-21l with variation around aromatic nitroalkenes	241
7.5.5 Adducts 22a-22d from aromatic conjugated nitroalkenes	252
7.5.6 Characterization of adducts 23a-23g with aliphatic nitroalkenes	256
7.5.7 Characterization of adducts 8-9 from chapter II	263
7.5.8 Characterization of other adducts with other pronucleophiles.....	267
7.5.9 Experimental section for Cascade Michael addition.....	273
7.5.9.1 Synthesis of precursors for Cascade Michael addition.....	273
7.5.9.2 Characterization of cyclized adducts from Cascade Michael reaction	277
7.5.10 Experimental section for Henry reaction	281

7.5.11 Experimental section for the Juliá-Colonna epoxidation	283
7.5.11.1 <i>Synthesis of chalcone 36</i>	283
7.5.11.2 <i>General procedure for Juliá-Colonna epoxidation</i>	283
7.5.11.3 <i>Characterization of Juliá-Colonna adducts</i>	283
7.6 EXPERIMENTAL PART OF CHAPTER V	285
7.6.1 Characterization of catalyst 41 and precursors	285
7.6.2 Procedure for synthesis of catalyst 35	289
7.6.2 Procedure for the synthesis of catalyst 43	291

7.1 MATERIALS AND GENERAL TECHNIQUES

7.1.1 Solvents and reagents

Unless otherwise specified, reagents were obtained from commercial sources (Sigma-Aldrich, Acros, Alfa Aesar, Fluka, TCI, Merck, etc.), stored as suppliers indicated and used without purification. When anhydrous solvents were required, they were dried following established protocols. In Guichard laboratory, tetrahydrofuran, toluene and dichloromethane were dried by filtration through activated alumina (Sigma-Aldrich). In Palomo laboratory, dichloromethane was dried over CaH_2 , toluene was dried over sodium. Triethylamine, *N,N*-diisopropylethylamine, diethyl malonate and dimethyl malonate were purified by distillation.

7.1.2 General methods

Yields refer to chromatographically purified and spectroscopically pure compounds, unless otherwise specified.

7.1.3 Chromatography

Reactions were monitored by either $^1\text{H-NMR}$ analysis of reaction aliquots or thin layer chromatography (TLC) using Merck silica gel 60 F254 plates and visualized by fluorescence quenching under UV light, Ficher Bioblock lamp VL-4LC, $\lambda = 254$ and 365 nm. For products from catalysed reactions, visualization of TLC was accomplished with a solution of potassium permanganate (1 g) in 100 mL of water (limited lifetime), followed by heating. For oligourea compounds, visualization of TLC was accomplished with a solution of ninhydrin (5 g) in 100 mL of ethanol, followed by heating.

Flash column chromatography was carried out on silica gel (40-63 μm). RP-HPLC purification was performed on a column VP 250/10 Nucleodur 100-5 C18 ec at a flow rate of 1 mL/min. The mobile phase was composed of H_2O (solvent A) in CH_3OH (solvent B) with gradient from 40% to 100% in 10 min.

7.1.4 Mass spectra

ESI-MS analyses were carried out with a ThermoElectron LCQ Advantage spectrometer equipped with an ion-trap mass analyzer. High resolution electrospray ionization time-of-flight (ESI-TOF) mass spectra were measured in the positive ion mode on a Waters/Micromass Q-ToF Ultima.

7.1.5 NMR spectra

^1H NMR and ^{13}C NMR spectra were recorded using a Bruker Spectrometer 300 MHz or 400 MHz and 75 MHz or 100 MHz, respectively. The chemical shifts (δ) are reported in parts per million (ppm) relative to the residual solvent peak, CDCl_3 ($= 7.36$), CD_3OH ($= 3.31, 4.87$), DMSO-d_6 ($= 2.50$) for ^1H NMR and relative to CDCl_3 ($= 77.0$), CD_3OD ($= 49.2$), DMSO-d_6 ($= 39.5$) and for ^{13}C NMR. Registered spectra process and edition were done using MestReNova MNova 8.1 program and Bruker TopSpin 3.5pl7. The multiplicity of each signal is designated using the following abbreviations: s,

singlet; d, doublet; t, triplet; q, quartet; m, multiplet; brs, broad singlet. The coupling constants (J) are reported in Hertz (Hz).

7.1.6 Determination of enantiomeric excesses

Enantiomeric excesses were determined using analytical high performance liquid chromatography (HPLC) performed on Waters-600E (equipped with 2996 and 2998 photodiode array UV detector) using Daicel Chiralpak IA, IB, IC, AD-H, OD-H and OJ-H columns.

7.1.7 Optical rotations

Optical rotations were recorded using a Jasco P-2000 polarimeter; specific rotations (SR) ($[\alpha]_D$) are reported in $10^{-1} \text{ deg}\cdot\text{cm}^2\cdot\text{g}^{-1}$; concentrations (c) are quoted in g/100 mL; D refers to the D-line of sodium (589 nm); temperatures (T) are given in degree Celsius ($^{\circ}\text{C}$).

7.1.8 X-Ray diffraction analysis

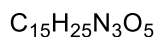
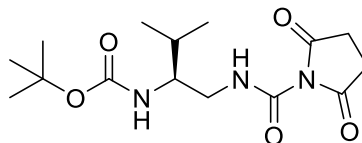
Single crystal X-ray diffraction experiments were performed at the IECB X-ray facility (CNRS UMS 3033 – INSERM US001, University of Bordeaux) on two rotating anodes: a 3kW microfocus Rigaku FRX for compound 1a and a 1.2 kW Rigaku MM007 HF for compounds 2a, 1b, 15 and 20. Both sources are equipped with high flux Osmic Varimax HF mirrors. The powerful FRX is combined with a hybrid Dectris Pilatus 200K detector. The MM007 detector is a cylindrical IP (imaging plate) optimized for small molecule single crystal structural analysis. All data were collected at the copper $\text{K}\alpha$ wavelength with a partial chi goniometer that decreases blind areas and enables automatic axial adjustment. Cylindrical IPs are used to permit wide angular measurement ranges of -60° to $+144^{\circ}$ (circumferential direction) and $\pm 45^{\circ}$ (axial direction). Measurement of the entire area is possible even with Cu $\text{K}\alpha$ radiation. The Rigaku CrystalClear suite was used to index and integrate all data with a multi-scan absorption correction. All structures were solved with Shelxt2 and refined by full matrix least-squares method on F with Shelxl-2014. Data collection, structures refinement statistics and CCDC deposition numbers are presented in the tables below. The final cif files were checked using IUCR's checkcif algorithm. Few B Alerts remain but mainly concern disordered groups or solvent molecules. As a rule of thumb, every time where disorder could be modelled with partial occupation, it was so. SHELX DFIX and RIGU restraints were used in the refinement strategy, as listed in the cif files, mostly for disordered CF₃ phenyl substituents. For disordered solvent water molecules, hydrogen atoms were not modelled if not seen in the Fourier difference maps.

X-ray diffraction experiments were performed with a high-flux RIGAKU FRX rotating anode at the Cu-K α wavelength.

7.2 SYNTHESIS OF BUILDING BLOCKS

Building blocks were synthesized as described in literature¹ with Boc-protected group strategy, from natural amino acids.

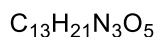
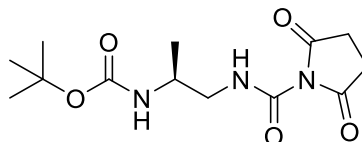
7.2.1 Valine-derivative Building Block



¹H NMR (300 MHz, CDCl₃) δ (ppm) 6.14 (br. s., 1H), 4.60 (d, *J* = 8.5 Hz, 1H), 3.59 (m, 1H), 3.40-3.47 (m, 1H), 3.24-3.34 (m, 1H), 2.84 (s, 4H), 1.83 (sext, *J* = 7.5 Hz, 1H), 1.49 (s, 1H), 1.00 (d, *J* = 7.8 Hz, 3H), 0.97 (d, *J* = 7.9 Hz, 3H).

¹³C NMR (75 MHz, CDCl₃) δ (ppm) 169.7, 55.4, 45.5, 30.3, 28.3, 19.3, 18.1.

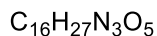
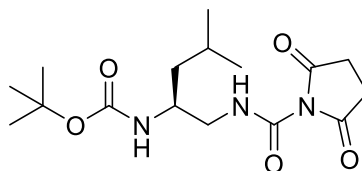
7.2.2 Alanine-derivative Building Block



¹H NMR (300 MHz, CDCl₃) δ (ppm) 6.29 (br. s., 1H), 4.65 (br. s., 1H), 3.86 (br. s., 1H), 3.40 (dt, *J* = 4.3 Hz, 13.5 Hz, 1H), 3.26 (m, 1H), 2.85 (s, 4H), 1.49 (s, 9H), 1.22 (d, *J* = 7.8 Hz, 3H).

¹³C NMR (75 MHz, CDCl₃) δ (ppm) 169.8, 151.9, 80.2, 48.3, 47.4, 28.2, 18.4.

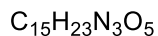
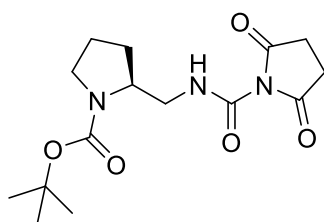
7.2.3 Leucine-derivative Building Block



¹H NMR (300 MHz, CDCl₃) δ (ppm) 6.27 (br. s., 1H), 4.59 (m, 1H), 3.81 (br. s., 1H), 3.38 (dt, *J* = 4.4 Hz, 13.4 Hz, 1H), 3.23 (m, 1H), 2.83 (s, 4H), 1.70 (sext, *J* = 7.6 Hz, 1H), 1.47 (s, 9H), 1.34 (m, 2H), 0.95 (s, *J* = 7.5 Hz, 3H), 0.94 (d, *J* = 7.4 Hz, 3H).

¹³C NMR (75 MHz, CDCl₃) δ (ppm) 169.86, 151.91, 48.59, 47.62, 41.50, 28.32, 24.76, 22.96, 22.02.

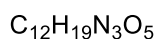
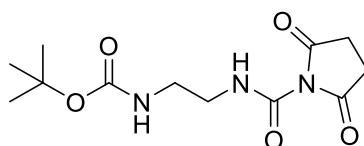
7.2.4 Proline-derivative Building Block



$^1\text{H NMR}$ (300 MHz, CDCl_3) δ (ppm) 4.06 (br. s., 1H), 3.21-3.41 (m, 4H), 2.84 (s, 4H), 2.08 (m, 1H), 1.88-1.93 (m, 2H), 1.71 (br. s., 2H), 1.50 (s, 9H).

$^{13}\text{C NMR}$ (75 MHz, CDCl_3) δ (ppm) 169.85, 151.70, 56.55, 47.85, 47.32, 29.64, 28.45, 25.49, 23.93.

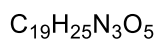
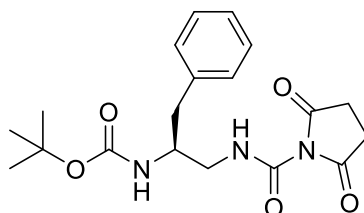
7.2.5 Glycine-derivative Building Block



$^1\text{H NMR}$ (300 MHz, CDCl_3) δ (ppm) 6.33 (br. s., 1H), 5.03 (br. s., 1H), 3.38 (m, 4H), 2.84 (s, 4H), 1.47 (s, 9H).

$^{13}\text{C NMR}$ (75 MHz, CDCl_3) δ (ppm) 170.0, 151.8, 80.1, 42.8, 39.9, 28.4, 25.5.

7.2.6 Phenylalanine-derivative Building Block

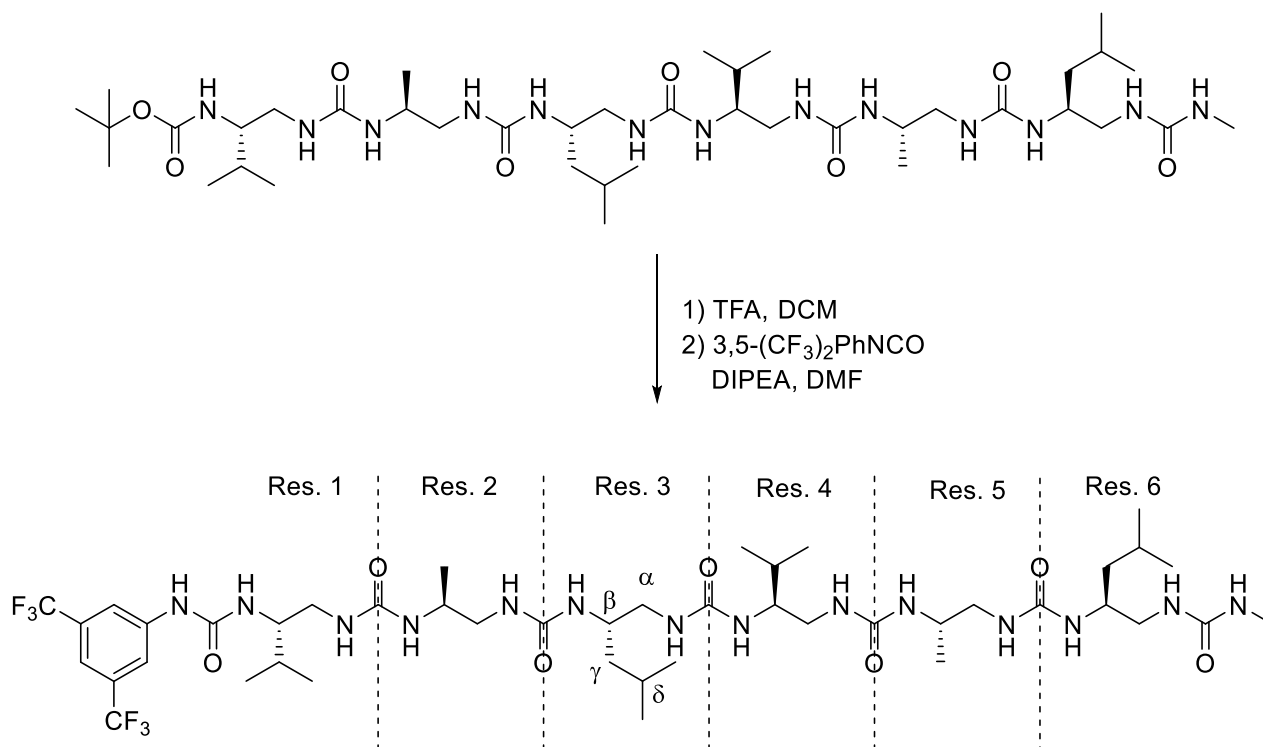


$^1\text{H NMR}$ (300 MHz, CDCl_3) δ (ppm) 7.21-7.37 (m, 5H), 5.99 (br. s., 1H), 4.61 (br. s., 1H), 4.61 (br. s., 1H), 4.01 (br. s.), 3.43-3.53 (m, 1H), 3.34 (m, 1H), 2.04 (s, 4H), 1.49 (s, 9H).

$^{13}\text{C NMR}$ (75 MHz, CDCl_3) δ (ppm) 176.1, 160.3, 157.3, 143.9, 134.3, 133.3, 131.2, 82.9, 56.7, 42.6, 33.4, 30.5.

7.3 SYNTHESIS OF CATALYSTS OF CHAPTER II

7.3.1 Synthesis of (CF₃)₂PhNHCO-Val^α-Ala^α-Leu^α-Val^α-Ala^α-Leu^α-NHMe (1a)



Scheme S1 : Synthesis of the hexamer 1a

To a solution of **BocVal^α-Ala^α-Leu^α-Val^α-Ala^α-NHMe** (800 mg, 0.88 mmol) in CH₂Cl₂ (2 mL) was added TFA (2 mL) and the reaction mixture was stirred at RT for 4 h. After completion of the reaction, TFA and CH₂Cl₂ were evaporated under reduced pressure. To the resulting TFA salt dissolved in DMF (4 mL) were successively added DIPEA (480 μL, 2.72 mmol) and 3,5-bis(trifluoromethyl)phenyl isocyanate (240 μL, 1.36 mmol). The reaction mixture was stirred at RT for 16 h. NaHCO₃ solution (30 mL) was added which led to gel formation which was recovered after filtration, dissolved in MeOH, concentrated and dried under high vacuum. The recovered orange solid was reprecipitated in acetonitrile to lead to the titled oligourea as a white solid (731mg, 81%).

¹H NMR (400 MHz, CD₃OH) δ (ppm) 9.01 (s, 1H), 8.00 (br. s., 2H), 7.52 (br. s., 1H), 6.56 (dd, *J* = 10.2 and 2.7 Hz, 1H), 6.50 (dd, *J* = 9.8 and 2.3 Hz, 1H), 6.37-6.45 (m, 2H), 6.26 (d, *J* = 10.7 Hz, 1H), 6.24 (d, *J* = 10.3 Hz, 1H), 6.21 (q, *J* = 4.9 Hz, 1H), 6.03-7.11 (m, 2H), 6.00 (dd, *J* = 9.6 and 3.6 Hz, 1H), 5.97 (d, *J* = 10.6 Hz, 1H), 5.93 (d, *J* = 10.6 Hz, 1H), 5.86 (d, *J* = 10.1 Hz, 1H), 4.00-4.15 (m, 1H), 3.75-4.00 (m, 4H), 3.48-3.75 (m, 7H), 2.70 (d, *J* = 4.8 Hz, 3H), 2.57-2.74 (m, 2H), 2.24-2.47 (m, 4H), 1.64-1.85 (m, 3H), 1.49-1.64 (m, 1H), 1.12-1.32 (m, 4H), 1.00-1.06 (m, 9H), 0.98 (d, *J* = 7.0 Hz, 3H), 0.88-0.95 (m, 15 H), 0.86 (d, *J* = 7.0 Hz, 3H) ppm.

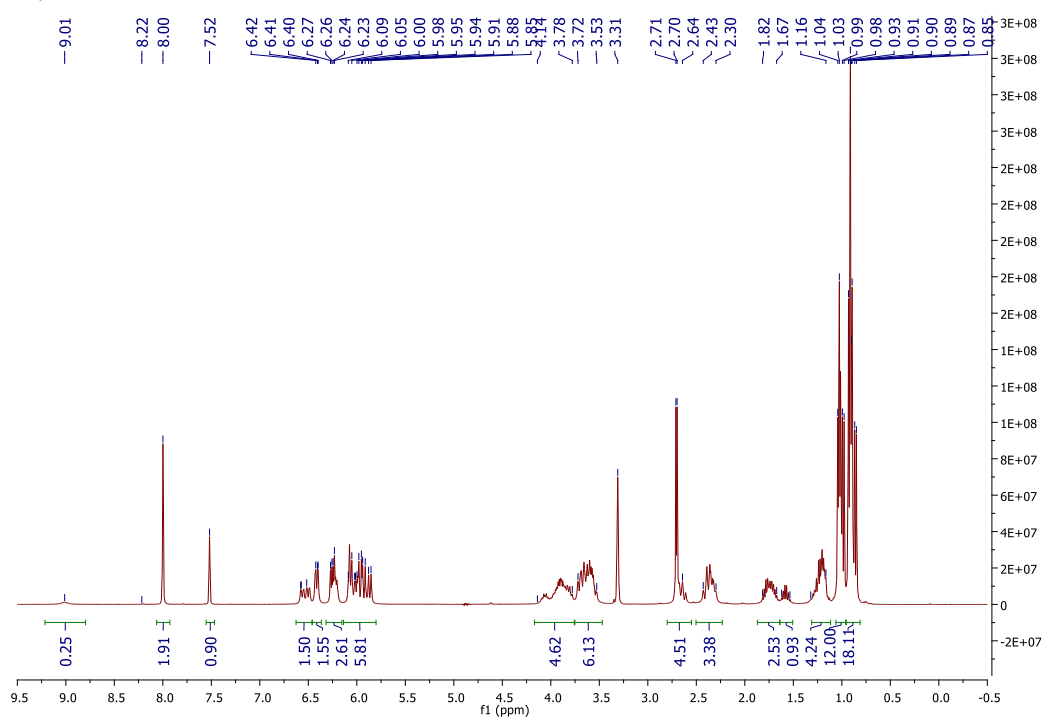
¹³C NMR (100 MHz, CD₃OH) δ (ppm) 162.1 (C), 162.0 (C), 161.8 (C), 161.6 (C), 161.4 (C), 160.9 (C), 158.2 (C), 143.2 (C), 133.1 (q, *J* = 33 Hz, 2 × C), 124.6 (q, *J* = 27 Hz, 2 × C), 118.8-119.1 (m, 2 × CH), 115.5-115.8 (m, CH), 56.7 (CH), 56.2 (CH), 49.4 (CH), 49.1 (CH), 48.2 (2 × CH₂), 47.4 (CH₂), 46.8 (CH), 46.3 (CH₂), 46.1 (CH), 44.7 (CH₂), 44.4 (CH₂), 43.8 (CH₂), 42.7 (CH₂), 31.91 (CH), 31.88 (CH), 26.8 (CH₃), 26.1 (CH), 25.8 (CH), 23.6 (CH₃), 23.5 (CH₃), 22.7 (CH₃), 22.4 (CH₃), 20.1 (CH₃), 20.0 (CH₃), 18.7 (CH₃), 18.5 (CH₃), 18.3 (CH₃), 18.2 (CH₃).

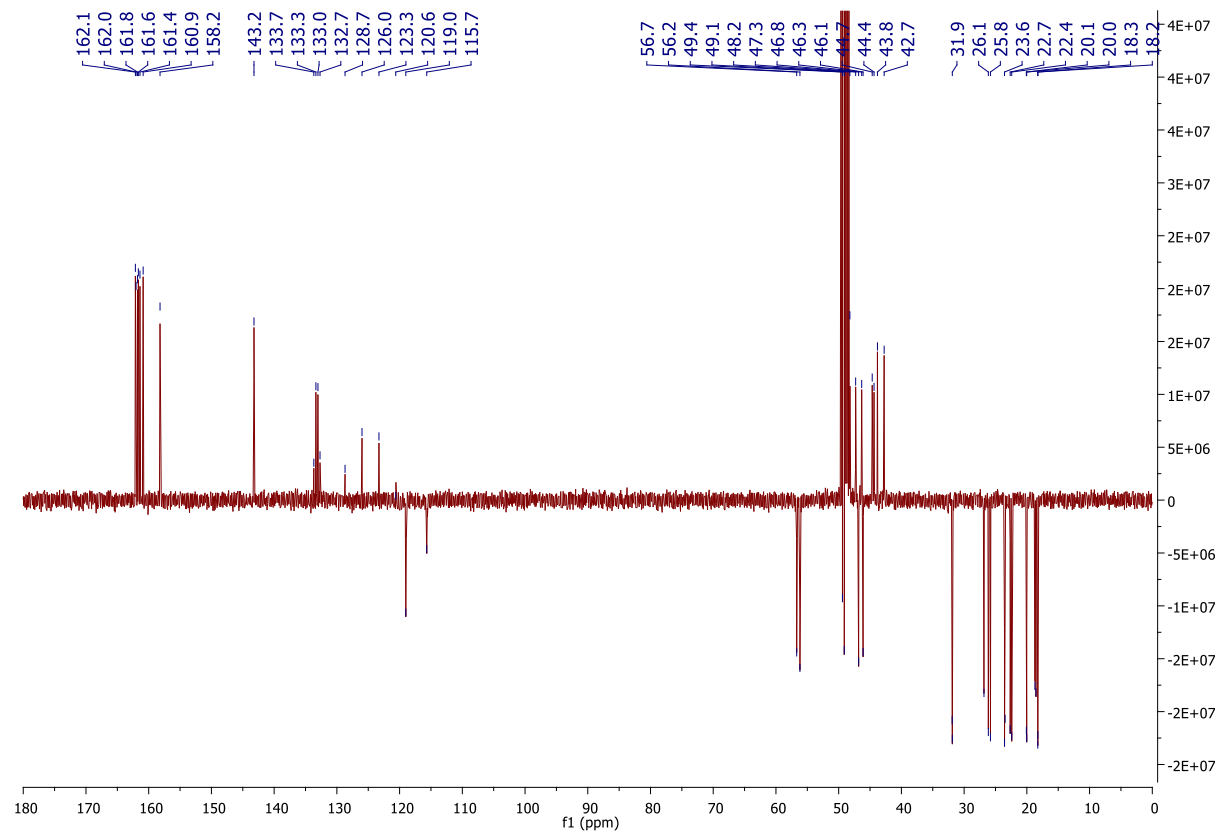
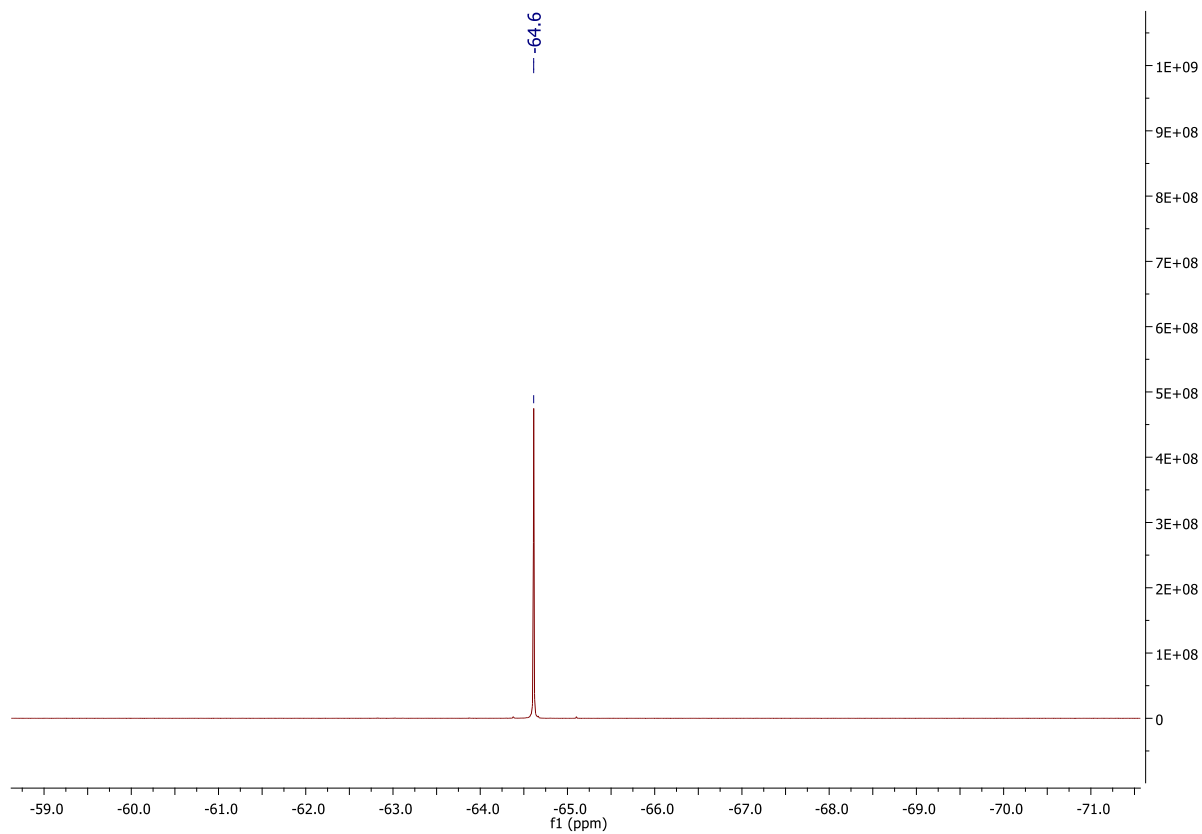
¹⁹F NMR (376 MHz, CD₃OH) δ -64.6 ppm.

HRMS (ES⁺, MeOH) calcd for C₄₄H₇₆F₆N₁₄O₇ = 1027.69984; found 1027.60173.

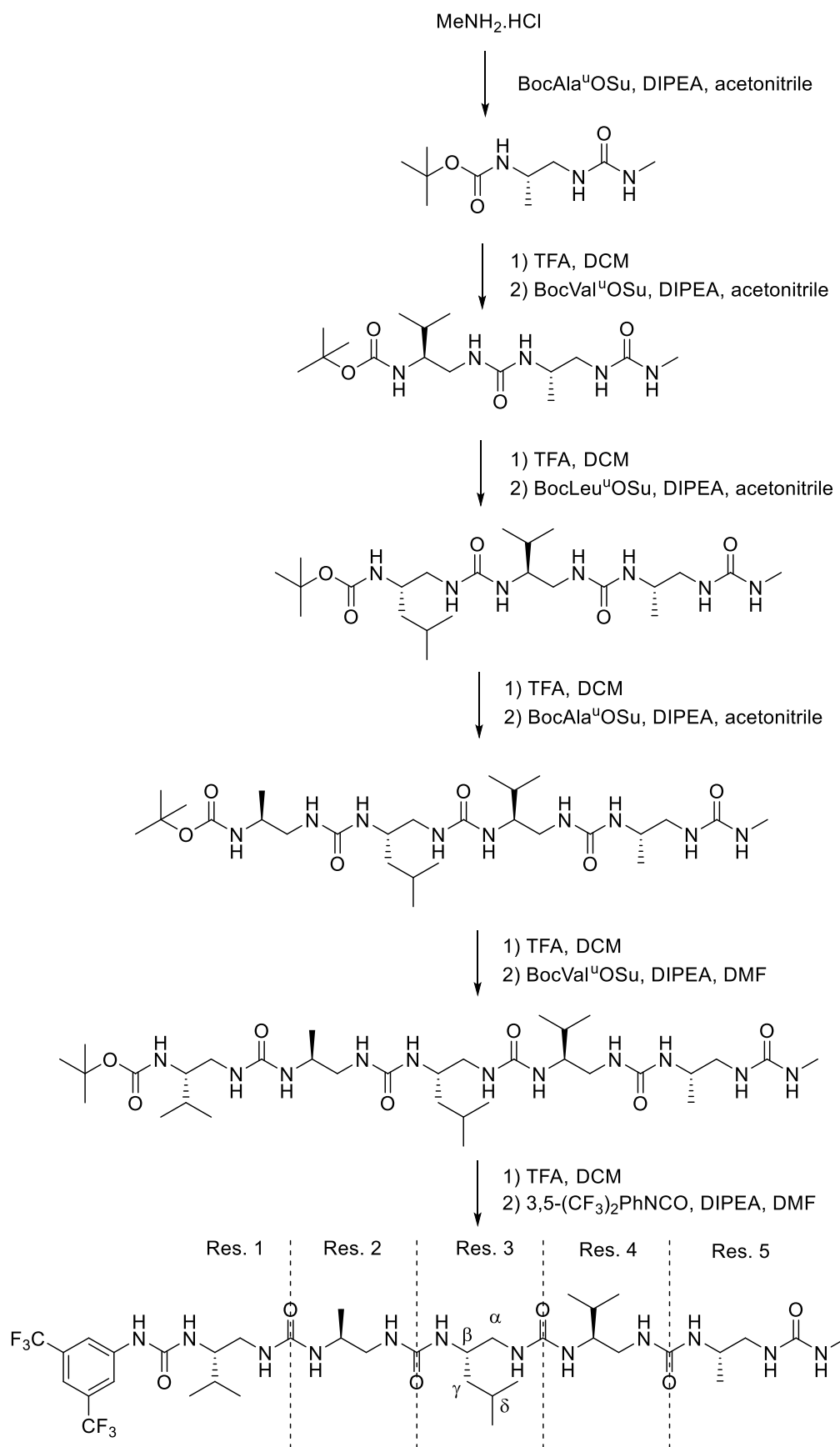
Table S1: ^1H NMR Chemical Shifts (ppm) of 3,5-(CF₃)₂PhNHCO-Val^u-Ala^u-Leu^u-Val^u-Ala^u-Leu^u-NHMe (1a) in CD₃OH at 293K.

Residue	NH	NH'	αCH^a	αCH^b	βCH	γCH	δCH	ϵCH	Term CH	$\Delta\delta(\alpha\text{CH})$
ArNHCO		9.01							8.00	
									7.62	
Val ^u	1	6.24	6.07	2.68	3.68	3.82	1.77	0.98 + 1.02		1.00
Ala ^u	2	5.83	6.00	2.33	3.61	3.88	1.01			1.28
Leu ^u	3	5.93	6.56	2.35	3.69	3.95	1.18	1.73	0.90	1.34
Val ^u	4	7.26	6.50	2.39	3.66	3.59	1.57	0.86 + 0.90		1.27
Ala ^u	5	5.97	6.41	2.36	3.56	4.06	1.03			1.20
Leu ^u	6	6.06	6.41	2.65	3.60	3.90	1.23	1.70	0.92	0.95
NHMe		6.21								2.70

 ^1H NMR:

^{13}C NMR: **^{19}F NMR:**

7.3.2 Synthesis of (CF₃)₂PhNHCO-Val^u-Ala^u-Leu^u-Val^u-Ala^u-NHMe (1b)



Scheme S2: Synthesis of the pentamer **1b**

7.3.2.1 *Boc-Ala^u-NHMe*

To a 0°C cooled suspension of methylamine hydrochloride (641 mg, 9.5 mmol) in acetonitrile (20 mL) were added DIPEA (3.3 mL, 1.9 mmol) and **BocAla^uOSu** (1.5 g, 4.8 mmol) and the mixture was stirred overnight at room temperature. Acetonitrile was evaporated under reduced pressure and 1 N KHSO₄ (20 mL) was added. The aqueous layer was extracted with EtOAc (3 x 20 mL) and the combined organic layers were washed with brine (20 mL) and dried over MgSO₄. After evaporation of the solvent under reduced pressure, purification of the crude by column chromatography (DCM:MeOH 95:5) followed by recrystallization from a mixture of EtOAc and Et₂O provided the titled compound as a white solid (658 mg, 59%).

¹H NMR (300 MHz, CDCl₃) δ (ppm) 4.92-5.33 (br s, 3H), 3.72 (m, 1H), 3.22 (m, 2H), 2.80 (s, 3H), 1.46 (s, 9H), 1.17 (d, *J* = 7.9 Hz, 3H).

¹³C NMR (75 MHz, CDCl₃) δ (ppm) 159.6 (CO), 156.4 (CO), 79.6 (C), 47.4 (CH), 46.8 (CH₂), 28.4 (3 x CH₃), 27.3 (CH₃), 18.5 (CH₃).

MS (ESI): *m/z* [M-tBu+H]⁺ 132.1, [M+H]⁺ 232.1.

7.3.2.2 *Boc-Val^u-Ala^u-NHMe*

To a solution of **Boc-Ala^u-NHMe** (155 mg, 0.67 mmol) in CH₂Cl₂ (2 mL) was added TFA (1.5 mL) and the reaction mixture was stirred at RT for 4 h. After completion of the reaction, TFA and CH₂Cl₂ were evaporated under reduced pressure. To the resulting TFA salt dissolved in acetonitrile (1.5 mL) were successively added DIPEA (2.01 mmol, 350 μL) and a solution of **BocVal^uOSu** (317 mg, 1.0 mmol) in acetonitrile (1.5 mL) and the reaction mixture was stirred at RT for 16 h. Acetonitrile was evaporated under reduced pressure and the residue was dissolved in EtOAc. The organic layer was washed with saturated NaHCO₃ (15 mL), 1 N KHSO₄ (15 mL) and water (15 mL) and was dried over MgSO₄. After evaporation of the solvent under reduced pressure, purification of the crude by column chromatography (MeOH/CH₂Cl₂ 2:98→10:90) followed by recrystallization from acetonitrile provided the titled oligourea as a white solid (168 mg, 70%).

¹H NMR (400 MHz, CD₃OH) δ (ppm) 6.41 (d, *J* = 10.0 Hz, 1H), 6.08 (s, 1H), 5.92-5.98 (m, 3H), 3.80 (sext, *J* = 7.8 Hz, 1H), 3.43-3.50 (m, 1H), 3.33-3.39 (m, 1H), 3.22-3.28 (m, 1H), 2.99-3.06 (m, 1H), 2.75 (d, *J* = 4.6 Hz, 3H), 1.76 (sept, *J* = 7.8 Hz, 1H), 1.48 (s, 9H), 1.13 (d, *J* = 7.8 Hz, 3H), 0.99 (d, *J* = 7.8 Hz, 3H), 0.95 (d, *J* = 7.0 Hz, CH₃)

¹³C NMR (100 MHz, CD₃OH) δ 162.9 (C), 161.7 (C), 159.7 (C), 80.7 (C), 58.5 (C), 48.5 (CH), 47.9 (CH₂), 44.0 (CH₂), 32.6 (CH), 29.6 (3 x C), 27.9 (CH₃), 20.7 (CH₃), 19.8 (CH₃), 19.2 (CH₃).

MS (ESI): *m/z* [M+H]⁺ 359.1

7.3.2.3 *Boc-Leu^u-Val^u-Ala^u-NHMe*

To a solution of **Boc-Val^u-Ala^u-NHMe** (553 mg, 1.5 mmol) in CH₂Cl₂ (2 mL) was added TFA (2 mL) and the reaction mixture was stirred at RT for 4 h. After completion of the reaction, TFA and CH₂Cl₂ were evaporated under reduced pressure. To the resulting TFA salt dissolved in acetonitrile (5 mL) were successively added DIPEA (4.62 mmol, 804 μL) and a solution of **BocLeu^uOSu** (631 mg, 1.5 mmol) in acetonitrile (3 mL) and the reaction mixture was stirred at RT for 16 h. Acetonitrile was evaporated under reduced pressure and saturated NaHCO₃ was added. The aqueous layer was extracted with CH₂Cl₂ (3x20 mL) and the combined organic layers were washed with 1 N KHSO₄ (20 mL) and water (20 mL) and were dried over MgSO₄. After evaporation of the solvent under reduced pressure, purification of the crude by column chromatography (MeOH/CH₂Cl₂ 5:95→10:90) provided the titled oligourea as a white solid (534 mg, 69%).

¹H NMR (400 MHz, CD₃OH) δ 7.55 (s, 1H), 6.52 (s, 1H), 6.05 (s, 1H), 6.04 (s, 1H), 5.87 (d, $J = 8.8$ Hz, 1H), 5.80 (s, 1H), 5.77 (s, 1H), 3.76-3.85 (m, 2H), 3.55-3.61 (m, 2H), 3.41-3.49, 2.80 (dd, $J = 8.5$ Hz, 1H), 2.70 (s, 3H), 2.50-2.66 (m, 2H), 1.66 (sext x 2, $J = 7.3$ Hz, 2H), 1.44 (s, 9H), 1.15-1.26 (m, 2H), 1.05 (d, $J = 7.8$ Hz, 3H), 0.94 (d, $J = 7.3$ Hz, 3H), 0.92 (d, $J = 7.3$ Hz, 3H), 0.89 (d, $J = 7.8$ Hz, 3H), 0.88 (d, $J = 7.4$ Hz, 3H).

¹³C NMR (100 MHz, CD₃OH) δ 162.1 (C), 161.5 (C), 161.2 (C), 159.1 (C), 80.1 (C), 56.5 (CH), 50.1 (CH), 49.1 (CH), 47.4 (CH), 46.8 (CH₂), 46.6 (CH₂), 46.7 (CH₂), 42.4 (CH₂), 31.9 (CH), 28.9 (3 x CH₃), 27.1 (CH₃), 26.2 (CH), 23.7 (CH₃), 22.4 (CH₃), 20.1 (CH₃), 19.3 (CH₃), 18.4 (CH₃).

MS (ESI): m/z : [M+H]⁺ 502.2.

7.3.2.4 Boc-Ala^u-Leu^u-Val^u-Ala^u-NHMe

To a solution of **Boc-Leu^u-Val^u-Ala^u-NHMe** (500 mg, 1.0 mmol) in CH₂Cl₂ (2 mL) was added TFA (2 mL) and the reaction mixture was stirred at RT for 4 h. After completion of the reaction, TFA and CH₂Cl₂ were evaporated under reduced pressure. To the resulting TFA salt dissolved in acetonitrile (2 mL) were successively added DIPEA (2.99 mmol, 521 μ L) and a solution of **BocAla^uOSu** (471 mg, 1.5 mmol) in acetonitrile (3 mL). The reaction mixture was stirred at RT for 16 h. The reaction mixture was stirred at RT for 16 h and saturated NaHCO₃ (20 mL) was added. The solid which precipitated was filtered off, was washed with 1 N KHSO₄ (20 mL), and water (20 mL) and was dried under high vacuum. Purification of the crude by column chromatography (MeOH/CH₂Cl₂ 5:95 \rightarrow 10:90) provided the titled oligourea as a white solid (480 mg, 80%).

¹H NMR (400 MHz, CD₃OH) δ (ppm) 6.72 (d, $J = 9.8$ Hz, 1H), 6.46 (d, $J = 9.5$ Hz, 1H), 6.30 (m, 1H), 6.26 (m, 1H), 6.13 (m, 1H), 6.07 (d, $J = 8.0$ Hz, 1H), 6.04 (d, $J = 8.5$ Hz, 1H), 5.96 (dd, $J = 9.0$ Hz, 3.4 Hz, 1H), 5.80 (d, $J = 10.2$ Hz, 1H), 3.97-4.03 (m, 1H), 3.88-3.94 (m, 1H), 3.74-3.81 (m, 1H), 3.66-3.71 (m, 2H), 3.46-3.59 (m, 2H), 2.80-2.84 (m, 1H), 2.77 (d, $J = 4.5$ Hz, 3H), 2.59-2.66 (m, 1H), 2.48-2.55 (m, 1H), 2.35-2.41 (m, 1H), 1.71 (sept, $J = 7.0$ Hz, 2H), 1.51 (s, 9H), 1.18-1.26 (m, 2H), 1.11 (d, $J = 7.9$ Hz, 3H), 1.10 (d, $J = 7.0$ Hz, 3H), 0.98 (d, $J = 7.2$ Hz, 3H), 0.96 (d, $J = 7.6$ Hz, 3H), 0.92 (d, $J = 7.7$ Hz, 3H), 0.91 (d, $J = 7.0$ Hz, 3H).

¹³C NMR (100 MHz, CD₃OH) δ (ppm) 162.8 (C), 162.7 (C), 162.3 (C), 162.1 (C), 159.7 (C), 81.2 (C), 56.8 (CH), 49.6 (CH), 48.8 (CH), 48.5 (CH₂), 48.3 (CH₂), 47.9 (CH), 47.5 (CH₂), 45.3 (CH₂), 43.1 (CH), 32.8 (C), 29.6 (3 x CH₃), 27.8 (C), 27.0 (CH), 24.5 (CH₃), 23.3 (CH₃), 20.9 (CH₃), 20.1 (CH₃), 19.1 (CH₃), 18.8 (CH₃).

MS (ESI): m/z : [M+H]⁺ 602.3, [2M+H]⁺ 1203.3.

7.3.2.5 Boc-Val^u-Ala^u-Leu^u-Val^u-Ala^u-NHMe

To a solution of **Boc-Ala^u-Leu^u-Val^u-Ala^u-NHMe** (450 mg, 0.75 mmol) in CH₂Cl₂ (2 mL) was added TFA (2 mL) and the reaction mixture was stirred at RT for 4 h. After completion of the reaction, TFA and CH₂Cl₂ were evaporated under reduced pressure. To the resulting TFA salt dissolved in DMF (1.5 mL) were successively added DIPEA (2.24 mmol, 391 μ L) and a solution of **BocVal^uOSu** (385 mg, 1.12 mmol) in DMF (1.5 mL). The reaction mixture was stirred at RT for 16 h and saturated NaHCO₃ (20 mL) was added. The solid which precipitated was filtered off, was washed with 1 N KHSO₄ (20 mL), and water (20 mL) and was dried under high vacuum. Purification of the residue by column chromatography (MeOH/CH₂Cl₂ 10:90) provided the titled oligourea as a white solid (380 mg, 69%).

¹H NMR (400 MHz, CD₃OH) δ (ppm) 6.68 (d, *J* = 10.4 Hz, 1H), 6.60 (dd, *J* = 10.4 Hz, 2.8 Hz, 1H), 6.49 (d, *J* = 10.3 Hz, 1H), 6.29-7.34 (m, 2H), 6.25 (d, *J* = 10.6 Hz, 1H), 6.12 (d, *J* = 9.4 Hz, 1H), 6.05 (m, 1H), 5.98 (d, *J* = 10.6 Hz, 1H), 5.93 (d, *J* = 9.8 Hz, 1H), 5.85 (dd, *J* = 9.7 Hz, 3.2 Hz, 1H), 3.99-4.06 (m, 1H), 3.87-3.96 (m, 2H), 3.60-3.75 (m, 4H), 3.50-3.57 (m, 2H), 2.79-2.83 (m, 1H), 2.77 (d, *J* = 4.5 Hz, 3H), 2.58-2.65 (m, 1H), 2.40-2.49 (m, 1H), 2.33-2.38 (m, 2H), 1.65-1.78 (m, 3H), 1.52 (s, 9H), 1.17-1.21 (m, 2H), 1.11 (d, *J* = 7.8 Hz, 3H), 1.08 (d, *J* = 7.3 Hz, 3H), 1.01 (d, *J* = 7.8 Hz, 3H), 0.98 (d, *J* = 7.0 Hz, 3H), 0.96 (d, *J* = 7.8 Hz, 3H), 0.95 (d, *J* = 7.4 Hz, 3H), 0.93 (d, *J* = 7.0 Hz, 3H), 0.92 (d, *J* = 7.9 Hz, 3H).

¹³C NMR (100 MHz, CD₃OH) 162.1 (C), 162.0 (C), 161.6 (C), 161.5 (C), 160.8 (C), 160.8 (C), 159.6 (C), 80.3 (C), 57.8 (CH), 55.9 (CH), 49.8 (CH), 48.8 (CH₂), 47.6 (CH), 47.0 (CH₂), 46.8 (CH), 46.6 (CH₂), 44.5 (CH₂), 44.0 (CH₂), 42.7 (CH), 32.0 (CH), 28.8 (3 x CH₃), 27.9 (CH), 27.2 (CH₂), 23.7 (CH₃), 22.5 (CH₃), 20.1 (CH₃), 20.0 (CH₃), 19.3 (CH₃), 19.0 (CH₃), 18.2 (CH₃), 18.1 (CH₃).

MS (ESI): *m/z*: [M+H]⁺ 730.5, [2M+H]⁺ 1459.4.

7.3.2.6 (CF₃)₂PhNHCO-Val^μ-Ala^μ-Leu^μ-Val^μ-Ala^μ-NHMe (1b)

To a solution of Boc-Val^μ-Ala^μ-Leu^μ-Val^μ-Ala^μ-NHMe (100 mg, 0.14 mmol) in CH₂Cl₂ (2 mL) was added TFA (2 mL) and the reaction mixture was stirred at RT for 4 h. After completion of the reaction, TFA and CH₂Cl₂ were evaporated under reduced pressure. To the resulting TFA salt dissolved in DMF (4 mL) were successively added DIPEA (0.41 mmol, 72 μL) and 3,5-bis(trifluoromethyl)phenyl isocyanate (36 μL, 0.21 mmol). The reaction mixture was stirred at RT for 16 h and saturated NaHCO₃ solution (20 mL) was added. The aqueous layer was extracted with CH₃Cl/*i*-PrOH 7:3 (3 × 30 mL) and the combined organic layers were washed with water (30 mL) and dried over MgSO₄. After evaporation of the solvent under reduced pressure, purification of the residue by column chromatography (MeOH/CH₂Cl₂ 5:95) provided the titled oligourea **1b** as a white solid (76 mg, 61%).

¹H NMR (400 MHz, CD₃OH) δ (ppm) 9.07 (s, 1H), 8.00 (br. s., 2H), 7.60 (br. s., 1H), 6.53 (dd, *J* = 9.2 and 2.0 Hz, 1H), 6.44 (dd, *J* = 8.9 and 1.4 Hz, 1H), 6.33-7.40 (m, 1H), 6.29 (d, *J* = 10.3 Hz, 1H), 6.17-6.26 (m, 2H), 6.14 (d, *J* = 8.9 Hz, 1H), 6.08-6.10 (m, 1H), 6.04 (dd, *J* = 9.3 and 3.0 Hz, 1H), 5.95 (d, *J* = 10.4 Hz, 1H), 5.90 (d, *J* = 10.0 Hz, 1H), 3.72-4.06 (m, 4H), 3.42-3.72 (m, 5H), 3.24-3.37 (m, 1H), 2.85-3.02 (m, 1H), 2.71 (d, *J* = 4.7 Hz, 3H), 2.67-2.80 (m, 1H), 2.50-2.63 (m, 1H), 2.31-2.50 (m, 2H), 1.56-1.87 (m, 3H), 1.13-1.20 (m, 2H), 1.08 (d, *J* = 7.0 Hz, 3H), 1.01 (d, *J* = 7.8 Hz, 3H), 1.00 (d, *J* = 7.1 Hz, 3H), 0.97 (d, *J* = 7.1 Hz, 3H), 0.94 (d, *J* = 7.0 Hz, 3H), 0.83-0.91 (m, 9H).

¹³C NMR (100 MHz, CD₃OH) δ (ppm) 162.0 (C), 161.8 (C), 161.6 (C), 161.2 (C), 160.8 (C), 158.2 (C), 143.3 (C), 133.1 (q, *J* = 33 Hz, 2 × C), 124.6 (q, *J* = 270 Hz, 2 × C), 118.7-119.2 (m, 2 × CH), 115.2-115.8 (m, CH), 56.6 (CH), 56.0 (CH), 55.8 (CH), 48.1 (CH₂), 47.5 (CH₂), 47.1 (CH), 46.81 (CH), 46.76 (CH₂), 44.4 (CH₂), 44.2 (CH₂), 42.7 (CH₂), 31.8 (CH), 31.7 (CH), 27.0 (CH₃), 27.1 (CH), 23.6 (CH₃), 22.4 (CH₃), 20.1 (CH₃), 20.0 (CH₃), 19.0 (CH₃), 18.5 (CH₃), 18.2 (CH₃), 18.0 (CH₃) ppm.

¹⁹F NMR (376 MHz, CD₃OH) δ (ppm) -64.6.

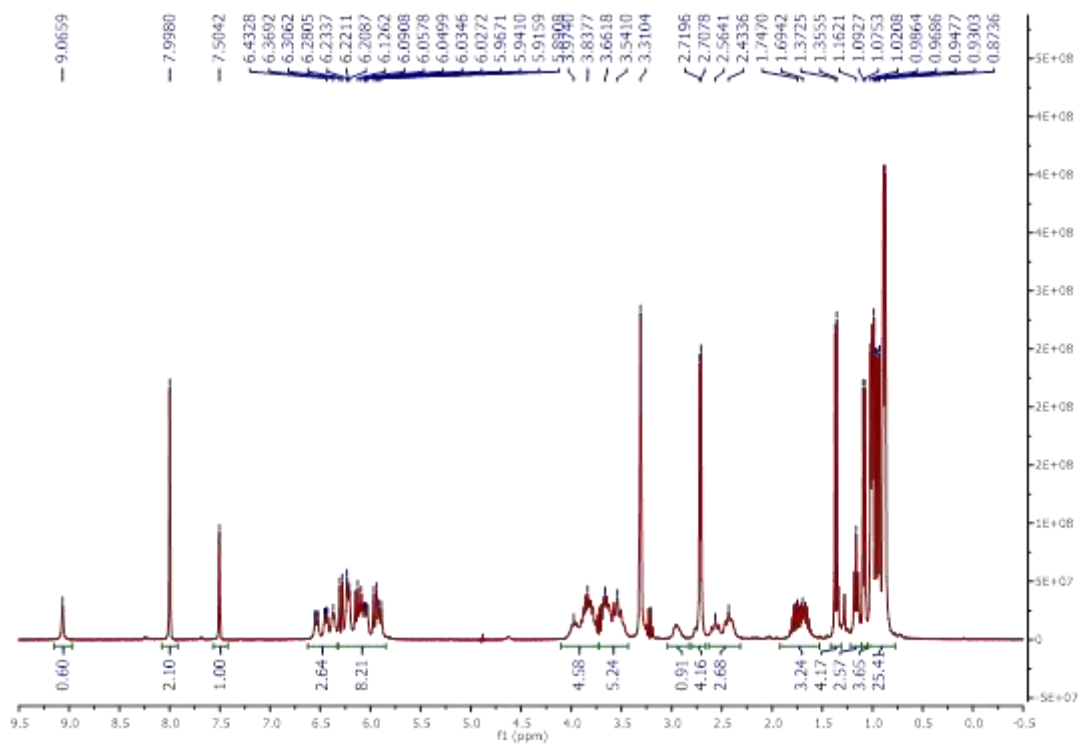
HRMS (ES⁺, MeOH) calcd for C₃₇H₆₂F₆N₁₂O₆ = 885.48922; found 885.49179.

Note: presence of an impurity which is visible on the ¹H NMR spectra (1.36 ppm) and the ¹⁹F NMR spectra (-77 ppm).

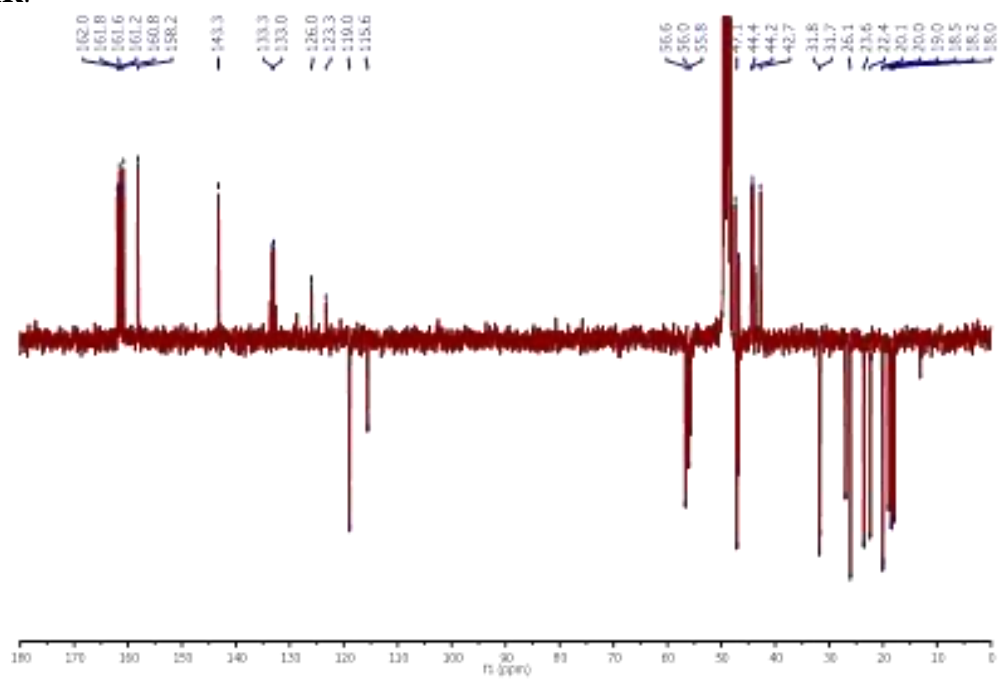
Table S2 : ^1H NMR Chemical Shifts (ppm) of **3,5-(CF₃)₂PhNHCO-Val^u-Ala^u-Leu^u-Val^u-Ala^u-NHMe** (**1b**) in CD₃OH at 293K.

Residue	NH	NH'	αCH^1	αCH^2	βCH	γCH	δCH	ϵCH	Term CH	$\Delta\delta(\alpha\text{CH})$
ArNHCO		9.07							8.00	
									7.60	
Val ^u 1	6.29	6.09	2.73	3.65	3.79	1.77	0.97 + 1.01			0.92
Ala ^u 2	5.90	6.04	2.41	3.50	3.87	1.00				1.09
Leu ^u 3	5.95	6.53	2.43	3.54	3.97	1.16	1.71	0.88 + 0.89		1.11
Val ^u 4	6.22	6.44	2.56	3.58	3.66	1.66	0.88			1.02
Ala ^u 5	6.14	6.36	2.94	3.29	3.83	1.08	0.94			0.35
NHMe	6.22								2.71	

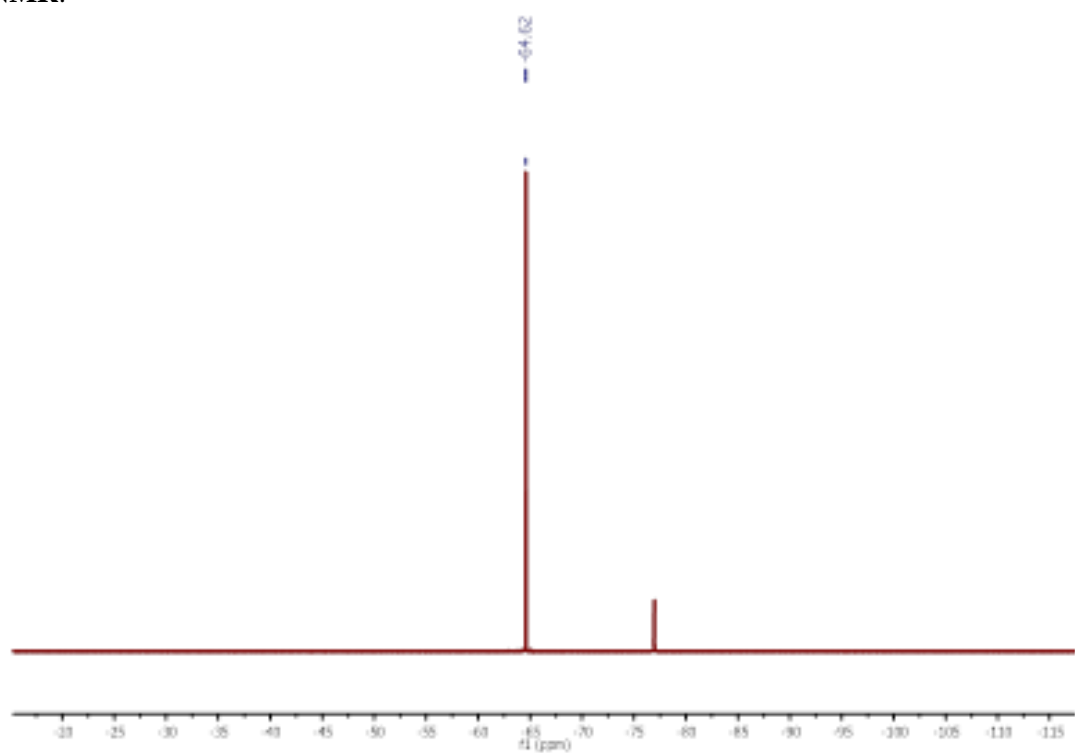
^1H NMR:



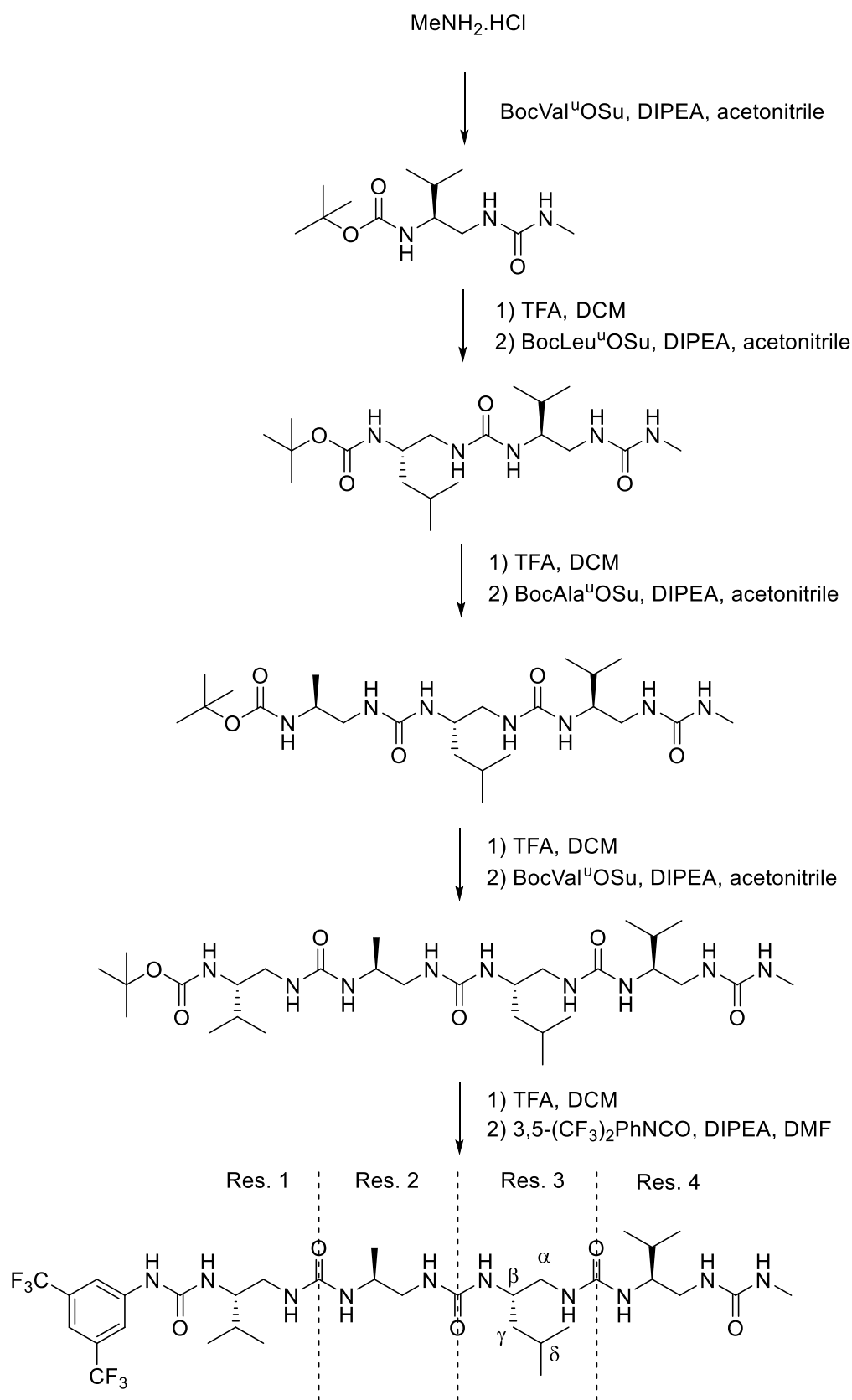
¹³C NMR:



¹⁹F NMR:



7.3.3 Synthesis of $(\text{CF}_3)_2\text{PhNHCO-Val}^u\text{-Ala}^u\text{-Leu}^u\text{-Val}^u\text{-NHMe}$ (**1c**)



Scheme S3: Synthesis of the tetramer 1c

7.3.3.1 Boc-Val^u-NHMe

To a suspension of methylamine hydrochloride (1.18 g, 17.58 mmol) in CH₃CN (30 mL) was added at 0 °C DIPEA (34.94 mmol, 7.09 mL) and a solution of **BocVal^uOSu** (11.65 mmol, 4.00 g) in CH₃CN (30 mL). The reaction mixture was stirred at RT for 16 h and the insoluble were filtered off. The filtrate was evaporated under reduced pressure and EtOAc (300 mL) was added to the residue. The organic layer was washed with 1 M KHSO₄ (2 × 100 mL), saturated NaHCO₃ (2 × 100 mL) and brine (100 mL) and was dried over MgSO₄. After evaporation of the solvent under reduced pressure, recrystallization from a mixture of EtOAc and cyclohexane (1:1) provided the titled compound as a white solid (1.96 g, 49%).

¹H NMR (300 MHz, DMSO-d₆) δ (ppm) 6.50 (d, *J* = 9.0 Hz, 1 H), 5.78 (q, *J* = 4.6 Hz, 1 H), 5.70 (t, *J* = 5.5 Hz, 1 H), 3.09-3.28 (m, 2 H), 2.88 (ddd, *J* = 5.5 and 8.2 and 13.4 Hz, 1 H), 2.52 (d, *J* = 4.7 Hz, 3 H), 1.62 (app.oct, *J* = 7.6 Hz, 1 H), 1.37 (s, 9H), 0.82 (d, *J* = 7.0 Hz, 3 H), 0.79 (d, *J* = 7.9 Hz, 3H).

¹³C NMR (75 MHz, DMSO-d₆) δ (ppm) 158.7 (CO), 155.8 (CO), 77.4 (C), 55.9 (CH), 41.0 (CH₂), 29.8 (CH), 28.3 (3 × CH₃), 27.3 (CH₃), 19.3 (CH₃), 17.9 (CH₃).

HRMS (ES⁺, MeOH) calcd for C₁₂H₂₅N₃O₃ = 260.19687 found 885.49179.

7.3.3.2 Boc-Leu^u-Val^u-NHMe

To a solution of **Boc-Val^u-NHMe** (800 mg, 3.08 mmol) in CH₂Cl₂ (10 mL) was added TFA (10 mL) and the mixture was stirred at RT until completion of the reaction. TFA and CH₂Cl₂ were evaporated under reduced pressure. Last traces of TFA were removed by co-evaporation with toluene (3 × 10 mL). To the resulting TFA salt dissolved CH₃CN (30 mL) were successively added DIPEA (9.24 mmol, 1.59 mL) and a solution of **BocLeu^uOSu** (4.75 mmol, 1.70 g) in CH₃CN (15 mL). The reaction mixture was stirred at RT for 16 h and the solvent was evaporated under reduced pressure. EtOAc (30 mL) was added to the residue and the organic layer was washed with 1 M KHSO₄ (2 × 10 mL) and brine (2 × 10 mL) and was dried over MgSO₄. After evaporation of the solvent under reduced pressure, trituration with a mixture of Et₂O and pentane (30:70) followed by column chromatography (CH₂Cl₂/MeOH 1:99→3:97) provided the titled oligourea as a white solid (1.05 g, 85%).

¹H NMR (400 MHz, DMSO-d₆) δ (ppm) 6.55 (d, *J* = 8.8 Hz, 1H), 5.80-5.87 (m, 1H), 5.78 (q, *J* = 4.4 Hz, 1H), 5.66-5.75 (m, 2H), 3.35-3.52 (m, 2H), 3.04-3.16 (m, 1H), 2.94-3.04 (m, 1H), 2.75-2.94 (m, 2H), 2.52 (d, *J* = 4.6 Hz, 3H), 1.48-1.73 (m, 2H), 1.37 (s, 9H), 1.07-1.27 (m, 2H), 0.77-0.88 (m, 12H).

¹³C NMR (75 MHz, DMSO-d₆) δ (ppm) 158.8 (C), 158.4 (C), 155.5 (C), 77.5 (C), 54.4 (CH), 48.9 (CH), 43.8 (CH₂), 41.9 (CH₂), 41.4 (CH₂), 29.6 (CH), 28.2 (3 × CH₃), 26.3 (CH₃), 24.3 (CH₃), 23.1 (CH₃), 22.0 (CH₃), 19.5 (CH₃), 17.5 (CH₃).

HRMS (ES⁺, MeOH) calcd for C₁₉H₃₉N₅O₄ = 402.30748; found 402.330767, 302.25509.

7.3.3.3 Boc-Ala^u-Leu^u-Val^u-NHMe

To a solution of **Boc-Leu^u-Val^u-NHMe** (950 mg, 2.36 mmol) in CH₂Cl₂ (10 mL) was added TFA (10 mL) and the mixture was stirred at RT until completion of the reaction. TFA and CH₂Cl₂ were evaporated under reduced pressure. Last traces of TFA were removed by co-evaporation with toluene (3 × 10 mL). To the resulting TFA salt dissolved in CH₃CN (30 mL) were successively added DIPEA (1.23 mL, 7.08 mmol) and a solution of **BocAla^uOSu** (1.15 g, 3.65 mmol) in CH₃CN (15 mL). The reaction mixture was stirred at RT for 16 h and the solvent was evaporated under reduced pressure. CH₂Cl₂ (30 mL) was added to the residue. The organic layer was washed with 1N KHSO₄ (2 × 15 mL) and water (2 × 15 mL) and was dried over MgSO₄. After evaporation of the solvent under reduced pressure, trituration with Et₂O followed by column chromatography (CH₂Cl₂/MeOH from 2:98 to 6:94) provided the titled oligourea as a white solid (1.07 g, 90%).

¹H NMR (400 MHz, DMSO-d₆) δ (ppm) 6.74 (d, *J* = 8.1 Hz, 1H), 5.91-5.99 (m, 1H), 5.88 (q, *J* = 4.6 Hz, 1H), 5.77-5.82 (m, 1H), 5.77 (d, *J* = 9.2 Hz, 1H), 5.73 (d, *J* = 9.4 Hz, 1H), 5.65-5.72 (m, 1H), 3.58-3.74 (m, 1H), 3.36-3.55 (m, 2H), 3.19-3.29 (m, 1H), 3.08-3.18 (m, 1H), 2.94-3.04 (m, 1H), 2.78-2.88 (m, 1H), 2.64-2.74 (m, 1H), 2.55-2.64 (m, 1H), 2.53 (d, *J* = 4.6 Hz, 3H), 1.52-1.68 (m, 2H), 1.38 (s, 9H), 1.14 (t, *J* = 7.0 Hz, 2H), 0.94 (d, *J* = 7.6 Hz, 3H), 0.86 (d, *J* = 7.6 Hz, 3H), 0.82 (d, *J* = 7.5 Hz, 3H), 0.81 (d, *J* = 7.8 Hz, 3H), 0.78 (d, *J* = 7.8 Hz, 3H).

¹³C NMR (75 MHz, DMSO-d₆) δ (ppm) 158.8 (C), 158.6 (C), 158.5 (C), 155.5 (C), 77.7 (C), 54.2 (CH), 47.6 (CH), 46.6 (CH), 45.0 (CH₂), 44.8 (CH₂), 41.9 (2 × CH₂), 30.0 (CH), 28.2 (3 × CH₃), 26.3 (CH₃), 24.3 (CH), 23.2 (CH₃), 21.9 (CH₃), 19.5 (CH₃), 18.2 (CH₃), 17.6 (CH₃).

HRMS (ES⁺, MeOH) calcd for C₂₃H₄₇N₇O₅ = 502.37114; found 402.31892, 502.37145.

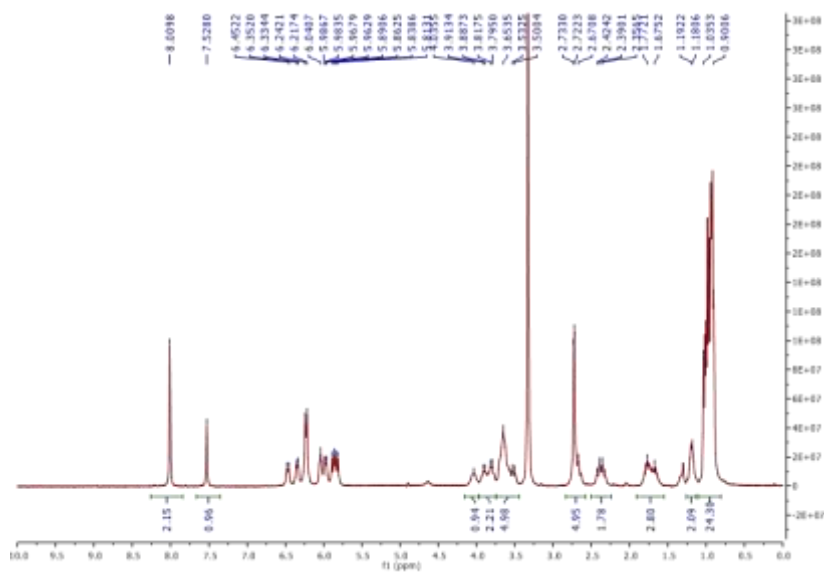
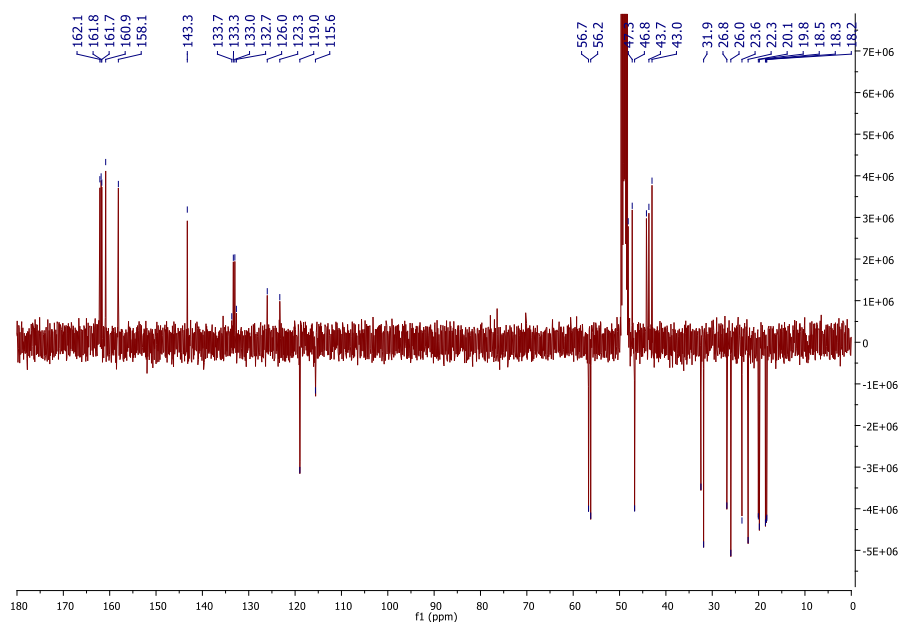
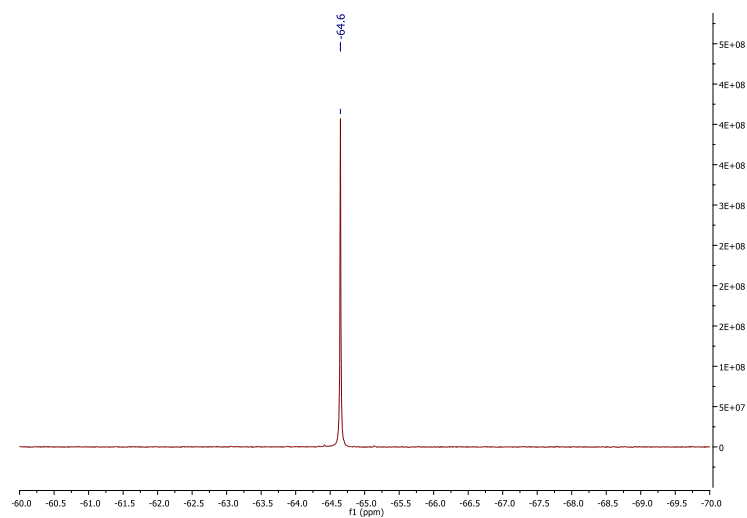
7.3.3.4 Boc-Val^u-Ala^u-Leu^u-Val^u-NHMe

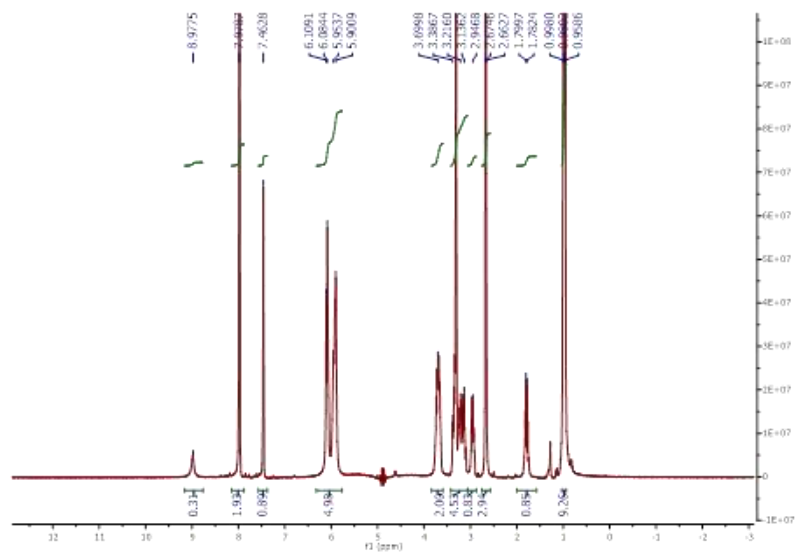
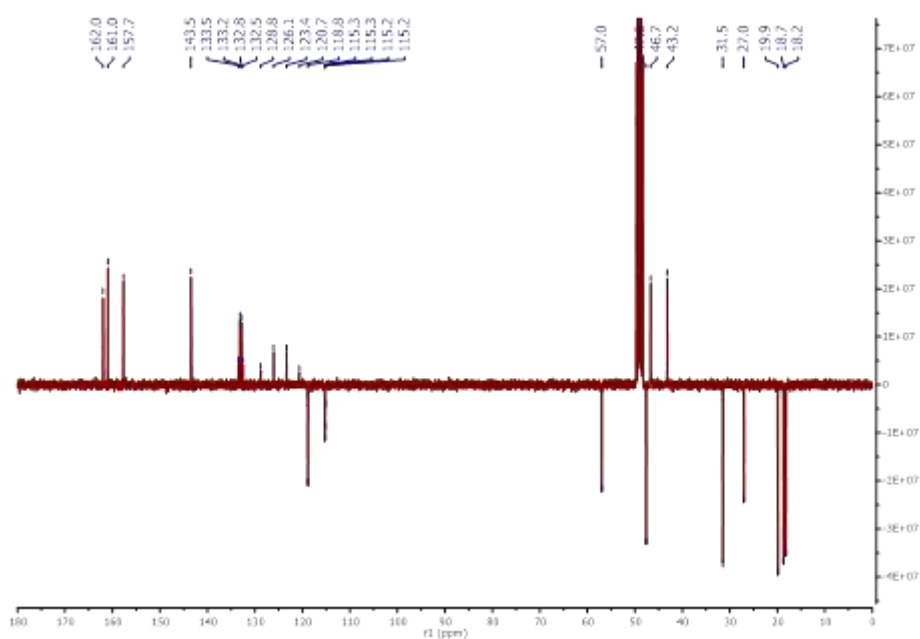
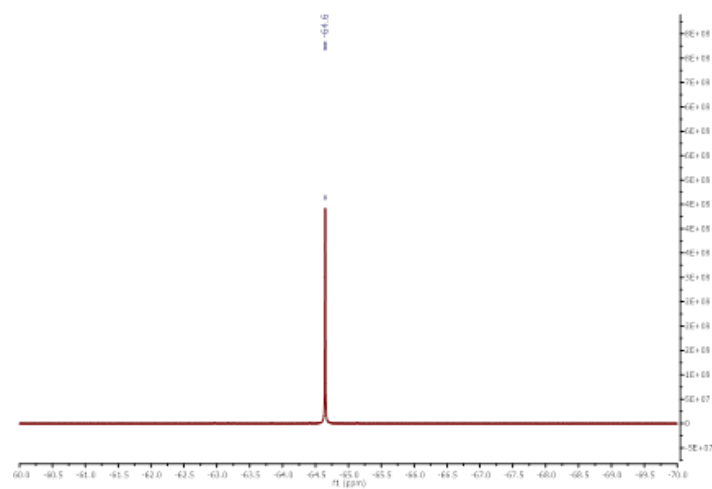
To a solution of **Boc-Ala^u-Leu^u-Val^u-NHMe** (940 mg, 1.87 mmol) in CH₂Cl₂ (10 mL) was added TFA (10 mL) and the mixture was stirred at RT until completion of the reaction. TFA and CH₂Cl₂ were evaporated under reduced pressure. Last traces of TFA were removed by co-evaporation with toluene (3 × 10 mL). To the resulting TFA salt dissolved in CH₃CN (30 mL) were successively added DIPEA (1.00 mL, 5.74 mmol) and a solution of **BocVal^uOSu** (933 mg, 2.72 mmol) in CH₃CN (15 mL). The reaction mixture was stirred at RT for 16 h and the solvent was evaporated under reduced pressure. CH₂Cl₂ (50 mL) was added to the residue. The organic layer was washed with 1 M KHSO₄ (2 × 30 mL) and water (2 × 30 mL) and was dried over MgSO₄. After evaporation of the solvent under reduced pressure, trituration with a mixture of Et₂O and EtOAc (30:70) followed by crystallization from a mixture of methanol and Et₂O (10:90) provided the titled oligourea as a white solid (580 mg, 49%).

¹H NMR (400 MHz, DMSO-d₆) δ (ppm) 6.72 (d, *J* = 9.1 Hz, 1H), 6.82-5.99 (m, 6H), 5.78 (d, *J* = 9.6 Hz, 1H), 5.74 (dd, *J* = 5.8 and 3.8 Hz, 1H), 3.61-3.80 (m, 2H), 3.13-3.47 (m, 6H), 2.65-2.77 (m, 1H), 2.54 (d, *J* = 4.6 Hz, 3H), 2.41-2.60 (m, 2H), 2.28-2.41 (m, 1H), 1.49-1.69 (m, 3H), 1.40 (s, 9H), 1.03-1.18 (m, 2H), 0.91 (d, *J* = 7.7 Hz, 3H), 0.79-0.88 (m, 15H), 0.78 (d, *J* = 7.7 Hz, 3H).

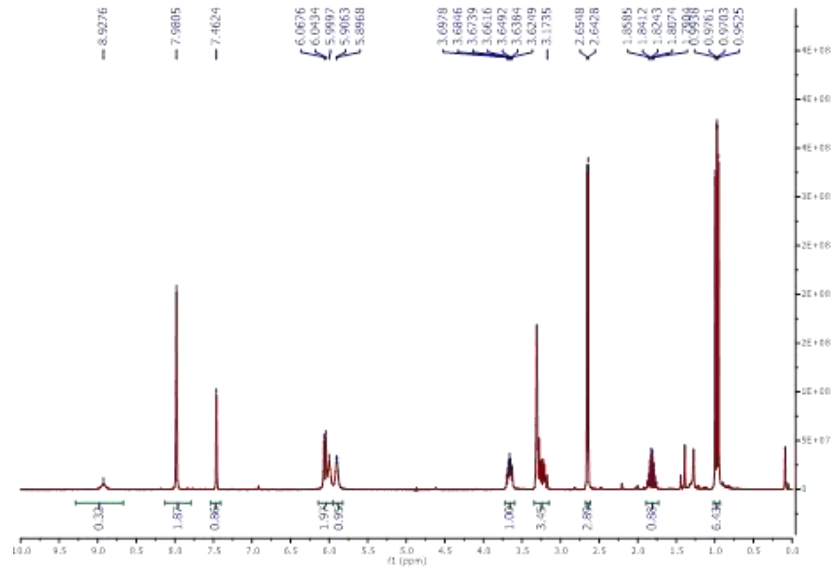
¹³C NMR (100 MHz, DMSO-d₆) δ (ppm) 159.0 (C), 158.8 (C), 158.7 (C), 158.6 (C), 156.6 (C), 77.9 (C), 56.0 (CH), 54.1 (CH), 47.3 (CH), 47.3 (CH₂), 45.31 (CH₂), 45.25 (CH), 41.9 (CH₂), 41.7 (CH₂), 41.4 (CH₂), 30.3 (CH), 30.1 (CH), 28.2 (3 × CH₃), 27.3 (CH₃), 24.5 (CH), 23.1 (CH₃), 22.0 (CH₃), 19.5 (CH₃), 19.3 (CH₃), 18.4 (CH₃), 18.3 (CH₃), 17.8 (CH₃).

HRMS (ES⁺, MeOH) calcd for C₂₉H₅₉N₉O₆ = 630.46611; found 630.46682, 302.25509.

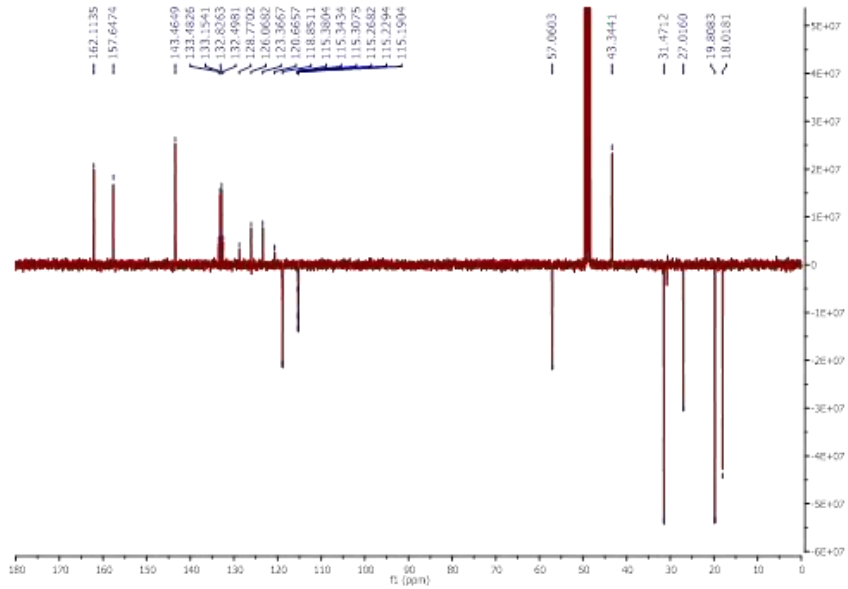
¹H NMR:**¹³C NMR:****¹⁹F NMR:**

^1H NMR: **^{13}C NMR:** **^{19}F NMR:**

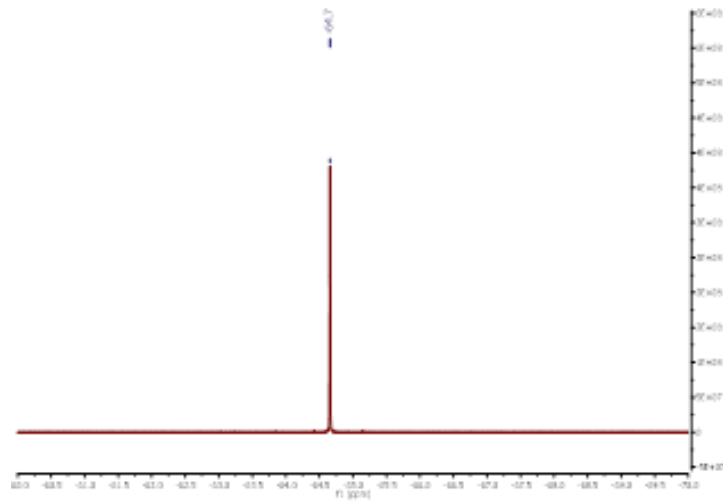
¹H NMR:

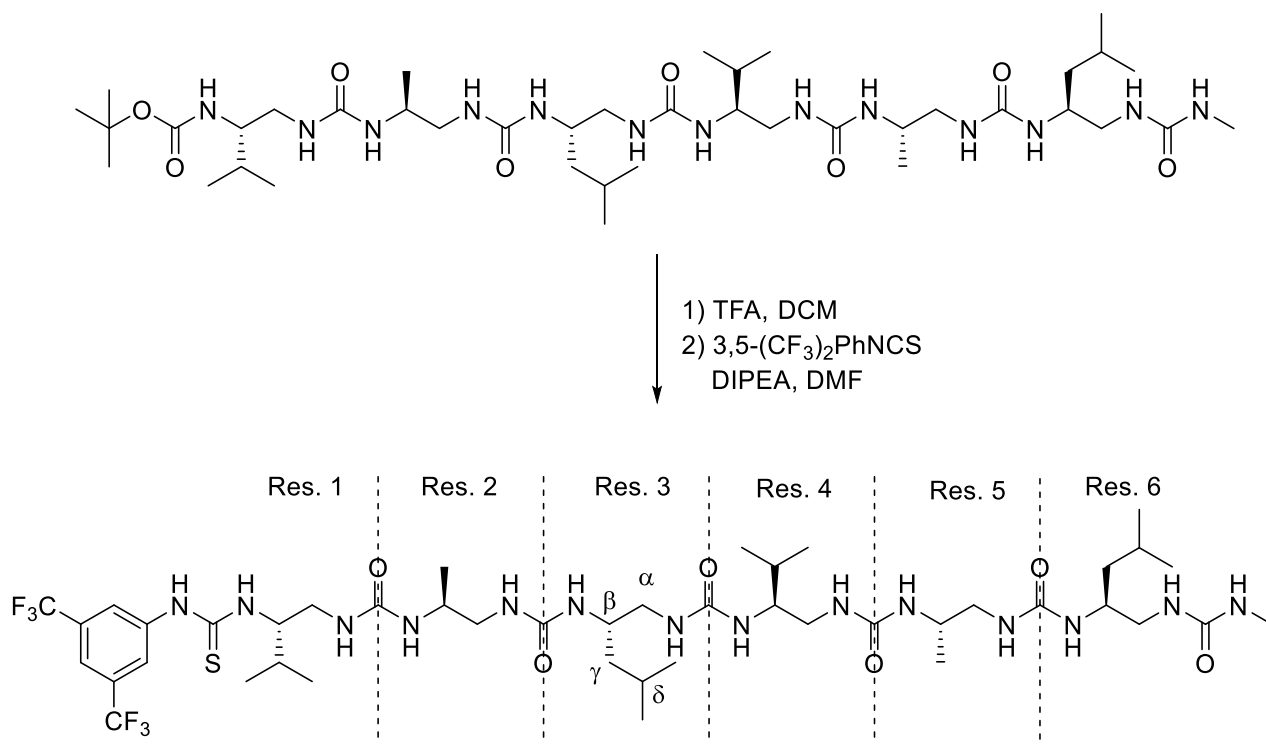


¹³C NMR :



¹⁹F NMR:



7.3.6 Synthesis of (CF₃)₂PhNHCS-Val^u-Ala^u-Leu^u-Val^u-Ala^u-Leu^u-NH^u-Me (**5a**)Scheme S6: Synthesis of the hexamer **5a**

To a solution of **Boc-Val^u-Ala^u-Leu^u-Val^u-Ala^u-Leu^u-NH^u-Me** (300 mg, 0.34 mmol) in CH₂Cl₂ (2 mL), TFA (1 mL) was added and reaction mixture was stirred at RT for 4 h. After completion of the reaction, TFA and CH₂Cl₂ were evaporated under reduced pressure. To the resulting TFA salt dissolved in DMF (1.5 mL) were successively added DIPEA (0.18 mL, 1.03 mmol) and 3,5-bis(trifluoromethyl)phenyl isothiocyanate (140 μ L, 0.76 mmol). The resulting solution was stirred at room temperature. After 36 hours, the mixture in DMF was cooled to 0°C and cold water (10 mL followed by 5 mL) was added with rapid stirring. The white powder obtained was filtered, washed with water (3 x 10 mL) and dried under vacuum. The crude residue was purified by chromatography on silica gel (DCM:MeOH 93:7 to 90:10) leading to the titled thiourea **5a** as a white solid (230 mg, 64%).

¹H NMR (400 MHz, CD₃OH): δ (ppm) 8.08 (s, 2H), 7.69 (s, 1H), 6.30-6.35 (m, 3H), 6.17-6.23 (m, 2H), 6.09-6.23 (m, 1H), 5.97 (m, 2H), 5.85-5.88 (m, 2H), 5.80-5.88 (m, 2H), 5.46 (m, 1H), 3.91-4.00 (m, 1H), 3.78-3.85 (m, 3H), 2.96 (m, 1H), 2.61 (d, J = 4.8 Hz, 3H), 2.53 -2.59 (m, 1H), 2.24-2.47 (m, 4H), 1.83 (sext, J = 7.8 Hz, 1H), 1.60 (sext, J = 7.0 Hz, 2H), 1.47 (sext, J = 7.4 Hz, 1H), 1.06-1.23 (m, 2H), 0.92-0.95 (4xd, J = 7.8 Hz, 4x3H), 0.83 (3xd, J = 7.4 Hz, 3x3H), 0.80 (d, J = 7.3 Hz, 2x3H), 0.77 (d, J = 7.8 Hz, 2x3H).

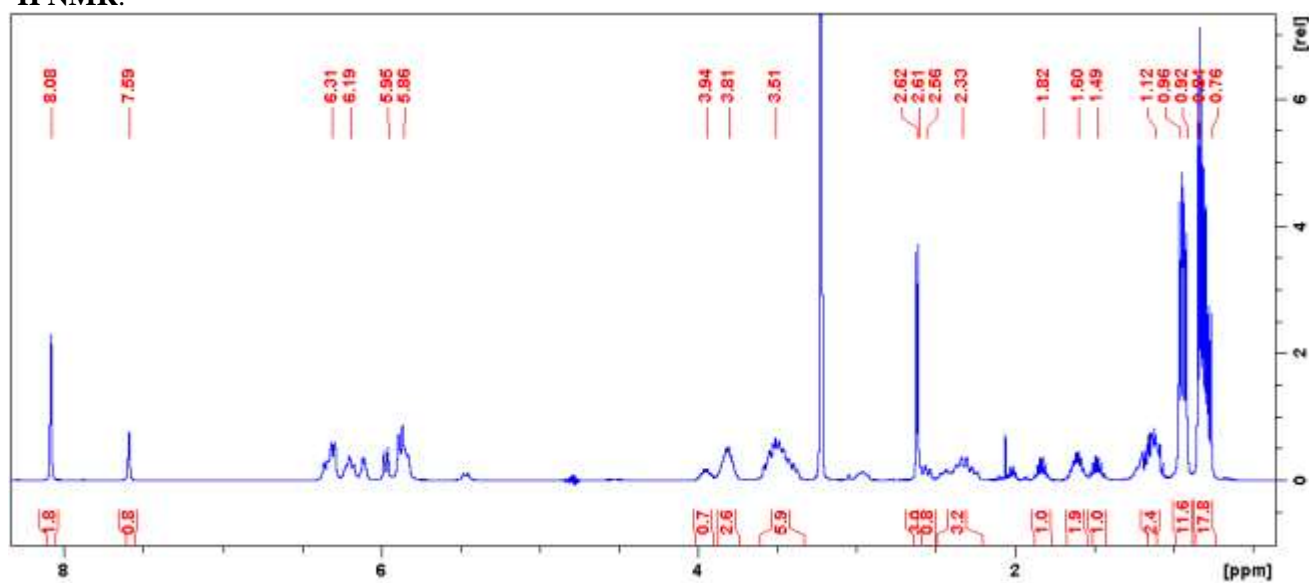
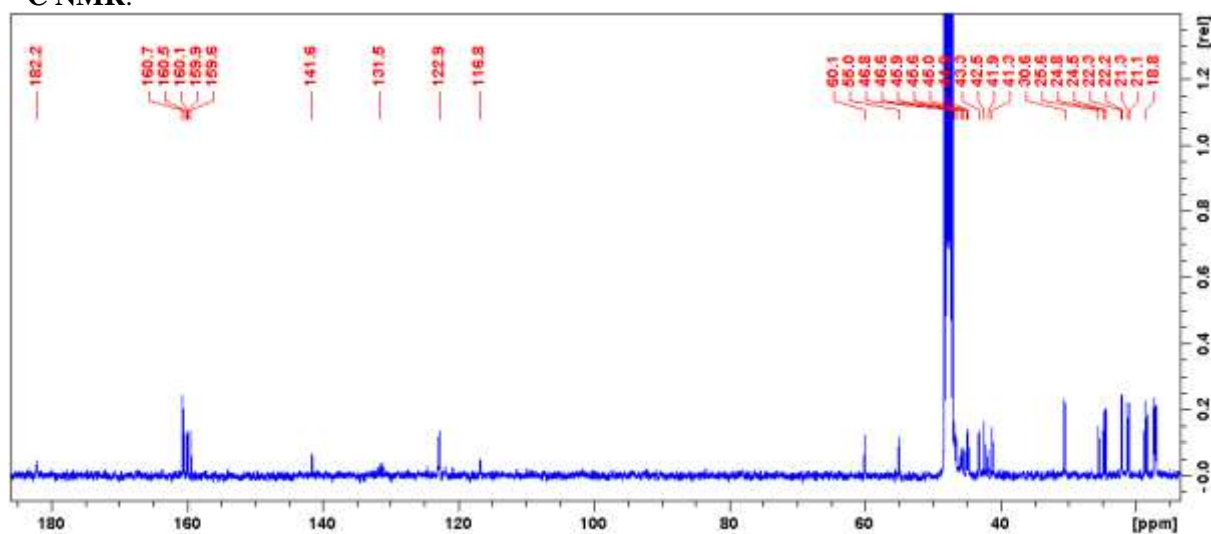
¹³C NMR (100 MHz, CD₃OH): δ (ppm) 182.2 (C), 160.7(C), 160.5 (C), 160.1 (C), 159.9 (C), 159.6 (C), 141.6 (q, J = 27 Hz, C), 131.5 (C), 122.9 (CH), 116.8 (CH), 60.1 (CH), 55.0 (CH), 46.8 (CH₂), 46.6 (CH₂), 45.9 (CH), 45.0 (CH₂), 44.9 (CH), 43.3 (CH₂), 42.5 (CH₂), 41.9 (CH₂), 41.3 (CH₂), 30.6 (CH₃), 25.6 (CH₃), 24.8 (CH₃), 24.5 (CH₃), 22.3 (CH₃), 22.2 (CH₃), 21.3 (CH₃), 21.1 (CH₃), 18.8 (CH₃), 18.5 (CH₃), 17.5 (CH₃).

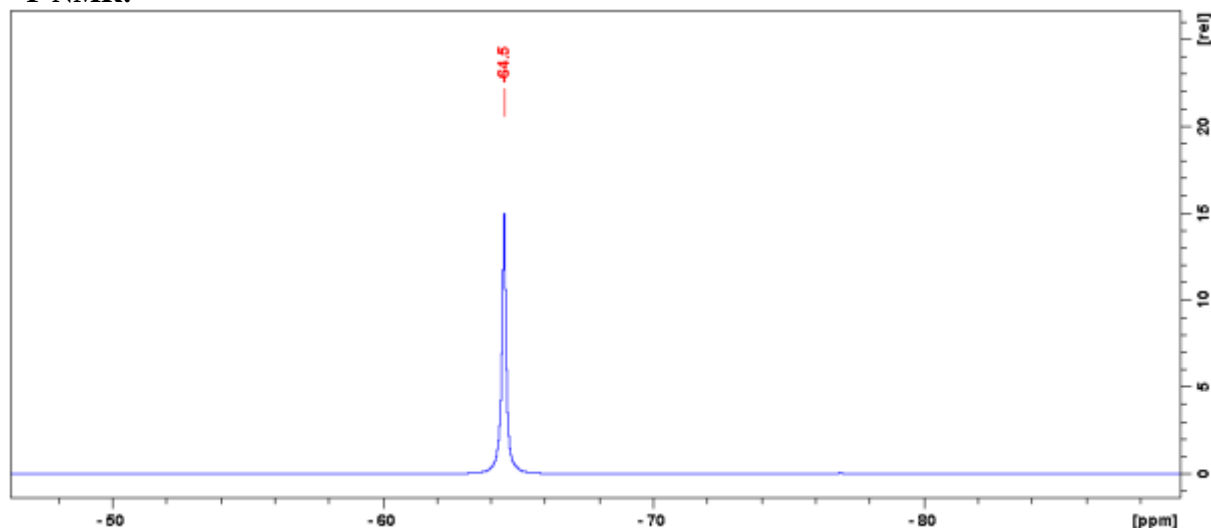
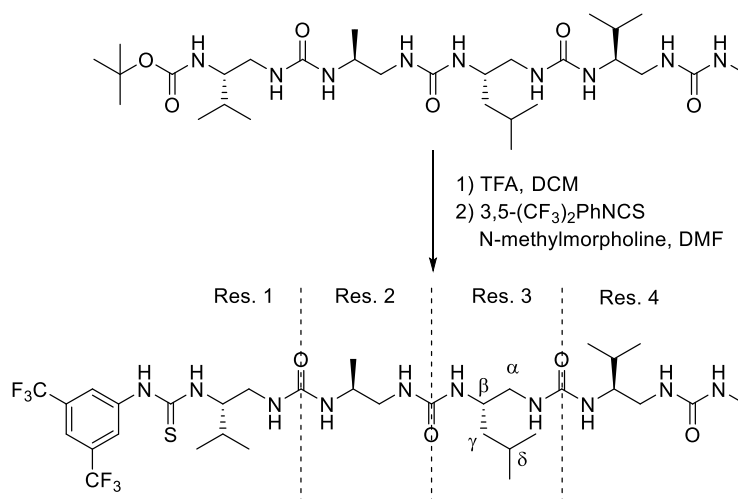
¹⁹F NMR (376 MHz, CD₃OH): δ (ppm) -64.5.

HRMS (ES⁺, MeOH) calcd for C₄₄H₇₆F₆N₁₄O₆S = 1043.57699; found 1043.57582.

Table S6 : ^1H NMR Chemical Shifts (ppm) of 3,5-(CF_3) $_2\text{PhNHCS-Val}^u\text{-Ala}^u\text{-Leu}^u\text{-Val}^u\text{-Ala}^u\text{-Leu}^u\text{-NHMe}$ (**5a**) in CD_3OH at 293K.

Residue		NH	NH'	$^{\alpha}\text{CH}^1$	$^{\alpha}\text{CH}^2$	$^{\beta}\text{CH}$	$^{\gamma}\text{CH}$	$^{\delta}\text{CH}$	$^{\epsilon}\text{CH}$	Term CH	$\Delta\delta(^{\alpha}\text{CH})$
	ArNHCS		ND							--	
Val ^u	1	5.89	5.75	3.52	2.97	4.49	1.83	0.77			0.55
Ala ^u	2	5.98	5.84	3.40	2.43	3.84	0.95				0.97
Leu ^u	3	5.46	6.21	3.54	2.34	3.84	1.10	1.60	0.92		1.20
Val ^u	4	6.17	6.33	3.54	2.32	3.47	1.48	0.80			1.22
Ala ^u	5	5.88	6.31	3.46	2.27	3.94	0.92				1.19
Leu ^u	6	5.96	6.29	3.49	2.58	3.80	1.13	1.61	0.83		0.91
	NHMe	7.10								2.62	

 ^1H NMR: ^{13}C NMR:

¹⁹F NMR:**7.3.7 Synthesis of (CF₃)₂PhNHCS-Val^u-Ala^u-Leu^u-Val^u-NHMe (5c)***Scheme S7: Synthesis of the tetramer 5c*

To a solution of **Boc-Val^u-Ala^u-Leu^u-Val^u-NHMe** (150 mg, 0.24 mmol) in DCM (2 mL) was added TFA (1 mL) at room temperature and reaction mixture was stirred for 4h. After completion of the reaction, TFA and CH₂Cl₂ were evaporated under reduced pressure. To the resulting TFA salt dissolved in DMF (2 mL) were successively added 4-methylmorpholine (78 μ L, 0.71 mmol) and 3,5-bis(trifluoromethyl)phenyl isothiocyanate (176 μ L, 0.96 mmol). The resulting solution was stirred at room temperature. After 24 hours, the crude material in DMF was cooled to 0°C and cold water (15 mL and 10 mL) was added. The crude residue was then extracted with CH₂Cl₂/MeOH (60 mL/40 mL). The organic layer was washed with 0.5 M aqueous KHSO₄ (60 mL) followed by water (2 x 60 mL), dried over Na₂SO₄, filtered and concentrated under vacuum to yield a crude residue which crystallised from CH₂Cl₂/MeOH upon standing overnight. The crystals were rinsed with CH₂Cl₂, isolated and purified by column chromatography on silica gel (7% to 8% MeOH in CH₂Cl₂) to yield the titled thiourea catalyst **2c** as a colourless powder (62 mg, 33%).

¹H NMR (400 MHz, CD₃OH): δ (ppm) 8.21 (s, 2H), 7.67 (s, 1H), 6.17-7.26 (m, 3H), 5.99 (m, 1H), 5.93 (m, 2H), 5.91 (m, 1H), 5.63 (m, 1H), 4.63 (s, 1H), 3.91 (m, 2H), 3.59 (m, 3H), 3.42 (m, 1H), 3.15 (m, 1H), 2.72 (m, 1H), 2.71 (d, $J = 4.4$ Hz, 3H), 2.58 (m, 1H), 1.93 (sext, $J = 7.4$ Hz, 1H), 1.68 (m, 2H),

1.22 (m, 2H), 1.05 (d, $J = 7.3$ Hz, 3H), 1.05 (d, $J = 7.3$ Hz, 3H), 1.03 (d, $J = 7.3$ Hz, 3H), 1.02 (d, $J = 5.6$ Hz, 3H), 0.95 (d, $J = 7.3$ Hz, 3H), 0.93 (d, $J = 7.6$ Hz, 3H), 0.91 (d, $J = 7.3$ Hz, 2x3H).

^{13}C NMR (100 MHz, CD_3OH): δ (ppm) 182.1 (C), 160.8 (C), 160.4 (C), 159.9 (C), 159.6 (C), 141.8 (C), 122.7, 116.7, 60.0 (CH), 55.1 (CH), 46.2 (CH_2), 45.7 (CH), 45.4 (CH_2), 42.3 (CH_2), 41.5 (CH_2), 30.9 (CH_3), 30.5 (CH_3), 25.6 (CH_3), 24.7 (CH_3), 22.3 (CH_3), 21.0 (CH_3), 18.6 (CH_3), 18.4 (CH_3), 17.5 (CH_3), 17.4 (CH_3), 17.1 (CH_3).

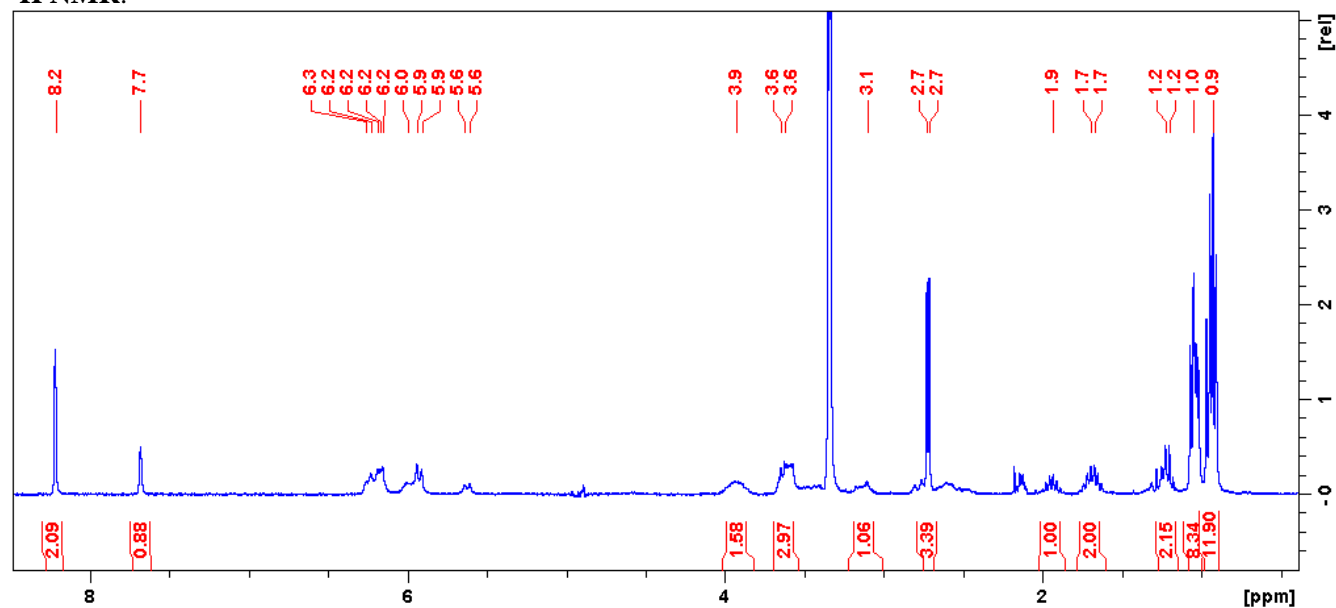
^{19}F NMR (282 MHz, CD_3OH): δ (ppm) -64.5

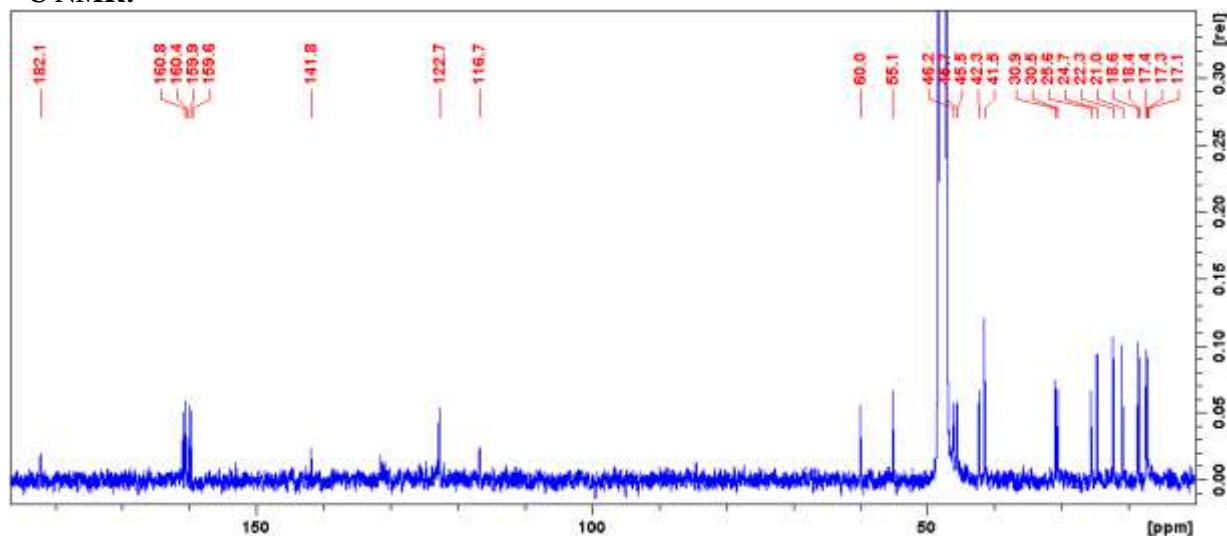
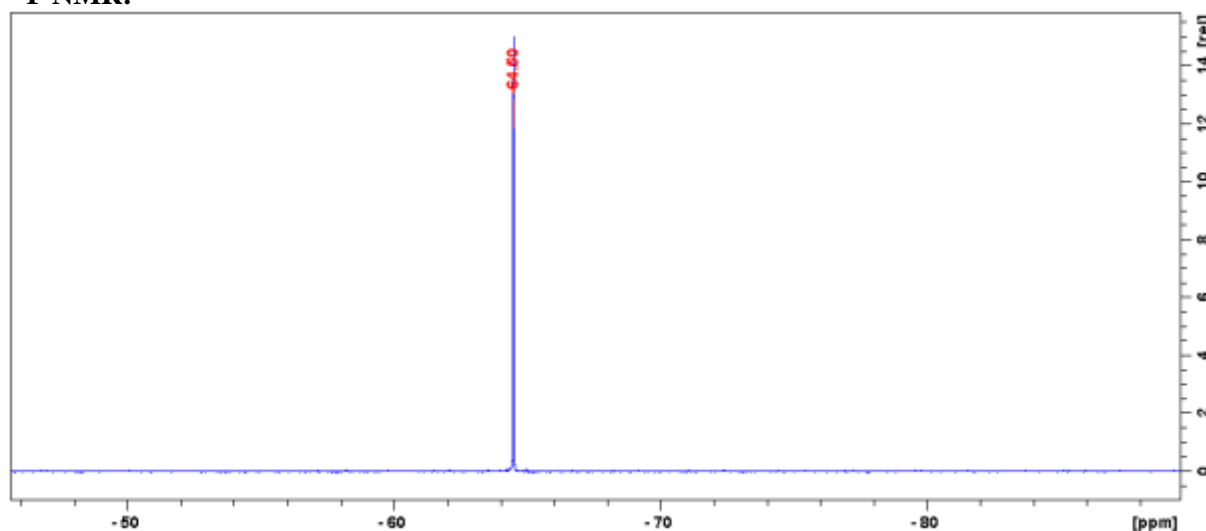
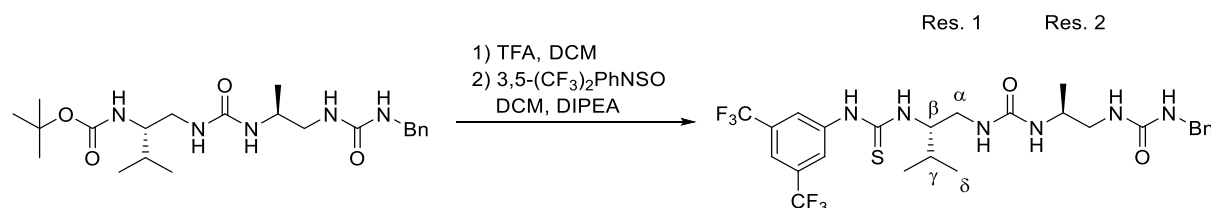
HRMS (ES^+ , MeOH) calcd for $\text{C}_{33}\text{H}_{54}\text{F}_6\text{N}_{10}\text{O}_5 = 801.40272$; found 801.40261.

Table S7 : ^1H NMR Chemical Shifts (ppm) of 3,5-(CF_3) $_2\text{PhNHCO-Val}^u\text{-Ala}^u\text{-Leu}^u\text{-Val}^u\text{-NHMe}$ (5c) in CD_3OH at 293K.

Residue	NH	NH'	αCH^1	αCH^2	βCH	γCH	δCH	ϵCH	Term CH	$\Delta\delta(\alpha\text{CH})$
ArNHCO		ND							-- 7.67	
Val ^u	1	5.94	6.00	3.61	3.16	4.56	1.94	0.93+0.95		0.83
Ala ^u	2	5.92	5.91	3.45	2.54	3.88	1.02			0.91
Leu ^u	3	5.64	6.20	3.57	2.55	3.95	1.20	1.68	0.91	1.02
Val ^u	4	6.23	6.26	3.58	2.75	3.62	1.68	1.03+1.05		0.99
NHMe		6.15							2.71	

^1H NMR:



¹³C NMR:**¹⁹F NMR:****7.3.8 Synthesis of (CF₃)₂PhNHCS-Valⁿ-Alaⁿ-NHBn (5d)***Scheme S8: Synthesis of the dimer 5d*

A solution of the corresponding Boc-protected urea (307 mg, 0.71 mmol) in CH₂Cl₂ (2 mL) was treated with TFA (1 mL) at room temperature until the starting material disappeared by TLC (4 hours). After completion, the reaction mixture was concentrated under vacuum. The resulting TFA salt was solubilised in DMF (1.5 mL) and the solution was made alkaline by the addition of diisopropylethylamine (300 μL, 1.73 mmol). Then, 3,5-bis(trifluoromethyl)phenyl isothiocyanate (193 μL, 1.07 mmol) was added and the resulting solution was stirred at room temperature. The reaction progress was monitored by TLC. After one night, water (10 mL) was added, then dichloromethane (40 mL) was added to solubilize the organic crude. Aqueous layer was extracted with DCM, organic layer was washed with water, then 1N HCl, then NaHCO₃, dried over Na₂SO₄ then concentrated under vacuum. Silica gel chromatography (DCM:MeOH from 99:1 to 90:10) provided the titled thiourea **5d** as a white solid (260 mg, 60%).

¹H NMR (400 MHz, CD₃OH) δ (ppm) 9.68 (s, 1H), 8.10 (s, 2H), 7.60 (d, $J = 9.1$ Hz, 1H), 7.61 (s, 1H), 7.08-7.18 (m, 5H), 6.44 (m, 1H), 6.18 (m, 1H), 5.93 (m, 1H), 4.20 (d, $J = 7.0$ Hz, 2H), 3.62 (sext, $J = 7.4$ Hz, 1H), 3.34 (m, 1H), 3.23 (m, 1H), 3.17 (m, 1H), 3.05 (m, 1H), 1.80 (sext, $J = 7.4$ Hz, 1H), 0.95 (d, $J = 7.8$ Hz, 3H), 0.92 (d, $J = 7.8$ Hz, 3H), 0.91 (d, $J = 7.8$ Hz, 3H).

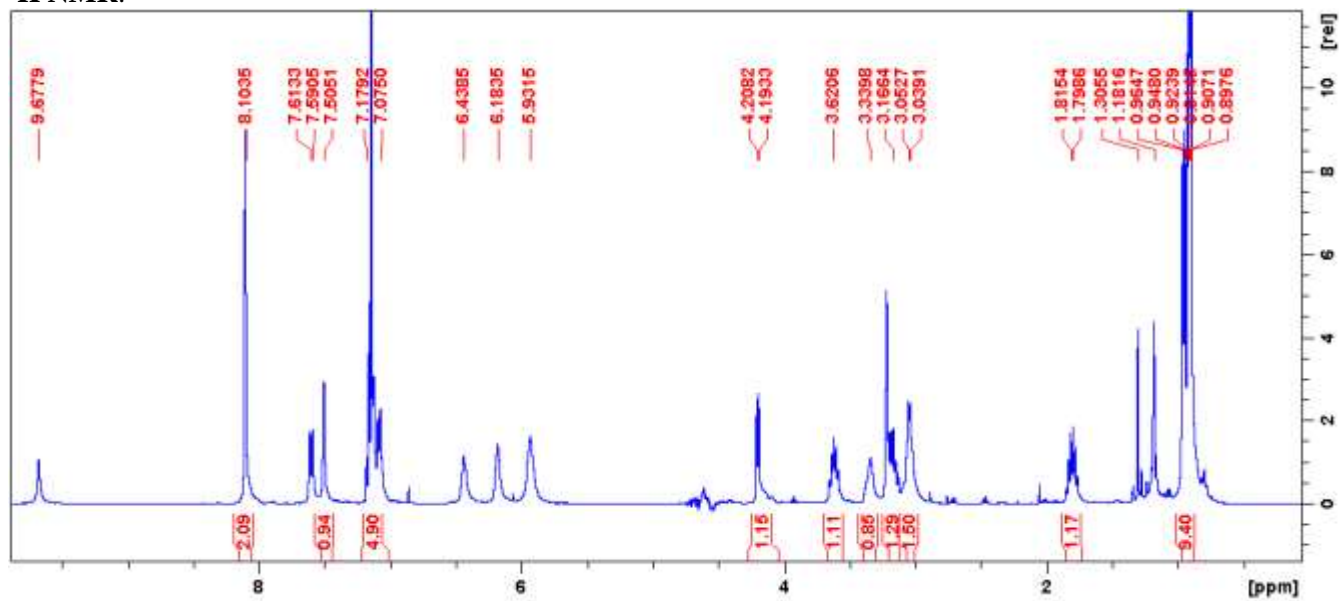
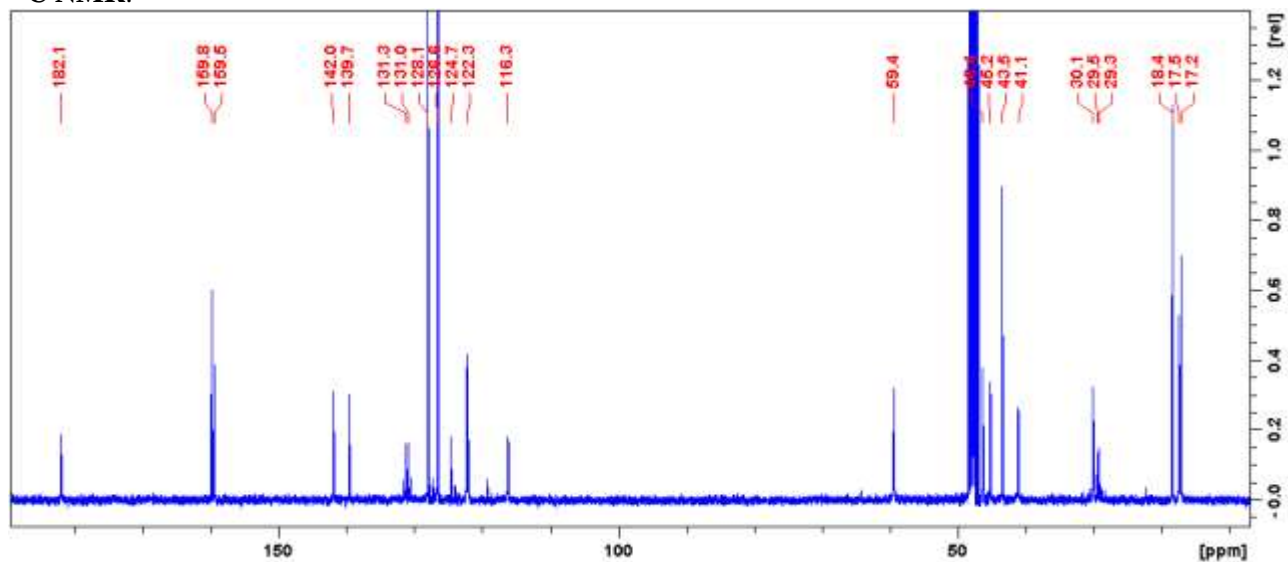
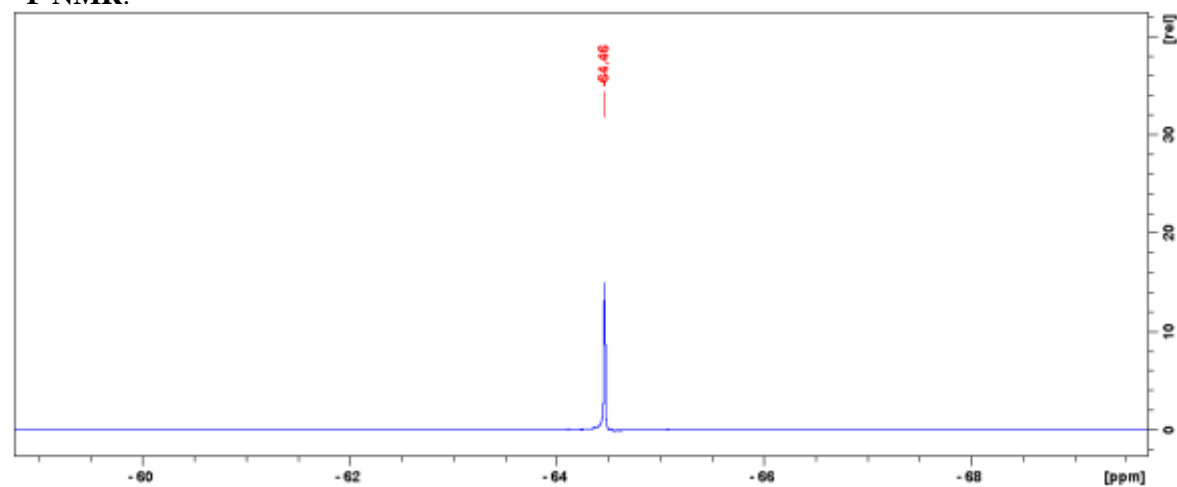
¹³C NMR (100 MHz, CD₃OH) δ (ppm) 182.1 (C), 159.8 (C), 159.5 (C), 142.0 (C), 139.7 (C), 131.2 (q, $J = 30$ Hz, C), 128.1 (CH), 126.6 (CH), 124.7 (CH), 122.3 (CH), 116.3 (CH), 59.4 (CH), 46.4 (CH), 45.2 (CH₂), 43.5 (CH₂), 41.1 (CH₂), 30.1 (CH₃), 29.5 (CH₃), 29.3 (CH₃), 18.4 (CH₃), 17.6 (CH₃), 17.3 (CH₃).

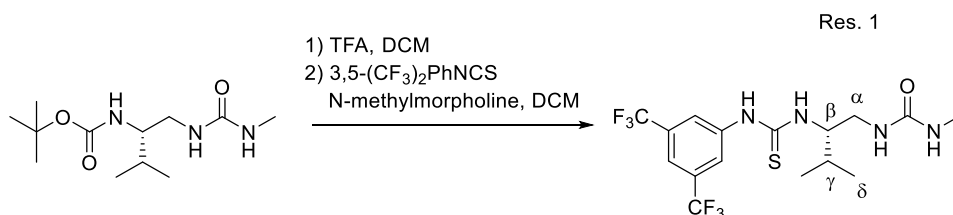
¹⁹F NMR (376 MHz, CD₃OH) δ (ppm) -64.5

HRMS (ES⁺, MeOH) calcd for C₂₆H₃₃F₆N₆O₂S = 607.63640 ; found 607.32971.

Table S8: ¹H NMR Chemical Shifts (ppm) of 3,5-(CF₃)₂PhNHCO-Val^u-Ala^u-NHBn (5d) in CD₃OH at 293K

Residue		NH	NH'	α CH ¹	α CH ²	β CH	γ CH	δ CH	ϵ CH	Term CH ₂ Ph	$\Delta\delta(\alpha$ CH)
	ArNHCO		9.69								
Val ^u	1	7.60	5.94	3.17	3.34	4.43	1.81	0.91			0.17
Ala ^u	2	5.98	6.18	3.23	3.04	3.62	0.95				0.19
	NHCH ₂ Ph	6.44								4.20 + 7.10	

¹H NMR:**¹³C NMR:****¹⁹F NMR:**

7.3.9 Synthesis of (CF₃)₂PhNHCS-Val^u-NHMe (**5e**)Scheme S9: Synthesis of the monomer **5e**

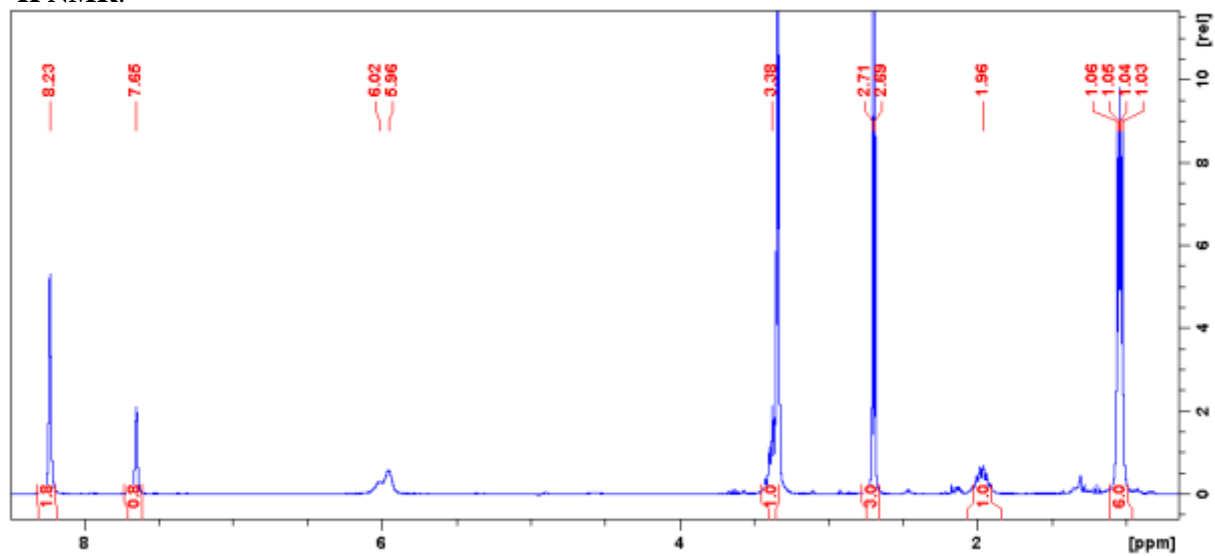
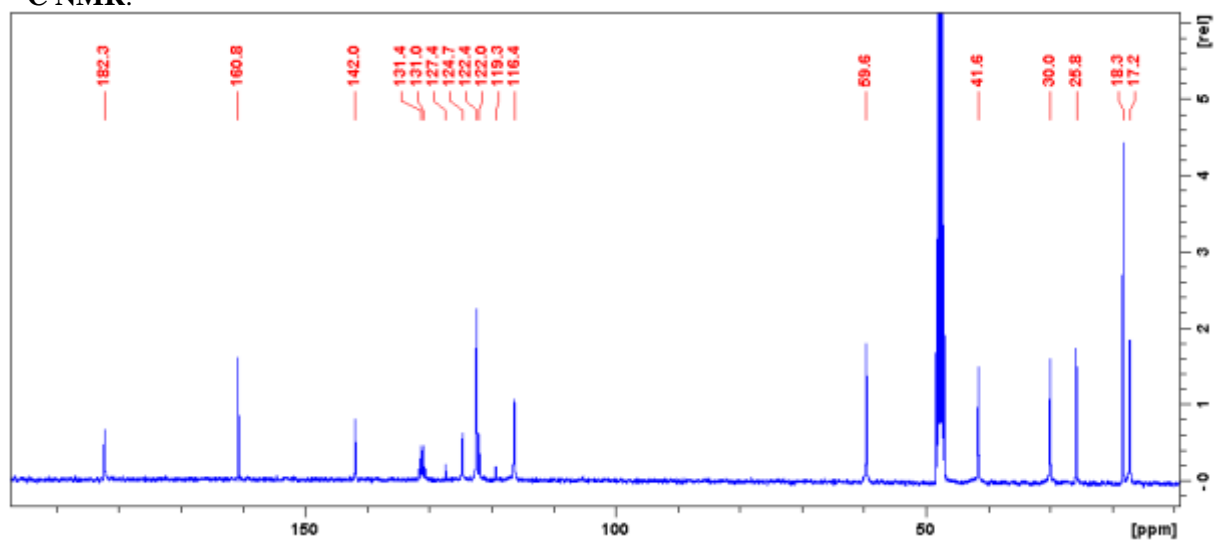
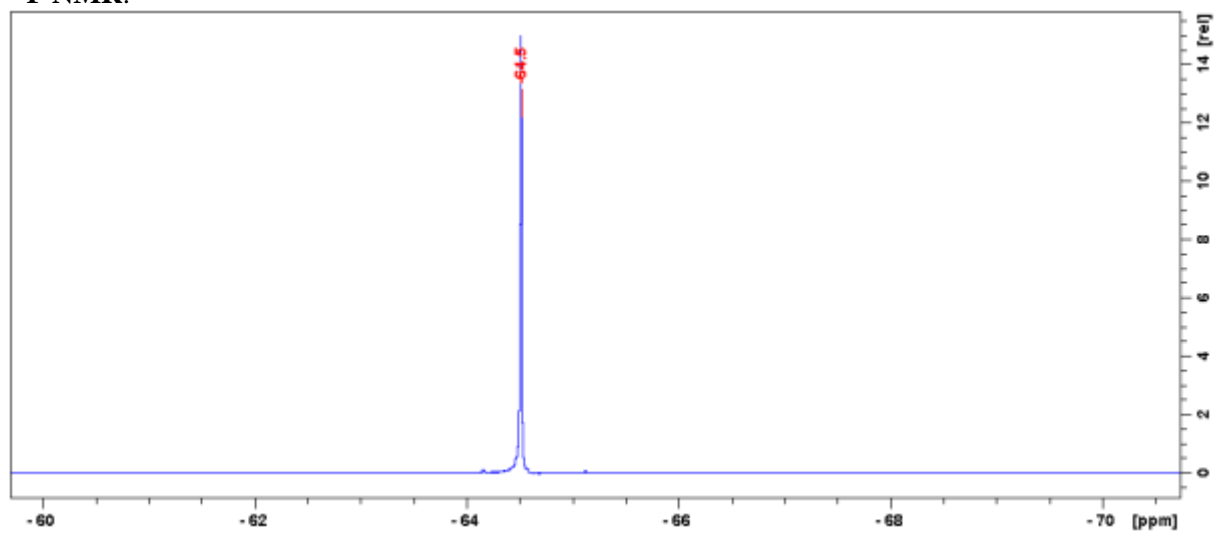
A solution of the corresponding Boc-protected urea (450 mg, 1.74 mmol) in CH₂Cl₂ (2 mL) was treated with TFA (1.5 mL) at room temperature until the starting material disappeared by TLC (4 hours). After completion, the reaction mixture was concentrated under vacuum. The resulting TFA salt was solubilised in CH₂Cl₂ (15 mL) and the solution was made alkaline by the addition of 4-methylmorpholine (400 μ L, 3.64 mmol). Then, 3,5-bis(trifluoromethyl)phenyl isothiocyanate (820 μ L, 4.51 mmol) was added and the resulting solution was stirred at room temperature. The reaction progress was monitored by analytic HPLC. After 40 hours, the crude was diluted with CH₂Cl₂ (30 mL) and washed with 1 M aqueous KHSO₄ (2 x 20 mL) followed by water (3 x 30 mL). Afterwards, the organic layer was dried over Na₂SO₄, filtered and concentrated. Silica gel chromatography (DCM:MeOH 98:1 to 98:2) provided the titled thiourea **5e** as a white solid (681 mg, 91%).

¹H NMR (300 MHz, CD₃OH) δ (ppm) 8.23 (s, 2H), 7.65 (s, 1H), 6.02 (m, 1H), 5.96 (m, 3H), 3.38 (m, 1H), 2.70 (d, J = 4.8 Hz, 3H), 1.96 (sext, J = 7.6 Hz, 1H), 1.05 (d, J = 7.9 Hz, 3H), 1.04 (d, J = 7.9 Hz, 3H).

¹³C NMR (100 MHz, CD₃OH) δ (ppm) 182.3 (C), 160.8 (C), 142.0 (C), 131.2 (C, q, J = 30 MHz), 127.5 (C), 124.7 (C), 122.4 (CH), 122.0 (CH₂), 119.3 (CH₂), 116.4 (CH), 59.6 (CH), 41.6 (CH₂), 30.0 (CH), 25.8 (CH₃), 18.3 (CH₃), 17.3 (CH₃).

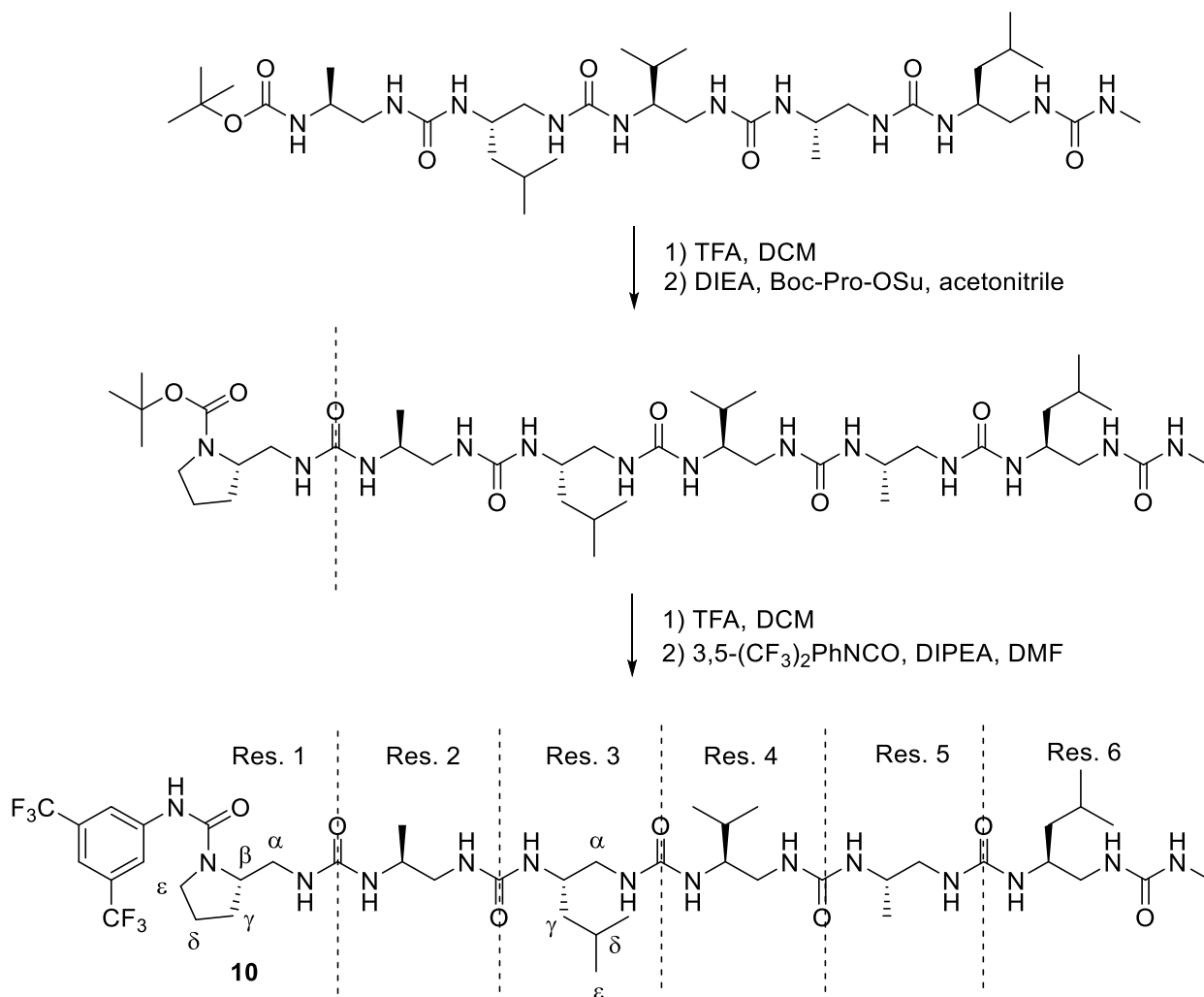
¹⁹F NMR (376 MHz, CD₃OH) δ (ppm) - 64.5.

HRMS (ES⁺, MeOH) calcd for C₂₆H₃₃F₆N₆O₂S = 607.63640; found 607.32971.

¹H NMR:**¹³C NMR:****¹⁹F NMR:**

7.4 SYNTHESIS OF CATALYSTS FROM CHAPTER III

7.4.1 Synthesis of 3,5-(CF₃)₂PhNHCO-Pro^u-Ala^u-Leu^u-Val^u-Ala^u-Leu^u-NHMe (10)



Scheme S10: Synthesis of the hexamer **10**

7.4.1.1 Boc-Pro^u-Ala^u-Leu^u-Val^u-Ala^u-Leu^u-NHMe

A solution of the corresponding Boc-protected urea (200 mg, 0.27 mmol) in CH₂Cl₂ (2 mL) was treated with TFA (2 mL) at room temperature until the starting material disappeared by TLC (1 hour). After completion, the reaction mixture was concentrated under vacuum. The resulting TFA salt was suspended in acetonitrile (2 mL) and the solution was made alkaline by the addition of DIPEA (141 μL, 0.81 mmol). Then, **BocPro^uOSu** (138 mg, 0.40 mmol) in acetonitrile (2 mL) was added and the resulting solution was stirred at room temperature overnight. Acetonitrile was removed under reduced pressure. Saturated NaHCO₃ solution was added and led to the formation of a white solid. The precipitate was purified on silica gel chromatography (DCM:MeOH 95:5 to 90:10), then purified fractions were recrystallized in acetonitrile : methanol providing the titled oligourea as white crystals (101 mg, 43%).

¹H NMR (400 MHz, pyridine-d₅) δ (ppm) 7.04-7.14 (m, 6H), 6.78 (m, 3H), 6.44 (s, 1H), 6.42 (s, 1H), 4.72 (m, 1H), 4.55 (s, 1H), 4.25-4.33 (m, 4H), 4.10-4.25 (m, 3H), 3.95-4.10 (m, 2H), 3.56 (m, 1H), 3.29 (m, 1H), 3.21 (m, 1H), 3.05 (m, 2H), 2.97 (d, *J* = 4.4 Hz, 3H), 2.65-2.75 (m, 3H), 2.45 (m, 1H), 1.78-1.92 (m, 4H), 1.66-1.74 (m, 3H), 1.52 (s, 9H), 1.05-1.36 (m, 15H), 0.92-0.99 (m, 9H), 0.78 (d, *J* = 7.4Hz, 3H).

¹³C NMR (100 MHz, pyridine-d₅) δ (ppm) 162.4 (2 x C), 161.9 (C), 161.6 (C), 161.3 (C), 157.6 (C), 125.2 (C), 81.1 (C), 59.1 (CH), 58.7 (CH), 56.6 (CH), 49.8 (CH), 49.6 (CH), 49.4 (CH₂), 49.1 (CH₂), 48.1 (CH₂), 48.0 (CH₂), 47.8 (CH), 47.6 (CH₂), 46.6 (CH), 45.8 (CH₂), 44.9 (CH₂), 43.0 (CH₂), 32.4 (CH), 29.8 (3 x CH₃), 29.7 (CH₂), 28.4 (CH), 26.7 (CH₃), 27.3 (CH₃), 25.0 (CH₃), 24.7 (CH₃), 23.6 (CH₃), 21.4 (CH₃), 20.4 (CH₃), 19.8 (CH₃), 19.5 (CH₃).

HRMS (ES⁺, MeOH) calcd for C₄₀H₈₀N₁₃O₈ = 870.62473; found 870.62537.

7.4.1.2 3,5-(CF₃)₂PhNHCO-Pro^u-Ala^u-Leu^u-Val^u-Ala^u-Leu^u-NHMe (10)

To a solution of **Boc-Pro^u-Ala^u-Leu^u-Val^u-Ala^u-Leu^u-NHMe** (100 mg, 115 μmol) in CH₂Cl₂ (1 mL) was added TFA (1 mL) and the reaction mixture was stirred at RT for 4 h. After completion of the reaction, TFA and CH₂Cl₂ were evaporated under reduced pressure. To the resulting TFA salt dissolved in DMF (2 mL) were successively added DIPEA (0.345 mmol, 60 μL) and 3,5-bis(trifluoromethyl)phenyl isocyanate (0.172 mmol, 31 μL). The reaction mixture was stirred at RT for 16 h and a saturated solution of NaHCO₃ (20 mL) was added (20 mL) was added. Desired compound was extracted with Isopropanol:Chloroform 3:7 (100 mL). Organic combined layers were washed with distilled water, dried over MgSO₄, filtered and concentrated under reduced pressure. Purification of the residue by column chromatography (MeOH/CH₂Cl₂ from 5:95 to 0:90) followed by purification with chromatotron (MeOH/CH₂Cl₂ 90:10) provided the titled oligopeptide **10** as a white solid (44 mg, 37%).

¹H NMR (400 MHz, CD₃OH) δ (ppm) 8.83 (s, 1H), 8.16 (s, 2H), 7.64 (s, 1H), 6.45 (m, 1H), 6.40 (d, *J*=9.2Hz, 1H), 6.37 (d, *J*=9.6Hz, 1H), 6.19 (m, 2H), 6.12 (m, 2H), 6.06 (d, *J* = 9.6 Hz, 1H), 5.97 (m, 2H), 5.72 (d, *J* = 10.4 Hz, 1H), 4.00-4.08 (m, 1H), 3.85-3.95 (m, 3H), 3.50-3.67 (m, 8H), 3.11 (m, 1H), 2.70 (d, *J* = 4.0 Hz, 3H), 2.63 (m, 1H), 2.27-2.43 (m, 3H), 1.94-2.13 (m, 1H), 1.80-1.85 (m, 1H), 1.69 (sext, *J* = 7.6 Hz, 2H), 1.57 (sext, *J* = 7.8 Hz, 3H), 1.20-1.29 (m, 1H), 1.16 (t, *J* = 7.3 Hz, 1H), 1.05 (d, *J* = 7.3 Hz, 3H), 1.02 (d, *J* = 7.8 Hz, 3H), 0.92 (d, *J*=7.4Hz, 3H), 0.92 (d, *J* = 7.3 Hz, 3H), 0.89 (d, *J* = 7.8Hz, 3x3H), 0.85 (d, *J* = 7.3 Hz, 3H).

¹³C NMR (100 MHz, CD₃OH) δ (ppm) 162.1 (C), 162.1 (C), 162.0 (C), 161.7 (C), 161.5 (C), 161.2 (C), 143.5 (C), 120.9 (CH), 116.3 (CH), 59.0 (CH), 56.4 (CH), 47.6 (CH₂), 47.5 (CH₂), 47.3 (CH), 46.3 (CH), 45.1 (CH₂), 44.8 (CH₂), 32.0 (CH), 27.0 (CH₂), 26.2 (CH₂), 25.9 (CH), 23.7 (CH₃), 23.6 (CH₃), 22.8 (CH₃), 22.6 (CH₃), 20.2 (CH₃), 18.9 (CH₃), 18.7 (CH₃), 18.4 (CH₃).

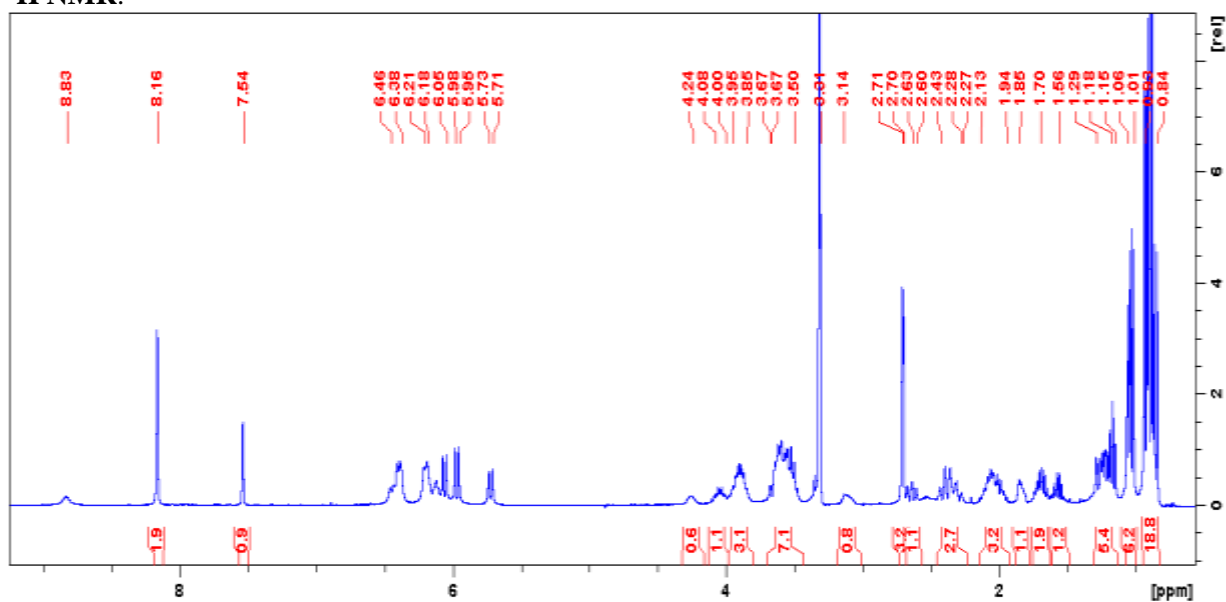
¹⁹F NMR (376 MHz, CD₃OH) δ -64.5.

HRMS (ES⁺, MeOH) calcd for C₄₄H₇₅F₆N₁₄O₇ = 1025.14804; found 1025.58729.

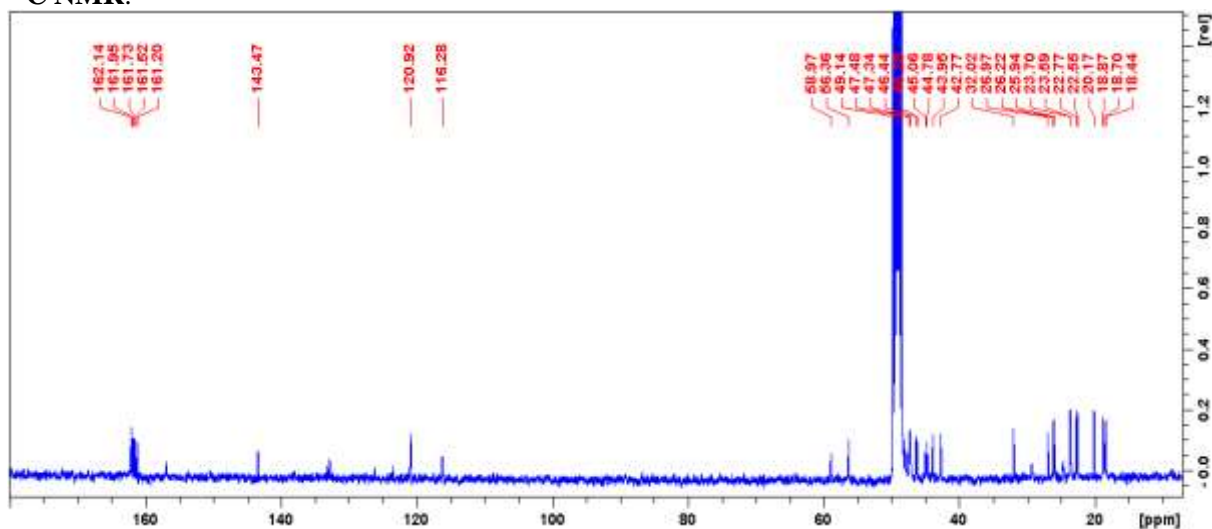
Table S9 : ^1H NMR Chemical Shifts (ppm) of 3,5-(CF_3) $_2\text{PhNHCO-Pro}^u\text{-Ala}^u\text{-Leu}^u\text{-Val}^u\text{-Ala}^u\text{-Leu}^u\text{-NHMe}$ (10) in CD_3OH at 293K

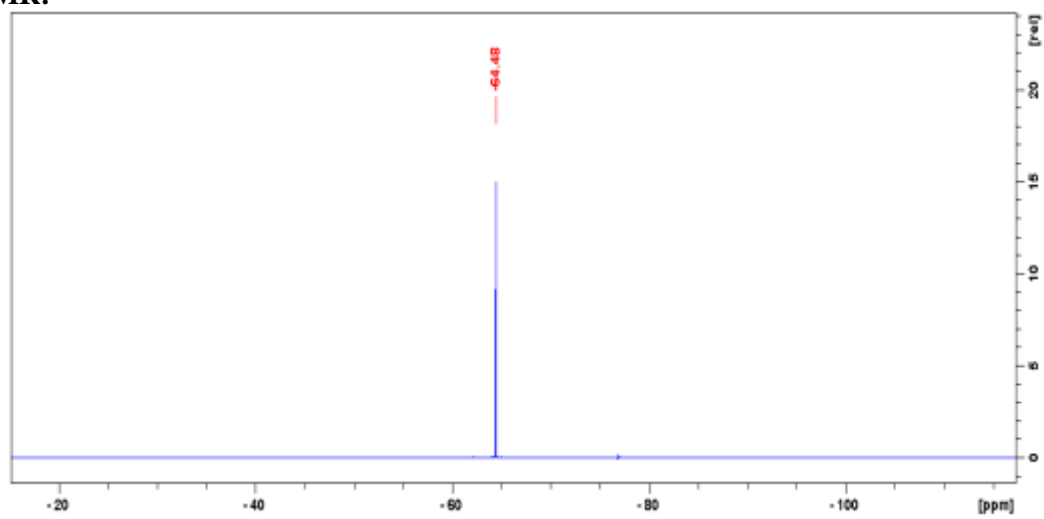
Residue	NH	NH'	$^{\alpha}\text{CH}^1$	$^{\alpha}\text{CH}^2$	βCH	γCH	δCH	$^{\epsilon}\text{CH}$	Term CH	$\Delta\delta(^{\alpha}\text{CH})$
ArNHCO		8.83								
Pro ^u 1	-	6.12	3.57	3.11	4.28	2.07	1.85	3.55		0.46
Ala ^u 2	5.97	6.21	3.53	2.73	3.87	1.05				0.80
Leu ^u 3	5.72	6.37	3.58	2.31	3.92	1.17	1.68	0.88		1.27
Val ^u 4	7.19	6.45	3.65	2.44	3.59	1.56	0.88+0.89			1.21
Ala ^u 5	5.97	6.40	3.51	2.35	4.08	1.02				1.16
Leu ^u 6	6.06	6.11	3.57	2.63	3.92	1.22	1.70	0.92		0.94
NHMe	6.25								2.70	

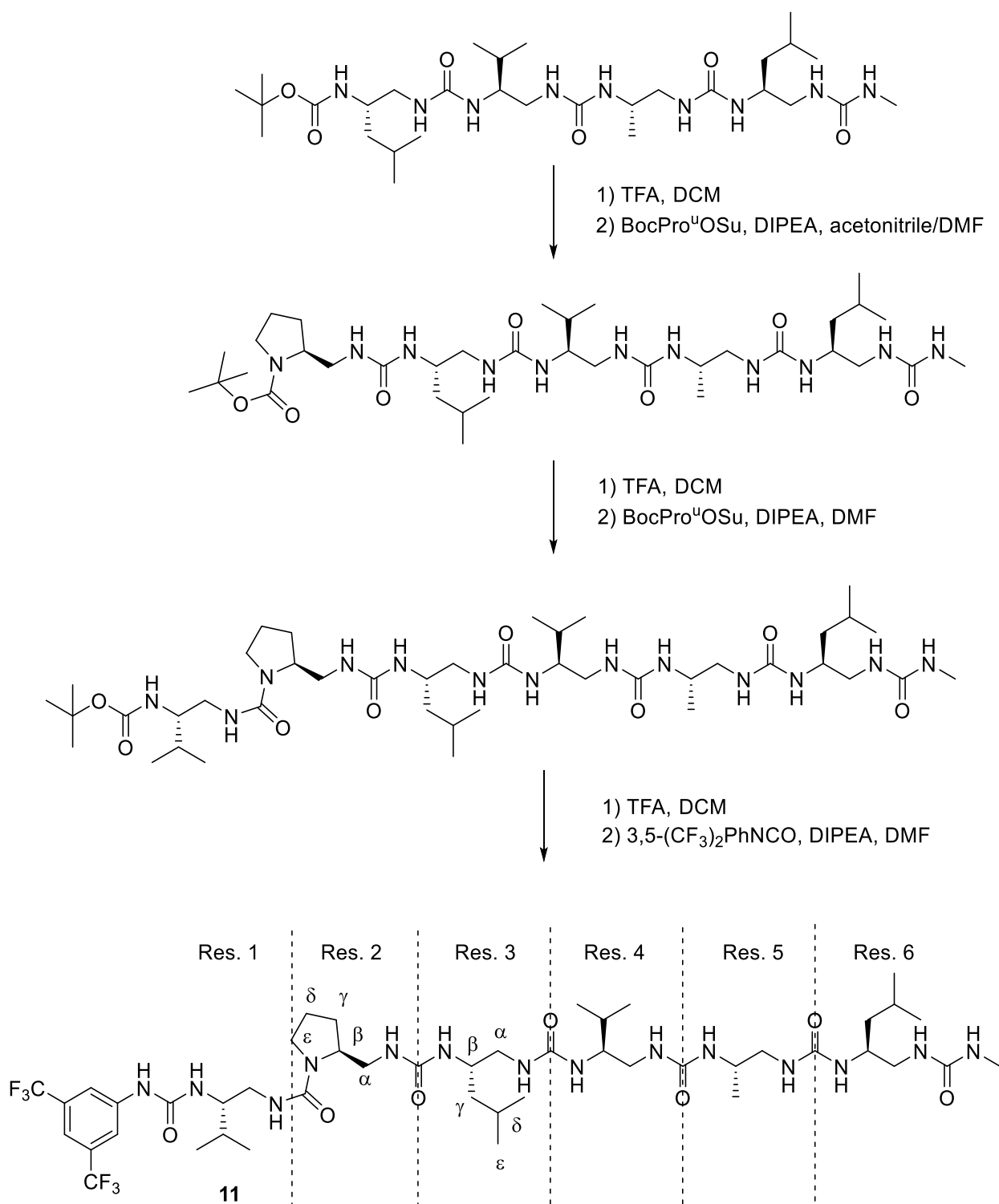
^1H NMR:



^{13}C NMR:



^{19}F NMR:

7.4.2 Synthesis of 3,5-(CF₃)₂PhNHCO-Val^u-Pro^u-Leu^u-Val^u-Ala^u-Leu^u-NHMe (**11**)Scheme S11 : Synthesis of the hexamer **11**

7.4.2.1 Boc-Pro^u-Leu^u-Val^u-Ala^u-Leu^u-NHMe

Boc-Leu^u-Val^u-Ala^u-Leu^u-NHMe (700 mg, 1.02 mmol) was dissolved in TFA (5 mL) and the mixture was stirred at RT until completion of the reaction (4 h). TFA was evaporated under reduced pressure. Last traces of TFA were removed by co-evaporation with toluene (3 × 10 mL). To the resulting TFA salt dissolved in a mixture of CH₃CN (6 mL) and DMF (6 mL) were added DIPEA (5.1 mmol, 0.89 mL) and a solution of **BocPro^uOSu** (383 mg, 1.20 mmol) in CH₃CN (3.5 mL). The reaction mixture was stirred at RT for 16 h and CH₃CN was evaporated under pressure. Saturated NaHCO₃ (40 mL) was added to the residue. The solid which precipitated was filtered off and was washed with water (10 mL), 0.25 M KHSO₄ (10 mL) and water (10 mL). The precipitate was dried under high vacuum and purification by column chromatography (MeOH/CH₂Cl₂ 7:93) followed by recrystallization from a mixture of MeOH, CH₂Cl₂ and Et₂O provided the titled oligourea as a white solid (385 mg, 49%).

¹H NMR (400 MHz, pyridine-d₅) δ (ppm) 6.90-7.12 (m, 4H), 6.84 (d, *J* = 7.7 Hz, 1H), 6.66-6.77 (m, 2H), 6.31-6.44 (m, 2H), 6.21 (d, *J* = 7.5 Hz, 1H), 4.68-4.83 (m, 1H), 4.52-4.65 (m, 1H), 3.84-4.49 (m, 7H), 3.40-3.77 (m, 1H), 3.22-3.36 (m, 1H), 3.11-3.21 (m, 1H), 2.98-3.11 (m, 2H), 2.96 (d, *J* = 4.4 Hz, 3H), 2.45-2.75 (m, 3H), 1.46-2.08 (m, 7H), 1.53 (s, 9H), 1.16-1.44 (m, 4H), 1.12 (d, *J* = 7.4 Hz, 3H), 1.08 (d, *J* = 7.5 Hz, 3H), 0.87-1.04 (m, 9H), 0.91 (d, *J* = 7.3 Hz, 3H), 0.79 (d, *J* = 7.6 Hz, 3H).

¹³C NMR (100 MHz, pyridine-d₅) δ (ppm) 161.6 (C), 161.4 (C), 160.9 (2 × C), 160.3 (C), 156.9 (C), 80.4 (C), 57.8 (CH), 56.0 (CH), 49.0 (2 × CH), 48.6 (CH₂), 47.5 (CH₂), 47.0 (CH₂), 46.7 (CH₂), 45.8 (CH), 45.1 (2 × CH₂), 44.2 (CH₂), 41.8 (CH₂), 31.6 (CH), 29.0 (3 × CH₃), 28.8 (CH₂), 27.6 (CH₃), 25.8 (CH), 25.5 (CH), 24.1 (CH₂), 23.8 (2 × CH₃), 22.9 (CH₃), 22.8 (CH₃), 20.6 (CH₃), 19.5 (CH₃), 18.8 (CH₃).

MS (ES⁺, MeOH): 770.6 ([M+H]⁺, 100%). **HRMS** (ES⁺, MeOH) calcd for C₃₆H₇₂N₁₁O₇ = 770.56107; found 770.56182.

7.4.2.2 Boc-Val^u-Pro^u-Leu^u-Val^u-Ala^u-Leu^u-NHMe

Boc-Pro^u-Leu^u-Val^u-Ala^u-Leu^u-NHMe (300 mg, 0.39 mmol) was dissolved in TFA (5 mL) and the reaction mixture was stirred at RT until completion of the reaction. TFA was evaporated under reduced pressure. Last traces of TFA were removed by co-evaporation with toluene (3 × 10 mL). To the resulting TFA salt dissolved in DMF (1.5 mL) were successively added DIPEA (203 μL, 1.17 mmol) and a solution of **BocVal^uOSu** (147 mg, 0.43 mmol) in CH₃CN (1.5 mL). The reaction mixture was stirred at RT for 16 h and CH₃CN was evaporated under reduced pressure. A saturated solution of NaHCO₃ (30 mL) was then added to the residue. The solid which precipitated was filtered off, was washed with H₂O (10 mL), 0.25 M KHSO₄ (10 mL) and H₂O (10 mL) and was dried under high vacuum. Purification of the residue by column chromatography (MeOH/CH₂Cl₂ 5:95→10:90) followed by precipitation from a mixture of EtOAc and Et₂O provided the titled oligourea as a white solid (230 mg, 66%).

¹H NMR (400 MHz, CH₃CN) δ (ppm) 6.76 (d, *J* = 9.2 Hz, 1H), 6.45 (d, *J* = 9.0 Hz, 1H), 6.27 (d, *J* = 7.7 Hz, 1H), 6.18 (d, *J* = 8.4 Hz, 1H), 5.98 (q, *J* = 4.5 Hz, 1H), 5.93 (d, *J* = 10.7 Hz, 1H), 5.85 (d, *J* = 10.4 Hz, 1H), 5.74 (d, *J* = 8.7 Hz, 1H), 5.70 (d, *J* = 9.6 Hz, 1H), 5.54 (t, *J* = 5.4 Hz, 1H), 5.37-5.49 (m, 2H), 4.12-4.26 (m, 1H), 3.91-4.07 (m, 1H), 3.75-3.91 (m, 2H), 3.42-3.74 (m, 8H), 3.22-3.32 (m, 1H), 3.18 (q, *J* = 8.8 Hz, 1H), 2.63 (d, *J* = 4.5 Hz, 3H), 2.53-2.64 (m, 1H), 2.14-2.52 (m, 5H), 1.94-2.04 (m, 2H), 1.40-1.86 (m, 6H), 1.43 (s, 9H), 1.10-1.22 (m, 4H), 0.96 (d, *J* = 7.9 Hz, 3H), 0.93 (d, *J* = 7.8 Hz, 3H), 0.86-0.92 (m, 15H), 0.83 (d, *J* = 7.7 Hz, 3H), 0.78 (d, *J* = 7.7 Hz, 3H).

¹³C NMR (100 MHz, CH₃CN) δ (ppm) 161.8 (C), 161.1 (2 × C), 160.5 (C), 160.0 (C), 159.5 (C), 158.9 (C), 80.1 (C), 56.6 (CH), 57.4 (CH), 55.7 (CH), 49.0 (CH), 48.6 (CH), 48.2 (CH₂), 46.7 (CH₂), 46.0 (2 × CH₂), 45.5 (CH), 44.6 (CH₂), 44.4 (CH₂), 44.3 (CH₂), 44.0 (CH₂), 42.5 (CH₂), 31.5 (CH), 28.7 (3 × CH₃), 27.8 (CH₂), 26.9 (CH₃), 26.0 (CH), 25.6 (CH), 24.5 (CH₂), 23.6 (CH₃), 23.5 (CH₃), 22.7 (CH₃), 22.4 (CH₃), 20.1 (CH₃), 19.9 (CH₃), 19.4 (CH₃), 19.1 (CH₃), 18.4 (CH₃).

MS (ES⁺, MeOH): 898.7 ([M+H]⁺, 100%). **HRMS** (ES⁺, MeOH) calcd for C₄₂H₈₄N₁₃O₈ = 898.65603; found 898.65540.

7.4.2.3 3,5-(CF₃)₂PhNHCO-Val^u-Pro^u-Leu^u-Val^u-Ala^u-Leu^u-NHMe (11)

To a solution of **Boc-Val^u-Pro^u-Leu^u-Val^u-Ala^u-Leu^u-NHMe** (186 mg, 0.207 mmol) in CH₂Cl₂ (2 mL) was added TFA (2 mL) and the mixture was stirred at RT until completion of the reaction. TFA and CH₂Cl₂ were evaporated under reduced pressure. Last traces of TFA were removed by co-evaporation with toluene (3 × 10 mL). To the resulting TFA salt dissolved in DMF (3 mL) were successively added DIPEA (162 μL, 0.910 mmol) and 3,5-bis(trifluoromethyl)phenyl isocyanate (54 μL, 0.310 mmol). The reaction mixture was stirred at RT for 16 h and a saturated solution of NaHCO₃ (20 mL) was added. The solid which precipitated was filtered off, was washed with H₂O (10 mL), 0.25 M KHSO₄ (10 mL) and H₂O (10 mL) and was dried under high vacuum. Purification of the residue by column chromatography (MeOH/CH₂Cl₂ 4:96→11:89) followed by precipitation from a mixture of EtOAc and MeOH provided the titled oligourea **11** as a white solid (112 mg, 51%). **MS** (ES⁺, MeOH): ([M+Na]⁺, 50%), ([M+H]⁺, 100%).

¹H NMR (400 MHz, CD₃OH) δ (ppm) 8.98 (s, 1H), 7.98 (brs, 2H), 7.61 (brs, 1H), 6.62 (brs, 1H), 6.26-6.48 (m, 4 H), 6.14-7.25 (m, 1H), 5.90-7.14 (m, 5H), 5.80 (d, *J* = 9.1 Hz, 1H), 4.11-4.25 (m, 1H), 4.00-4.11 (m, 1H), 3.81-4.00 (m, 3H), 3.48-3.73 (m, 6H), 3.31-3.47 (m, 1H), 3.18-3.31 (m, 2H), 2.80-2.99 (m, 1H), 2.70 (d, *J* = 4.2 Hz, 3H), 2.56-2.73 (m, 2H), 2.27-2.49 (m, 3H), 1.86-2.00 (m, 2H), 1.47-1.85 (m, 6H), 1.14-1.27 (m, 4H), 0.96-1.06 (m, 9H), 0.86-0.95 (m, 15 H), 0.84 (d, *J* = 7.5 Hz, 3H).

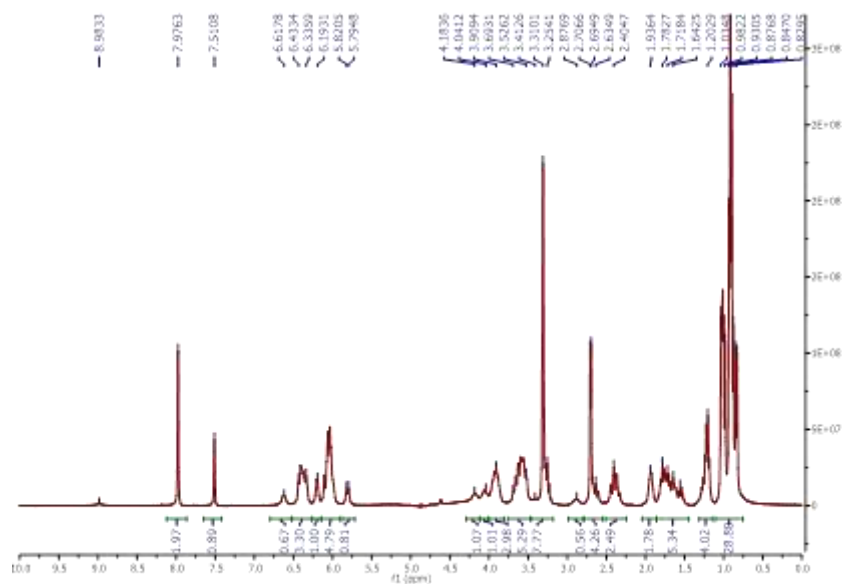
¹³C NMR (100 MHz, CD₃OH) δ 162.3 (C), 162.0 (C), 161.6 (2 × C), 161.4 (C), 160.1 (C), 158.1 (C), 143.3 (C), 133.1 (q, *J* = 33 Hz, 2 × C), 124.7 (q, *J* = 270 Hz, 2 × C), 118.7-119.1 (m, 2 × CH), 115.3-115.7 (m, CH), 57.5 (CH), 56.3 (CH), 56.1 (CH), 49.4 (2 × CH), 48.2 (CH₂), 47.0 (CH₂), 46.4 (CH₂), 46.3 (CH₂), 46.1 (CH), 44.9 (CH₂), 44.75 (CH₂), 44.70 (CH₂), 43.8 (CH₂), 42.8 (CH₂), 31.9 (2 × CH), 28.5 (CH₂), 26.8 (CH₃), 26.1 (CH), 25.8 (CH), 24.5 (CH₂), 23.5 (CH₃), 23.4 (CH₃), 22.7 (CH₃), 22.4 (CH₃), 20.04 (CH₃), 20.01 (CH₃), 18.7 (CH₃), 18.5 (CH₃), 18.3 (CH₃) ppm.

¹⁹F NMR (376 MHz, CD₃OH) δ -64.6 ppm.

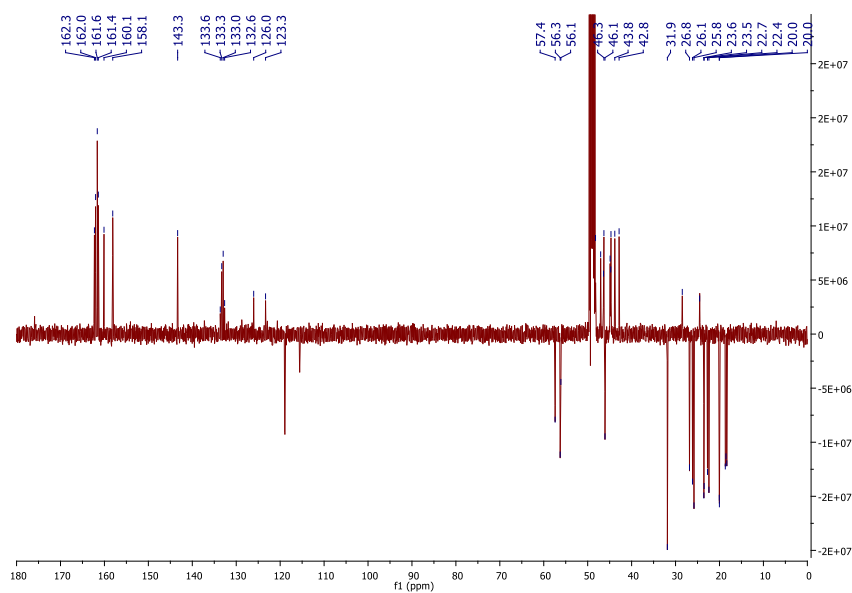
Table S10: ^1H NMR Chemical Shifts (ppm) of 3,5-(CF₃)₂PhNHCO-Val^u-Pro^u-Leu^u-Val^u-Ala^u-Leu^u-NHMe (11) in CD₃OH at 293K.

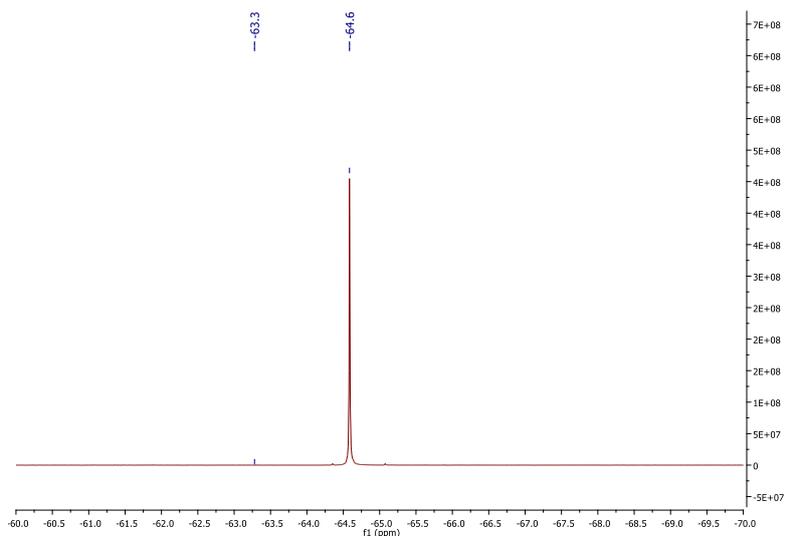
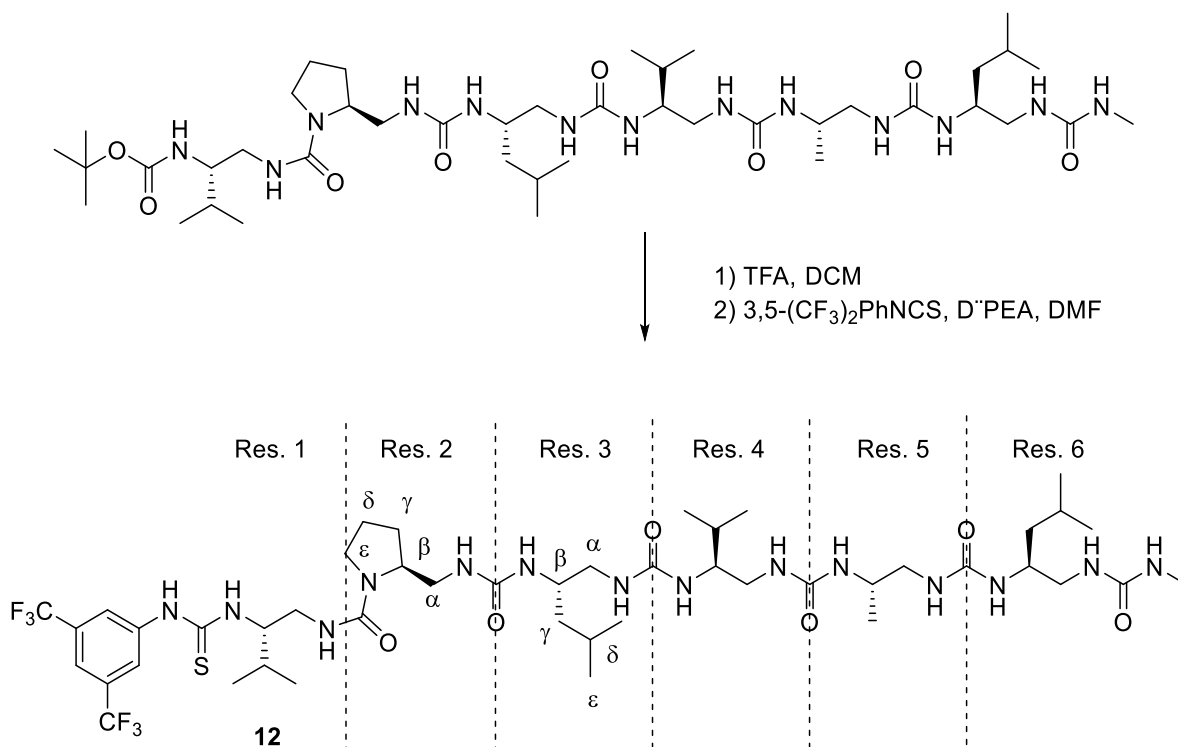
Residue	NH	NH'	αCH^a	αCH^b	βCH	γCH	δCH	ϵCH	Term CH	$\Delta\delta(^{\circ}\text{CH})$
		8.98							7.98	
	ArNHCO								7.61	
Val ^u	1	6.04	6.33	2.89	3.56	3.95	1.77	1.01		0.67
Pro ^u	2	-	5.99	2.70	3.41	4.18	1.63	1.94	3.26	0.71
Leu ^u	3	5.80	6.62	2.41	3.66	3.91	1.20	1.71	0.90	1.23
Val ^u	4	6.09	6.39	2.41	3.63	3.57	1.55	0.84		1.22
Ala ^u	5	6.05	6.38	2.37	3.55	4.06	1.03	0.88		1.18
Leu ^u	6	6.03	6.43	2.64	3.60	3.89	1.24	1.70	0.93	0.96
	NHMe	6.20							2.70	

^1H NMR:



^{13}C NMR:



¹⁹F NMR:**7.4.3 Synthesis of (CF₃)₂PhNHCS-Val^u-Pro^u-Leu^u-Val^u-Ala^u-Leu^u-NHMe (12)***Scheme S12: Synthesis of the hexamer 12*

Boc-Pro^u-Leu^u-Val^u-Ala^u-Leu^u-NHMe (300 mg, 0.39 mmol) was dissolved in TFA (5 mL) and the reaction mixture was stirred at RT until completion of the reaction. TFA was evaporated under reduced pressure. Last traces of TFA were removed by co-evaporation with toluene (3 × 10 mL). To the resulting TFA salt dissolved in DMF (1.5 mL) were successively added DIPEA (203 μL, 1.17 mmol) and a solution of **BocVal^uOSu** (147 mg, 0.43 mmol) in CH₃CN (1.5 mL). The reaction mixture was stirred at RT for 16 h and CH₃CN was evaporated under reduced pressure. A saturated solution of NaHCO₃ (30 mL) was then added to the residue. The solid which precipitated was filtered off, was washed with H₂O (10 mL), 0.25 M KHSO₄ (10 mL) and H₂O (10 mL) and was dried under high vacuum. Purification of the residue by column chromatography (MeOH/CH₂Cl₂ 5:95→10:90) followed by precipitation from a mixture of EtOAc and Et₂O provided the titled oligourea **12** as a white solid (230 mg, 66%).

¹H NMR (400 MHz, CD₃OH) δ (ppm) 8.08 (s, 2H), 7.66 (s, 1H), 6.34 (m, 1H), 6.32 (m, 1H), 6.21 (m, 3H), 6.10 (m, 1H), 5.98 (m, 1H), 5.93 (m, 1H), 5.87 (m, 2H), 5.63 (m, 1H), 3.94 (m, 1H), 3.80 (m, 2H), 3.35-3.56 (m, 8H), 3.17 (m, 1H), 2.61 (d, *J* = 4.4 Hz, 4H), 2.55-2.60 (m, 1H), 2.25-2.42 (m, 4H), 1.72-1.83 (m, 4H), 1.48-1.61 (m, 3H), 1.46 (sext, *J* = 7.8 Hz, 1H), 1.08-1.20 (m, 4H), 0.94 (m, 8H), 0.83 (3d, *J* = 7.4 Hz, 3x3H), 0.80 (d, *J* = 7.4 Hz, 2x3H), 0.76 (d, *J* = 7.8 Hz, 3H).

¹³C NMR (100 MHz, CD₃OH) δ (ppm) 182.4 (C), 160.7 (C), 160.3 (C), 160.1 (C), 160.0 (C), 158.7 (C), 141.9 (C), 131.4 (C), 131.1 (C), 124.7 (C), 122.7 (2 x CH), 122.0 (CH), 116.6 (CH), 59.7 (CH), 56.6 (CH), 55.0 (CH), 47.8 (CH₂), 45.9 (CH), 45.7 (CH₂), 45.0 (CH), 44.8 (CH₂), 43.5 (CH₂), 42.8 (CH₂), 42.5 (CH), 41.5 (CH₂), 30.7 (CH), 30.5 (CH₂), 29.3 (CH), 27.9 (CH₂), 25.6 (CH₃), 24.9 (CH₂), 24.5 (CH₃), 22.9 (CH₂), 22.3 (CH₂), 22.2 (CH₃), 21.5 (CH₃), 21.1 (CH₃), 18.8 (CH₃), 18.5 (CH₃), 17.5 (CH₃), 17.4 (CH₃), 17.3 (CH₃).

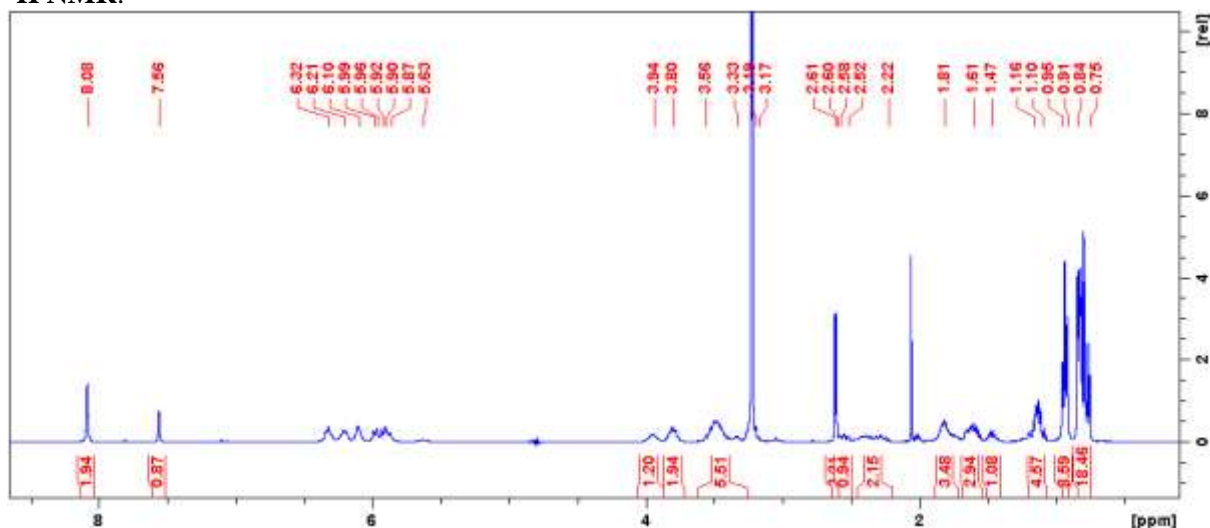
¹⁹F NMR (282 MHz, CD₃OH): δ (ppm) -64.5

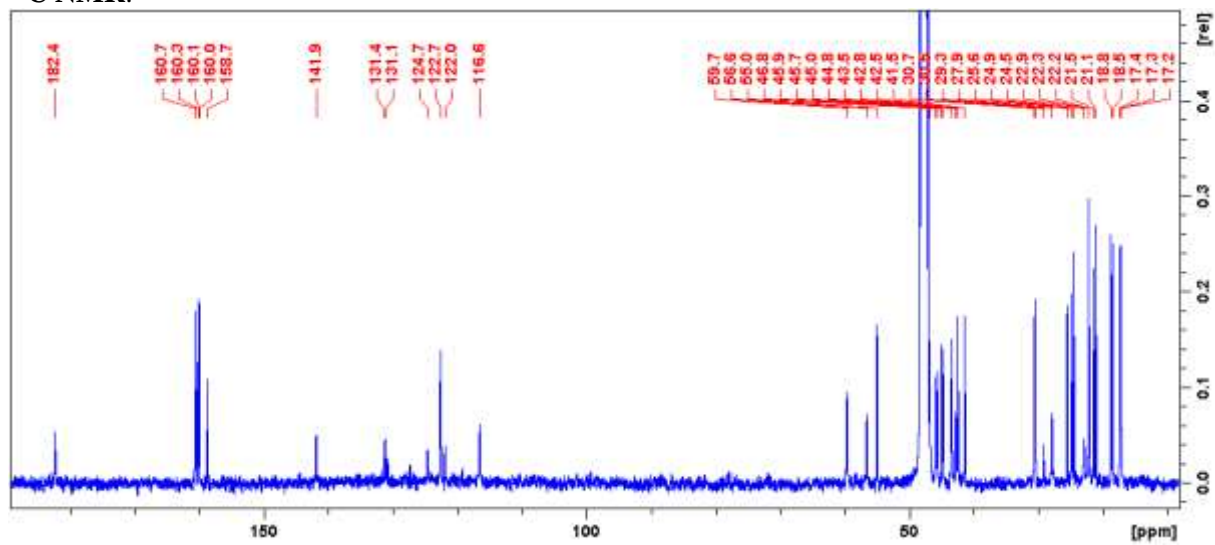
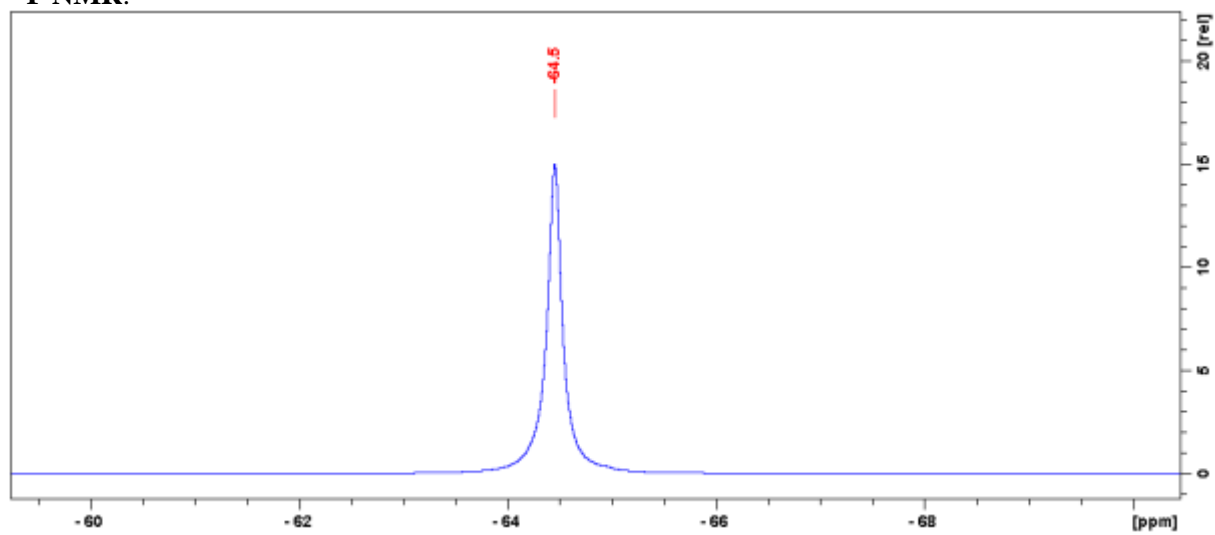
HRMS (ES⁺, MeOH) calcd for C₄₆H₇₈F₆N₁₄O₆S = 1069.59264; found 1069.59347.

Table S20: ¹H NMR Chemical Shifts (ppm) of 3,5-(CF₃)₂PhNHCO-Val^S-Pro^u-Leu^u-Val^u-Ala^u-Leu^u-NHMe (**12**) in CD₃OH at 293K.

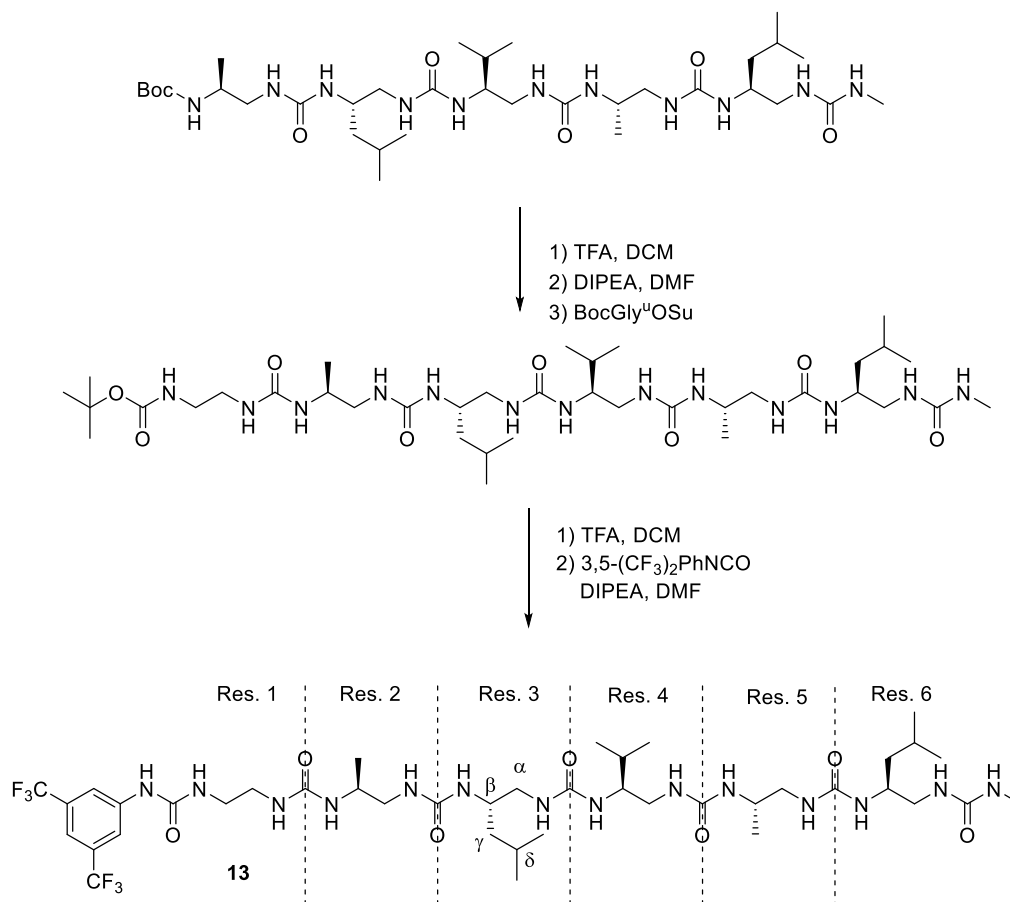
Residue		NH	NH'	^α CH ¹	^α CH ²	^β CH	^γ CH	^δ CH	^ε CH	Term CH	Δδ(^α CH)
	ArNHCO		ND								
Val^S	1	5.87	6.17	3.48	2.46	3.50	1.48	0.76			1.02
Pro^u	2	-	6.09	3.35	2.63	3.17	1.80	0.94			0.72
Leu^u	3	5.63	6.21	3.50	2.39	3.80	1.13	1.72	0.83		1.11
Val^u	4	5.87	6.19	3.52	2.46	3.48	1.48	0.80			1.06
Ala^u	5	5.98	6.32	3.48	2.28	3.96	1.08				1.20
Leu^u	6	5.93	6.34	3.48	2.54	3.80	1.13	1.61	0.94		0.94
	NHMe									2.61	

¹H NMR:



^{13}C NMR: **^{19}F NMR:**

7.4.4 Synthesis of 3,5-(CF₃)₂PhNHCO-Gly^u-Ala^u-Leu^u-Val^u-Ala^u-Leu^u-NHMe (13)



Scheme S13: Synthesis of the hexamer **13**

7.4.4.1 BocGly^u-Ala^u-Leu^u-Val^u-Ala^u-Leu^u-NHMe

Boc-Ala^u-Leu^u-Val^u-Ala^u-Leu^u-NHMe (75 mg, 0.10 mmol) was dissolved in TFA (1 mL) and the reaction mixture was stirred at RT until completion of the reaction. TFA was evaporated under reduced pressure. Last traces of TFA were removed by co-evaporation with toluene (3 × 10 mL). To the resulting TFA salt dissolved in DMF (1 mL) were successively added DIPEA (52 μL, 0.30 mmol) and a solution of **BocGly^uOSu** (46 mg, 0.15 mmol) in DMF (1 mL). The reaction mixture was stirred at RT for 16 h and NaHCO₃ solution (10 mL) was added which allowed the appearance of a precipitate. The solid was filtered off, was washed with H₂O (10 mL), dissolved in MeOH (10 mL) and concentrated under vacuum. Purification of the residue by column chromatography (MeOH/CH₂Cl₂ 5:95→15:85) provided the titled oligourea as a white solid (75 mg, 75%).

¹H NMR (400 MHz, CD₃OH) δ (ppm) 6.63 (s, 1H), 6.39-7.30 (m, 4H), 6.10 (m, 1H), 5.89-6.00 (m, 4H), 5.80 (m, 1H), 5.76 (m, 1H), 3.75-3.95 (m, 4H), 3.39-3.54 (m, 5H), 2.62 (d, *J* = 4.4 Hz, 4H), 2.26-2.37 (m, 4H), 1.61 (m, *J* = 7.8 Hz, 2H), 1.49 (sext, *J* = 7.8 Hz, 1H), 1.36 (s, 9H), 1.18 (m, 4H), 0.96 (d, *J* = 7.8 Hz, 3H), 0.93 (d, *J* = 7.8 Hz, 3H), 0.80-0.84 (d, *J* = 7.8 Hz, 5x3H), 0.76 (s, *J* = 7.8 Hz, 3H).

¹³C NMR (75 MHz, CD₃OH) δ (ppm) 160.6 (C), 129.4 (CH), 127.6 (CH), 54.9 (CH), 45.7 (CH), 42.2 (CH₂), 41.3 (CH₂), 30.5 (CH), 29.4 (CH₂), 27.5 (3xCH₃), 25.5 (CH₃), 24.9 (CH₃), 24.6 (CH₃), 22.2 (CH₃), 21.3 (CH₃), 21.1 (CH₃), 18.8 (CH₃), 17.5 (CH₃), 17.1 (CH₃), 16.9 (CH₃).

MS (ESI): *m/z* [M+H]⁺ 830.7.

7.4.4.2 3,5-(CF₃)₂PhNHCO-Gly^u-Ala^u-Leu^u-Val^u-Ala^u-Leu^u-NHMe (13)

To a solution of **Boc-Gly^u-Ala^u-Leu^u-Val^u-Ala^u-Leu^u-NHMe** (63 mg, 0.075 mmol) in CH₂Cl₂ (1 mL) was added TFA (1 mL) and the reaction mixture was stirred at RT for 4 h. After completion of the reaction, TFA and CH₂Cl₂ were evaporated under reduced pressure. To the resulting TFA salt dissolved in DMF (1 mL) were successively added DIPEA (0.225 mmol, 39 μL) and 3,5-bis(trifluoromethyl)phenyl isocyanate (0.113 mmol, 20 μL). The reaction mixture was stirred at RT for 16 h and a saturated solution of NaHCO₃ (10 mL) was added. The solid which precipitated was filtered off, was washed with H₂O (10 mL), 0.25 M KHSO₄ (10 mL) and H₂O (10 mL) and was dried under high vacuum. Purification of the residue by column chromatography (MeOH/CH₂Cl₂ from 5:95 to 15:85) followed by preparative HPLC purification (MeOH/H₂O 30:100→0:100 in 5 min, then 5 min methanol isocratic) provided the titled oligourea **13** as an orange solid (47 mg, 64%).

¹H NMR (400 MHz, DMSO-d₆) δ (ppm) 8.14 (s, 2H), 7.69 (s, 1H), 6.28-6.32 (m, 1H), 6.16-6.22 (m, 4H), 6.05-6.12 (m, 2H), 5.96-6.02 (m, 1H), 5.86-5.89 (m, 1H), 5.71-5.73 (m, 1H), 4.18 (m, 1H), 3.68-3.91 (m, 3H), 3.40-3.51 (m, 3H), 3.36 (m, 2H), 3.24-3.29 (m, 1H), 3.12-3.20 (m, 2H), 2.59 (m, 1H), 2.59 (d, *J* = 4.4Hz, 3H), 2.24-2.41 (m, 3H), 2.11 (m, 2H), 1.64 (sext, *J* = 7.8 Hz, 2H), 1.52 (sext, *J* = 7.0Hz, 1H), 1.28 (m, 1H), 1.15 (t, *J* = 7.8Hz, 1H), 1.01 (d, *J* = 7.4Hz, 3H), 0.95 (d, *J* = 7.8Hz, 3H), 0.88 (d, *J* = 7.4Hz, 3H), 0.88 (d, *J* = 7.4 Hz, 2x3H), 0.85 (d, *J* = 7.6 Hz, 3H), 0.81 (d, *J* = 7.8Hz, 3H), 0.79 (d, *J* = 7.8Hz, 3H).

¹³C NMR (100 MHz, DMSO-d₆) δ (ppm) 169.9 (C), 169.7 (C), 169.5 (C), 169.0 (C), 168.5 (C), 165.5 (C), 159.8 (C), 159.5 (C), 159.2 (C), 152.9 (C), 141.1 (C, m), 127.6 (CH), 64.3 (CH), 57.7 (CH), 55.7 (CH), 54.8 (CH), 54.6 (CH), 53.3 (CH₂), 52.9 (CH₂), 51.3 (CH₂); 40.3 (CH₂), 36.6 (CH₂), 34.8 (CH₃), 34.5 (CH₃), 33.4 (CH₃), 33.3 (CH₃), 32.3 (CH₃), 29.7 (CH₃), 29.0 (CH₃), 28.8 (CH₃), 27.9 (CH₃).

¹⁹F NMR (376 MHz, DMSO-d₆) δ -65.2

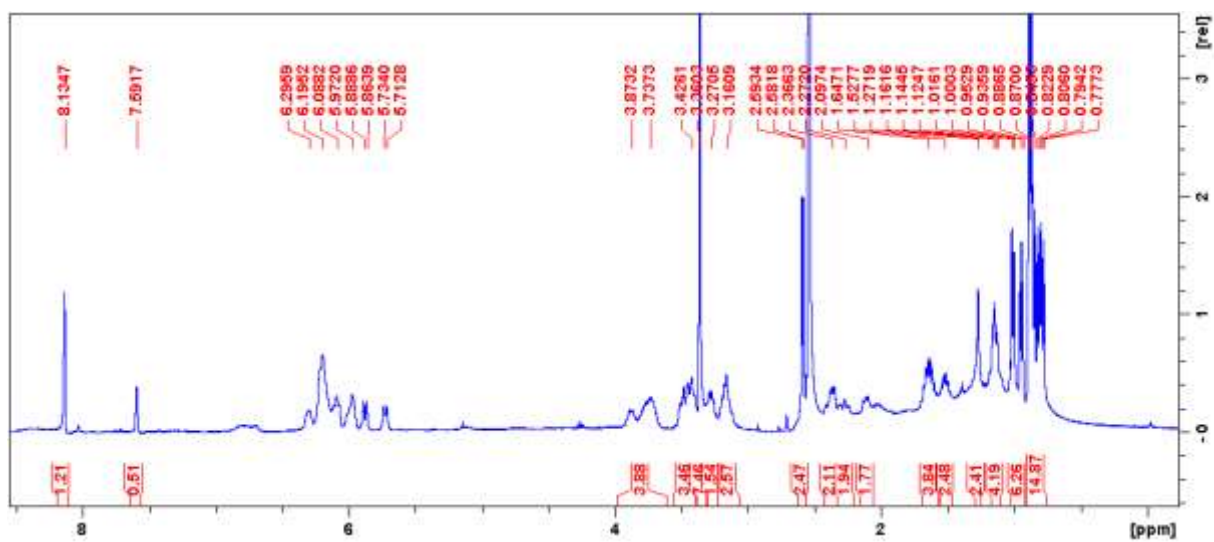
HRMS (ES⁺, MeOH) calcd for C₄₁H₇₀F₆N₁₄O₇ = 985.55289; found: 985.55203.

Note: Presence of a small impurity visible on ¹⁹F.

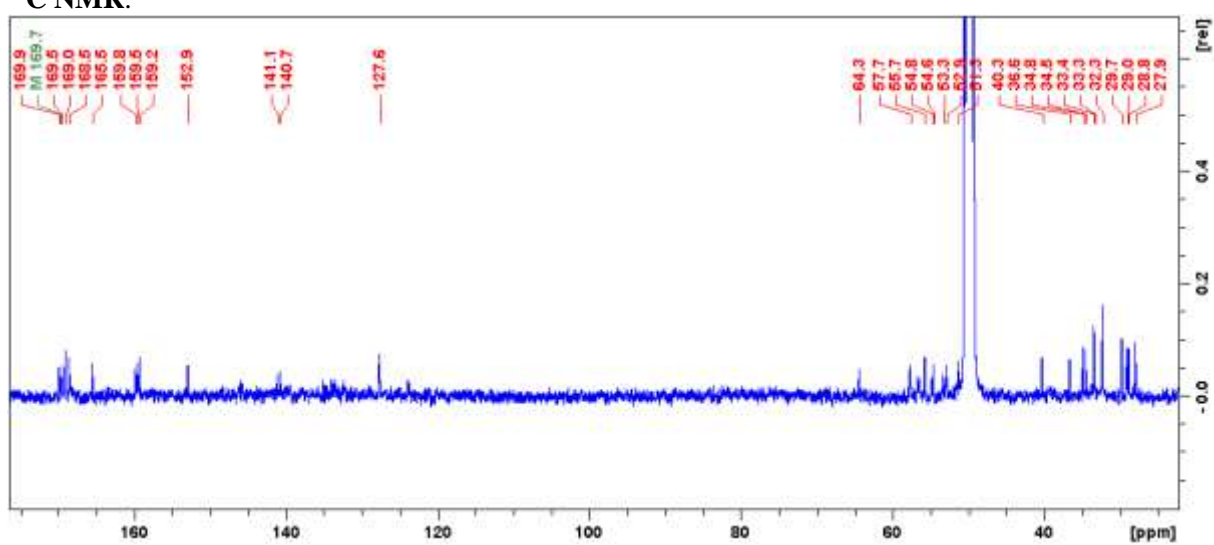
Table S 11: ¹H NMR Chemical Shifts (ppm) of 3,5-(CF₃)₂PhNHCO-Gly^u-Ala^u-Leu^u-Val^u-Ala^u-Leu^u-NHMe (**13**) in DMSO-d₆ at 293K.

Residue	NH	NH'	^α CH ₁	^α CH ₂	^β CH	^γ CH	^δ CH	^ε CH	Term CH	Δδ(^α CH)
ArNHCO		ND								
Gly ^u 1	5.97	6.18	3.30	2.51	3.75+2.52					0.79
Ala ^u 2	6.18	6.09	3.38	2.37	3.72	1.01				1.01
Leu ^u 3	6.71	6.05	3.40	2.34	3.71	1.12	1.63	0.85		1.06
Val ^u 4	6.16	5.96	3.39	2.37	3.77	1.67	0.86			1.02
Ala ^u 5	6.18	5.84	3.41	2.28	3.90	0.95				1.13
Leu ^u 6	6.28	6.19	3.35	2.36	3.46	1.28	1.52	0.78		0.99
NHMe	5.93								2.59	

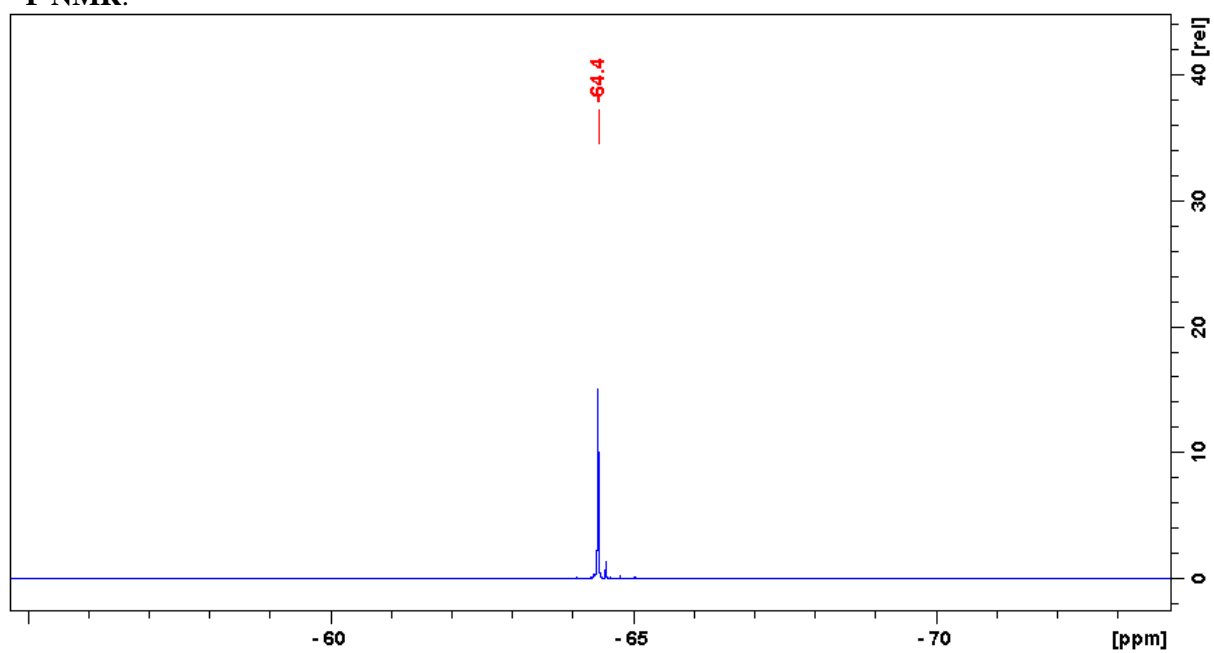
¹H NMR:



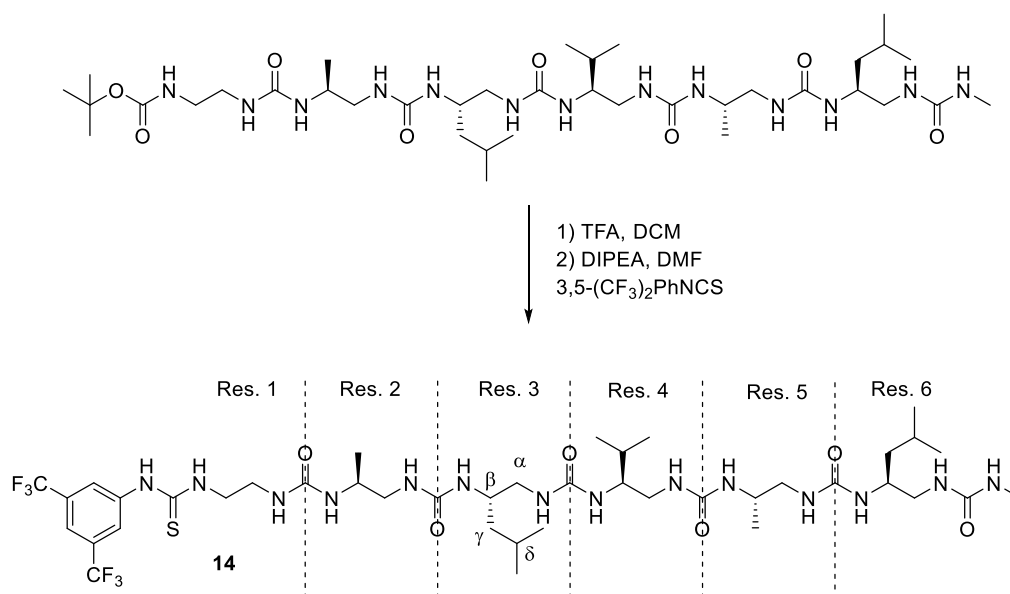
¹³C NMR:



¹⁹F NMR:



7.4.5 Synthesis of 3,5-(CF₃)₂PhNHCS-Gly^u-Ala^u-Leu^u-Val^u-Ala^u-Leu^u-NHMe (**14**)



Scheme S14 : Synthesis of the hexamer **14**

Boc-protected hexamer (300 mg, 0.40 mmol) was dissolved in DCM (5 mL) and TFA (5 mL) was added. After completion of the reaction, reaction mixture was concentrated. DIPEA (420 μ L, 2.41 mmol) and activated monomer **4** (182 mg, 0.60 mmol) were added in the residue dissolved in DMF (10 mL). After 16h, NaHCO₃ solution (20 mL) was added and led to precipitation. The resulting solid was recovered by filtration, dissolved in CH₂Cl₂ (50 mL) and washed with water (3 x 10 mL). The organic layer was dried over Na₂SO₄, filtered and concentrated under reduced pressure. Purification by chromatography on silica gel with a gradient of 7% to 11% MeOH in CH₂Cl₂ gave 315 mg (94%) of the titled oligourea **14** as a white solid.

¹H NMR (400 MHz, CD₃OH) δ 8.14 (s, 2H), 7.63 (s, 1H), 6.35-6.42 (m, 3H), 6.17-6.23 (m, 2H), 5.95-6.09 (m, 5H), 5.72 (m, 2H), 4.00-4.08 (m, 1H), 3.87-3.95 (m, 3H), 3.68-3.81 (m, 2H), 3.48-3.68 (m, 6H), 3.34-3.41 (m, 2H), 2.71 (d, J = 4.8 Hz, 3H), 2.61-2.68 (m, 2H), 2.40-2.44 (m, 3H), 1.69 (2 x sext, 2 x J = 7.3 Hz, 2H), 1.58 (sext, J = 7.8 Hz, 1H), 1.17-1.29 (m, 2H), 1.06 (d, J = 7.8 Hz, 3H), 0.99 (d, J = 7.3 Hz, 3H), 0.90 (d, J = 7.8 Hz, 2 x 3H), 0.89 (d, J = 7.8 Hz, 3H), 0.86 (d, J = 7.8 Hz, 2 x 3H), 0.83 (d, J = 7.8 Hz, 3H).

¹³C NMR (100 MHz, CD₃OH): δ 160.7(C), 160.7 (C), 160.5 (C), 160.0 (C), 159.6 (C), 141.7 (C), 131.5 (q, J = 30 Hz, CF₃), 124.7 (C), 122.6 (C), 122.0 (2 x CH), 116.7 (CH), 55.1 (CH), 47.8 (CH), 46.6 (CH₂), 45.9 (CH₂), 45.0 (CH₂), 44.9 (CH₂), 44.3 (CH), 43.2 (CH), 42.4 (CH₂), 41.2 (CH₂), 39.1 (CH), 30.6 (CH), 25.6 (CH₃), 24.9 (CH₃), 24.5 (CH), 22.3 (CH₃), 22.2 (CH₃), 21.3 (CH₃), 18.8 (CH₃).

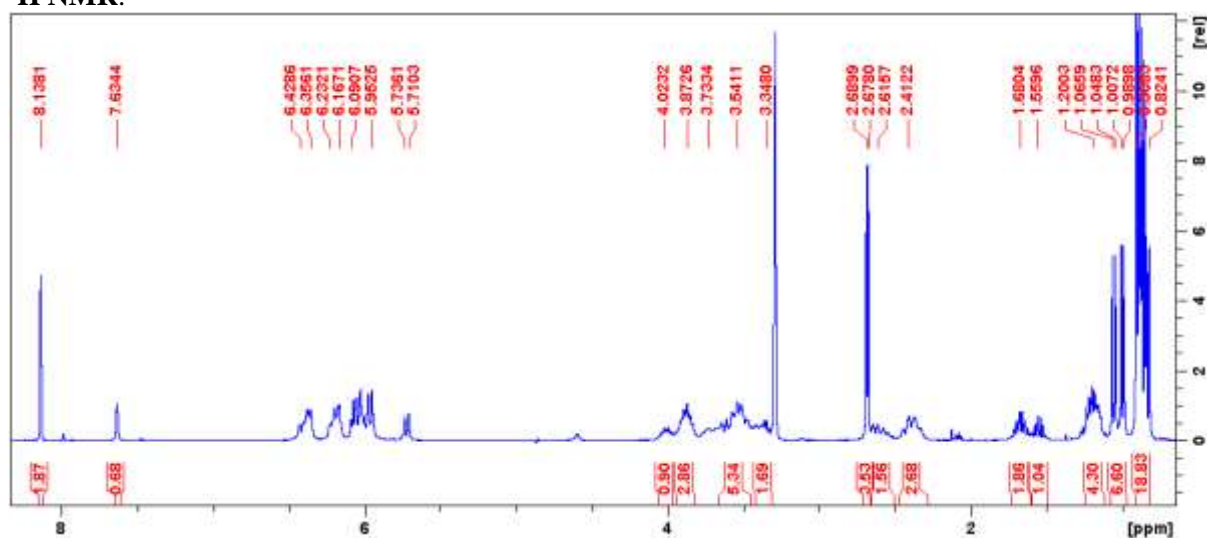
¹⁹F NMR (376 MHz, CD₃OH) : δ -64.6

HRMS (ES⁺, MeOH) calcd for C₄₁H₇₁F₆N₁₄O₆S = 1001.53004 ; found: 1001.53342. Note: Presence of a small impurity visible on ¹⁹F.

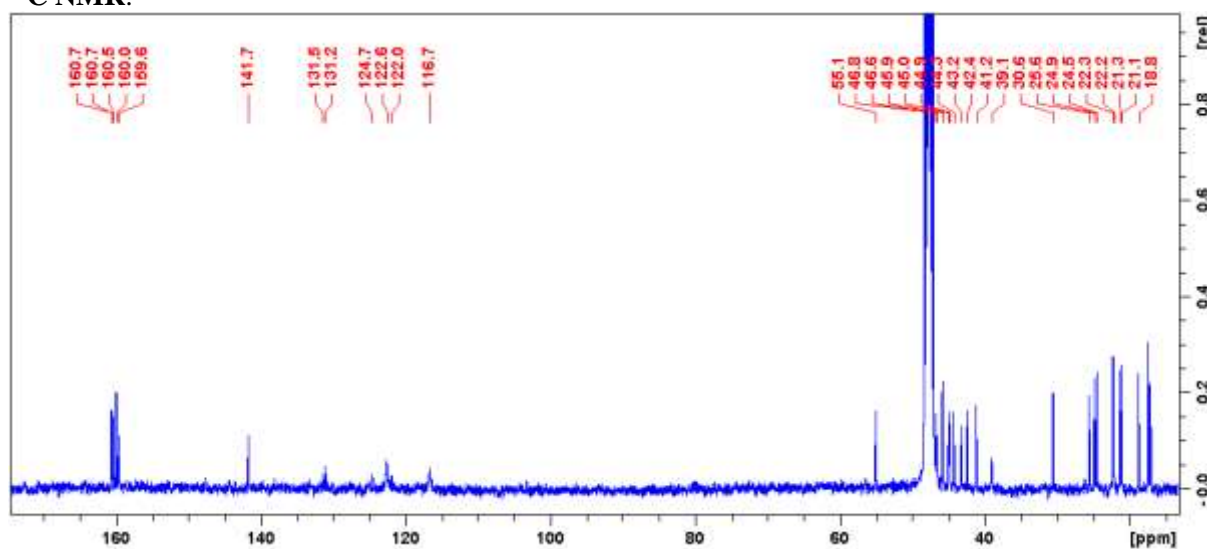
Table S 12 : ^1H NMR Chemical Shifts (ppm) of 3,5-(CF_3) $_2\text{PhNHCS-Gly}^u\text{-Ala}^u\text{-Leu}^u\text{-Val}^u\text{-Ala}^u\text{-Leu}^u\text{-NHMe}$ (**14**) in CD_3OH at 293K

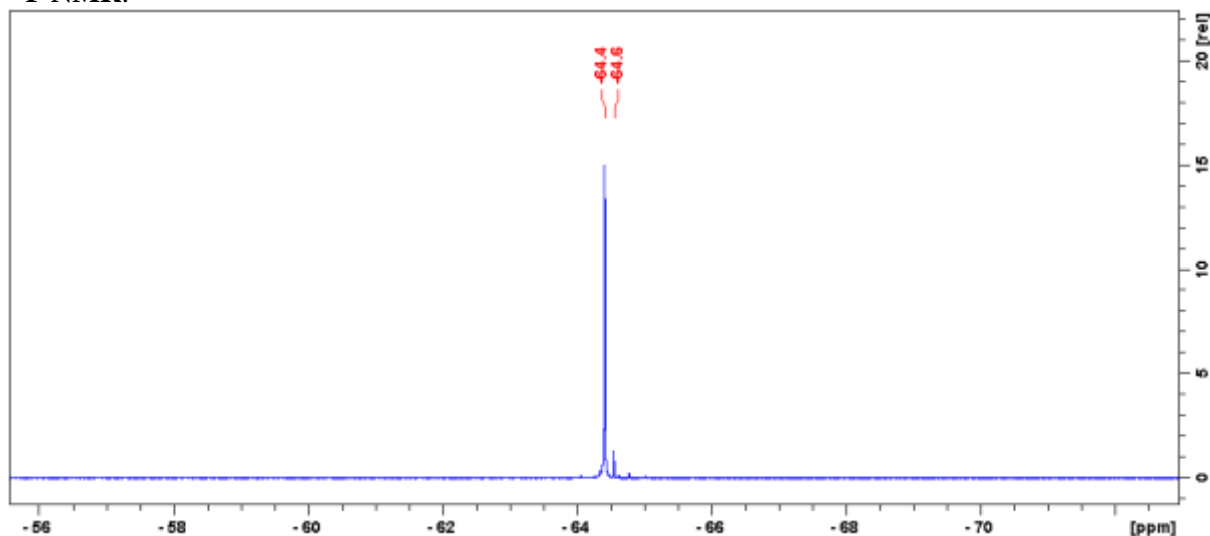
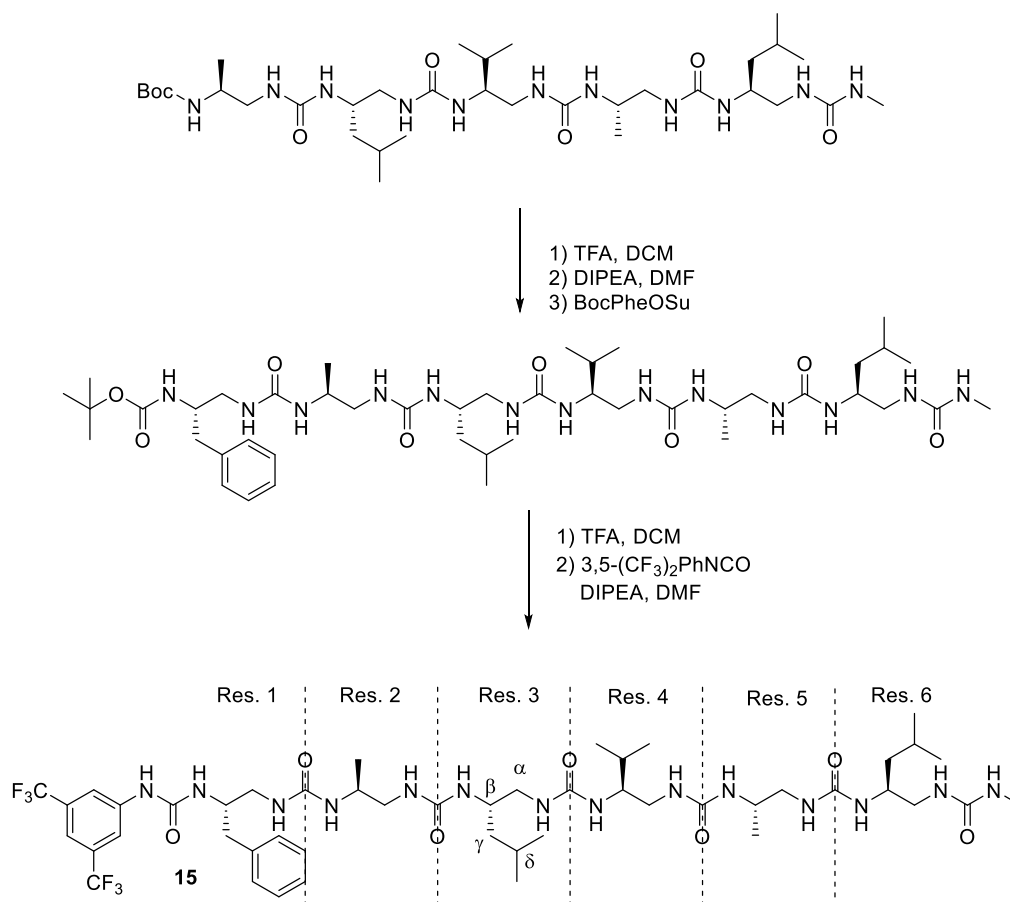
Residue	NH	NH'	αCH^1	αCH^2	βCH	γCH	δCH	ϵCH	Term CH	$\Delta\delta(\alpha\text{CH})$
ArNHCS	ND									
Gly ^u	1	6.10	6.10	3.74	3.39	3.58+3.40				0.35
Ala ^u	2	5.98	6.39	3.54	2.60	4.06	1.02			0.94
Leu ^u	3	5.75	6.25	3.56	2.39	3.90	1.24	1.69	0.86+0.92	1.17
Val ^u	4	6.21	6.46	3.63	2.44	3.54	1.58	0.89+0.92		1.19
Ala ^u	5	6.06	5.82	3.48	2.42	3.95	1.08			1.06
Leu ^u	6	6.09	6.40	3.59	2.68	3.88	1.22	1.64	0.93+0.93	0.91
NHMe	6.21								2.71	

^1H NMR:



^{13}C NMR:



¹⁹F NMR:**7.4.6 Synthesis of 3,5-(CF₃)₂PhNHCO-Phe^u-Ala^u-Leu^u-Val^u-Ala^u-Leu^u-NHMe (15)**Scheme S15: Synthesis of the hexamer **15****7.4.7.1 Boc-Phe^u-Ala^u-Leu^u-Val^u-Ala^u-Leu^u-NHMe**

To a solution of **Boc-Ala^u-Leu^u-Val^u-Ala^u-Leu^u-NHMe** (75 mg, 0.1 mmol) in CH₂Cl₂ (1 mL) was added TFA (1 mL) and the reaction mixture was stirred at RT for 4 h. After completion of the reaction, TFA and CH₂Cl₂ were evaporated under reduced pressure. To the resulting TFA salt dissolved in DMF (1 mL) were successively added DIPEA (0.3 mmol, 52 μL) and **BocPhe^uOSu** (0.15 mmol, 59 mg). The

reaction mixture was stirred at RT for 16 h and a saturated solution of NaHCO₃ (10 mL) was added. The solid which precipitated was filtered off, was washed with H₂O (10 mL), 1N KHSO₄ (10 mL) and H₂O (10 mL) and was dried under high vacuum. Purification of the residue by column chromatography (MeOH/CH₂Cl₂ 5:95→15:85) provided the titled oligourea as a transparent solid (79 mg, 86%).

¹H NMR (400 MHz, CD₃OH) δ (ppm) 7.08-7.31 (m, 5H), 6.71 (d, *J* = 9.6 Hz, 1H), 6.31-6.40 (m, 4H), 6.09-6.13 (m, 1H), 6.03-6.07 (m, 1H), 5.98 (d, *J* = 9.4 Hz, 1H), 5.87 (d, *J* = 10.4 Hz, 1H), 5.73 (m, 1H), 5.67 (d, *J* = 10.4 Hz, 2H), 3.92-3.98 (m, 1H), 3.68-3.86 (m, 4H), 3.43-3.59 (m, 6H), 2.62 (d, *J* = 4.4 Hz, 3H), 2.62 (m, 2H), 2.46-2.57 (m, 3H), 2.18-2.30 (m, 3H), 2.06-2.12 (m, 1H), 1.60-1.67 (m, 1H), 1.48-1.56 (m, 2H), 1.45 (s, 3H), 1.28 (s, 9H), 1.13-1.19 (m, 3H), 0.95 (d, *J* = 8.0 Hz, 3H), 0.92 (d, *J* = 7.3 Hz, 3H), 0.85 (d, *J* = 7.8 Hz, 2x3H), 0.82 (d, *J* = 7.8 Hz, 3H), 0.78 (d, *J* = 7.8 Hz, 2x3H), 0.76 (d, *J* = 7.8 Hz, 3H).

¹³C NMR (100 MHz, CD₃OH) δ (ppm) 160.1 (C), 160.1 (C), 159.5 (C), 159.5 (C), 157.8 (C), 157.7 (C), 156.8 (C), 138.7 (C), 136.4 (C), 129.2, 129.0, 128.7 (2 x CH), 128.3 (CH), 128.0 (2 x CH), 127.9, 126.5, 126.0, 79.0, 55.9, 54.8, 54.7, 52.6, 52.5, 45.8, 45.7, 45.0, 44.8, 43.4, 42.6, 42.5, 41.4, 40.7, 38.8, 38.3, 35.6, 30.6, 30.3, 27.5, 27.0, 25.6, 25.4 (CH₃), 24.8 (CH), 24.5 (CH), 22.3 (CH₃), 22.2 (CH₃), 21.3 (CH₃), 21.2 (CH₃), 18.8 (CH₃).

MS (ESI): *m/z* [M+H]⁺ 921.7. Note: Presence of an impurity visible on ¹³C.

7.4.7.2 3,5-(CF₃)₂PhNHCO-Phe^u-Ala^u-Leu^u-Val^u-Ala^u-Leu^u-NHMe (15)

To a solution of **Boc-Phe^u-Ala^u-Leu^u-Val^u-Ala^u-Leu^u-NHMe** (79 mg, 0.086 mmol) in CH₂Cl₂ (1 mL) was added TFA (1 mL) and the reaction mixture was stirred at RT for 4 h. After completion of the reaction, TFA and CH₂Cl₂ were evaporated under reduced pressure. To the resulting TFA salt dissolved in DMF (1 mL) were successively added DIPEA (0.225 mmol, 39 μL) and 3,5-bis(trifluoromethyl)phenyl isocyanate (0.113 mmol, 20 μL). The reaction mixture was stirred at RT for 16 h and a saturated solution of NaHCO₃ (10 mL) was added. The solid which precipitated was filtered off, was washed with H₂O (10 mL), 1N KHSO₄ (10 mL) and H₂O (10 mL) and was dried under high vacuum. Purification of the residue by column chromatography (MeOH/CH₂Cl₂ from 5:95 to 10:90) followed by preparative HPLC purification (MeOH/H₂O 30:100→0:100 in 5 min, then 5 min methanol isocratic) provided the titled oligourea **15** as a purple solid (35 mg, 38%).

¹H NMR (400 MHz, CD₃OH) δ (ppm) 7.96 (s, 2H), 7.64 (s, 1H), 7.32-7.44 (m, 10H), 6.51-6.55 (m, 2H), 6.47 (dd, *J* = 3.2 Hz, 10.0 Hz, 1H), 6.45 (dd, *J* = 2.8 Hz, 8.8 Hz, 1H), 6.37 (d, *J* = 10 Hz, 1H), 6.25 (m, 2H), 6.19 (m, 2H), 6.12 (d, *J* = 10.0 Hz, 1H), 6.07 (dd, *J* = 3.6 Hz, 9.6 Hz, 1H), 6.01 (d, *J* = 10.4 Hz, 1H), 5.91 (d, *J* = 10.0 Hz, 1H), 5.79 (d, *J* = 10.8 Hz, 1H), 4.05-4.14 (m, 1H), 3.86-4.00 (m, 4H), 3.57-3.73 (m, 7H), 2.79-2.83 (m, 1H), 2.75 (d, *J* = 4.8 Hz, 3H), 2.35-2.46 (m, 2H), 2.25-2.33 (m, 1H), 1.75 (2x oct, *J* = 7.8 Hz, 1H+1H), 1.62 (oct, *J* = 7.8 Hz, 1H), 1.27-1.38 (m, 3H), 1.11-1.20 (m, 1H), 1.08 (d, *J* = 7.8 Hz, 3H), 1.06 (d, *J* = 7.8 Hz, 3H), 0.99 (d, *J* = 7.8 Hz, 3H+3H), 0.95 (d, *J* = 7.3 Hz, 3H), 0.93 (d, *J* = 7.8 Hz, 3H), 0.91 (d, *J* = 7.4 Hz, 3H), 0.90 (d, *J* = 7.8 Hz, 3H).

¹³C NMR (100 MHz, CD₃OH) δ (ppm) 162.2 (C), 162.2 (C), 162.0 (C), 161.9 (C), 161.5 (C), 161.0 (C), 157.8 (C), 143.3 (C), 139.6 (C), 133.4 (C), 133.1 (C), 130.1 (2 x CH), 129.6 (2 x CH), 127.6 (CH), 119.3 (2 x CH), 115.8 (CH), 56.3 (CH), 53.0 (CH), 49.6 (CH₂), 48.5 (CH₂), 47.4 (CH₃), 47.1 (CH₂), 46.5 (CH₂), 46.4 (CH₃), 46.3 (CH₂), 44.8 (CH₂), 44.0 (CH₂), 42.8 (CH₂), 40.0, 32.0 (CH), 27.0, 26.2 (CH), 26.0 (CH₃), 23.7 (CH₃), 23.6 (CH₃), 22.8 (CH₃), 22.6 (CH₃), 20.2 (CH₃), 18.9 (CH₃), 18.4 (CH₃), 18.4 (CH₃).

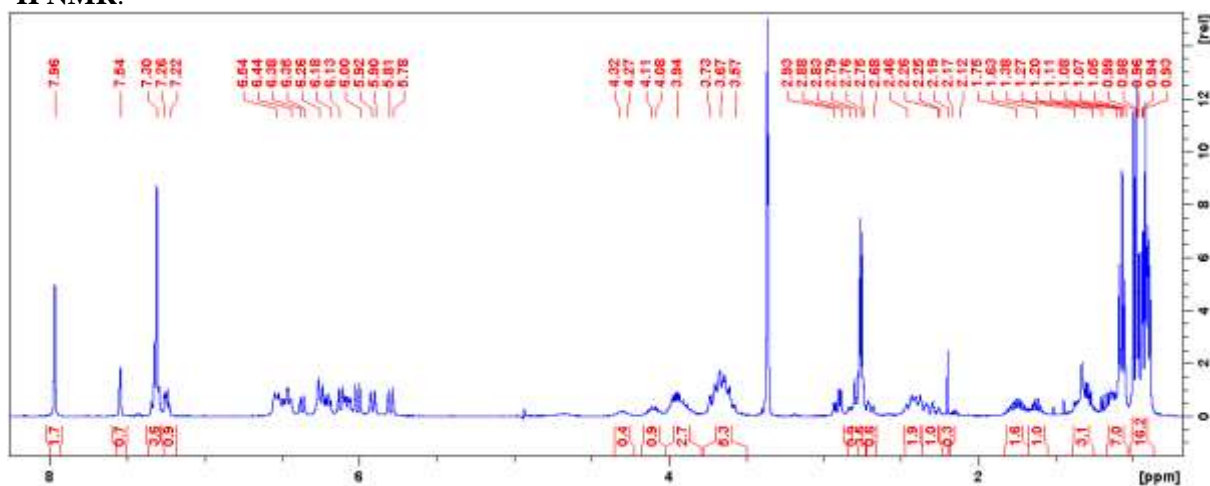
¹⁹F NMR (376 MHz, CD₃OH) δ (ppm) -64.7.

HRMS (ES⁺, MeOH) calcd for C₄₈H₇₆F₆N₁₄O₇ = 1075.59984 ; found: 1075.60095

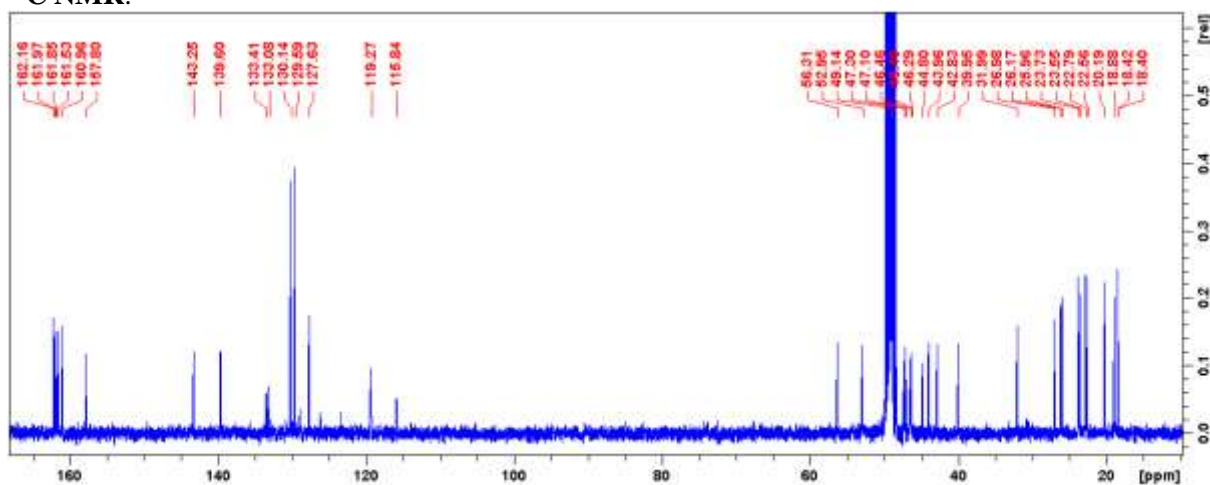
Table S13 : ^1H NMR Chemical Shifts (ppm) of 3,5-(CF_3) $_2\text{PhNHCO-Phe}^u\text{-Ala}^u\text{-Leu}^u\text{-Val}^u\text{-Ala}^u\text{-Leu}^u\text{-NHMe}$ (15) in CD_3OH at 293K

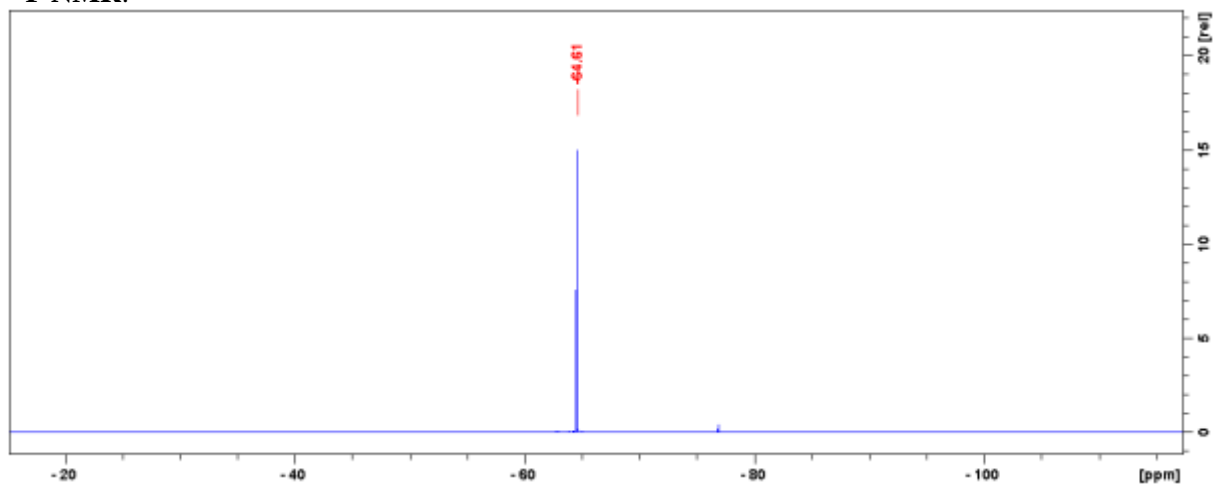
Residue		NH	NH'	αCH^1	αCH^2	βCH	γCH	δCH	ϵCH	Term CH	$\Delta\delta(\alpha\text{CH})$
ArNHCO			6.21								
Phe ^u	1	6.35	6.19	3.68	2.84	4.29					0.84
Ala ^u	2	6.00	6.46	3.60	2.39	4.09	1.08				1.21
Leu ^u	3	5.79	6.54	3.66	2.29	3.96	1.72	1.14	0.90+0.91		1.37
Val ^u	4	6.24	6.51	3.70	2.41	3.65	1.74	0.99			1.29
Alau	5	5.90	6.07	3.62	2.37	3.88	1.06				1.25
Leu ^u	6	6.11	6.44	3.66	2.44	3.94	1.72	1.10	0.95+0.96		1.22
NHMe		6.19								2.75	

^1H NMR:



^{13}C NMR:

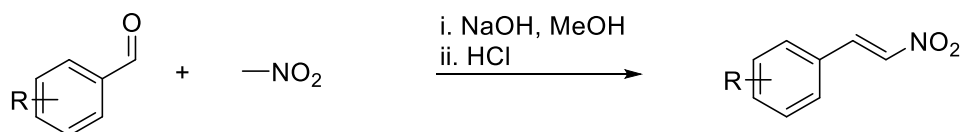


^{19}F NMR:

7.5 EXPERIMENTAL PART OF CHAPTER IV

7.5.1 General procedure for synthesis of nitroalkenes

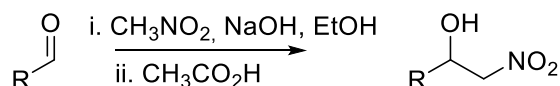
7.5.1.1 General procedure to synthesize aromatic nitroalkenes



Scheme S16: Synthesis of aromatic nitroalkenes

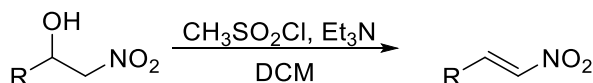
Aldehyde and nitromethane were solubilized in methanol and cooled down at 0°C. NaOH solution was added. Reaction mixture was stirred at 0°C for 15min. The resulting solution was added on 6NHCl solution. Desired compound was extracted with DCM. Organic combined layers were washed with brine, dried with MgSO₄, filtered and concentrated. The crude was triturated in Et₂O.

7.5.1.2 General procedure to synthesize aliphatic nitroalkenes



Scheme S17: Synthesis of aliphatic nitroalkene – Formation of nitroalcohol

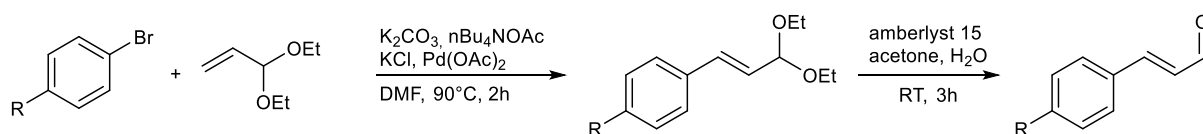
To an aldehyde (20 mmol, 1 eq.) and nitromethane (20 mmol, 1 eq.), solution in EtOH (5 mL), cooled at 0°C was added dropwise NaOH 6M (20 mmol, 1 eq.). Reaction mixture was stirred at room temperature for 10 min then acetic acid (2 mL) was added. Aqueous layer was extracted with Et₂O. Organic combined layers were washed with water till pH = 6, dried on MgSO₄, filtered and concentrated. Crude was directly used for next step without further purification.



Scheme S18: Synthesis of aliphatic nitroalkene - Elimination

To the previous alcohol (20 mmol, 1 eq.) solution in DCM (20 mL) was added sulfonyl chloride (20 mmol, 1 eq.) then trimethylamine (80 mmol, 4 eq.) at 0°C. Reaction mixture was stirred at 0°C for 45 min. Water was added and organic layer was recovered, washed with 1N HCl, brine, dried over MgSO₄, filtered and concentrated.

7.5.1.3 General procedure to synthesize aromatic conjugated nitroalkenes



Scheme S19 : Synthesis of conjugated aromatic aldehyde

Heck coupling

In a dry flask under N_2 loaded with the substituted bromophenyl (20 mmol) and diethyl acetal acrolein (9.73 mL, 60 mmol) dissolved in DMF (80 mL), were added K_2CO_3 (4.15 g, 30 mmol), tetrabutylammonium acetate (12.44 g, 40 mmol), potassium chloride (1.5 g, 20 mmol) and palladium (II) acetate (136 mg, 0.6 mmol, 3mol%). The resulting mixture was stirred at $90^\circ C$ for 2h.

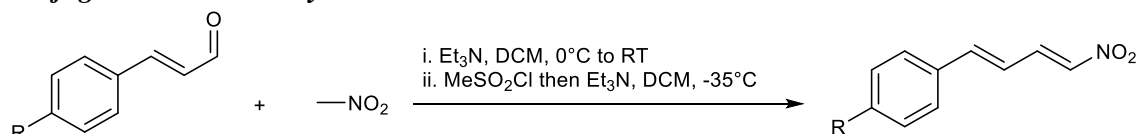
After cooling down the reaction mixture to room temperature were added diethyl ether (50 mL) and water (30 mL). Aqueous layer was extracted with Et_2O . Combined organic layers were washed with brine, dried over $MgSO_4$, filtered then concentrated. The crude was directly used for next step without further purification.

Acetal deprotection

In a flask loaded with the previous acetal in acetone (30 mL) with water (15 mL) was added the resin *Amberlyst 15* (600 mg), reaction mixture was vigorously stirred for 3h at room temperature.

Acetone was concentrated, aqueous layer was extracted with Et_2O . Combined organic layers were washed with brine, dried over $MgSO_4$, filtered then concentrated. Crude was purified on Silica Gel Chromatography with Hexane:EtOAc 95:5 to 90:10.

Conjugated nitroalkene synthesis

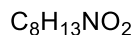
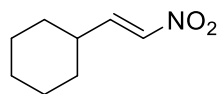


Scheme S20: Synthesis of conjugated aromatic nitroalkene

The procedure for nitromethane addition on the conjugated aldehyde was the same than for aliphatic nitroalkene (see 7.5.1.2).

7.5.1.4 Characterization of synthesized nitroalkenes

(E)-(2-nitrovinyl)cyclohexane

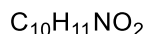
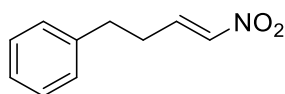


The crude was purified on Silica Gel Chromatography with Hexane:DCM gradient from 100:0 to 80:20.

$^1\text{H NMR}$ (CDCl_3 , 300MHz) δ (ppm) 7.31 (dd, $J = 7.9$ Hz, $J = 13.2$ Hz, 1H), 6.93 (dd, $J = 1.2$ Hz, $J = 13.5$ Hz, 1H), 2.17-2.29 (m, 1H), 1.70-1.83 (m, 5H), 1.13-1.41 (m, 6H).

$^{13}\text{C NMR}$ (CDCl_3 , 75MHz) δ (ppm) 138.4, 146.5, 138.4, 36.7, 31.6, 25.8, 25.7.

(E)-(4-nitrobut-3-en-1-yl) benzene

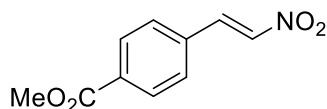


The crude was purified on Silica Gel Chromatography with Hexane:DCM gradient from 100:0 to 80:20.

$^1\text{H NMR}$ (CDCl_3 , 300MHz) δ (ppm) 6.38 (m, 5H), 4.41 (m, 2H), 2.72-2.94 (m, 2H), 1.87 (m, 2H).

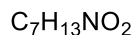
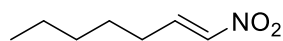
$^{13}\text{C NMR}$ (CDCl_3 , 75MHz) δ (ppm) 128.4, 128.6, 128.4, 126.3, 80.7, 67.9, 35.3, 31.4, 15.0.

(E)-methyl-4-(2-nitrovinyl)benzoate



$^1\text{H NMR}$ (CDCl_3 , 300MHz) δ (ppm) 8.10 (m, 2H), 8.01 (d, $J = 13.8$ Hz, 1H), 7.61 (m, 3H), 3.96 (s, 3H).

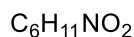
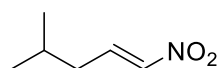
(E)-1-nitrohept-1-ene



$^1\text{H NMR}$ (CDCl_3 , 300MHz) δ (ppm) 7.33-7.42 (m, 1H), 6.98 (d, $J = 13.2$ Hz, 1H), 2.26 (qd, $J = 1.5$ Hz, $J = 7.3$ Hz, 2H), 1.47-1.57 (m, 3H), 1.31-1.57 (m, 6H).

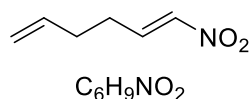
$^{13}\text{C NMR}$ (CDCl_3 , 75MHz) δ (ppm) 142.9, 139.7, 31.4, 31.1, 28.6, 26.6, 22.5, 14.0.

(E)-4-methyl-1-nitropent-1-ene



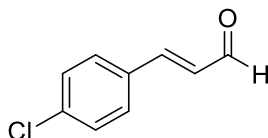
$^1\text{H NMR}$ (CDCl_3 , 300MHz) δ (ppm) 7.33-7.40 (m, 1H), 6.98 (dt, $J = 1.2$ Hz, $J = 13.5$ Hz, 1H), 2.15 (t, $J = 7.8$ Hz, 2H), 1.84 (sept., $J = 6.9$ Hz, 1H), 0.98 (s, 3H), 0.96 (s, 3H).

$^{13}\text{C NMR}$ (CDCl_3 , 75MHz) δ (ppm) 141.7, 140.3, 37.5, 23.0, 22.4.

(E)-1-nitrohexa-1,5-diene

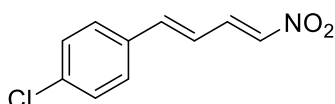
1H NMR ($CDCl_3$, 300MHz) δ (ppm) 7.37 (m, 1H), 6.99 (dt, $J = 1.5$ Hz, $J = 13.5$ Hz, 1H), 5.78 (sext.+dd, $J = 7.2$ Hz, $J = 2.4$ Hz, $J = 17.1$ Hz, 1H), 5.08 (m, 2H), 2.24-2.42 (m, 4H).

^{13}C NMR ($CDCl_3$, 75MHz) δ (ppm) 141.9, 140.0, 136.0, 117.6, 31.7, 27.8.

(E)-3-(4-chlorophenyl)acrylaldehyde

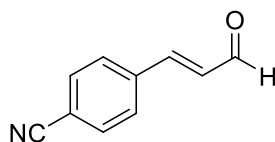
1H NMR ($CDCl_3$, 300MHz) δ (ppm) 9.70 (d, $J = 7.6$ Hz, 1H), 7.51-7.62 (m, 4H), 6.71 (d, $J = 7.8$ Hz, 1H), 6.66 (d, $J = 7.8$ Hz, 1H)

^{13}C NMR ($CDCl_3$, 75MHz) δ (ppm) 193.5, 151.2, 129.8, 129.6, 129.1

1-chloro-4-((1E,3E)-4-nitrobuta-1,3-dien-1-yl)benzene

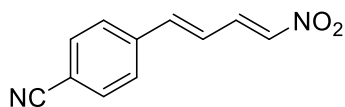
1H NMR (300 MHz, $CDCl_3$) δ (ppm) 7.79 (dd, $J = 11.4$ Hz, 12.9 Hz, 1H), 7.50-7.60 (m, 4H), 7.37 (d, $J = 13.2$ Hz, 1H), 7.13 (d, $J = 15.6$ Hz, 1H), 6.87 (dd, $J = 11.4$ Hz, 15.6 Hz, 1H).

^{13}C NMR (75 MHz, $CDCl_3$) δ (ppm) 144.5, 139.1, 138.8, 129.5, 129.0, 121.3.

(E)-4-(3-oxoprop-1-en-1-yl)benzotrile

1H NMR (300 MHz, $CDCl_3$) δ (ppm) 9.76 (d, $J = 7.6$ Hz, 1H), 7.69 (m, 4H), 7.58 (d, $J = 17.2$ Hz, 1H), 6.77 (dd, $J = 7.6$ Hz, 17.2 Hz, 1H).

^{13}C NMR (75 MHz, $CDCl_3$) δ (ppm) 193.0, 149.6, 138.3, 133.0, 131.3, 128.9.

4-((1E,3E)-4-nitrobuta-1,3-dien-1-yl)benzotrile

1H NMR (300 MHz, $CDCl_3$) δ (ppm) 7.69 (dd, $J = 11.4$ Hz, 13.2 Hz, 1H), 7.61-7.64 (m, 4H), 7.33 (d, $J = 12.9$ Hz, 1H), 7.08 (d, $J = 15.6$ Hz, 1H), 6.87 (dd, $J = 11.4$ Hz, 15.6 Hz, 1H).

^{13}C NMR (75 MHz, $CDCl_3$) δ (ppm) 143.1, 140.4, 137.8, 132.9, 128.1, 124.1

7.5.2 General procedure for the asymmetric conjugate addition of 1,3-dicarbonyl compounds to nitroalkenes

7.5.2.1 *Asymmetric reaction*

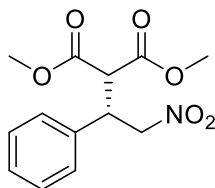
To a vial charged with **1a** (0.51 mg, 0.5 μ mol) were added the nitroalkene (0.5 mmol) and a solution of freshly distilled dimethyl malonate (0.11 mL, 1.0 mmol) in dry toluene (0.5 mL). The reaction mixture was cooled down to -20°C and tertiary amine (0.15 mmol) was added. After complete consumption of the nitroalkene, the reaction mixture was quenched with 1N hydrochloric acid solution, extracted three times with dichloromethane, washed with brine, dried over magnesium sulfate, filtered and concentrated. The crude was purified on Silica Gel Chromatography as described in Supporting Information. The enantiomeric excess was determined by Chiral HPLC as described in Supporting Information.

7.5.2.2 *Racemic reaction*

To a vial charged with the nitroalkene (0.5 mmol) in distilled DCM (500 μ L) and a solution of freshly distilled dimethyl malonate (0.11 mL, 1.0 mmol) was added triethylamine (520 μ L, 0.15 mmol) at room temperature. After complete consumption of the nitroalkene, the reaction mixture was quenched with 1N hydrochloric acid solution, extracted three times with dichloromethane, washed with brine, dried over magnesium sulfate, filtered and concentrated. The crude was purified on Silica Gel Chromatography as described in Supporting Information.

7.5.3 Characterisation of adducts 4, 18c-e, 16a with variation of malonate hindrance

(+)-(S)-Dimethyl 2-(2-nitro-1-phenylethyl)malonate (16a)



Chemical Formula: C₁₃H₁₅NO₆

Analytical data are consistent with previously reported valuesⁱⁱ.

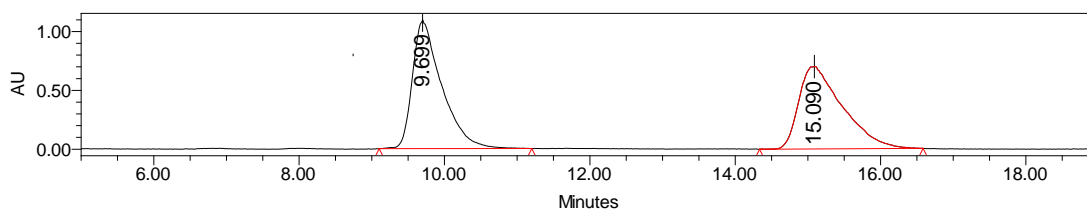
Purification on Silica Gel Chromatography with Hexane:Ethyl Acetate, from 90:10 to 80:20.

¹H NMR (300 MHz, CDCl₃) δ (ppm) 7.18-7.41 (m, 5H), 4.80-4.94 (m, 2H), 4.21 (dt, *J* = 5.4 Hz, *J* = 9.0 Hz, 1H), 3.70 (s, 3H), 3.50 (s, 3H).

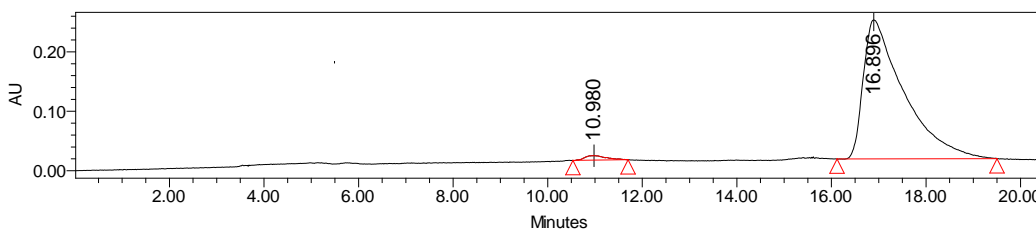
¹³C NMR (75 MHz, CDCl₃) δ (ppm) 168.43, 167.82, 136.59, 129.32, 128.72, 128.23, 77.54, 54.61, 52.82, 52.62, 42.77.

Enantiomeric excess of 97% was determined by HPLC [Chiralpak® AD-H ; flow: 1.0 mL/min ; hexane/*i*-PrOH: 75:25 ; λ = 210 nm ; major enantiomer *t*_R = 16.9 min ; minor enantiomer *t*_R = 11.0 min]. [α]_D²³ + 22.7 (c 0.18, CH₂Cl₂, 97% *ee*)

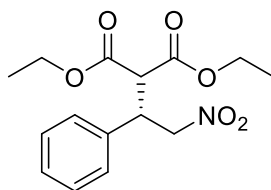
HPLC traces:



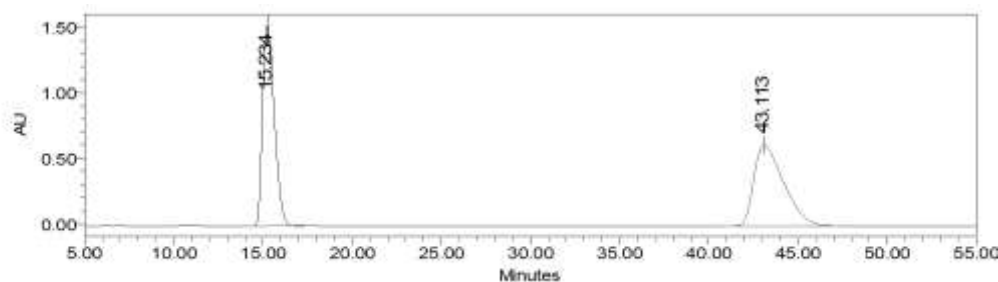
	Retention Time	% Area
1	15.090	48.84
2	9.699	51.16



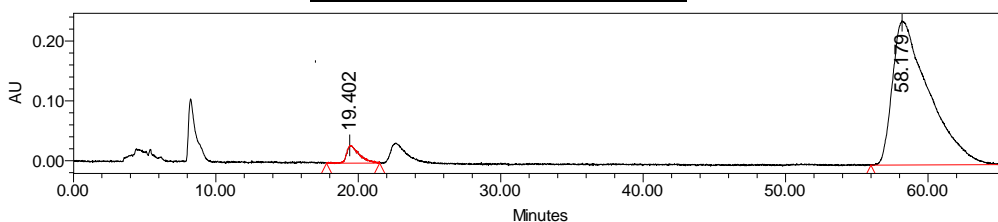
	Retention Time	% Area
1	10.980	1.68
2	16.896	98.32

(+)-(S)-Diethyl 2-(2-nitro-1-phenylethyl)malonate (4)Chemical Formula: C₁₅H₁₉NO₆Analytical data are consistent with previously reported values⁸.

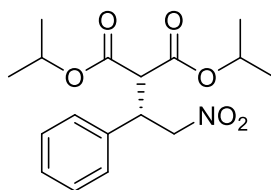
Purification on Silica Gel Chromatography with Hexane:Ethyl Acetate, from 95:5 to 80:20.

¹H NMR (300 MHz, CDCl₃) δ (ppm) 7.16-7.35 (m, 5H), 4.83 (m, 2H), 4.13 (m, 3H), 3.91 (q, *J* = 7.3 Hz, 2H), 3.75 (d, *J* = 9.3 Hz, 1H), 1.19 (t, *J* = 8.1 Hz, 3H), 0.98 (t, *J* = 7.3 Hz, 3H).¹³C NMR (75 MHz, CDCl₃) δ (ppm) 168.2, 167.6, 136.8, 129.4, 128.8, 128.5, 77.8, 62.2, 61.9, 55.0, 42.9, 13.7, 13.5.Enantiomeric excess of 92% was determined by HPLC [Chiralpak® AD-H; flow: 1.0 mL/min ; hexane/*i*-PrOH: 90:10 ; λ = 210 nm ; major enantiomer *t*_R = 58.2 min ; minor enantiomer *t*_R = 19.4 min]. [α]_D²³ + 30.8 (c 0.11, CH₂Cl₂, 92% *ee*)**HPLC traces:**

	Retention Time	% Area
1	15.234	49.43
2	43.113	50.57



	Retention Time	% Area
1	19.402	4.06
2	58.179	95.94

(+)-(S)-Diisopropyl 2-(2-nitro-1-phenylethyl)malonate (16c)Chemical Formula: C₁₇H₂₃NO₆

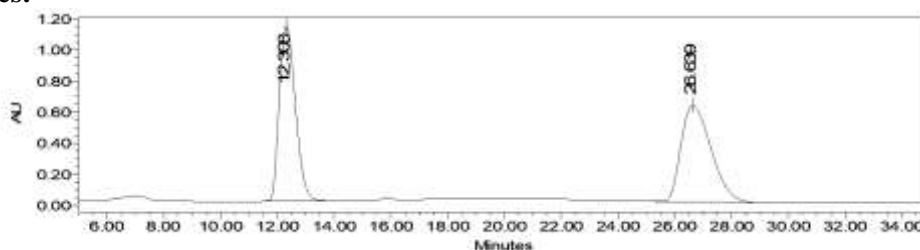
Analytical data are consistent with previously reported valuesⁱⁱⁱ.

Purification on Silica Gel Chromatography with Hexane:Ethyl Acetate, from 95:5 to 90:10.

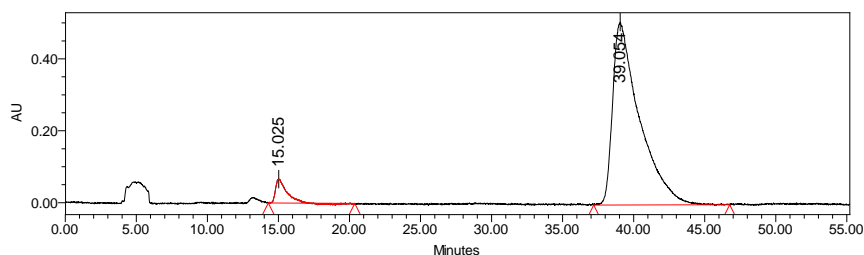
¹H NMR (300 MHz, CDCl₃) δ (ppm) 7.18-7.31 (m, 5H), 5.01 (quint, *J* = 7.3 Hz, 1H), 4.73-4.89 (m, 3H), 4.13 (dt, *J* = 4.8 Hz, 9.6Hz, 1H), 3.68 (d, *J* = 9.6 Hz, 1H), 1.17 (d, *J* = 7.3 Hz, 6H), 0.99 (d, *J* = 7.3 Hz, 3H), 0.94 (d, *J* = 7.3 Hz, 3H).

¹³C NMR (75 MHz, CDCl₃) δ (ppm) 167.0, 166.4, 137.3, 128.8, 128.3, 128.1, 77.9, 69.9, 69.5, 55.2, 42.9, 21.6, 21.4, 21.2.

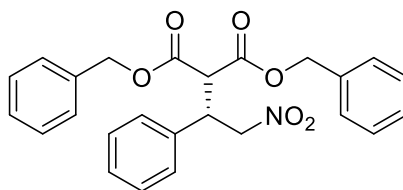
Enantiomeric excess of 89% was determined by HPLC [Chiralpak® AD-H ; flow: 1.0 mL/min ; hexane/*i*-PrOH: 90:10 ; λ = 210 nm ; major enantiomer *t*_R = 39.1 min ; minor enantiomer *t*_R = 15.0 min]. [α]_D²³ + 9.0 (c 0.3, CH₂Cl₂, 89% *ee*)

HPLC traces:

	Retention Time	% Area
1	12.308	49.57
2	27.639	50.43



	Retention Time	% Area
1	15.025	5.69
2	39.054	94.31

(S)-Dibenzyl 2-(2-nitro-1-phenylethyl)malonate (16d)Chemical Formula: C₂₅H₂₃NO₆

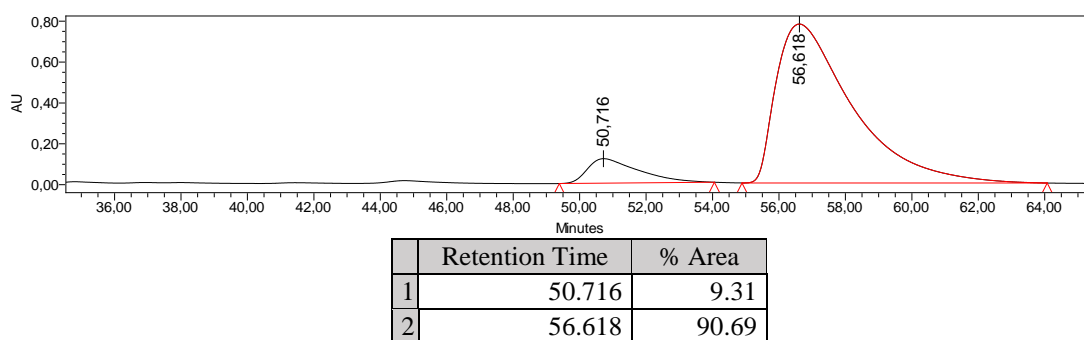
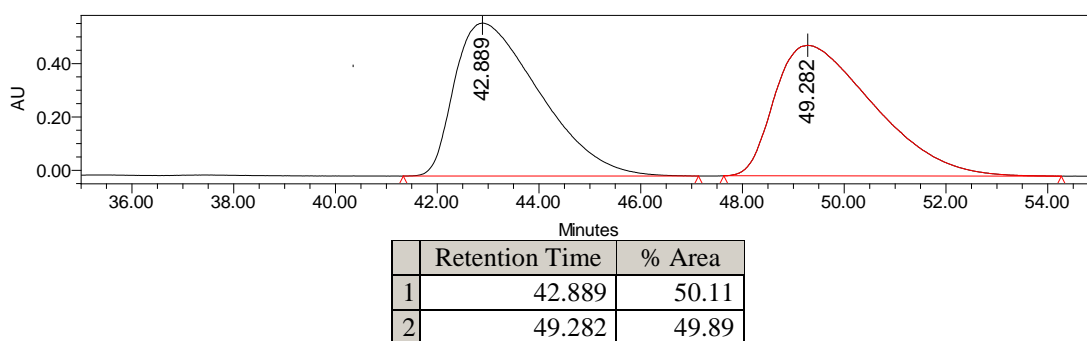
Analytical data are consistent with previously reported values⁸.

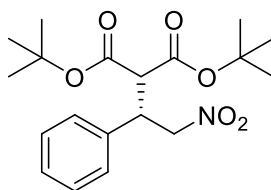
Purification on Silica Gel Chromatography with Hexane:Ethyl Acetate, from 90:10 to 80:20.

¹H NMR (300 MHz, CDCl₃) δ (ppm) 7.69-7.97 (m, 15H), 4.79 (d, *J* = 2.7 Hz), 4.56 (s, 2H), 4.47 (dd, *J* = 5.4 Hz, 3.0 Hz, 2H), 3.90 (td, *J* = 5.7 Hz, 9.0 Hz, 1H), 3.58 (d, *J* = 9.3 Hz, 1H).

¹³C NMR (75 MHz, CDCl₃) δ (ppm) 167.74, 167.13, 136.42, 135.17, 135.08, 129.31, 128.97, 128.93, 128.86, 128.77, 128.65, 128.56, 128.29, 77.54, 67.70, 67.62, 54.80, 42.76.

Enantiomeric excess of 81% was determined by HPLC [Chiralpak® AD-H ; flow: 0.75 mL/min ; hexane/*i*-PrOH: 90:10 ; λ = 210 nm ; major enantiomer *t*_R = (50.7 min; minor enantiomer *t*_R = 57.6 min)].

HPLC traces:

***rac*-Di-*tert*-butyl 2-(2-nitro-1-phenylethyl)malonate (16e)**Chemical Formula: C₁₉H₂₇NO₆

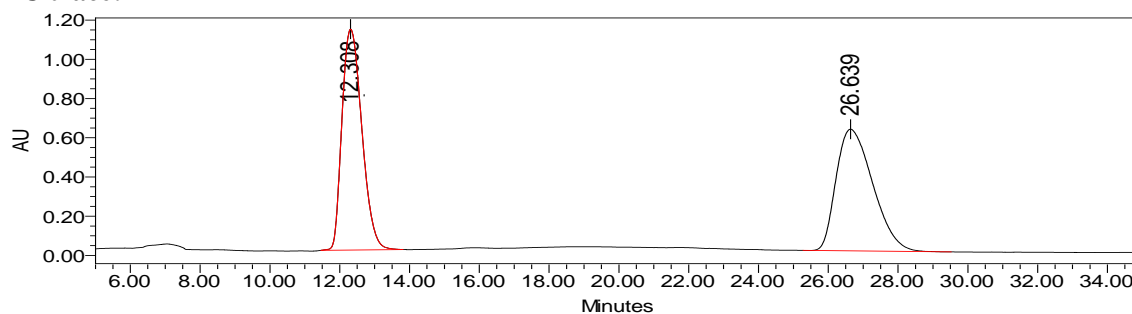
Analytical data are consistent with previously reported values^{iv}.

Purification on Silica Gel Chromatography with Hexane:Ethyl Acetate, from 100:0 to 95:5.

¹H NMR (300 MHz, CDCl₃) δ (ppm) 7.33-7.42 (m, 5H), 4.93 (dd, *J* = 4.5 Hz, *J* = 12.9 Hz, 1H), 4.80 (dd, *J* = 9.6 Hz, *J* = 12.9 Hz, 1H), 4.12 (dt, *J* = 4.5 Hz, *J* = 9.6 Hz, 1H), 3.62 (d, *J* = 7.6 Hz, 1H), 1.47 (s, 9H), 1.23 (s, 9H).

¹³C NMR (75 MHz, CDCl₃) δ (ppm) 167.6, 166.7, 137.1, 129.2, 128.8, 128.6, 83.1, 82.5, 78.4, 57.5, 43.0, 27.7, 27.4.

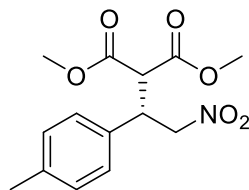
Enantiomers were separated by HPLC [Chiralpak® AD-H ; flow: 0.5 mL/min ; hexane/*i*-PrOH: 70:30 ; λ = 210 nm ; t_R = 12.3 min ; t_R = 27.6 min].

HPLC trace:

	% Area	Retention Time
1	49.57	12.308
2	50.43	27.639

7.5.4 Characterisation of adducts 21b-21l with variation around aromatic nitroalkenes

(+)-(S)-Dimethyl 2-(2-nitro-1-(*p*-tolyl)ethyl)malonate (21b)



Chemical Formula: C₁₄H₁₇NO₆

Analytical data are consistent with previously reported values⁸.

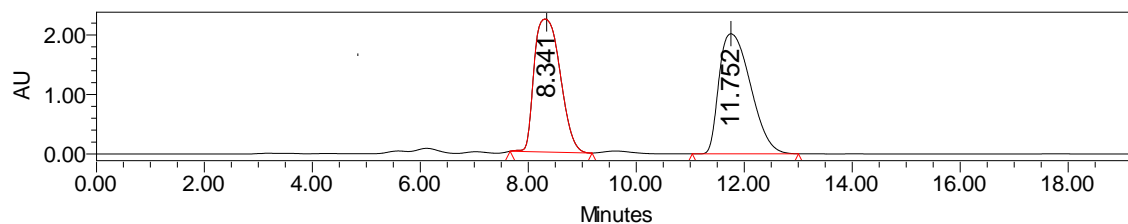
Purification on Silica Gel Chromatography with Hexane:Ethyl Acetate, from 90:10 to 80:20.

¹H NMR (300 MHz, CDCl₃) δ (ppm) 7.26 (s, 4H), 4.95-5.09 (m, 2H), 4.35 (dt, *J* = 5.4 Hz, *J* = 9.0 Hz, 1H), 3.99 (d, *J* = 9.0 Hz, 1H), 3.90 (s, 3H), 3.71 (s, 3H), 2.45 (s, 3H).

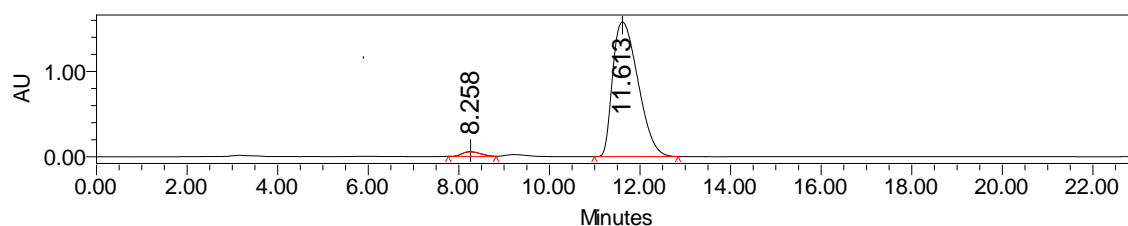
¹³C NMR (75 MHz, CDCl₃) δ (ppm) 168.5, 167.9, 138.6, 133.5, 130.1, 128.1, 77.6, 54.7, 52.8, 52.7, 42.5, 30.6, 20.7.

Enantiomeric excess of 95% was determined by HPLC [Chiralpak® AD-H ; flow: 1.0 mL/min; hexane/*i*-PrOH: 75:25 ; λ = 210 nm ; major enantiomer *t*_R = 11.6 min ; minor enantiomer *t*_R = 8.3 min].
[α]_D²³ + 2.9 (c 0.42, CH₂Cl₂, 95% *ee*)

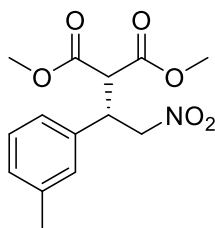
HPLC traces:



	Retention Time	% Area
1	8.341	47.76
2	11.752	52.24



	Retention Time	% Area
1	8.258	2.37
2	11.613	97.63

(+)-(S)-Dimethyl 2-(2-nitro-1-(*m*-tolyl)ethyl)malonate (21c)Chemical Formula: C₁₄H₁₇NO₆

Analytical data are consistent with previously reported values^v.

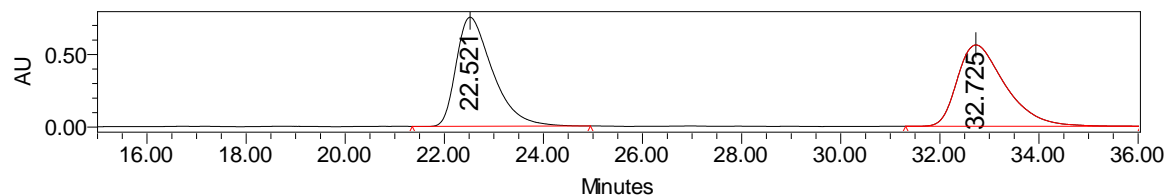
Purification on Silica Gel Chromatography with Hexane:Ethyl Acetate 90:10.

¹H NMR (300 MHz, CDCl₃) δ (ppm) 7.34-7.56 (m, 4H), 5.06-5.19 (m, 2H), 4.20 (dt, *J* = 5.7 Hz, *J* = 8.7 Hz, 2H), 4.08 (d, *J* = 9.0 Hz, 1H), 3.99 (s, 3H), 3.81 (s, 3H), 2.55 (s, 3H).

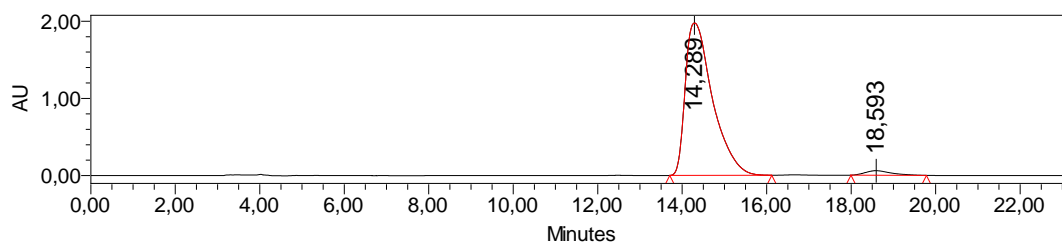
¹³C NMR (75 MHz, CDCl₃) δ (ppm) 168.0, 167.5, 138.8, 136.2, 129.3, 129.0, 128.8, 124.8, 77.7, 77.68, 54.9, 53.1, 52.9, 43.0, 21.5.

Enantiomeric excess of 94% was determined by HPLC [Chiralpak® IC ; flow: 1.0 mL/min ; hexane/*i*-PrOH: 90:10 ; λ = 210 nm ; major enantiomer *t*_R = 14.3 min ; minor enantiomer *t*_R = 18.6 min].

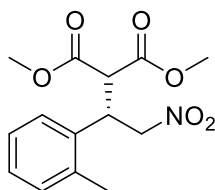
[α]_D²³ + 5.2 (c 0.51, CH₂Cl₂, 94% *ee*)

HPLC traces:

	Retention Time	% Area
1	32.725	49.60
2	22.521	50.40



	Retention Time	% Area
1	14.289	97.21
2	18.593	2.79

(+)-(S)-Dimethyl 2-(2-nitro-1-(*o*-tolyl)ethyl)malonate (21d)Chemical Formula: C₁₄H₁₇NO₆

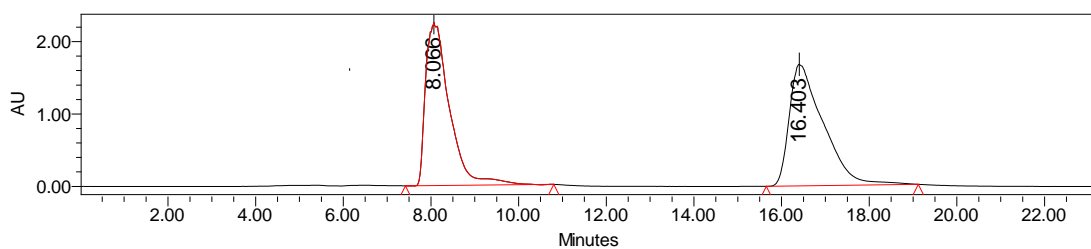
Analytical data are consistent with previously reported values^{vi}.

Purification on Silica Gel Chromatography with Hexane:Ethyl Acetate, from 90:10 to 80:20.

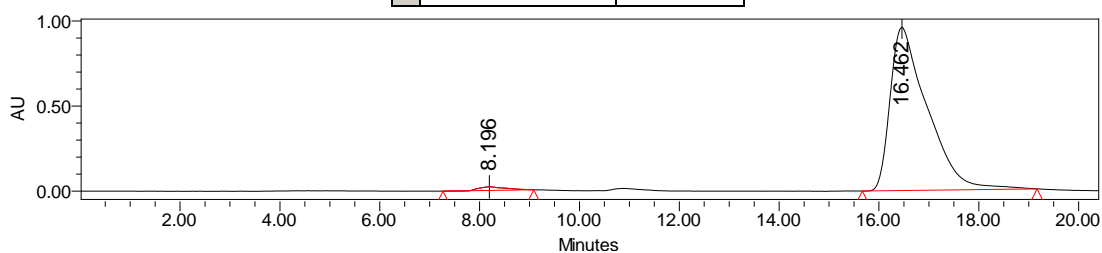
¹H NMR (300 MHz, CDCl₃) δ (ppm) 7.30-7.37 (m, 4H), 4.91-5.05 (m, 2H), 4.68 (dt, *J* = 5.4 Hz, *J* = 8.7 Hz, 1H), 3.86 (s, 3H), 3.63 (s, 3H), 2.54 (s, 3H).

¹³C NMR (75 MHz, CDCl₃) δ (ppm) 168.1, 167.5, 137.1, 134.6, 131.4, 128.2, 126.6, 125.9, 77.5, 54.6, 53.1, 52.9, 37.9, 19.5.

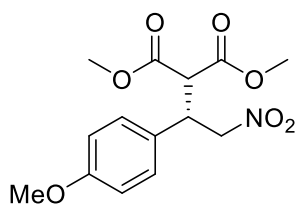
Enantiomeric excess of 97% was determined by HPLC [Chiralpak® AD-H ; flow: 1.0 mL/min ; hexane/*i*-PrOH: 75:25 ; λ = 210 nm ; major enantiomer *t*_R = 17.5 min ; minor enantiomer *t*_R = 8.2 min]. [α]_D²³ + 5.2 (c 0.54, CH₂Cl₂, 97% *ee*)

HPLC traces:

	Retention Time	% Area
1	8.066	48.49
2	16.403	51.51



	Retention Time	% Area
1	8.196	1.60
2	16.462	98.40

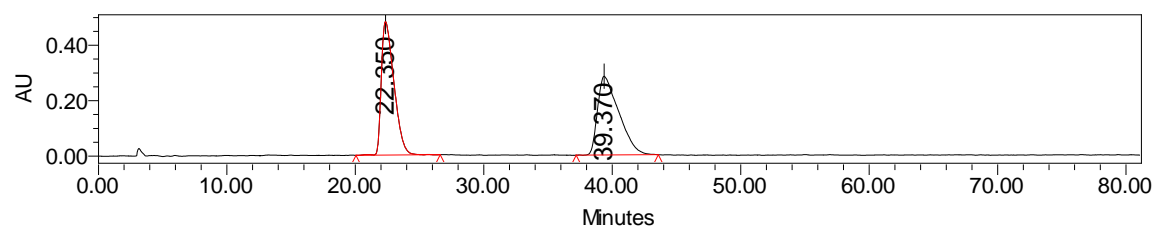
(+)-(S)-Dimethyl 2-(1-(4-methoxyphenyl)-2-nitroethyl)malonate (21e)Chemical Formula: C₁₄H₁₇NO₇Analytical data are consistent with previously reported values⁸.

Purification on Silica Gel Chromatography with Hexane:Ethyl Acetate, 80:20.

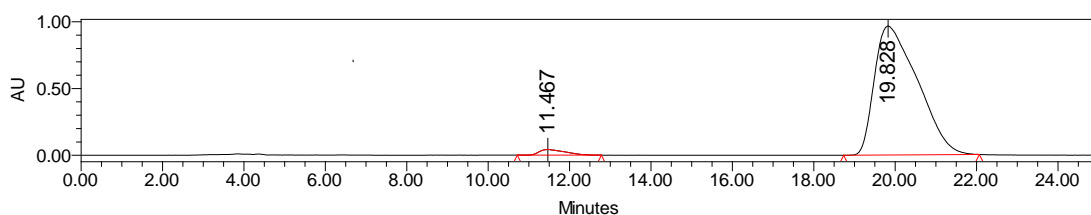
¹H NMR (300 MHz, CDCl₃) δ (ppm) 7.14 (d, *J* = 9.0 Hz, 2H), 7.83 (d, *J* = 8.7 Hz, 2H), 4.78-4.92 (m, 2H), 4.18 (dt, *J* = 5.4 Hz, *J* = 9.0 Hz, 1H), 3.82 (d, *J* = 9.3 Hz, 1H), 3.77 (s, 3H), 3.76 (s, 3H), 3.57 (s, 3H).

¹³C NMR (75 MHz, CDCl₃) δ (ppm) 167.8, 167.3, 159.4, 128.9, 127.8, 114.3, 76.5, 55.1, 54.8, 52.9, 52.7, 42.2.

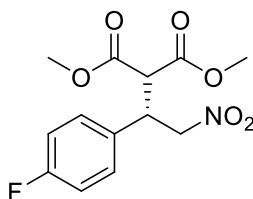
Enantiomeric excess of 95% was determined by HPLC [Chiralpak® AD-H ; flow: 1.0 mL/min ; hexane/*i*-PrOH: 90:10 ; λ = 210 nm ; major enantiomer *t*_R = 19.8 min ; minor enantiomer *t*_R = 11.5 min]. [α]_D²³ + 17.2 (c 0.38, CH₂Cl₂, 95% *ee*)

HPLC traces:

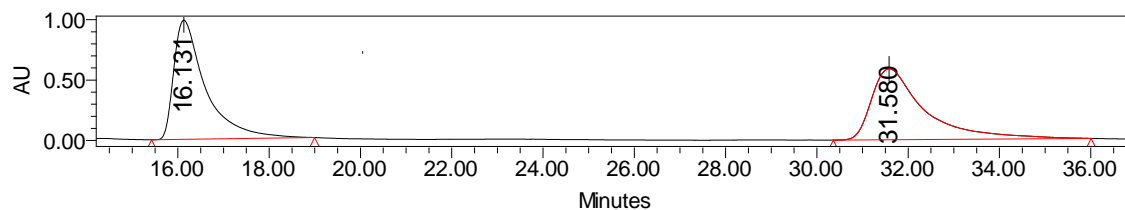
	Retention Time	% Area
1	22.350	50.24
2	39.370	49.76



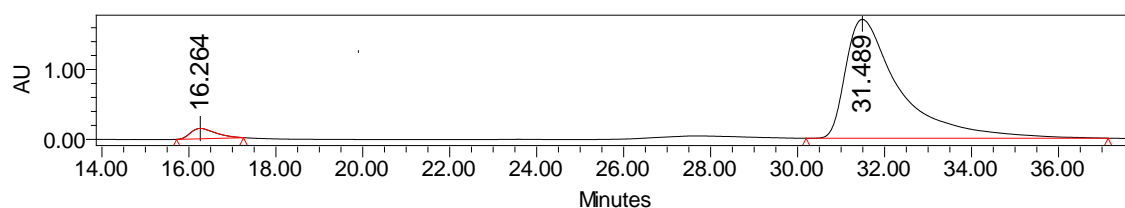
	Retention Time	% Area
1	11.467	2.52
2	19.828	97.58

(+)-(S)-Dimethyl 2-(1-(4-fluorophenyl)-2-nitroethyl)malonate (21f)Chemical Formula: C₁₃H₁₄FNO₆Analytical data are consistent with previously reported values⁸.

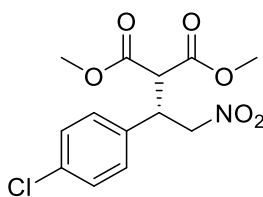
Purification on Silica Gel Chromatography with Hexane:Ethyl Acetate from 90:10 to 80:20.

¹H NMR (300 MHz, CDCl₃) δ (ppm) 7.13-7.19 (m, 2H), 7.92-7.98 (m, 2H), 4.82 (dq, *J* = 5.1 Hz, 13.2 Hz, 2H), 4.15 (sext, *J* = 5.1 Hz, 1H), 3.76 (d, *J* = 9.0 Hz, 1H), 3.70 (s, 3H), 3.51 (s, 3H).¹³C NMR (75 MHz, CDCl₃) δ (ppm) 167.8, 167.3, 164.3, 161.0, 129.9, 129.8, 116.3, 116.0, 77.6, 54.8, 53.2, 53.0, 42.4.Enantiomeric excess of 92% was determined by HPLC [Chiralpak® IA ; flow: 1.0 mL/min ; hexane/*i*-PrOH: 90:10 ; λ = 210 nm ; major enantiomer *t*_R = 31.5 min ; minor enantiomer *t*_R = 17.3 min].[α]_D²³ + 11.8 (c 0.17, CH₂Cl₂, 92% *ee*)**HPLC traces:**

	Retention Time	% Area
1	16.131	50.21
2	31.580	49.79



	Retention Time	% Area
1	16.264	3.90
2	31.489	96.10

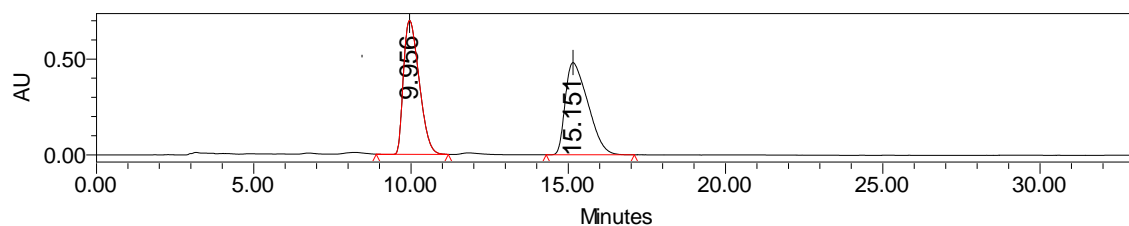
(+)-(S)-Dimethyl 2-(1-(4-chlorophenyl)-2-nitroethyl)malonate (21g)Chemical Formula: C₁₃H₁₄ClNO₆

Analytical data are consistent with previously reported values⁸.

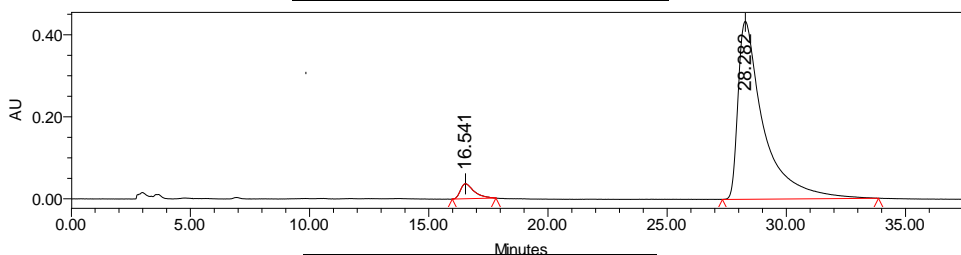
Purification on Silica Gel Chromatography with Hexane:Ethyl Acetate, from 90:10 to 80:20.

¹H NMR (300 MHz, CDCl₃) δ (ppm) 7.37-7.41 (m, 2H), 7.17-7.31 (m, 2H), 4.81-4.95 (m, 2H), 4.23 (dt, *J* = 5.4 Hz, *J* = 9.0 Hz, 1H), 3.82 (d, *J* = 9.0 Hz, 1H), 3.77 (s, 3H), 3.59 (s, 3H). ¹³C NMR (75 MHz, CDCl₃) δ (ppm) 167.93, 167.46, 135.00, 134.73, 129.63, 77.60, 54.85, 53.41, 53.26, 42.67.

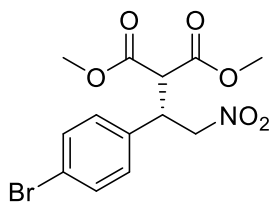
Enantiomeric excess of 91% was determined by HPLC [Chiralpak® AD-H ; flow: 1.0 mL/min ; hexane/*i*-PrOH: 90:10 ; λ = 210 nm ; major enantiomer *t*_R = 28.3 min ; minor enantiomer *t*_R = 16.5 min]. [α]_D²³ + 42.2 (c 0.16, CH₂Cl₂, 91% *ee*)

HPLC traces:

	Retention Time	% Area
1	9.956	50.19
2	15.151	49.81



	Retention Time	% Area
1	16.541	4.34
2	28.282	95.66

(+)-(S)-Dimethyl 2-(1-(4-bromophenyl)-2-nitroethyl)malonate (21h)Chemical Formula: C₁₃H₁₄BrNO₆

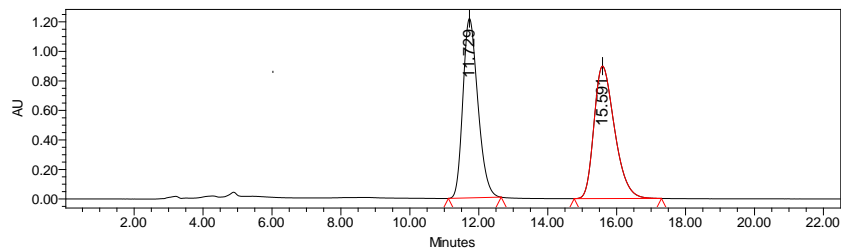
Analytical data are consistent with previously reported values⁸.

Purification on Silica Gel Chromatography with Hexane:Ethyl Acetate from 90:10 to 70:30.

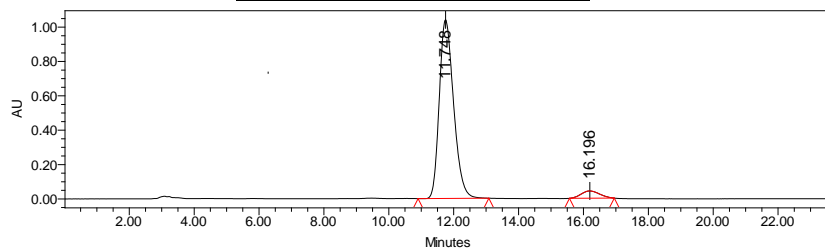
¹H NMR (300 MHz, CDCl₃) δ (ppm) 7.48 (d, *J* = 8.4 Hz, 2H), 7.05 (d, *J* = 8.4 Hz, 2H), 4.81 (dq, *J* = 5.1 Hz, 13.2Hz, 2H), 4.14 (td, *J* = 5.1 Hz, 9.0Hz, 1H), 3.76 (d, *J* = 9.3 Hz, 1H), 3.68 (s, 3H), 3.51 (s, 3H).

¹³C NMR (75 MHz, CDCl₃) δ (ppm) 167.6, 167.1, 135.3, 132.2, 129.7, 122.6, 77.3, 54.5, 53.2, 53.0, 42.4

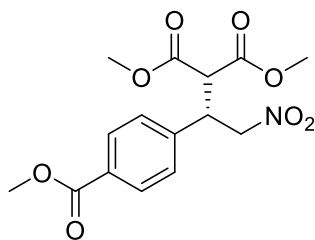
Enantiomeric excess of 90% was determined by HPLC [Chiralpak® OD-H ; flow: 1.0 mL/min ; hexane/*i*-PrOH: 70:30 ; λ = 210 nm ; major enantiomer *t*_R = 11.7 min ; minor enantiomer *t*_R = 16.2 min]. [α]_D²³ + 18.2 (c 0.22, CH₂Cl₂, 90% *ee*)

HPLC traces:

	Retention Time	% Area
1	11.729	49.70
2	15.591	50.30



	Retention Time	% Area
1	11.748	95.03
2	16.196	4.97

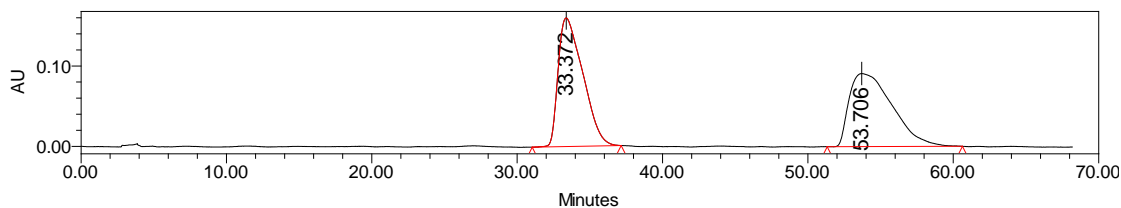
(+)-(S)-Dimethyl 2-(1-(4-(methoxycarbonyl)phenyl)-2-nitroethyl)malonate (21i)Chemical Formula: C₁₅H₁₇NO₈

Purification on Silica Gel Chromatography with Hexane:Ethyl Acetate from 90:10 to 80:20.

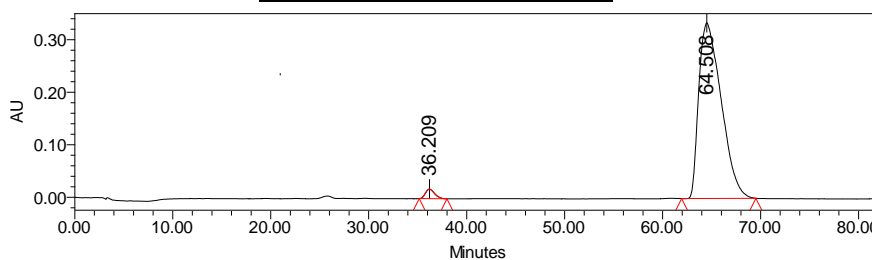
¹H NMR (300 MHz, CDCl₃) δ (ppm) 7.99 (d, *J* = 8.4 Hz, 2H), 7.42 (d, *J* = 8.4 Hz, 2H), 4.92 (dq, *J* = 5.7 Hz, 13.5Hz, 2H), 4.31 (dt, *J* = 5.7 Hz, 8.7Hz, 1H), 3.90 (s, 3H), 3.86 (d, *J* = 9.0 Hz, 1H), 3.76 (s, 3H), 3.57 (s, 3H).

¹³C NMR (75 MHz, CDCl₃) δ (ppm) 167.8, 167.3, 166.6, 141.5, 130.5, 128.2, 77.3, 54.6, 53.3, 53.2, 52.4, 43.0, 31.1.

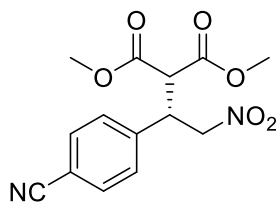
Enantiomeric excess of 95% was determined by HPLC [Chiralpak® AD-H ; flow: 1.0 mL/min ; hexane/*i*-PrOH: 90:10 ; λ = 210 nm ; major enantiomer *t*_R = 64.5 min ; minor enantiomer *t*_R = 37.2 min]. [α]_D²³ + 11.5 (c 0.23, CH₂Cl₂, 95% *ee*)

MS (ES⁺, MeOH): 340.11 ([M+H]⁺)**HPLC traces:**

	Retention Time	% Area
1	33.372	50.14
2	53.706	49.86



	Retention Time	% Area
1	36.209	2.17
2	64.508	97.83

(+)-(S)-Dimethyl 2-(1-(4-cyanophenyl)-2-nitroethyl)malonate (21j)Chemical Formula: C₁₄H₁₄N₂O₆Analytical data are consistent with previously reported values^{vii}.

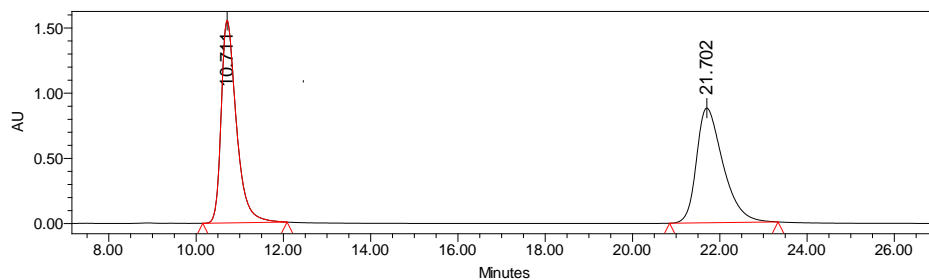
Purification on Silica Gel Chromatography with Hexane:Ethyl Acetate from 80:20 to 70:30.

¹H NMR (300 MHz, CDCl₃) δ (ppm) 7.62 (d, *J* = 8.4 Hz, 2H), 7.47 (d, *J* = 8.4 Hz, 2H), 4.92 (dq, *J* = 5.4 Hz, 13.5Hz, 2H), 4.31 (dt, *J* = 5.4 Hz, 8.7Hz, 1H), 3.84 (d, *J* = 9.0 Hz, 1H), 3.77 (s, 3H), 3.60 (s, 3H).

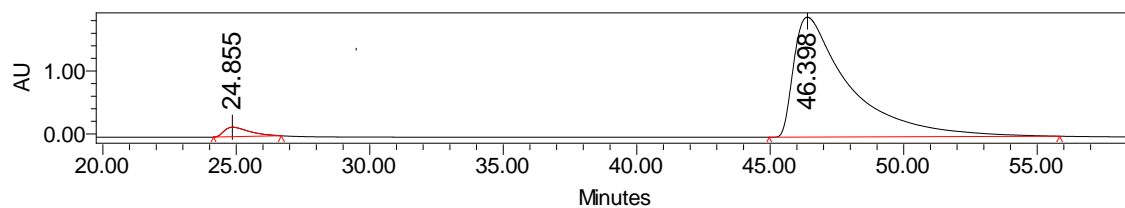
¹³C NMR (75 MHz, CDCl₃) δ (ppm) 167.6, 166.9, 141.7, 132.9, 129.0, 118.2, 112.8, 76.7, 54.3, 53.4, 53.2, 42.9.

Enantiomeric excess of 93% was determined by HPLC [Chiralpak® IA ; flow: 1.0 mL/min ; hexane/*i*-PrOH: 70:30 ; λ = 210 nm ; major enantiomer *t*_R = 47.4 min ; minor enantiomer *t*_R = 24.9 min].

[α]_D²³ + 12.8 (c 0.58, CH₂Cl₂, 93% *ee*)

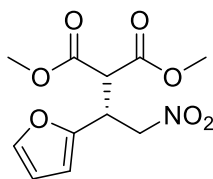
HPLC traces:

	Retention Time	% Area
1	10.711	50.27
2	21.702	49.73



	Retention Time	% Area
1	24.855	3.47
2	47.398	97.53

(-)-Dimethyl (R)-2-(1-(furan-2-yl)-2-nitroethyl)malonate (21k)



Chemical Formula: C₁₁H₁₃NO₇

Analytical data are consistent with previously reported values¹¹.

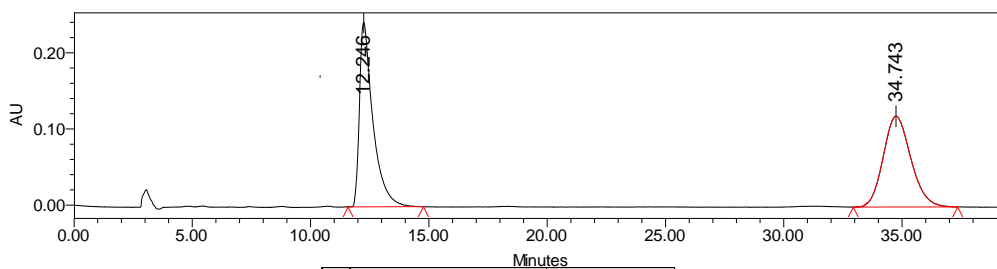
Purification on Silica Gel Chromatography with Hexane:Ethyl Acetate from 90:10 to 80:20.

¹H NMR (300 MHz, CDCl₃) δ (ppm) 7.44 (t, *J* = 0.9 Hz, 1H), 7.29 (d, *J* = 1.8 Hz, 1H), 7.21 (t, *J* = 3.3 Hz, 1H), 4.85-4.96 (m, 2H), 4.39 (dt, *J* = 5.4 Hz, *J* = 7.8 Hz, 1H), 3.93 (d, *J* = 7.8 Hz, 1H), 3.75 (s, 3H), 3.69 (s, 3H).

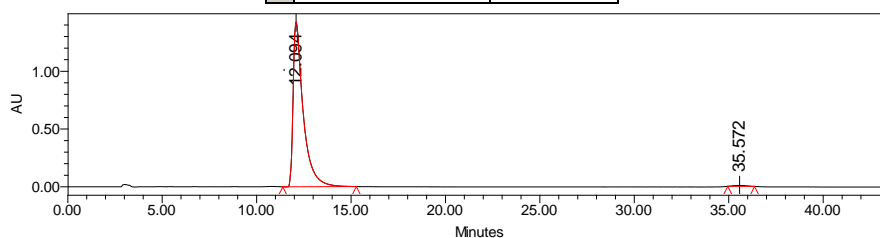
¹³C NMR (75 MHz, CDCl₃) δ (ppm) 167.6, 167.4, 149.5, 143.0, 110.7, 108.5, 75.4, 53.2, 52.8, 37.0.

Enantiomeric excess of 98% was determined by HPLC [Chiralpak® OD-H ; flow: 1.0 mL/min ; hexane/*i*-PrOH: 90:10 ; λ = 210 nm ; major enantiomer *t*_R = 12.1 min ; minor enantiomer *t*_R = 35.6 min]. [α]_D²³ - 2.8 (c 0.64, CH₂Cl₂, *ee* 98%)

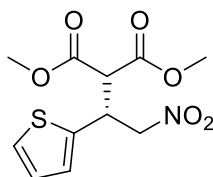
HPLC traces:



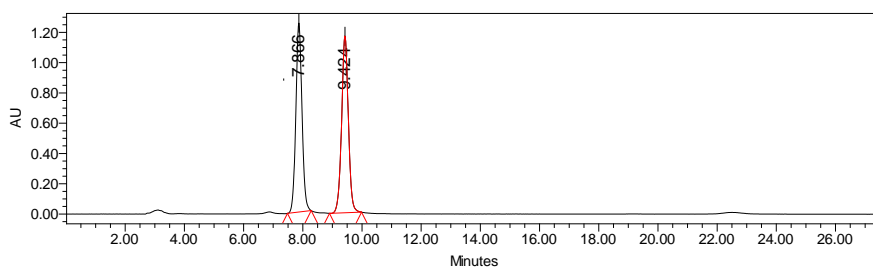
	Retention Time	% Area
1	12.246	49.72
2	34.743	50.28



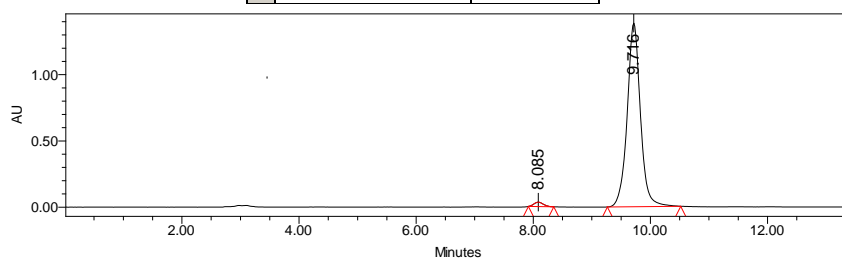
	Retention Time	% Area
1	12.094	99.22
2	35.572	0.78

(-)-Dimethyl (R)-2-(2-nitro-1-(thiophen-2-yl)ethyl)malonate (211)Chemical Formula: C₁₁H₁₃NO₆SAnalytical data are consistent with previously reported values⁸.

Purification on Silica Gel Chromatography with Hexane:Ethyl Acetate from 90:10 to 80:20.

¹H NMR (300 MHz, CDCl₃) δ (ppm) 7.31-7.33 (m, 1H), 7.91-7.95 (m, 2H), 4.86-4.98 (m, 2H), 4.57 (dt, *J* = 5.7 Hz, *J* = 7.8 Hz, 1H), 3.91 (d, *J* = 7.8 Hz, 1H), 3.76 (s, 3H), 3.66 (s, 3H).¹³C NMR (75 MHz, CDCl₃) δ (ppm) 167.7, 167.3, 138.5, 127.3, 126.8, 125.7, 77.9, 53.4, 53.2, 38.5.Enantiomeric excess of 97% was determined by HPLC [Chiralpak® IA ; flow: 1.0 mL/min ; hexane/*i*-PrOH: 80:20 ; λ = 210 nm ; major enantiomer *t*_R = 9.7 min ; minor enantiomer *t*_R = 8.1 min].[α]_D²³ + 7.0 (c 0.40, CH₂Cl₂, 97% *ee*)**HPLC traces:**

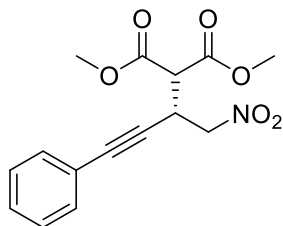
	Retention Time	% Area
1	7.866	49.30
2	9.424	50.70



	Retention Time	% Area
1	8.085	1.70
2	9.716	98.30

7.5.5 Adducts 22a-22d from aromatic conjugated nitroalkenes

(+)-Dimethyl-(S)-2-(1-nitro-4-phenylbut-3-yn-2-yl)malonate (22a)



Chemical Formula: C₁₅H₁₅NO₆

Analytical data are consistent with previously reported values^{viii}.

Purification on Silica Gel Chromatography with Hexane:Ethyl Acetate from 95:5 to 80:20.

¹H NMR (300 MHz, CDCl₃) δ (ppm) 7.31-7.44 (m, 5H), 4.69-4.82 (m, 2H), 4.06-4.14 (m, 1H), 3.84 (d, 1H, *J* = 7.8 Hz), 3.77 (s, 6H).

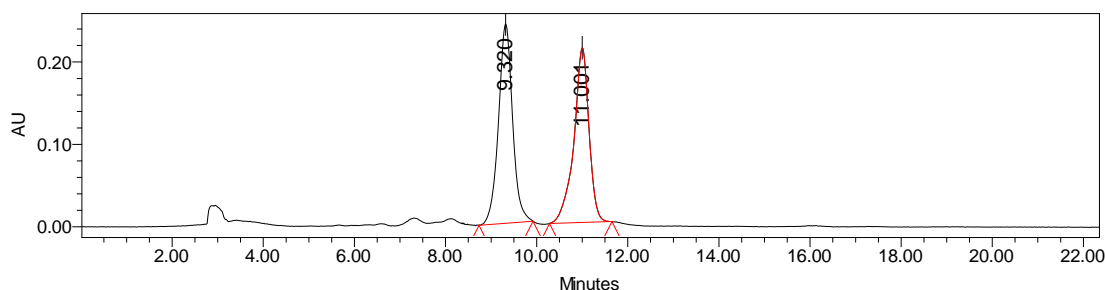
¹³C NMR (75 MHz, CDCl₃) δ (ppm) 167.3, 167.0, 131.9, 128.9, 128.4, 121.9, 85.9, 83.2, 76.1, 53.2, 53.1, 30.9.

Enantiomeric excess of 91% was determined by HPLC [Chiralpak® IA ; flow: 1.0 mL/min ; hexane/*i*-PrOH: 90:10 ; λ = 210 nm ; major enantiomer *t*_R = 9.5 min ; minor enantiomer *t*_R = 11.0 min].

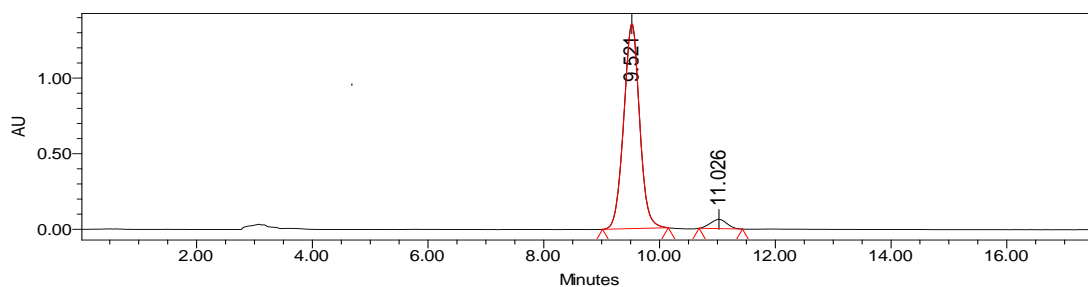
[α]_D²³ + 20.5 (c 0.1, CH₂Cl₂, 91% *ee*)

MS (ES⁺, MeOH): 328.13 ([M+Na+H]⁺)

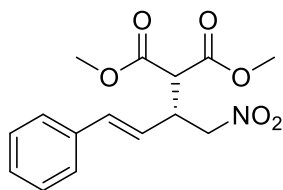
HPLC traces:



	Retention Time	% Area
1	9.320	51.43
2	11.001	48.57



	Retention Time	% Area
1	9.521	95.53
2	11.026	4.47

(+)-Dimethyl (*R,E*)-2-(1-nitro-4-phenylbut-3-en-2-yl)malonate (22b)Chemical Formula: C₁₅H₁₇NO₆

Analytical data are consistent with previously reported values^{ix}.

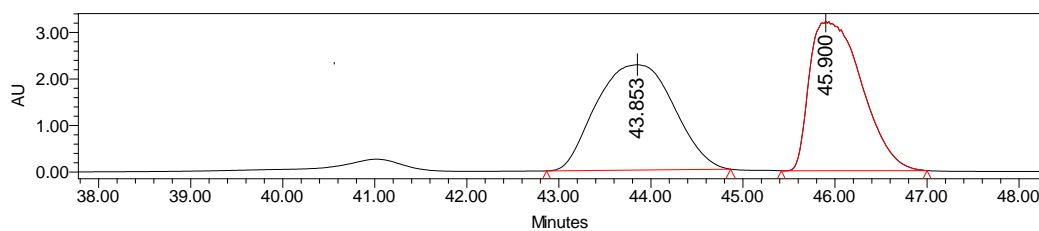
Purification on Silica Gel Chromatography with Hexane:Ethyl Acetate from 95:5 to 80:20.

¹H NMR (300 MHz, CDCl₃) δ (ppm) 7.33-7.45 (m, 5H), 7.57 (d, *J* = 15.9 Hz, 1H), 7.10 (dd, *J* = 9.0 Hz, *J* = 15.9 Hz, 1H), 4.65-4.79 (m, 2H), 3.73-3.76 (m, 2H), 3.77 (s, 3H), 3.73 (s, 3H).

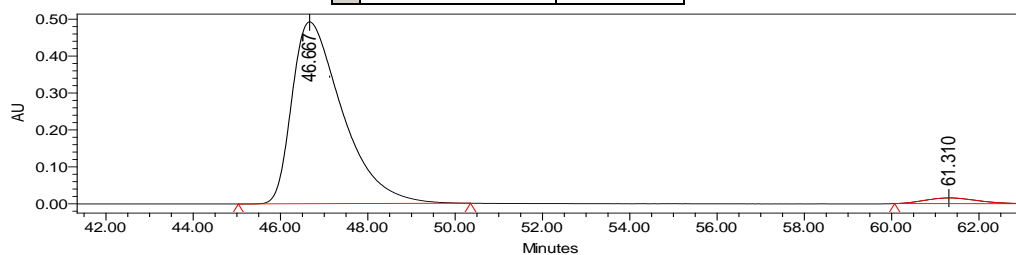
¹³C NMR (75 MHz, CDCl₃) δ (ppm) 167.8, 167.7, 136.0, 128.7, 128.4, 126.7, 123.4, 77.1, 53.5, 53.0, 41.4.

Enantiomeric excess of 94% was determined by HPLC [Chiralpak® IC ; flow: 1.0 mL/min ; hexane/*i*-PrOH: 99:1 ; λ = 210 nm ; major enantiomer *t*_R = 45.9 min ; minor enantiomer *t*_R = 43.9 min].

[α]_D²³ + 14.2 (c 0.35, CH₂Cl₂, 94% *ee*)

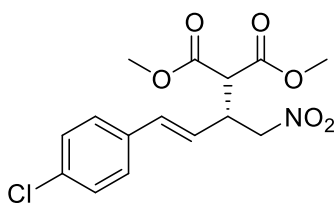
HPLC traces:

	Retention Time	% Area
1	43.853	51.28
2	45.900	48.72



	Retention Time	% Area
1	46.667	97.88
2	61.310	3.12

(+)-Dimethyl (*R,E*)-2-(4-(4-chlorophenyl)-1-nitrobut-3-en-2-yl)malonate (22c**)**



Chemical Formula: C₁₅H₁₆ClNO₆

Analytical data are consistent with previously reported values¹⁵.

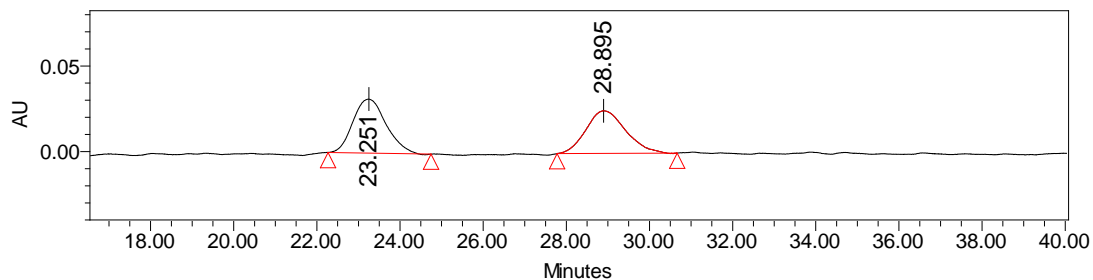
Purification on Silica Gel Chromatography with Hexane:Ethyl Acetate from 90:10 to 70:30.

¹H NMR (300 MHz, CDCl₃) δ (ppm) 7.19-7.48 (m, 4H), 7.53 (d, *J* = 15.9 Hz, 1H), 7.08 (dd, *J* = 9.0 Hz, 15.6 Hz, 1H), 4.65-4.76 (m, 2H), 3.77 (m, 3H), 3.73 (s, 3H), 3.59-3.73 (m, 2H).

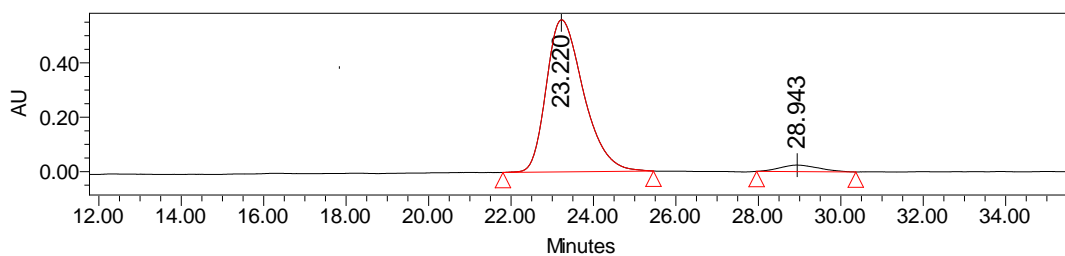
¹³C NMR (75 MHz, CDCl₃) δ (ppm) 167.8, 134.5, 134.2, 129.4, 129.4, 128.0, 124.2, 77.16, 53.4, 53.1, 41.4.

Enantiomeric excess of 92% was determined by HPLC [Chiralpak® OD-H ; flow: 1.0 mL/min ; hexane/*i*-PrOH: 90:10 ; λ = 210 nm ; major enantiomer *t*_R = 23.2 min ; minor enantiomer *t*_R = 28.9 min]. [α]_D²³ + 8.7 (c 0.69, CH₂Cl₂, 92% *ee*)

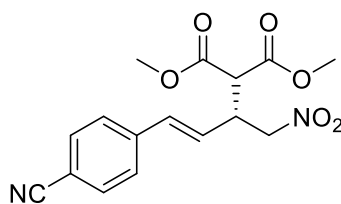
HPLC traces:



	Retention Time	% Area
1	23.251	51.48
2	28.895	48.52



	Retention Time	% Area
1	23.220	95.77
2	28.943	4.23

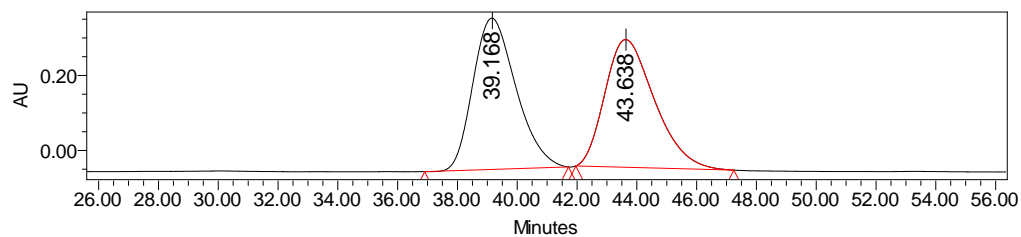
Dimethyl (*R,E*)-2-(4-(4-cyanophenyl)-1-nitrobut-3-en-2-yl)malonate (22d)

 Chemical Formula: C₁₆H₁₆N₂O₆

Purification on Silica Gel Chromatography with Hexane:Ethyl Acetate from 90:10 to 70:30.

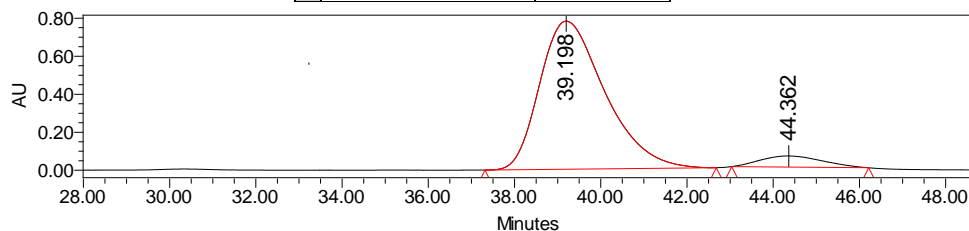
¹H NMR (300 MHz, CDCl₃) δ (ppm) 7.69 (d, *J* = 8.1 Hz, 2H), 7.51 (d, *J* = 8.4 Hz, 2H), 7.59 (d, *J* = 15.9 Hz, 1H), 7.26 (dd, *J* = 9.0 Hz, 15.9 Hz, 1H), 4.66-4.79 (m, 2H), 3.78 (s, 3H), 3.74 (s, 3H), 3.72-3.75 (m, 2H).

¹³C NMR (75 MHz, CDCl₃) δ (ppm) 167.7, 140.5, 134.2, 132.8, 127.8, 127.5, 119.0, 111.9, 77.0, 53.3, 41.4.

 Enantiomeric excess of 87% was determined by HPLC [Chiralpak® OD-H ; flow: 0.5 mL/min ; hexane/*i*-PrOH: 70:30 ; λ = 210 nm ; major enantiomer t_R = 38.7 min ; minor enantiomer t_R = 43.8 min].

HPLC traces:


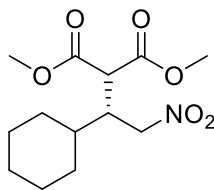
	Retention Time	% Area
1	39.168	50.66
2	43.638	49.34



	Retention Time	% Area
1	39.198	93.32
2	44.362	7.68

7.5.6 Characterization of adducts 23a-23g with aliphatic nitroalkenes

(+)-Dimethyl (*R*)-2-(1-cyclohexyl-2-nitroethyl)malonate (23a)



Chemical Formula: C₁₃H₂₁NO₆

Analytical data are consistent with previously reported values⁸.

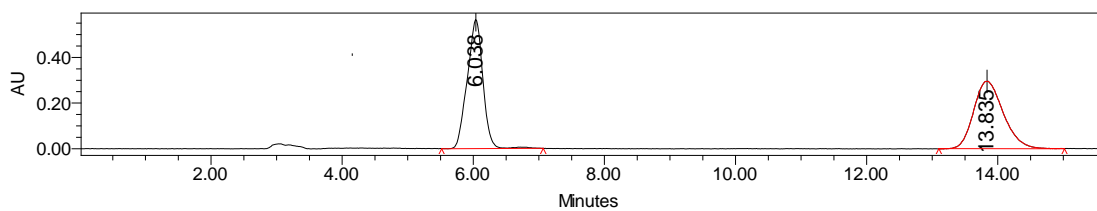
Purification on Silica Gel Chromatography with Hexane:Ethyl Acetate from 97:3 to 80:20.

¹H NMR (300 MHz, CDCl₃) δ (ppm) 4.73 (dd, *J* = 4.5 Hz, *J* = 14.7 Hz), 4.61 (dd, *J* = 7.3 Hz, *J* = 14.4 Hz), 3.75 (d+d, *J* = 7.0 Hz, *J* = 7.0 Hz, 6H+1H), 2.88 (m, 1H), 1.65-1.78 (m, 5H), 1.45 (m, 1H), 0.80-1.28 (m, 5H).

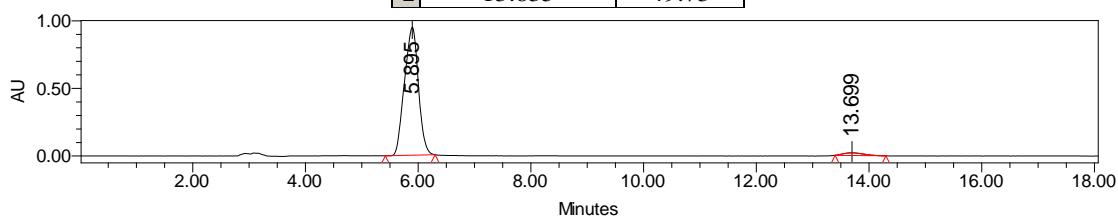
¹³C NMR (75 MHz, CDCl₃) δ (ppm) 160.1, 168.7, 75.5, 53.1, 52.9, 51.2, 42.3, 39.8, 30.3, 30.0, 26.4, 26.3, 26.1.

Enantiomeric excess of 94% was determined by HPLC [Chiralpak® OD-H ; flow: 1.0 mL/min ; hexane/*i*-PrOH: 90:10 ; λ = 210 nm ; major enantiomer *t*_R = 5.9 min ; minor enantiomer *t*_R = 13.7 min]. [α]_D²³ + 17.4 (c 0.38, CH₂Cl₂, 94% *ee*)

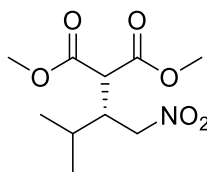
HPLC traces:



	Retention Time	% Area
1	7.038	50.27
2	13.835	49.73



	Retention Time	% Area
1	5.895	97.08
2	13.699	2.92

(+)-Dimethyl (R)-2-(3-methyl-1-nitrobutan-2-yl)malonate (23b)Chemical Formula: C₁₀H₁₇NO₆

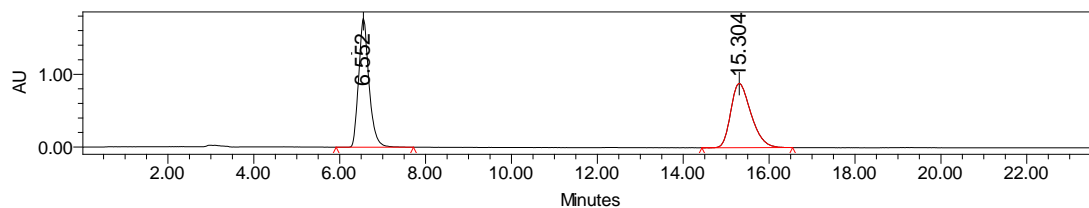
Analytical data are consistent with previously reported values^x.

Purification on Silica Gel Chromatography with Hexane:Ethyl Acetate 95:5.

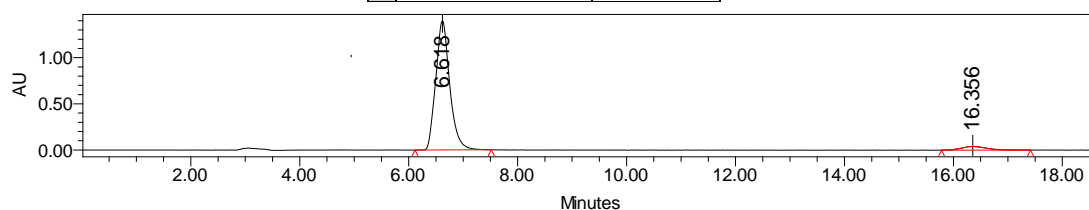
¹H NMR (300 MHz, CDCl₃) δ (ppm) 4.72 (dd, *J* = 4.5 Hz, *J* = 14.4 Hz, 1H), 4.56 (dd, *J* = 7.3 Hz, *J* = 14.4 Hz, 1H), 3.75 (s, 3H), 3.72 (s, 3H), 3.70 (d, *J* = 5.4 Hz, 1H), 2.89 (m, 1H), 1.84 (m, 1H), 0.95 (d+d, *J* = 7.9 Hz, *J* = 7.8 Hz, 3H+3H).

¹³C NMR (75 MHz, CDCl₃) δ (ppm) 168.9, 168.7, 75.3, 53.1, 52.8, 51.4, 42.8, 29.7, 19.9, 19.2.

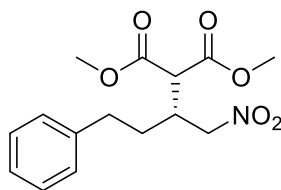
Enantiomeric excess of 91% was determined by HPLC [Chiralpak® OD-H ; flow: 1.0 mL/min ; hexane/*i*-PrOH: 90:10 ; λ = 210 nm ; major enantiomer *t*_R = 17.4 min ; minor enantiomer *t*_R = 7.5 min]. [α]_D²³ + 45.8 (c 0.18, CH₂Cl₂, 91% *ee*)

HPLC traces:

	Retention Time	% Area
1	7.552	50.71
2	15.304	49.29



	Retention Time	% Area
2	17.356	4.71
1	7.618	95.29

(+)-Dimethyl (R)-2-(1-nitro-4-phenylbutan-2-yl)malonate (23c)Chemical Formula: C₁₅H₁₉NO₆

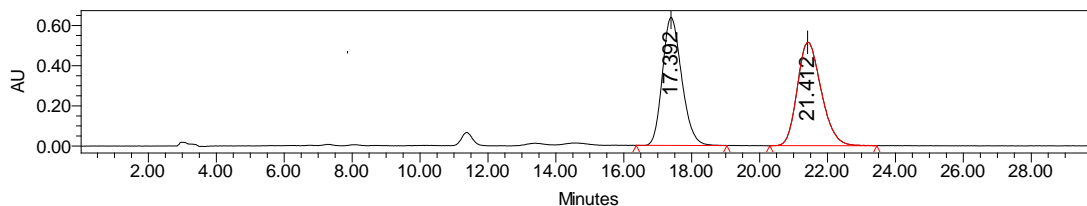
Analytical data are consistent with previously reported values⁸.

Purification on Silica Gel Chromatography with Hexane:Ethyl Acetate from 95:5 to 90:10.

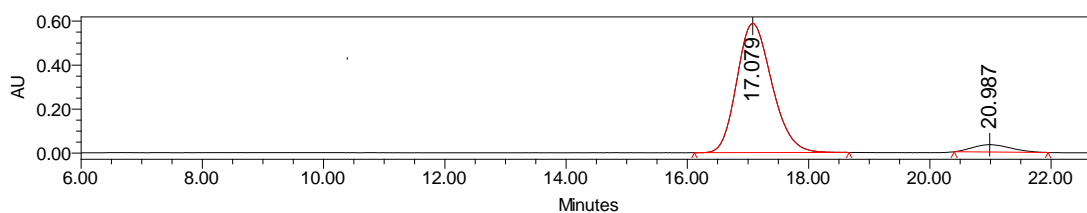
¹H NMR (300 MHz, CDCl₃) δ (ppm) 7.18-7.45 (m, 5H), 4.78 (dd, *J* = 5.4 Hz, *J* = 13.5 Hz, 1H), 4.60 (dd, *J* = 7.6 Hz, *J* = 13.5 Hz, 1H), 3.79 (s, 6H), 3.75 (d, *J* = 7.0 Hz, 1H), 3.00 (sext, *J* = 7.0 Hz, 1H), 2.74 (m, 2H), 1.83 (m, 2H).

¹³C NMR (75 MHz, CDCl₃) δ (ppm) 168.24, 168.14, 140.36, 128.66, 128.31, 126.4, 76.4, 52.9, 52.8, 52.4, 37.6, 33.0, 31.8.

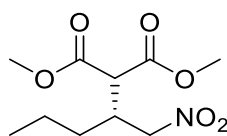
Enantiomeric excess of 88% was determined by HPLC [Chiralpak® OD-H ; flow: 1.0 mL/min ; hexane/*i*-PrOH: 90:10; λ = 210 nm ; major enantiomer *t*_R = 17.0 min ; minor enantiomer *t*_R = 21.0 min]. [α]_D²³ + 24.5 (c 0.18, CH₂Cl₂, 88% *ee*)

HPLC traces:

	Retention Time	% Area
1	17.492	49.96
2	21.412	50.04



	Retention Time	% Area
1	17.079	94.22
2	20.987	5.78

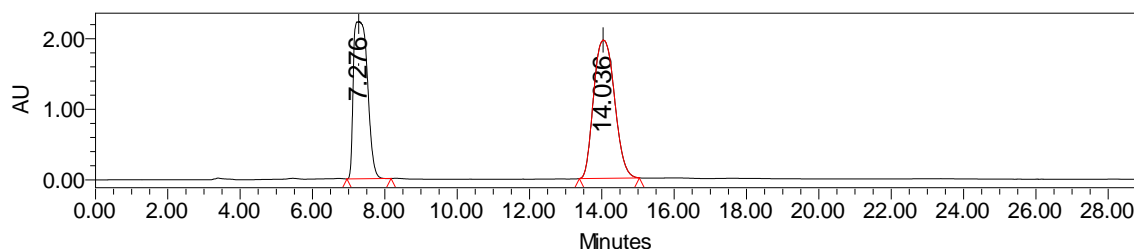
(+)-Dimethyl (R)-2-(1-nitropentan-2-yl)malonate (23d)Chemical Formula: C₁₀H₁₇NO₆Analytical data are consistent with previously reported values^{xi}.

Purification on Silica Gel Chromatography with Hexane:Ethyl Acetate from 99:1 to 95:5.

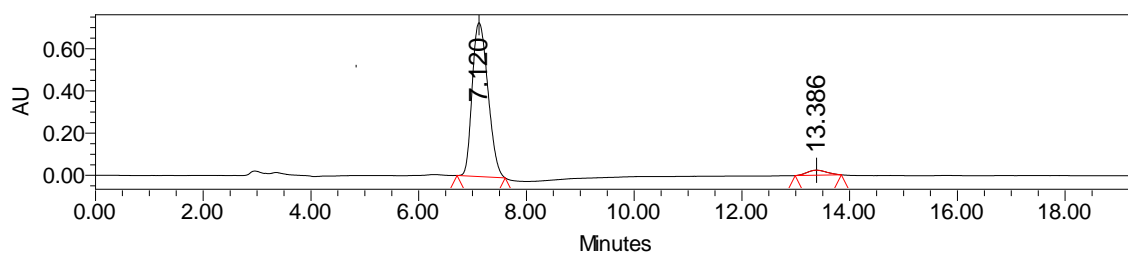
¹H NMR (300 MHz, CDCl₃) δ (ppm) 4.70 (dd, *J* = 5.1 Hz, *J* = 13.5 Hz, 1H), 4.53 (dd, *J* = 7.9 Hz, *J* = 13.5 Hz, 1H), 3.76 (s, 3H), 3.75 (s, 3H), 3.66 (d, *J* = 5.7 Hz, 1H), 2.91 (sext, *J* = 5.7 Hz, 1H), 1.41 (m, 4H), 0.93 (t, *J* = 7.9 Hz, 3H).

¹³C NMR (75 MHz, CDCl₃) δ (ppm) 168.5, 168.3, 78.7, 53.0, 52.8, 52.4, 36.9, 32.3, 20.0, 13.8.

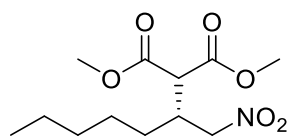
Enantiomeric excess of 92% was determined by HPLC [Chiralpak® OD-H ; flow: 1.0 mL/min ; hexane/*i*-PrOH: 90:10 ; λ = 210 nm ; major enantiomer *t*_R = 7.1 min ; minor enantiomer *t*_R = 13.4 min]. [α]_D²³ + 33.4 (c 0.15, CH₂Cl₂, 92% *ee*)

HPLC traces:

	Retention Time	% Area
1	7.376	43.37
2	14.036	57.63



	Retention Time	% Area
1	7.120	97.11
2	13.386	3.89

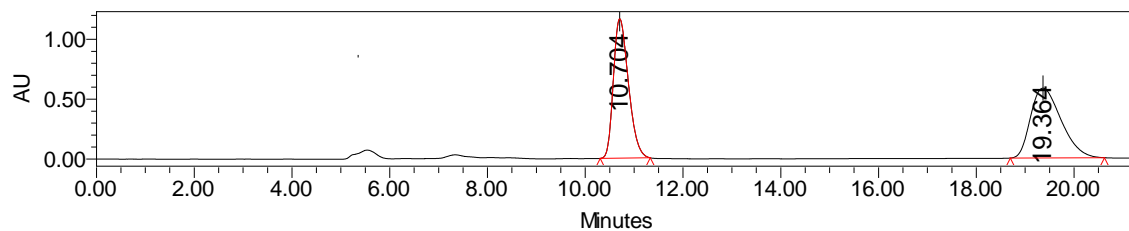
(+)-Dimethyl (R)-2-(1-nitroheptan-2-yl)malonate (23e)Chemical Formula: C₁₂H₂₁NO₆Analytical data are consistent with previously reported values¹¹.

Purification on Silica Gel Chromatography with Hexane:Ethyl Acetate from 95:5.

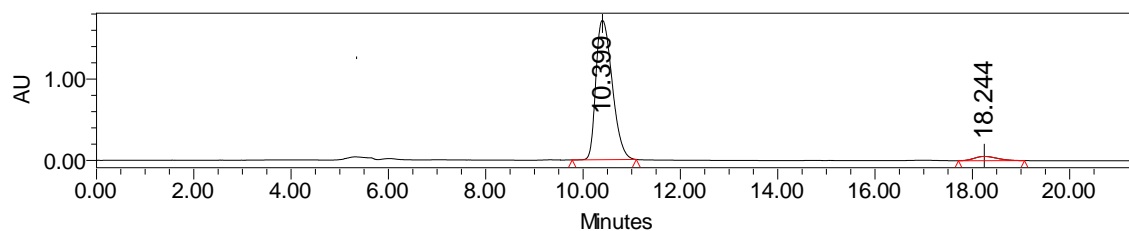
¹H NMR (300 MHz, CDCl₃) δ (ppm) 4.69 (dd, *J* = 5.1 Hz, *J* = 13.2 Hz, 1H), 4.51 (dd, *J* = 7.6 Hz, *J* = 13.2 Hz, 1H), 3.75 (s, 3H), 3.75 (s, 3H), 3.65 (d, *J* = 7.0 Hz, 1H), 2.88 (sext, *J* = 5.7 Hz, 1H), 1.24-1.48 (m, 6H), 0.87 (t, *J* = 7.6 Hz, 3H).

¹³C NMR (75 MHz, CDCl₃) δ (ppm) 168.50, 168.31, 76.67, 52.94, 52.82, 52.43, 37.09, 31.49, 30.06, 26.36, 22.44, 13.99.

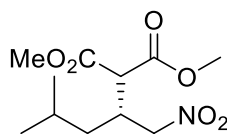
Enantiomeric excess of 92% was determined by HPLC [Chiralpak® OD-H ; flow: 1.0 mL/min ; hexane/*i*-PrOH: 90:10 ; λ = 210 nm ; major enantiomer *t*_R = 10.4 min ; minor enantiomer *t*_R = 18.2 min]. [α]_D²³ + 12.2 (c 0.34, CH₂Cl₂, 92% *ee*)

HPLC traces:

	Retention Time	% Area
1	10.704	49.60
2	19.364	50.40



	Retention Time	% Area
1	10.399	95.92
2	18.244	4.08

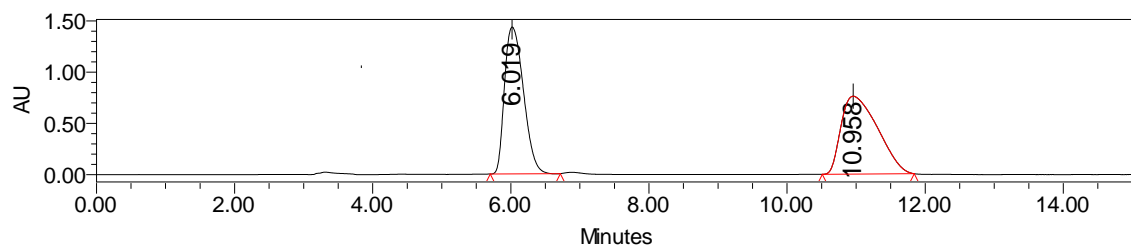
(+)-Dimethyl (R)-2-(4-methyl-1-nitropentan-2-yl)malonate (23f)Chemical Formula: C₁₁H₁₉NO₆Analytical data are consistent with previously reported values⁸.

Purification on Silica Gel Chromatography with Hexane:Ethyl Acetate 97:3.

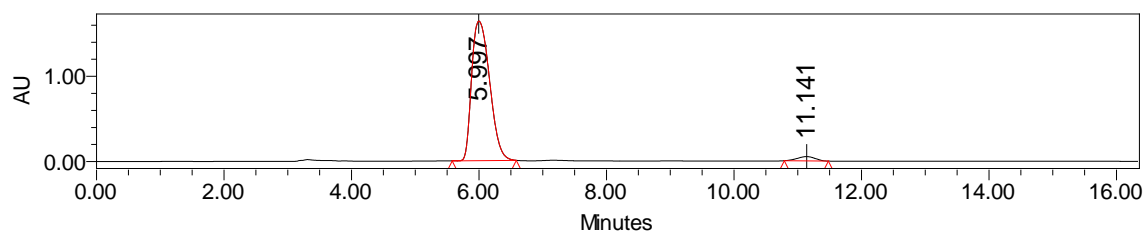
¹H NMR (300 MHz, CDCl₃) δ (ppm) 4.69 (dd, *J* = 5.1 Hz, *J* = 13.2 Hz, 1H), 4.50 (dd, *J* = 7.3 Hz, *J* = 13.2 Hz, 1H), 3.75 (s, 6H), 3.65 (d, *J* = 5.7 Hz, 1H), 2.94 (sext, *J* = 7.6 Hz, 1H), 1.61 (sept, *J* = 7.9 Hz, 1H), 1.30 (dt, *J* = 2.1 Hz, *J* = 7.3 Hz, 2H), 0.92 (d, *J* = 2.7 Hz, 3H), 0.90 (d, *J* = 2.7 Hz, 3H).

¹³C NMR (75 MHz, CDCl₃) δ (ppm) 168.5, 168.3, 76.7, 52.9, 52.5, 39.1, 35.1, 25.3, 22.5, 22.3.

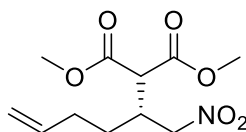
Enantiomeric excess of 94% was determined by HPLC [Chiralpak® OD-H ; flow: 1.0 mL/min ; hexane/*i*-PrOH: 90:10 ; λ = 210 nm ; major enantiomer *t*_R = 7.0 min ; minor enantiomer *t*_R = 11.1 min]. [α]_D²³ + 5.4 (c 0.40, CH₂Cl₂, 94% *ee*)

HPLC traces:

	Retention Time	% Area
1	7.019	49.49
2	10.958	50.51



	Retention Time	% Area
1	5.997	97.04
2	11.141	2.96

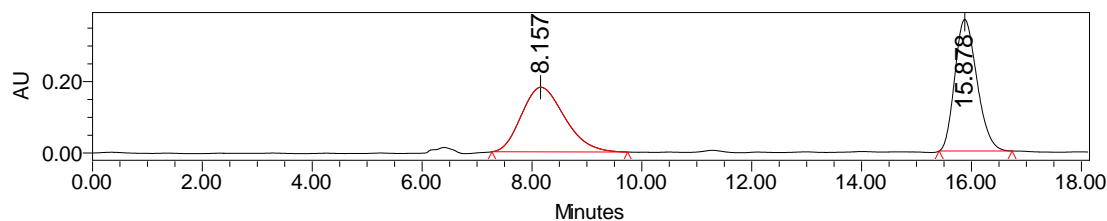
(+)-Dimethyl (R)-2-(1-nitrohex-5-en-2-yl)malonate (23g)Chemical Formula: C₁₁H₁₇NO₆

Purification on Silica Gel Chromatography with Hexane:Ethyl Acetate from 99:1 to 95:5.

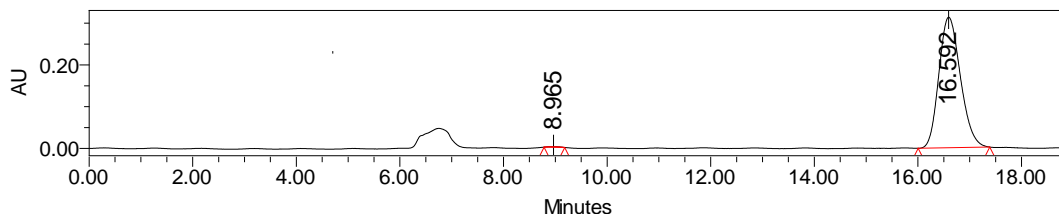
¹H NMR (300 MHz, CDCl₃) δ (ppm) 5.73 (sext+dd, *J* = 7.6 Hz, *J* = 3.0 Hz, *J* = 17.1 Hz, 1H), 5.01-5.09 (m, 2H), 4.71 (dd, *J* = 5.1 Hz, *J* = 13.5 Hz, 1H), 4.54 (dd, *J* = 7.6 Hz, *J* = 13.5 Hz, 1H), 3.77 (s, 6H), 3.68 (d, *J* = 5.7 Hz, 1H), 2.92 (sext, *J* = 5.7 Hz, 1H), 2.11-2.18 (m, 2H), 1.54-1.62 (m, 2H).

¹³C NMR (75 MHz, CDCl₃) δ (ppm) 168.5, 168.3, 137.7, 116.4, 76.6, 53.1, 53.0, 52.4, 37.5, 30.9, 29.3.

Enantiomeric excess of 92% was determined by HPLC [Chiralpak® OD-H ; flow: 1.0 mL/min ; hexane/*i*-PrOH: 90:10 ; λ = 210 nm ; major enantiomer *t*_R = 16.7 min ; minor enantiomer *t*_R = 9.0 min]. [α]_D²³ + 40.9 (c 0.12, CH₂Cl₂, >99% *ee*)

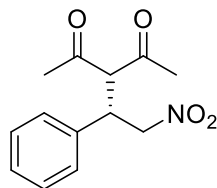
HPLC traces:

	Retention Time	% Area
1	8.157	48.84
2	15.878	51.16

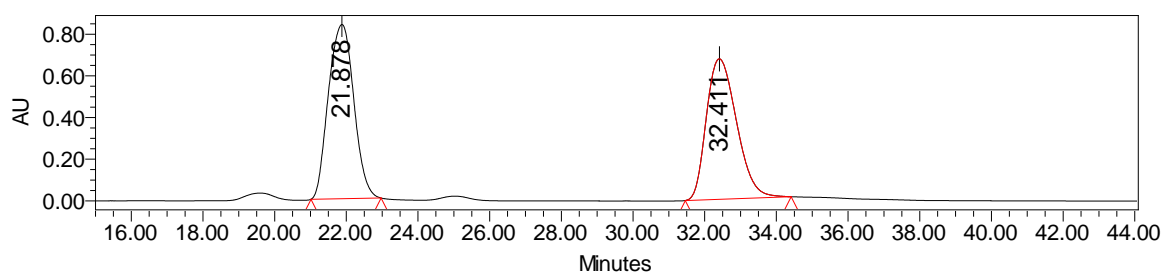


	Retention Time	% Area
1	8.965	0.27
2	16.592	99.73

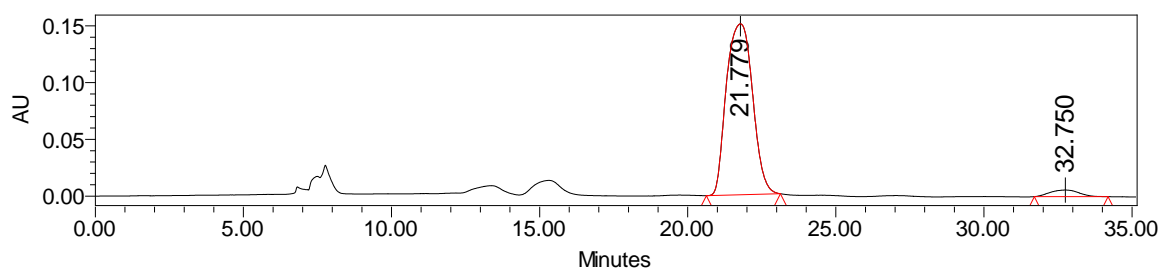
7.5.7 Characterization of adducts 8-9 from chapter II

(S)-3-(2-nitro-1-phenylethyl)pentane-2,4-dione (8a)Chemical Formula: C₁₃H₁₅NO₄Analytical data are consistent with previously reported values¹⁸.

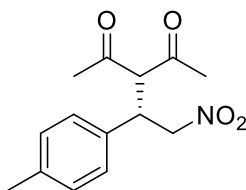
Purification on Silica Gel Chromatography with Hexane:Ethyl Acetate from 90:10 to 80:20.

¹H NMR (300 MHz, CDCl₃) δ (ppm) 7.30-7.47 (m, 5H), 4.66 (m, 2H), 4.40 (d, *J* = 10.7 Hz, 1H), 4.28 (m, 1H), 2.33 (s, 3H), 1.98 (s, 3H).¹³C NMR (75 MHz, CDCl₃) δ (ppm) 129.4, 128.6, 128.0, 78.2, 70.8, 42.8, 30.4, 29.5.Enantiomeric excess of 92% was determined by HPLC [Chiralpak® IC ; flow: 0.5 mL/min ; hexane/*i*-PrOH: 80:20 ; λ = 210 nm ; major enantiomer *t*_R = 21.8 min ; minor enantiomer *t*_R = 32.8 min].**HPLC traces:**

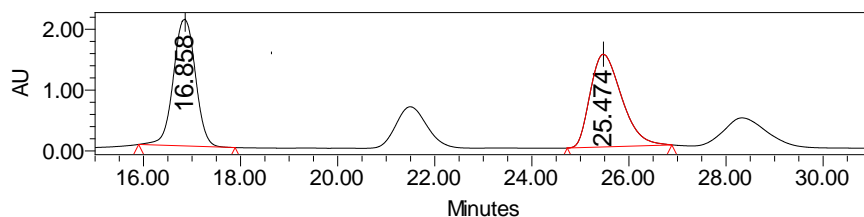
	Retention Time	% Area
1	21.878	51.07
2	32.411	48.93



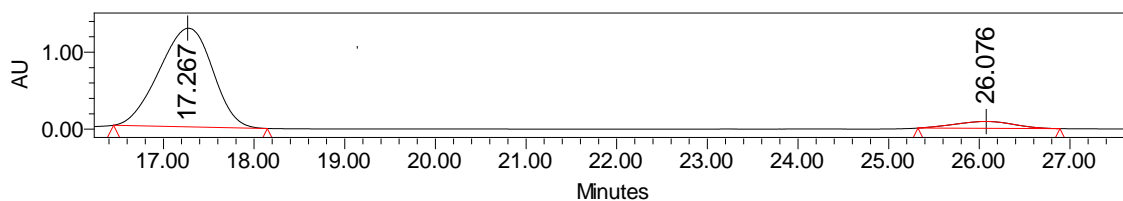
	Retention Time	% Area
1	21.779	95.88
2	32.750	4.12

(S)-3-(2-nitro-1-(*p*-tolyl)ethyl)pentane-2,4-dione (8b)Chemical Formula: C₁₄H₁₇NO₄Analytical data are consistent with previously reported values^{xiii}.¹H NMR (300 MHz, CDCl₃) δ (ppm) 7.33-7.44 (m, 4H), 4.78 (d, *J* = 7.3 Hz, 2H), 4.54 (d, *J* = 10.8 Hz, 1H), 4.37 (m, 1H), 2.46 (s, 6H), 2.12 (s, 3H).¹³C NMR (75 MHz, CDCl₃) δ (ppm) 201.9, 201.2, 138.3, 132.9, 130.0, 127.8, 78.4, 70.7, 42.5, 30.5, 29.6, 21.1.

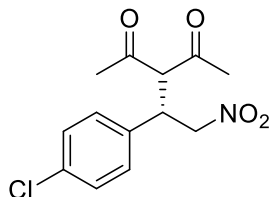
Purification on Silica Gel Chromatography with Hexane:Ethyl Acetate from 80:20 to 70:30.

Enantiomeric excess of 86% was determined by HPLC [Chiralpak® IC ; flow: 1.0 mL/min ; hexane/*i*-PrOH: 90:10 ; λ = 210 nm ; major enantiomer *t*_R = 17.4 min ; minor enantiomer *t*_R = 27.1 min].[α]_D²³ + 111.0 (c 0.32, CH₂Cl₂, 86% *ee*)**HPLC traces:**

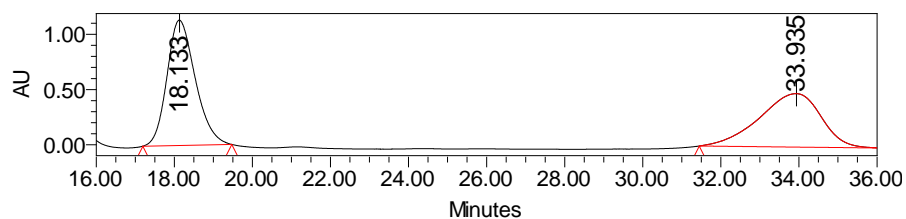
	Retention Time	% Area
1	17.858	49.05
2	25.474	50.95



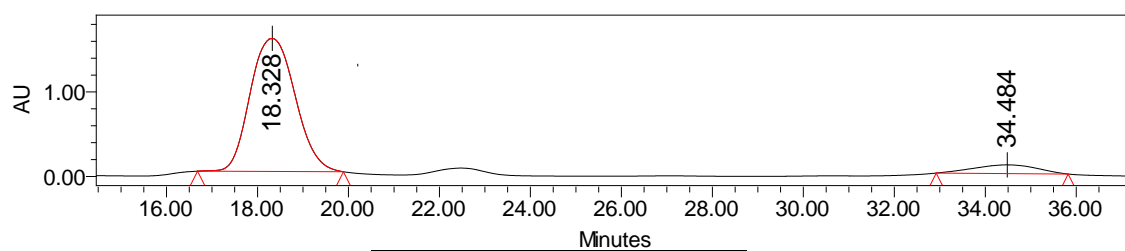
	Retention Time	% Area
1	17.367	92.86
2	27.076	7.14

(+)-(S)-3-(1-(4-chlorophenyl)-2-nitroethyl)pentane-2,4-dione (8g)Chemical Formula: C₁₃H₁₄ClNO₄Analytical data are consistent with previously reported values¹⁸.

Purification On Silica Gel Chromatography with Hexane:Ethyl Acetate from 80:20 to 70:30.

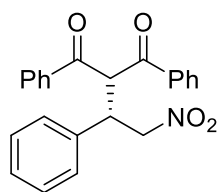
¹H NMR (300 MHz, CDCl₃) δ (ppm) 7.33 (d, *J* = 8.4 Hz, 2H), 7.07 (d, *J* = 8.7 Hz, 2H), 4.55 (d, *J* = 7.3 Hz, 2H), 4.26 (d, *J* = 10.5 Hz, 1H), 4.18 (m, 1H), 2.20 (s, 3H), 1.90 (s, 3H).¹³C NMR (75 MHz, CDCl₃) δ (ppm) 201.5, 200.7, 134.7, 134.5, 129.6, 129.4, 78.0, 70.5, 42.2, 30.5, 29.9Enantiomeric excess of 83% was determined by HPLC [Chiralpak® IA ; flow: 1.0 mL/min ; hexane/*i*-PrOH: 80:20 ; λ = 210 nm ; major enantiomer *t*_R = 18.3 min ; minor enantiomer *t*_R = 34.5 min].[α]_D²³ + 75.2 (c 0.2, CH₂Cl₂, ee 83%)**HPLC traces:**

	Retention Time	% Area
1	18.133	51.83
2	33.935	48.17



	Retention Time	% Area
1	18.328	91.60
2	34.484	8.40

(+)-(S)-2-(2-nitro-1-phenylethyl)-1,3-diphenylpropane-1,3-dione (9)



Chemical Formula: C₂₃H₁₉NO₄

Analytical data are consistent with previously reported values^{xiii}.

Purification on Silica Gel Chromatography with Hexane:Ethyl Acetate 90:10.

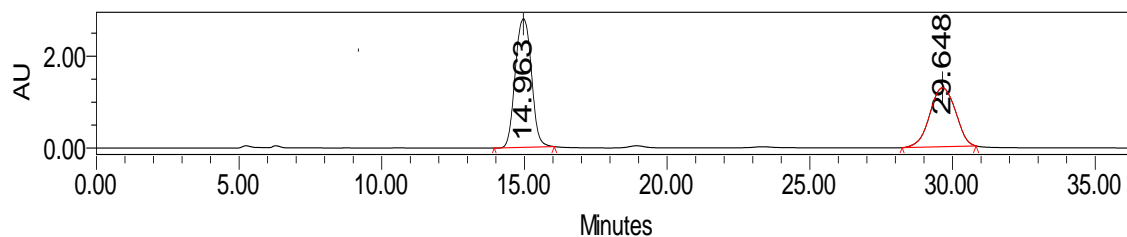
¹H NMR (300 MHz, CDCl₃) δ (ppm) 7.80-8.05 (m, 5H), 7.19-7.60 (m, 10H), 5.89 (d, *J* = 7.8 Hz, 1H), 5.03 (d, *J* = 7.9 Hz, 2H), 4.67 (q, *J* = 7.9 Hz, 1H).

¹³C NMR (75 MHz, CDCl₃) δ (ppm) 194.3, 193.7, 137.9, 137.3, 135.9, 134.2, 133.9, 132.6, 129.0, 128.9, 128.9, 128.7, 128.4, 128.3, 127.4, 77.5, 59.9, 44.2.

Enantiomeric excess of 100% was determined by HPLC [Chiralpak® IA ; flow: 1.0 mL/min ; hexane/*i*-PrOH: 90:10 ; λ = 210 nm ; major enantiomer *t*_R = 18.3 min ; minor enantiomer *t*_R = 34.5 min].

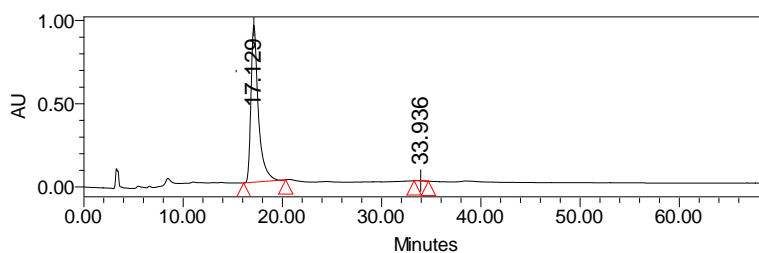
[α]_D²³ + 59.6 (c 0.08, CH₂Cl₂, 100% *ee*)

HPLC traces:



	Retention Time	% Area
1	14.963	57.85
2	29.648	42.15

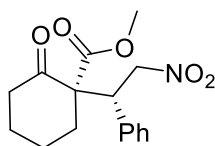
Note: Chromatogram was obtained with **1a** 0.1mol%, in DCM with DABCO 30mol%.



	Retention Time	% Area
1	17.129	99.73
2	33.936	0.27

7.5.8 Characterization of other adducts with other pronucleophiles

(-)-Methyl (S)-1-((R)-2-nitro-1-phenylethyl)-2-oxocyclohexane-1-carboxylate (20)



Chemical Formula: C₁₆H₁₉NO₅

Analytical data are consistent with previously reported values^{xiv}.

Purification on Silica Gel Chromatography with Hexane:Ethyl Acetate 90:10.

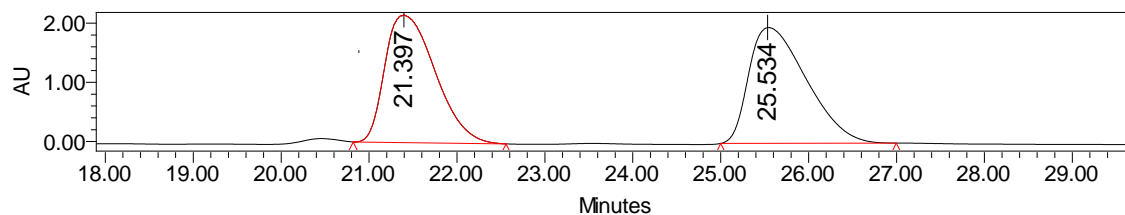
¹H NMR (300 MHz, CDCl₃) δ (ppm) 7.00-7.63 (m, 5H), 4.97 (dd, *J* = 3.3 Hz, 13.5 Hz, 1H), 4.72 (dd, *J* = 13.2 Hz, 11.1 Hz, 1H), 3.92 (dd, *J* = 3.3 Hz, 11.4 Hz, 1H), 2.32-2.46 (m, 2H), 1.90-2.04 (m, 2H), 1.34-1.48 (m, 4H), 1.17 (s, 3H).

¹³C NMR (75 MHz, CDCl₃) δ (ppm) 207.1, 169.7, 135.5, 129.5, 128.4, 128.2, 77.6, 62.0, 41.5, 37.1, 28.0, 22.4, 14.0

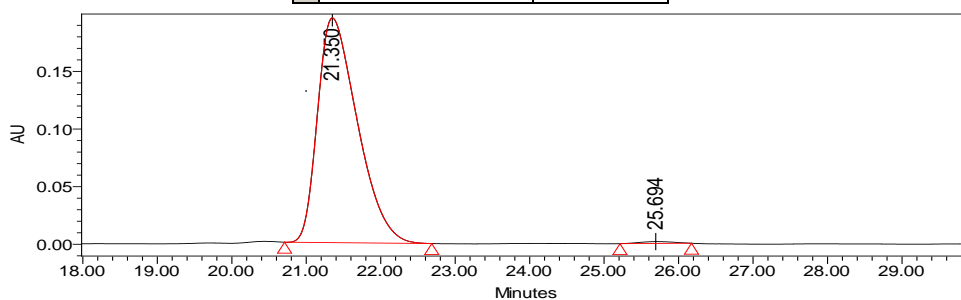
Enantiomeric excess of 98% and diastereo ratio of 100:0 were determined by HPLC [Chiralpak® IC ; flow: 0.5 mL/min; hexane/*i*-PrOH: 80:20 ; λ = 210 nm ; major enantiomer *t*_R = 21.4 min ; minor enantiomer *t*_R = 25.7 min].

[α]_D²³ – 47.9 (c 0.3, CH₂Cl₂, 99% *ee*, d.r.: 100:0)

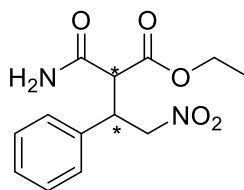
HPLC traces :



	Retention Time	% Area
1	21.397	49.06
2	25.534	50.94



	Retention Time	% Area
1	21.350	99.32
2	25.694	0.68

Ethyl 2-carbamoyl-4-nitro-3-phenylbutanoate (25)

 Chemical Formula: C₁₃H₁₆N₂O₅

Purification on Silica Gel Chromatography with Hexane:Ethyl Acetate 50:50.

 Diastereomeric excesses 75:25 (without and with catalyst) were determined by HPLC [Chiralpak® IA ; flow: 1.0 mL/min ; hexane/i-PrOH: 90:10 ; λ = 210 nm ; major diastereomer t_R = 18.1 min and t_R = 21.7 min ; minor enantiomer t_R = 43.1 min and 55.7 min]

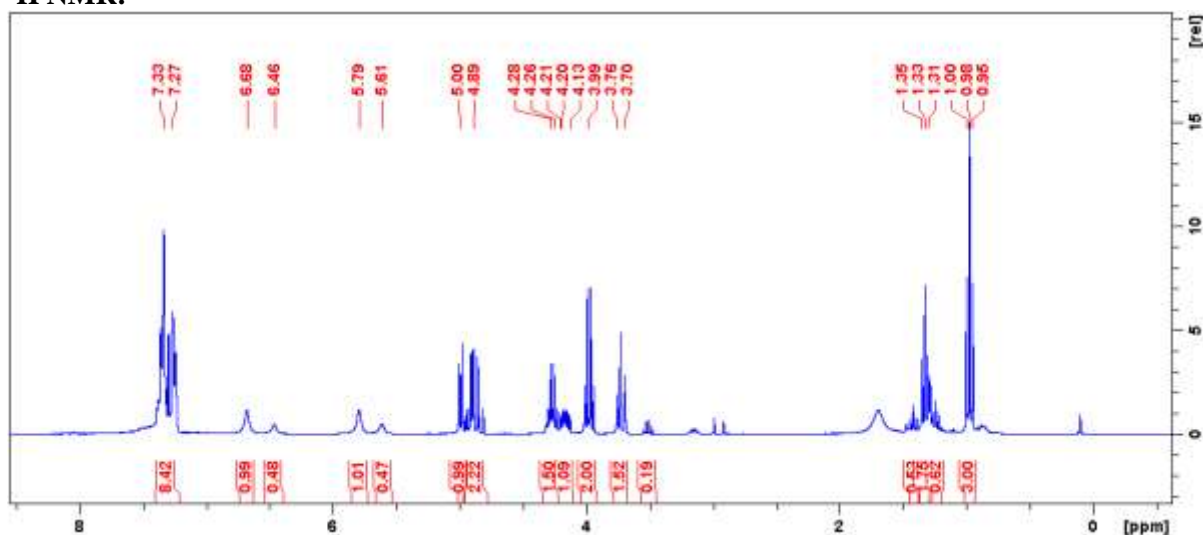
Note: crystallization studies should be performed to determine the absolute configuration of each centres, and attribute properly the nature of each diastereomer to each HPLC peak.

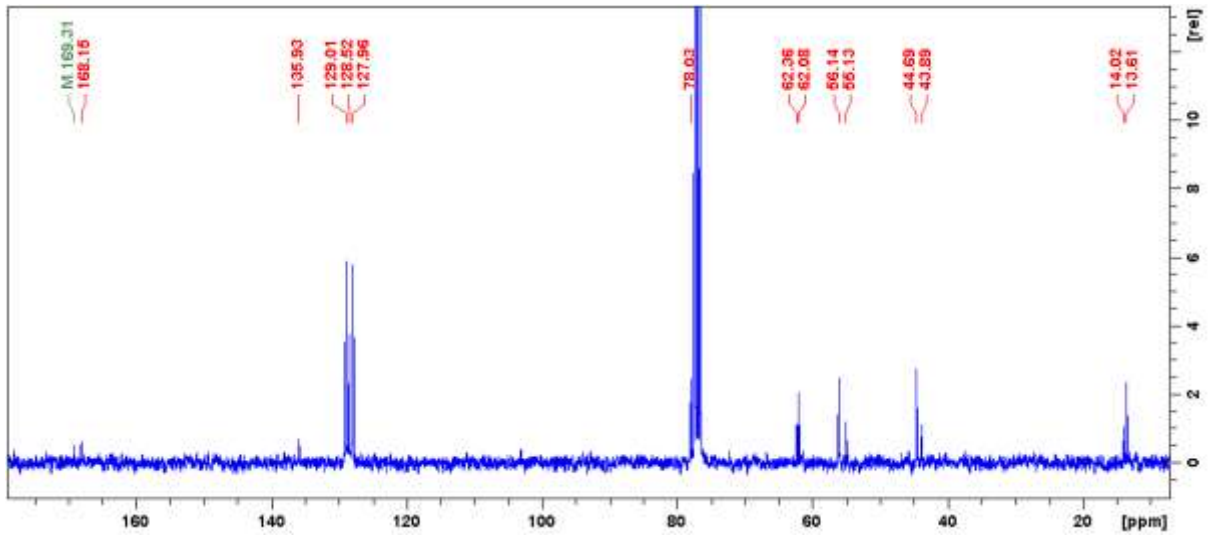
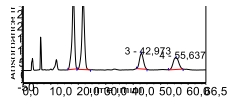
Minor diastereomers
¹H NMR (300 MHz, CDCl₃) δ (ppm) 7.27-7.34 (m, 5H, H^{aromatic}), 7.46 (br. s., 1H, NH₂), 5.61 (br. s., 1H, NH₂), 4.27 (d, J = 7.1 Hz, 1H, CO-CH-CO), 4.13-4.21 (m, CH₂NO₂), 3.70-3.76 (m, OCH₂CH₃+ CHCH₂NO₂), 1.33 (t, J = 7.1 Hz, 3H, OCH₂CH₃).

¹³C NMR (75 MHz, CDCl₃) δ (ppm) 135.9, 129.0, 128.5, 128.0, 78.0, 62.4, 55.1, 43.9, 13.7.

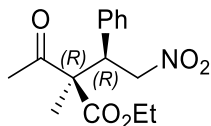
Major diastereomers
¹H NMR (300 MHz, CDCl₃) δ (ppm) 7.27-7.34 (m, 5H, H^{aromatic}), 7.68 (br. s., 1H, NH₂), 5.79 (br. s., 1H, NH₂), 4.99 (d, J = 7.1 Hz, 1H, CO-CH-CO), 4.90 (qd, J = 7.8 Hz, 9.0 Hz, 2H, CH₂NO₂), 4.23-4.32 (m, 1H, CHCH₂NO₂), 3.97 (q, J = 7.1 Hz, 2H, OCH₂CH₃), 0.98 (t, J = 7.1 Hz, 3H, OCH₂CH₃).

¹³C NMR (75 MHz, CDCl₃) δ (ppm) 135.9, 129.0, 128.5, 128.0, 78.0, 62.1, 57.1, 44.7, 14.0.

¹H NMR:


^{13}C NMR:**HPLC traces:**

	Retention Time	Relative Area
1	18.193	37.32
2	21.767	37.78
3	42.973	11.97
4	55.637	12.93

(2*R*,3*R*)-ethyl 2-acetyl-2-methyl-4-nitro-3-phenylbutanoate (27)Chemical Formula: C₁₅H₁₉NO₅

Diastereomeric excesses of 71:29 and enantiomeric excess of 79% for the major enantiomer were determined by HPLC [Chiralpak® OD-H ; flow: 1.0 mL/min ; hexane/*i*-PrOH: 95:5 ; λ = 210 nm; major diastereomer t_R = 14.6 min and t_R = 21.6 min ; minor enantiomer t_R = 13.3 min and 27.0 min] (in the study with 0.1 mol% catalyst **1a** and 30mol% Et₃N).

Minor diastereomers

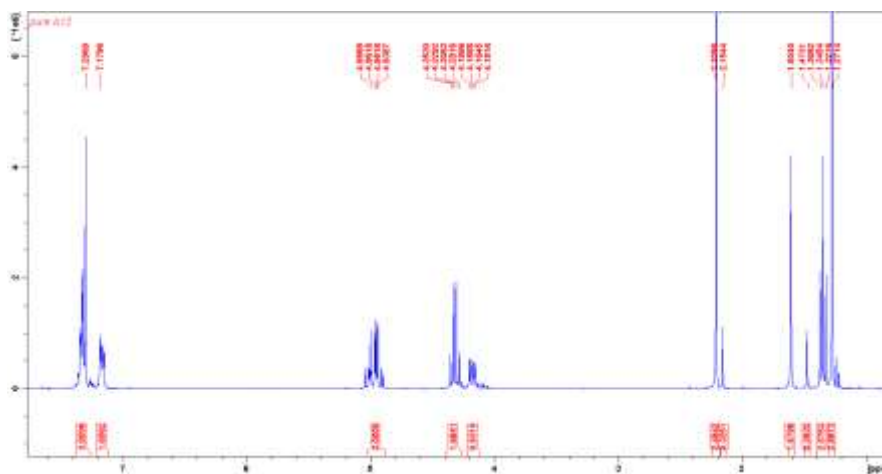
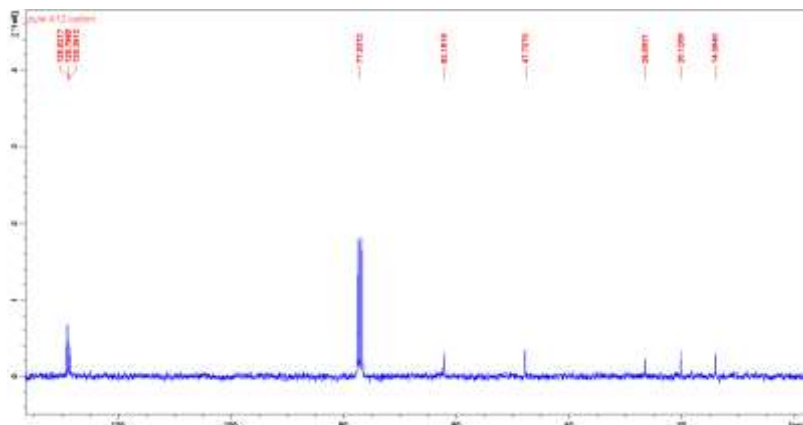
¹H NMR (300 MHz, CDCl₃) δ (ppm) 7.26-7.32 (m, 3H), 7.14-7.19 (m, 2H), 4.94-5.00 (m, 2H), 4.31 (q, J = 7.1 Hz, 2H), 4.17 (dd, J = 3.9 Hz, 10.6 Hz, 1H), 2.21 (s, 3H), 1.35 (t, J = 7.1 Hz, 3H), 1.27 (s, 3H).

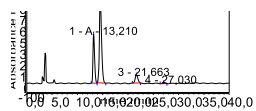
¹³C NMR (75 MHz, CDCl₃) δ (ppm) 129.0, 128.8, 128.4, 62.2, 47.7, 27.5, 20.1, 14.0. Note: the two carbonyl functions were not visible on this experiment.

Major diastereomers

¹H NMR (300 MHz, CDCl₃) δ (ppm) 7.28-7.39 (m, 3H), 7.18-25 (m, 2H), 4.98 (d, J = 7.9 Hz, 2H), 4.27 (t, J = 7.3 Hz, 1H), 4.10-4.23 (m, 2H), 2.15 (s, 3H), 1.47 (s, 3H), 1.23 (t, J = 7.1 Hz, 3H).

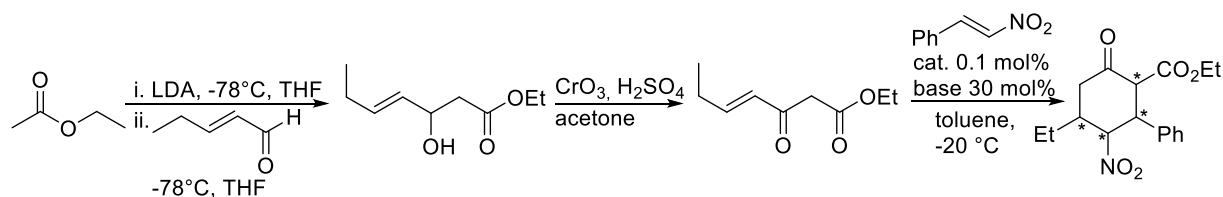
¹³C NMR (75 MHz, CDCl₃) 129.3, 128.7, 128.4, 62.1, 47.4, 27.6, 27.9, 18.1, 13.9. Note: the two carbonyl functions were not visible on this experiment.

Minor diastereomers¹H NMR:¹³C NMR:



	Retention Time (min)	% Relative Area
1	13.210	27.79
2	14.513	63.60
3	21.663	7.45
4	27.030	1.16

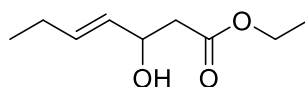
7.5.9 Experimental section for Cascade Michael addition



Scheme S21: Synthesis of adduct **30b** by Tandem Michael addition

7.5.9.1 Synthesis of precursors for Tandem Michael addition

Preparation of ethyl (E)-3-hydroxyhept-4-enoate (**28b**)



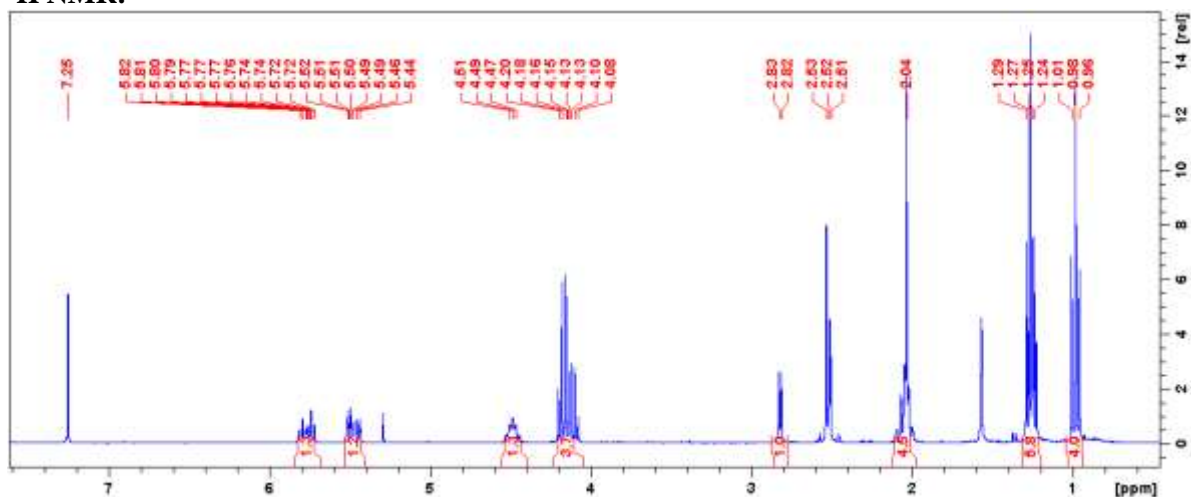
Chemical Formula: $C_9H_{16}O_3$

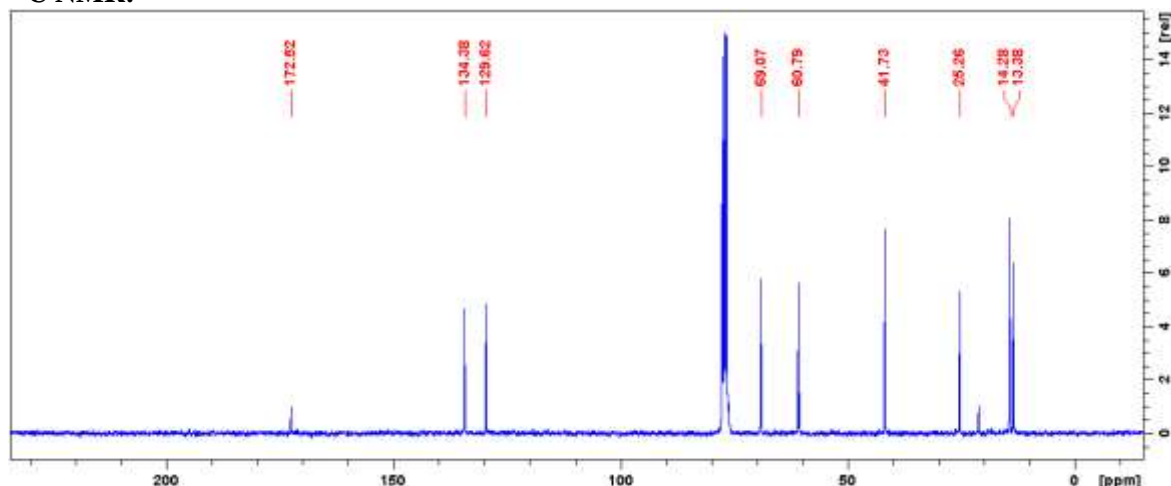
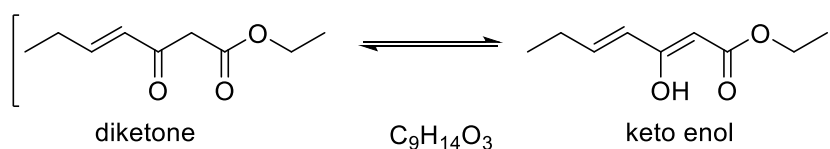
To a stirred solution of distilled THF (80 mL) and diisopropylamine (3 mL, 20 mmol, 1 eq.) at -79°C was added *n*-BuLi (8.8 mL, 22 mmol, 2.5 M in hexanes, 1.1 eq.). The reaction was stirred at -78°C for 15 min followed by the dropwise addition to ethyl acetate (2 mL, 20 mmol, 1 eq.). Upon completion of EtOAc addition, the reaction was stirred 50 min at -78°C . (E)-pent-2-enal (2 mL, 20 mmol, 1 eq.) was added and the reaction mixture was warmed to room temperature and stirred till complete conversion. Reaction mixture turned intense orange. The reaction was quenched by the addition of saturated NH_4Cl solution (10 mL). Desired compound was extracted with Et_2O , washed with brine, dried over MgSO_4 , filtered and concentrated under reduced pressure. Purification on Silica Gel Chromatography with Hexane:EtOAc from 100:0 to 70:30 led to a colorless oil (1.45 g, 8.4 mmol, yield 42%).

$^1\text{H NMR}$ (300 MHz, CDCl_3) δ (ppm) 5.73-5.82 (m, 1H, $\text{CH}^{\text{alcene}}$), 5.44-5.52 (m, 1H, $\text{CH}^{\text{alcene}}$), 4.42 (m, 1H, CHOH), 4.17 (q, $J = 7.9$ Hz, 2H, $\text{CO}_2\text{CH}_2\text{CH}_3$), 2.84 (d, $J = 3.9$ Hz, 1H, OH), 2.54 (s, 1H, $\text{CH}_2\text{CO}_2\text{Et}$), 2.52 (d, $J = 2.4$ Hz, 1H, $\text{CH}_2\text{CO}_2\text{Et}$), 2.04 (m, 2H, CH_2CH_3), 1.30 (m, 3H, $\text{CO}_2\text{CH}_2\text{CH}_3$), 0.99 (t, $J = 7.3$ Hz, 3H, CH_2CH_3)

$^{13}\text{C NMR}$ (100 MHz, CDCl_3) δ (ppm) 172.5, 134.4, 129.6, 69.1, 60.8, 41.7, 25.3, 14.3, 13.4.

$^1\text{H NMR}$:



^{13}C NMR:**Preparation of ethyl (E)-3-oxohept-4-enoate (29b)**

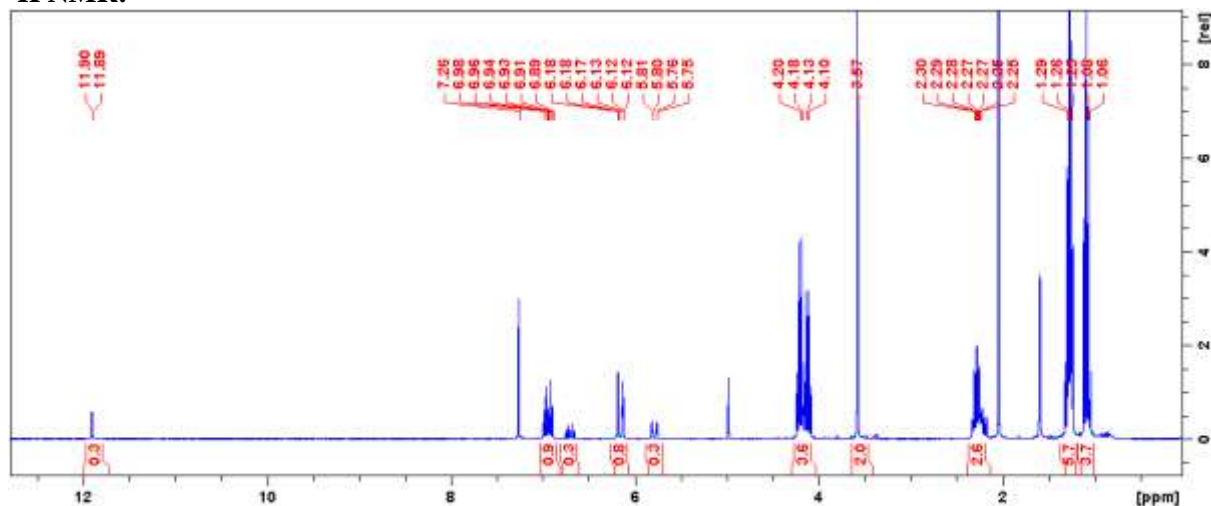
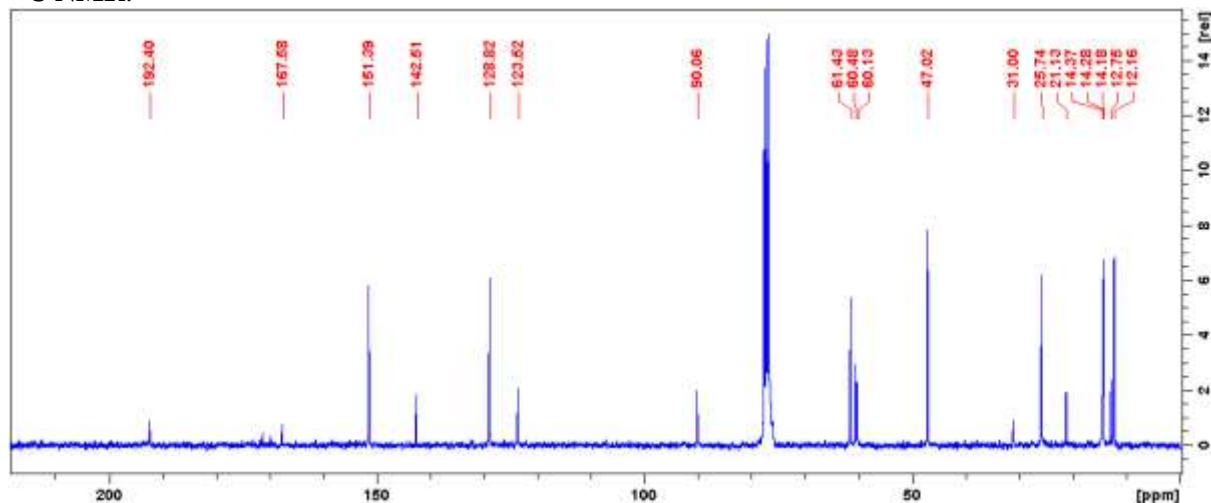
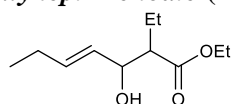
Jones' reagent was prepared by the addition of distilled water (8.8 mL) to CrO_3 (1.34 g) followed by the careful addition at 0°C of concentrated H_2SO_4 (1.2 mL).

Jones' reagent was added dropwise to a stirred solution of β -hydroxy ester (1.45 g, 8.4 mmol), in acetone (25 mL) at 0°C and reaction mixture was warmed to room temperature. After complete conversion, methanol was added to quench the excess of Jones' reagent. Desired compound was extracted with Et_2O , washed with brine, dried over MgSO_4 , filtered and concentrated under reduced pressure.

Purification on Silica Gel Chromatography with Hexane:EtOAc from 100:0 to 90:10 led to a colourless oil (400 mg, 1.3 mmol, yield 15%).

^1H NMR (300 MHz, CDCl_3) δ (ppm) 11.9 (s, 1H, OH^{enol}), 7.94 (dt, $J = 7.3$ Hz, $J = 15.9$ Hz, 1H, $\text{Et-CH}=\underline{\text{CH}}-\text{CO}^{\text{enone}}$), 7.70 (dt, $J = 7.6$ Hz, $J = 15.6$ Hz, 1H, $\text{Et-CH}=\text{C}(\underline{\text{OH}})^{\text{enol}}$), 7.18 (dt, $J = 1.8$ Hz, $J = 15.9$ Hz, 1H, $\text{CH}=\underline{\text{CH}}^{\text{enone}}$), 7.78 (dq, $J = 1.8$ Hz, $J = 15.6$ Hz, 1H, $\text{CH}=\underline{\text{CH}}^{\text{enol}}$), 4.98 (q, $J = 7.3$ Hz, 2H, $\text{OCH}_2\text{CH}_3^{\text{enone}}$), 4.22 (q, $J = 7.3$ Hz, 2H, $\text{OCH}_2\text{CH}_3^{\text{enol}}$), 3.58 (s, 2H, COCH_2CO), 2.32 (m, 2H, CH_2CH_3 + 2H, $\text{CH}_2\text{CH}_2\text{CH}_3$), 1.25 (m, 3H, $\text{CO}_2\text{CH}_2\text{CH}_3$), 1.08 (m, 3H, CH_2CH_3).

^{13}C NMR (100 MHz, CDCl_3) δ (ppm) 192.4, 167.6, 151.4, 142.5, 128.8, 123.5, 90.1, 61.4, 60.5, 60.1, 31.0, 25.7, 21.1, 14.4, 14.3, 12.8, 12.2.

¹H NMR:**¹³C NMR:****Preparation of ethyl (E)-2-ethyl-3-hydroxyhept-4-enoate (28c)**Chemical Formula: C₁₁H₂₀O₃

To a stirred solution of distilled THF (80 mL) and diisopropylamine (3 mL, 20 mmol, 1.3 eq.) at -79°C was added *n*-BuLi (8.8 mL, 22 mmol, 2.5 M in hexanes, 1.4 eq.). The reaction was stirred at -78°C for 15 min followed by the dropwise addition to ethyl propanoate (2.6 mL, 20 mmol, 1.3 eq.). Upon completion of ethyl propanoate addition, the reaction was stirred 50 min at -78°C. (E)-pent-2-enal (1.5 mL, 15 mmol, 1 eq.) was added and the reaction mixture was warmed to room temperature and stirred till complete conversion. Reaction mixture turned intense orange. The reaction was quenched by the addition of saturated NH₄Cl solution (10 mL). Desired compound was extracted with Et₂O, washed with brine, dried over MgSO₄, filtered and concentrated under reduced pressure.

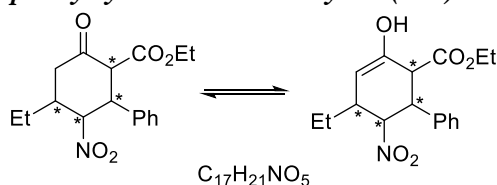
Purification on Silica Gel Chromatography with Hexane:EtOAc from 95:5 to 70:30 led to a colourless oil (1.12 g, 5.6mmol, yield 37%).

¹H NMR (300 MHz, CDCl₃) δ (ppm) 5.79 (m, 1H, Et-CH=CH), 5.48 (tt, *J* = 1.5 Hz, 7.0 Hz, 1H, Et-CH=CH), 4.18 (m, 3H, CHOH + OCH₂CH₃), 2.40 (m, 2H, OH + CH-Et), 1.67 (m, 2H, CH=CH-CH₂-CH₃), 1.27-1.34 (m, 5H, CH-CH₂-CH₃), 0.93-1.06 (m, 6H, 2 x CH-CH₂-CH₃).

A peak of DCM was present in the sample.

7.5.9.2 Characterization of cyclized adducts from Cascade Michael reaction

Ethyl 4-ethyl-3-nitro-6-oxo-2-phenylcyclohexanecarboxylate (30b)



Purification on Silica Gel Chromatography with Hexane:Ethyl Acetate from 98:2 to 80:20.

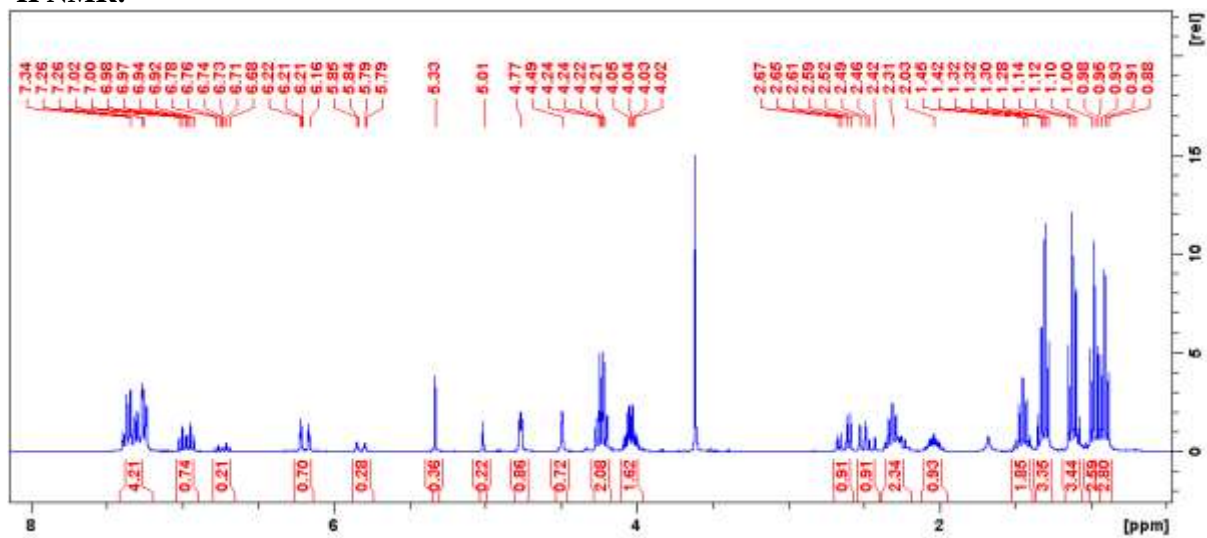
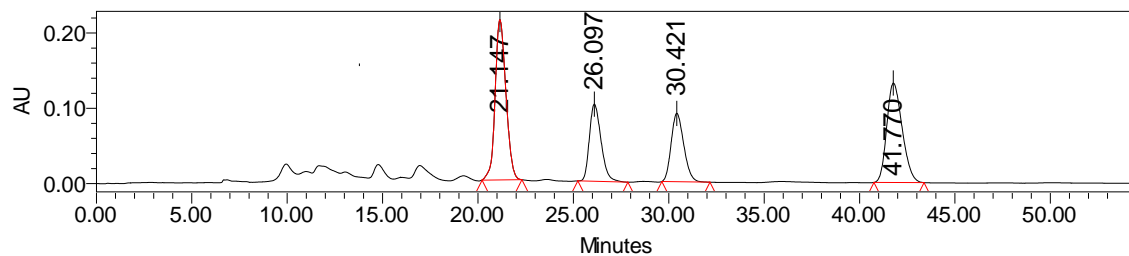
Major diastereomers

1H NMR (300 MHz, $CDCl_3$) δ (ppm) 12.61 (s, 1H, OH), 7.31-7.46 (m, 5H, C_6H_5), 6.73 (dt, $J = 15.5$ Hz, 7.6 Hz, 1H, $CHNO_2$), 6.18 (dt, $J = 15.9$ Hz, 1.7 Hz, 1H, $CH-Ph$), 4.22 (q+q, $J = 7.1$ Hz, 2H, OCH_2CH_3), 2.64 (dd, $J = 18.8$ Hz, 7.9 Hz, 1H, CH_2^{cycle}), 2.47 (dd, $J = 10.8$ Hz, 18.7 Hz, 1H, CH_2^{cycle}), 2.18-2.36 (m, 2H, $CHCH_2CH_3$), 2.03 (m, 1H, $CHCH_2CH_3$), 1.30 (t, $J = 7.1$ Hz, 3H, OCH_2CH_3), 0.91 (t, $J = 7.6$ Hz, 3H, $CHCH_2CH_3$).

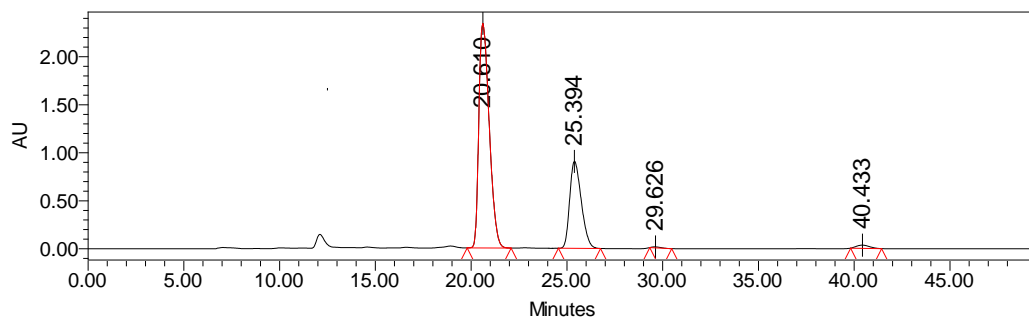
Minor diastereomers

1H NMR (300 MHz, $CDCl_3$) δ (ppm), 11.93 (d, $J = 1.4$ Hz, 1H, OH), 7.31-7.46 (m, 5H, C_6H_5), 6.96 (dt, $J = 7.3$ Hz, 15.9 Hz, 1H, $CHNO_2$), 5.82 (dq, $J = 15.5$ Hz, 1.5 Hz, 1H, $CH-Ph$), 4.03 (dq, $J = 7.1$ Hz, 2.9 Hz, 2H, OCH_2CH_3), 2.64 (dd, $J = 18.8$ Hz, 7.9 Hz, 1H, CH_2^{cycle}), 2.47 (dd, $J = 10.8$ Hz, 18.7 Hz, 1H, CH_2^{cycle}), 2.18-2.36 (m, 2H, $CHCH_2CH_3$), 2.03 (m, 1H, $CHCH_2CH_3$), 1.44 (t, $J = 7.5$ Hz, 3H, OCH_2CH_3), 0.97 (t, $J = 7.1$ Hz, 2.59 H, $CHCH_2CH_3$).

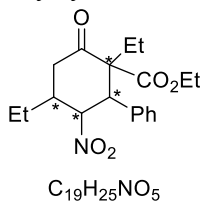
Enantiomeric excess of 98% and diastereo ratio of 70:30:0:0 were determined by HPLC [Chiralpak® IC ; flow: 0.5 mL/min ; hexane/i-PrOH: 80:20 ; $\lambda = 210$ nm ; **major diastereomers**: major enantiomer $t_R = 20.6$ min, minor enantiomer $t_R = 40.4$ min ; **minor diastereomers**: major enantiomer $t_R = 25.4$ min, minor enantiomer $t_R = 29.6$ min].

¹H NMR:**HPLC traces:**

	Retention Time	% Area
1	21.147	34.40
2	27.097	17.94
3	30.421	17.14
4	41.770	30.52



	Retention Time	% Area
1	20.610	68.74
2	25.394	29.80
3	29.626	0.23
4	40.433	1.23

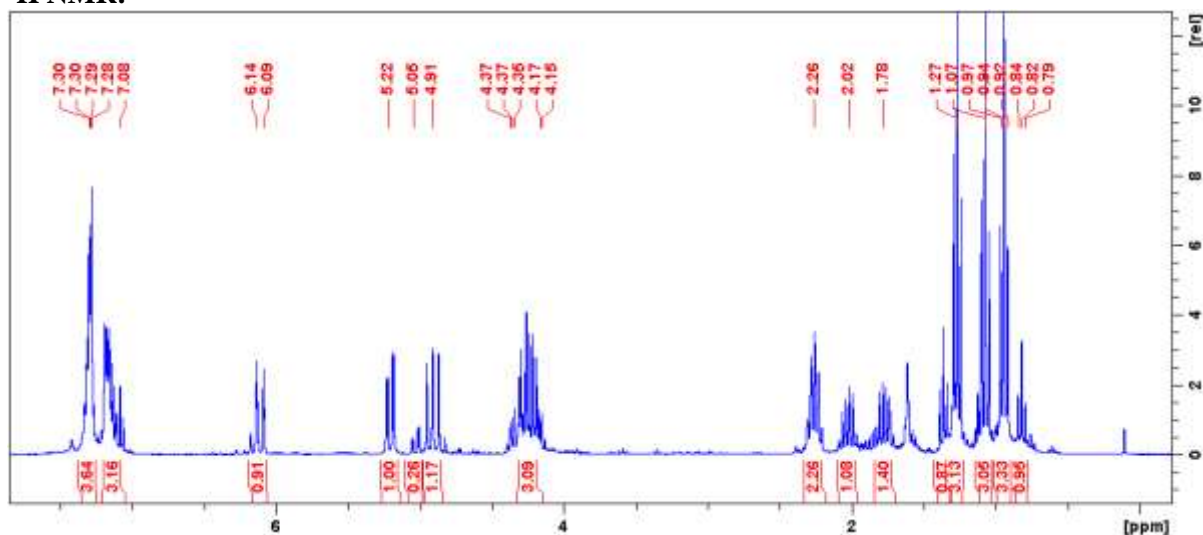
Ethyl 4-ethyl-1-methyl-3-nitro-6-oxo-2-phenylcyclohexanecarboxylate (30c)

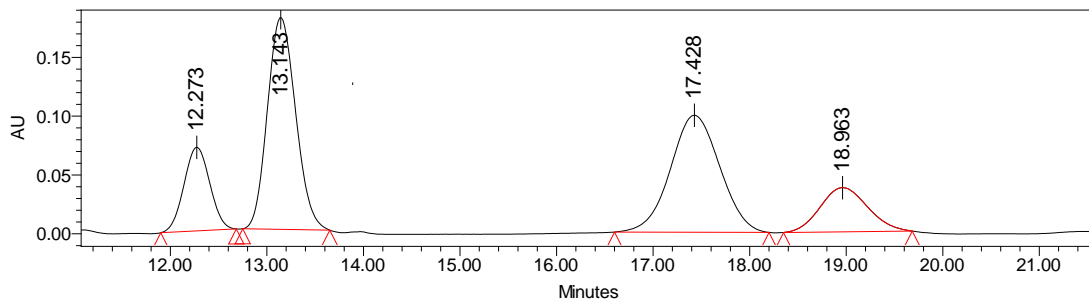
Purification on Silica Gel Chromatography with Hexane:Ethyl Acetate from 98:2 to 90:10.

1H NMR (300 MHz, $CDCl_3$) δ (ppm) 7.08-7.43 (m, 5H, H^{ar}), 6.11 (dt, $J = 1.6$ Hz, 15.2 Hz, 1H, $CHPh$), 5.21 (dd, $J = 3.3$ Hz, 13.2 Hz, 1H, $CHNO_2^{maj}$), 5.03 (dd, $J = 3.1$ Hz, 13.4 Hz, 1H, $CHNO_2^{min}$), 4.91 (dd, $J = 13.2$ Hz, 11.4 Hz, 1H, 1H from $COCH_2$), 4.15-4.37 (m, 3H, 1H from $COCH_2 + OCH_2CH_3$), 2.26 (m, 2H, $CHCH_2CH_3$), 2.02 (sept, $J = 7.8$ Hz, 1H, $CHCH_2CH_3$), 1.78 (sext, $J = 7.9$ Hz, 2H, $C-CH_2CH_3$), 1.36 (t, $J = 7.1$ Hz, 3H, $OCH_2CH_3^{min}$), 1.27 (t, $J = 7.3$ Hz, 3H, $OCH_2CH_3^{maj}$), 1.07 (t, $J = 7.5$ Hz, 3H, $CHCH_2CH_3$), 0.94 (t, $J = 7.5$ Hz, 3H, $CCH_2CH_3^{maj}$), 0.82 (t, $J = 7.6$ Hz, $CCH_2CH_3^{min}$).

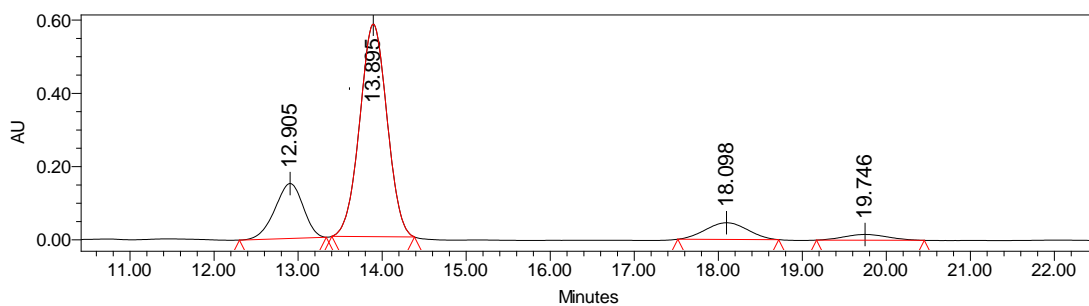
Enantiomeric excess of 78% and diastereo ratio of 78:22:0:0 were determined by HPLC [Chiralpak® IC ; flow: 1.0 mL/min ; hexane/*i*-PrOH: 95:5 ; $\lambda = 210$ nm ; **major diastereomers**: major enantiomer $t_R = 13.9$ min, minor enantiomer $t_R = 18.1$ min ; **minor diastereomers**: major enantiomer $t_R = 12.9$ min, minor enantiomer $t_R = 19.7$ min].

1H NMR:



HPLC traces:

	Retention Time	% Area
1	12.273	13.48
2	13.143	37.45
3	17.528	37.06
4	18.963	13.11



	Retention Time	% Area
1	12.905	18.68
2	13.895	69.87
3	18.098	8.43
4	19.746	3.02

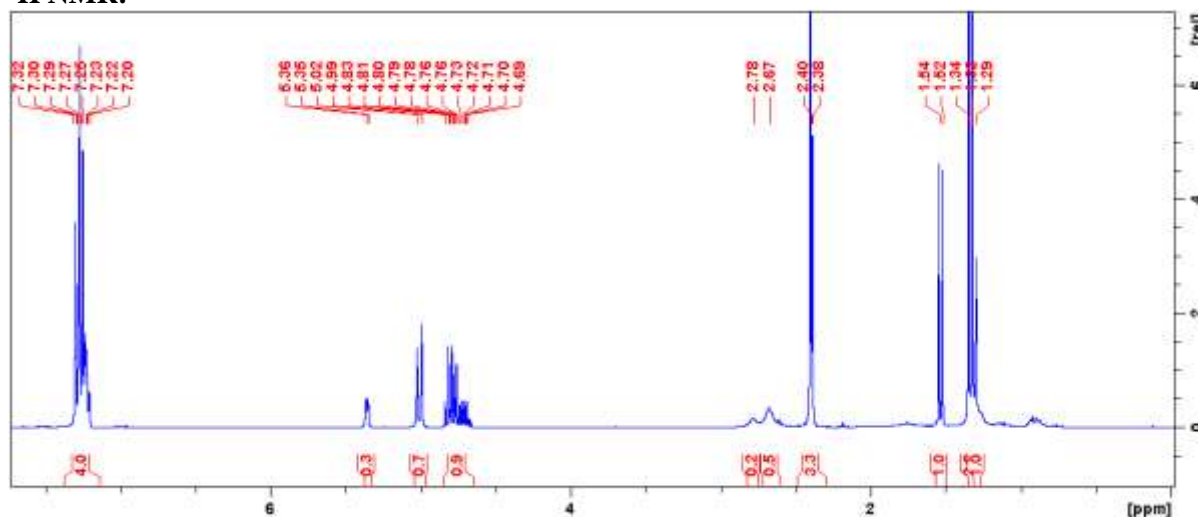
7.5.10 Experimental section for Henry reaction

2-nitro-1-(p-tolyl)propan-1-ol (40)

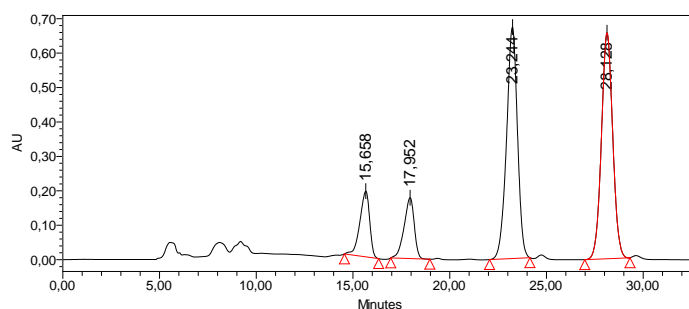
Major Diastereomer: $^1\text{H NMR}$ (300 MHz, CDCl_3) δ (ppm) 7.30-7.42 (m, 4H), 5.00 (d, $J = 9.1$ Hz, 1H), 4.75 (m, 1H), 2.67 (br. s., 1H), 2.40 (s, 3H), 1.33 (d, $J = 7.8$ Hz, 3H).

Minor Diastereomer: $^1\text{H NMR}$ (300 MHz, CDCl_3) δ (ppm) 7.30-7.42 (m, 4H), 5.35 (d, $J = 3.7$ Hz, 1H), 4.69-4.76 (m, 1H), 2.78 (br. s., 1H), 2.38 (s, 3H), 1.53 (d, $J = 7.8$ Hz, 3H).

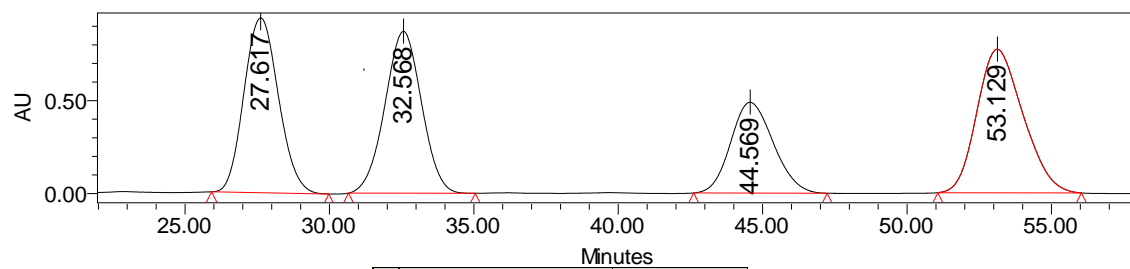
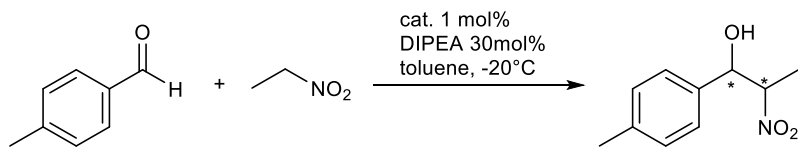
$^1\text{H NMR}$:



Enantiomeric excess of 26% and diastereo ratio of 53:47 were determined by HPLC [Chiralpak® AD-H ; flow: 0.5 mL/min ; hexane/*i*-PrOH: 95:5 ; $\lambda = 210$ nm; **major diastereomers:** major enantiomer $t_R = 53.1$ min, minor enantiomer $t_R = 44.6$ min ; **minor diastereomers:** enantiomer $n^{\circ}1$ $t_R = 27.6$ min, enantiomer $n^{\circ}2$ $t_R = 32.6$ min].



	Migration Time	% Area
1	15.658	10.14
2	17.952	9.74
3	23.244	39.84
4	28.128	40.28

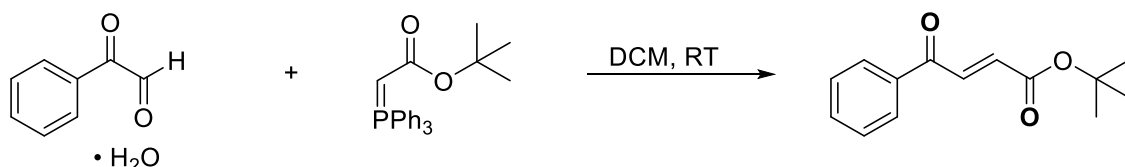


	Retention Time	% Area
1	27.617	27.88
2	32.568	27.43
3	44.569	17.35
4	53.129	29.44

7.5.11 Experimental section for the Juliá-Colonna epoxidation

7.5.11.1 Synthesis of chalcone 36

(E)-3-(furan-2-yl)-1-phenylprop-2-en-1-one (36)



In a flask under argon were added phenylglyoxal monohydrate (152 mg, 1.0 mmol, 1 eq.) and *tert*-butoxycarbonylmethylene triphenylphosphorane (376 mg, 1.0 mmol, 1 eq.) in dry DCM (2 mL) and stirred all day at room temperature. The reaction mixture was then concentrated and directly purified on Silica Gel Chromatography with Cyclohexane:EtOAc from 95:5 to 90:10 to lead to yellow oil (undetermined yield).

$^1\text{H NMR}$ (300 MHz, CDCl_3) δ (ppm) 8.01-8.05 (m, 2H), 7.85 (d, $J = 15.4$ Hz, 1H), 7.65 (tt, $J = 1.4$ Hz, 7.5 Hz, 1H), 7.62-7.68 (m, 2H), 6.85 (d, $J = 15.6$ Hz, 1H).

$^{13}\text{C NMR}$ (75 MHz, CDCl_3) δ (ppm) 190.0, 164.8, 136.8, 135.7, 134.6, 133.7, 128.9, 82.0, 28.0.

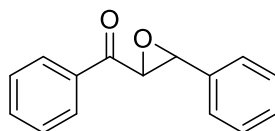
7.5.11.2 General procedure for Juliá-Colonna epoxidation

To a vial charged with **1a** (0.51 mg, 0.5 μmol) were added the urea-peroxide hydrogen (56 mg, 0.6 mmol, 1.2 eq) in dry toluene (500 μL) and DBU was added at the desired temperature. After 5 min, the chalcone (0.5 mmol, 1 eq) was added and reaction mixture was stirred at room temperature until complete conversion. The crude was directly purified on Silica Gel Chromatography as described in Supporting Information. The enantiomeric excess was determined by Chiral HPLC as described in Supporting Information.

7.5.11.3 Characterization of Juliá-Colonna adducts

Phenyl (3-phenyloxiran-2-yl)methane (32)

Enantiomeric ratio was determined by HPLC [Chiralpak® IC ; flow: 1.0 mL/min ; hexane/*i*-PrOH: 90:10 ; $\lambda = 210$ nm ; $t_{\text{R}} = 21.5$ min, minor enantiomer $t_{\text{R}} = 23.6$ min].

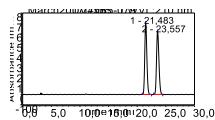


Chemical Formula: $\text{C}_{15}\text{H}_{12}\text{O}_2$

$^1\text{H NMR}$ (300 MHz, CDCl_3) δ (ppm) 8.04-8.07 (m, 2H), 7.66 (tt, $J = 1.3$ Hz, 7.5 Hz, 1H), 7.60-7.66 (m, 2H), 7.51-7.54 (m, 5H), 4.33 (d, $J = 1.9$ Hz, 1H), 4.12 (d, $J = 1.9$ Hz, 1H).

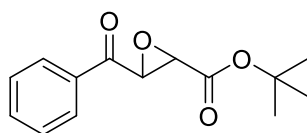
$^{13}\text{C NMR}$ (75 MHz, CDCl_3) δ (ppm) 135.5, 134.0, 129.1, 128.9, 128.9, 128.8, 128.4, 125.8, 61.1, 59.4.

HPLC traces:



	Retention Time	% Area
1	21,483	49,97
2	23,557	50,03

Tert-butyl 3-benzoyloxirane-2-carboxylate (37)

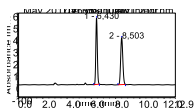


Chemical Formula: C₁₄H₁₆O₄

¹H NMR (300 MHz, CDCl₃) δ (ppm) 8.04-8.07 (m, 2H), 7.65-7.71 (tt, *J* = 1.3 Hz, 7.5 Hz, 1H), 7.62-7.68 (m, 3H), 4.41 (d, *J* = 1.8 Hz, 1H), 3.62 (d, *J* = 1.8 Hz, 1H), 1.56 (9H, s). Boc and H₂O peaks were confounded.

¹³C NMR (75 MHz, CDCl₃) δ (ppm) 192.3, 167.2, 135.1, 129.0, 128.6, 83.6, 55.3, 53.8, 28.0.

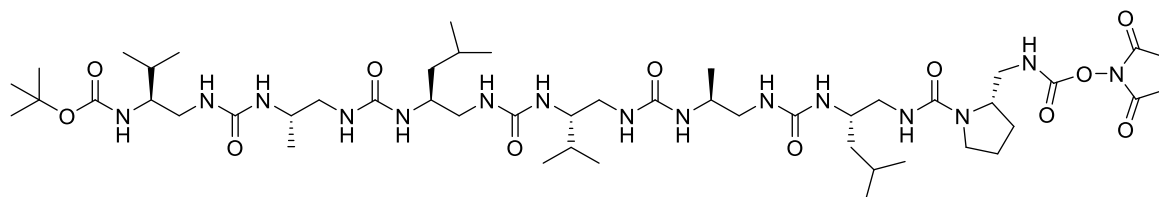
HPLC traces :



	Retention Time	% Area
1	6.43	49.65
2	8.50	50.35

7.6 EXPERIMENTAL PART OF CHAPTER V

7.6.1 Characterization of catalyst 41 and precursors

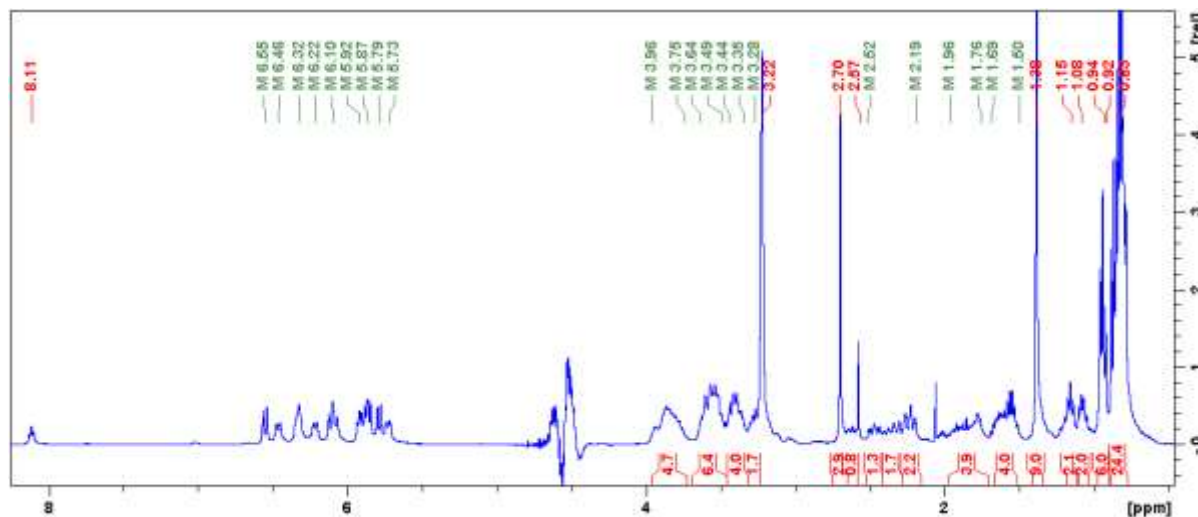
Oligourea 34

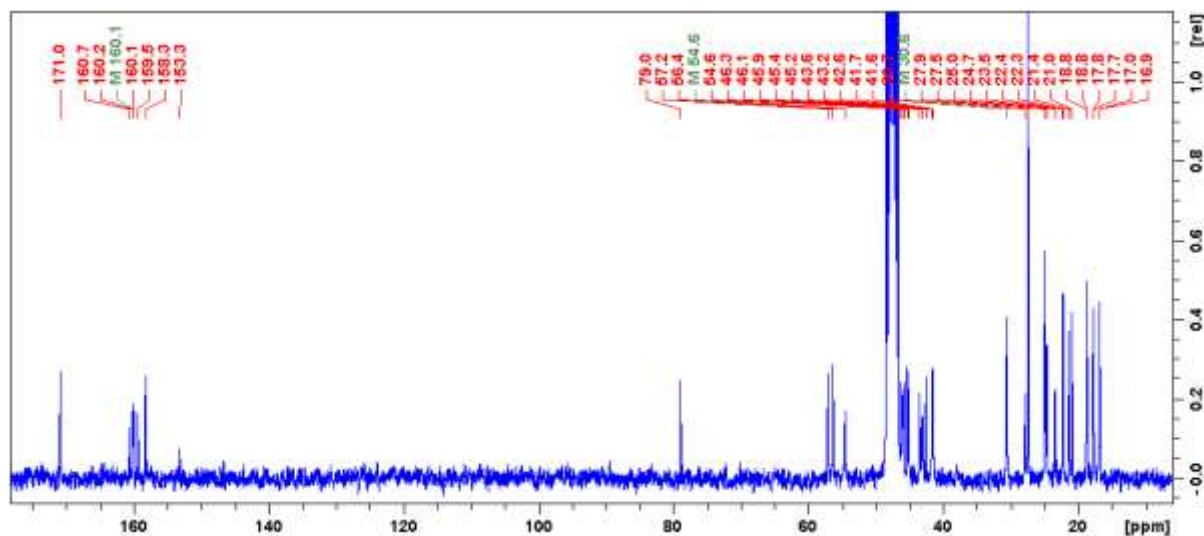
$^1\text{H NMR}$ (400 MHz, CD_3OH) δ (ppm) 8.11 (m, 1H), 6.55 (d, $J = 10.1$ Hz, 1H), 6.46 (m, 1H), 6.32 (m, 2H), 6.21 (d, $J = 8.6$ Hz, 1H), 6.06-6.12 (m, 2H), 5.91 (m, 1H), 5.87 (d, $J = 9.4$ Hz, 2H), 5.78 (d, $J = 9.7$ Hz, 1H), 5.73 (dd, $J = 9.4$ Hz, 3.3 Hz, 1H), 3.75-3.96 (m, 4H), 3.49-3.64 (m, 7H), 3.35-3.47 (m, 3H), 3.25 (m, 1H), 2.70 (s, 4H), 2.40-2.64 (m, 3H), 2.19-2.32 (m, 3H), 1.50-1.69 (m, 4H), 1.38 (s, 9H), 1.14-1.17 (m, 2H), 1.07-1.10 (m, 2H), 0.94 (2 x d, $J = 7.4$ Hz, 2 x 3H), 0.78-0.96 (m, 8 x 3H).

$^{13}\text{C NMR}$ (75 MHz, CD_3OD) δ (ppm) 171.0, 160.7, 160.2, 160.1, 160.1, 159.5, 158.3, 153.3, 79.0, 57.2, 57.4, 54.6, 54.6, 46.3, 46.1, 45.9, 45.4, 45.2, 43.6, 43.2, 42.7, 41.7, 41.6, 30.7, 30.6, 27.9, 27.6, 25.0, 24.7, 23.5, 22.4, 22.3, 21.4, 21.0, 18.8, 18.8, 17.8, 17.8, 18.0, 16.9.

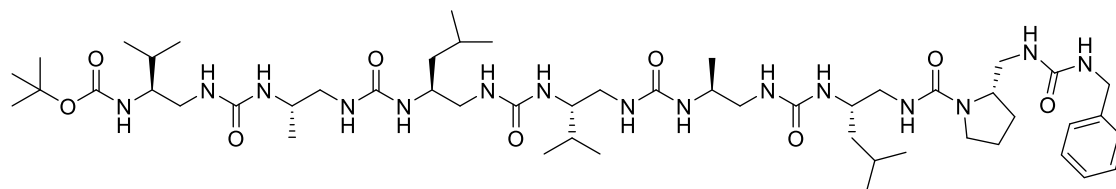
Table S 14: $^1\text{H NMR}$ Chemical Shifts (ppm) of *Boc-Val^u-Ala^u-Leu^u-Val^u-Ala^u-Leu^u-Pro^uOSu (34)* in CD_3OH at 293K.

Residue	NH	NH'	$^{\alpha}\text{CH}^a$	$^{\alpha}\text{CH}^b$	βCH	γCH	δCH	ϵCH	Term CH	$\Delta\delta(^{\alpha}\text{CH})$
Boc									1.38	
Val^u	1	6.55	5.91	3.54	2.48	3.40	1.56	0.84		1.06
Ala^u	2	5.87	6.20	3.56	2.40	3.86	0.94			1.16
Leu^u	3	5.87	6.45	3.56	2.24	3.56	1.08	0.82		1.32
Val^u	4	6.11	6.31	3.58	2.32	3.62	1.56	0.82		1.26
Ala^u	5	5.78	6.73	3.52	2.24	3.80	0.96			1.28
Leu^u	6	6.06	6.31	3.40	2.64	3.90	1.18	1.66	0.82	0.76
Pro^u	7	-	8.10	3.44	3.25	3.93	1.87	1.76	1.96	0.19
OSu									2.70	

 $^1\text{H NMR}$:

¹³C NMR:

tert-butyl ((4*S*,9*S*,14*S*,19*S*,24*S*,29*S*)-1-((*S*)-2-((3-benzylureido)methyl)pyrrolidin-1-yl)-4,19-diisobutyl-14-isopropyl-9,24,30-trimethyl-1,6,11,16,21,26-hexaoxo-2,5,7,10,12,15,17,20,22,25,27-undecazahentriacontan-29-yl)carbamate – Boc-41



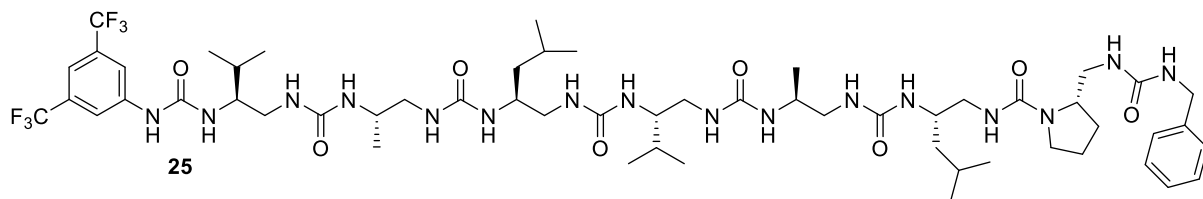
¹H NMR (400 MHz, CDCl₃) δ (ppm) 7.43 (m, 4H), 7.35 (m, 1H), 6.69 (m, 1H), 6.60 (m, 1H), 6.53 (m, 1H), 6.44 (m, 1H), 6.37 (m, 1H), 6.32 (m, 1H), 6.25 (d, *J* = 10.3 Hz, 1H), 6.14 (d, *J* = 9.3 Hz, 1H), 6.06 (m, 1H), 6.00 (2 x d, *J* = 9.5 Hz, 10.2 Hz, 2H), 5.93 (d, *J* = 7.4 Hz, 1H), 5.86 (dd, *J* = 3.2 Hz, 7.1 Hz, 1H), 3.86-4.04 (m, 5H), 3.62-3.78 (m, 5H), 3.43-3.57 (m, 4H), 3.35 (m, 1H), 2.73-2.80 (m, 1H), 2.57-2.64 (m, 1H), 2.32-2.50 (m, 4H), 1.85-2.01 (m, 6H), 1.65-1.81 (m, 4H), 1.52 (s, 9H), 1.27-1.33 (m, 1H), 1.17-1.22 (m, 2H), 1.07 (m, 3H), 0.91-1.01 (m, 8 x 3H).

¹³C NMR (100 MHz, CD₃OH) δ (ppm) 160.8, 160.3, 160.1, 160.0, 159.5, 158.4, 158.3, 128.1, 126.9, 126.6, 79.0, 57.6, 56.5, 54.5, 46.3, 46.2, 46.0, 45.5, 45.3, 43.5, 43.3, 42.8, 42.0, 41.8, 41.5, 30.7, 30.6, 28.5, 27.6, 24.9, 24.7, 23.3, 22.4, 22.3, 21.4, 20.9, 18.8, 17.9, 17.7, 16.9.

Table S ^{15}H NMR Chemical Shifts (ppm) of **Boc-Val^u-Ala^u-Leu^u-Val^u-Ala^u-Leu^u-Pro^u-CH₂Ph** (**Boc-41**) in CD_3OH at 293K

Residue		NH	NH'	αCH^a	αCH^b	βCH	γCH	δCH	ϵCH	Term CH	$\Delta\delta(\alpha\text{CH})$
	Boc										
Val^u	1	6.69	6.06	3.69	2.60	3.54	1.69	1.01			1.09
Ala^u	2	6.00	6.32	3.47	2.48	3.93	0.99				0.99
Leu^u	3	6.00	6.61	3.69	2.36	3.98	1.21	1.74	0.94		1.33
Val^u	4	6.25	6.44	3.68	2.46	3.74	1.69	0.96			1.22
Ala^u	5	5.93	5.86	3.67	2.39	3.93	1.07				1.28
Leu^u	6	6.14	6.53	3.52	2.77	4.00	1.28	1.78	0.99		0.75
Pro^u	7	-	6.37	3.50	3.35	3.98	2.00	1.88	1.95		0.15
CH₂Ph		7.74			4.33					7.42	

(*S*)-2-((3-benzylureido)methyl)-*N*-((3*S*,8*S*,13*S*,18*S*,23*S*,28*S*)-1-((3,5-bis(trifluoromethyl)phenyl)amino)-13,28-diisobutyl-3,18-diisopropyl-8,23-dimethyl-1,6,11,16,21,26-hexaoxo-2,5,7,10,12,15,17,20,22,25,27-undecaazanacosan-29-yl)pyrrolidine-1-carboxamide (**41**)



^1H NMR (400 MHz, CD_3OH) δ (ppm) 7.91 (s, 2H), 7.52 (s, 1H), 7.19 (m, 4H), 7.11 (m, 1H), 6.45-6.50 (m, 2H), 6.31 (m, 1H), 6.14-6.23 (m, 3H), 6.06 (d, $J = 9.0$ Hz, 1H), 5.97-6.00 (m, 1H), 5.88-5.92 (m, 2H), 5.84 (d, $J = 10.2$ Hz, 1H), 5.79 (d, $J = 9.7$ Hz, 1H), 3.68-3.87 (m, 5H), 3.48-3.62 (m, 5H), 3.28-3.39 (m, 5H), 2.77 (m, 1H), 2.57-2.65 (m, 1H), 2.20-2.42 (m, 4H), 1.77-1.91 (m, 6H), 1.60-1.73 (m, 5H), 1.51-1.58 (m, 1H), 1.15-1.19 (m, 2H), 1.06 (t, $J = 7.4$ Hz, 2H), 0.78-0.93 (10 x 3H, m).

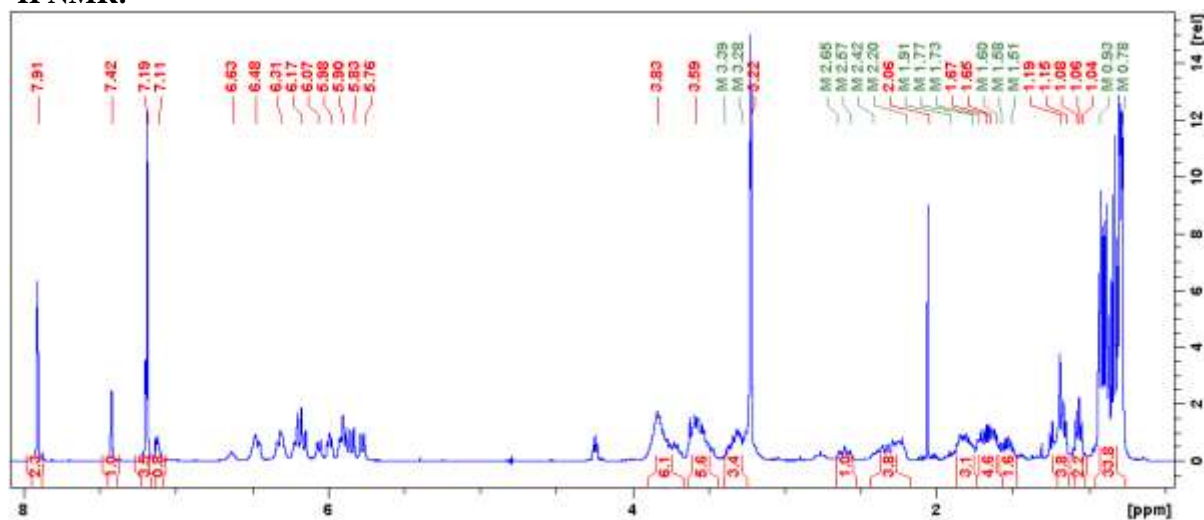
^{13}C NMR (75 MHz, CD_3OH) δ (ppm) 160.8, 160.4, 160.1, 159.6, 158.3, 156.9, 142.0, 139.9, 132.1, 131.7, 131.2, 128.1, 126.9, 126.7, 125.2, 121.6, 117.7, 114.4, 57.7, 55.4, 54.6, 45.6, 45.3, 43.5, 43.2, 43.0, 42.3, 41.8, 41.8, 41.6, 30.6, 29.3, 28.4, 24.8, 24.7, 23.3, 22.5, 22.3, 21.4, 20.9, 18.8, 17.9, 17.4, 17.01, 17.0.

^{19}F NMR (376 MHz, CD_3OH) δ (ppm) -64.60

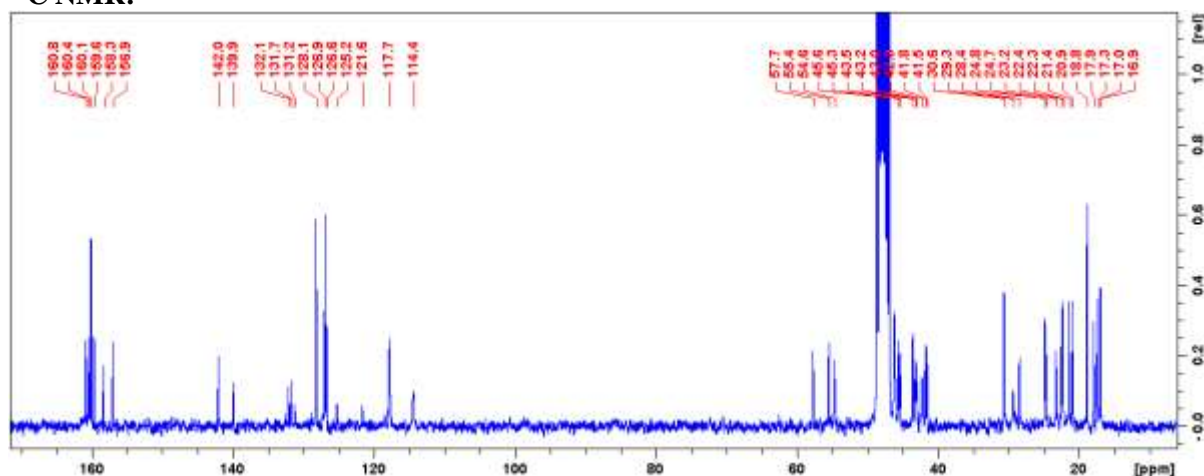
Table S16: ^1H NMR Chemical Shifts (ppm) of 3,5-(CF_3) $_2\text{PhNHCO-Val}^u\text{-Ala}^u\text{-Leu}^u\text{-Val}^u\text{-Ala}^u\text{-Leu}^u\text{-Pro}^u\text{-CH}_2\text{Ph}$ (**41**) in CD_3OH at 293K.

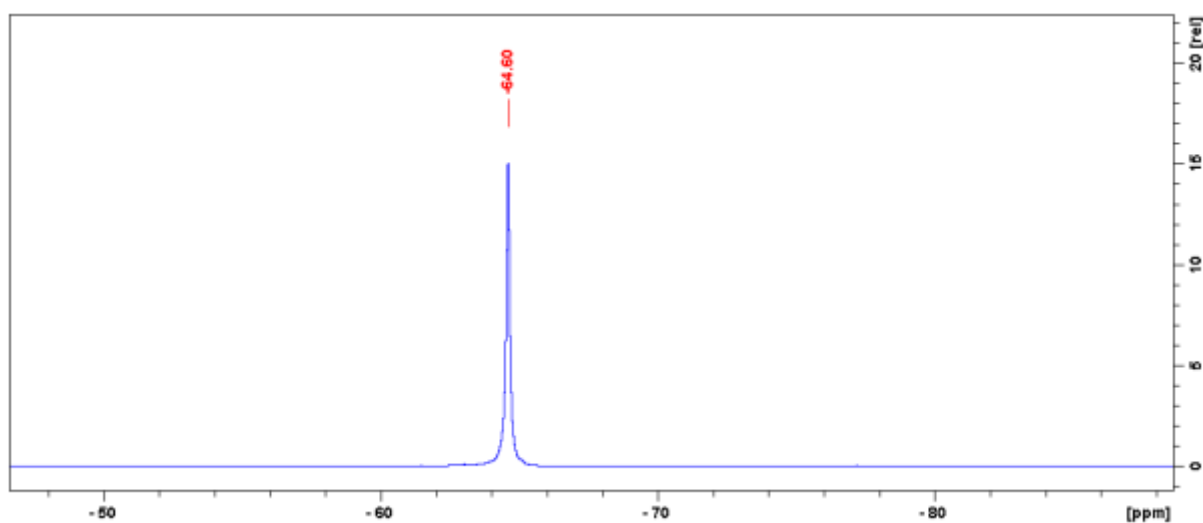
Residue	NH	NH'	$^{\alpha}\text{CH}^a$	$^{\alpha}\text{CH}^b$	$^{\beta}\text{CH}$	$^{\gamma}\text{CH}$	$^{\delta}\text{CH}$	$^{\epsilon}\text{CH}$	Term CH	$\Delta\delta(^{\alpha}\text{CH})$
Ar	7.65								7.52 + 7.91	
Val ^u 1	6.18	5.98	3.62	2.61	3.71	1.69	0.89			1.01
Ala ^u 2	5.91	6.21	3.34	2.40	3.82	0.89				0.94
Leu ^u 3	5.84	6.45	3.57	2.27	3.87	1.06	1.65	0.87		1.30
Val ^u 4	6.14	6.32	3.58	2.36	3.62	1.56	0.89			1.22
Ala ^u 5	5.79	5.92	3.50	2.24	3.80	0.89				1.24
Leu ^u 6	6.06	6.50	3.27	2.77	3.87	1.19	1.69	0.82		0.5
Pro ^u 7	-	6.30	3.30	3.25	3.84	1.85	1.77	1.91		0.05
CH ₂ Ph									4.24	
									7.11 + 7.19	

^1H NMR:

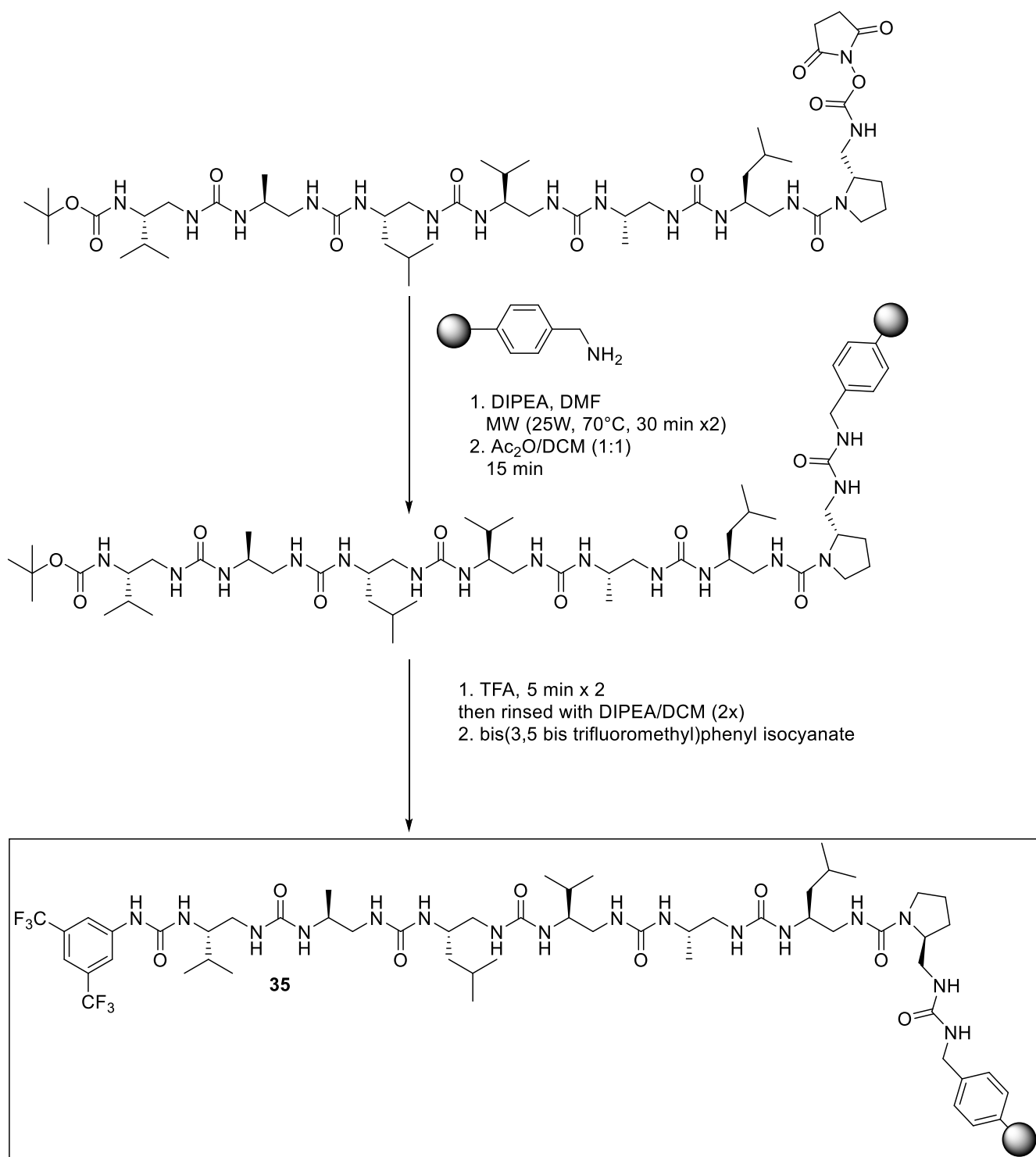


^{13}C NMR:



¹⁹F NMR:**7.6.2 Procedure for synthesis of catalyst 35**

Before synthesis, the resin was washed in DMF three times and let swollen 30 min in DMF. Kaiser test (ninhydrin, phenol, pyridine in ethanol) will be performed all along the synthesis to follow the couplings. Beads are blue in presence of free amines, they are colourless when the amines are capped. In a microwave reactor were added the polystyrene resin (100 mg, 37 μ mol, 1 eq., loading = 0.37 mmol/g), Boc-protected oligourea (48 mg, 44.4 μ mol, 1.2 eq) in DMF (500 μ L) and DIPEA (19 μ L, 111 μ mol, 3 eq.). The reaction mixture was heated at microwave at 25W and 70 °C for 30 min. The remaining free amines were capped with a solution acetic anhydride:DCM (1:1 v:v). Then beads were filtered, rinsed three times with DCM. The amine was deprotected through the addition of TFA (1 mL) at room temperature for 5 min, followed by being rinsed three times with DCM. Reaction mixture was basified with a solution DIPEA:DCM (1:1 v:v) for 5 min at RT, then beads were rinsed three times with DCM. 3,5-bis (trifluoromethyl)phenyl isocyanate (34 μ L, 185 μ mol, 5 eq.) was added to the reaction mixture in DCM (1 mL), and it was stirred for 20 min at room temperature until complete amine coupling. Beads were rinsed three times with DCM and dried under high vacuum. The grafted beads were orange ($m_{\text{total}} = 159$ mg, grafted resin loading = 0.23 mmol/g, quantitative).

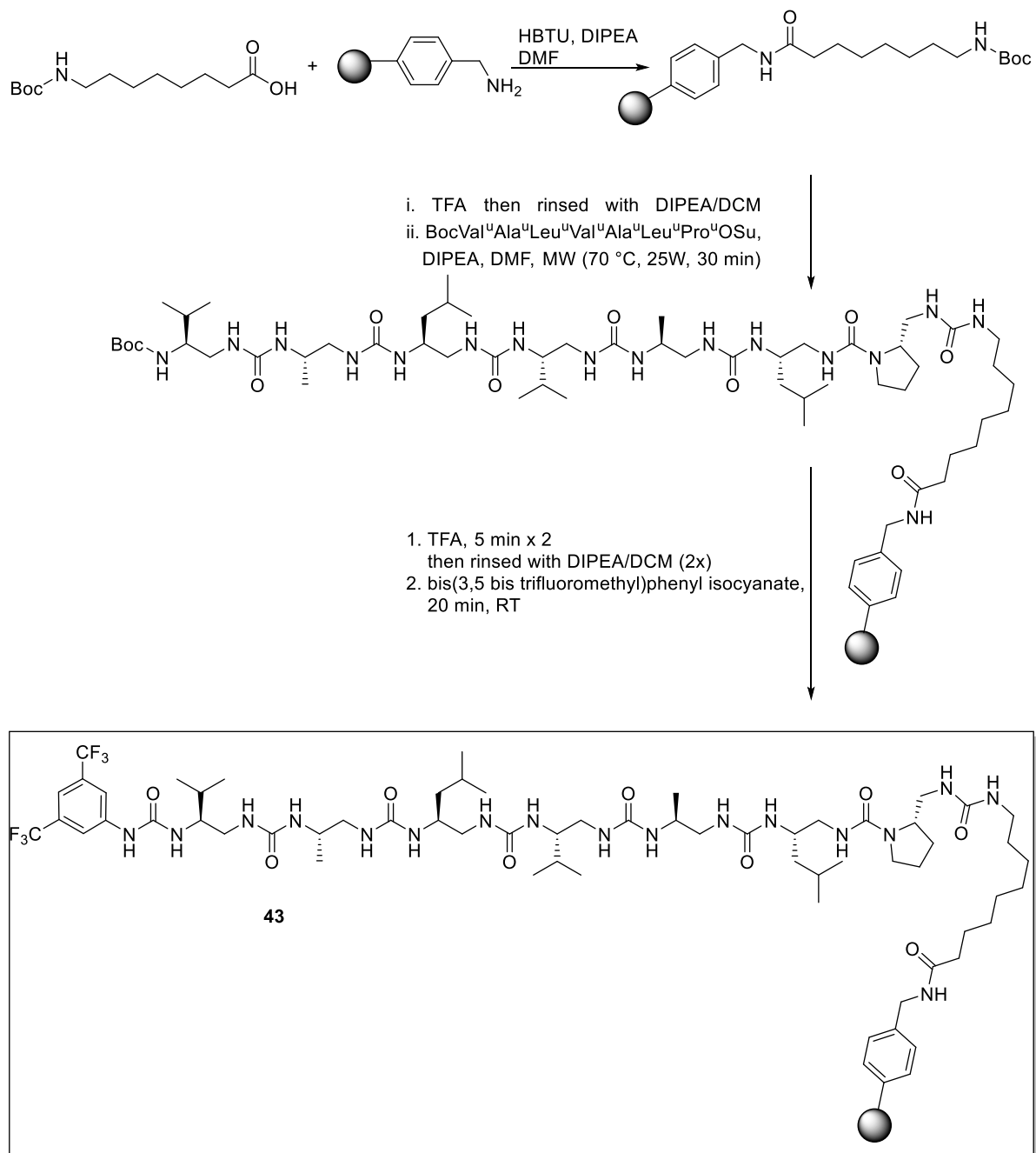


Scheme S22: Synthesis of solid-support catalyst **35**

7.6.2 Procedure for the synthesis of catalyst 43

Before synthesis, the resin was washed in DMF three times and let swollen 30 min in DMF. Kaiser test will be performed all along the synthesis to follow the couplings.

In a microwave reactor were added the polystyrene resin (50 mg, 18.5 μmol , 1 eq., loading = 0.37 mmol/g), HBTU (53.7 μmol , 20 mg, 2.9 eq.), Boc-8-Aoc (14 mg, 55.5 μmol , 3 eq.) and DIPEA (10 μL , 55.5 μmol , 3 eq) were added and stirred overnight at room temperature. Then beads were filtered, rinsed three times with DCM and dried under vacuum to lead to yellow beads (60.2 mg, quantitative). The complete coupling of amine functions was checked with Kaiser test. Beads were swollen 20 min in DCM then filtered and TFA (2 mL) was added and deprotection was run for 5 min at RT. Then beads were filtered, rinsed three times with DCM and reaction mixture was basified with a solution DIPEA:DCM (1 mL, 1:1 v:v). Boc-protected oligourea (60 mg, 55.5 μmol , 3 eq) was dissolved in DMF (500 μL) and added to reaction mixture which was heated for 30 min at 25W and 70 °C. Complete coupling was checked with Kaiser test and Chloranyl test. Beads were filtered and rinsed three times with DCM. TFA (1 mL) was added at room temperature for 5 min to deprotect the amine. Reaction mixture was basified with a solution DIPEA:DCM (1 mL, 1:1 v:v), then beads were rinsed and DMF (500 μL) was added. Isocyanate (10.2 μL , 55.5 μmol , 3 eq.) was added and reaction mixture was stirred overnight at room temperature. Because all the beads were not coupled, additional isocyanate (3 eq) and DIPEA (10 μL) were added. After stirring for 20 min at RT, coupling was complete. Beads were filtered, washed three times with DCM, dried under high vacuum to lead to yellow beads (73.8 mg, grafted resin loading = 0.25 mmol/g, quantitative).



Scheme S23: Synthesis of solid-supported catalyst 43

7.7 Crystallographic data

Table S17: Crystal data and refinement details for molecule **1a**

ccdc code	CCDC 1534525
Chemical formula	C ₁₇₆ H ₃₀₄ F ₂₄ N ₅₆ O ₃₀
Formula weight	4140.73 g/mol
Temperature	120 (2) K
Wavelength	1.54178 Å
Crystal system	Monoclinic
Space group	<i>P</i> 2 ₁
Unit cell dimensions	<i>a</i> = 26.850(5) Å, α = 90°
	<i>b</i> = 12.056(2) Å, β = 109.18(3)°
	<i>c</i> = 36.707(7) Å, γ = 90(3)°
Volume	11222(4) Å ³
<i>Z</i>	4 (<i>Z'</i> =2)
Density (calculated)	1.225 Mg/m ³
Absorption coefficient	0.834 mm ⁻¹
Absorption correction	Multi-scan
Crystal size	0.30 × 0.30 × 0.20 mm ³
Completeness to theta max	94.8%
Reflections collected	148910
Reflections observed [<i>I</i> > 2σ(<i>I</i>)]	35357
<i>R</i> _{int}	0.0896
Data/parameters/restrains	148910/2619/26
Goodness-of-fit on F ²	0.967
Final R indices [<i>I</i> > 4σ(<i>I</i>)]	R1 = 0.0656, wR2 = 0.0.1520
R indices (all data)	R1 = 0.0977, wR2 = 0.1689
Largest diff. peak and hole	0.686 and -0.271 e Å ⁻³

Table S 18: Crystal data and refinement details for molecule **5a**

ccdc code	CCDC 1534523
Chemical formula	C ₄₅ H ₇₉ F ₆ N ₁₄ O ₇ S
Formula weight	1074.28 g/mol
Temperature	120 (2) K
Wavelength	1.54178 Å
Crystal system	Triclinic
Space group	<i>P</i> -1
Unit cell dimensions	$a = 12.085(2)$ Å, $\alpha = 108.71(3)^\circ$ $b = 16.110(3)$ Å, $\beta = 104.35(3)^\circ$ $c = 16.872(3)$ Å, $\gamma = 97.82(3)^\circ$
Volume	2929.9 (12) Å ³
<i>Z</i> '	2
Density (calculated)	1.218 Mg/m ³
Absorption coefficient	1.134 mm ⁻¹
Absorption correction	Multi-scan
Crystal size	0.20 × 0.10 × 0.10 mm ³
Completeness to theta max	98.1%
Reflections collected	40075
Reflections observed [<i>I</i> > 2(<i>I</i>)]	15651
<i>R</i> _{int}	0.0336
Data/parameters/restrains	40075/1413/162
Goodness-of-fit on <i>F</i> ²	1.153
Final <i>R</i> indices [<i>I</i> > 4σ (<i>I</i>)]	<i>R</i> 1 = 0.0754, <i>wR</i> 2 = 0.1771
<i>R</i> indices (all data)	<i>R</i> 1 = 0.0763, <i>wR</i> 2 = 0.1795
Largest diff. peak and hole	1.611 and -0.431 e Å ⁻³

Table S 19: Crystal data and refinement details for molecule **1b**

ccdc code	CCDC 1534527
Chemical formula	$C_{37}H_{64}F_6N_{12}O_8 \cdot$
Formula weight	919.00 g/mol
Temperature	120 (2) K
Wavelength	1.54178 Å
Crystal system	Orthorhombic
Space group	$P2_12_12_1$
Unit cell dimensions	$a = 9.799(2)$ Å, $\alpha = 90^\circ$
	$b = 21.455(4)$ Å, $\beta = 90(3)^\circ$
	$c = 24.701(5)$ Å, $\gamma = 90(3)^\circ$
Volume	5193.1 (18) Å ³
Z	4
Density (calculated)	1.175 Mg/m ³
Absorption coefficient	0.837 mm ⁻¹
Absorption correction	Multi-scan
Crystal size	0.30 × 0.02 × 0.02 mm ³
Completeness to theta = 68.246°	98.6%
Reflections collected	19777
Reflections observed [$I > 2\sigma(I)$]	8776
R_{int}	0.0337
Data/parameters/restraints	19777/643/204
Goodness-of-fit on F^2	1.018
Final R indices [$I > 4\sigma(I)$]	R1 = 0.0455, wR2 = 0.1132
R indices (all data)	R1 = 0.0626, wR2 = 0.1190
Largest diff. peak and hole	0.229 and -0.222 e Å ⁻³

Table S 20: Crystal data and refinement details for molecule **12**

ccdc code	CCDC 1534528
Chemical formula	(C ₄₆ H ₇₈ F ₆ N ₁₄ O ₆ S)
Formula weight	1069.28 g/mol
Temperature	120 (2) K
Wavelength	1.54178 Å
Crystal system	Orthorhombic
Space group	<i>P</i> 2 ₁ 2 ₁ 2 ₁
Unit cell dimensions	<i>a</i> = 15.2126(8) Å, α = 90°
	<i>b</i> = 15.6715(5) Å, β = 90°
	<i>c</i> = 23.6347(8) Å, γ = 90°
Volume	5634.6 (4) Å ³
<i>Z</i>	4
Density (calculated)	1.260 Mg/m ³
Absorption coefficient	1.164 mm ⁻¹
Absorption correction	Multi-scan
Crystal size	0.4 × 0.06 × 0.06 mm ³
Completeness to theta = 72.286°	98.8%
Reflections collected	16496
Reflections observed [<i>I</i> > 2σ(<i>I</i>)]	8560
<i>R</i> _{int}	0.1024
Data/parameters/restraints	16496/668/18
Goodness-of-fit on F ²	1.121
Final <i>R</i> indices [<i>I</i> > 4σ(<i>I</i>)]	<i>R</i> 1 = 0.0986, <i>wR</i> 2 = 0.2249
<i>R</i> indices (all data)	<i>R</i> 1 = 0.1131, <i>wR</i> 2 = 0.2685
Largest diff. peak and hole	0.828 and -0.311 e Å ⁻³

Table S21: Crystal data and refinement details for molecule **Boc-11**

ccdc code	CCDC 1534526
Chemical formula	C ₄₂ H ₈₅ N ₁₃ O ₉
Formula weight	916.22 g/mol
Temperature	103 (2) K
Wavelength	1.54178 Å
Crystal system	Orthorhombic
Space group	<i>P</i> 2 ₁ 2 ₁ 2 ₁
Unit cell dimensions	<i>a</i> = 13.9547(3) Å, α = 90°
	<i>b</i> = 16.1574(3) Å, β = 90°
	<i>c</i> = 22.4255(16) Å, γ = 90°
Volume	5056.3 (4) Å ³
<i>Z</i>	4
Density (calculated)	1.204 Mg/m ³
Absorption coefficient	0.697 mm ⁻¹
Absorption correction	Multi-scan
Crystal size	0.30 × 0.20 × 0.20 mm ³
Completeness to theta = 72.090°	99.2%
Reflections collected	71085
Reflections observed [<i>I</i> > 2σ(<i>I</i>)]	9803
<i>R</i> _{int}	0.0278
Data/parameters/restrains	71085/633/0
Goodness-of-fit on F ²	1.074
Final R indices [<i>I</i> > 4σ(<i>I</i>)]	R1 = 0.0343, wR2 = 0.0844
R indices (all data)	R1 = 0.0365, wR2 = 0.0826
Largest diff. peak and hole	0.220 and -0.244 e Å ⁻³

Bibliography

-
- i Guichard, G.; Semetey, V.; Didierjean, C.; Aubry, A.; Briand, J.-P.; Rodriguez, M., *J. Org. Chem.* **1999**, *64*, 8702-8705.
- ii Bae H.Y.; Song C.E, *ACS Catal.* **2015** *5*, 3613–3619.
- iii M. Işık, Unver, C. Tanyeli, *J. Org. Chem.* **2015**, *80*, 828–835.
- iv Evans, D.A.; Mito, S.; Seidel, D., *J. Am. Chem. Soc.* **2007**, *129*, 11583–11592.
- v Li, H.; Wang, Y.; Tang, L.; Deng, L., *J. Am. Chem. Soc.* **2004**, *126*, 9906–9907.
- vi McCooey, S.H.; Connon, S.J., *Angew. Chem. Int. Ed.* **2005**, *44*, 6367–6370.
- vii Zhang, L., *Adv. Synth. Catal.* **2009**, *351*, 3063–3067.
- viii Li, X.; Peng, F.; Shao, Z., *Adv. Synth. Catal.* **2012**, *354*, 2873–2885.
- ix Ghosh, S.K.; Ganzmann, C.; Bhuvanesh, N.; Gladysz, J.A., *Angew. Chem. Int. Ed.* **2016**, *55*, 4356–4360.
- x Terada, M., *J. Am. Chem. Soc.* **2005**, *128* 1454-1455.
- xi Chowdhury, R.; Vamisetti, G.B.; Ghosh, S.K., *Tetrahedron Asymmetry* **2014**, *25*, 516–522.
- xii Wang, Y.F., *Green Chem.* **2012**, *14*, 893.
- xiii Chen, J.; Huang, Y., *Nat. Commun.* **2014**, *5*.
- xiv Rao, K.; Trivedi, R.; Kantam, M., *Synlett* **2014**, *26*, 221–227.